N°d'ordre NNT : 2017LYSET006

DOCTORAL THESIS OF THE UNIVERSITY OF LYON
prepared at
Ecole Nationale des Travaux Publics de l'Etat

Doctoral School N° 162
Mécanique, Energétique, Génie Civil et Acoustique (MEGA)

Specialty: **Civil Engineering**

Publicly defended the 15th of September 2017 by:

Lucas Babadopulos

Phenomena occurring during cyclic loading and fatigue tests on bituminous materials: Identification and quantification

---

before the committee composed of:

DJERAN-MAIGRE, Irini	Prof., INSA Lyon	President
AIREY, Gordon	Prof., University of Nottingham, UK	Reviewer
SOARES, Jorge Barbosa	Prof., Federal University of Ceará, Brazil	Reviewer
BAAJ, Hassan	Dr., University of Waterloo, Canada	Examiner
POUGET, Simon	Dr., EIFFAGE Routes	Examiner
DI BENEDETTO, Hervé	Prof., University of Lyon/ENTPE	Advisor
SAUZÉAT, Cédric	Prof., University of Lyon/ENTPE	Co-advisor

N°d'ordre NNT : 2017LYSET006

THESE de DOCTORAT DE L'UNIVERSITE DE LYON
opérée au sein de
l'Ecole Nationale des Travaux Publics de l'Etat

Ecole Doctorale N° 162
Mécanique, Energétique, Génie Civil et Acoustique (MEGA)

Spécialité / discipline de doctorat : Génie Civil

Soutenue publiquement le 15/09/2017, par :

Lucas Babadopulos

Phénomènes apparaissant dans les matériaux bitumineux lors de chargements cycliques et d'essais de fatigue : Identification et quantification

---

Devant le jury composé de :

DJERAN-MAIGRE, Irini	Prof., INSA Lyon	Présidente
AIREY, Gordon	Prof., Université de Nottingham, RU	Rapporteur
SOARES, Jorge Barbosa	Prof., Université Fédérale de Ceará, Brésil	Rapporteur
BAAJ, Hassan	Dr., Université de Waterloo, Canada	Examinateur
POUGET, Simon	Dr., EIFFAGE Routes	Examinateur
DI BENEDETTO, Hervé	Prof., Université de Lyon/ENTPE	Directeur de thèse
SAUZÉAT, Cédric	Prof., Université de Lyon/ENTPE	Co-Directeur de thèse

TABLE OF CONTENTS

Table of contents ..... **iii**

Acknowledgements ..... **ix**

Résumé ..... **xi**

Abstract ..... **xiii**

List of Tables ..... **xv**

List of Figures ..... **xviii**

Main Symbols ..... **xxxv**

Chapter 1: Introduction **1**

Chapter 2: Generalities on the Mechanical Behaviour of Bituminous Materials **6**

2.1. Bituminous materials composition 8

2.1.1. Bitumen 9

2.1.2. Mastic 10

2.1.3. Bituminous mixture 10

2.2. Mechanical behaviour and the effects of time and temperature 11

2.2.1. General experimental observations 11

2.2.2. Thermo-sensitivity (temperature dependence) 16

2.2.3. Time (or frequency) dependence (viscosity aspects) 16

2.2.4. Time-temperature (or frequency-temperature) superposition 19

2.2.4.1. In linear viscoelasticity 21

2.2.4.2. In nonlinear viscoelasticity 22

2.2.4.3. In plasticity 23

2.2.4.4. In crack propagation 24

2.2.4.5. In fatigue 25

2.2.4.6. Relation between bitumen, mastic and bituminous mixtures 26
2.2.4.7. Non thermorheologically simple bituminous materials 26
2.3. Linear viscoelasticity for non-ageing materials 27
2.3.1. Experimental assessment of time domain properties 27
2.3.2. Experimental assessment of frequency domain properties 28
2.3.3. Convolution integral and relationships between properties 30
2.3.4. Discrete spectrum models 31
2.3.4.1. Springs and Dashpots 31
2.3.4.2. Dashpot 31
2.3.4.3. Generalised Kelvin-Voigt (GKV) model 32
2.3.4.4. Generalised Maxwell-Wiechert (GMW) model 32
2.3.4.5. Interconversion between linear viscoelastic properties from models 33
2.3.5. Continuum spectrum models 33
2.3.5.1. The parabolic element 33
2.3.5.2. Huet model and Huet-Sayegh model 33
2.3.5.3. 2S2P1D model 34
2.3.6. Normalised complex modulus and SHStS transformation 36
2.4. Nonlinear viscoelasticity 39
2.4.1. Equivalent complex modulus as a function of loading amplitude 39
2.4.2. Mathematical formulations for nonlinear viscoelastic behaviour 41
2.5. Fatigue damage 41
2.5.1. Experimental observations 42
2.5.2. Damage modelling 43
2.6. Failure 44
2.6.1. Experimental observations 44
2.6.2. Failure modelling 45
2.6.2.1. Whöler curves and Miner’s law 46

2.7. Thixotropy 46
2.8. General formulation to interpret fatigue tests considering biasing phenomena 50
Chapter 3: Experimental Devices and Programme 55
3.1. Experimental set-ups 56
3.1.1. Annular Shear Rheometer (ASR) tests 57
3.1.2. Tension-Compression (T-C) tests 59
3.2. Experimental analysis 60
3.2.1. Annular Shear Rheometer (ASR) tests 60
3.2.2. Tension-Compression (T-C) tests 62
3.2.3. Signal analysis and stiffness measurements 63
3.2.4. Geometrical biases in ASR tests stiffness measurements 66
3.2.4.1. Effect of an eccentricity between internal and external moulds 66
3.2.4.2. Effect of a material loss due to flow under gravity 67
3.2.4.3. Effect of the formation of a circular section meniscus 68
3.2.4.4. Geometrical biases analysis conclusion 69
3.3. Materials and designation 69
3.3.1. Bitumen 69
3.3.1.1. Description 69
3.3.1.2. Specimen preparation for ASR tests 69
3.3.2. Glass beads mastic 70
3.3.2.1. Description 71
3.3.2.2. Fabrication process 71
3.3.2.3. Specimen preparation for ASR tests 71
3.3.3. Bituminous mixtures 72
3.3.3.1. Bituminous mixture specimen fabrication process for T-C tests 72
3.3.3.2. BM1 (C. V. Phan, Di Benedetto, Sauzéat, Lesueur, et al., 2017) 72
3.3.3.3. BM2 (Q. T. Nguyen, 2011) 73

3.3.3.4. BM3 (Q. T. Nguyen, 2011) 73
3.4. Experimental campaign overview 73
Chapter 4: Nonlinearity of Bituminous Materials 76
4.1. Introduction 77
4.2. Tension-compression experiments on bituminous mixture specimens 80
4.2.1. Complex modulus test at 50μm/m 80
4.2.2. Strain Amplitude Sweep Tests for NonLinearity Evaluation (SASTENOLE) 83
4.2.3. Analysis of SASTENOLE test results on BM1_B 85
4.2.4. Analysis of SASTENOLE test results on BM1_C 101
4.2.4.1. Strain dependence of norm of complex modulus and phase angle 102
4.2.4.2. Strain dependence of norm and phase angle of complex Poisson's ratio 109
4.2.5. Transient effects during SASTENOLE tests 113
4.3. Annular shear experiments on bitumen and mastic specimens 115
4.3.1. Complex shear modulus test at "low" amplitudes 115
4.3.2. Strain Amplitude Sweep (SAS) tests on bitumen and mastic 118
4.3.2.1. Cyclic effects during Strain Amplitude Sweep (SAS) tests 119
4.3.3. Analysis of Strain Amplitude Sweep (SAS) test results 121
4.4. LVE limits of bituminous materials 127
4.5. Conclusion on nonlinearity 130
Chapter 5: Initial Modulus Decrease and Self-heating During Cyclic Loading 132
5.1. Introduction 133
5.2. Tension-compression experiments description 135
5.2.1. Complex modulus test (H. M. Nguyen, 2010) 135
5.2.2. Phase I Fatigue test (Q. T. Nguyen, 2011) 136
5.3. Considered heterogeneous cell and relationship with the grading curve 137
5.4. Thermomechanical coupling and preliminary calculations 139
5.5. Performed calculations without heat diffusion 142

5.5.1. Homogeneous heat distribution in the bituminous mixture 142
5.5.2. Homogeneous heat distribution only in the bitumen 142
5.5.3. 3D heterogeneous calculation 143
5.6. Results and analysis without heat diffusion 147
5.6.1. Example: test on BM3_A at 12.3°C and 3Hz and 116μm/m 147
5.6.2. Analysis of initial slopes of norm of complex modulus for all tests 149
5.6.3. Time intervals when calculated slopes are observed in experiments 154
5.7. 3D heterogeneous calculation with heat diffusion 156
5.7.1. FEM Calculations 157
5.7.1.1. FEM characteristics 159
5.7.1.2. Thermal and Mechanical FEM calculations 160
5.8. Results and analysis with heat diffusion 161
5.9. Conclusion on bituminous mixture self-heating 163
Chapter 6: Combined Effects of Different Phenomena During Cyclic Tests 165
6.1. Introduction 166
6.2. Annular Shear Rheometer experiments description 168
6.2.1. Complex shear modulus tests 168
6.2.2. Alternating Strain Amplitudes (ASA) test 168
6.2.3. Load and Rest Periods (LRP) tests 169
6.3. Complex shear modulus test results: the effect of temperature 171
6.4. ASA test results 173
6.5. LRP test results: quantification of biasing effects on bitumen and mastic specimens 177
6.5.1. An example of LRP test results: 5 LRP loops with 10,000 cycles and 4h rest on bitumen submitted to 20,000μm/m sinusoidal loading 177
6.5.2. Damage 184
6.5.3. Nonlinearity and self-heating 187
6.5.4. Thixotropy 194

6.6. Number of cycles and rest time effect 196
6.7. Failure analysis 199
6.8. Conclusion on biasing effects on bitumen and mastic 202
Chapter 7: Conclusions and Perspectives 204
Résumé en Français 209
Introduction 210
Généralités sur les matériaux bitumineux 214
Matériaux et Matériels 216
Non-linéarité 216
Auto-échauffement 217
Effets combinés des différents phénomènes lors des essais cycliques 219
Conclusions et Perspectives 220
REFERENCES 223
Appendix A – Utilised PID control parameters 252
Appendix B – Bitumen and Mastic Nonlinearity Characterisation Results 254
Appendix C – Bitumen and Mastic Load and Rest Period Test Results 261
LRP test results on Bitumen 262
B5070_C with 3,600μm/m strain amplitude 262
B5070_A with 10,000μm/m strain amplitude 268
B5070_B with 20,000μm/m strain amplitude 274
B5070_D with 20,000μm/m strain amplitude 280
LRP test results on Mastic 286
M5070_30pc40-70_C with 1,000μm/m strain amplitude 286
M5070_30pc40-70_A with 3,300μm/m strain amplitude 292
M5070_30pc40-70_B with 8,500μm/m strain amplitude 298

ACKNOWLEDGEMENTS

I know the preparation of a PhD thesis is considered an individual work. Ok, it is a huge effort, both from an intellectual and from a manual point of view. I think most people cannot even imagine the pressure we put on ourselves as PhD students, and the hard work that is required to become doctor. Even if other people participate in the tasks, we are the ones being measured by the work produced… and it was a really hard work, and I found myself multiple times thinking I could not manage all the required tasks. So, I understand the character of individuality of this work, but it is clear that I needed people from around me. I needed family to cheer me up. I needed help… and I got it! *I got by with a little help from my friends*. And not only during crisis, such as the two fires that interrupted my experimental plan, but also on a day-to-day basis, within our research team and group of colleagues and from my supervisors, and from close friends and family… So, okay, an individual work, but I wished that the people who accompanied me through this adventure could feel the pride and the happiness of its success as I do. I enjoyed the time as a PhD student, and I will miss it. But I am just incredibly happy it is finished! I wanted to try to express all my gratitude to all the people directly or indirectly involved in my PhD experience. Hope you all feel acknowledged even if these small pages do not clearly state you name…

Firstly, I wanted to thank my PhD advisors, Profs. Hervé Di Benedetto and Cédric Sauzéat, who have directed this work and found ways to keep going on even when the conditions were hard. I advanced much faster and I went much further than I could imagine, thanks to your work. I am positively sure that a made the good choice of coming here for my PhD (despite many problems I had with different spheres of public administration, from the Prefecture to my own school, for which I also had much help from guardian angels like Mrs. Francette Pignard, among others). This work, that started focused on local self-heating, ended-up covering also nonlinearity, thixotropy and damage with comparable importance, and I am really proud of what we have done during these 3 years and 3 months. A special thanks goes to Cédric, who many times acted as my personal psychologist…

I would like to thank the PhD reviewers, Profs. Gordon Airey and Jorge Soares, who worked really hard in evaluating this thesis. I really appreciate your comments and beautifully prepared reports, of which I am very proud. I am honoured by your participation in this work. I am also grateful for the participation in this thesis' Committee of Prof. Irini Djeran-Maigre and Drs. Hassan Baaj and Simon Pouget. The discussions we had during the PhD defence were very interesting, and I feel motivated to continue with this work, and glad that I chose the path of research. I also appreciate all the advice I got from all of you.

I thank our research team (and friends) at ENTPE. I wish all people facing the challenges of a PhD work such a good team as I had here. Special thanks goes to Gabriel Orozco for his friendship and all the support with the experimental plan we managed on bitumen and mastic, and also to Dr. Salvatore Mangiafico, for our work on nonlinearity and many passionate discusions that builded up our friendship. I also thank our past master's students Khanh Phan and Wen Fan for the experimental support. I wish all the best for your careers and I am grateful I had the opportunity to work on your supervision team.

I would like to thank the Brazilian agency CAPES and its Science without Borders (*Ciência sem Fronteiras* - CsF) programme for the grant I had within my PhD project (BEX 13.551/13-2). I also thank ENTPE and its *Chaire* with Eiffage, for its support to this investigation.

Finally, I would like to thank (a lot) my family (o Familhão Baba), who has always been there for me. I had the perfect conditions during all my education, so if this work is done, it is also because they were always there for me from the very beginning. I feel privileged, grateful and lucky, and I think a have somewhat a supplementary responsibility for all I do. I thank especially my wife Priscilla not only for all the unconditional support I had from her, but also because I would not have finished this work on time to see my first baby arrive if it weren't for her help. I am full of hope for the future thanks to you and Gaël. **I dedicate this thesis to you two**, and hope we will enjoy our time together with all our love.

Thank you all!

Lucas Babadopulos, 27.09.2017

"I hear babies crying, I watch them grow

They'll learn much more than I'll never know

And I think to myself what a wonderful world

Yes I think to myself what a wonderful world…"

RESUME

La fatigue est un des principaux mécanismes de dégradation des chaussées. En laboratoire, la fatigue est simulée en utilisant des essais de chargement cyclique, généralement sans période de repos. L'évolution du module complexe (une propriété du matériau utilisée dans la caractérisation de la rigidité des matériaux viscoélastiques) est suivie de manière à caractériser l'endommagement. Son changement est généralement interprété comme étant dû au dommage, alors que d'autres phénomènes (se distinguant du dommage par leur réversibilité) apparaissent.

Des effets transitoires, propres aux matériaux viscoélastiques, apparaissent lors des tout premiers cycles (2 ou 3) et produisent une erreur dans la détermination du module complexe. La non-linéarité (dépendance du module complexe avec le niveau de déformation) est caractérisée par une diminution réversible instantanée du module et une augmentation de l'angle de phase qui est observée avec l'augmentation de l'amplitude de déformation. De plus, pendant le chargement, de l'énergie mécanique est dissipée en raison du caractère visqueux du comportement du matériau. Cette énergie se transforme principalement en chaleur ce qui induit une augmentation de température. Cela produit une diminution de module liée à cet auto-échauffement. Quand le matériau revient à la température initiale, le module initial est alors retrouvé. La partie restante du changement de module peut être expliquée, d'une part par un autre phénomène réversible, appelé dans la littérature « thixotropie », et d'autre part par le dommage « réel », qui est irréversible.

Cette thèse explore ces phénomènes dans les bitumes, mastics (bitume mélangé avec des particules fines, dont le diamètre est inférieur à 80µm) et enrobés bitumineux. Un chapitre (sur la nonlinearité) présente des essais de « balayage d'amplitude de déformation » avec augmentation ou/et diminution des amplitudes sont présentés. Un autre se concentre sur l'auto-échauffement. Il comprend une proposition de procédures de modélisation dont les résultats sont comparés avec des résultats des cycles initiaux d'essais de fatigue. Finalement, un chapitre est dédié à l'analyse du module complexe mesuré pendant le chargement et les phases de repos. Des essais de chargement et repos ont été réalisés sur bitume (où le phénomène de thixotropie est supposé avoir lieu) et mastic, de manière à déterminer l'effet de chacun des phénomènes identifiés sur l'évolution du module complexe des matériaux testés.

Les résultats de l'étude sur la nonlinearité suggèrent que son effet vient principalement du comportement non linéaire du bitume, qui est déformé de manière très non-homogène dans les enrobés bitumineux.

Il est démontré qu'un modèle de calcul thermomécanique simplifié de l'échauffement local, ne considérant aucune diffusion de chaleur, peut expliquer le changement initial de module complexe observé au cours des essais cycliques sur enrobés. Néanmoins, la modélisation de la diffusion de chaleur a démontré que cette diffusion est excessivement rapide. Cela indique que la distribution de l'augmentation de température nécessaire pour expliquer complètement le module complexe observé ne peut pas être atteinte. Un autre phénomène réversible, qui a des effets sur le module complexe similaires à ceux d'un changement de température, doit donc avoir lieu. Ce phénomène est considéré être de la thixotropie.

Finalement, à partir des essais de chargement et repos, il est démontré qu'une partie majeure du changement de module complexe au cours des essais cycliques vient des processus réversibles. Le dommage se cumule de manière approximativement linéaire par rapport au nombre de cycles. Le phénomène de thixotropie semble partager la même direction sur l'espace complexe que la non-linéarité. Cela indique que les deux phénomènes sont possiblement liés par la même origine micro-structurelle. Des travaux supplémentaires sur le phénomène de thixotropie sont nécessaires.

Mots-clés : matériaux bitumineux, essais de fatigue, non-linéarité, auto-échauffement, thixotropie, dommage, bitumes, mastics, enrobés bitumineux, modélisation, comportement cyclique.

ABSTRACT

Fatigue is a main pavement distress. In laboratory, fatigue is simulated using cyclic loading tests, usually without rest periods. Complex modulus (a material stiffness property used in viscoelastic materials characterisation) evolution is monitored, in order to characterise damage evolution. Its change is generally interpreted as damage, whereas other phenomena (distinguishable from damage by their reversibility) occur.

Transient effects, proper to viscoelastic materials, occur during the very initial cycles (2 or 3) and induce an error in the measurement of complex modulus. Nonlinearity (strain-dependence of the material's mechanical behaviour) is characterised by an instantaneous reversible modulus decrease and phase angle increase observed when strain amplitude increases. Moreover, during loading, mechanical energy is dissipated due to the viscous aspect of material behaviour. This energy turns mainly into heat and produces a temperature increase. This produces a modulus decrease due to self-heating. When the material is allowed to cool back to its initial temperature, initial modulus is recovered. The remaining stiffness change can be explained partly by another reversible phenomenon, called in the literature "thixotropy", and, then, by the "real" damage, which is irreversible.

This thesis investigates these phenomena in bitumen, mastic (bitumen mixed with fine particles, whose diameter is smaller than 80µm) and bituminous mixtures. One chapter (on nonlinearity) presents increasing and/or decreasing strain amplitude sweep tests. Another one focuses on self-heating. It includes a proposition of modelling procedures whose results are compared with the initial cycles from fatigue tests. Finally, a chapter is dedicated to the analysis of the measured complex modulus during both loading and rest periods. Loading and rest periods tests were performed on bitumen (where the phenomenon of thixotropy is supposed to happen) and mastic in order to determine the effect of each of the identified phenomena on the complex modulus evolution of the tested materials.

Results from the nonlinearity investigation suggest that its effect comes primarily from the nonlinear behaviour of the bitumen, which is very non-homogeneously strained in the bituminous mixtures.

It was demonstrated that a simplified thermomechanical model for the calculation of local self-heating (non-uniform temperature increase distribution), considering no heat diffusion, could explain the initial complex modulus change observed during cyclic tests on bituminous mixtures. However, heat diffusion modelling demonstrated that this diffusion is excessively fast. This indicates that the temperature increase distribution necessary to completely explain the observed complex modulus decrease cannot be reached. Another reversible phenomenon, which has effects on complex modulus similar to the ones of a temperature change, needs to occur. That phenomenon is hypothesised as thixotropy.

Finally, from the loading and rest periods tests, it was demonstrated that a major part of the complex modulus change during cyclic loading comes from the reversible processes. Damage was

found to cumulate in an approximately linear rate with respect to the number of cycles. The thixotropy phenomenon seems to share the same direction in complex space as the one of nonlinearity. This indicates that both phenomena are possibly linked by the same microstructural origin. Further research on the thixotropy phenomenon is needed.

Keywords: bituminous materials, fatigue tests, nonlinearity, self-heating, thixotropy, damage, bitumen, mastic, bituminous mixtures, modelling, cyclic behaviour.

LIST OF TABLES

Table 3-1. Overview of the analysed experiments on bitumen (B5070). 75

Table 3-2. Overview of the analysed experiments on mastic (M5070_30pc40-70). 75

Table 3-3. Overview of the analysed experiments on bituminous mixtures (BM1, BM2 and BM3). 75

Table 4-1. 2S2P1D model and WLF equation parameters used to model the LVE behaviour of the studied bituminous mixtures. 81

Table 4-2. Regression parameters p_E and p_φ obtained from nonlinearity envelopes of, respectively, norm and phase angle of complex modulus obtained from all SASTENOLE tests on BM1_B at different temperatures and frequencies, for increasing strain amplitude loading paths. 92

Table 4-3. Maximum strain amplitude values satisfying the $|p_E \cdot \varepsilon_0| \leq 0.05$ condition, according to p_E coefficients obtained from increasing sweeps of SASTENOLE tests on BM1_B (Table 4-2). 95

Table 4-4. Values of p_E/p_φ and α obtained for all temperatures and frequencies from linear regressions for BM1_B in (a) Cole-Cole and (b) Black spaces. Each value was obtained by combining data from both decreasing and increasing strain amplitude sweeps. 100

Table 4-5. Summary of SASTENOLE test conditions on BM1_C (test scheme for BM1_B on Figure 4-3). 102

Table 4-6. Regression parameters p_E and p_φ obtained from nonlinearity envelopes of, respectively, norm and phase angle of complex modulus obtained from all SASTENOLE tests on BM1_C (BM1_B results on Table 4-2) at different temperatures and frequencies, for increasing strain amplitude loading paths. 104

Table 4-7. Maximum strain amplitude values satisfying the $|p_E \cdot \varepsilon_0| \leq 0.05$ condition (5% decrease in norm of complex modulus, similar to the considered LVE limit definition), according to p_E coefficients obtained from increasing sweeps of SASTENOLE tests on BM1_C (Table 4-6) (cf. BM1_B results on Table 4-3). 106

Table 4-8. Values of p_E/p_φ and α obtained for all temperatures and frequencies from linear regressions for BM1_C (results for BM1_B on Table 4-4) in (a) Cole-Cole and (b) Black spaces. Each value was obtained by combining data from both decreasing and increasing strain amplitude sweeps. 108

Table 4-9. Generalised Kelvin-Voigt model (at 14.44°C) with 40 viscoelastic elements and one free elastic constant used to simulate transient effects in the tested bituminous mixture, following numerical calculation from the literature (Gayte et al. 2016). This set of KVG parameters is a discretised form to describe LVE behaviour of BM1, equivalent to 2S2P1D model for BM1_A (cf. Table 4-1, where WLF parameters are also given). 114

Table 4-10. 2S2P1D model and WLF equation parameters used to model the LVE behaviour of the studied bitumen and mastic. 118

Table 5-1. 2S2P1D model and WLF equation parameters used to model the LVE behaviour of the studied bituminous mixtures 136

Table 5-2. *M* parameter values obtained from 2S2P1D model and WLF equation (constants given in Table 5-1) for BM2 141

Table 5-3. *M* parameter values obtained from 2S2P1D model and WLF equation (constants given in Table 5-1) for BM3 141

Table 5-4. Strain amplitude, norm of complex modulus, phase angle and initial modulus decrease (from the experiment and from simplified 3D thermomechanical calculation using e = 58.6μm/m and R = 2.32mm) for BM2 151

Table 5-5. Strain amplitude, norm of complex modulus, phase angle and initial modulus decrease (from the experiment and from simplified 3D thermomechanical calculation using e = 35.1μm/m and R = 2.32mm) for BM3 152

Table 5-6. Time interval correspondence between calculated and experimental slopes (both for the case of homogeneous heat in the bitumen and homogeneous heat in the bituminous mixture) observed for Phase I Fatigue tests on BM2. 155

Table 5-7. Time interval correspondence between calculated and experimental slopes (both for the case of homogeneous heat in the bitumen and homogeneous heat in the bituminous mixture) observed for Phase I Fatigue tests on BM3. 155

Table 5-8. Bituminous mastic Generalised Maxwell model constants (cf. Eq. 5-10), chosen to give, for R = 2.32mm, a bituminous mixture with initial norm of complex modulus of 14,500MPa and phase angle of 14.5° at 11.6°C and 10Hz, compatible with BM3 characterisation. 157

Table 5-9. Calculated temperatures at points A (hottest one) and B (coldest one) in the EHeV and calculated bituminous mixture relative modulus decrease after 10s of loading at 10Hz and 150μm/m (with different values of mastic half-thickness, 3, 10, and 100μm, particle radius R = 2.32mm, and mastic's Generalised Maxwell model constants given in Table 5-8. 162

Table 6-1. Specimens used in Loading and Rest Periods (LRP) tests and tested loading conditions (strain amplitude, number of cycles during loading loops and rest time applied during rest loops). All tests were performed using 5 LRP loops, started with mean in-specimen temperature of 11°C. 171

Table 6-2. Results from the fatigue tests performed immediately after the last rest loop of the LRP tests, in terms of the number of cycles at failure defined considering changes in trend on the rate of change in modulus and on the phase angle. 202

Table A-1. MTS® press's (FlexTest SE) Proportional-Derivative-Integral (PID) controller parameters (controlled channel is the mean shear strain for three extensometers) used for tests on

mastic M5070_30pc40-70 at the given approximate values of targeted shear strain amplitude (γ_0). 253

Table A-2. Instron® 8800 press's Proportional-Derivative-Integral (PID) controller parameters (controlled channel is the mean axial strain for three extensometers*) used for tests on BM1 at the given approximate values of targeted axial strain amplitude (ε_0). 253

LIST OF FIGURES

Figure 2-1. Bituminous materials seen in different length-scales: a) bituminous mixture cross-section, b) mastic schematic representation, c) bitumen scanning electron microscopy (SEM) image (Loeber et al. 1996), and d) schematic representation of bitumen and some of its components (Read et al. 2003). 9

Figure 2-2. Schematic representation of loading (strain, in figures a and b, or stress, in figures c and d) and response (stress or strain) (Di Benedetto and Corté 2005). 12

Figure 2-3. Schematic representation of different conceptual mechanical behaviour regions depending on the applied strain levels (ε) and the material temperature (T) for bitumen (Olard et al. 2005). T_g represents the glass transition temperature, where a brittle-to-ductile fracture behaviour is observed. 13

Figure 2-4. Schematic representation of different conceptual mechanical behaviour regions depending on the applied strain levels (ε) and the number of applied loading cycles (N) for bitumen (Mangiafico 2014). 13

Figure 2-5. Schematic representation of different conceptual mechanical behaviour regions depending on the applied strain levels (ε) and the number of applied loading cycles (N) for bituminous mixtures (Di Benedetto et al. 2013). 14

Figure 2-6. Linear viscoelasticity limits determined experimentally in bitumen and bituminous mixtures (Airey and Rahimzadeh 2004). 15

Figure 2-7. Schematic representation of different loading and response paths: different plots and time effect sensitivity. If curves I and II are always superimposed in the axes $l_{ij} - r_{ij}$ (which correspond to stress-strain curve) and in the axes r_{ij} -r_{kl}, the material is not sensitive to time effects (non viscous and non sensitive to ageing) in the considered loading domain (Di Benedetto et al. 2003). 17

Figure 2-8. Schematic representation of the evolution of an intrinsic material property with time, no evolution during Δt meaning that the material is non-aging for that time span, possibly being either time-independent or viscous (Di Benedetto et al. 2003). 18

Figure 2-9. Vertical modulus (E_v), at strain amplitude close to 10^{-5}m/m, as a function of strain rate (or equivalent strain rate for cyclic tests) for different geomaterials. The very important viscous sensitivity for bituminous mix is clearly visible (Di Benedetto et al. 2003). 19

Figure 2-10. Schematic representation of the time temperature superposition principle application, using the time-shift factor a_T (Di Benedetto et al. 2008). In the left-hand side, loading and response signals are plotted as functions of the equivalent time (after time-shift). In the bottom right corner, the graph indicates that same values in the y-axis from the bottom left graph (response) are also plotted in the x-axis of the upper right graph. 20

Figure 2-11. Example of time-temperature superposition principle verification for linear viscoelasticity of bituminous mixture (Nguyen et al. 2013b). 22

Figure 2-12. Example of time-temperature superposition principle verification for the nonlinear domain (nonlinear viscoelasticity) of bituminous mixture (Nguyen et al. 2015). 23

Figure 2-13. Example of time-temperature superposition principle verification for the nonlinear domain (plastic deformations) of bituminous mixture (Nguyen et al. 2009). 24

Figure 2-14. Example of time-temperature superposition principle verification for crack propagation in bituminous mixture (Nguyen et al. 2013a). 25

Figure 2-15. Example of time-temperature superposition principle verification for the fatigue behaviour of bituminous mixture (Phan et al. 2017a). 26

Figure 2-16. Mechanical analogues - a) spring, b) dashpot, c) parabolic element, d) GKV, e) GMW, f) 2S2P1D – and g) 2S2P1D model interpretation in Cole-Cole plot (Specht et al. 2017)..36

Figure 2-17. Example of coincidence of various normalised complex modulus curves from linear viscoelastic characterisation of different bituminous materials containing the same base bitumen (Pham et al. 2015a). Nine materials, differing with respect to the manufacturing process, fabrication temperature, the percentage of Recycled Asphalt Pavement (RAP), the use of additives and the air void content. 37

Figure 2-18. Schematic representation of the SHStS transformation (Mangiafico 2014).....38

Figure 2-19. Example of bituminous mixture prediction using the SHStS transformation and bitumen linear viscoelastic characterisation from two different experimental procedures (using the Dynamic Shear Rheometer and using the *Métravib*) (Mangiafico 2014). 39

Figure 2-20. Example of bituminous mixture fatigue test experimental data (Tapsoba 2011): norm of complex modulus and phase angle (above), and measured surface temperature (below)..43

Figure 2-21. Relationship between loading amplitude and number of cycles at fatigue (fatigue life) (Di Benedetto and Corté 2005). The figure presents schematically two different approaches: fitting Wöhler curve to describe this dependence, or searching for a “endurance limit” (Carpenter et al. 2003), which is the loading amplitude below which an infinite fatigue life would be expected. 46

Figure 2-22. Schematic representation of breakdown and build-up of thixotropic structure (Barnes 1997). Among possible explanation for shear-thinning and thixotropic behaviour are: alignment of elongated particles in the flow direction, loss of junctions in polymer solutions, rearrangement of microstructure in suspension and emulsion, and breakdown of flocs. 47

Figure 2-23. Equilibrium values of shear stress during “step” constant shear experiments, where the applied shear rate is changed in different loading blocks (Barnes 1997). 48

Figure 2-24. Verification of time temperature superposition for thixotropy (Nguyen 2011): norm of complex modulus variation (above), and phase angle variation (below). 49

Figure 2-25. Schematic representation of the contributions of the different physical phenomena (nonlinearity, heating, thixotropy and damage) on the measured norm of complex modulus during a cyclic loading test (at strain amplitude ε_{01}) including rest (Nguyen 2011). 51

Figure 2-26. Directions of different phenomena on Black space (Nguyen 2011): example of experimental results (above), and schematic representation of the directions of the variation in complex (below). 52

Figure 2-27. Example of experimental results from tests on bituminous mixture consisting in the application of 100,000 cycles at 100μm/m followed by 24h of rest (Mangiafico 2014). Variations in norm of complex modulus (figure a) and phase angle (figure b) corresponding to different physical phenomena are represented: nonlinearity, heating, thixotropy and damage (called “unrecovered” in the figure, since an asymptotic value had not yet been obtained). 53

Figure 3-1. (a) ASR tests on bitumen and mastic hollow cylinder specimens mounted on a MTS® hydraulic press testing frame, and (b) T-C tests on bituminous mixture cylindrical specimens mounted on an Instron® hydraulic press testing frame. 57

Figure 3-2. Focus on the ASR test apparatus in the MTS® press (from Figure 3-1a), and details on the test specimen with mounted sensors 58

Figure 3-3. Focus on the T-C test apparatus in the Instron® press (from Figure 3-1b), and details on the test specimen with mounted sensors. 60

Figure 3-4. ASR specimen deformation during tests and interpretation of the applied shear strain. 61

Figure 3-5. Example of sinusoidal signals fitting in order to obtain amplitude and phase for experimental signals (sequence of two cycles for the stress, the radial strain, and the three axial strain measurements during a T-C test – example from nonlinearity investigation, Chapter 4)..... 65

Figure 3-6. Error on shear modulus introduced by the eccentricity between the external and the internal mould during ASR tests. a) Definition of studied eccentricity. b) Illustration of the specimen having a certain eccentricity, and its Finite Elements mesh (example with 3mm eccentricity). c) Mean error in shear modulus obtained with an eccentric specimen for different values of eccentricity. d) Zoom for eccentricities between 0 and 3mm. 67

Figure 3-7. Error on shear modulus introduced by a material loss due to flow under gravity. a) Definition of studied material loss (Mat_loss in %). b) Illustration of the specimen having a circular meniscus (diameter equals specimen thickness) due to material loss and its Finite Elements mesh (example with 0.01m Mat_loss). c) Mean error in shear modulus obtained with a specimen after a certain material loss. d) Zoom for material loss between 0 and 25%. 68

Figure 3-8. Bitumen ASR specimen preparation process. a) Clean mould before specimen preparation. b) Mould prepared for pouring with its protective adhesive tape. c) Mould with a

poured specimen (material is poured in excess in order to compensate for thermal expansion/contraction). d) Finished specimen. 70

Figure 3-9. Apparatus for mastic preparation..... 71

Figure 4-1. Scheme of the bituminous mixture complex modulus test (T-C setup, cf. Figure 3-3) loading path. 81

Figure 4-2. 2S2P1D model and WLF equation fitting of experimental data (BM1_A and BM1_C specimens) obtained from Tension/Compression (T-C) complex modulus tests at 50μm/m: a) Cole-Cole plot; b) Black diagram; c) normalized complex modulus master curve (at 15C); e) norm and f) phase angle of complex modulus; g) norm and h) phase angle of complex Poisson's ratio master curve (at 15°C) with details on tested temperatures. 82

Figure 4-3. Detailed scheme of the 16 Strain Amplitude Sweep Tests for NonLinearity Evaluation (SASTENOLE) applied on BM1_B, with an example of results obtained for the norms of complex modulus and Poisson's ratio during the eight sequences of the SASTENOLE test #13, at 14°C, 0.3Hz. A total of 128 sequences were performed and analysed on BM1_B. 85

Figure 4-4. Results obtained from SASTENOLE tests at 8°C, 10Hz (a, b, c) and 14°C, 0.3Hz (d, e, f), for maximum targeted strain amplitude of 110μm/m: norm of complex modulus $|E^*|$ (top), phase angle φ (middle) and dissipated energy per cycle W_N (bottom) are plotted as functions of strain amplitude. 87

Figure 4-5. Norm of the complex modulus $|E^*|$ (a, top) and phase angle φ (b, bottom) obtained from the SASTENOLE test at 14°C, 0.3Hz, for the four increasing strain amplitude loading paths: s_E and p_φ are the slopes of the nonlinearity envelopes of, respectively, $|E^*|$ and φ. 90

Figure 4-6. Norm of the complex modulus $|E^*|$ (a, top) and phase angle φ (b, bottom) obtained from the SASTENOLE test at 14°C, 0.3Hz, for decreasing strain amplitude loading paths: R^2 values are calculated for the regressions of the initial points with lines of, respectively, s_E and p_φ slopes (as calculated in Figure 4-5 for increasing strain amplitude loading paths). 91

Figure 4-7. Linear regression of p_E values as a function of corresponding p_φ values obtained from all SASTENOLE tests on BM1_B at different temperatures and frequencies, for increasing strain amplitude loading paths (Figure 4-5). 93

Figure 4-8. Schemes of nonlinearity directions in Black (top) and Cole-Cole (bottom) spaces (cf. Eq. 4-6 and Eq. 4-8). 95

Figure 4-9. Results obtained from all SASTENOLE tests on BM1_B (scheme on Figure 4-3) at different temperatures and frequencies, for both decreasing and increasing strain amplitude loading paths, in Cole-Cole space: zooms are provided for data obtained at 14°C, 0.3Hz (bottom, left) and 8°C, 10Hz (bottom, right). For each combination of temperature and frequency, the regression was performed by combining data from both decreasing and increasing strain amplitude sweeps. 97

Figure 4-10. Results obtained from all SASTENOLE tests on BM1_B (scheme on Figure 4-3) at different temperatures and frequencies, for both decreasing and increasing strain amplitude

loading paths, in Black space: zooms are provided for data obtained at 8°C, 10Hz (bottom, left) and 14°C, 0.3Hz (bottom, right). For each combination of temperature and frequency, the regression was performed by combining data from both decreasing and increasing strain amplitude sweeps. 98

Figure 4-11. Results obtained from all SASTENOLE tests on BM1_B at different temperatures and frequencies, for both decreasing and increasing strain amplitude loading paths, in normalized Black space.....101

Figure 4-12. Comparison between the test conditions range for the first experimental campaign on bituminous mixture nonlinearity (BM1_B, cf. Figure 4-3) and for the second experimental campaign (on BM1_C). Including all testing sequences (increasing and decreasing sweeps at three different maximum targeted strain amplitudes) a total of 162 sequences were performed and analysed on BM1_C. 102

Figure 4-13. Results obtained from all SASTENOLE tests on BM1_C at different temperatures and frequencies, for both decreasing and increasing strain amplitude loading paths, in (a) Cole-Cole plot (comparable to Figure 4-9 for BM1_B), (b) Black space (comparable to Figure 4-10 for BM1_B), and (c) normalized black space (comparable to Figure 4-11 for BM1_B). 103

Figure 4-14. p_E and p_φ results obtained from all SASTENOLE tests on BM1_C (BM1_B results on Figure 4-7 also represented here) at different temperatures and frequencies, for increasing strain amplitude loading paths: a) p_E as a function of corresponding p_φ; b) p_E (intensity of nonlinearity effect) as a function of corresponding p_E/p_φ (which gives nonlinearity direction); c) isotherms for p_E; and d) p_E master curve, d) p_E/p_φ master curve, and f) p_φ master curve, all constructed using WLF parameters from LVE characterisation (Table 4-1). The master curves are presented at 15°C. 105

Figure 4-15. LVE limit (in terms of axial strain amplitude, $\varepsilon_{0.95\%}$, figs. a and b, and axial stress amplitude, $\sigma_{0.95\%}$, figs. c and d) obtained from SASTENOLE results (cf. $|p_E \cdot \varepsilon_0| \leq 0.05$ results in Table 4-7) on bitumen BM1_C as a function of norm of complex modulus (figs. a and c) and time-shifted frequency (figs b and d).....107

Figure 4-16. Norm and phase angle of complex modulus ($|E^*|$, φ, figures a and b) and of Poisson's ratio ($|\nu^*|$, φ_ν, figures c and d) obtained during increasing and decreasing strain sweeps of SASTENOLE test for maximum targeted strain amplitude of 110µm/m at -4°C, 1Hz. 110

Figure 4-17. Norm and phase angle of complex modulus ($|E^*|$, φ, figures a and b) and of Poisson's ratio ($|\nu^*|$, φ_ν, figures c and d) obtained during increasing and decreasing strain sweeps of SASTENOLE test for maximum targeted strain amplitude of 110µm/m at 28°C, 0.1Hz. 111

Figure 4-18. Norm $|\nu^*|$ (top) and phase angle φ_ν of Poisson's ratio (bottom) obtained from SASTENOLE test at -4°C, 1Hz, for the three increasing strain amplitude (figures a and b) and for the three decreasing strain amplitude loading paths (figures c and d): s_ν and $p_{\varphi\nu}$ are the slopes of the nonlinearity envelopes of, respectively, $|\nu^*|$ and φ_ν. 112

Figure 4-19. Norm $|v^*|$ (top) and phase angle φ_v of Poisson's ratio (bottom) obtained from SASTENOLE test at 28°C, 0.1Hz, for the three increasing strain amplitude (figures a and b) and for the three decreasing strain amplitude loading paths (figures c and d): s_v and $p_{\varphi v}$ are the slopes of the nonlinearity envelopes of, respectively, $|v^*|$ and φ_v. 112

Figure 4-20. Example of results for the simulation of perfectly linear viscoelastic response of BM1_A (using KVG model parameters given in Table 4-9, and specimen diameter 75.3mm), including transient effects, to the SASTENOLE loading path (increasing and decreasing sweeps), obtained at 14°C and 0.3Hz with maximum strain amplitude of 100µm/m: a) Modulus from increasing and decreasing sweeps as a function of loading cycles; a) Modulus from increasing and decreasing sweeps as a function of the applied strain amplitude; and examples of hysteresis loop (including the actual response and the fitted sine functions used to obtain modulus) at c) the 2nd cycle and d) the 10th cycle. 115

Figure 4-21. Scheme of the bitumen and mastic complex modulus test (ASR setup, cf. Figure 3-2, and Figure 3-4 for a deformation scheme) loading path. 116

Figure 4-22. 2S2P1D fitting of experimental data (BM1_A and BM1_C specimens) obtained from ASR complex shear modulus tests at low strain amplitude (force signal amplitude around 0.3kN): a) Cole-Cole plot; (b) Black diagram; c) normalized complex modulus master curve (at 15°C); d) norm of complex modulus, and e) phase angle master curves (at 15°C) with details on tested temperatures; and f) comparison of norm of axial complex modulus master curves (at 15°C) for the three studied materials. 117

Figure 4-23. Detailed scheme of the Strain Amplitude Sweep (SAS) tests conducted using the ASR, with an example of results for B5070 at 11.1°C, presenting the obtained norm of complex shear modulus and the in-specimen temperature during the loading sequences at 3Hz. 119

Figure 4-24. Maximum temperature increase during SAS tests on bitumen and mastic (at the last cycle of loading at a given frequency and strain amplitude, cf. Figure 4-23). The figure presents the temperature increase for tests on bitumen at 11.1°C and all frequencies (figure a), on mastic at 11.1°C and all frequencies (figure b), on bitumen and mastic at 10Hz and all temperatures (figure c) and a zoom on these last results (figure d). 120

Figure 4-25. Example of a set of experimental results (norm and phase angle of complex shear modulus) for SAS tests using the ASR (tests at 6.3°C on mastic M5070_30pc40-70), with details on the method for determination of the asymptotic "linear" values (at 0µm/m) and of the LVE limit in terms of strain amplitude. 122

Figure 4-26. SAS experimental results in normalized Black curves (normalized equivalent complex modulus as a function of the normalized phase angle) for all tested temperatures and frequencies on bitumen B5070 and mastic M5070_30pc40-70. 123

Figure 4-27. SAS experimental results at 0.1Hz for all tested temperatures in normalized Black curves (normalized equivalent complex modulus as a function of the normalized phase angle) for bitumen B5070 and mastic M5070_30pc40-70. 124

Figure 4-28. p_E/p_φ results obtained from all SAS tests on B5070 and on M5070_30pc40-70 at different temperatures and frequencies: a) p_E/p_φ as a function of frequency; b) p_E/p_φ master curves, constructed using WLF parameters from LVE characterisation (Table 4-10); c) p_E/p_φ master curves including BM1_C results (cf. Figure 4-14). The master curves are presented at 15°C. 125

Figure 4-29. LVE limit (in terms of shear strain amplitude, $\gamma_{0.95\%}$, figs. a, b, e, and f, and shear stress amplitude, $\tau_{0.95\%}$, figs. c, d, and g) obtained from SAS test results (cf. example in Figure 4-25) on bitumen B5070 and mastic M5070_30pc40-70 as a function of norm of complex shear modulus (a through e) and time-shifted frequency at 15°C (f and g). 126

Figure 4-30. Comparison of the determined LVE limits (in terms of axial or shear strain amplitude, $\varepsilon_{0.95\%}$ or $\gamma_{0.95\%}$, figure a, and axial or shear stress amplitude, $\sigma_{0.95\%}$ or $\tau_{0.95\%}$, figure b) obtained from SASTENOLE and SAS test results (cf. Figure 4-15 and Figure 4-29) on bitumen B5070, mastic M5070_30pc40-70 and BM1_C as a function of norm of complex shear modulus. 127

Figure 4-31. Comparison of the determined LVE limits (in terms of axial or shear strain amplitude, $\varepsilon_{0.95\%}$ or $\gamma_{0.95\%}$, figure a, and axial or shear stress amplitude, $\sigma_{0.95\%}$ or $\tau_{0.95\%}$, figure b) obtained from SASTENOLE and SAS test results (cf. Figure 4-15 and Figure 4-29) on bitumen B5070, mastic M5070_30pc40-70 and BM1_C as a function of the time-shifted frequency (with the same WLF parameters as for linear characterisation, cf. Table 4-1 and Table 4-10). The results are presented as master curves at 15°C. 129

Figure 5-1. Scheme for the proposed thermomechanical calculations. 135

Figure 5-2. Loading scheme (Nguyen 2011) of a Phase I Fatigue test (example of tests on BM2_A). 137

Figure 5-3. a) Considered idealized heterogeneous bituminous mixture (monodisperse spherical particles in a mastic phase) and b) Zoom on the elementary cell called “Elementary Heterogeneous Volume” (EHeV) used for 3D heterogeneous calculation. 138

Figure 5-4. Aggregate gradation of the two studied materials: in mass (left axis, classical representation without bitumen) and in volume (right axis, considering air voids and bitumen)..138

Figure 5-5. Scheme of the steps necessary to the simplified thermomechanical calculations. 139

Figure 5-6. Schematic definition of the normalized parameter (M) giving the influence of temperature on $|E^*|$ for a given loading frequency. 141

Figure 5-7. Explanation of strain calculation from displacement δ (applied load F in tension-compression): a) Case of the Elementary Homogeneous Volume (EHoV) and b) Case of the Elementary Heterogeneous Volume (EHeV) 143

Figure 5-8. 3D heterogeneous calculation results with e/R = 0.015 (fixed parameters corresponding to the studied bituminous mixture, tested at 12.3°C and 3Hz for a strain amplitude of 116μm/m, cf. also test results in Figure 5-10 and Figure 5-11): (above) strain amplitude and

cumulated force on a disc of radius *r* and (below) temperature increase per cycle for local adiabatic conditions (i.e. no heat transfer) as a function of relative position (*r*/*R*) 146

Figure 5-9. Modulus (left axis) and relative modulus (right axis) decrease per cycle as a function of *e*/*R* (fixed parameters correspond to BM3 and tested at 12.3°C and 3Hz for a strain amplitude of around 116µm/m, see also test results Figure 5-10) 147

Figure 5-10. Initial decrease of norm of complex modulus for BM3_A, tested at 12.3°C and 3Hz for a strain amplitude of 116µm/m (cf. also test results in Figure 5-11): data and prediction considering the 3 considered calculations: i) homogeneous heat in the mix, ii) Homogeneous heat in bituminous phase and iii) 3D heterogeneous thermomechanical calculation. Up to 10,000 cycles (b) and, zoom up to 100 cycles (a). 149

Figure 5-11. For BM2, modelled (3D heterogeneous thermomechanical calculation, cf. Section 5.5.3 and Figure 5-10a) normalized initial modulus decrease ($-d|E_{bm}^{*}|/dN)/|E_{bm}^{*}|$) as a function of the results obtained from experiments (for cycles between 5 and 7s of loading) at different temperatures and frequencies with different strain amplitudes (10 tests): a) labelled by frequencies, and b) labelled by temperatures. 153

Figure 5-12. For BM3, modelled (3D heterogeneous thermomechanical calculation, cf. Section 5.5.3 and Figure 5-10a) normalized initial modulus decrease ($-d|E_{bm}^{*}|/dN)/|E_{bm}^{*}|$) as a function of the results obtained from experiments (for cycles between 5 and 7s of loading) at different temperatures and frequencies with different strain amplitudes (13 tests): a) labelled by frequencies, and b) labelled by temperatures. 153

Figure 5-13. Investigation of relationships of the time for correspondence between calculated and experimental slopes of norm of complex modulus observed for Phase I Fatigue tests. Example on BM3. a) Time correspondence (beginning and end of correspondence) for the calculation considering homogeneous heat in bitumen as a function of the time-shifted frequency. b) Number of cycles for the beginning of correspondence for the calculation considering homogeneous heat in bitumen and homogeneous heat in mixture as a function of the number of cycles for the beginning of correspondence for the calculation considering heterogeneous heat in mastic. c) A normalised parameter (involving correspondence time, strain amplitude, and complex modulus) as a function of the time-shifted frequency. 156

Figure 5-14. Flowchart describing performed FEM calculations: thermal analysis and mechanical analysis. 158

Figure 5-15. a) Idealized heterogeneous bituminous mixture; b) Zoom on the meshed elementary cell called “Elementary Heterogeneous Volume” (EHeV) used for 3D FEM analysis; c) considerations for FEM thermal analysis; d) considerations for FEM mechanical analysis. 160

Figure 5-16. Temperature distribution and bituminous mixture relative modulus change at a) 0.1s; b) 1s; and c) 10s for *e* = 3µm and sinusoidal loading at 10Hz and 150µm/m strain amplitude applied on the bituminous mixture (the model represents BM3). 161

Figure 5-17. Results for the first 100 cycles of sinusoidal loading for e = 3µm. a) Modulus and temperature changes calculated with a "linearized" heat production during each cycle; and b) and c) zoom for cycles #99 and #100 including the temperature change considering "real" heat production at points A (maximum temperature change) and B (minimum temperature change)..162

Figure 6-1. Scheme of the Alternating Strain Amplitude test loading path, including details on the applied strain amplitudes during loading (no rest periods are applied). 169

Figure 6-2. Scheme of Load and Rest Periods tests loading path, including representation of the applied strain amplitudes during loading and of the applied small strain amplitudes during rest. 170

Figure 6-3. 2S2P1D model (cf. Chapter 4, Figure 4-22 and Table 4-10) for bitumen (B5070) and mastic (M5070_30pc40-70), with indications of complex modulus obtained at 10Hz at various temperatures from 10 to 21°C: Representation on a) Cole-Cole plot and b) Black diagram (with arithmetic scale for the norm of complex modulus). 172

Figure 6-4. Alternating Strain Amplitudes (ASA) test results for bitumen (B5070_G): a) Norm of complex modulus, b) phase angle, c) mean in-specimen temperature, and d) shear strain amplitude as a function of time, for a test performed at constant frequency of 10Hz (1s = 10cycles).....176

Figure 6-5. Alternating Strain Amplitudes (ASA) test results for bitumen (B5070_G) represented in Black space (natural non-log axis for norm of complex modulus as a function of the phase angle. 177

Figure 6-6. Experimental results (B5070_D) for LRP tests: 5 LRP loops with 10,000 cycles and 4h rest on bitumen submitted to 20,000µm/m sinusoidal loading: a) Norm of complex modulus and phase angle as a function of time, and b) shear strain amplitude and temperature as a function of time. 181

Figure 6-7. Experimental results (B5070_D) for LRP tests: 5 LRP 20,000µm/m sinusoidal loading loops with 10,000 cycles each on bitumen: a) Norm of complex shear modulus, b) phase angle, c) mean in-specimen temperature, and d) dissipated energy per cycle as a function of the number of applied cycles.....182

Figure 6-8. Experimental results (B5070_D) for LRP tests: 5 LRP 20,000µm/m sinusoidal loading loops with 10,000 cycles each on bitumen: representation on a) Black space, and b) Cole-Cole diagram. 183

Figure 6-9. Experimental results (B5070_D) for LRP tests: 5 LRP 20,000µm/m sinusoidal loading loops with 10,000 cycles each on bitumen: a) Normalised (the initial modulus being considered as the result at the 3rd cycle) norm of complex shear modulus, and b) normalised phase angle as a function of number of applied cycles; and c) representation of the results on a normalised Black space. 184

Figure 6-10. Experimental results for LRP tests: analysis of the unrecovered relative change in complex modulus after 4h rest: a) bitumen (B5070_C) with 3,600µm/m sinusoidal loading, b)

bitumen (B5070_A) with 10,000μm/m, c) bitumen (B5070_B and B5070_D) with 20,000μm/m, d) mastic (M5070_30pc40-70_C) with 1,000μm/m, e) mastic (M5070_30pc40-70_A) with 3,300μm/m, and f) mastic (M5070_30pc40-70_B) with 8,800μm/m. 186

Figure 6-11. Slopes of the unrecovered change in norm of complex modulus obtained from LRP tests on bitumen and mastic as a function of the applied shear strain amplitude. 187

Figure 6-12. Scheme of the utilised correction for the temperature effect (T-effect) on the complex modulus, with an example for bitumen (the hypothesis for correction is the same for mastic). The correction uses as input parameters the 2S2P1D complex moduli (G^*_{2S2P1D}, fitted for low strain amplitudes) at the initial (Tini) and the current (T) measured temperatures, and the measured complex modulus (G^*) during the LRP test (performed at higher strain amplitudes). a) Complex modulus at different temperatures on a Black diagram (cf. Figure 4-22 and Table 4-10 and Figure 6-3). b) Temperature effect on the calculated 2S2P1D complex modulus (low strain amplitude, $\gamma_{0,1}$) and indication of nonlinearity effect on . c) Scheme of the temperature effect on the measured complex modulus (at higher strain amplitude, $\gamma_{0,2}$), after the effect of nonlinearity is obtained (cf. Chapter 4). 189

Figure 6-13. Temperature evolution as a function of the number of applied cycles during the first loading loop of LRP test on bitumen specimen B5070_D. Three temperature evolution curves are presented: measured mean in-specimen temperature, necessary temperature to explain phase angle variation during loading, and necessary temperature to explain modulus variation during loading. 190

Figure 6-14. Experimental results (B5070_D) for LRP tests (5 LRP tests with 10,000 cycles of 20,000μm/m sinusoidal loading and 4h rest loops on bitumen): a) Black diagram representation of the results including details of the number of cycles during loading and the time of rest during rest periods, and a representation of the nonlinearity effect; b) results after temperature correction. The figure present also a 2S2P1D model prediction, with indication of LVE complex modulus at 10Hz and three temperatures, 11.1°C (Tini), 15°C and 19°C. 193

Figure 6-15. Experimental results (B5070_D) for LRP tests (5 LRP tests with 10,000 cycles of 20,000μm/m sinusoidal loading and 4h rest loops on bitumen): Black diagram representation of a) the raw experimental results and the results after the temperature correction and b) the experimental results after temperature and damage correction. The figure present also a 2S2P1D model prediction, with indication of LVE complex modulus at 10Hz and three temperatures, 11.1°C (Tini), 15°C and 19°C. 195

Figure 6-16. Experimental results (B5070_E) for LRP tests: 5 LRP loops with 20,000 cycles and 14h rest on bitumen submitted to 20,000μm/m sinusoidal loading. a) Norm of complex modulus and phase angle as a function of time, and b) shear strain amplitude and temperature as a function of time. 198

Figure 6-17. Comparison (in Black space) of LRP test results with different test parameters: LRP test with 10,000 cycles of sinusoidal loading at 20,000μm/m and 4h rest loops and 20,000

cycles of sinusoidal loading at 20,000μm/m and 14h rest loops on bitumen (B5070_E) at 11.0°C and 10Hz. 199

Figure 6-18. Experimental results (B5070_D) for the fatigue test performed immediately after the last rest loop of the LRP test (cf. Figure 6-6) with to 20,000μm/m sinusoidal loading and determination of the number of cycles at failure (*Nf*). a) Norm of complex modulus and phase angle as a function of the number of applied cycles, and b) shear strain amplitude and temperature as a function of the number of applied cycles. 201

Figure 6-19. Experimental results from the fatigue tests performed immediately after the last rest loop of the LRP tests: number of cycles at failure (*Nf*), defined considering changes in trend on the rate of change in modulus and on the phase angle, as a function of the shear strain amplitude (Whöler curves). a) Results considering only cycles from the fatigue test, and b) results considering both the cycles from the LRP and the cycles from the fatigue test (the effect of all cycles on the fatigue damage is considered to cumulate). 202

Figure B-1. Set of experimental results (norm and phase angle of complex shear modulus) for SAS tests using the ASR (tests at 6.3°C on bitumen B5070), with details on the method for determination of the asymptotic “linear” values (at 0μm/m) and of the LVE limit in terms of strain amplitude. 255

Figure B-2. Set of experimental results (norm and phase angle of complex shear modulus) for SAS tests using the ASR (tests at 11.1°C on bitumen B5070), with details on the method for determination of the asymptotic “linear” values (at 0μm/m) and of the LVE limit in terms of strain amplitude. 256

Figure B-3. Set of experimental results (norm and phase angle of complex shear modulus) for SAS tests using the ASR (tests at -3.2°C on mastic M5070_30pc40-70), with details on the method for determination of the asymptotic “linear” values (at 0μm/m) and of the LVE limit in terms of strain amplitude. 257

Figure B-4. Set of experimental results (norm and phase angle of complex shear modulus) for SAS tests using the ASR (tests at 6.3°C on mastic M5070_30pc40-70), with details on the method for determination of the asymptotic “linear” values (at 0μm/m) and of the LVE limit in terms of strain amplitude. 258

Figure B-5. Set of experimental results (norm and phase angle of complex shear modulus) for SAS tests using the ASR (tests at 11.1°C on mastic M5070_30pc40-70), with details on the method for determination of the asymptotic “linear” values (at 0μm/m) and of the LVE limit in terms of strain amplitude. 259

Figure B-6. Set of experimental results (norm and phase angle of complex shear modulus) for SAS tests using the ASR (tests at 15.0°C on mastic M5070_30pc40-70), with details on the method for determination of the asymptotic “linear” values (at 0μm/m) and of the LVE limit in terms of strain amplitude. 260

Figure C-1. Experimental results (B5070_C) for LRP tests: 5 LRP loops with 10,000 cycles and 4h rest on bitumen submitted to 3,600μm/m sinusoidal loading: a) Norm of complex modulus and phase angle as a function of time, and b) shear strain amplitude and temperature as a function of time. 262

Figure C-2. Experimental results (B5070_C) for LRP tests: 5 LRP 3,600μm/m sinusoidal loading loops with 10,000 cycles each on bitumen: a) Norm of complex shear modulus, b) phase angle, c) mean in-specimen temperature, and d) dissipated energy per cycle as a function of the number of applied cycles.....263

Figure C-3. Experimental results (B5070_C) for LRP tests: 5 LRP 3,600μm/m sinusoidal loading loops with 10,000 cycles each on bitumen: representation on a) Black space, and b) Cole-Cole diagram. 264

Figure C-4. Experimental results (B5070_C) for LRP tests: 5 LRP 3,600μm/m sinusoidal loading loops with 10,000 cycles each on bitumen: a) Normalised (the initial modulus being considered as the result at the 3rd cycle) norm of complex shear modulus, and b) normalised phase angle as a function of number of applied cycles; and c) representation of the results on a normalised Black space. 265

Figure C-5. Experimental results (B5070_C) for LRP tests (5 LRP tests with 10,000 cycles of 3,600μm/m sinusoidal loading and 4h rest loops on bitumen): a) Black diagram representation of the results including details of the number of cycles during loading and the time of rest during rest periods, and a representation of the nonlinearity effect; b) results after temperature correction. The figure present also a 2S2P1D model prediction, with indication of LVE complex modulus at 10Hz and three temperatures, 11.1°C (Tini), 11.4°C and 11.7°C. 266

Figure C-6. Experimental results (B5070_C) for LRP tests (5 LRP tests with 10,000 cycles of 3,600μm/m sinusoidal loading and 4h rest loops on bitumen): Black diagram representation of a) the raw experimental results and the results after the temperature correction and b) the experimental results after temperature and damage correction. The figure present also a 2S2P1D model prediction, with indication of LVE complex modulus at 10Hz and three temperatures, 11.1°C (Tini), 11.4°C and 11.7°C. 267

Figure C-7. Experimental results (B5070_A) for LRP tests: 5 LRP loops with 10,000 cycles and 4h rest on bitumen submitted to 10,000μm/m sinusoidal loading: a) Norm of complex modulus and phase angle as a function of time, and b) shear strain amplitude and temperature as a function of time. 268

Figure C-8. Experimental results (B5070_A) for LRP tests: 5 LRP 10,000μm/m sinusoidal loading loops with 10,000 cycles each on bitumen: a) Norm of complex shear modulus, b) phase angle, c) mean in-specimen temperature, and d) dissipated energy per cycle as a function of the number of applied cycles.....269

Figure C-9. Experimental results (B5070_A) for LRP tests: 5 LRP 10,000μm/m sinusoidal loading loops with 10,000 cycles each on bitumen: representation on a) Black space, and b) Cole-Cole diagram. 270

Figure C-10. Experimental results (B5070_A) for LRP tests: 5 LRP 10,000μm/m sinusoidal loading loops with 10,000 cycles each on bitumen: a) Normalised (the initial modulus being considered as the result at the 3rd cycle) norm of complex shear modulus, and b) normalised phase angle as a function of number of applied cycles; and c) representation of the results on a normalised Black space. 271

Figure C-11. Experimental results (B5070_A) for LRP tests (5 LRP tests with 10,000 cycles of 10,000μm/m sinusoidal loading and 4h rest loops on bitumen): a) Black diagram representation of the results including details of the number of cycles during loading and the time of rest during rest periods, and a representation of the nonlinearity effect; b) results after temperature correction. The figure present also a 2S2P1D model prediction, with indication of LVE complex modulus at 10Hz and three temperatures, 11.0°C (Tini), 12.5°C and 14°C. 272

Figure C-12. Experimental results (B5070_A) for LRP tests (5 LRP tests with 10,000 cycles of 10,000μm/m sinusoidal loading and 4h rest loops on bitumen): Black diagram representation of a) the raw experimental results and the results after the temperature correction and b) the experimental results after temperature and damage correction. The figure present also a 2S2P1D model prediction, with indication of LVE complex modulus at 10Hz and three temperatures, 11.0°C (Tini), 12.5°C and 14°C. 273

Figure C-13. Experimental results (B5070_B) for LRP tests: 5 LRP loops with 10,000 cycles and 4h rest on bitumen submitted to 20,000μm/m sinusoidal loading: a) Norm of complex modulus and phase angle as a function of time, and b) shear strain amplitude and temperature as a function of time. 274

Figure C-14. Experimental results (B5070_B) for LRP tests: 5 LRP 20,000μm/m sinusoidal loading loops with 10,000 cycles each on bitumen: a) Norm of complex shear modulus, b) phase angle, c) mean in-specimen temperature, and d) dissipated energy per cycle as a function of the number of applied cycles 275

Figure C-15. Experimental results (B5070_B) for LRP tests: 5 LRP 20,000μm/m sinusoidal loading loops with 10,000 cycles each on bitumen: representation on a) Black space, and b) Cole-Cole diagram. 276

Figure C-16. Experimental results (B5070_B) for LRP tests: 5 LRP 20,000μm/m sinusoidal loading loops with 10,000 cycles each on bitumen: a) Normalised (the initial modulus being considered as the result at the 3rd cycle) norm of complex shear modulus, and b) normalised phase angle as a function of number of applied cycles; and c) representation of the results on a normalised Black space. 277

Figure C-17. Experimental results (B5070_B) for LRP tests (5 LRP tests with 10,000 cycles of 20,000μm/m sinusoidal loading and 4h rest loops on bitumen): a) Black diagram representation of the results including details of the number of cycles during loading and the time of rest during rest periods, and a representation of the nonlinearity effect; b) results after temperature correction. The figure present also a 2S2P1D model prediction, with indication of LVE complex modulus at 10Hz and three temperatures, 10.9°C (Tini), 15°C and 19°C. 278

Figure C-18. Experimental results (B5070_B) for LRP tests (5 LRP tests with 10,000 cycles of 20,000μm/m sinusoidal loading and 4h rest loops on bitumen): Black diagram representation of a) the raw experimental results and the results after the temperature correction and b) the experimental results after temperature and damage correction. The figure present also a 2S2P1D model prediction, with indication of LVE complex modulus at 10Hz and three temperatures, 10.9°C (Tini), 15°C and 19°C. 279

Figure C-19. Experimental results (B5070_D) for LRP tests: 5 LRP loops with 10,000 cycles and 4h rest on bitumen submitted to 20,000μm/m sinusoidal loading: a) Norm of complex modulus and phase angle as a function of time, and b) shear strain amplitude and temperature as a function of time. 280

Figure C-20. Experimental results (B5070_D) for LRP tests: 5 LRP 20,000μm/m sinusoidal loading loops with 10,000 cycles each on bitumen: a) Norm of complex shear modulus, b) phase angle, c) mean in-specimen temperature, and d) dissipated energy per cycle as a function of the number of applied cycles..... 281

Figure C-21. Experimental results (B5070_D) for LRP tests: 5 LRP 20,000μm/m sinusoidal loading loops with 10,000 cycles each on bitumen: representation on a) Black space, and b) Cole-Cole diagram. 282

Figure C-22. Experimental results (B5070_D) for LRP tests: 5 LRP 20,000μm/m sinusoidal loading loops with 10,000 cycles each on bitumen: a) Normalised (the initial modulus being considered as the result at the 3rd cycle) norm of complex shear modulus, and b) normalised phase angle as a function of number of applied cycles; and c) representation of the results on a normalised Black space. 283

Figure C-23. Experimental results (B5070_D) for LRP tests (5 LRP tests with 10,000 cycles of 20,000μm/m sinusoidal loading and 4h rest loops on bitumen): a) Black diagram representation of the results including details of the number of cycles during loading and the time of rest during rest periods, and a representation of the nonlinearity effect; b) results after temperature correction. The figure present also a 2S2P1D model prediction, with indication of LVE complex modulus at 10Hz and three temperatures, 11.0°C (Tini), 15°C and 19°C. 284

Figure C-24. Experimental results (B5070_D) for LRP tests (5 LRP tests with 10,000 cycles of 20,000μm/m sinusoidal loading and 4h rest loops on bitumen): Black diagram representation of a) the raw experimental results and the results after the temperature correction and b) the experimental results after temperature and damage correction. The figure present also a 2S2P1D model prediction, with indication of LVE complex modulus at 10Hz and three temperatures, 11.0°C (Tini), 15°C and 19°C. 285

Figure C-25. Experimental results (M5070_30pc40-70_C) for LRP tests: 5 LRP loops with 10,000 cycles and 4h rest on bitumen submitted to 1,100μm/m sinusoidal loading: a) Norm of complex modulus and phase angle as a function of time, and b) shear strain amplitude and temperature as a function of time. 286

Figure C-26. Experimental results (M5070_30pc40-70_C) for LRP tests: 5 LRP 1,100µm/m sinusoidal loading loops with 10,000 cycles each on bitumen: a) Norm of complex shear modulus, b) phase angle, c) mean in-specimen temperature, and d) dissipated energy per cycle as a function of the number of applied cycles. 287

Figure C-27. Experimental results (M5070_30pc40-70_C) for LRP tests: 5 LRP 1,100µm/m sinusoidal loading loops with 10,000 cycles each on bitumen: representation on a) Black space, and b) Cole-Cole diagram. 288

Figure C-28. Experimental results (M5070_30pc40-70_C) for LRP tests: 5 LRP 1,100µm/m sinusoidal loading loops with 10,000 cycles each on bitumen: a) Normalised (the initial modulus being considered as the result at the 3rd cycle) norm of complex shear modulus, and b) normalised phase angle as a function of number of applied cycles; and c) representation of the results on a normalised Black space. 289

Figure C-29. Experimental results (M5070_30pc40-70_C) for LRP tests (5 LRP tests with 10,000 cycles of 1,100µm/m sinusoidal loading and 4h rest loops on bitumen): a) Black diagram representation of the results including details of the number of cycles during loading and the time of rest during rest periods, and a representation of the nonlinearity effect; b) results after temperature correction. The figure present also a 2S2P1D model prediction, with indication of LVE complex modulus at 10Hz and three temperatures, 11.1°C (Tini), 11.2°C and 11.4°C.....290

Figure C-30. Experimental results (M5070_30pc40-70_C) for LRP tests (5 LRP tests with 10,000 cycles of 1,100µm/m sinusoidal loading and 4h rest loops on bitumen): Black diagram representation of a) the raw experimental results and the results after the temperature correction and b) the experimental results after temperature and damage correction. The figure present also a 2S2P1D model prediction, with indication of LVE complex modulus at 10Hz and three temperatures, 11.1°C (Tini), 11.2°C and 11.4°C. 291

Figure C-31. Experimental results (M5070_30pc40-70_A) for LRP tests: 5 LRP loops with 10,000 cycles and 4h rest on bitumen submitted to 3,300µm/m sinusoidal loading: a) Norm of complex modulus and phase angle as a function of time, and b) shear strain amplitude and temperature as a function of time. 292

Figure C-32. Experimental results (M5070_30pc40-70_A) for LRP tests: 5 LRP 3,300µm/m sinusoidal loading loops with 10,000 cycles each on bitumen: a) Norm of complex shear modulus, b) phase angle, c) mean in-specimen temperature, and d) dissipated energy per cycle as a function of the number of applied cycles. 293

Figure C-33. Experimental results (M5070_30pc40-70_A) for LRP tests: 5 LRP 3,300µm/m sinusoidal loading loops with 10,000 cycles each on bitumen: representation on a) Black space, and b) Cole-Cole diagram. 294

Figure C-34. Experimental results (M5070_30pc40-70_A) for LRP tests: 5 LRP 3,300µm/m sinusoidal loading loops with 10,000 cycles each on bitumen: a) Normalised (the initial modulus being considered as the result at the 3rd cycle) norm of complex shear modulus, and b) normalised

phase angle as a function of number of applied cycles; and c) representation of the results on a normalised Black space. 295

Figure C-35. Experimental results (M5070_30pc40-70_A) for LRP tests (5 LRP tests with 10,000 cycles of 3,300μm/m sinusoidal loading and 4h rest loops on bitumen): a) Black diagram representation of the results including details of the number of cycles during loading and the time of rest during rest periods, and a representation of the nonlinearity effect; b) results after temperature correction. The figure present also a 2S2P1D model prediction, with indication of LVE complex modulus at 10Hz and three temperatures, 11.1°C (Tini), 12°C and 13°C. 296

Figure C-36. Experimental results (M5070_30pc40-70_A) for LRP tests (5 LRP tests with 10,000 cycles of 3,300μm/m sinusoidal loading and 4h rest loops on bitumen): Black diagram representation of a) the raw experimental results and the results after the temperature correction and b) the experimental results after temperature and damage correction. The figure present also a 2S2P1D model prediction, with indication of LVE complex modulus at 10Hz and three temperatures, 11.1°C (Tini), 12°C and 13°C. 297

Figure C-37. Experimental results (M5070_30pc40-70_B) for LRP tests: 5 LRP loops with 10,000 cycles and 4h rest on bitumen submitted to 8,500μm/m sinusoidal loading: a) Norm of complex modulus and phase angle as a function of time, and b) shear strain amplitude and temperature as a function of time. 298

Figure C-38. Experimental results (M5070_30pc40-70_B) for LRP tests: 5 LRP 8,500μm/m sinusoidal loading loops with 10,000 cycles each on bitumen: a) Norm of complex shear modulus, b) phase angle, c) mean in-specimen temperature, and d) dissipated energy per cycle as a function of the number of applied cycles. 299

Figure C-39. Experimental results (M5070_30pc40-70_B) for LRP tests: 5 LRP 8,500μm/m sinusoidal loading loops with 10,000 cycles each on bitumen: representation on a) Black space, and b) Cole-Cole diagram. 300

Figure C-40. Experimental results (M5070_30pc40-70_B) for LRP tests: 5 LRP 8,500μm/m sinusoidal loading loops with 10,000 cycles each on bitumen: a) Normalised (the initial modulus being considered as the result at the 3rd cycle) norm of complex shear modulus, and b) normalised phase angle as a function of number of applied cycles; and c) representation of the results on a normalised Black space. 301

Figure C-41. Experimental results (M5070_30pc40-70_B) for LRP tests (5 LRP tests with 10,000 cycles of 8,500μm/m sinusoidal loading and 4h rest loops on bitumen): a) Black diagram representation of the results including details of the number of cycles during loading and the time of rest during rest periods, and a representation of the nonlinearity effect; b) results after temperature correction. The figure present also a 2S2P1D model prediction, with indication of LVE complex modulus at 10Hz and three temperatures, 11.1°C (Tini), 16°C and 21°C. 302

Figure C-42. Experimental results (M5070_30pc40-70_B) for LRP tests (5 LRP tests with 10,000 cycles of 8,500μm/m sinusoidal loading and 4h rest loops on bitumen): Black diagram representation of a) the raw experimental results and the results after the temperature correction

and b) the experimental results after temperature and damage correction. The figure present also a 2S2P1D model prediction, with indication of LVE complex modulus at 10Hz and three temperatures, 11.1°C (Tini), 16°C and 21°C. 303

MAIN SYMBOLS

All chapters

Symbol	Definition
$\sigma(t)$ and $\tau(t)$	Normal stress and shear stress signals, as a function of time
$\varepsilon_1(t)$ and $\gamma(t)$	Axial strain and shear strain signals, as a function of time
$\varepsilon_2(t)$ and $\varepsilon_2(t)$	Orthogonal transverse strains with respect to $\varepsilon_1(t)$
ε_{0j}, σ_0, γ_0, τ_0	Amplitude of a given signal
f	Loading frequency
ω	Loading pulsation (angular frequency)
N	Number of applied cycles
Nf	Number of cycles at fatigue failure
T	Temperature
Tini	Initial temperature
Tref	Reference temperature for a mastercurve
Tg	Glassy transition temperature
a_T	Time-shift factor from Time-Temperature Superposition
E and D	Elastic Young's modulus and elastic compliance
G	Elastic shear modulus
ν	Elastic Poisson's ratio
E^*, G^*, and ν^*	Complex modulus, complex shear modulus, and complex Poisson's ratio
$\|E^*\|$, $\|G^*\|$, and $\|\nu^*\|$	Norm of a given complex property
φ_{E^*}, φ_{G^*}, and φ_{ν^*}	Phase angle of a given complex property
φ	Phase angle
$E_1 = Re(E^*)$ or G_1	Real part of complex modulus or of complex shear modulus
$E_2 = Im(E^*)$ or G_2	Imaginary part of complex modulus or of complex shear modulus
W_N	Dissipated strain energy in a sinusoidal loading cycle

Chapter 4 - Nonlinearity

s_E	Strain dependence of the norm of complex modulus
$\|E_0^*\|$ or $\|G_0^*\|$	Norm of complex modulus at very small strain amplitude (near 0μm/m)
p_E	Normalised ($/\|E_0^*\|$) strain dependence of the norm of complex modulus
s_E	Strain dependence of the norm of complex modulus
p_φ	Strain dependence of the phase angle of complex modulus
φ_0	Phase angle of complex modulus at very small strain amplitude (near 0μm/m)
$\varepsilon_{0,95\%}$	Axial strain amplitude that induce a 5% change in $\|E^*\|$ with respect to $\|E_0^*\|$
$\gamma_{0,95\%}$	Shear strain amplitude that induce a 5% change in $\|G^*\|$ with respect to $\|G_0^*\|$
$\sigma_{0,95\%}$	Normal stress amplitude that induce a 5% change in $\|E^*\|$ with respect to $\|E_0^*\|$
$\tau_{0,95\%}$	Shear stress amplitude that induce a 5% change in $\|G^*\|$ with respect to $\|G_0^*\|$

Chapter 5 – Self-heating

F	Applied force on a unit cell
S_e	Surface where the force F is distributed
R	Characteristic radius of spherical particles in the 3D thermomechanical model
e	Minimum half-thickness of mastic (half of the distance between two particles in the 3D thermomechanical model)
M_m	Temperature derivative of norm of complex modulus of mastic
M_{bm}	Temperature derivative of norm of complex modulus of bituminous mixture
M	Normalised (with respect to the norm of complex modulus of the given material) temperature derivative of norm of complex modulus

Chapter 6 – Combined Effects

$\|G_0^*\|$	Initial value of norm of complex modulus (evaluated at the 3rd loading cycle)

Chapter 1: INTRODUCTION

Roadways are main infrastructures necessary for the economic development of a country. Bituminous pavements (which include one or more bituminous mixture layers) are the most common technical solution for the construction of roads presenting relatively high traffic volume. In some design methods, those pavements are conceived for a certain design life, which can be determined following mechanistic and empirical considerations. Information from the designed structure and its use (climate, structural geometry, loads, etc.) and from the applied materials (assessed by laboratory tests) is used as input for prediction of the structural integrity over time (performance simulation). One of the main distresses occurring in bituminous pavements, and that need to be simulated for design purposes, is fatigue cracking.

Fatigue cracking of the bituminous mixture layer is originated from the accumulation of damage under traffic. Even if a single loading cycle is unable to produce failure in the bituminous mixture, the repetition of the loads may induce, after many cycles, the failure of the material, accelerating pavement degradation. Damage is seen as the development of microcracks within a material, which induces macroscopically an apparent loss of stiffness. In laboratory, fatigue testing of bituminous materials consists more commonly in applying continuously repeated load cycles until failure. The continuously applied cycles accelerate the damage process that is seen in the bituminous mixtures applied in real pavements. Material stiffness may be monitored during tests, and its change can be used as an indicator of damage in the material (Di Benedetto et al., 2004, Tapsoba et al., 2015). In some approaches, those changes are used to fit damage models, used afterwards for performance simulation. So, it is particularly important to correctly interpret the changes in stiffness during fatigue tests, identifying the occurring physical phenomena.

It is possible to distinguish three phases during fatigue tests on bituminous mixtures (Di Benedetto, de La Roche, Baaj, Pronk, & Lundström, 2004). The first phase (Phase I) is characterized by a relatively rapid and non-linear change in stiffness (as measured through a material property known as the complex modulus) with the repetition of cycles at the beginning of the test. In that phase, other phenomena than damage seem to be predominant. Those phenomena may be listed as transient effects (Gayte, Di Benedetto, Sauzéat, & Nguyen, 2016), strain dependence or nonlinearity (Airey, Rahimzadeh, & Collop, 2003; Di Benedetto, Nguyen, & Sauzéat, 2011; Gauthier, Bodin, Chailleux, & Gallet, 2010; Mangiafico et al., 2015; Mangiafico, Babadopulos, Sauzéat, & Di Benedetto, 2017), bulk self-heating (Di Benedetto, Nguyen, et al., 2011; Lundström, Ekblad, & Isacsson, 2004; Riahi et al., 2016) and thixotropy (Barnes, 1997; Di Benedetto, Nguyen, et al., 2011; Mangiafico et al., 2015; Riahi et al., 2017). Phase II presents a quasi-linear evolution of complex modulus. Phase III presents generally a change in trend of complex modulus evolution with respect to Phase II. This change indicates that defects coalesced into a macrocrack (Goodrich, 1991) and results are no longer exploitable to obtain volumetric material properties such as stiffness. For instance, in the case of tension-compression fatigue tests, stress and strain fields are not homogeneous anymore, whereas it is the case before macrocrack

coalescence. The boundary between Phases II and III is interpreted as the moment of the failure of the specimen and is an important output of fatigue tests (called number of cycles to failure, *Nf*). Nevertheless, that boundary may not systematically manifest itself very clearly. Experimental results (Di Benedetto, Nguyen, et al., 2011; Isailović, Wistuba, & Cannone Falchetto, 2017; Mangiafico, 2014; Mangiafico et al., 2017; Q. T. Nguyen, 2011; C. V. Phan, Di Benedetto, Sauzéat, Dayde, & Pouget, 2017; Riahi et al., 2017; Soltani & Anderson, 2005) show that most of the effects observed during Phase I are completely reversible. These effects are produced by processes that may be classified as bulk (occurring in a distributed manner in the material volume) recoverable phenomena.

In order to estimate performance, material models are necessary. They need to describe material properties as simple and accurate as possible, respecting material behaviour. In order to determine material properties, tests are performed. The present work treats the fundamental behaviour of bituminous materials observed in laboratory tests. It concentrates in the different phenomena capable of producing effects on material stiffness. Those effects directly impact the interpretation of fatigue tests, for which literature (Bahia et al. 1999; Carpenter et al. 2003; Darabi et al. 2013; Ghuzlan and Carpenter 2000; Ghuzlan and Carpenter 2006; Ghuzlan and Carpenter 2003; Kim et al. 1997; Shen et al. 2006; Underwood et al. 2012; You et al. 2014, among others) commonly considers that only fatigue damage induces stiffness changes.

The phenomena treated in this thesis are:

- Nonlinearity, which is a reversible phenomenon that causes stiffness to be dependent of the loading levels (such as the strain amplitude in sinusoidal loading). Since fatigue tests are usually performed to determine the amount of loading cycles necessary to produce failure as a function of the loading level, different loading levels are to be used in tests and an effect of nonlinearity is expected. Moreover, during cyclic tests, some cycles may be necessary before the targeted loading amplitude is reached, so nonlinearity is expected to produce effects on stiffness at least at the beginning of cyclic tests;
- Self-heating, which is a consequence of the dissipative viscoelastic behaviour of the material. The material dissipates mechanical energy in its volume when loaded. That dissipated energy turns into heat and produces a temperature increase in the material. As a consequence, a stiffness decrease is observed in the bituminous material, which is thermo-sensitive. Also, due to the stiffness difference between aggregate particles and mastic, and to the distribution of different thicknesses of mastic covering particles, heterogeneous self-heating is expected in the material. In thin coatings, these local self-heating effects may produce a relatively high local stiffness change, impacting more pronouncedly the stiffness of the whole material. The temperature increase due to local self-heating is difficult to measure since the scale in which it may happen is of few tens of microns. That makes local self-heating a phenomenon likely to be confounded with thixotropy (explained next). The effects of self-heating in a heterogeneous material, such as the bituminous mixture, are also evaluated in this work. If the material is allowed to cool to the original temperature, the original stiffness is recovered, i.e. self-heating is a reversible phenomenon;

- Thixotropy, which is a phenomenon occurring in some fluids, such as colloids (of which bitumen is an example), presenting under continuous loading a decrease of viscosity (or stiffness) through time. That change occurs until an equilibrium viscosity (or stiffness) is reached. When loading is stopped (rest period applied to the material) the original viscosity (or stiffness) is recovered after some time, i.e. the phenomenon is reversible. Both the decrease and the recovery of material properties are manifestations of thixotropy. The phenomenon can be seen as the combination of two sub-phenomena, known as the breakdown and the build-up of the material's microstructure, both occurring simultaneously. The equilibrium of those two sub-phenomena leads to the equilibrium viscosity (or stiffness), which is loading level dependent;
- Damage, which in continuum mechanics is seen as a phenomenon of loss of resistant cross-section at a scale inferior to the one of the studied continuum (phenomenon distributed in the material volume), producing a change in apparent stiffness. The apparent stiffness may be used as an indicator of the damage evolution. Since the loss of resistant cross-section produces in the microscopic level a material discontinuity, unless the material is capable of flowing back to the voids created before, damage is an irreversible phenomenon. It is observed that some authors believe that this material "flowing back" phenomenon that repairs microcracks occurs in bituminous mixtures at a sufficiently high temperature. That phenomenon is commonly called "self-healing" of microcracks. The combination of damage and self-healing could be easily confounded with thixotropy. As an additional comment, it is observed that during fatigue tests, the other phenomena, which are reversible, are considered to produce biasing effects for the test, which is supposed to give information on damage and failure. Those phenomena are sometimes referred to in this thesis as biasing effects.

As it can be seen from the past comments, the assessment of bituminous materials properties from tests may be complicated since the aforementioned physical phenomena need to be taken into account. Otherwise, simplification hypotheses necessary to the analysis of some tests may not hold and consequently impact the determined material properties. In addition to the method of experiments analysis, the test geometry itself needs to be carefully chosen in order to obtain reliable fundamental material properties. If the effects of the aforementioned phenomena are relatively important, test geometries producing non-homogeneous stress and strain fields (e.g. bending tests, indirect tensile tests, cylinder torsion etc.) are not suitable for obtaining material properties. Analysing those tests (i.e. to obtain stress and strain fields from force and displacement measurements) requires a supplementary hypothesis on the material behaviour (e.g. isotropic linear viscoelasticity), whose determination is the purpose itself of the tests. In addition, as mentioned before, the phenomena occurring during the tests are dependent on stress/strain level. Since non-homogeneous tests produce non-uniform stress and strain distributions, the necessary supplementary hypothesis needs to take into account stress/strain dependence, i.e. be based on the known type of material behaviour. This type of behaviour is not accessible without homogeneous tests.

Regarding the presented context, the research problem treated in this thesis is the misinterpretation of general cyclic tests and fatigue tests on bituminous materials, which makes it difficult to obtain reliable fundamental material properties, due to the combined effect of different

physical phenomena. The general objective of the work is to identify and to quantify the effects of each of the physical phenomena, in order to improve the interpretation of cyclic tests. Specifically, the goals of the thesis are:

- To evaluate the effect of nonlinearity in bitumen, mastic and bituminous mixture at different conditions of temperature and frequency and investigate how nonlinearity in these different material scales relate to each other;
- To analyse the effect of local self-heating during cyclic tests in bituminous mixtures at different conditions of temperature, frequency and loading amplitude. Also, it should be verified whether local self-heating could explain the initial modulus decrease observed in tests. This would indicate that no other reversible phenomenon (such as thixotropy) is required to produce the observed experimental results;
- To experimentally demonstrate the combined effects of the studied phenomena (nonlinearity, self-heating, thixotropy and damage) and how to decompose those effects.

As seen, this doctoral thesis is concentrated in the field of Mechanics of Materials, applied to bituminous materials. It was developed at the Laboratory of Tribology and Dynamics of Systems (LTDS – *Laboratoire de Tribologie et Dynamique des Systèmes*) at the *Ecole Nationale des Travaux Publics de l'Etat* (ENTPE), France, with the support of the Brazilian Science without Borders (CsF – *Ciência sem Fronteiras*) programme (PhD grant), and the participation of ENTPE through its research cooperation (*Chaire*) with the company *Eiffage Routes*. In addition to this Introduction (Chapter 1) presenting the context of the study and its objectives, the thesis comprises experimental and modelling approaches, organised as follows.

- Chapter 2 presents generalities on the mechanical behaviour of bituminous materials. It communicates main points from the literature relevant for the work herein, such as the composition of bituminous materials and the description of their thermomechanical behaviour. The chapter is concluded with the description of a general approach to interpret fatigue tests taking into account reversible physical phenomena (nonlinearity, self-heating and thixotropy) occurring during cyclic loading of bituminous materials;
- Chapter 3 describes the experimental devices used for the tests presented in the thesis. It also gives details on the evaluated materials and introduces the procedure to interpret test results (signals treatment);
- Chapter 4 treats the phenomenon of nonlinearity in bituminous materials, intended in this thesis as the strain-dependence of a material's mechanical behaviour. The effects of loading amplitude on materials stiffness are analysed for bitumen, mastic and bituminous mixture. Comparisons are made and a proposition for the physical origin of the phenomenon in bituminous mixtures is given;
- Chapter 5 covers the phenomenon of self-heating due to thermomechanical coupling in bituminous materials. It describes the investigation to verify whether local self-heating could explain the initial modulus decrease observed in tests. This would indicate that no other reversible phenomenon (such as thixotropy) is required to produce the observed experimental results;
- Chapter 6 describes the experimental work designed to determine the contributions of each of the aforementioned behaviours during cyclic tests on bitumen and on mastic. A

description of the separation of the impact of the studied phenomena is presented and a framework for the interpretation of material behaviour during tests, and consequently modelling material behaviour, is presented.

- Chapter 7 presents the general conclusion of the thesis with impact on the analysis of cyclic loading tests, and recommendations for future work.

Chapter 2: GENERALITIES ON THE MECHANICAL BEHAVIOUR OF BITUMINOUS MATERIALS

Chapter 2: Generalities on the Mechanical Behaviour of Bituminous Materials 6
2.1. Bituminous materials composition 8
2.1.1. Bitumen 9
2.1.2. Mastic 10
2.1.3. Bituminous mixture 10
2.2. Mechanical behaviour and the effects of time and temperature 11
2.2.1. General experimental observations 11
2.2.2. Thermo-sensitivity (temperature dependence) 16
2.2.3. Time (or frequency) dependence (viscosity aspects) 16
2.2.4. Time-temperature (or frequency-temperature) superposition 19
2.2.4.1. In linear viscoelasticity 21
2.2.4.2. In nonlinear viscoelasticity 22
2.2.4.3. In plasticity 23
2.2.4.4. In crack propagation 24
2.2.4.5. In fatigue 25
2.2.4.6. Relation between bitumen, mastic and bituminous mixtures 26
2.2.4.7. Non thermorheologically simple bituminous materials 26
2.3. Linear viscoelasticity for non-ageing materials 27
2.3.1. Experimental assessment of time domain properties 27
2.3.2. Experimental assessment of frequency domain properties 28
2.3.3. Convolution integral and relationships between properties 30
2.3.4. Discrete spectrum models 31
2.3.4.1. Springs and Dashpots 31
2.3.4.2. Dashpot 31
2.3.4.3. Generalised Kelvin-Voigt (GKV) model 32
2.3.4.4. Generalised Maxwell-Wiechert (GMW) model 32
2.3.4.5. Interconversion between linear viscoelastic properties from models 33
2.3.5. Continuum spectrum models 33
2.3.5.1. The parabolic element 33
2.3.5.2. Huet model and Huet-Sayegh model 33
2.3.5.3. 2S2P1D model 34

2.3.6. Normalised complex modulus and SHStS transformation....36
2.4. Nonlinear viscoelasticity....39
2.4.1. Equivalent complex modulus as a function of loading amplitude....39
2.4.2. Mathematical formulations for nonlinear viscoelastic behaviour....41
2.5. Fatigue damage....41
2.5.1. Experimental observations....42
2.5.2. Damage modelling....43
2.6. Failure....44
2.6.1. Experimental observations....44
2.6.2. Failure modelling....45
2.6.2.1. Whöler curves and Miner's law....46
2.7. Thixotropy....46
2.8. General formulation to interpret fatigue tests considering biasing phenomena....50

This chapter presents some generalities on the mechanical behaviour of bituminous materials. The information provided is useful for understanding the experimental analysis presented in this thesis. From the main aspects of bitumen composition through the mechanical behaviour aspects of bituminous materials, information linked to the physical phenomena observed during cyclic loading is provided. Then, a general approach for the analysis of cyclic tests results is presented, based in past developments.

Literature demonstrated experimentally the existence of different physical phenomena during the cyclic loading of bituminous materials: transient effects (Gayte et al., 2016); strain dependence or nonlinearity (Airey et al., 2003; Di Benedetto, Nguyen, et al., 2011; Gauthier et al., 2010; Mangiafico et al., 2015, 2017); bulk self-heating (Di Benedetto, Nguyen, et al., 2011; Lundström et al., 2004; Riahi et al., 2016); thixotropy (Di Benedetto, Nguyen, et al., 2011; Mangiafico et al., 2015; Riahi et al., 2017; Soltani & Anderson, 2005); damage (Baaj, 2002; Bahia et al., 1999; Di Benedetto, Ashayer Soltani, & Chaverot, 1996; Di Benedetto, de La Roche, et al., 2004; K. A. Ghuzlan & Carpenter, 2003, 2006, Y. R. Kim et al., 1997, 1997; N. Tapsoba, Sauzéat, & Di Benedetto, 2013; N. Tapsoba, Sauzéat, Di Benedetto, Baaj, & Ech, 2015; B. Underwood et al., 2012; Van Rompu, Di Benedetto, Buannic, Gallet, & Ruot, 2012); and possibly self-healing (Bhasin, Little, Bommavaram, & Vasconcelos, 2008; Canestrari, Virgili, Graziani, & Stimilli, 2015; Karki, Li, & Bhasin, 2015; Q. Liu, Schlangen, van de Ven, & García, 2010; Moreno-Navarro, Sol-Sánchez, & Rubio-Gámez, 2015; Palvadi, Bhasin, & Little, 2012; Shan, Tan, Underwood, & Kim, 2010). The interpretation of these physical phenomena is necessary before drawing conclusions based on cyclic tests results, depending on the main aspect investigated. For example, during fatigue tests, the damage evolution (from stiffness measurements) and the fatigue life (also related to the stiffness measurements) of the material can be assessed. However, in order to investigate damage evolution from the measured stiffness during fatigue tests, it seems reasonable to consider correcting the effect of the other phenomena on the measured stiffness, which is seldom the case in the literature. This would be even more important if the effect of these other phenomena showed to be relatively more important than damage in bituminous materials, which seems to be systematically the case (Di Benedetto, Nguyen, et al., 2011; Mangiafico et al., 2015; Q. T. Nguyen, Di Benedetto, & Sauzéat, 2015; Soltani & Anderson, 2005). During tests involving rest periods, the intrinsic reversibility of the phenomena of nonlinearity, self-heating and thixotropy can easily be confounded with the phenomenon called in the literature self-healing (Canestrari et al., 2015; Palvadi et al., 2012; Shan et al., 2010).

Among the referred phenomena, only damage, and possibly self-healing present some kind of irreversibility, one producing the opposite effect of the other on the material mechanical properties. The remaining phenomena produce completely reversible changes in the material.

2.1. Bituminous materials composition

“Bituminous material” is the general term used to refer to a material that contains bitumen. Three main types of bituminous material can be defined: bituminous mixture, mastic and bitumen. These materials differ by their bitumen content (from about 5% in mass in the case of bituminous mixture up to 100% in the case of neat unmodified bitumen), and by the size of their biggest

particles (from few nanometres in the case of bitumen to about 20mm in the case of bituminous mixtures). Figure 2-1 presents these materials and their heterogeneities in different scales.

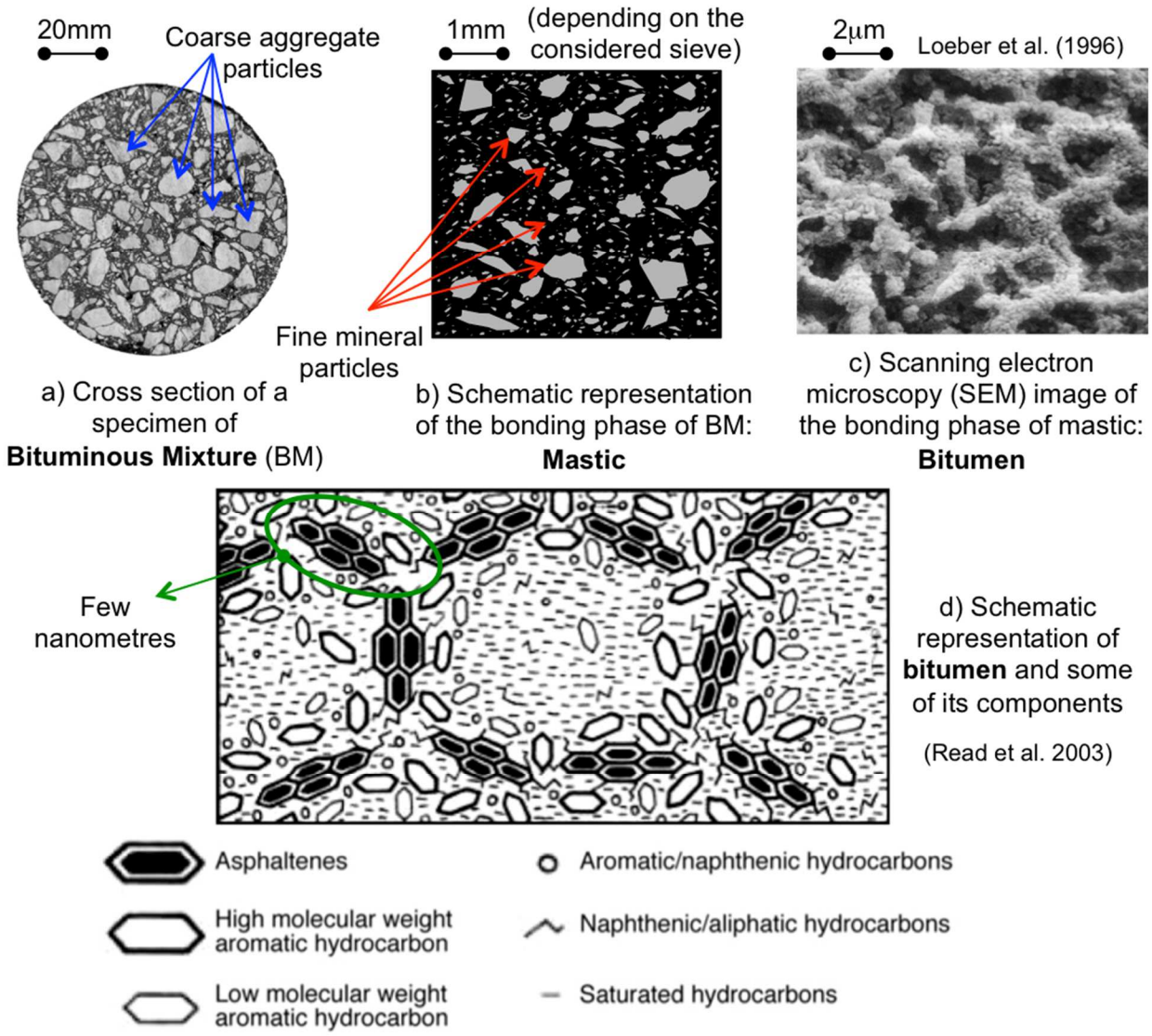

Figure 2-1. Bituminous materials seen in different length-scales: a) bituminous mixture cross-section, b) mastic schematic representation, c) bitumen scanning electron microscopy (SEM) image (Loeber, Sutton, Morel, Valleton, & Muller, 1996), and d) schematic representation of bitumen and some of its components (Read, Whiteoak, & Hunter, 2003).

2.1.1. Bitumen

Bitumen (cf. Figure 2-1c) is a "virtually involatile, adhesive and waterproofing material derived from crude petroleum, or present in natural asphalt, which is completely or nearly completely soluble in toluene, and very viscous or nearly solid at ambient temperatures" (NF EN 12597, 2014). It is used as binder for producing bituminous mixtures, which constitute an important infrastructure material used for paving roadways. Nowadays, most of the bitumen available in the market is the vacuum residue of the crude oil after its distillation process (Lesueur, 2009). The material obtained this way is called straight-run bitumen. It is composed mainly by

carbon and hydrogen (more than 90% by weight), disposed in saturate, cyclic or aromatic structures. The composition of bitumen depends primarily on its crude source. It is used for the preparation of bituminous materials either as is or after modification (by polymer, rubber, among other materials used as modifiers).

Bitumen is typically composed of many different chemicals, divided mainly into two main blends of hydrocarbons: asphaltenes (which is a solid phase, insoluble in n-heptane) and maltenes. The latter are sub-divided into saturates, aromatics and resins. This division is called in the literature SARA fractions. The most accepted description for bitumen structure is a colloidal dispersion of solid asphaltenes particles, or micelles (with radius of few nanometres), in an oily liquid matrix formed by the maltenes (cf. Figure 2-1d).

In Europe, bitumen is generally classified by penetration before being commercialised (NF EN 1426, 2007). Needle penetration is a measurement of consistency at 25°C. In North America, the most used system of classification is the Superpave Performance Grade (PG), which indicates service temperatures for a bituminous mixture containing the bitumen (AASHTO M320, 2009; AASHTO PP6, 1994). These service temperatures are based on rheological (or mechanical) tests at different temperatures (AASHTO T313, 2012; AASHTO T314, 2012; AASHTO T315, 2012; Bahia & Anderson, 1995). The indicated service temperatures are, then, somewhat of the temperatures for which an arbitrary measure of consistency is obtained.

2.1.2. Mastic

Mastic (cf. Figure 2-1b) is a mixture of bitumen (modified or not) and “fine” aggregate particles. These particles are normally understood as the mineral filler, considered generally as particles passing through the 0.075mm sieve (following American standards) or the 0.063mm sieve (following European standards). In this case, mastics can also be seen as suspensions of the mineral filler particles in the bitumen phase (Rigden, 1947), and the change in material properties from the bitumen to the mastic is driven by the filler volume fraction, as in classical theories of solid inclusions in fluids (Einstein, 1906; Goddard & Miller, 1967). In these cases, the mineral particles are seen as a filling inert material that changes the rheology of the mastic.

In Chapter 5, mastic is intended as the bituminous matrix that bonds coarser particles in a bituminous mixture. In that case, different sieves can be used to determine what are “fine” and what are coarse particles (cf. Figure 2-1b), even if these sieves correspond to particles presenting diameter of the order of some millimetres. Literature sometimes uses another terminology (such as Fine Aggregate Matrix, FAM) for such mastics with “coarser” fine particles.

2.1.3. Bituminous mixture

Bituminous mixtures (cf. Figure 2-1a) are mixes of bitumen (modified or not), aggregate particles, and air voids, possibly containing additives used in its fabrication. The performance of the bituminous mixture is influenced by many different factors, such as the bitumen and its content, the presence and type of modifiers, type of fillers, the aggregate particles size distribution

(grading curve, and nominal maximum aggregate size), the compatibility between aggregate and bitumen, and by the voids content (Anderson & Goetz, 1973; Baaj, Di Benedetto, & Chaverot, 2005; Bari & Witczak, n.d.; S. H. Carpenter & Vandam, 1987; Chen & Peng, 1998; Di Benedetto, Olard, Sauzéat, & Delaporte, 2004; Doan, 1977; Isacsson & Zeng, 1998; King, Muncy, & Prudhomme, 1986; Lira, Jelagin, & Birgisson, 2013; Little & Petersen, 2005; Moutier, 1991; Roberts, Khandal, Brown, Lee, & Kennedy, 1996; Romeo, Birgisson, Montepara, & Tebaldi, 2010; Tayebali, Goodrich, Sousa, & Monismith, 1991; Vavrik, Pine, Huber, Carpenter, & Bailey, 2001; Von Quintus, Mallela, & Buncher, 2007).

2.2. Mechanical behaviour and the effects of time and temperature

The mechanical behaviour is described by the relationships between stress and strain in a material (Lemaître & Chaboche, 1990). In bituminous materials, different types of mechanical behaviour (linear elastic, linear viscoelastic, nonlinear viscoelastic, plastic, damage) are observed, depending on their composition, and on loading conditions (temperature, frequency, strain/stress amplitude, number of applied cycles) (S.-C. Huang & Di Benedetto, 2015; Y. H. Huang, 2004; Hunter, Self, & Read, 2015; Y. R. Kim, 2009; Roberts et al., 1996; Whiteoak & Shell Bitumen, 1991).

2.2.1. General experimental observations

In order to investigate the mechanical behaviour of bituminous materials, cyclic tests are commonly used (Di Benedetto et al., 2013, 1996; Di Benedetto & Corté, 2005; Di Benedetto, de La Roche, et al., 2004; Di Benedetto, Partl, Francken, & De La Roche Saint André, 2001; S.-C. Huang & Di Benedetto, 2015; Y. H. Huang, 2004; Y. R. Kim, 2009; Roberts et al., 1996). Cyclic tests consist in the application of a varying loading, customarily sinusoidal (or a function derived from sinusoidal functions). Depending on the chosen loading path, a different type of observed response is to be expected. Figure 2-2 presents schematically some typical loading paths and response examples from tests on bituminous materials.

In Figure 2-2 it is seen that in the case of loading being controlled in terms of strain (figures a and b) with constant amplitude, the response, given in terms of stress, presents decreasing amplitude. Also, the mean value of the response stress signal is bounded and tends not to vary much with respect to the initial mean value for both the cases where the strain signal is not centred to zero (figure a) or in the cases where it is (figure b). In the case of loading being controlled in terms of stress with constant amplitude (figures c and d), the strain tends to increase until failure of the specimen. In the case where the stress signal is not centred to zero (Figure 2-2d), the material flows and the strain amplitude may be negligible in comparison to this flow. In this case, the specimen is likely to fail mainly due to the cumulated flow than due to the application of the cycles itself, as it is the case for the classical indirect tensile tests (Babadopulos, Soares, & Castelo Branco, 2015).

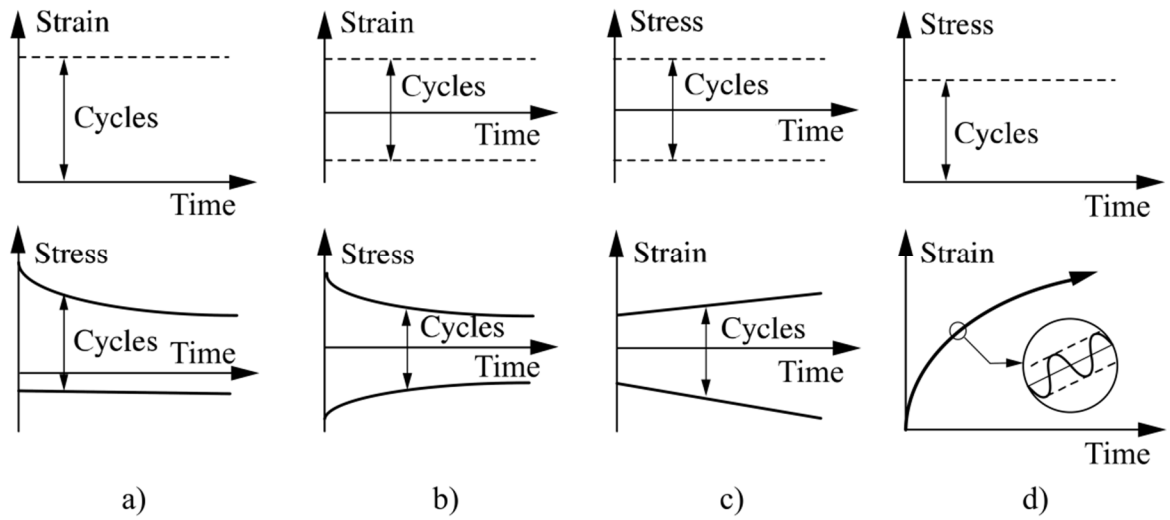

Figure 2-2. Schematic representation of loading (strain, in figures a and b, or stress, in figures c and d) and response (stress or strain) (Di Benedetto & Corté, 2005).

Figure 2-3 presents schematically, in a strain level versus temperature diagram, regions where different conceptual mechanical behaviour is expected. When the strain level is small, linear behaviour is expected. This linearity level may be dependent on the temperature level. The linear behaviour can either be represented by an elastic behaviour (at very low temperatures, near the glassy transition of the material), characterised by the axial Young's modulus and the shear Coulomb's modulus (E and G in the figure) or by a linear viscoelastic behaviour at higher temperatures, characterised by a complex Young's modulus (E*) and a complex shear modulus (G*) in the frequency domain. These material properties are formally defined in Section 2.3. In constant shear strain rate (high cumulated strain levels), the mechanical behaviour of neat bitumen may be approximated to the one of a Newtonian fluid, with a viscosity independent of the strain rate. In other cases, nonlinearity is expected. Figure 2-4 complements the information in the previous figure, presenting a strain level versus number of cycles diagram of the behaviour of bitumen. In this diagram, the effect of the repetition of cycles on bitumen behaviour is seen. Analogously, Figure 2-5 presents the same conceptual types of mechanical behaviour for bituminous mixtures. In addition to the presented conceptual types of mechanical behaviour, the effect of the thixotropy (Barnes, 1997; Mewis & Wagner, 2009) phenomenon should be expected on the mechanical response of bituminous materials, due to its colloidal structure and asphaltene flocs formation (Lesueur, 2009; Read et al., 2003). The effects of the different phenomena (nonlinearity, thixotropy, self-heating, damage) produce changes on the measured material parameter (E* and G*). Then, measuring these properties provides a means of evaluating the effect of the different phenomena.

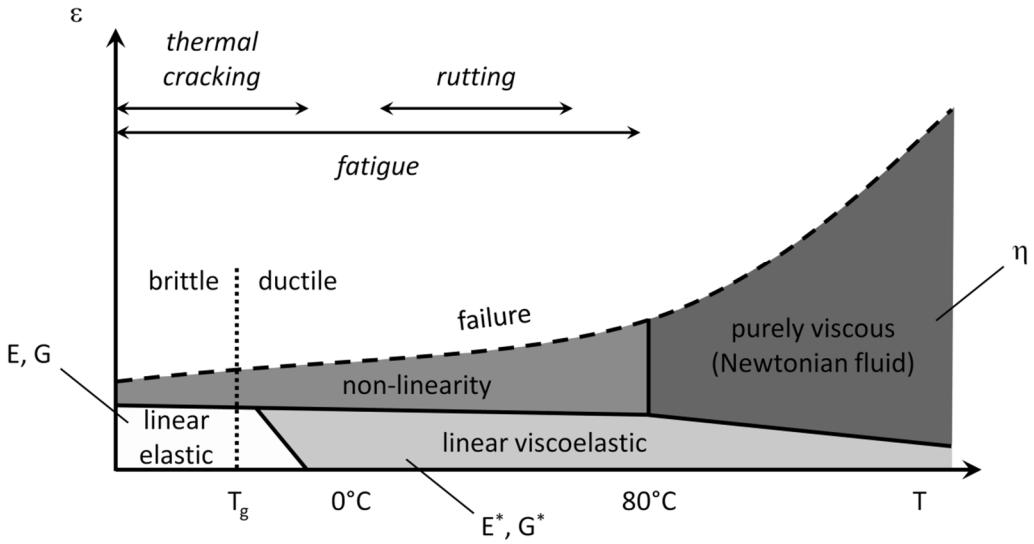

Figure 2-3. Schematic representation of different conceptual mechanical behaviour regions depending on the applied strain levels (ε) and the material temperature (T) for bitumen (Olard, Di Benedetto, Dony, & Vaniscote, 2005). T_g represents the glass transition temperature, where a brittle-to-ductile fracture behaviour is observed.

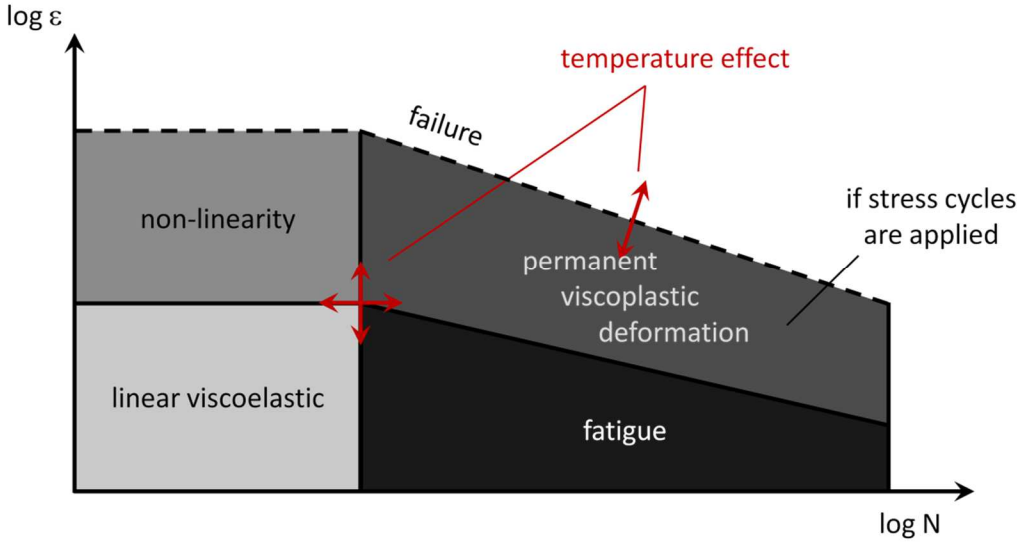

Figure 2-4. Schematic representation of different conceptual mechanical behaviour regions depending on the applied strain levels (ε) and the number of applied loading cycles (N) for bitumen (Mangiafico, 2014).

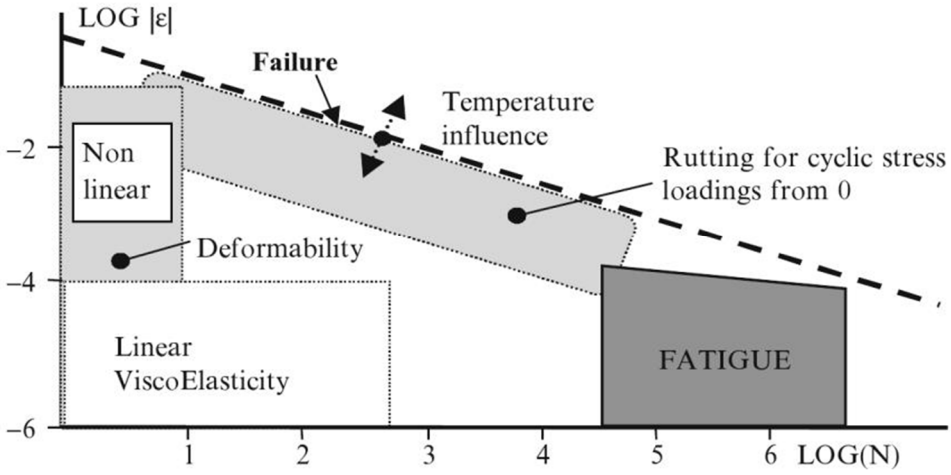

Figure 2-5. Schematic representation of different conceptual mechanical behaviour regions depending on the applied strain levels (ε) and the number of applied loading cycles (N) for bituminous mixtures (Di Benedetto et al., 2013).

(Doubbaneh, 1995) was the first to study the limit between the regions presenting linear and nonlinear viscoelasticity. The idea of defining this transition, which is rather gradually observed when increasing strain amplitude, as the strain amplitude that induces a 5% decrease in norm of complex modulus appears later (Airey & Rahimzadeh, 2004; Airey, Rahimzadeh, & Collop, 2002; Airey et al., 2003). Figure 2-6 presents, for bitumen and bituminous mixtures, separation limits between the linear and the nonlinear regions (Airey & Rahimzadeh, 2004) seen in the previous figures. As seen, bitumen nonlinearity appears with 1% shear strain amplitude (for higher modulus conditions, corresponding to lower temperatures and higher frequencies). For bituminous mixtures, nonlinearity seems to appear with an approximate axial strain of 100μm/m, independently of the loading conditions which is also in agreement with previous results, obtained for temperatures between 5 and 41°C (Doubbaneh, 1995). However, other authors present experimental results demonstrating that the effect of nonlinearity and the LVE limit are temperature- and frequency- dependent (Coutinho, Babadopulos, Freire, Castelo Branco, & Soares, 2014; Mangiafico et al., 2017). It seems that at the bituminous mixtures LVE limit can change from few tens to few hundreds of μm/m when changing from high to low temperatures.

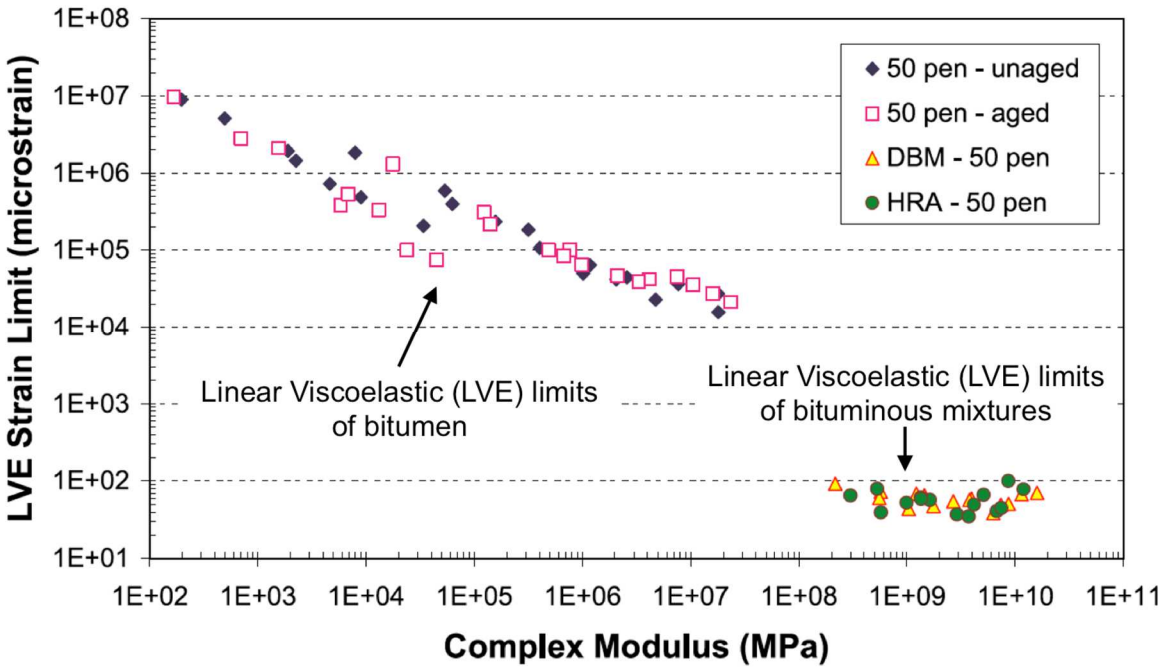

Figure 2-6. Linear viscoelasticity limits determined experimentally in bitumen and bituminous mixtures (Airey & Rahimzadeh, 2004).

Some references (in a non-extensive list) are recommended for the reader for each conceptual behaviour region: linear viscoelasticity (Delaporte et al. 2009; Delaporte et al. 2007; Di Benedetto et al. 2016; Di Benedetto et al. 2009; Di Benedetto et al. 2007; Di Benedetto et al. 2004b; Di Benedetto et al. 2001; Dougan et al. 2003; Gayte et al. 2016; Gudmarsson et al. 2015; Mounier et al. 2012; Olard and Di Benedetto 2003; Phan et al. 2017; Specht et al. 2017, among others), nonlinearity (Airey et al. 2003; Airey et al. 2002; Airey and Rahimzadeh 2004; Bahia et al. 1999; Coutinho et al. 2014; Di Benedetto et al. 2011; Gauthier et al. 2010; Mangiafico et al. 2017; Mangiafico et al. 2015; Nguyen et al. 2015; Underwood and Kim 2013; Underwood and Kim 2012, among others), rutting (Bastos, Babadopulos, & Soares, 2017; Bastos, Torquato e Silva, Soares, Nascimento, & Kim, 2016; Yeong-Tae Choi & Kim, 2014; Yeong-Tae Choi, Subramanian, Guddati, & Kim, 2012; Y.-T. Choi & Kim, 2013; Di Benedetto, Mondher, Sauzéat, & Olard, 2007; Di Benedetto, Nguyen, Pouget, & Sauzéat, 2008; Neifar, 1997; Neifar & Di Benedetto, 2001; H. M. Nguyen, Pouget, Di Benedetto, & Sauzéat, 2009), and fatigue (Baaj et al. 2005; Baaj 2002; Babadopulos et al. 2016a; Bahia et al. 1999; Bodin et al. 2004; Carpenter et al. 2003; Daniel and Kim 2001; Darabi et al. 2013; Di Benedetto et al. 2004a; Di Benedetto et al. 1996; Doan 1977; Ghuzlan and Carpenter 2006; Karki et al. 2015; Kim et al. 1997; Lundström et al. 2004; Moreno-Navarro et al. 2017; Moreno-Navarro et al. 2015a; Moreno-Navarro et al. 2015b; Moutier 1991; Phan et al. 2017; Shan et al. 2010; Shen et al. 2006; Soltani and Anderson 2005; Tapsoba et al. 2015; Tapsoba et al. 2013; Underwood et al. 2012; Underwood and Kim 2013; Van Rompu et al. 2012; You et al. 2014, among others).

2.2.2. Thermo-sensitivity (temperature dependence)

Bituminous materials present high thermo-sensitivity (Behzadfar & Hatzikiriakos, 2014; Bodin et al., 2004; Di Benedetto, Sauzeat, et al., 2011; Di Benedetto, Olard, et al., 2004; Moreno-Navarro et al., 2017). Bituminous mixtures may be about 1,000 times stiffer when tested at low temperatures when compared to experimental results at high temperature (Babadopulos, Ferreira, & Soares, 2016; Di Benedetto et al., 2001; Dougan et al., 2003). When looking at the asymptotic behaviour of these materials, it is seen that that difference may be higher, of the order of 10,000 times (Cardona, 2016; Di Benedetto et al., 2001; Olard & Di Benedetto, 2003; C. V. Phan, Di Benedetto, Sauzéat, Lesueur, et al., 2017). Around the temperature commonly used in fatigue tests (10°C), a 1°C change in temperature produces a stiffness change of the order of 10% (Babadopulos, Sauzéat, & Di Benedetto, 2017a, 2017b). This temperature dependence in bituminous mixtures is inherited from the bitumen (Delaporte et al., 2007; Di Benedetto, Olard, et al., 2004; Olard & Di Benedetto, 2003) and possibly its modifiers.

2.2.3. Time (or frequency) dependence (viscosity aspects)

The stress-strain response of a material may change with time. This includes changes with respect to the time chosen for the beginning of loading (and with changes in loading rate), and also changes that occur over time, independently of loading. These changes need to be separated into different types of behaviour in order to allow for correct analysis. For example, changes with time may come from inertia, or dynamic, effects (such as wave propagation), which is not due to the rheological behaviour of the material. Then, among the time effects that are relevant for the study of material rheology, two main classes may be defined: ageing effects, and viscous or loading rate effects (Di Benedetto, Tatsuoka, Lo Presti, Sauzéat, & Geoffroy, 2003). These effects are intimately related to basic mechanisms, such as physical-chemical changes due to material oxidation (Herrington & Ball, 1996; Petersen et al., 1993), time-dependent properties of the constituents in the mixture, sliding and entanglement of long molecules etc (Brinson & Brinson, 2015; Doolittle & Doolittle, 1957; Emri, 2005; Ferry, 1980; Oakley, Giacomin, & Yosick, 1998). Figure 2-7 presents a schematic representation of loading (l_{ij}) and response (r_{ij}) curves (i and j used to represent a general six-dimensional case of loading, including shear and axial loading cases in three different space directions) as functions of time, and also cross-plotted. It may be used as a means to determine if time effects (both ageing and viscous) exist in the material or not. If in a given domain of loading the response curve is independent of the chronology of loading (or loading rate), the material is not sensitive to time effects.

Non-ageing materials give theoretically the same stress-strain response for two identical loading histories started at different instants (Di Benedetto et al., 2003). On the contrary, this is not the case for ageing materials. This is schematised in Figure 2-8. In the figure, it is seen that a rheological parameter (giving material stiffness, for example) may evolve with time (due to ageing) or not (non-ageing material). Also, it is seen that during a certain time interval Δt, it is possible to represent the behaviour of a material presenting ageing over a wide time interval as it was non-ageing. During mechanical tests at low and moderate temperatures (up to about 50°C) for few tens of hours, bituminous materials can be considered as non-ageing. This is not the case

during mixing and compaction (due to high temperatures, above 135°C), and also during long periods of time in the field. Aging in bituminous materials is linked to a physical phenomenon such as volatilisation of light fractions in the bitumen, more common during construction, and also a chemical process, known as oxidation. For references on ageing, on its chemical description and on its consequences on bitumen and bituminous mixtures rheology, the reader may refer to the recommended literature (R. K. Abu Al-Rub, Darabi, Kim, Little, & Glover, 2013; Alavi, Hajj, & Morian, 2013; Babadopulos, 2014; Babadopulos, Ferreira, & Soares, 2016; Babadopulos, Ferreira, Soares, et al., 2016; Baek, Underwood, & Kim, 2012; Daniel, Kim, & Lee, 1998; Glover et al., 2008; Herrington & Ball, 1996; Lau, Lunsford, Glover, Davison, & Bullin, 1992; D. Y. Lee & Huang, 1973; M. Liu, Ferry, Davison, Glover, & Bullin, 1998; M. Liu, Lunsford, Davison, Glover, & Bullin, 1996; Partl et al., 2013; Petersen et al., 1993; Qin, Schabron, Boysen, & Farrar, 2014; Wright, 1965). In this thesis, due to the analyses concentrated on laboratory tests at moderate temperatures, with materials prepared always following the same temperature history, ageing is not evaluated. Tested materials are considered as non-ageing.

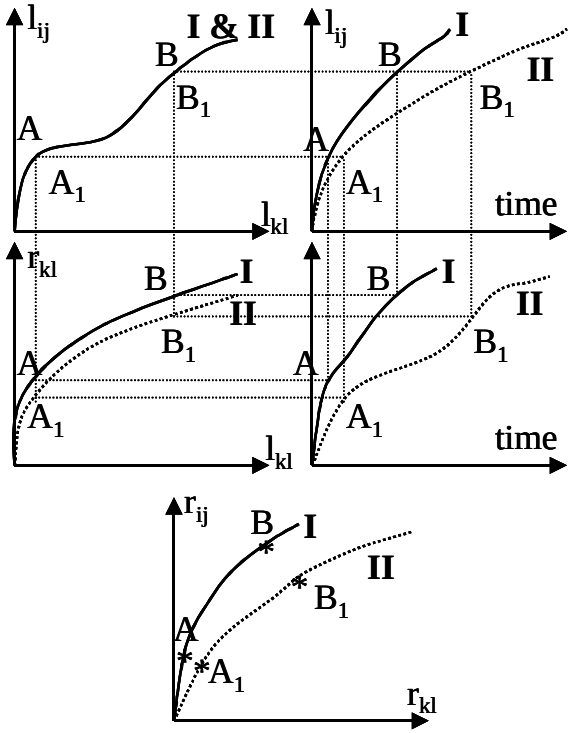

Figure 2-7. Schematic representation of different loading and response paths: different plots and time effect sensitivity. If curves I and II are always superimposed in the axes $l_{ij} – r_{ij}$ (which correspond to stress-strain curve) and in the axes r_{ij} -r_{kl}, the material is not sensitive to time effects (non viscous and non sensitive to ageing) in the considered loading domain (Di Benedetto et al., 2003).

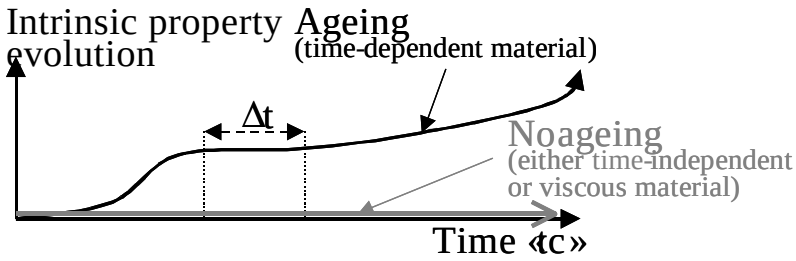

Figure 2-8. Schematic representation of the evolution of an intrinsic material property with time, no evolution during Δt meaning that the material is non-aging for that time span, possibly being either time-independent or viscous (Di Benedetto et al., 2003).

Bituminous mixtures present a particularly important sensitivity to loading rate effects among the geo-materials, as it can be seen in Figure 2-9 (Di Benedetto et al., 2003). Sensitivity to loading rate effects is commonly assessed through sinusoidal loading tests known as complex modulus tests, at different frequencies. The figure presents experimental data from the linear domain (cf. Figure 2-5) covering the range between 0.0004 Hz and 4Hz. Norm of complex modulus gives a measure of material stiffness. For elastic materials, the norm of complex modulus corresponds to the classical Young's modulus (represented in the y-axis in the figure as E_v).

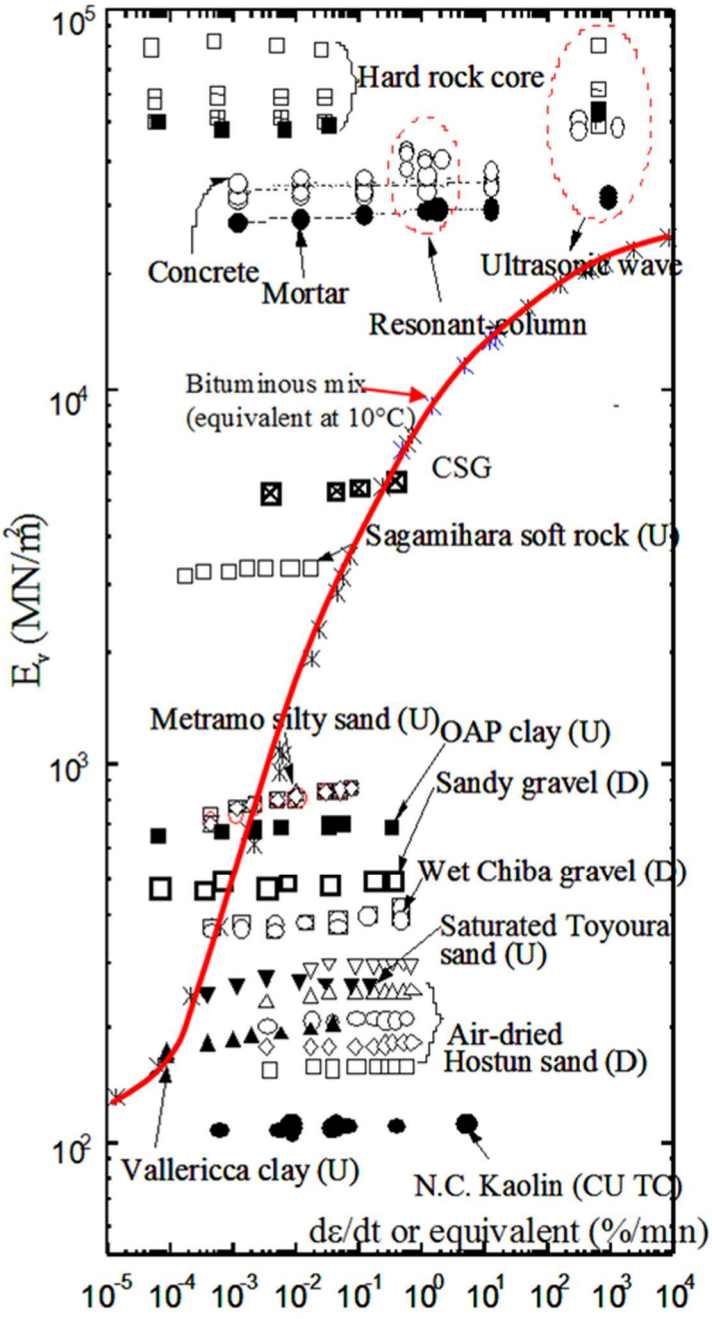

Figure 2-9. Vertical modulus (E_v), at strain amplitude close to 10^{-5}m/m, as a function of strain rate (or equivalent strain rate for cyclic tests) for different geomaterials. The very important viscous sensitivity for bituminous mix is clearly visible (Di Benedetto et al., 2003).

2.2.4. Time-temperature (or frequency-temperature) superposition

For a given material presenting viscous time effects, at two different temperatures, the material behaviour can be equivalent if the same stress-strain (loading-response) is observed. The loading and the response can be plotted as a function of an "equivalent time" in order to obtain the same curves (Di Benedetto et al., 2008). Figure 2-10 presents schematically this concept. The equivalent

time consists in the time divided by a certain factor, a_T, which represents the time-shift related to the change in temperature. This time-shift factor may be determined experimentally.

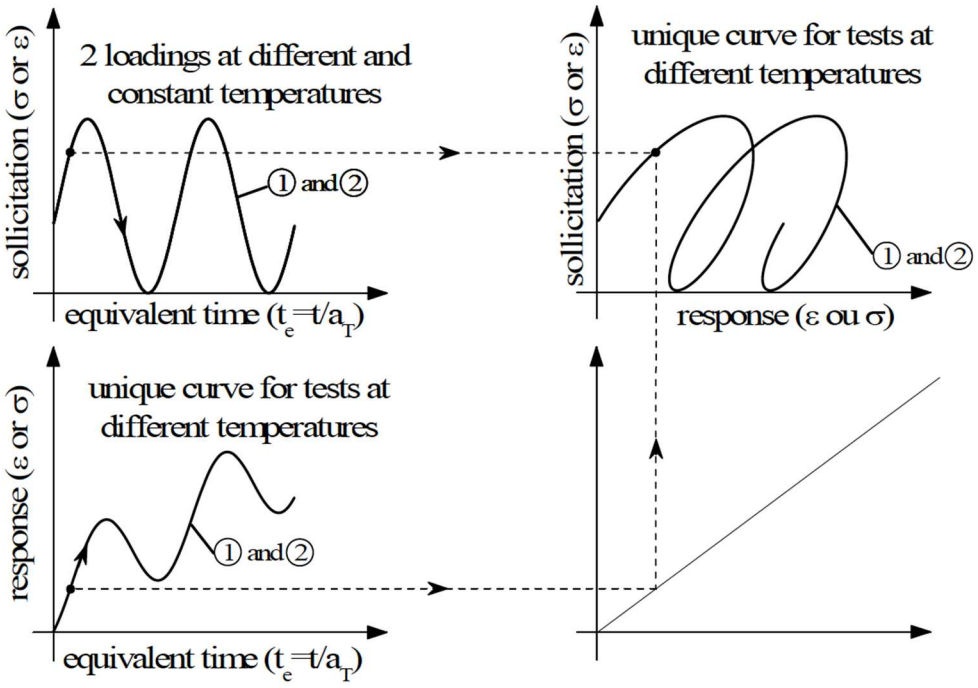

Figure 2-10. Schematic representation of the time temperature superposition principle application, using the time-shift factor a_T (Di Benedetto et al., 2008). In the left-hand side, loading and response signals are plotted as functions of the equivalent time (after time-shift). In the bottom right corner, the graph indicates that same values in the y-axis from the bottom left graph (response) are also plotted in the x-axis of the upper right graph.

Among others (Arrhenius equation, polynomial fittings etc), the Williams-Landel-Ferry (WLF) equation (Williams, Landel, & Ferry, 1955) can be used to describe this phenomenon, relating two different temperatures where, at different loading times (or frequencies), the same material response is observed. WLF equation is presented in Eq. 2-1. In this relation, the definition of time-shift factors appears (a_T, cf. Figure 2-10). If the material behaviour respects this time-shift, i.e., if the Time-Temperature Superposition Principle (TTSP) is valid, it is considered as "thermorheologically simple" (Ferry, 1980; Gross, 1968). In this case, all viscoelastic spectrum of the material is changed by the same factor after a temperature change, and this factor is represented by a unique value of a_T at a given temperature (Gross, 1968). Time-temperature superposition may be related to the mobility of long molecules in the material (Brinson & Brinson, 2015; Emri, 2005; Ferry, 1980; Oakley et al., 1998). This is linked to the inter-molecular (or "free") volume (not occupied by molar mass) (Doolittle & Doolittle, 1957; Emri, 2005). (Emri, 2005) demonstrates that the Doolittle equation (Doolittle & Doolittle, 1957) for the relationship between free volume and viscosity of a fluid may be used to derive the WLF equation. As it will be seen in Section 2.2.4, this will have an impact in the different types of mechanical behaviour of bituminous materials: linear viscoelasticity, nonlinearity, plasticity, crack propagation and fatigue. As it will be shown, it seems that the same time-shift for all these behaviours is observed for a

given bituminous mixture, i.e., the same WLF equation parameters can be used to model time-temperature superposition for all the referred behaviours.

$$\log a_T(T) = -\frac{C_1\left(T - T_{ref}\right)}{C_2 + \left(T - T_{ref}\right)} \qquad \text{Eq. 2-1}$$

2.2.4.1. *In linear viscoelasticity*

For bituminous mixtures, in the case of linear viscoelasticity, the TTSP verification can be done by plotting the complex modulus (stiffness complex property further detailed in the next section) in complex representations (either Cole-Cole plot, where the imaginary part of complex modulus is represented as a function of its real part, or Black space, where the norm of complex modulus is plotted against phase angle). At different frequencies and temperatures, the material will change behaviour, but coincidence of points will be obtained at different pairs of temperature and frequency (cf. Figure 2-11e for a Black diagram representation, with a unique curve, which indicates that the TTSP is valid). Figure 2-11 presents experimental results (Q. T. Nguyen, Di Benedetto, Sauzéat, & Tapsoba, 2013) for the complex modulus and complex Poisson's ratio characterisation of a bituminous mixture commonly used in France (*Béton Bituminex Semi-Grenu* - BBSG). On the graphs, the isotherms (curves where all points are obtained at the same temperature) for each material property are presented. These are the data before time-shift, which is schematically represented on Figure 2-11a. In Figure 2-11, different representations are given, such as master curves for norm of complex modulus (figure a), phase angle (figure b) norm of complex modulus (figure c), phase angle of complex modulus (figure c). In master curves, a material property is plotted as a function of the time-shifted frequency, i.e., the frequency multiplied by the shift factor a_T. This frequency is frequently called as "equivalent frequency" or "reduced frequency" in the literature. Master curves are obtained after the time-shift of the isotherms, forming a unique smooth curve. In Figure 2-11f, this mixture's shift factors are plotted as a function of the temperature, and the WLF equation fitting is presented. All results are presented at a reference temperature of 9.5°C.

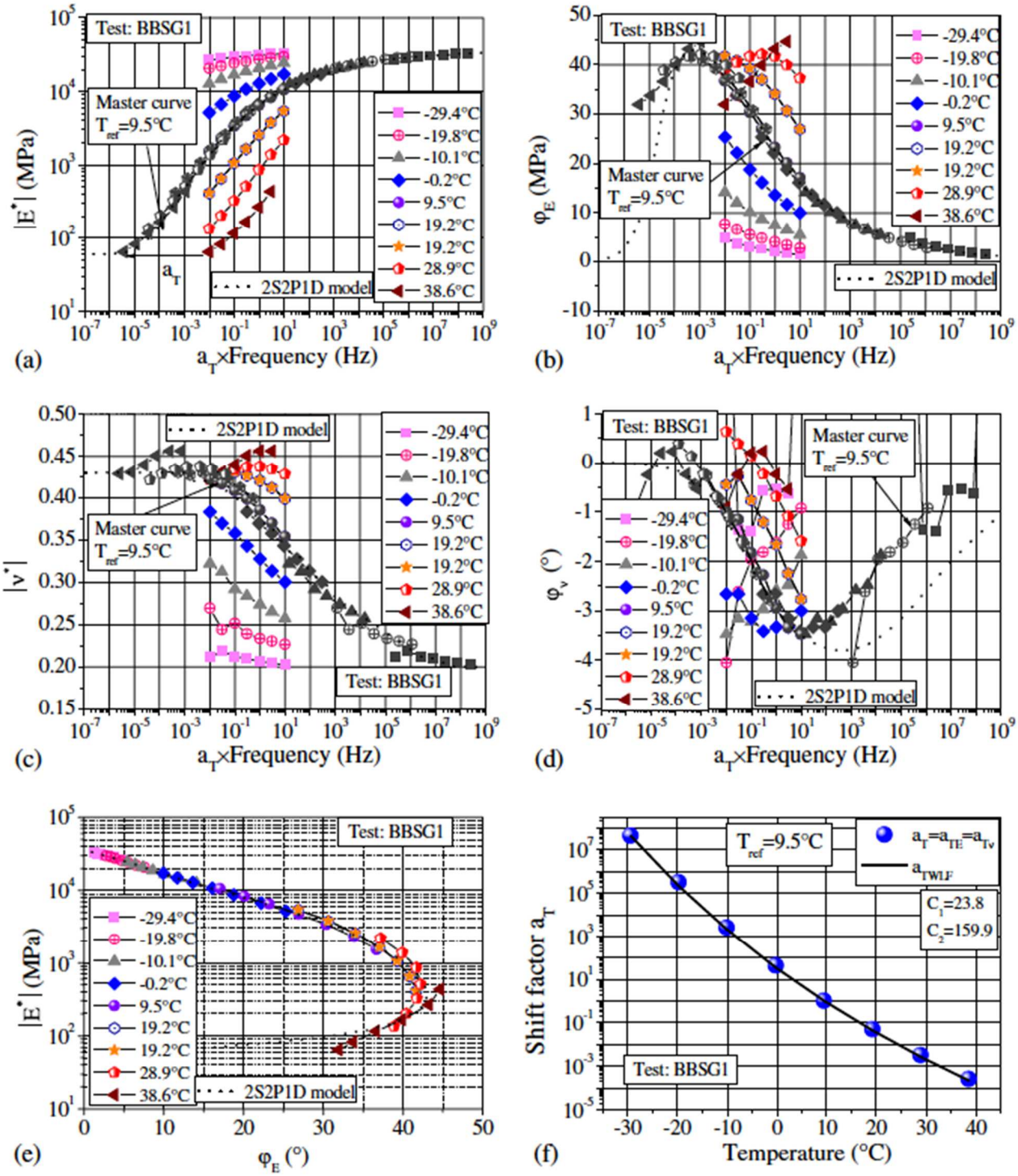

Figure 2-11. Example of time-temperature superposition principle verification for linear viscoelasticity of bituminous mixture (Q. T. Nguyen et al., 2013).

2.2.4.2. *In nonlinear viscoelasticity*

In the case of nonlinearity, (Q. T. Nguyen et al., 2015) presented master curves for different material parameters. As an example, the axial strain amplitude ($\varepsilon_{01_95\%}$), for which 5% decrease in stiffness is obtained with respect to asymptotic small strain stiffness, is plotted as a function of time-shifted frequencies (Figure 2-12). In the figure, the change in phase angle with respect to

small strain phase angle is also represented in a master curve. Both time-shifted curves form a unique smooth curve, indicating that the TTSP is also valid for nonlinearity parameters. The shift factors (a_T) used in the referred work are the same as the ones obtained from the linear viscoelastic characterisation of the bituminous mixture. That means that the same WLF equation parameters can be used both for linear viscoelasticity (LVE) modelling and for nonlinear viscoelasticity modelling of this mixture.

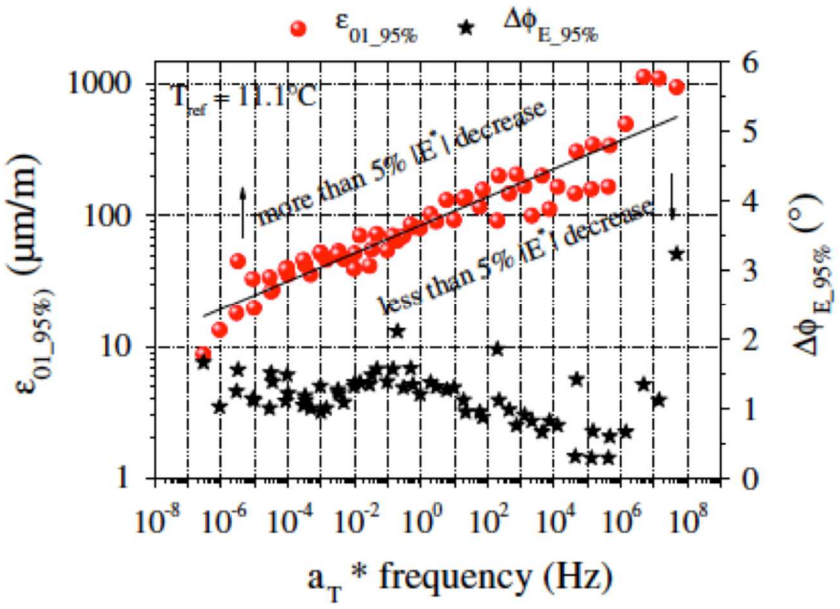

Figure 2-12. Example of time-temperature superposition principle verification for the nonlinear domain (nonlinear viscoelasticity) of bituminous mixture (Q. T. Nguyen et al., 2015).

2.2.4.3. *In plasticity*

The TTSP may also verify for bituminous mixtures plastic behaviour (H. M. Nguyen et al., 2009). Figure 2-13 presents plastic deformations in two directions (1 and 2, axial and radial) obtained as a function of equivalent time (t/a_T) at two pairs of temperature and frequency. In the referred work, the pairs of temperature and frequency were chosen using the LVE WLF equation parameters. As seen, the chosen pair of temperatures and frequencies gives the same plastic deformations (mechanical response) before plastic failure. It was then concluded, that for that bituminous mixtures (and possibly others), time-temperature superposition in plasticity can use the same WLF equation parameters as for linear viscoelasticity.

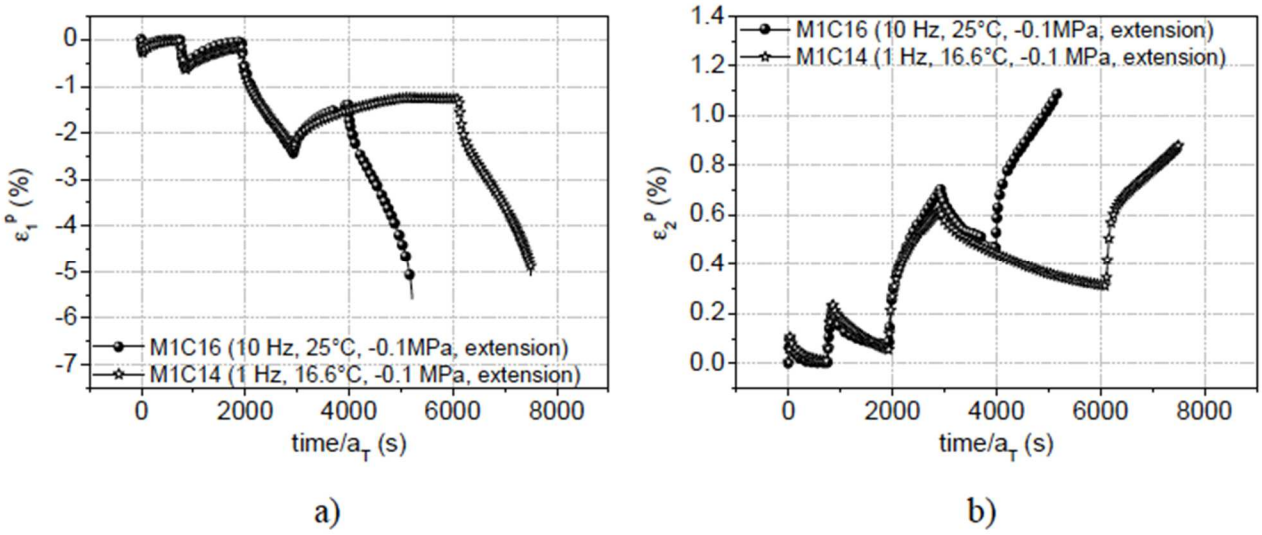

Figure 2-13. Example of time-temperature superposition principle verification for the nonlinear domain (plastic deformations) of bituminous mixture (H. M. Nguyen et al., 2009).

2.2.4.4. *In crack propagation*

The TTSP is also verified for crack propagation in bituminous mixtures (M. L. Nguyen, Sauzéat, Di Benedetto, & Tapsoba, 2013). Figure 2-14 presents experimental results at different conditions of temperature and frequency, chosen using the LVE WLF equation for the tested bituminous mixture. As seen, the same mechanical responses are obtained at the different chosen temperatures, verifying the TTSP for crack propagation with the same shift factors as for linear viscoelasticity.

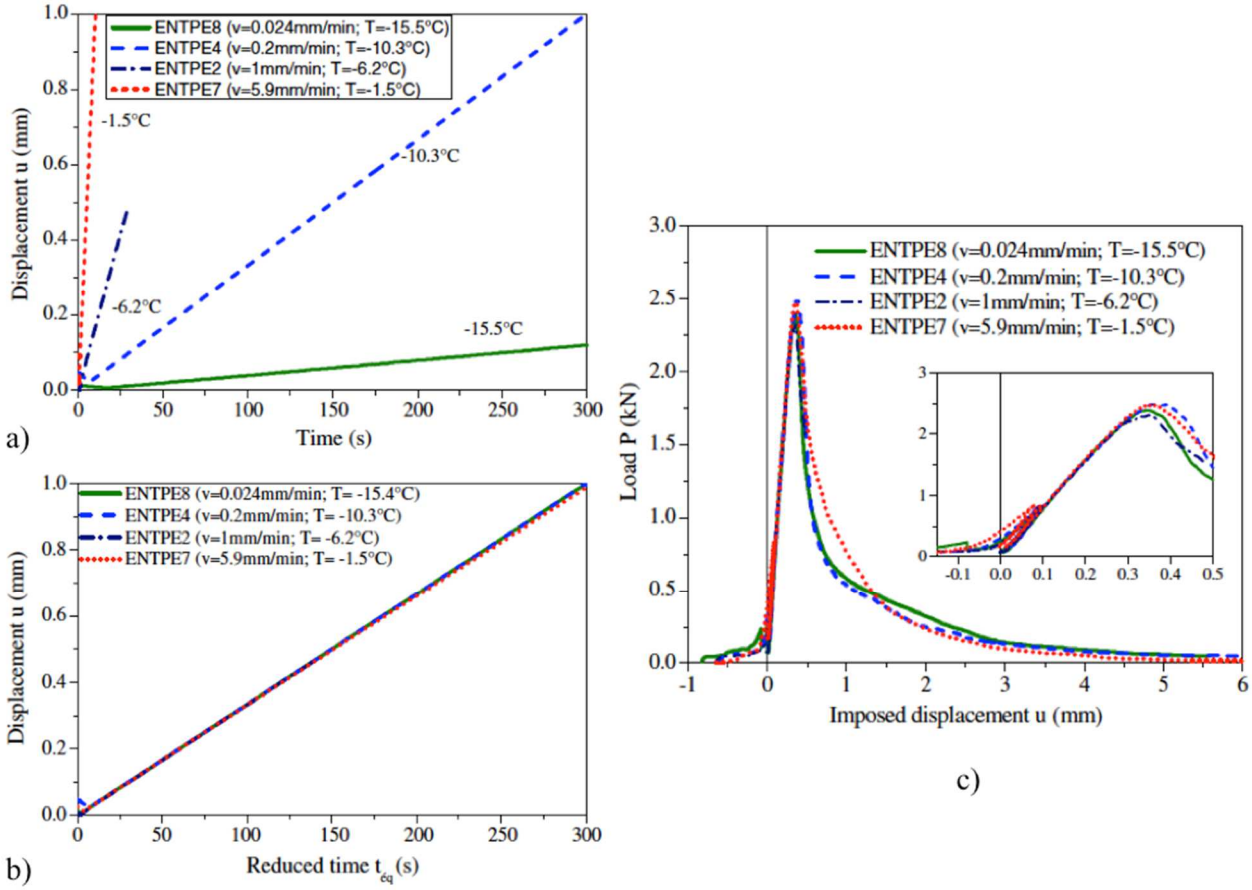

Figure 2-14. Example of time-temperature superposition principle verification for crack propagation in bituminous mixture (M. L. Nguyen et al., 2013).

2.2.4.5. *In fatigue*

(C. V. Phan, Di Benedetto, Sauzéat, Dayde, et al., 2017) performed a similar study for the fatigue behaviour of bituminous mixtures. In Figure 2-15, fatigue tests experimental results (norm of complex modulus in figures a and b, and specimen surface temperature in figure c) at three different pairs of temperature and frequency are given. Two of them were predicted using LVE WLF equation to give the same mechanical response: 10Hz, 10°C; and 3Hz, 6.7°C. Again, before failure similar mechanical responses were obtained, giving an indication that the TTSP is also verified for fatigue with the same shift factors as for linear viscoelasticity.

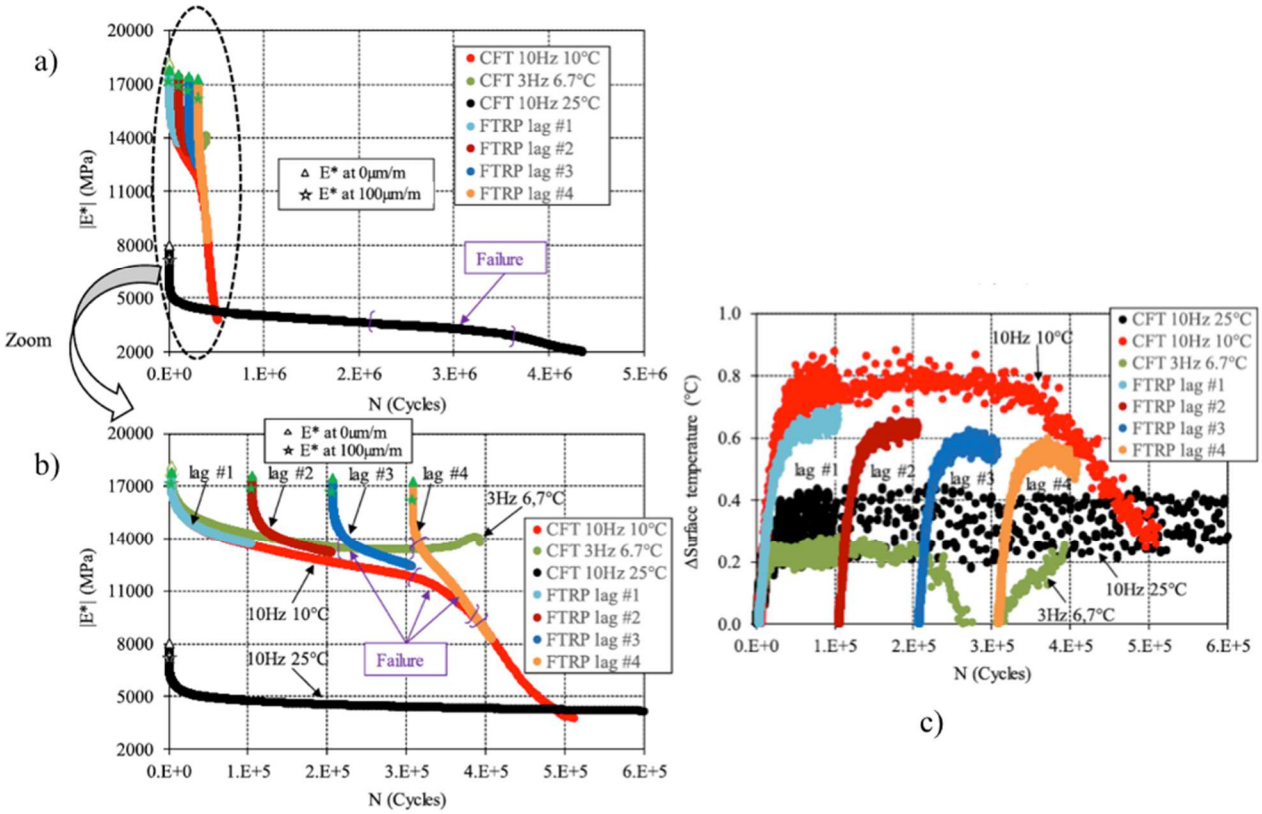

Figure 2-15. Example of time-temperature superposition principle verification for the fatigue behaviour of bituminous mixture (C. V. Phan, Di Benedetto, Sauzéat, Dayde, et al., 2017).

2.2.4.6. *Relation between bitumen, mastic and bituminous mixtures*

Experimental results available in the literature demonstrate that the time-temperature superposition observed in bituminous mixtures is similar to the one observed in the bitumen with which it is fabricated. The same time-shift coefficients (same WLF equation parameters) can be used. This also works for mastics (Delaporte et al., 2007; Di Benedetto, Olard, et al., 2004; Olard & Di Benedetto, 2003). It appears that the time-shift behaviour is inherited from the bitumen. Depending on the volume content of particles, however, a change in characteristic time for the LVE behaviour of the material is observed (Di Benedetto, Delaporte, et al., 2007).

2.2.4.7. *Non thermorheologically simple bituminous materials*

For some bituminous materials, usually presenting high degree of polymer modification, the Black diagrams and Cole-Cole plots do not form a unique curve. Hence, the TTSP is not verified when analysing the linear viscoelastic behaviour. Yet, it is possible to construct master curves for the norm of complex modulus, but the resulting phase angle master curve will present discontinuities. For some applications, this is acceptable. It is then said that the Partial Time-Temperature Superposition Principle (PTTSP) is applied (Olard, 2003; Olard & Di Benedetto, 2003).

2.3. Linear viscoelasticity for non-ageing materials

Linear viscoelastic (LVE) materials present mechanical response mixing viscous and elastic characteristics. Both purely viscous and purely elastic behaviours are linear. This means that the mechanical response obtained from a loading that can be decomposed into two parts is equal to the sum of the responses for each of these loading parts. Equivalently, this means that the Boltzmann superposition principle applies for LVE materials. For example, if the stress signal is multiplied by a certain factor, the strain needs to be multiplied by the exact same factor. While for the instant application of loading LVE materials behave as elastic solids, they may present purely viscous Newtonian behaviour at very long times of loading. As established before (cf. Section 2.2.4), equivalently, at very high loading frequencies (or low temperatures) the material behaves as elastic solid, while at very low loading frequencies (or high temperatures) the material may behave as Newtonian fluid. As it will be seen, this behaviour at high temperature may also tend to another elastic-like behaviour, which is different from the one obtained at low temperature (it is the case for bituminous mixtures, for example, where the granular skeleton is responsible for providing this high temperature elastic-like behaviour).

The LVE behaviour of materials can be characterised by different material properties, either in the time domain, or in the frequency domain. The most common material properties used to characterised elastic materials, such as modulus (E) and compliance (D, equal to $1/E$ in elasticity), Poisson's ratio (ν), shear modulus (G), among others, are also used in the characterisation of LVE materials. However, in the case of LVE materials, these properties are time-dependent (a characteristic of viscous materials, cf. Section 2.2.3), obtained when maintaining constant a loading parameter, and comparing this constant loading value with the response function. In this case, time domain properties are obtained. Experiments can also be performed using sinusoidal loading at a certain frequency. In this case, for LVE materials, sinusoidal loading and responses (at steady state) are obtained after few cycles. These sinusoidal signals can be compared, with respect to the ratio of their amplitudes, and with respect to the observed phase lag. In this case, frequency domain properties are obtained. They will be represented as complex numbers, which will contain information on both the amplitudes and phase lags relations. In this section, the main time domain and frequency domain properties are presented. Also, a brief review on LVE models used to represent them is given.

2.3.1. Experimental assessment of time domain properties

Two classical tests may be used to characterise LVE materials: the relaxation test and the creep test. In the first one (relaxation test), an instant strain is applied to the material (initially at rest), and kept constant over time. The stress signal value is observed to decrease. This is called the relaxation phenomenon. From this test, the relaxation modulus (or relaxation function, $E(t)$) is defined, as the ratio between the variable stress and the constant strain applied to the material (cf. Eq. 2-2). In the second one (creep test), an instant stress is applied to the material (initially at rest), and kept constant over time. The strain signal value is observed to increase. This is called the creep phenomenon, and consists in material flow. From this test, the creep compliance (or creep

function, *D*(t)) is defined, as the ratio between the variable strain and the constant stress applied to the material (cf. Eq. 2-3).

In the case of an elastic material, both functions reduce to constants, the Young's modulus and the elastic compliance. While for elastic materials one function is the reciprocal of the other, this is not the general case for LVE material (cf. Eq. 2-4).

$$E(t) = \frac{\sigma(t)}{\varepsilon_0} \quad ; \quad with\ \varepsilon(t) = \varepsilon_0 \quad for \quad t > 0 \qquad \text{Eq. 2-2}$$

$$D(t) = \frac{\varepsilon(t)}{\sigma_0} \quad ; \quad with\ \sigma(t) = \sigma_0 \quad for \quad t > 0 \qquad \text{Eq. 2-3}$$

$$D(t) \neq \frac{1}{E(t)} \qquad \text{Eq. 2-4}$$

2.3.2. Experimental assessment of frequency domain properties

In the frequency domain, either sinusoidal strain (with amplitude ε_0 and frequency *f*) or sinusoidal stress (with amplitude σ_0 and frequency *f*) is applied to the material as loading. In any case, the obtained response is sinusoidal after few cycles (steady state), with a phase lag corresponding to φ. The analysis of the test results can be made in complex notation. In this case, the complex modulus can be defined as the ratio between sinusoidal stress and sinusoidal strain in complex notation (cf. Eq. 2-5). The superscripts "*" indicate a complex quantity. In the equation, ω=2πf is known as the pulsation or the angular frequency. From this definition, the norm of complex modulus can be defined as the complex modulus magnitude, which presents also a phase angle (relating the imaginary and real parts of complex modulus), as in Eq. 2-6 and Eq. 2-7. For elastic materials, no phase lag is observed between stress and strain signals, and the complex modulus presents only a real part, which is equivalent to the elastic properties. The same reasoning can be done to define the complex compliance, as the ratio between sinusoidal strain and sinusoidal stress in complex notation. It is then clear that in the case of sinusoidal loading complex modulus and complex compliance are reciprocals (cf. Eq. 2-8).

$$E^* = \frac{\sigma^*}{\varepsilon^*} = \frac{\sigma_0 e^{i\omega t}}{\varepsilon_0 e^{i(\omega t - \varphi)}} = \frac{\sigma_0}{\varepsilon_0} e^{i\varphi} \qquad \text{Eq. 2-5}$$

$$|E^*| = \frac{\sigma_0}{\varepsilon_0}\ (norm\ of\ complex\ modulus)\ \ and \quad \varphi\ (phase\ angle) \qquad \text{Eq. 2-6}$$

$$E^*(\omega) = E1(\omega) + i.E2(\omega) \quad ; \quad E1 = |E^*|\cos\varphi \quad and \quad E2 = |E^*|\sin\varphi \qquad \text{Eq. 2-7}$$

$$D^* = \frac{1}{E^*} \quad \text{Eq. 2-8}$$

In sinusoidal axial loading, in addition to the axial response, a radial response is also expected due to Poisson's effect. The radial strain signal may present a phase lag with respect to the axial strain signal, represented by $\pi+\varphi_\nu$ (where π denotes that while the axial strain is decreasing – contraction - , the radial strain is increasing – extension). The same reasoning used for complex modulus can also be used to define the complex Poisson's ratio (cf. Eq. 2-9).

$$\nu^* = -\frac{\varepsilon_2^*}{\varepsilon_1^*} = -\frac{\varepsilon_{02} e^{i(\omega t-\varphi+\pi+\varphi_\nu)}}{\varepsilon_{01} e^{i(\omega t-\varphi)}} = \frac{\varepsilon_{02}}{\varepsilon_{01}} e^{i\varphi_\nu} \quad \text{Eq. 2-9}$$

If a shear loading sinusoidal test is used, then instead of an axial complex modulus, a complex shear modulus is obtained (cf. Eq. 2-10). In the equation, τ represents the shear stress and γ the shear strain applied to the material, while φ_G represents the phase lag between the two signals. In the case of isotropic behaviour, Eq. 2-11 applies (similar to elastic equation relating the corresponding elastic properties).

$$G^* = \frac{\tau^*}{\gamma^*} = \frac{\tau_0 e^{i\omega t}}{\gamma_0 e^{i(\omega t-\varphi_G)}} = \frac{\tau_0}{\gamma_0} e^{i\varphi_G} \quad \text{Eq. 2-10}$$

$$G^* = \frac{E^*}{2(1+\nu^*)} \quad \text{Eq. 2-11}$$

These experimentally determined frequency domain material properties can be analysed using different graphs. The most frequently used are:

- Cole-Cole plots, which consist in presenting data points in a diagram relating the imaginary part of complex modulus (or complex Poisson's ratio) as a function of its real part. One point in this graph represents the complex modulus, which can be seen as a vector in this representation. If the Cole-Cole plot is an orthogonal space (with same length scales corresponding to same modulus values in the y-axis and in the x-axis) the norm of complex modulus corresponds to the distance from the origin to the data point, and the phase angle to the angle between the vector and the x-axis. This representation is particularly useful to analyse the behaviour of bituminous materials at low temperatures. It can be used to verify the validity of the TTSP for the LVE behaviour.
- Black diagrams, which consist in plotting the norm of complex modulus (or complex Poisson's ratio) as a function of its phase angle. The axis of modulus is frequently represented in log scale, and in this case this representation is particularly useful to analyse the behaviour of bituminous materials at high temperatures. It can also be used to verify the validity of the TTSP for the LVE behaviour (cf. Figure 2-11).

- Isotherms, where norm of complex modulus (or complex Poisson's ratio) is plotted as a function of the tested frequency (or the tested pulsation). The same can be done with the phase angle. These curves give, at a fixed temperature, the effect of frequency on a material property.
- Isochrones, where norm of complex modulus (or complex Poisson's ratio) is plotted as a function of the tested temperature. The same can be done with the phase angle. These curves give, at a fixed loading frequency (or fixed pulsation), the effect of temperature on a material property.
- Master curves (obtained after the application of the TTSP). In this case, after verifying the validity of the TTSP, time-shift factors are used to obtain a unique curve for norm of complex modulus (or complex Poisson's ratio) and for phase angle as functions of the equivalent frequency (cf. Section 2.2.4.1). If the TTSP is valid, both curves will be unique and smooth, using the same shift factors. If only the PTTSP is valid, even if the norm of complex modulus (or complex Poisson's ratio) may be smooth and unique, the phase angle will present discontinuities.

2.3.3. Convolution integral and relationships between properties

From the application of Bolztmann superposition principle, equations relating stress and strain can be written for linear viscoelastic materials. In Eq. 2-12, a convolution integral relating the stress signal response (σ) to the applied strain history (ε) is presented. In the equation, u is a time-variable used in the integration, and $E(t)$ is the material property known as relaxation modulus. Analogously, Eq. 2-13 presents the calculation of the strain signal from the stress signal, where the material property known as the creep compliance ($D(t)$) intervenes.

$$\sigma(t) = \int_0^t E(t-u)\frac{\partial \varepsilon}{\partial u}du \qquad ; \qquad t > 0 \qquad \text{Eq. 2-12}$$

$$\varepsilon(t) = \int_0^t D(t-u)\frac{\partial \sigma}{\partial u}du \qquad ; \qquad t > 0 \qquad \text{Eq. 2-13}$$

Laplace-Carson transformation can be used to take these convolution relations written in the time domain, to algebraic relations in a transformed space (space of variable p instead of time t). In this transformed space, it can be demonstrated that the time-domain properties and frequency domain properties are intimately related. The complex modulus, for example, corresponds to the Laplace-Carson transformed of the relaxation modulus obtained at the point $p=i\omega$. It can be concluded that these material properties describe equivalently the linear viscoelastic behaviour of a material.

In Laplace-Carson transformed space, elastic-like equations are obtained. They can be used to obtain the linear viscoelastic solution to a given boundary value problem from the elastic solution

for the same problem, by taking the inverse Laplace-Carson transformation. This procedure to obtain linear viscoelastic solutions from known elastic solutions is known in the literature as the Elastic-Viscoelastic correspondence Principle (Biot, 1955).

From the application of the Bolztmann superposition principle, Eq. 2-14 can also be obtained. The equation demonstrates the relationship between relaxation modulus and creep compliance, and may be used as a tool for interconverting these material properties (obtain one of them from the other) (Park & Schapery, 1999; Tiouajni, Di Benedetto, Sauzéat, & Pouget, 2011).

$$\int_0^t E(t-u)D(u)du = t \qquad ; t > 0$$
$$\text{or} \quad \int_0^t E(t)D(t-u)du = t \qquad ; t > 0 \qquad \text{Eq. 2-14}$$

2.3.4. Discrete spectrum models

In this section, some LVE models available in the literature are presented. Focus is given to models based on mechanical analogues (associations of springs and dashpots) presenting discrete spectra. After, Figure 2-16 shows schematically the presented models.

2.3.4.1. *Springs and Dashpots*

A spring (cf. Figure 2-16a) is a purely elastic mechanical analogue, characterised by its modulus E. This modulus appears as a constant term in the complex modulus of the spring, in its relaxation modulus or in its creep compliance ($1/E$).

$$\sigma = E\varepsilon \qquad \text{Eq. 2-15}$$

2.3.4.2. *Dashpot*

A dashpot (cf. Figure 2-16b) is a purely viscous mechanical analogue, characterised by its Newtonian viscosity η. It appears in creep compliance with the flow term t/η, but does not appear in relaxation modulus functions, since the purely viscous material relaxes stress instantly (it may appear just as a punctual contribution, explicitly formulated with a Dirac delta).

$$\sigma = E\dot{\varepsilon} \qquad \text{Eq. 2-16}$$

2.3.4.3. *Generalised Kelvin-Voigt (GKV) model*

The Generalised Kelvin-Voigt (GKV) model consists in the association in series of spring-dashpot pairs linked in parallel (cf. Figure 2-16d). Its creep compliance is given analytically by Eq. 2-17, for a GKV model with *n* viscoelastic elements. Its complex modulus is given by Eq. 2-18. In both cases, no free dashpot element was included, which is the general case for the GKV model. However, in bituminous mixtures modelling, these free viscosity elements are seldom used (it is also not the case in this thesis). For a given viscoelastic element *j* in the model, τ_j represents the ratio between the dashpot viscosity η_j and the spring modulus E_j, and is a characteristic time for this element.

$$D(t) = \frac{\varepsilon(t)}{\sigma_0} = \frac{1}{E_\infty} + \sum_{j=1}^{n} \frac{1}{E_j}(1 - e^{-t/\tau_j}) = D_g + \sum_{j=1}^{n} D_j(1 - e^{-t/\tau_j}) \qquad \text{Eq. 2-17}$$

$$E^*(\omega) = \left(\frac{1}{E_0} + \sum_{j=1}^{n} \frac{E_j}{E_j^2 + i\omega\tau_j} \right)^{-1} \qquad \text{Eq. 2-18}$$

2.3.4.4. *Generalised Maxwell-Wiechert (GMW) model*

The Generalised Maxwell-Wiechert (GMW) model consists in the association in parallel of spring-dashpot pairs linked in series (cf. Figure 2-16e). Its relaxation modulus is given analytically by Eq. 2-19. Its complex modulus is given by Eq. 2-20. In both cases, no free dashpot element was included, which is the general case for the GMW model. However, in bituminous mixtures modelling, these free viscosity elements are seldom used (it is also not the case in this thesis). For a given viscoelastic element *j* in the model, ρ_j represents the ratio between the dashpot viscosity η_j and the spring modulus E_j, and is a characteristic time for this element.

$$E(t) = \frac{\sigma(t)}{\varepsilon_0} = E_0 + \sum_{j=1}^{n} E_j . e^{(-t/\rho_j)} \qquad \text{Eq. 2-19}$$

$$E^*(\omega) = E_0 + \sum_{j=1}^{n} E_j \frac{i\omega\rho_j}{1 + i\omega\rho_j} \qquad \text{Eq. 2-20}$$

2.3.4.5. *Interconversion between linear viscoelastic properties from models*

Using the Boltzmann superposition principle, it is possible to derive relationships between the presented rheological models (cf. 2.3.3). Approximate relationships are available in the literature to obtain a GKV model from a GMW and vice-versa (Park & Schapery, 1999; Tiouajni et al., 2011).

2.3.5. Continuum spectrum models

In this section, some LVE models available in the literature are presented. Focus is given to models based on mechanical analogues presenting continuous spectra. After, Figure 2-16 shows schematically the presented models with more details on the 2S2P1D model.

2.3.5.1. *The parabolic element*

A parabolic element (cf. Figure 2-16c) is a mechanical analogue presenting creep compliance of the form given in Eq. 2-21, where a, τ and h are model constants, with τ the characteristic time. No explicit expression of the relaxation modulus is available. The parabolic element's complex modulus (given in Eq. 2-22) can be obtained by applying the convolution integrals in Eq. 2-14. In Eq. 2-22, $\Gamma(1+h)$ is the Gamma function (cf. Eq. 2-23) applied to the argument $(1+h)$.

$$D(t) = a\left(\frac{t}{\tau}\right)^h \qquad \text{Eq. 2-21}$$

$$E^*(\omega) = \frac{(i\omega\tau)^h}{a.\Gamma(1+h)} \qquad \text{Eq. 2-22}$$

$$\Gamma(n) = \int_0^\infty x^{n-1}e^{-x}dx \quad , \quad n > 0 \qquad \text{Eq. 2-23}$$

2.3.5.2. *Huet model and Huet-Sayegh model*

The Huet model (Huet, 1963) present two parabolic elements and a spring, all associated in series. The two parabolic elements (1 and 2) have creep compliances given in Eq. 2-24. The compliance of the Huet model is given by Eq. 2-25 and its complex modulus by Eq. 2-26. No explicit expression of the relaxation modulus is available. Due to the use of only one purely elastic constant, this model cannot model correctly the asymptotic elastic behaviour of bituminous mixtures at high temperature and low frequency.

$$D_1(t) = a\left(\frac{t}{\tau}\right)^h \quad \text{and} \quad D_2(t) = b\left(\frac{t}{\tau}\right)^k \qquad \text{Eq. 2-24}$$

$$D(t) = \frac{1}{E_0}\left[1 + \delta\frac{\left(\frac{t}{\tau}\right)^k}{\Gamma(1+k)} + \frac{\left(\frac{t}{\tau}\right)^h}{\Gamma(1+h)}\right] \quad \text{Eq. 2-25}$$

$$E^*(i\omega\tau) = \frac{E_0}{1 + \delta(i\omega\tau)^{-k} + (i\omega\tau)^{-h}} \quad \text{Eq. 2-26}$$

In order to solve the lack of ability of the Huet model to represent the high temperature asymptotic behaviour of bituminous mixtures, the Huet-Sayegh model (Sayegh, 1965) includes a spring associated in parallel with the Huet model. No explicit expression is available for the relaxation function or for the creep compliance. The complex modulus of the Huet-Sayegh model is given by Eq. 2-27.

$$E^*(i\omega\tau) = E_{00} + \frac{E_0 - E_{00}}{1 + \delta(i\omega\tau)^{-k} + (i\omega\tau)^{-h}} \quad \text{Eq. 2-27}$$

2.3.5.3. *2S2P1D model*

Although the Huet-Sayegh model may rather well represent the LVE behaviour of bituminous mixtures, it cannot represent asymptotic viscous behaviour, such as observed experimentally for neat bitumen. In order to improve that, a viscosity term has been added to the Huet-Sayegh model, as represented in Figure 2-16f. 2S2P1D model's complex modulus is reported in Eq. 2-28, where complex modulus E^* is expressed as a function of pulsation ω (ω = 2π*f*, where *f* is the loading frequency). The seven parameters needed to calibrate the model are:

- E_{00}, the asymptotic static modulus (when $\omega \to 0$)

- E_0, the asymptotic glassy modulus (when $\omega \to \infty$)

- *h* and *k*, dimensionless constants of the two parabolic elements (related to, respectively, initial and final slopes of complex modulus curve in Cole-Cole plot)

- *δ*, a dimensionless shape factor

- *τ*, a characteristic time and the only parameter depending on temperature

- *β*, dimensionless parameter related to the viscosity *η* of the linear dashpot ($\eta=(E_0-E_{00})\beta\tau$).

The characteristic time *τ* can be obtained at any temperature by applying the time-shift factors, as in Eq. 2-29. This is done using its value τ_0 at a reference temperature Tref and the time-temperature shift factor at the temperature *T*, $a_T(T)$. This rule to obtain time-shifted characteristic times can be used with any of the LVE mechanical analogues presented here, which is compatible

with the assumption of thermorheologically simple materials (Ferry, 1980; Gross, 1968). The WLF equation may be used (cf. Section 2.2.4.1).

$$E^*(i\omega\tau) = E_{00} + \frac{E_0 - E_{00}}{1 + \delta(i\omega\tau)^{-k} + (i\omega\tau)^{-h} + (i\omega\beta\tau)^{-1}} \quad \text{Eq. 2-28}$$

$$\tau(T) = a_T(T)\tau_0 \quad \text{Eq. 2-29}$$

The 2S2P1D model is suitable for modelling bitumen, mastic and bituminous mixtures linear viscoelastic behaviours (Delaporte et al., 2007; Di Benedetto, Olard, et al., 2004; Olard & Di Benedetto, 2003). There is no explicit analytical expression for the creep compliance or for the relaxation function of the 2S2P1D model. Then, a discretisation of its spectrum is necessary. The discretisation procedure consists of finding a *n*-element GKV model, which gives approximately the same complex modulus results as the 2S2P1D model. This is done by fitting a GKV model to the 2S2P1D model complex modulus (Pouget, Sauzéat, Di Benedetto, & Olard, 2012b; Tiouajni et al., 2011). An approximated analytical expression for the creep compliance can then be obtained. If the relaxation function is needed, an interconversion of properties is used (Tiouajni et al., 2011). The model has also been extended for the three-dimensional case, including the modelling of the complex Poisson's ratio (Di Benedetto, Delaporte, et al., 2007). A thorough application of the model has been presented for the viscoelastic analysis of the Millau Bridge, in France (Pouget, 2011). It is to be observed that, since theoretically a GKV or a GMW model with an infinite number of elements (continuous spectrum) represents the LVE behaviour of a real material (Biot, 1954), the 2S2P1D model is the closest presented representation of the real material behaviour. This representation is given with a fixed number of model parameters: 7 2S2P1D model constants, plus 3 WLF equation constants (10 in total for 1D modelling), and possibly 3 more constants for the 3D case describing also the Poisson's ratio (13 in total for 3D modelling). The three constants needed for 3D modelling are the asymptotic Poisson's ratio values at low and high temperatures (ν_0 and ν_{00}) and possibly a factor accounting for a different characteristic time between the complex modulus and the complex Poisson's ratio. Eq. 2-30 presents the equation to obtain the 2S2P1D model complex Poisson's ratio (combined with Eq. 2-27), in the case where characteristic times are coincident. In the cases where the characteristic time for the complex Poisson's ratio cannot be assumed as the same as for the complex modulus for bituminous mixtures, a simple factor multiplying the characteristic time of complex modulus can be used to obtain the characteristic time of Poisson's ratio (Pham, Sauzéat, Di Benedetto, et al., 2015).

$$\nu^*(\omega) = \nu_{00} + (\nu_0 - \nu_{00})\frac{E^*(\omega) - E_{00}}{E_0 - E_{00}} \quad \text{Eq. 2-30}$$

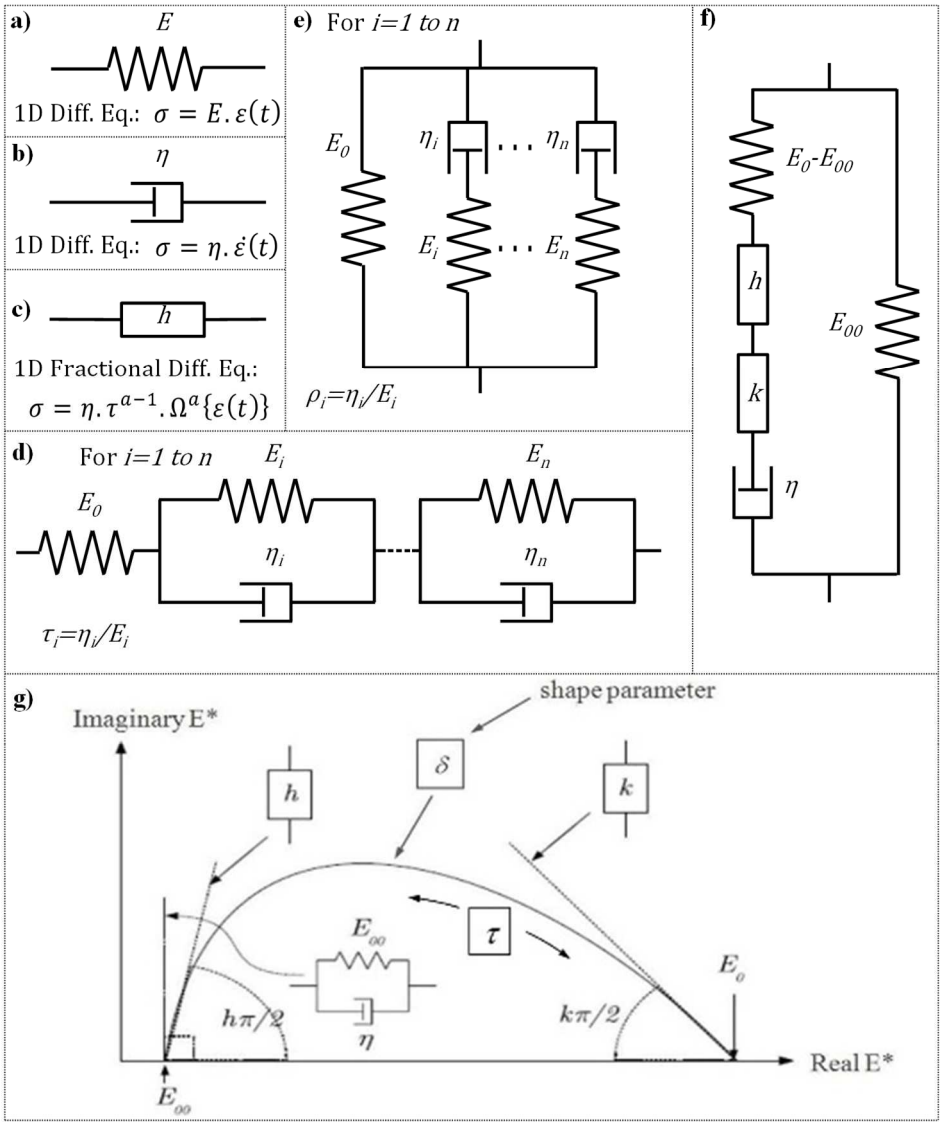

Figure 2-16. Mechanical analogues - a) spring, b) dashpot, c) parabolic element, d) GKV, e) GMW, f) 2S2P1D – and g) 2S2P1D model interpretation in Cole-Cole plot (Specht et al., 2017).

2.3.6. Normalised complex modulus and SHStS transformation

Literature demonstrates that the linear viscoelastic behaviour of bituminous materials (mixtures and mastics) is intimately related to the linear viscoelastic behaviour of the bitumen used in their fabrication (Delaporte et al., 2007; Di Benedetto, Delaporte, et al., 2007; Di Benedetto, Olard, et al., 2004; Olard & Di Benedetto, 2003). Using a normalisation procedure (as in Eq. 2-31), it can be shown that unique curves are obtained for all bituminous materials produced with a given bitumen (cf. example in Figure 2-17). This provides a means to obtain the LVE properties of a bituminous material from the LVE properties of another one containing the same bitumen (Delaporte et al., 2007; Di Benedetto, Olard, et al., 2004; Pouget, Sauzéat, Di Benedetto, & Olard, 2012a; Pouget et al., 2012b). The method is independent of any rheological model. It is called Shift-Homothety-Shift in time-Shift (SHStS) presented schematically in Figure 2-18.

$$E^*_{normalised} = \frac{E^* - E_{00}}{E_0 - E_{00}} \qquad \text{Eq. 2-31}$$

Figure 2-17 presents experimental results for normalised complex modulus (Cole-Cole plot in figure a, and Black diagram in figure b) and complex Poisson's ratio (master curve in figure c) (Pham, Sauzéat, Di Benedetto, et al., 2015). A coincidence of the normalised parameters (modulus or Poisson's ratio) is obtained for all materials.

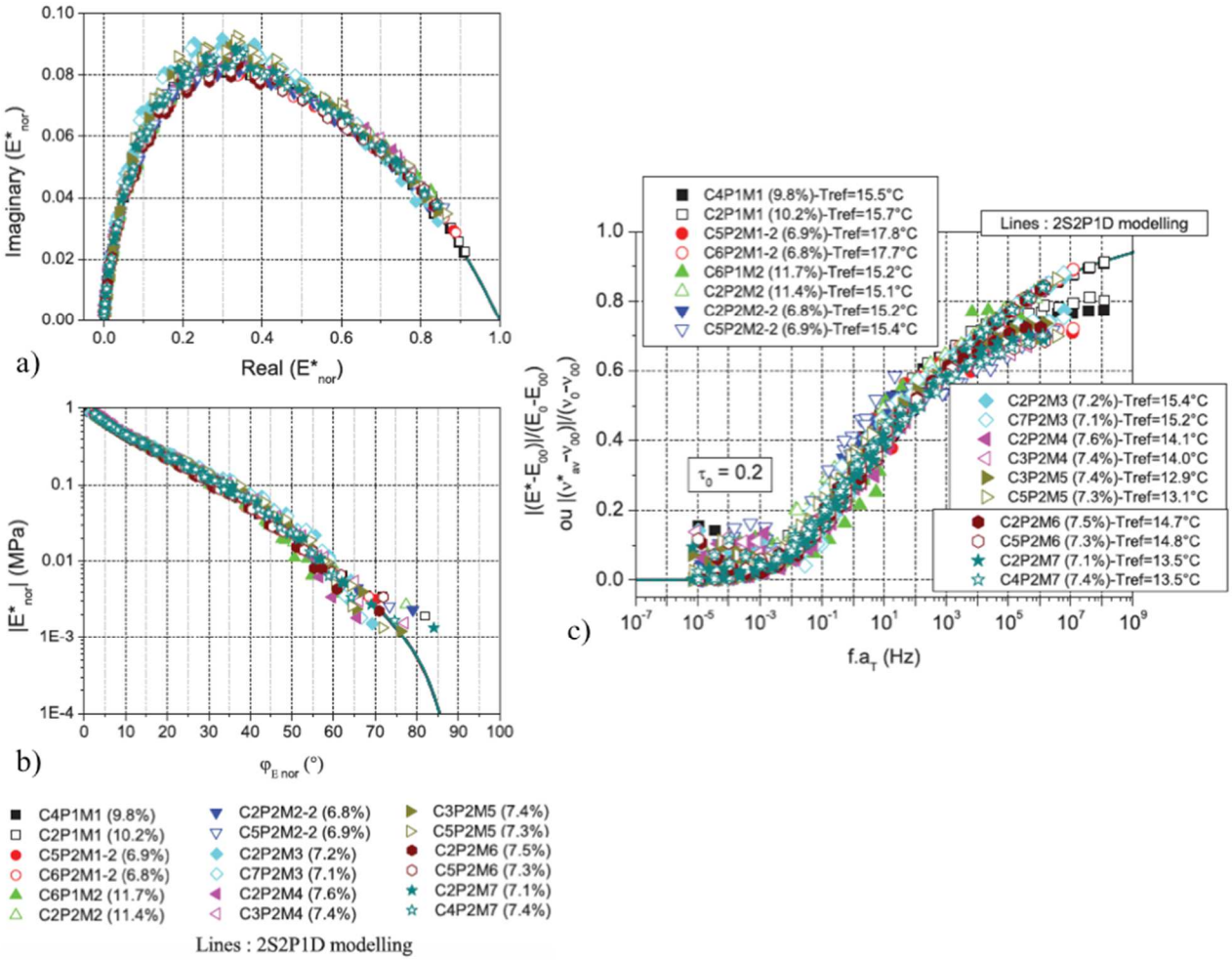

Figure 2-17. Example of coincidence of various normalised complex modulus curves from linear viscoelastic characterisation of different bituminous materials containing the same base bitumen (Pham, Sauzéat, Di Benedetto, et al., 2015). Nine materials, differing with respect to the manufacturing process, fabrication temperature, the percentage of Recycled Asphalt Pavement (RAP), the use of additives and the air void content.

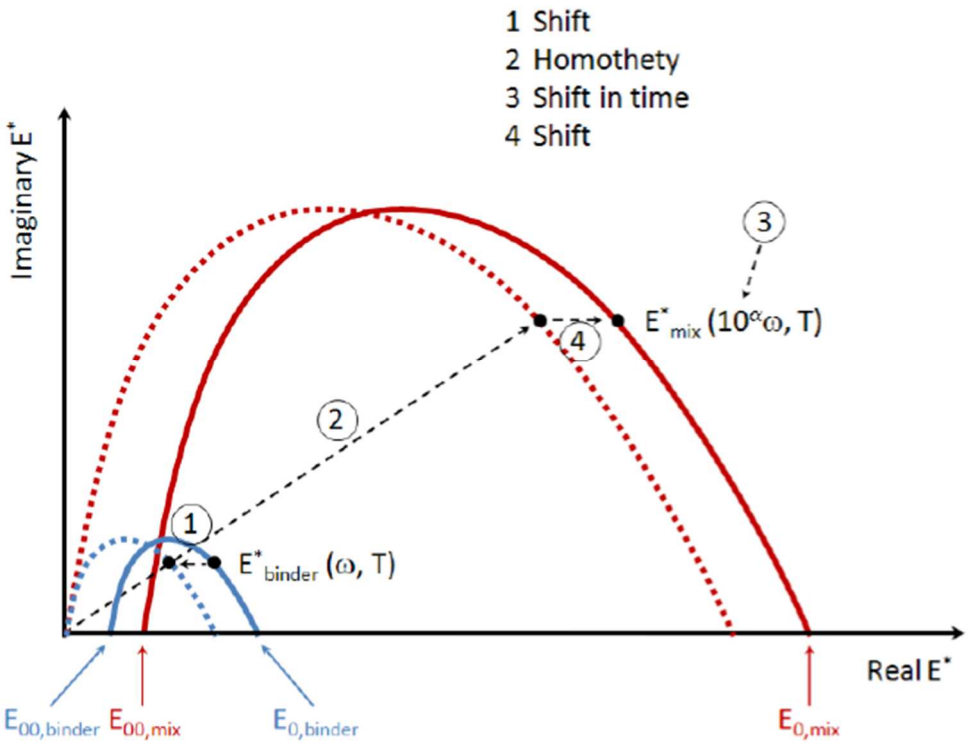

Figure 2-18. Schematic representation of the SHStS transformation (Mangiafico, 2014).

Using the SHStS transformation, literature demonstrates that bituminous mixture LVE behaviour can be obtained from LVE behaviour of bitumen (which is easier to obtain in laboratory with less costly procedures). Figure 2-19 presents an example of the estimation of bituminous mixture LVE behaviour from bitumen LVE behaviour (Mangiafico, 2014), as determined from two experimental procedures: tests with the Dynamic Shear Rheometer (DSR, that works in torsional shear) and tests with the *Métravib* (that works in axial tension-compression).

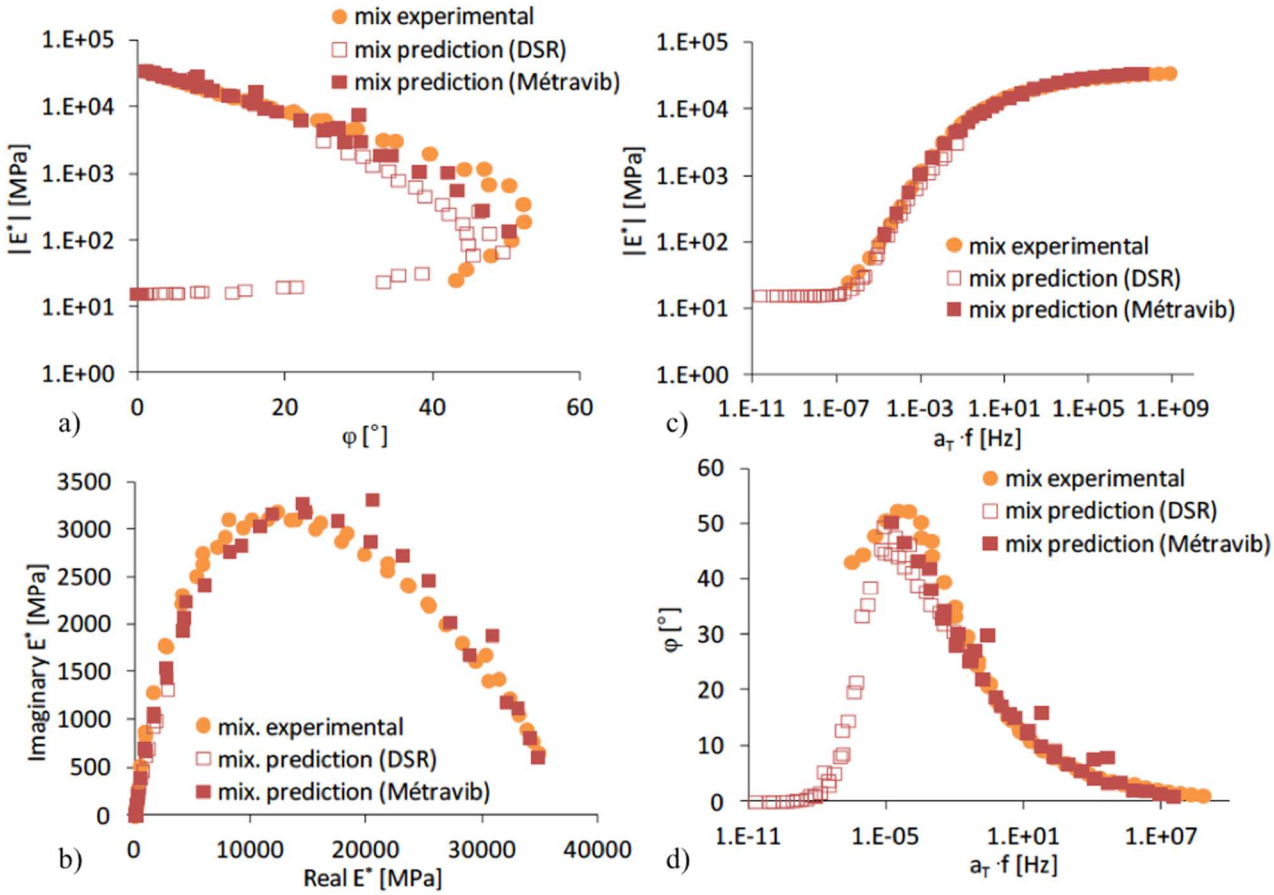

Figure 2-19. Example of bituminous mixture prediction using the SHStS transformation and bitumen linear viscoelastic characterisation from two different experimental procedures (using the Dynamic Shear Rheometer and using the *Métravib*) (Mangiafico, 2014).

2.4. Nonlinear viscoelasticity

2.4.1. Equivalent complex modulus as a function of loading amplitude

During approximately the 3 first sinusoidal cycles in bituminous materials, transient effects are still non negligible and a steady state cannot be assumed (Gayte et al., 2016). This is a consequence of the LVE behaviour of the bituminous material, and non-negligible distortion with respect to a sinusoidal function should be expected in the measured stress/strain signals. Hence, during these first cycles the experimental result for complex modulus is not a reliable measurement of the complex modulus.

After the referred first few cycles, many physical phenomena may influence the material response during cyclic loading, such as nonlinearity, self-heating, thixotropy and damage (Coutinho et al., 2014; Di Benedetto et al., 1996; Di Benedetto, de La Roche, et al., 2004; Di Benedetto, Olard, et al., 2004; Gauthier et al., 2010; Gayte et al., 2016; Mangiafico, 2014; Mangiafico et al., 2015, 2017; Q. T. Nguyen, 2011; Q. T. Nguyen et al., 2015; C. V. Phan, Di Benedetto, Sauzéat, Dayde, et al., 2017; Riahi et al., 2017; Soltani & Anderson, 2005). During a given cycle, however, the effects of self-heating, thixotropy and damage may usually be neglected,

i.e. their effects may be considered as constant during the period of one loading cycle, not distorting the sinusoidal signal. However, the effect of nonlinearity (strain dependence of material response) could still influence the measured signals, which could deviate from sinusoidal functions for strong nonlinearity. As it will be seen in this work, the measured signals during tests on bituminous materials at different amplitudes can still be well approximated by sinusoidal functions for small nonlinearity. Then, using the same signal treatment as for the determination of a "very small strain" complex modulus, the "equivalent" complex modulus is obtained from experiments (or "apparent" complex modulus, as in (Gauthier et al., 2010).

The equivalent complex modulus may be dependent on strain (nonlinearity), and on the number of applied of loading cycles (cyclic effects such as thixotropy and damage). Hence, the variation in equivalent complex modulus may be an indicator of the contributions of different physical phenomena (transient effects, physical nonlinearity, self-heating, thixotropy and damage). These phenomena (including self-heating) induce an apparently nonlinear response in the material with respect to its stress and strain signals (if the analysis is done considering an isothermal test).

Rigorously, in the case of nonlinear viscoelasticity the complex modulus could not be defined. Moreover, since the Boltzmann superposition principle does not apply, the relationship between the complex modulus and time-domain material properties cannot be derived (cf. 2.3.3). However, the equivalent complex modulus may be used as a parameter to interpret the mechanical behaviour of bituminous materials, with small nonlinearity (inducing negligible distortion in sinusoidal signals).

It is to be observed that the vast majority of practitioners and researchers in the domain of bituminous materials assume that the equivalent complex modulus remains constant in the so called "small strain domain" (where LVE behaviour would be obtained, cf. Figure 2-4 and Figure 2-5), fixed approximately below strain amplitude of 100μm/m for bituminous mixtures and between 1% and 10% for bitumen (cf. Figure 2-6) (Airey & Rahimzadeh, 2004; Airey et al., 2002, 2003). In this thesis, an investigation questions the validity of that assumption (cf. Chapter 4), by obtaining experimentally a quantification of material nonlinearity with respect to strain amplitude. In this investigation, results obtained from tests carried out at varying strain amplitude are analysed in terms of equivalent complex modulus, called sometimes just "complex modulus" (as in the literature) for simplicity.

As presented in the literature (Mangiafico, 2014; Mangiafico et al., 2015; Q. T. Nguyen, 2011; Q. T. Nguyen et al., 2015), due to the servo-control systems of hydraulic presses used for testing bituminous mixtures, some tens of cycles are sometimes needed before reaching the desired strain amplitude of a test. Then, since strain amplitude is increasing, the measured complex modulus will change as a consequence of nonlinearity. (Delaporte, 2007) recommended using small sinusoidal tests in order to verify linearity conditions before testing bitumen and mastic for its LVE properties (complete complex modulus test).

2.4.2. Mathematical formulations for nonlinear viscoelastic behaviour

General theories of nonlinear viscoelasticity, which may be applied to any material, based on stress-strain relationships written as sums of multiple integrals are found in the literature (Green & Rivlin, 1957; Green, Rivlin, & Spencer, 1997; Lockett, 1965, 1972; Rivlin, 1965). In the case of linear viscoelasticity, only one integral was necessary (cf. Section 2.3.3). Due to the complexity of the nonlinear viscoelastic models presenting multiple integrals, to the fact that many kernel functions need to be experimentally determined (which may require prohibitive testing efforts), and to the difficulty to extract a physical interpretation of these parameters, these general models need to be simplified. This can be done by taking advantage of certain aspects of the behaviour of certain materials such as bituminous materials (Schapery, 1969), with sufficient accuracy for engineering applications (Delgadillo, Bahia, & Lakes, 2012; Findley, Lai, & Onaran, 1976). Single integral models can be obtained from this simplification process (Findley et al., 1976; Pipkin & Rogers, 1968; Schapery, 1969). This is done by assuming that time and frequency dependence in the nonlinear range can be expressed in terms of linear viscoelastic properties, and leads to a single integral nonlinear model that is very similar in form to the convolution integral used in linear viscoelasticity. In the referred models, additional material functions taking into account the influence of the applied strain (or the applied stress) appear in the equations, and need to be experimentally determined. In Schapery's model, for example, 4 new material functions need to be determined: 3 for stress/strain influence on the mechanical response and 1 for modified time-temperature superposition due to nonlinearity.

2.5. Fatigue damage

Damage can be investigated following two classical methods: the michomechanics approach, and the continuum mechanics approach. While the first tries to model in details each phenomenon at the microstructural scale and tries to recompose the material scale behaviour (observed in experiments) from this perspective, the latter makes experimental observations directly on the material scale, and proposes phenomenological explanations. As it will be seen in this thesis, relevant complexity is associated to the combined effects of the different phenomena occurring during cyclic loading of bituminous materials. Moreover, computational costs still make micromechanical models to be prohibitive sometimes, even with models not including all the physical aspects of bituminous mixtures. Due to these reasons, correct micromechanical modelling of bituminous mixtures considering the different phenomena presented in this thesis seems to still require improvement. Micromechanical damage models are not in the scope of this thesis.

In continuum damage mechanics, damage is seen as the loss of resistant cross-section in the material (Kachanov, 1958, 1986; Lemaître & Chaboche, 1990). Due to this loss of resistant cross-section, a loss in apparent stiffness is expected. This apparent loss in stiffness is measurable in laboratory and can be used as a means to characterise the damage state of a material.

The loss of resistance- cross-section in the material happens as a consequence of the application of loading, not necessarily the maximum load that the material is able to bear without breaking. Eventually, failure comes from the repetition of these loads, which individually could

not produce failure in the material. In this case of damage produced by the repetition of loads, the term fatigue is used (Poncelet, 1839). Fatigue damage accumulation rate depends on the applied stress levels (Wöhler, 1870).

2.5.1. Experimental observations

In bituminous materials, during the so-called fatigue tests, where continuous cyclic loading is applied, the norm of complex modulus is observed to decrease, in three distinct phases: Phase I, Phase II, and Phase III (Baaj, Di Benedetto, & Chaverot, 2003; Di Benedetto et al., 1996; Di Benedetto, de La Roche, et al., 2004). In Figure 2-20, strain-controlled homogeneous (tensions-compression) fatigue test results are presented (Nouffou Tapsoba, 2011). These phases can be conceptually separated as follows.

- Phase I: rapid nonlinear decrease in norm of complex modulus and increase in phase angle. In this phase, temperature also increases rapidly. It appears that fatigue damage is not the predominant phenomenon producing effects on the observed complex modulus change.
- Phase II: a quasi-linear decrease in norm of complex modulus is observed over the cycles. Phase angle also increases, but less than during Phase I, despite the much greater number of applied cycles in this example. Temperature stopped increasing (it slightly decreases). During Phase II, fatigue damage contributes to material deterioration. Microcracks are distributed in the material volume and continuum mechanics is still accurate in the description of the phenomenon.
- Phase III: perturbations in the measured complex modulus trends are observed (both in modulus and in phase angle). Microcracks probably coalesced into a macrocrack, and continuum mechanics is no longer accurate in the description of the phenomenon. Although it is hard to distinguish precisely when did coalescence happened, this transition between Phase II and Phase II is usually considered as fatigue failure (cf. Section 2.6).

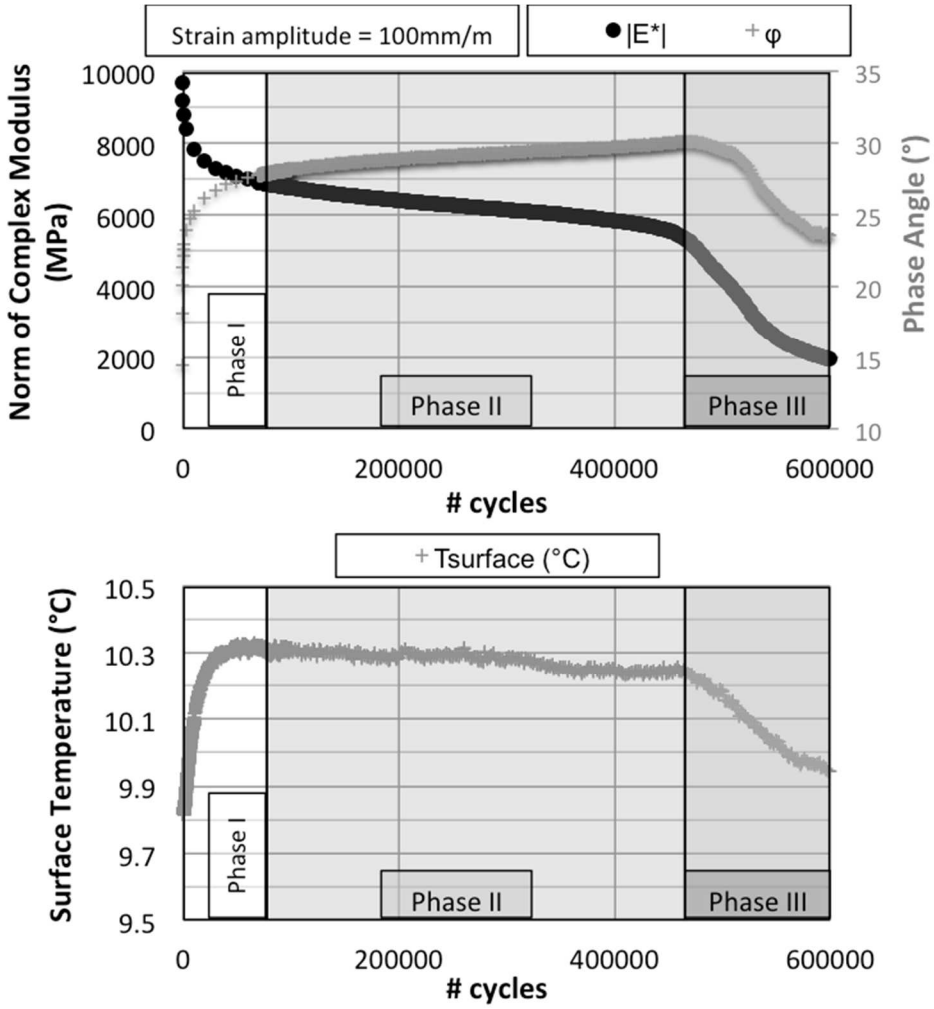

Figure 2-20. Example of bituminous mixture fatigue test experimental data (Nouffou Tapsoba, 2011): norm of complex modulus and phase angle (above), and measured surface temperature (below).

2.5.2. Damage modelling

Damage modelling involves predicting the evolution of the damage state of a material during its service life. From experiments, the damage state (as represented for example as a relative loss in resistant cross-section area) is not measurable directly. Then, damage models usually model the stiffness evolution with loading. Damage models based on dissipated strain energy (K. A. Ghuzlan & Carpenter, 2006; K. Ghuzlan & Carpenter, 2000; Shen et al., 2006), on Schapery's Work Potential theory (Y. R. Kim, 2009; Y. R. Kim et al., 1997; H.-J. Lee & Kim, 1998; Lundström et al., 2004; Lundstrom & Isacsson, 2003; Park, Kim, & Schapery, 1996; Park & Schapery, 1997; Schapery, 1991; B. Underwood et al., 2012; B. Underwood & Kim, 2013; B. S. Underwood, 2016), or on a series of constitutive models (hypothesised, than fitted to experimental results) (Rashid K. Abu Al-Rub, Darabi, Masad, & Little, 2011; M. Darabi et al., 2013; M. K. Darabi, Abu Al-Rub, Masad, & Little, 2013; Masad, Al-Rub, & Little, 2012; Masad, Tashman, Little, & Zbib, 2005; You, Masad, Al-Rub, Kassem, & Little, 2014) are available in the literature. These models are used to predict stiffness evolution (translated into damage) for a given loading history. However, the referred analysis procedures consider that all loss in norm of complex modulus

during tests is due to damage, and modulus recovery can only come from another irreversible phenomenon, called self-healing, producing opposite effect with respect to damage. Although all referred models seem somewhat to accurately fit experimental results in terms of modulus change, the problem is that the modulus change in experiments does not come only from damage. More dramatically, careful analysis of experimental results seem actually to demonstrate that damage is the phenomenon producing less modulus change in the material (Mangiafico, 2014; Q. T. Nguyen, 2011) during continuous cyclic loading. Then, if in the field, bituminous mixtures do not experience other phenomena such as thixotropy or self-heating due to long rest periods and few applications of loading (not continuous loading), the ability of the referred models to predict field fatigue damage seems compromised.

In order to account for these biasing phenomena in the analysis of damage from laboratory fatigue tests, the ENTPE/University of Lyon proposed a damage model (Baaj, 2002; Baaj et al., 2003, 2005; Di Benedetto, de La Roche, et al., 2004; N. Tapsoba et al., 2015). This method, called D_{IIIC}, describes the evolution of "real" damage (evaluated for cycles where the other phenomena reached a state where no further change in complex modulus is expected) with the number of cycles.

2.6. Failure

Another aspect investigated when it comes to fatigue damage of bituminous materials is failure. As previously commented (cf. Section 2.5.1), after a certain damage accumulation in the material, a macrocrack may appear, and perturb measurements of force and displacement, altering complex modulus during the test. This is believed to occur between Phase II and Phase III. The investigation of failure in laboratory is of great importance to the asphalt community, since laboratory failure (from fatigue tests) is related to field fatigue failure of the bituminous mixtures layers in pavements. This link between lab results and field results is still an important aspect of investigation in the asphalt community. In this thesis, only laboratory fatigue failure is investigated, since the investigation is focused on bitumen and bituminous mixtures at the material level.

2.6.1. Experimental observations

A precise determination of the cycle where macrocrack coalescence occurs is a difficult task. As seen before, changes in the complex modulus evolution trend are observed during fatigue tests (cf. Figure 2-20). These changes are an indication of fatigue failure, but they are influenced by other phenomena occurring during fatigue tests. Different criteria are proposed in the literature to determine fatigue failure, frequently related to the measured complex modulus evolution in the fatigue test. Some of the available criteria in the literature are given next.

- The most commonly used criterion for fatigue failure is a fixed change in norm of complex modulus. The value of 50% change in modulus decrease is used in most standards for fatigue analysis (NF EN 12697-24, 2012). This method neglects the

influence of other phenomena (which may be material-dependent) on the measured complex modulus. This also neglects the possibility that different materials could bear different damage accumulations without failing.

- By observing the trends of evolution of norm of complex modulus and phase angle, it is possible to detect a change in trend between Phase II and Phase III. Some authors use the peak phase angle as an indication of fatigue failure. However, if failure does not occur in between strain measurements, this peak phase angle may not be visible. Other authors propose to look for the second inflection point in the norm of complex modulus evolution (Y.-R. Kim, Little, & Lytton, 2003). This observation is usually in near the peak phase angle, when the latter is visible. Since temperature evolves during the tests, with cooling during Phase II in the case of strain-controlled tests (cf. Figure 2-20), and possibly other phenomena also induce changes in the phase angle, it is not clear that the peak phase angle is precisely associated with crack coalescence. Still, searching for changes in the trends of evolution of norm of complex modulus and phase angle seems a reasonable method.
- Observing the trend of evolution in other material parameters, such as dissipated energy, is also presented in the literature as a means to determine the number of cycles at fatigue failure (Hopman, Kunst, & Pronk, 1989). Since dissipated energy is calculated from norm of complex modulus and phase angle, this method keeps actually a fundamental similarity with the last one.
- Observing the trend of evolution of other parameters, such as the norm of complex modulus (or material integrity) multiplied by the number of cycles (Safaei, Castorena, & Kim, 2016). Yet, some relation between this method and the second one appear, but this time a test parameter (number of cycles) intervenes on the calculated parameter.

In order to avoid the influence of the other phenomena on the determination of failure, it is possible to look into “local” measurements in the tested specimen, such as each of the extensometers strain amplitudes (Baaj, 2002; Soltani, 1998). While during Phase I and Phase II, all extensometers strain amplitude measurements (usually three of them) are near the average strain amplitude, during Phase III these measurements may diverge very fast, giving a method to determine fatigue failure.

2.6.2. Failure modelling

After failure (fatigue life) is determined from tests, at different stress/strain levels, models relating the application of repeated loads and the fatigue life consumption (ratio between the number of already applied cycles and the number of cycles at failure for a given stress/strain amplitude) are useful for performance prediction. Some models in the literature try to relate fatigue failure to a material parameter measured during the test (K. A. Ghuzlan & Carpenter, 2006; K. Ghuzlan & Carpenter, 2000; Sabouri & Kim, 2014; Shen et al., 2006), such as the minimum rate of change in the dissipated energy. Yet, the main purpose of this modelling procedure is to predict

when failure is expected. For this Wöhler curves and Miner's hypothesis (Miner, 1945; Palmgreen, 1924) are classically used.

2.6.2.1. *Whöler curves and Miner's law*

Wöhler curves relate the fatigue life (number of cycles expected at failure) to the loading level (stress amplitude, strain amplitude or other parameters of this type). Figure 2-21 presents schematically an example of Wöhler curve fitted to experimental data (Di Benedetto & Corté, 2005). Each data point is obtained from a laboratory fatigue test at a different loading level.

In the field, each vehicle loading corresponds to a loading level in the Wöhler curve. Then, for this loading, a certain number of cycles at failure is expected. According to Miner's hypothesis, all loading cycles at a given loading level consume the same amount of fatigue life of the material. Then, with this simple hypothesis, it is possible to predict fatigue life for a more complex distribution of loading levels. This idea can be used for design purposes. Alternatively, (S. Carpenter et al., 2003) propose that under a certain loading level, fatigue life tends to infinite. Then, if a pavement structure is designed to present loading level in the bituminous mixture layer under this value, it should not present fatigue failure. This concept is known in the literature as perpetual pavement.

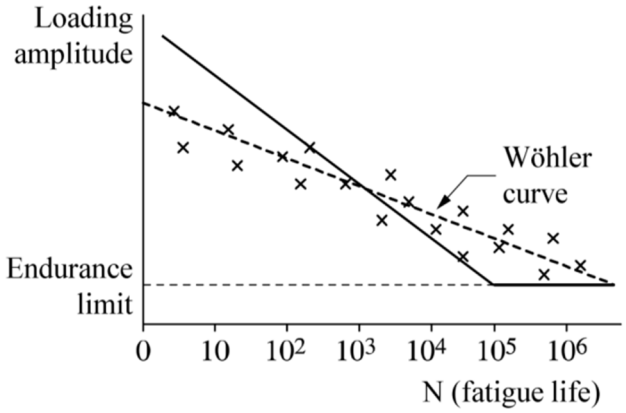

Figure 2-21. Relationship between loading amplitude and number of cycles at fatigue (fatigue life) (Di Benedetto & Corté, 2005). The figure presents schematically two different approaches: fitting Wöhler curve to describe this dependence, or searching for a "endurance limit" (S. Carpenter et al., 2003), which is the loading amplitude below which an infinite fatigue life would be expected.

2.7. Thixotropy

Some fluids present viscosity (or, more generally, for other materials, stiffness) that depends on the applied shear rate (or, more generally, strain level). In fluids rheology, if viscosity decreases with an increase in shear rate, this behaviour is called shear-thinning. If this change in viscosity occurs over time, and is reversible after rest is applied, this behaviour is called thixotropy . All

liquids with microstructure can show thixotropy (Barnes, 1997). These materials are usually shear-thinning. Shear thinning occurs due to many reasons, such as alignment of elongated particles in the flow direction, loss of junctions in polymer solutions, rearrangements of microstructure in suspension and emulsion and breakdown of flocs (which is reversible) (Barnes, 1997). If a finite time is required for these changes in the microstructure to happen, then thixotropy is observed at the material level, because changes in the measured viscosity will be observed over time. Thixotropy can be seen as the succession of metastable equilibrium states of the material microstructure, as a result of the combination of two sub-phenomena: breakdown and build-up of microstructure. Breakdown occurs as a result of the applied loading, and the more loading is applied, more microstructure breakdown is expected, until the equilibrium with the sub-phenomena of build-up. Build-up may be a result of Brownian motion (or other phenomena), which tends to rebuild the microstructure. Figure 2-22 presents schematically different metastable states for the microstructure of a material obtained after shearing and after resting. Figure 2-23 presents a typical schematic test result on a thixotropic material, from experiments with continuous shear separated in different blocks, each one with a different shear level ("step experiments"). As a result of the combination of breakdown and build-up of the microstructure, different equilibrium levels of shear stress are expected from the application of constant shear rate. The change from an equilibrium state to the other occurs over time. A similar test, but with sinusoidal strain instead of the constant strain rate, was used to evaluate thixotropy of bituminous mixtures during cyclic loading (Soltani & Anderson, 2005).

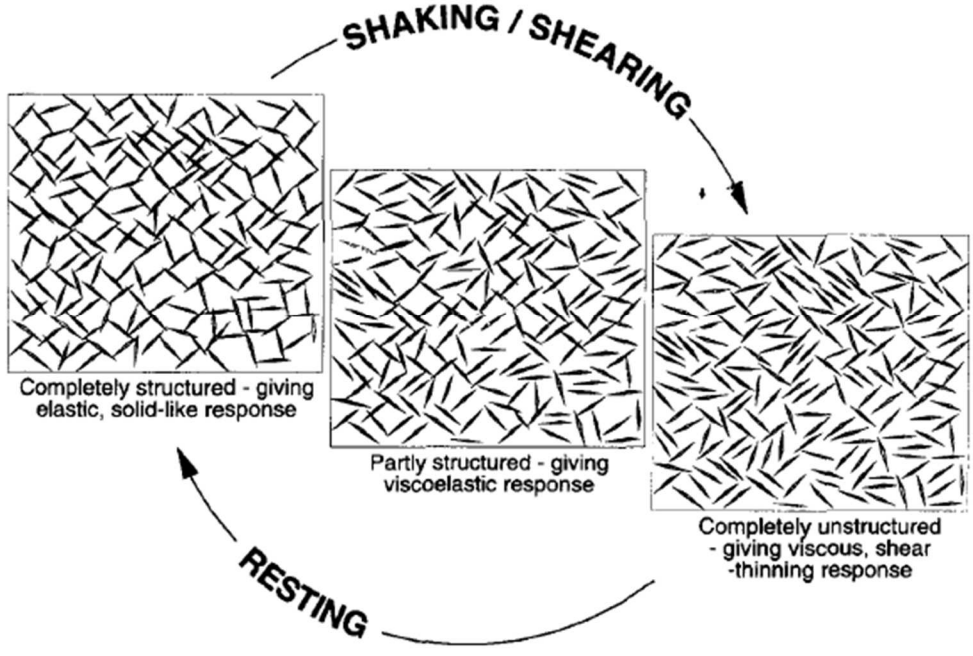

Figure 2-22. Schematic representation of breakdown and build-up of thixotropic structure (Barnes, 1997). Among possible explanation for shear-thinning and thixotropic behaviour are: alignment of elongated particles in the flow direction, loss of junctions in polymer solutions, rearrangement of microstructure in suspension and emulsion, and breakdown of flocs.

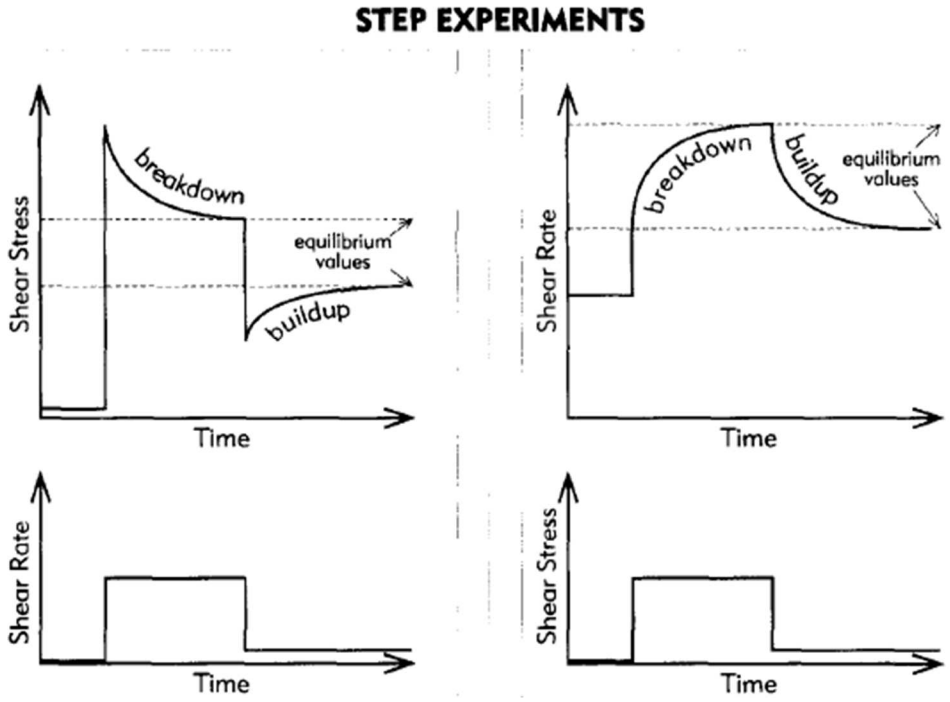

Figure 2-23. Equilibrium values of shear stress during "step" constant shear experiments, where the applied shear rate is changed in different loading blocks (Barnes, 1997).

Thixotropic behaviour has been observed experimentally in bituminous materials (Canestrari et al., 2015; Di Benedetto, Nguyen, et al., 2011; Isailović et al., 2017; Mangiafico et al., 2015; C. V. Phan, Di Benedetto, Sauzéat, Dayde, et al., 2017; Riahi et al., 2017; Shan, Tan, Underwood, & Kim, 2011; Soltani & Anderson, 2005; Van Rompu et al., 2012). In these materials, much confusion can be made when interpreting results from tests, because other physical phenomena (e.g. self-heating, damage) also produce changes in stiffness during tests. This is particularly more complicated when including the hypothesis of a phenomenon, called in the literature "self-healing" of microcracks (Bhasin et al., 2008; Canestrari et al., 2015; Daniel & Kim, 2001; Karki et al., 2015; Palvadi et al., 2012), which is responsible of recovering a stiffness loss due to damage. Much research in the literature neglects completely the thixotropic behaviour of bitumen and bituminous mixtures, and what is called "self-healing" of microcracks includes thixotropy. Bituminous materials literature lacks of clear distinction between the thixotropic behaviour and the combination of damage and self-healing phenomenon. Despite the fact that this may appear just as a semantic issue, it should be underlined that a fundamental difference between both explanations exists: the former presents no microcracks at all, and the latter presents appearance and disappearance of microcracks. This fundamental difference may change considerably the obtained material properties from laboratory experiments interpretation, and, hence, influence both the choice of materials and the performance prediction of these materials in the field. In the field, vehicle load produces only few applications of loading cycles (continuous loading is not applied), thus thixotropy is not expected. It can then be concluded that thixotropy in bituminous materials produces biasing effects on the measured stiffness for both the interpretations of damage and self-healing behaviour. It should be noticed that literature presents experimental data showing that,

after a rest period of 4h where significant recovery is observed in bituminous mixture material properties (following 25% modulus decrease during loading), but, from 4h to 8h of rest at 20°C, negligible effect is measured (Isailović et al., 2017). As additional information, Figure 2-24 presents experimental results (Q. T. Nguyen, 2011) that suggest that the thixotropy phenomenon respects also the TTSP with the same time-shift factors as for linear viscoelastic characterisation (cf. more information on time-temperature superposition in Section 2.2.4).

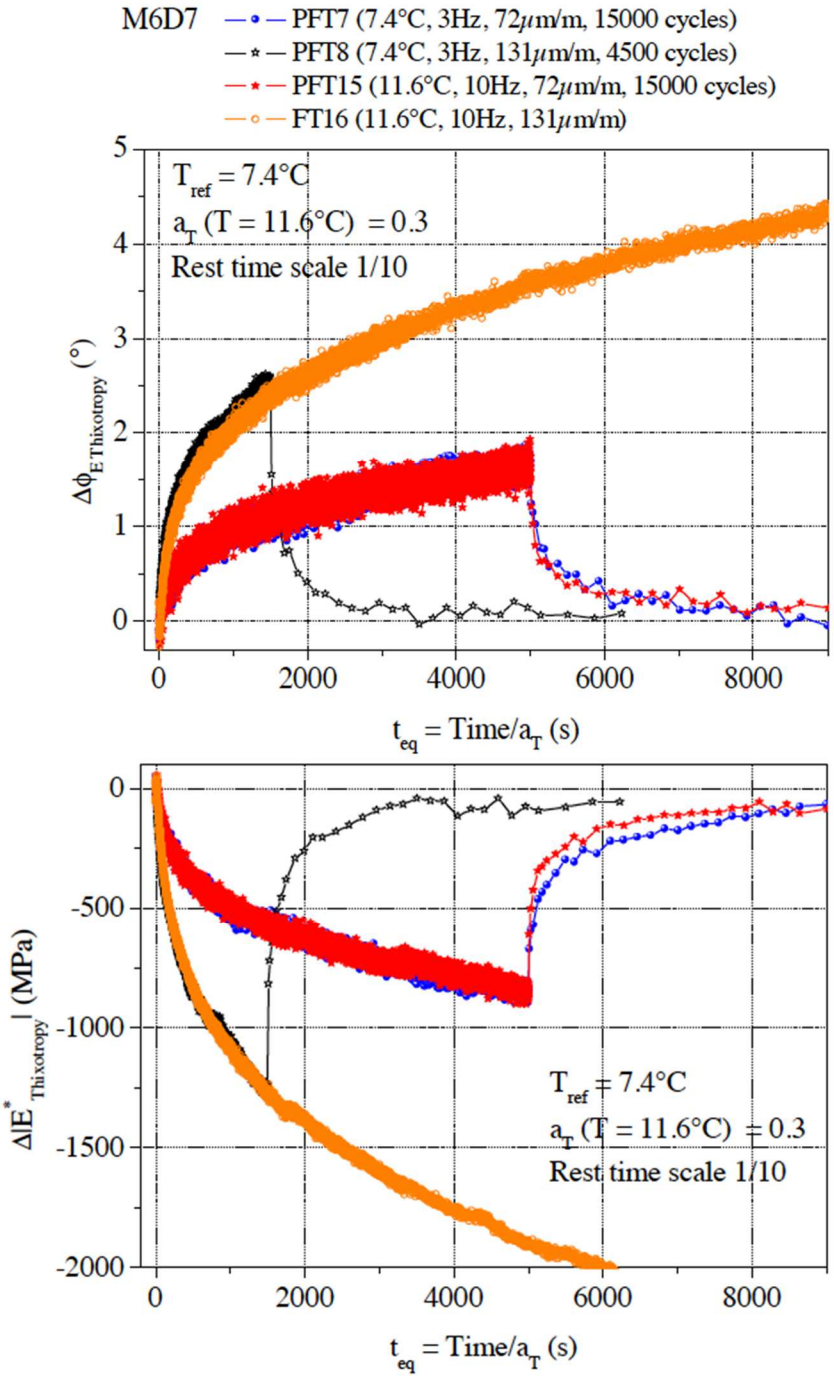

Figure 2-24. Verification of time temperature superposition for thixotropy (Q. T. Nguyen, 2011): norm of complex modulus variation (above), and phase angle variation (below).

2.8. General formulation to interpret fatigue tests considering biasing phenomena

A general framework has been developed at ENTPE/University of Lyon for the interpretation of experimental results from cyclic loading and fatigue tests (Mangiafico, 2014; Q. T. Nguyen, 2011). This includes the consideration of different physical phenomena (nonlinearity, self-heating, thixotropy and damage), which induce complex modulus variations during loading. Among these phenomena, the reversible ones are considered to induce biasing effects with respect to damage analysis. This consideration is done because during fatigue tests the reversible effects appear, but this is not the case during in-situ vehicle loading, where few cycles followed by rest are applied. To allow test interpretation considering all biasing phenomena, rest periods are necessary. During the test (both during loading, at high relative strain amplitude, and during rest, at low strain amplitude and for very punctual tests), complex modulus is measured. The changes in the measured norm of complex modulus (which is noted $E(\varepsilon_0,T,N)$, as a function of strain amplitude, temperature and number of cycles) and in the measured phase angle, can be due to the following physical phenomena:

- Nonlinearity: the effect of this phenomenon on the complex modulus is observed at the beginning of cyclic loading, when the hydraulic press servo-control changes strain amplitude until the test strain amplitude is obtained. This phenomenon is thoroughly investigated in Chapter 4. At fixed temperature and frequency, nonlinearity makes the measured complex modulus depend on the applied axial strain amplitude (ε_{01}). At very small strain amplitude (linear domain) the norm of complex modulus is noted $E(0,T_0,1)$. Then, this effect is observed when the strain amplitude is changing (beginning of the test), but no variation due to nonlinearity is expected after that. At the beginning of loading at the targeted axial strain amplitude, the norm of complex modulus is noted $E(\varepsilon_{01},T,1)$. The change in complex modulus due to nonlinearity is instantaneous and reversible, and noted here $\Delta E_{Nonlinearity}$. It can be calculated as:
    - $\Delta E_{Nonlinearity} = E(\varepsilon_{01},T_0,1) - E(0,T_0,1)$.
- Self-heating (and self-cooling during rest): the effect of this phenomenon on the complex modulus is observed when the specimen temperature is changing. Even in a thermal chamber at constant temperature, the specimen temperature may vary. During continuous cyclic loading, the bituminous material specimen, which is viscoelastic, dissipates mechanical energy, transforming it into heat. Then, a temperature increase is expected in the specimen. Since, the material is thermo-sensitive, a change in complex modulus occurs as a consequence of self-heating. Temperature measurements in the specimen, associated with rheological models (2S2P1D model and WLF equation), give information on this self-heating. Then, this effect is observed during loading as long as temperature increases, and is also observed during rest as long as temperature decreases. The change in complex modulus due to temperature variation is reversible. The variation of norm of complex modulus (at a given cycle N) due to self-heating is noted here $\Delta E_{Heating}$.
    - $\Delta E_{Heating} = E(\varepsilon_{01},T,N) - E(\varepsilon_{01},T_0,N)$.

- Thixotropy: the effect of this phenomenon on the complex modulus is observed during loading and during rest, when the material microstructure is rearranging (cf. Section 2.7). During loading stiffness decreases and during rest it increases up to an equilibrium value, theoretically the same as before loading (the phenomenon is reversible). The variation of norm of complex modulus due to thixotropy is noted here $\Delta E_{Thixotropy}$. The recovered modulus after rest is noted $E_{rev}(\varepsilon_{01},T_0,N)$.
    - $\Delta E_{Thixotropy} = E(\varepsilon_{01},T,N) - E_{rev}(\varepsilon_{01},T,N)$.
- Damage: the effect of this phenomenon on the complex modulus is observed during loading. During loading, the material cross-section reduces (microcracks) and the apparent stiffness is reduced. With damage accumulation, microcracks may coalesce into a macrocrack, and the material fails. The phenomenon is irreversible. The variation of norm of complex modulus due to damage is noted here $\Delta E_{Fatigue}$.
    - $\Delta E_{Fatigue} = E_{rev}(\varepsilon_{01},T,N) - E(\varepsilon_{01},T,1)$.
- Together, thixotropy and fatigue are called "cyclic effects", because both produce a change in stiffness with the repetition of loading cycles. The variation of norm of complex modulus due to cyclic effects is noted here $\Delta E_{Cyclic\ Effects}$.
    - $\Delta E_{Cyclic\ Effects} = \Delta E_{Fatigue} + \Delta E_{Thixotropy} = E(\varepsilon_{01},T,N) - E(\varepsilon_{01},T,1)$.

Then, the modulus at the initial temperature and at the test strain amplitude ($E(\varepsilon_{01},T_0,N)$) obtained during the test can be written as in Eq. 2-32. This same framework can be used to analyse phase angle evolution. Figure 2-25 presents schematically the changes in modulus expected during cyclic loading and during rest in bituminous materials (Q. T. Nguyen, 2011).

$$E(\varepsilon_{01},T_0,N) = E(0,T_0,1) + \Delta E_{Nonlinearity} + \Delta E_{Heating} + \Delta E_{Thixotropy} + \Delta E_{Fatigue} \quad \text{Eq. 2-32}$$

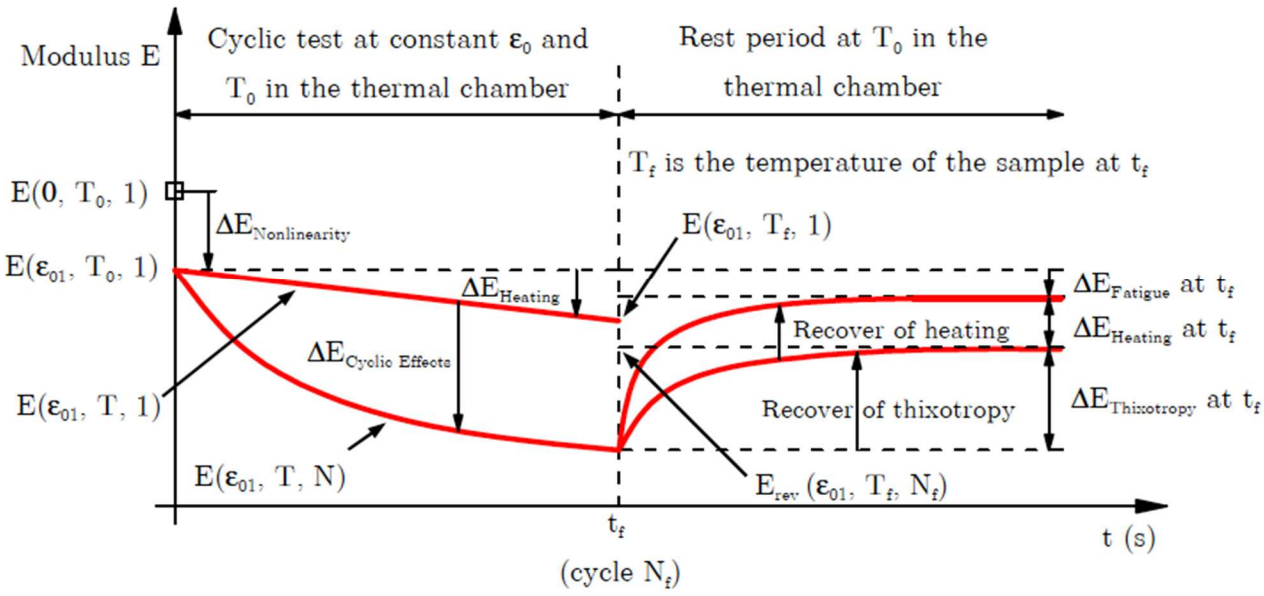

Figure 2-25. Schematic representation of the contributions of the different physical phenomena (nonlinearity, heating, thixotropy and damage) on the measured norm of complex modulus during a cyclic loading test (at strain amplitude ε_{01}) including rest (Q. T. Nguyen, 2011).

The evolution of complex modulus during cyclic loading and during rest can also be investigated in complex representations. The Black diagram is a useful tool for the referred analysis. (Q. T. Nguyen, 2011) investigated the effects of the combined physical phenomena commented before on the measured complex modulus of bituminous mixtures using Black diagrams. Figure 2-26 presents an example of test results and an interpretation of the evolution of the effects of each of the commented phenomena. In Black space, it is seen that each phenomena present a particular direction of complex modulus evolution. Before performing the continuous cyclic loading test, information on temperature-sensitivity may be obtained from classical complex modulus tests. If these tests include different strain amplitudes, nonlinearity effect can also be calculated (cf. Figure 2-26).

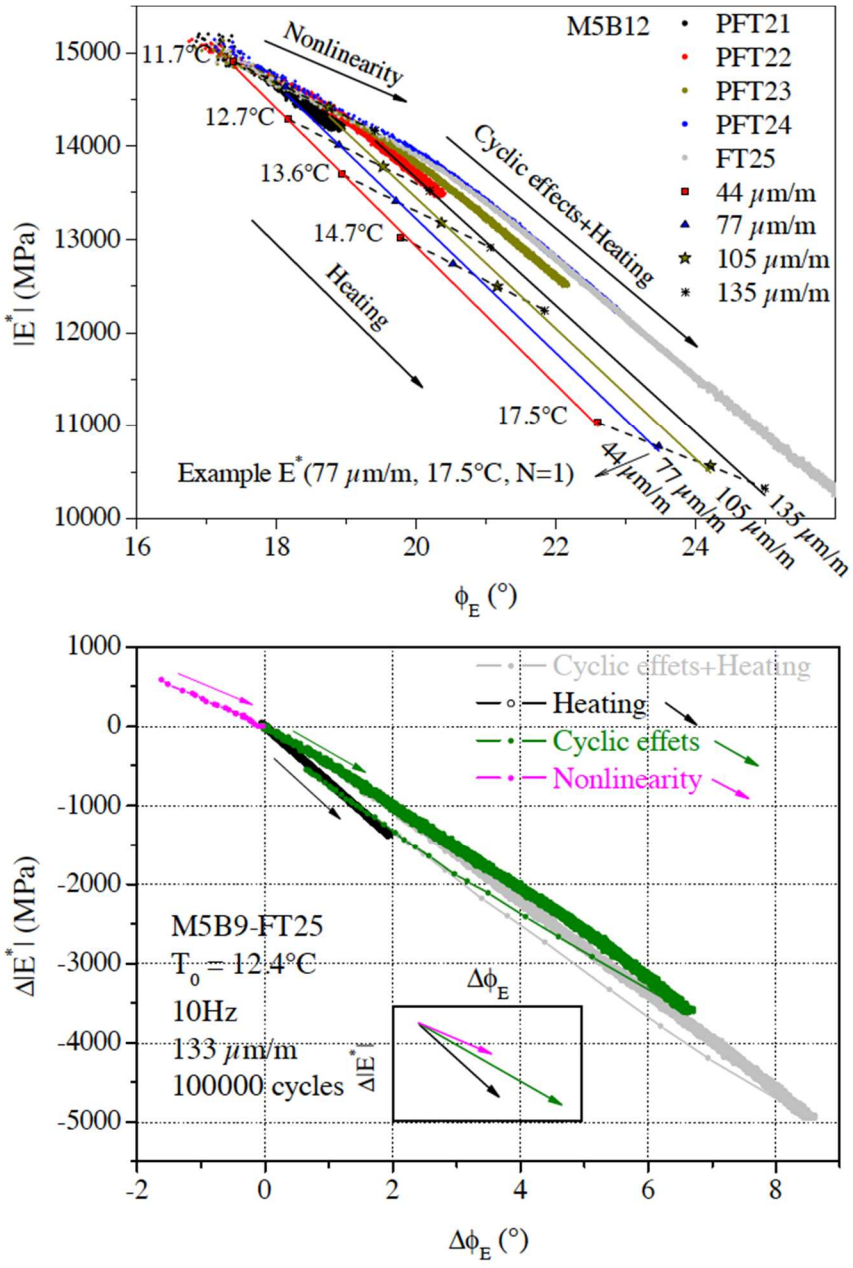

Figure 2-26. Directions of different phenomena on Black space (Q. T. Nguyen, 2011): example of experimental results (above), and schematic representation of the directions of the variation in complex (below).

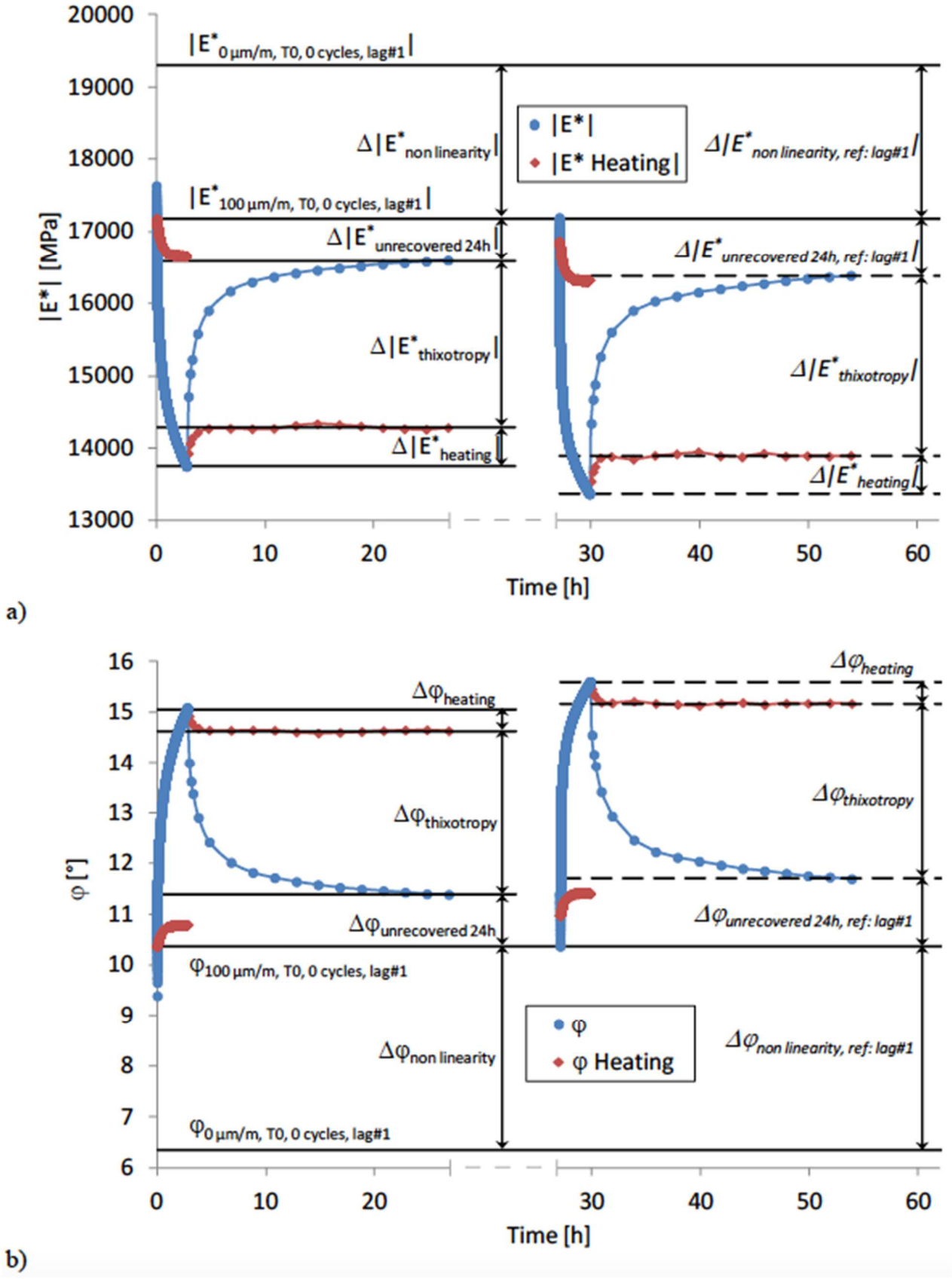

Figure 2-27. Example of experimental results from tests on bituminous mixture consisting in the application of 100,000 cycles at 100µm/m followed by 24h of rest (Mangiafico, 2014). Variations in norm of complex modulus (figure a) and phase angle (figure b) corresponding to different physical phenomena are represented: nonlinearity, heating, thixotropy and damage (called "unrecovered" in the figure, since an asymptotic value had not yet been obtained).

Figure 2-27 presents experimental results (norm of complex modulus and phase angle) from cyclic tests including rest periods, interpreted using the same framework (Mangiafico, 2014). In the referred work, these tests were performed on different bituminous mixtures, with application of 100,000 cycles at 100μm/m followed by 24h of rest. Five loops of loading and rest were applied. In the different tested mixtures, the unrecovered change in norm of complex modulus after 24h rest was of about 10% (with respect to the total change in modulus during loading) (Mangiafico, 2014). This was accompanied by around 1° change in the phase angle. This unrecovered change in norm of complex modulus is the one possibly associated with damage, which is the phenomenon considered as responsible for leading the material to fatigue failure. Due to its small relative importance with respect to the total modulus variation during loading, it is clear that the biasing effects need to be taken into account during fatigue analysis of bituminous mixtures. For the same reasons, self-healing analysis needs also to include considerations on thixotropy (Shan et al., 2011, 2010), although it seems that a more precise method for distinguishing thixotropy during rest from self-healing is still needed.

Chapter 3: EXPERIMENTAL DEVICES AND PROGRAMME

Chapter 3: Experimental Devices and Programme....55
3.1. Experimental set-ups....56
3.1.1. Annular Shear Rheometer (ASR) tests....57
3.1.2. Tension-Compression (T-C) tests....59
3.2. Experimental analysis....60
3.2.1. Annular Shear Rheometer (ASR) tests....60
3.2.2. Tension-Compression (T-C) tests....62
3.2.3. Signal analysis and stiffness measurements....63
3.2.4. Geometrical biases in ASR tests stiffness measurements....66
3.2.4.1. Effect of an eccentricity between internal and external moulds....66
3.2.4.2. Effect of a material loss due to flow under gravity....67
3.2.4.3. Effect of the formation of a circular section meniscus....68
3.2.4.4. Geometrical biases analysis conclusion....69
3.3. Materials and designation....69
3.3.1. Bitumen....69
3.3.1.1. Description....69
3.3.1.2. Specimen preparation for ASR tests....69
3.3.2. Glass beads mastic....70
3.3.2.1. Description....71
3.3.2.2. Fabrication process....71
3.3.2.3. Specimen preparation for ASR tests....71
3.3.3. Bituminous mixtures....72
3.3.3.1. Bituminous mixture specimen fabrication process for T-C tests....72
3.3.3.2. BM1 (C. V. Phan, Di Benedetto, Sauzéat, Lesueur, et al., 2017)....72
3.3.3.3. BM2 (Q. T. Nguyen, 2011)....73
3.3.3.4. BM3 (Q. T. Nguyen, 2011)....73
3.4. Experimental campaign overview....73

This chapter presents the experimental devices used for the tests performed. It also describes the tested materials and introduces the considered stress/strain paths used for experiments. Finally, an overview of the tests performed in each of the materials is given. It is to be observed that the test geometries are chosen in order to obtain homogeneous experiments (Di Benedetto, de La Roche, et al., 2004; Di Benedetto et al., 2001), i.e., tests that produce homogeneous stress and strain fields in the material (considering the hypothesis of material homogeneity in continuum mechanics, i.e. the biggest particles are relatively small when compared to the smallest specimen dimension). Homogeneous tests allow obtaining stress and strain fields directly from measurements on the boundaries of the material volume, without the need for supplementary hypotheses in the analysis. Thus, these tests give direct access to the constitutive behaviour of the studied material, which is a major interest. In the case of non-homogeneous tests, a supplementary hypothesis on the constitutive behaviour of the material is necessary in order to interpret test results, i.e. to obtain stress and strain fields and, then, access constitutive behaviour.

3.1. Experimental set-ups

This section describes the experimental set-ups used in this work: the Annular Shear Rheometer (ASR) set-up, used for testing bitumen and mastic; and the Tension-Compression (T-C) set-up, used for testing bituminous mixtures. Both set-ups lead to approximately homogeneous tests (Di Benedetto, de La Roche, et al., 2004; Di Benedetto et al., 2001). Figure 3-1 presents the two set-ups mounted in the testing frames of the two hydraulic presses used in this work.

Two thermal chambers (manufactured by BIA Climatic®) were used for thermal conditioning prior to all mechanical tests (both are represented in Figure 3-1). These thermal chambers are able to apply temperatures from −60°C to 80°C using a two stage compressor cooling process. Meanwhile, temperature homogeneity in the thermal chamber is provided by the action of a built-in fan. Before each test, a thermal conditioning time of at least 3h30 for bitumen and mastic hollow cylinder specimens was used, which has been experimentally determined in previous works with similar materials and equipment (Delaporte, 2007). For bituminous mixture cylinder specimens, the thermal conditioning time was of at least 4h, which can be determined either experimentally (Lamothe, 2014) or from a thermal calculation (Q. T. Nguyen, 2011).

Two types of temperature sensors were used in this thesis: thermocouples and resistance temperature detectors. Their signal responses were treated with two different types of signal conditioners.

The temperature sensors used to measure specimen temperature during ASR tests were thermocouples. Thermocouples consist of two different conductors forming an electrical junction at differing temperatures. That produces a temperature-dependent voltage due to the Seebeck effect. The voltage can be directly related to temperature, which gives the temperature measurement without the need of an electrical power input. Type T (copper/constantan, constantan being a copper-nickel alloy) thermocouples were chosen, with a 0.5mm diameter and 150mm-long sheath. This kind of thermocouples provides good measure repeatability (±0.1°C) within the range from −200°C to 200°C (TCSA, 2016). They present sufficiently small diameter (a tenth of

specimen's thickness) in order to be immerged in the ASR test specimens, without perturbing measurements. The standardised (IEC 60584-1, 2013) maximum tolerance (allowed difference between measured temperature and real temperature) for a given type T thermocouple is 0.5°C. In order to acquire data from measurements sufficiently fast and without data treatment lags, a special kind of signal conditioner was used (the transmitter TDMTC, manufactured by TCSA®). The referred transmitter presents a response time of less than 25ms. In addition, the response time of the thermocouples is also sufficiently small, and it is consequently possible to observe temperature changes from one cycle to the other during sinusoidal loading, even at 10Hz. In order to assess possible temperature inhomogeneity in the bitumen and mastic specimens, four thermocouples, placed 90° apart from each other (details in Figure 3-2), were used.

The temperature sensor used to measure specimen surface temperature during T-C tests was a resistance temperature detector known as Pt100. A resistance temperature detector is a sensor whose wire electrical resistance depends on temperature. The Pt100 is made of platinum (which presents a 100 ohms resistance at 0°C), a material for which electrical resistance as a function of temperature is documented. Then, it is possible to obtain temperature measurements from resistance measurements. As a consequence of its working mechanism, this device requires an electrical power input in order to perform measurements. The standardised (IEC 60751, 2008) maximum tolerance for a given Pt100 is 0.3°C at 0°C and 0.8°C at −100°C and 100°C. The signal conditioner used for Pt100 measurements was a Tracker 220 series. More details on the equipment are given next, in sections dedicated to each of the two types of test performed.

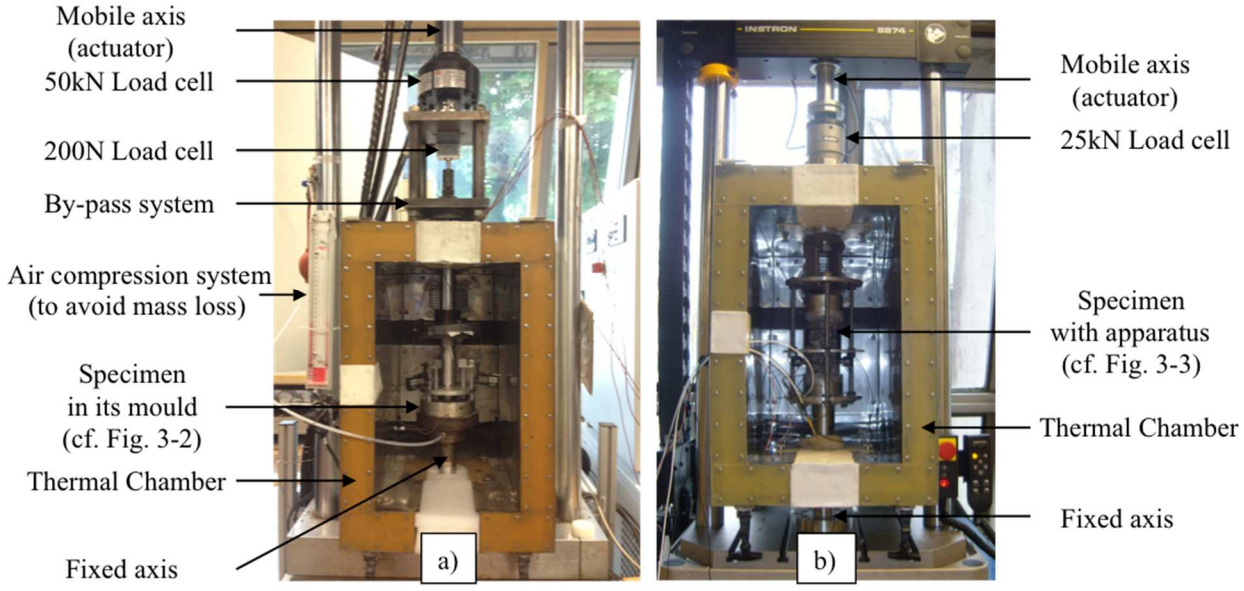

Figure 3-1. (a) ASR tests on bitumen and mastic hollow cylinder specimens mounted on a MTS® hydraulic press testing frame, and (b) T-C tests on bituminous mixture cylindrical specimens mounted on an Instron® hydraulic press testing frame.

3.1.1. Annular Shear Rheometer (ASR) tests

The ASR test set-up is designed to apply direct shear, in an approximately homogeneous fashion, to thin-wall hollow cylinder specimens of bitumen or mastic, using a hydraulic press. As

seen in Figure 3-1a, a mobile axis (actuator), which is fixed to the inner part of the mould holding the specimen, applies load, which generates shear on the specimen. Load is measured using a load cell. The external part of the mould holding the specimen is attached to a fixed axis. The displacement between these two parts is measured in order to measure shear strain in the material. Then constitutive behaviour of the material can be obtained from shear tests. Specimen temperature is measured during the tests using the four type T thermocouples.

A MTS® hydraulic press powered by a MTS® SilentFlo® 515.07 hydraulic supply was used for tests in bitumen and mastic hollow cylinders specimens (cf. Figure 3-1a). The press is equipped with a ±50kN capacity load cell (model 661.20F-02) with accuracy of 15N, and a ±200N capacity load cell (model FN3148-200N) with accuracy of 0.01N. A by-pass allows deciding whether to use or not the small capacity load cell. Measures from the load cell are used to obtain the applied shear stress on the tested material (details in Section 3.2.1). Three extensometers (model 632.11F-20) are used to measure shear strain on the bitumen and mastic hollow cylinder specimens (details in Section 3.2.1). Extensometer gauge length used is 50mm. The hydraulic press works with a servo control system using mainly Proportional-Integral-Derivative (PID) controllers. PID parameters were adjusted specifically to each ASR test performed in this work.

Figure 3-2 presents ASR tests set-up, including the location of the utilised sensors. In all ASR tests analysed in this thesis, the same location was used, in order to detect possible sources of bias, leading to systematic error, such as differences in the displacement measured in different parts of the specimen and non-homogeneity of temperature increase. This configuration was obtained after refining practices with the experience from previous works (Orozco, 2016).

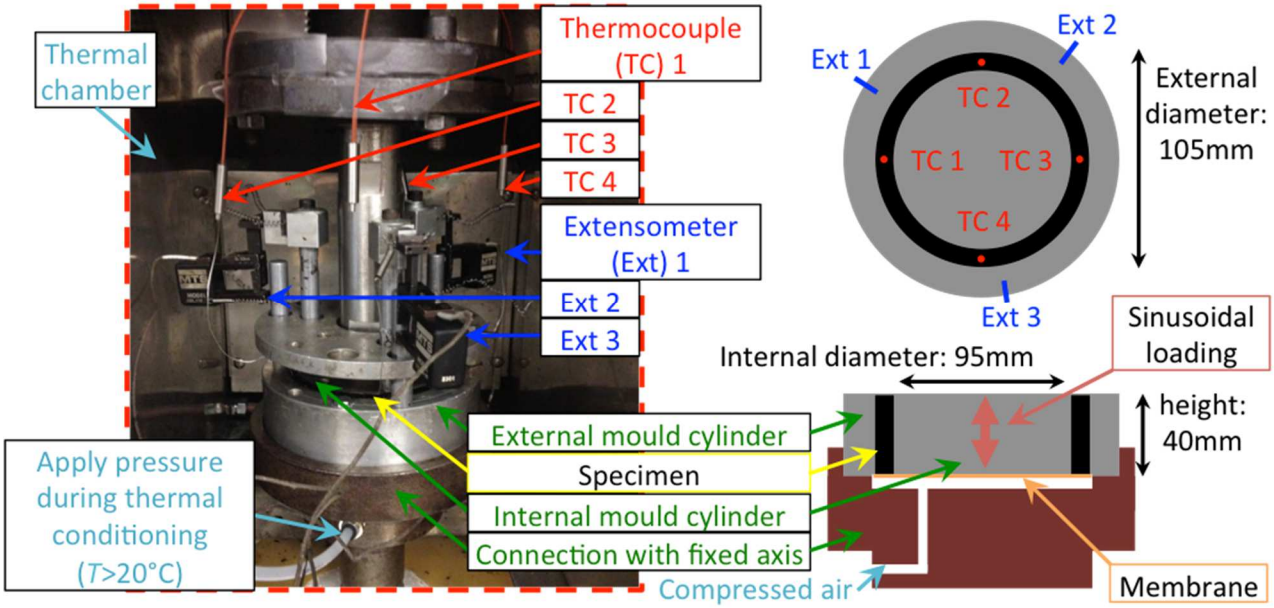

Figure 3-2. Focus on the ASR test apparatus in the MTS® press (from Figure 3-1a), and details on the test specimen with mounted sensors

The analysis of the load cell and extensometers results is made based on the hypothesis of uniform distribution of stress and strain in the specimen, valid for homogeneous tests. Annular shear test homogeneity is a good approximation for small specimen thickness in comparison to the radius. For the used geometry (5mm-thick specimen), error due to nonlinearity on the measured modulus is lower than 0.1%. A thorough discussion on the homogeneity of this test may be found in the literature (Delaporte, 2007).

An eccentricity fault between internal and external moulds would lead to non-uniformity of shear strain in the specimen (since specimen thickness would not be uniform), then leading to a non-uniform stiffness after the different physical phenomena (nonlinearity, self-heating, thixotropy and damage) had acted on the specimen. In Section 3.2.4, the effect of an eccentricity fault on stiffness measurements is investigated using numerical simulation, among other geometrical biases, such as possible material loss due to flow under gravity and material rearrangement inside the mould.

3.1.2. Tension-Compression (T-C) tests

The T-C tests are designed to apply axial loading homogeneously on cylindrical specimens of bituminous mixture using a hydraulic press. As seen in Figure 3-1b, a mobile axis (actuator), which is fixed to the upper cap glued to the specimen, applies load, which generates tension or compression on the specimen. The lower cap is attached to a fixed axis. Load is measured using a load cell. Axial strain is measured on-specimen using extensometers. Radial strain is measured using non-contact sensors placed along a specimen diameter. Then, three-dimensional constitutive behaviour of the material can be obtained. On-surface specimen temperature is measured during the tests using the Pt100.

Figure 3-3 presents T-C tests set-up and the used sensors. An Instron® 8874 series hydraulic press was used for Tension-Compression (T-C) tests on bituminous mixture cylindrical specimens (cf. Figure 3-1b). The Instron® press is equipped with a ±25kN capacity load cell (model Dynacell® 2527 series) with accuracy of 25N. Measures from the load cell are used to obtain the applied axial stress on the tested material (details in Section 3.2.2). Three extensometers (model 2620-601) are used to measure on-specimen axial strain on bituminous mixtures cylinder specimens (details in Section 3.2.2). Gauge length used is 75mm. Two non-contact sensors (Micro-Epsilon eddy current sensors with 0-0.5mm range), positioned along a specimen diameter, were used to measure radial displacement in order to obtain radial strain. The hydraulic press works with a servo control system using mainly Proportional-Integral-Derivative (PID) controllers.

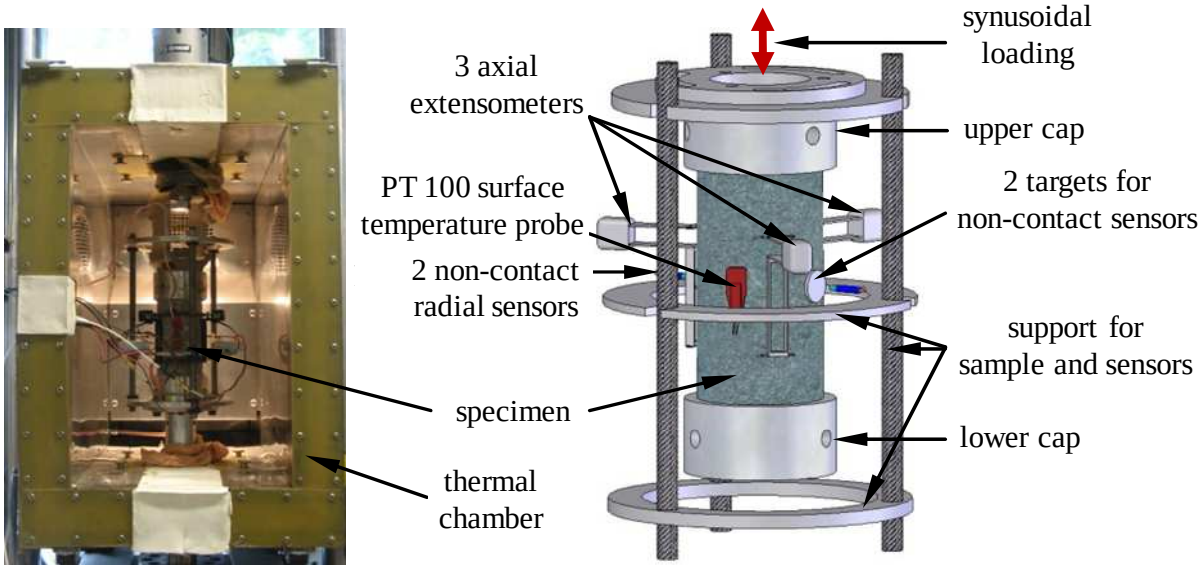

Figure 3-3. Focus on the T-C test apparatus in the Instron® press (from Figure 3-1b), and details on the test specimen with mounted sensors.

The analysis of the load cell and extensometers results is made based on the hypothesis of uniform distribution of stress and strain in the specimen. Test homogeneity is a good approximation for small temperature gradients along the specimen radius.

3.2. Experimental analysis

This section describes the signal treatment performed in order to obtain material properties from the performed tests. It also includes a discussion on possible geometrical biases that could influence test results, and establish tolerances for those biases.

3.2.1. Annular Shear Rheometer (ASR) tests

Extensometers measurements give access to the axial displacement between the internal and the external mould cylinders that contain the tested specimen. A given extensometer *i* measures a displacement ($\Delta\square_i$). Shear strain measured by extensometer *i* (Ext *i*, whose position is represented in Figure 3-2) at the instant *t* can then be obtained, as in Eq. 3-1. Specimen thickness is 5mm. A geometrical interpretation is given in Figure 3-4.

$$\gamma_i(t) = \frac{\Delta h_i(t)}{Specimen\ thickness} \qquad \text{Eq. 3-1}$$

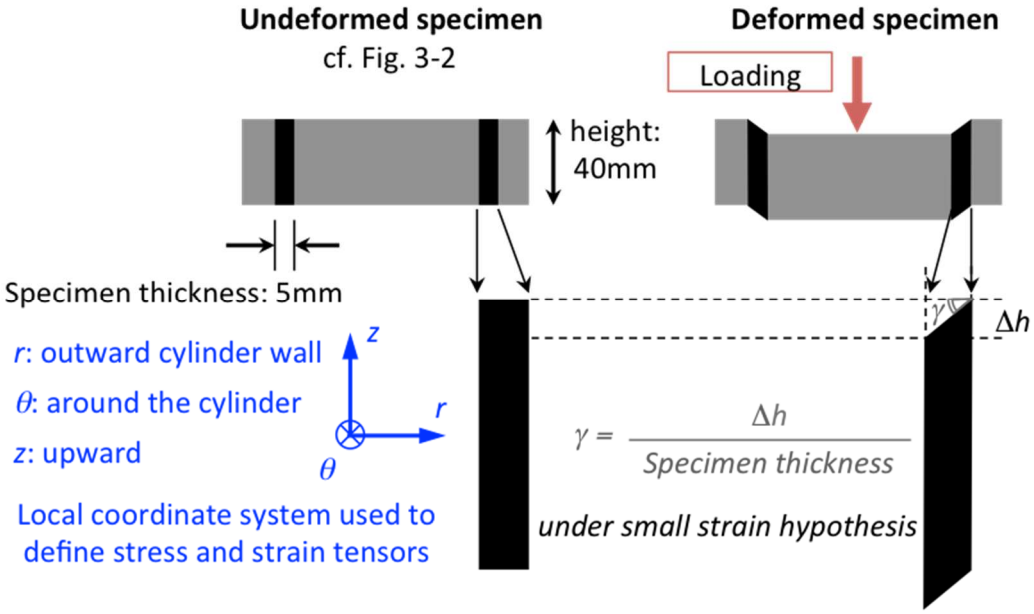

Figure 3-4. ASR specimen deformation during tests and interpretation of the applied shear strain.

From the three extensometers measurements, a mean shear strain is obtained, as in Eq. 3-2. All ASR tests in this thesis are controlled using that mean value $\gamma(t)$ (Eq. 3-2). PID controller for this signal needed to be meticulously adjusted for each testing condition in bitumen and in mastic, presenting relevant variation (cf. Appendix A, for information on the obtained MTS® press's PID adjustment).

$$\gamma(t) = \frac{\sum_{i=1}^{3} \gamma_i(t)}{3} \qquad \text{Eq. 3-2}$$

Load cell measurements give access to the shear stress applied on the specimen. Since the load cell is associated in series with the testing system, the force $P(t)$ applied on the specimen is the same as the force measured in the load cell (increased by the weight of the pieces between the specimen and the load cell, which is corrected in the signal analysis explained afterwards). The surface on which the load $P(t)$ is applied is calculated as the mean surface (A_{mean}) between the external and the internal cylindrical surface of the specimen (test homogeneity hypothesis). For a thin hollow cylinder, shear stress $\tau(t)$ in the specimen at the instant t is calculated as in Eq. 3-3.

$$\tau(t) = \frac{P(t)}{A_{mean}};\ A_{mean} = 2\pi \frac{(R_{int} + R_{ext})}{2} H \qquad \text{Eq. 3-3}$$

In Eq. 3-3, $P(t)$ represents the force measurement at the instant t, R_{int} and R_{ext} represent the internal and the external specimen radius, respectively, and H represents the specimen height. Values for these parameters are found in Figure 3-2. Then, the stress and strain tensors (defined with respect to the cylindrical coordinate system indicated in Figure 3-4) in the material tested in the ASR can be represented as in Eq. 3-4 and Eq. 3-5, respectively.

$$\underline{\underline{\varepsilon}}_{ASR} = \begin{bmatrix} \varepsilon_{rr} & \varepsilon_{r\theta} & \varepsilon_{rz} \\ \varepsilon_{r\theta} & \varepsilon_{\theta\theta} & \varepsilon_{\theta z} \\ \varepsilon_{rz} & \varepsilon_{\theta z} & \varepsilon_{zz} \end{bmatrix} = \begin{bmatrix} 0 & 0 & \gamma/2 \\ 0 & 0 & 0 \\ \gamma/2 & 0 & \varepsilon_{zz} \end{bmatrix} \quad \text{Eq. 3-4}$$

$$\underline{\underline{\sigma}}_{ASR} = \begin{bmatrix} \sigma_{rr} & \sigma_{r\theta} & \sigma_{rz} \\ \sigma_{r\theta} & \sigma_{\theta\theta} & \sigma_{\theta z} \\ \sigma_{rz} & \sigma_{\theta z} & \sigma_{zz} \end{bmatrix} = \begin{bmatrix} \sigma_{rr} & 0 & \tau \\ 0 & \sigma_{\theta\theta} & 0 \\ \tau & 0 & 0 \end{bmatrix} \quad \text{Eq. 3-5}$$

3.2.2. Tension-Compression (T-C) tests

The three extensometers measurements ($\varepsilon_i(t)$ for the ith extensometer) give directly the on-specimen axial strain $\varepsilon_{ax}(t)$ through an average, as in Eq. 3-6.

$$\varepsilon_{ax}(t) = \frac{\sum_{i=1}^{3} \varepsilon_i\,(t)}{3} \quad \text{Eq. 3-6}$$

All loading performed during T-C tests in this thesis is controlled using that mean value (mean on-specimen axial strain controlled tests). PID controller for this signal was adjusted for each testing condition in bituminous mixture, especially for nonlinearity tests (cf. Chapter 4), presenting relevant variation (cf. Appendix A, for information on the obtained Instron® press's PID adjustment).

The two non-contact sensors placed along a specimen diameter allow determining the change in diameter $\Delta\Phi(t)$ (difference between the measured displacements), with respect to the initial specimen diameter Φ. Then, radial strain $\varepsilon_{rad}(t)$ is obtained using Eq. 3-7.

$$\varepsilon_{rad}(t) = \frac{\Delta\Phi(t)}{\Phi} \quad \text{Eq. 3-7}$$

Load cell measurements give access to the normal stress applied axially on the specimen. The surface on which the load $P(t)$ is equivalent to the cross-section of the cylindrical specimen (of area A). Then, normal stress $\sigma(t)$ in the specimen at the instant t is calculated as in Eq. 3-8. The diameter D of the specimen is 75mm. Then, the strain and stress tensors (defined in cylindrical coordinates similarly to the ASR) in the material tested in the T-C configuration can be represented as in Eq. 3-9 and Eq. 3-10, respectively.

$$\sigma(t) = \frac{P(t)}{A};\ A = \frac{\pi D^2}{4} \quad \text{Eq. 3-8}$$

$$\underline{\underline{\varepsilon}}_{T-C} = \begin{bmatrix} \varepsilon_{rr} & \varepsilon_{r\theta} & \varepsilon_{rz} \\ \varepsilon_{r\theta} & \varepsilon_{\theta\theta} & \varepsilon_{\theta z} \\ \varepsilon_{rz} & \varepsilon_{\theta z} & \varepsilon_{zz} \end{bmatrix} = \begin{bmatrix} \varepsilon_{rr} & 0 & 0 \\ 0 & \varepsilon_{\theta\theta} & 0 \\ 0 & 0 & \varepsilon_{zz} \end{bmatrix} = \begin{bmatrix} \varepsilon_{rad} & 0 & 0 \\ 0 & \varepsilon_{rad} & 0 \\ 0 & 0 & \varepsilon_{ax} \end{bmatrix} = \quad \text{Eq. 3-9}$$

$$\underline{\underline{\sigma}}_{T-C} = \begin{bmatrix} \sigma_{rr} & \sigma_{r\theta} & \sigma_{rz} \\ \sigma_{r\theta} & \sigma_{\theta\theta} & \sigma_{\theta z} \\ \sigma_{rz} & \sigma_{\theta z} & \sigma_{zz} \end{bmatrix} = \begin{bmatrix} 0 & 0 & 0 \\ 0 & 0 & 0 \\ 0 & 0 & \sigma_{zz} \end{bmatrix} \quad \text{Eq. 3-10}$$

3.2.3. Signal analysis and stiffness measurements

The analysed tests use sinusoidal loading (shear strain controlled sinusoidal tests for ASR and axial strain controlled sinusoidal tests for T-C). After obtaining experimental data for stress and strain signals, a data treatment procedure is used in order to determine the amplitude and the phase of each of the sinusoidal functions fitted to the experimental signals for a given cycle. Signal treatment consists of a least squares method used to fit Eq. 3-11 to experimental data. In that equation, $X(t)$ represents the experimental sinusoidal signal to fit, $X_{centring\ correction}$ its mean value, X_0 its amplitude, ω its pulsation ($\omega = 2\pi f$, f being the applied test frequency) and ϕ_X the phase of the signal. This procedure is applied for all sinusoidal signals obtained at each of the loading cycles. For temperature, an arithmetic average for all points at a given cycle was used.

$$X(t) = X_{centring\ correction} + X_0 \sin(\omega t + \phi_X) \quad \text{Eq. 3-11}$$

An indicator of the fitting quality can be used in order to determine if the signal can be approximated by a sinusoidal function using the obtained fitting parameters. The fitting quality indicator (K_X) used in this work is obtained as in Eq. 3-12. It corresponds to an average difference between the measured and the modelled signal values in terms of a percentage with respect to the signal amplitude. In the equation, np represents the total number of data points in the analysed cycle. For a given data point j, X_j^{exp} represents the experimental value of the signal X, X_j^{mod} represents the value of the fitted signal at the same instant, and A_X represents the determined amplitude for the analysed cycle. For example, for the T-C tests, using the described procedure, the sinusoidal part of stress, axial strain, and radial strain signals can be represented as in Eq. 3-13, Eq. 3-14 and Eq. 3-15, respectively.

$$K_X = \frac{1}{np} . \sum_{j=1}^{np} \frac{\left| X_j^{exp} - X_j^{mod} \right|}{A_X} \times 100\% \quad \text{Eq. 3-12}$$

$$\sigma(t) = \sigma_0 \sin(\omega t) \quad \text{Eq. 3-13}$$

$$\varepsilon_{ax}(t) = \varepsilon_{0,ax} \sin(\omega t - \varphi_{E^*}) \quad \text{Eq. 3-14}$$

$$\varepsilon_{rad}(t) = -\varepsilon_{0,rad}\sin(\omega t - \varphi_{E^*} + \varphi_{\nu^*}) = \varepsilon_{0,rad}\sin(\omega t - \varphi_{E^*} + \pi + \varphi_{\nu^*}) \qquad \text{Eq. 3-15}$$

An example of sinusoidal signals fitting to experimental data is presented in Figure 3-5. The example is for a T-C test on BM1 at 14°C and 0.3Hz used in the nonlinearity investigation (for more details on the test, cf. Chapter 4). Signals presented in the figure have been centred to zero y coordinate (using $X_{centring\ correction}$ for each signal). The stress, the mean axial strain, and the radial strain signals are presented along with their sinusoidal fitting result. With the fitting results, stiffness (including Poisson's ratio, for T-C tests) is obtained. From the ASR tests, a complex shear modulus (norm and phase angle) is obtained as in Eq. 3-16. In that equation, τ_0 represents the shear stress amplitude, γ_0 the shear strain amplitude, φ_{G^*} the phase angle of the shear modulus. Analogously, from the T-C tests, a complex Young's modulus and a complex Poisson's ratio are obtained as in Eq. 3-17 and Eq. 3-18, respectively. In those equations σ_0 represents the axial stress amplitude, $\varepsilon_{0,ax}$ the axial strain amplitude, $\varepsilon_{0,rad}$ the radial strain amplitude, φ_{E^*} the phase angle of the Young's modulus.

$$G^* = |G^*|e^{i\varphi_{G^*}} \quad ; \quad |G^*| = \frac{\tau_0}{\gamma_0} \qquad \text{Eq. 3-16}$$

$$E^* = |E^*|e^{i\varphi_{E^*}} \quad ; \quad |E^*| = \frac{\sigma_0}{\varepsilon_0} \qquad \text{Eq. 3-17}$$

$$\nu^* = |\nu^*|e^{i\varphi_{\nu^*}} \quad ; \quad |\nu^*| = \frac{\varepsilon_{0,rad}}{\varepsilon_{0,ax}} \qquad \text{Eq. 3-18}$$

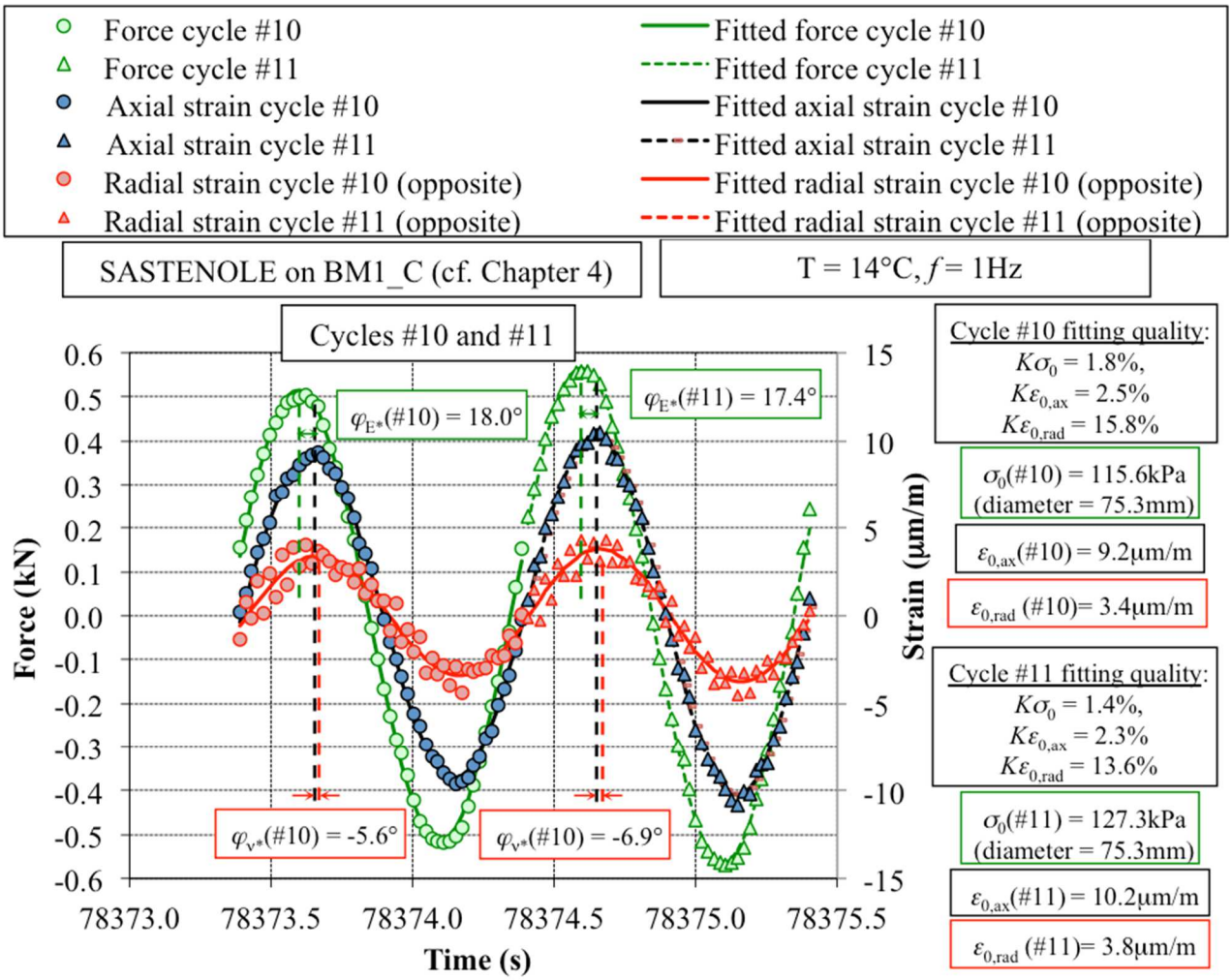

Figure 3-5. Example of sinusoidal signals fitting in order to obtain amplitude and phase for experimental signals (sequence of two cycles for the stress, the radial strain, and the three axial strain measurements during a T-C test – example from nonlinearity investigation, Chapter 4).

Since complex modulus is rigorously defined only in the case of linear response (validity of Boltzmann superposition principle), with stress and strain signals being perfectly sinusoidal (in steady state), it results that obtaining a complex modulus for bituminous materials is an approximation. Results obtained using the procedure presented before (Eq. 3-11 to Eq. 3-18) could only be interpreted as a "strictly speaking" complex modulus for sinusoidal loading at very small stress/strain, with steady state response. Then, since material behaviour is not linear for all stress/strain levels, there exists a need to define an "equivalent" complex modulus, which is the result obtained using the procedure for any cycle where nonlinearities in the response are sufficiently small in order to still obtain sinusoidal signals. This condition can be verified by setting a limit for the fitting quality indicator K_X. Noise in the signals is expected to produce imperfect signals, hence non-nil K_X. The signal quality indicator also depends on the signal amplitudes, since for higher applied amplitude, the noise of the signals becomes relatively less important. With the T-C test set-up used in this work, for a test with 10µm/m axial strain amplitude and 0.6kN force amplitude, K_X is around 2% for axial strain and stress signals. It is around 5% for 10µm/m radial strain amplitude. With the ASR test set-up used in this work, for a

test with 1500μm/m shear strain amplitude and 0.3kN force amplitude, K_X is around 2% for stress and axial strain signals. The referred strain amplitudes are very low and induce negligible nonlinearity in the behaviour of the tested materials (cf. example in Figure 3-5). Signal defects induced by nonlinear responses are indistinguishable from noise for those values of signal quality indicator. Signals with K_X around 5% were accepted as sinusoidal for the analyses performed in this work. Values up to 15% were accepted for the radial strain in T-C tests. This sinusoidal signals fitting was used in order to obtain "equivalent complex modulus", "equivalent complex shear modulus" and "equivalent complex Poisson's ratio". The term "equivalent" is frequently not included, for simplicity sake, even if the obtained results include nonlinear effects.

3.2.4. Geometrical biases in ASR tests stiffness measurements

The effects of some geometrical biases in ASR experiments were evaluated using Finite Element Method (FEM). Problems in isotropic linear elasticity representing the ASR experiment allowed obtaining displacement fields (in x, y and z directions) and stress tensor fields within the analysed volume. It is important to observe that the solution of the elasticity problems can be used to interpret sinusoidal linear viscoelasticity problems (using the Elastic Viscoelastic Correspondence Principle, (Biot, 1955). FEM solution was obtained using the software COMSOL Multiphysics®. The used finite element mesh consisted of tetrahedral elements, and it was refined until convergence of the solution. The used FEM meshes were generated automatically (using the functionality "physics-controlled mesh"), and are considered as "Fine" by the software (depending on the magnitude of the bias, the number of elements was increased). The applied boundary conditions were (cf. Figure 3-6 and Figure 3-7 for the referred surfaces):

- Top and bottom surfaces (z direction) were considered free (nil stress);
- Internal cylindrical surface was considered as fixed (nil displacement);
- External cylindrical surface undergoes a prescribed displacement (of 50μm).

To the material volume, a Young's modulus of 1MPa was affected, which does not influence the evaluated results in terms of calculated relative variations with respect to the assigned value of 1MPa. The calculated "apparent" shear modulus is obtained by evaluating the load necessary to impose the prescribed displacement, considering a non-biased specimen. The results are interpreted in terms of a mean error in shear modulus between the "apparent" modulus (with the geometrical bias) and the material modulus. Three studies of biased geometry were performed: an eccentricity between the internal and the external cylinder (cf. Figure 3-6), a material loss due to material flow under gravity (cf. Figure 3-7), and the formation of a meniscus both on the top and on the bottom surfaces (no material loss, only rearrangement).

3.2.4.1. *Effect of an eccentricity between internal and external moulds*

In Figure 3-6a, the parameter "eccentricity" (an indicator of non-coaxiality) is defined. In Figure 3-6b, results of mean error in shear modulus are presented as a function of the eccentricity, while Figure 3-6c presents the same results in a zoomed zone. It is seen that for eccentricities

smaller than 2mm, error is less than 10%. For 1mm, error is 1.85%, which justifies accepting results obtained with small (around 1mm) eccentricities in the mounting. The study was performed for values of eccentricity from 0.0mm to 4.5mm, for which the number of elements in the FEM mesh varied from 1,464 to 14,128, respectively. The example shown in the figure is for 3mm eccentricity, for which 3,137 elements were used.

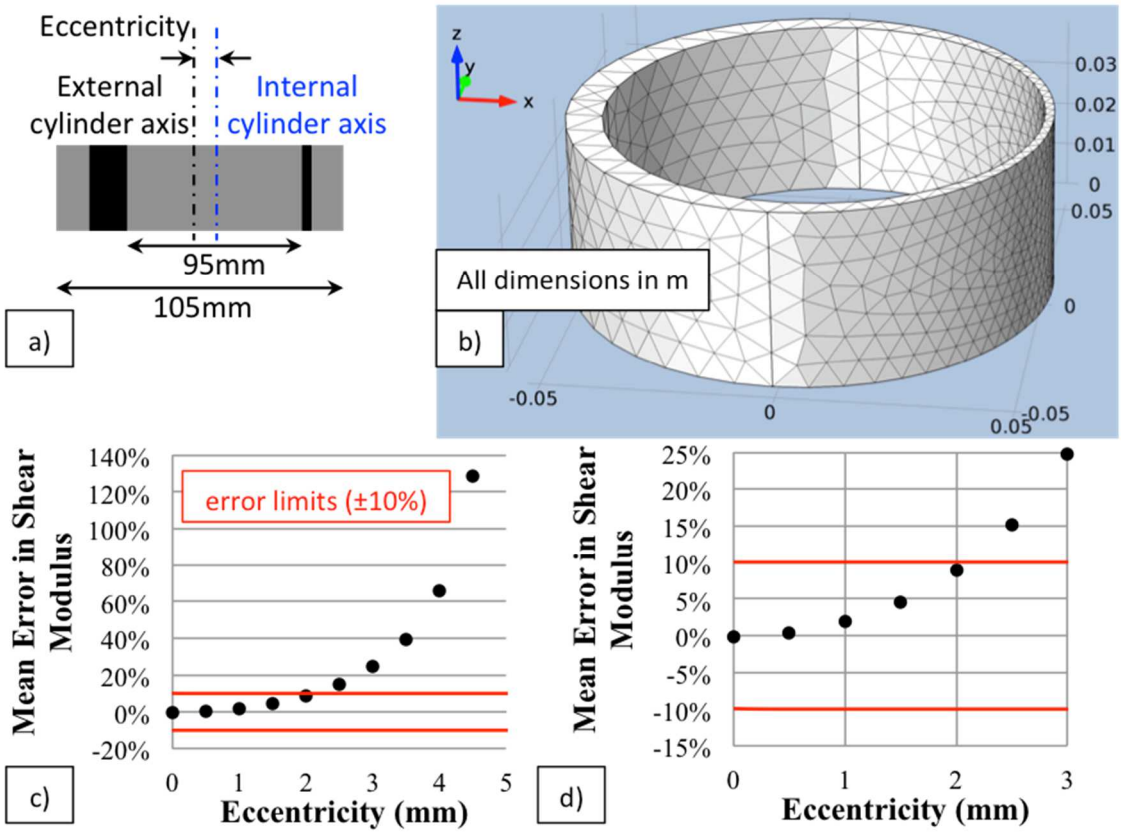

Figure 3-6. Error on shear modulus introduced by the eccentricity between the external and the internal mould during ASR tests. a) Definition of studied eccentricity. b) Illustration of the specimen having a certain eccentricity, and its Finite Elements mesh (example with 3mm eccentricity). c) Mean error in shear modulus obtained with an eccentric specimen for different values of eccentricity. d) Zoom for eccentricities between 0 and 3mm.

3.2.4.2. *Effect of a material loss due to flow under gravity*

In Figure 3-7a, the parameter “Mat_loss” (material loss, in length dimensions) is defined. It can be linked to the percentage material loss due to flow under gravity (cf. Figure 3-7a). Figure 3-7b shows results of mean error in shear modulus as a function of the percentage material loss, while Figure 3-7c presents the same results in a zoomed zone. It is seen that the percentage material loss is directly translated into the value of the error in the measured shear modulus (i.e. they are equal), which was expected since the relative loss of side contact of the specimen with the moulds is approximately the same. Consequently, a loss of 10% of material induces a loss of approximately 10% of contact area of the specimen with the moulds, then reducing the stress necessary to produce the prescribed displacement by the same quantity. The study was performed for values of

material loss between 0.0% and 99.9%, for which the number of elements in the FEM mesh varied from 2,278 to 33,497. The example shown in the figure is for a material loss of 0.01m, for which 32,755 elements were used.

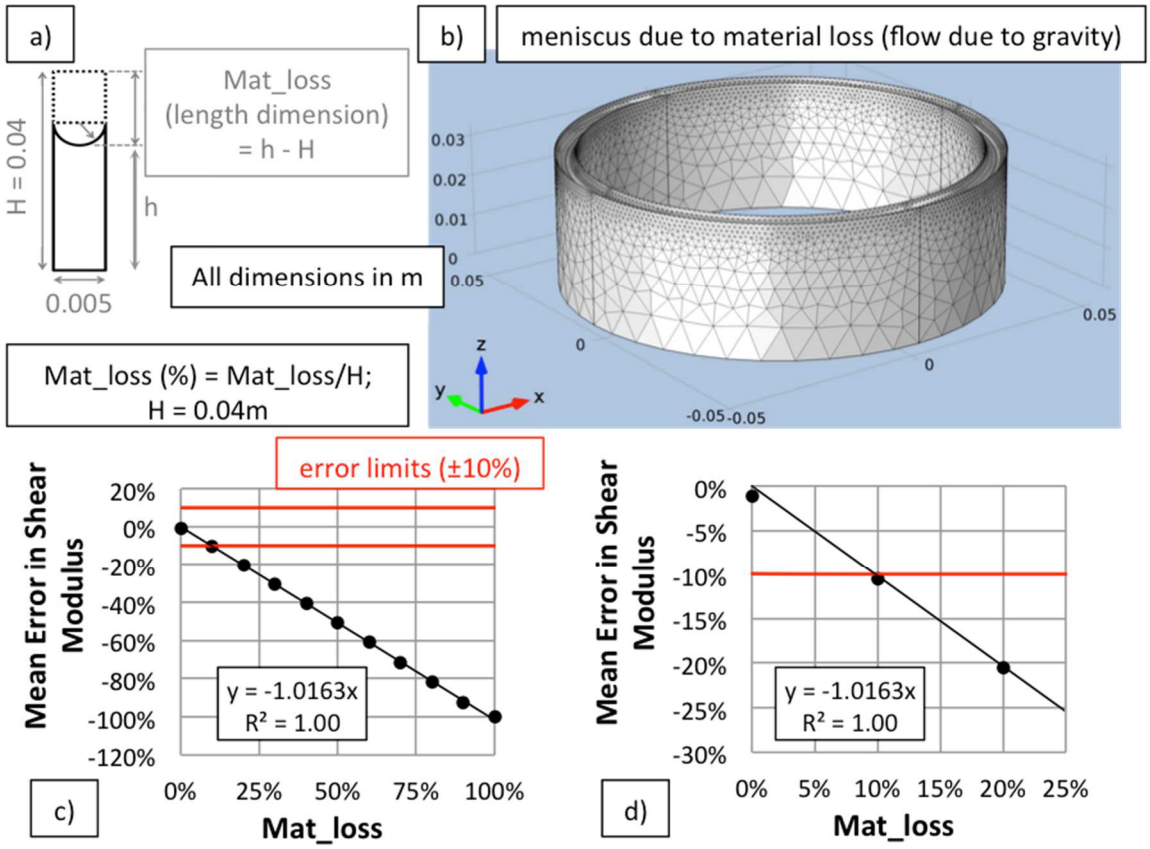

Figure 3-7. Error on shear modulus introduced by a material loss due to flow under gravity. a) Definition of studied material loss (Mat_loss in %). b) Illustration of the specimen having a circular meniscus (diameter equals specimen thickness) due to material loss and its Finite Elements mesh (example with 0.01m Mat_loss). c) Mean error in shear modulus obtained with a specimen after a certain material loss. d) Zoom for material loss between 0 and 25%.

3.2.4.3. *Effect of the formation of a circular section meniscus*

Finally, for the last bias investigated here (circular section meniscus with varying radius, from 5mm to 17.5mm), Poisson's ratio was observed to influence results. Error in the obtained modulus was less than 5% for a material with Poisson's ratio equal to 0.00, but that result lowered to less than 2% for a material with Poisson's ratio of 0.48. Varying the radius of the circular section meniscus from 5mm to 17.5mm decreased the error in shear modulus of about 1%. The circular section meniscus used in the study of material loss represents the worst-case scenario. Since the tested materials (bitumen and mastic) are expected to present Poisson's ratio near to 0.5, this bias was considered to introduce negligible error in the analysis of stiffness.

3.2.4.4. *Geometrical biases analysis conclusion*

From the study of the eccentricity bias, it was verified that less than 10% error on shear modulus is obtained for eccentricity lower than 2mm. From the study of the material loss bias, it was observed that less than 10% error on shear modulus is obtained for material loss lower than 10% (corresponding to a material loss, in mm, seen on the top of the specimens during tests, of 4mm). From the study of the shape of the circular meniscus, it was observed that for bitumen and mastic the error on shear modulus is lower than 2%.

Finally, it is concluded that ASR tests with eccentricity around 1mm, with material loss lower than 10% (4mm on the top of the specimen) associated with a meniscus, can still provide reliable stiffness measurements. This validates the measures obtained in this work. It is also observed that the biases presented in these studies may occur during the mounting and thermal conditioning processes, but do not significantly evolve during the test itself.

3.3. Materials and designation

3.3.1. Bitumen

3.3.1.1. *Description*

Straight-run bitumen produced by the company *Total*, and classified as a 50/70 penetration grade was used for the investigation of different phenomena during cyclic tests in this thesis. The bitumen is used in the French National Project (PN) IMPROVMURE. It presented 55dmm penetration in the needle penetration test (NF EN 1426, 2007), 49.4°C of softening point in the ring and ball test (NF EN 1427, 2007), and −15°C of Fraass breaking point (NF EN 12593, 2007). The 50/70 bitumen is designated in this thesis with the code B5070. It was also used in the fabrication of mastic, described next. The bitumen sample used throughout the entire thesis work was received in September 2015 and stocked at temperatures between 0 and 5°C in 1L containers (containing approximately 900mL of bitumen). Experimental results for B5070 are presented in Chapters 4 and 6.

3.3.1.2. *Specimen preparation for ASR tests*

Figure 3-8 presents the specimen preparation procedure. In order to prepare specimens for ASR tests, a 1L cylindrical container with bitumen was heated at 150°C for 3h30. For the preparation of the specimens, a given bitumen container was heated only once, in order to obtain similar aging condition for all tested specimens. The aluminium ASR moulds prepared to receive the bitumen (cf. Figure 3-8b) were heated at the same temperature (150°C) for 30min. The moulds have been previously meticulously cleaned using solvents and acetone, in order to guarantee good adherence between the bitumen and the metallic (aluminium) mould. The moulds are fixed with a centring accessory (cf. Figure 3-8a, situated at the bottom) in order to produce 5mm-thick annular specimens. A plastic film (sufficiently resistant to temperatures of the order of 150°C) is placed between this centring accessory and the cylindrical moulds in order to avoid material loss during

moulding. An adhesive tape is used in order to facilitate specimen finishing. Bitumen is poured with an excess of material, in order to compensate for thermal expansion/contraction and to ensure that, after specimen finishing, a 4cm-height specimen is obtained. Final aspect of the specimen is presented in Figure 3-8d. For each pouring process using a given 1L container, four specimens are prepared in four different moulds.

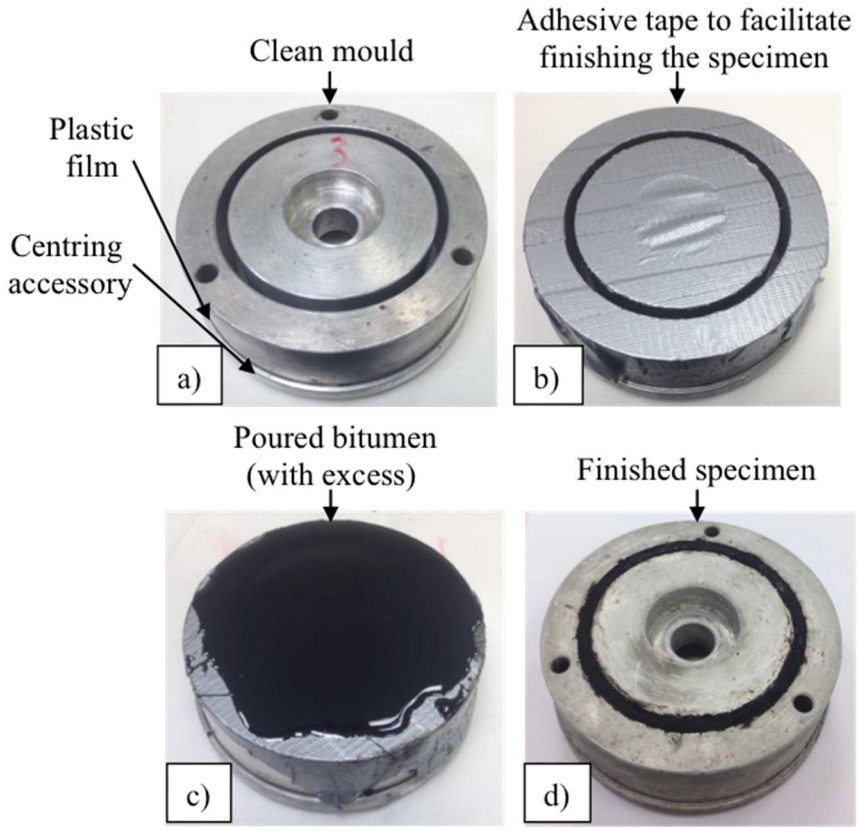

Figure 3-8. Bitumen ASR specimen preparation process. a) Clean mould before specimen preparation. b) Mould prepared for pouring with its protective adhesive tape. c) Mould with a poured specimen (material is poured in excess in order to compensate for thermal expansion/contraction). d) Finished specimen.

3.3.2. Glass beads mastic

Glass beads were used to fabricate mastic for this thesis. Using the beads allows having a model material with almost perfect spheres with controlled and relatively uniform diameter. The mastic prepared for this thesis presents 30% in volume of glass beads. It is designated M5070_30pc40-70. Experimental results for M5070_30pc40-70 are presented in Chapters 4 and 6.

3.3.2.1. *Description*

The bitumen used in the fabrication of Glass beads mastic is B5070, described in Section 3.3.1. The glass beads used for the fabrication of mastic were fabricated by the company *CVP Abrasif-Broyage*. The spherical glass beads present no free silica content and are chemically inert. Their chemical composition is mainly silicon dioxide (SiO_2, at least 70%), with also other oxides (at least 13% Na_2O, 7% CaO, 3% MgO, 0.5% Al_2O_3% and 0.2% K_2O). The specific gravity of the particles is 2.46g/cm^3. At least 80% in mass of the beads is of particles whose diameter is comprised between 40µm and 70µm.

3.3.2.2. *Fabrication process*

500g of B5070 were heated in a 1L cylindrical container at 150°C for 3h30. Then, 541.38g of glass beads were gradually added to the container, while mixing the fluid using a FARTOOLS bench drill equipped with a helical paddle (Figure 3-9). That was done in order to obtain mastic with a glass beads content of 30% in volume with respect to the total mixture (bitumen, with specific gravity of approximately 1.027g/cm^3, and glass beads). During the process, a hot plate was used in order to avoid stiffening of the bitumen due to cooling at room temperature during mixing. After, the mastic is allowed to cool at room temperature before being stocked at a temperature between 0 and 5°C.

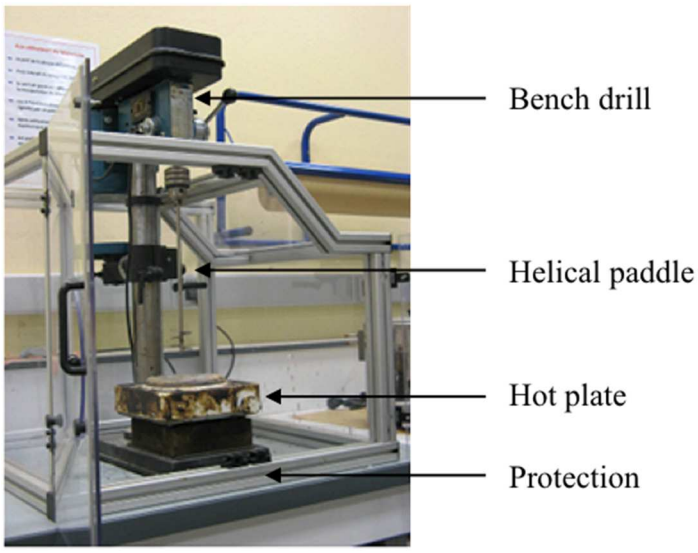

Figure 3-9. Apparatus for mastic preparation

3.3.2.3. *Specimen preparation for ASR tests*

In order to prepare specimens for ASR tests, a 1L cylindrical container with the prepared mastic was heated at 170°C for 3h30. The ASR moulds were heated at the same temperature for 30min. Specimen preparation process is similar to the one for bitumen (cf. Section 3.3.1.2), but

includes in addition mixing manually the mastic using a small paddle, in order to avoid segregation.

3.3.3. Bituminous mixtures

3.3.3.1. *Bituminous mixture specimen fabrication process for T-C tests*

The fabrication process follows the standard (NF EN 12697-35, 2007). The different materials (bitumen, aggregate and filler) are heated to the fabrication temperature of 150°C. Aggregate portions are weighted, and then mixed. The designed bitumen content is added and mixing is continued. The final mixture is then compacted in slabs following the standard (NF EN 12697-33, 2007) using a laboratory MLPC-type wheel compactor. The fabricated plates present dimensions of 60×40×12cm^3.

Cylindrical specimens for Tension-Compression (T-C) tests were obtained from the compacted slabs. The slabs are cut using a circular saw, and cored using a core drill, in order to obtain specimens with the desired geometry. Final geometry is a 75mm diameter and 140mm height cylinder. Cored cylindrical specimens present axial direction (where T-C loading is applied) coincident with the perpendicular direction to plate wheel compaction. Specimens produced this way can be considered as orthotropic (Di Benedetto et al., 2016, 2009), with at some conditions of loading frequency and temperature 25% difference in stiffness for axial and radial directions.

3.3.3.2. *BM1 (C. V. Phan, Di Benedetto, Sauzéat, Lesueur, et al., 2017)*

The bituminous mixture designated as BM1 in this thesis is the same as the one designated as E3550-5.1-2.5 in another study (C. V. Phan, Di Benedetto, Sauzéat, Lesueur, et al., 2017)(Q. T. Nguyen, 2011). Maximum theoretical specific gravity for BM1 is 2.486g/cm^3. Results for three specimens (BM1_A, BM1_B, BM1_C) were analysed in this thesis (cf. Chapter 4), presenting air voids contents of 2.9%, 2.4%, and 2.9%, respectively. BM1_A and BM1_B were used for complex modulus tests. BM1_B and BM1_C were used for an investigation of nonlinearity.

The bitumen used in the fabrication of BM1 is a pure straight-run 35/50 penetration grade. The bitumen content used is 5.1%. BM1 uses a continuous grading curve with nominal maximum aggregate size of 14mm. It is a High Modulus Asphalt (*Enrobé à Module Élevé* - EME) (NF EN 13108-1, 2007), containing hydrated lime (2.5% in total mixture mass). Except for the hydrated lime, aggregate's origin was the quarry "Haut-Lieu", France. Aggregate formulation presents 24.4% of 10/14 aggregate, 21.7% of 6/10 aggregate, 14.3% of 4/6 aggregate, 15.8% of 2/4 aggregate, 23.8% of 0/2 aggregate (including the hydrated lime).

3.3.3.3. *BM2 (Q. T. Nguyen, 2011)*

The bituminous mixture designated as BM2 in this thesis is the same as M5 (Q. T. Nguyen, 2011), whose experimental results were obtained in Q. T. Nguyen's thesis, and analysed in this work following a new approach (cf. Chapter 5). Maximum theoretical specific gravity for BM2 is 2.563g/cm^3. Results for two specimens (BM2_A, BM2_B) were analysed in this thesis, presenting air voids contents of 1.3% and 0.8%, respectively.

The bitumen used in this formulation is initially a 50/70 penetration grade, modified by 1.2% in mass of bitumen of polyphosphoric acid. The resulting modified bitumen is a 35/50. The bitumen content used in the mixture is 5.7%. BM2 uses a continuous grading curve of type BBSG (*Béton Bitumineux Semi-Grenu*) with nominal maximum aggregate size of 10mm. Aggregate is the same as in F. Olard's thesis (Olard, 2003), which is a crushed diorite (from the quarry "Moreau" at Mazières-en-Gatine, France). Aggregate formulation presents 43% of 6/10 aggregate, 23% of 2/6 aggregate, 32% of 0/2 aggregate, and 2% of added limestone filler. The specific gravities of each of those materials are 2.832, 2.789, 2.817, 2.689g/cm^3, respectively.

3.3.3.4. *BM3 (Q. T. Nguyen, 2011)*

The bituminous mixture designated as BM3 in this thesis is the same as M6 (Q. T. Nguyen, 2011), whose experimental results were obtained in Q. T. Nguyen's thesis, and analysed in this work following a new approach (cf. Chapter 5:). Maximum theoretical specific gravity for BM3 is 2.590g/cm^3. Results for two specimens (BM3_A, BM3_B) were analysed in this thesis, presenting air voids contents of 4.7% and 4.3%, respectively. As seen next, BM3 is similar to BM2, except for the bitumen modification.

The bitumen used in this formulation is the same 50/70 base bitumen as for BM2, without any modification. The bitumen content used in the mixture is 5.7%. BM3 also uses a continuous grading curve of type BBSG (*Béton Bitumineux Semi-Grenu*) with nominal maximum aggregate size of 10mm. Aggregate is the same as in Dr. Olard's thesis (Olard, 2003), which is a crushed diorite (from the quarry "Moreau" at Mazières-en-Gatine, France). Aggregate formulation presents 41% of 6/10 aggregate, 24% of 2/6 aggregate, 30.2% of 0/2 aggregate, and 4.8% of added limestone filler. The specific gravities of each of those materials are 2.832, 2.789, 2.817, 2.689g/cm^3, respectively.

3.4. Experimental campaign overview

Table 3-1 summarises the performed tests on the investigated materials. For all tested materials, complex modulus tests were performed in order to obtain stiffness information at very small strain levels. This information is required for the interpretation of all other tests used in this work. In order to accomplish each of the goals of this thesis (cf. Chapter 1), different experiments have been designed, as follows.

- In order to evaluate the effect of nonlinearity in bitumen, mastic and bituminous mixture, strain amplitudes sweeps were performed. Strain amplitude sweeps consist in applying sinusoidal loading to the material with different amplitudes, and evaluating the effect of this change in amplitude on the measured equivalent stiffness. For Bitumen and mastic, common Strain Amplitude Sweep (SAS) tests were used, i.e., few cycles at a given strain amplitude were applied in order to obtain a modulus. Then, another amplitude is tested, and so forth. For bituminous mixtures, a special kind of strain amplitude sweep was proposed in this work. It is called Strain Amplitude Sweep Test for Nonlinearity Evaluation (SASTENOLE). Different frequencies and temperatures were tested for all materials (cf. Chapter 4);
- In order to analyse the effect of local self-heating during cyclic tests in bituminous mixtures at different conditions of temperature, frequency and loading amplitude, cyclic loading was applied for many cycles (of the order of 10,000, depending on the test). These results have been previously obtained (Q. T. Nguyen, 2011), and analysed in this work from a different perspective. In this thesis, those tests are called Phase I Fatigue tests (cf. Chapter 5);
- In order to experimentally demonstrate the combined effects of the studied phenomena (nonlinearity, self-heating, thixotropy and damage), Load and Rest Periods (LRP) tests were used. These tests consist basically in applying sinusoidal loading cycles (observing modulus decrease), followed by rest periods in which modulus recovery is observed using “very small strain” sinusoidal loading (cf. Chapter 6). After LRP tests, a fatigue tests (until failure) was performed on some of the specimens.

Table 3-1. Overview of the analysed experiments on bitumen (B5070).

Test set-up	Material/Specimen	Complex Modulus (E^* and ν^*, or G^*)	Strain Amplitude Sweep (SAS or SASTENOLE)	Phase I Fatigue	Load and Rest Periods (LRP)	Fatigue until failure
ASR	**B5070_A**	X			X	X
ASR	**B5070_B**	X			X	X
ASR	**B5070_C**	X			X	
ASR	**B5070_D**				X	X
ASR	**B5070_E**				X	X
ASR	**B5070_F**		X			
ASR	**B5070_G**		X*			

*A complementary test, called Alternating Strain Amplitude test (ASA, Chapter 6), was performed in B5070_G.

Table 3-2. Overview of the analysed experiments on mastic (M5070_30pc40-70).

Test set-up	Material/Specimen	Complex Modulus (E^* and ν^*, or G^*)	Strain Amplitude Sweep (SAS or SASTENOLE)	Phase I Fatigue	Load and Rest Periods (LRP)	Fatigue until failure
ASR	**M5070_30pc40-70_A**	X			X	X
ASR	**M5070_30pc40-70_B**	X			X	X
ASR	**M5070_30pc40-70_C**		X		X	X

Table 3-3. Overview of the analysed experiments on bituminous mixtures (BM1, BM2 and BM3).

Test set-up	Material/Specimen	Complex Modulus (E^* and ν^*, or G^*)	Strain Amplitude Sweep (SAS or SASTENOLE)	Phase I Fatigue	Load and Rest Periods (LRP)	Fatigue until failure
T-C	**BM1_A**	X				
T-C	**BM1_B**	X	X			
T-C	**BM1_C**		X			
T-C	**BM2_A**			X		
T-C	**BM2_B**			X		
T-C	**BM3_A**			X		
T-C	**BM3_B**			X		

Chapter 4: NONLINEARITY OF BITUMINOUS MATERIALS

Chapter 4: Nonlinearity of Bituminous Materials.....76
4.1. Introduction.....77
4.2. Tension-compression experiments on bituminous mixture specimens 80
4.2.1. Complex modulus test at 50μm/m 80
4.2.2. Strain Amplitude Sweep Tests for NonLinearity Evaluation (SASTENOLE).....83
4.2.3. Analysis of SASTENOLE test results on BM1_B.....85
4.2.4. Analysis of SASTENOLE test results on BM1_C.....101
4.2.4.1. Strain dependence of norm of complex modulus and phase angle.....102
4.2.4.2. Strain dependence of norm and phase angle of complex Poisson's ratio.....109
4.2.5. Transient effects during SASTENOLE tests.....113
4.3. Annular shear experiments on bitumen and mastic specimens 115
4.3.1. Complex shear modulus test at "low" amplitudes 115
4.3.2. Strain Amplitude Sweep (SAS) tests on bitumen and mastic 118
4.3.2.1. Cyclic effects during Strain Amplitude Sweep (SAS) tests 119
4.3.3. Analysis of Strain Amplitude Sweep (SAS) test results 121
4.4. LVE limits of bituminous materials.....127
4.5. Conclusion on nonlinearity.....130

4.1. Introduction

This chapter presents the investigation on nonlinearity of bituminous materials. The part of the investigation dealing with bituminous mixtures resulted in the publication of a journal paper (Mangiafico et al., 2017), and involved the supervision of the works of two master's students (Fan, 2016; T. K. Phan, 2015).

In linear viscoelasticity, a sinusoidal loading (in steady state) with constant strain amplitude leads to a response in stress amplitude in such a way that the ratio between stress amplitude and strain amplitude is a constant, known as norm of complex modulus. The phase between the two signals is also a constant, known as phase angle, independent of the loading amplitude. Then, the complex modulus is independent of the loading level. For bituminous materials, this is generally considered true for a small number of applied cycles at sufficiently low strain amplitudes (Airey & Rahimzadeh, 2004; Airey et al., 2002, 2003; Bahia et al., 1999; Coutinho et al., 2014; Delaporte et al., 2007; Di Benedetto et al., 2001; Doubbaneh, 1995; Gauthier et al., 2010; Goodrich, 1991).

The phenomenon of nonlinearity is intended as the dependence of the material's stiffness on the loading level (stress or strain dependence). It may occur even for very small strain amplitudes (around some tens of μm/m). For a material presenting nonlinearity, under sinusoidal strain input, the stress output in the material (approximately sinusoidal – considering small nonlinearities – with constant amplitude for all cycles) is expected to deviate from the linear viscoelastic predicted response, i.e. the ratio between stress amplitude and strain amplitude, as well as their phase difference, is expected to depend on the loading level. This dependence on loading level is the object of the investigation presented in this chapter.

As presented in Section 2.3.2, complex modulus' definition considers a superposition principle, which is rigorously valid only in the case of linearity of the material mechanical response. Still, for small nonlinearities, the concept of "equivalent" complex modulus can be considered (cf. Sections 2.4.1 and 3.2.3). The norm of equivalent complex modulus is the ratio between the measured stress amplitude and the measured strain amplitude during sinusoidal loading, provided that nonlinearity is small (signals can be approximated by sinusoidal functions). The phase angle of equivalent complex modulus is the phase difference between stress and strain measured signals.

Although not tested separately in this work, granular materials are known to present nonlinearity, higher strain leading to lower modulus (Kongkitkul et al., 2008; Sauzéat, 2003; Tatsuoka, Kohata, & Lo Presti, 1995; Tatsuoka & Shibuya, 1992)(Sauzéat, 2003; Tatsuoka et al., 1995; Tatsuoka & Shibuya, 1992). This may be due to nonlinearity of the particle contacts' mechanical behaviour, and/or to strain-dependent changes in the force chains mobilised in the granular skeleton of the material.

Because of the large difference in stiffness between the bitumen phase and the aggregate particles, in the bituminous mixture, most of the bulk strain is concentrated in the binder. Using digital image analysis and a numerical modelling procedure, it can be shown that applying a shear strain of 1% in a typical bituminous mixture can result in a strain distribution in the bituminous matrix whose values vary from 0.3 to 32% (Bahia et al., 1999). At some points of the matrix, strains from 10 to 100 times higher than the bulk strain applied to the bituminous mixture are to be expected (Babadopulos et al., 2017a; Babadopulos, Sauzéat, & Di Benedetto, 2016) (further

discussion on this point is presented in Chapter 5). The fact that, locally, strain in bitumen is potentially beyond the LVE limit, could explain partially the origin of the strain dependence of modulus in bituminous mixtures, as pointed out in the literature (Airey & Rahimzadeh, 2004; Airey et al., 2002, 2003; Coutinho et al., 2014).

As it can be seen, bituminous mixtures could inherit a strain dependent mechanical behaviour from the heterogeneously loaded bitumen (due to the particles presence) or from the granular stacking itself. At present, the literature does not present further information on the relationship between the nonlinearity observed in bitumen, mastic and bituminous mixtures.

The most common procedure to investigate nonlinearity in bituminous materials is the application of amplitude sweeps, i.e. tests that include some loading cycles at different levels of stress or strain amplitude. If the loading is controlled in strain signal, the test is called a strain amplitude sweep. Most of the research available in the literature uses increasing amplitude sweeps. It was concluded for bituminous materials that, at fixed frequency and temperature, the norm of complex modulus decreases with increasing strain amplitude, while the phase angle increases (Airey & Rahimzadeh, 2004; Airey et al., 2002, 2003; Bahia et al., 1999; Coutinho et al., 2014; Di Benedetto, Nguyen, et al., 2011; Gauthier et al., 2010; Mangiafico et al., 2015; Q. T. Nguyen et al., 2015; B. Underwood & Kim, 2013; B. S. Underwood & Kim, 2012). (Gauthier et al., 2010) studied the directions of the biasing effects, including nonlinearity, in Black diagrams and Cole-Cole plots. The referred authors used experimental results from cyclic tests on trapezoidal bituminous mixture specimens and from Cone and Plate and Plate and Plate Dynamic Shear Rheometer (DSR) geometry for bitumen specimens. They observed, for testing at 10°C and 10Hz, non-negligible nonlinearity effects in the cyclic response of bituminous materials, following directions different from other effects such as self-heating or damage.

The strain amplitude level below which the assumption of Linear ViscoElastic (LVE) behaviour can be made is referred to as “LVE limit”. In the literature, the LVE limit has been investigated by applying loading to bituminous materials at different strain levels. Among others, (Airey & Rahimzadeh, 2004; Airey et al., 2002, 2003) performed amplitude sweep tests (varying either the controlled strain amplitude or the controlled stress amplitude) on different kinds of bitumen and bituminous mixtures. Those authors defined the LVE limit as the value of strain amplitude above which the material’s norm of complex modulus is decreased by more than 5% with respect to the modulus in the linear region (low strain levels). From that definition, it was found that the LVE limit of pure bitumen is around 1% (or 10,000μm/m) shear strain, while for mixtures it is of the order of 100μm/m axial strain (these values are approximate and depend on temperature). For bituminous mixtures LVE limit, a previous work had determined the same order of magnitude (Doubbaneh, 1995). While bitumen LVE limit seemed to depend on temperature and frequency, approximately constant values were obtained for mixtures.

In the previously referred works, the test geometry used for bituminous mixtures was a cylinder under tension-compression, which produces homogeneous states of stress and strain (Di Benedetto et al., 2001), and results with simple interpretation. The test geometry used for bitumen was a cylinder under torsion, which produces non-homogeneous states of stress and strain in the material (Di Benedetto et al., 2001), with non-sheared material in the centre of the cylinder and material submitted to maximum shear (whose value is inaccessible without prior knowledge of the

material behaviour) at the external radius of the cylinder. In this case, with significant nonlinearity, the hypothesis of homogeneous stiffness in the specimen, used to analyse test results (convert torque and rotation into stress and strain) to obtain a complex modulus, may not be valid. That means that the actual shear applied at a certain point in the material cannot be obtained in a simple manner, and that the obtained complex modulus results cannot represent actual material behaviour. However, it may be argued that for low nonlinearity effect (as below the LVE limit) results are sufficiently reliable, at least to estimate the LVE limit. (Gauthier et al., 2010) compared complex shear modulus results on bitumen specimens obtained both with the Cone and Plate (homogenous test) and Plate and Plate (non-homogeneous test) Dynamic Shear Rheometer (DSR) geometry. Results were obtained for bitumen specimens at 10°C and 10Hz. At these loading conditions, for a relative change in the measured modulus of less than 5% (which was observed at around 1% shear strain), results for both geometries seemed comparable. The difference increased up to 10% at 3% shear strain, when the measured modulus had changed by 30% and the measured phase angle by 2°. Then, it is clear that the use of a homogeneous test for investigating nonlinearity is more adequate.

Recent studies have shown that bituminous mixtures exhibit a non-negligible variation of their complex modulus even below 100μm/m (considered as the bituminous mixture LVE limit by many authors) (Dougan et al., 2003; Mangiafico et al., 2015; Q. T. Nguyen et al., 2015; B. S. Underwood & Kim, 2012; Uzan & Levenberg, 2007). These results suggest that it could be misleading to consider that nonlinearity is "triggered" when strain/stress amplitude is increased up to a certain limit. It seems that it actually manifests gradually with the amplitude increase. Nevertheless, using the definition involving a 5% change in norm of complex modulus can be of practical use. The definition is maintained in this work for purposes of comparison between the nonlinearity observed in bitumen, in mastic and in bituminous mixture.

It is important to highlight that, in this work, nonlinearity is intended purely as strain dependence of complex modulus. In fact, the repetition of loading cycles on the material can lead to the occurrence of other reversible phenomena influencing material properties, such as transient effects, self-heating and possibly thixotropy (Di Benedetto, Nguyen, et al., 2011; Di Benedetto et al., 2001; Mangiafico et al., 2015; Q. T. Nguyen et al., 2015). These phenomena can induce variations of complex modulus that could be interpreted as strain dependence if not correctly taken into account. During increasing strain amplitude sweeps, all mentioned phenomena, including nonlinearity, induce a decrease in the norm of complex modulus. For this reason, this kind of test alone cannot easily distinguish nonlinearity from other reversible phenomena. These phenomena, including nonlinearity, are known in the literature as biasing effects (due to the bias they produce during fatigue tests). Their identification and quantification represents a challenge when analysing tests on bituminous materials (Moreno-Navarro, Sol-Sánchez, et al., 2015). The reader may refer to other studies for more information about this subject (Bodin et al., 2004; Di Benedetto et al., 1996; Di Benedetto, de La Roche, et al., 2004; Gauthier et al., 2010; Y. R. Kim et al., 1997; Mangiafico et al., 2015; Q. T. Nguyen et al., 2015; Soltani & Anderson, 2005).

The objective of this investigation is to determine how nonlinearity affects the mechanical response of bituminous materials during cyclic loading. The phenomenon of nonlinearity is investigated on bitumen (B5070, cf. 3.3.1, for material description), mastic (M5070_30pc40_70, cf. 3.3.2) and bituminous mixture (BM1, cf. 3.3.3.2). Also, the investigation addresses the relation

between the nonlinearity observed in bituminous mixtures and the one observed in bitumen and mastic. For bitumen and mastic, shear strains up to 100,000μm/m (10%) were investigated. Higher strain amplitudes were not used in order to maintain the small strain hypothesis from continuum mechanics (and consequent linearity of the strain tensor, cf. Figure 3-4). For bituminous mixtures, nonlinearity was investigated at very small strains (below 150μm/m) domain. The effects of nonlinearity on the equivalent complex modulus are investigated in terms of variations of norm and phase angle as functions of the applied strain amplitude. The evolution of equivalent complex modulus with strain amplitude is studied in Black and Cole-Cole diagrams, allowing the investigation of directions of nonlinearity on those representations. For bituminous mixtures, a new test protocol is developed, composed of both increasing and decreasing strain amplitude sweeps, performed at different temperatures and frequencies. Results obtained during increasing and decreasing sweeps are compared, in order to separate the effects of nonlinearity from those of other phenomena related to cyclic loading.

4.2. Tension-compression experiments on bituminous mixture specimens

Tension-compression (T-C) tests were used (cf. Section 3.2.2 for test set-up) for the characterisation of bituminous mixture. A characterisation of the "linear" behaviour, given by the complex modulus (at fixed strain amplitude of 50μm/m), and a characterisation of the nonlinear behaviour (varying strain amplitude) were performed.

Two experimental campaigns on bituminous mixture BM1 were carried out, one involving specimens BM1_A and BM1_B and the other one involving specimen BM1_C. The first one focused on nonlinearity effects at temperatures near 10°C (chosen temperatures varied from 8 to 14°C, with frequencies from 0.3 to 10Hz), used for fatigue tests (NF EN 12697-24, 2012). For fatigue tests, nonlinearity is seen as a biasing phenomenon, whose effect during fatigue tests needs to be corrected. Hence, in order to better interpret fatigue tests at 10°C, a precise characterisation of nonlinearity around 10°C and 10Hz is required, since specimen temperature may vary significantly during fatigue tests (Babadopulos et al., 2017a; Bodin et al., 2004; Di Benedetto, Nguyen, et al., 2011; Mangiafico et al., 2015; Riahi et al., 2016, 2017). The second experimental campaign enlarged the spectrum of frequencies and temperatures tested (chosen temperatures varied from −4 to 28°C, with frequencies from 0.1 to 10Hz), in order to obtain a characterisation of the nonlinearity phenomenon at a wider range of temperature and frequency.

4.2.1. Complex modulus test at 50μm/m

LVE behaviour of BM1 was characterised by means of complex modulus tests at different temperatures (ranging from -25°C to 50°C) and frequencies (from 0.003 to 10Hz). Two specimens were tested (BM1_A for the first experimental campaign on nonlinearity, and BM1_C for the second one). Axial strain amplitudes (ε_0) of 50±5μm/m were applied. A scheme of the utilised loading path is presented in Figure 4-1. Results are presented in Figure 4-2.

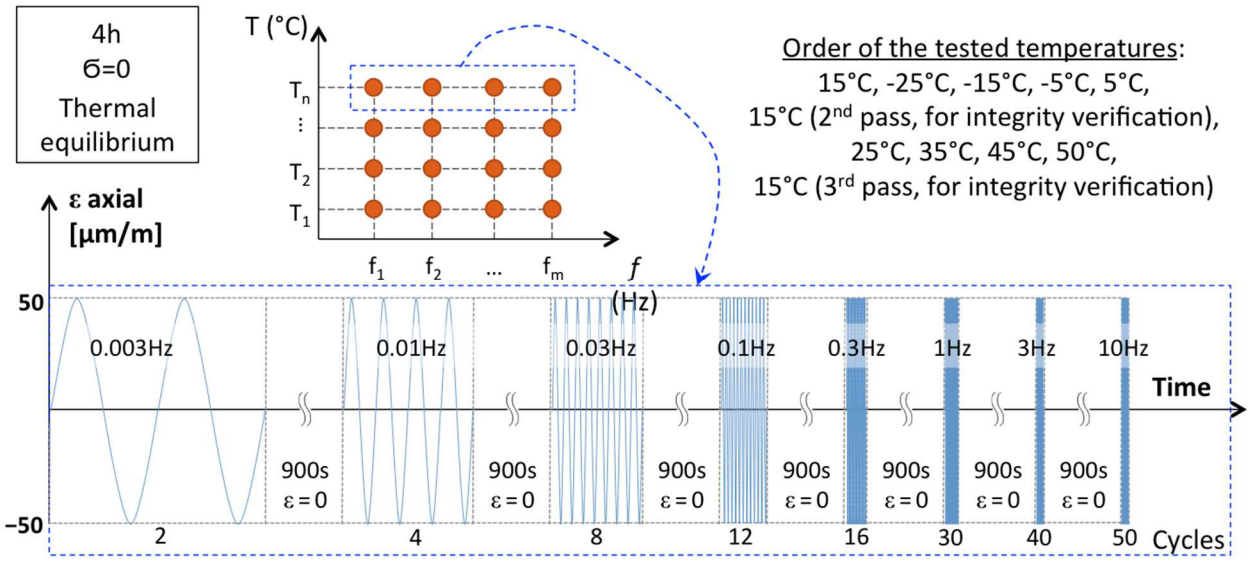

Figure 4-1. Scheme of the bituminous mixture complex modulus test (T-C setup, cf. Figure 3-3) loading path.

Obtained test results were then fitted using 2S2P1D (2 Springs, 2 Parabolic elements, 1 Dashpot) analogical model (Olard & Di Benedetto, 2003) (cf. Eq. 2-28 and Eq. 2-30), including the parameters used to describe three dimensional behaviour, i.e. to obtain Poisson's ratio (Di Benedetto, Delaporte, et al., 2007). Fitted 2S2P1D model is presented in Table 4-1.

Table 4-1. 2S2P1D model and WLF equation parameters used to model the LVE behaviour of the studied bituminous mixtures.

	2S2P1D model parameters (T_{ref} = 15°C)							3D 2S2P1D param.			WLF equation		
Specimen	**E_{00} (MPa)**	**E_0 (MPa)**	**k (-)**	**h (-)**	**δ (-)**	**$\tau_{0,E}$ (s)**	**β (-)**	**ν_{00} (-)**	**ν_0 (-)**	**$\tau_{0,\nu}$ (s)**	**T_{ref} (°C)**	**C_1 (-)**	**C_2 (°C)**
BM1_A	18	40,300	0.172	0.570	1.90	$1.22 \cdot 10^{-1}$	95	0.50	0.25	$1.20 \cdot 10^{2}$	15.0	36.5	238.5
BM1_C	25	39,200	0.172	0.570	1.90	$1.69 \cdot 10^{-1}$	95	0.47	0.28	$1.66 \cdot 10^{2}$	15.0	36.5	238.5

The first experimental campaign (complex modulus test performed on BM1_A) was carried out in 2015, while the second one was in 2016 (complex modulus test performed on BM1_C). Then, it was expected that the mixture in specimen BM1_C would be slightly aged with respect to the one in BM1_A. The aging explains the slight difference in the characteristic time for the two specimens aging (Mangiafico, 2014), also perceptible in Figure 4-2c (time-shift between master curves). Other slight differences may be explained by sample-to-sample variation (in E_0 may be influenced by the specimen air voids content, (Cardona, 2016) or by test conditions (E_{00} may be influenced by the mean strain applied to the specimen at the higher temperatures, (Cardona, 2016).

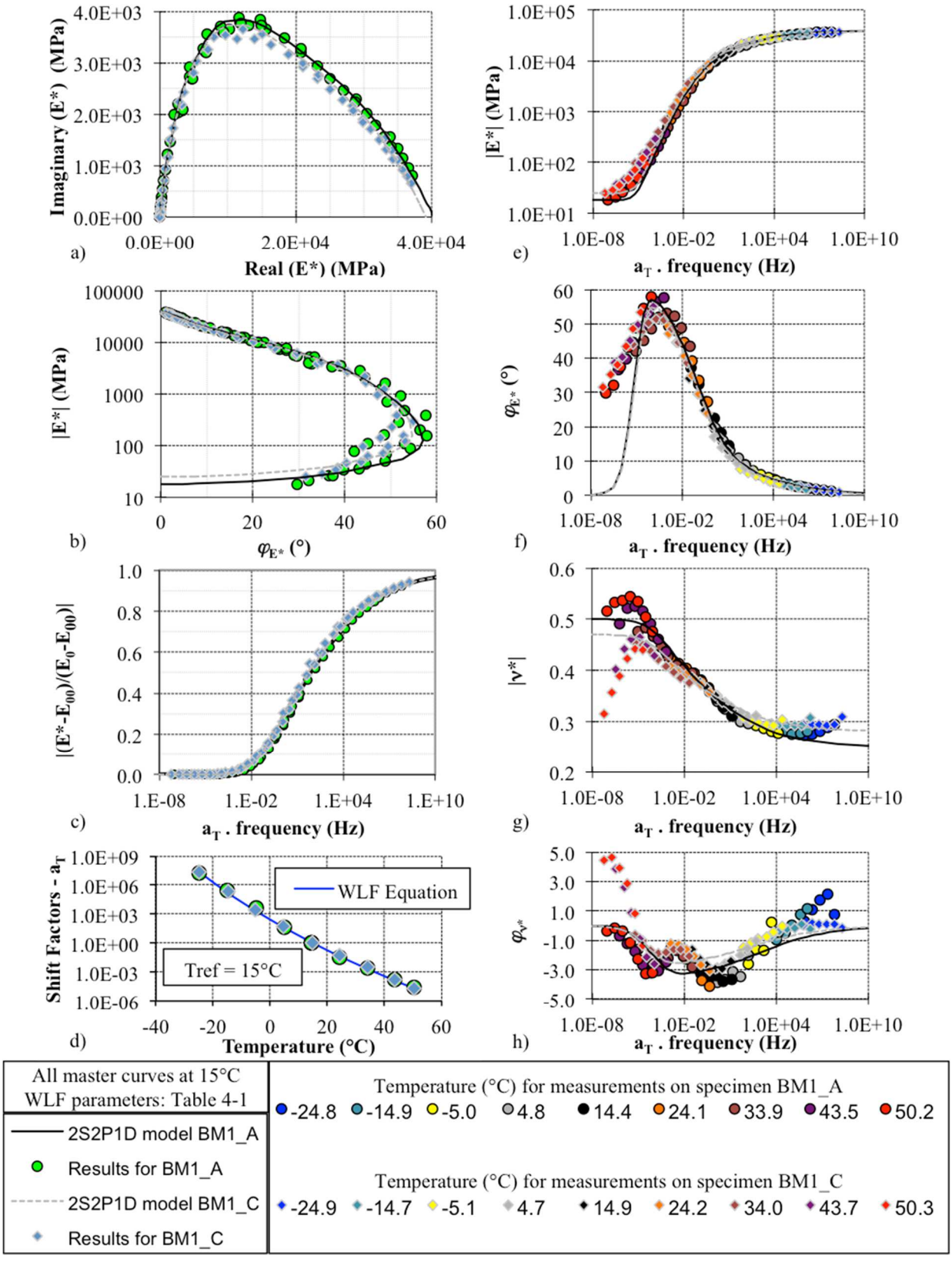

Figure 4-2. 2S2P1D model and WLF equation fitting of experimental data (BM1_A and BM1_C specimens) obtained from Tension/Compression (T-C) complex modulus tests at 50μm/m: a) Cole-Cole plot; b) Black diagram; c) normalized complex modulus master curve (at 15C); e) norm and f) phase angle of complex modulus; g) norm and h) phase angle of complex Poisson's ratio master curve (at 15°C) with details on tested temperatures.

4.2.2. Strain Amplitude Sweep Tests for NonLinearity Evaluation (SASTENOLE)

An original test protocol was designed in order to investigate nonlinearity of bituminous mixtures. The procedure is composed of a series of Strain Amplitude Sweep Tests for NonLinearity Evaluation (SASTENOLE). For BM1_B, 16 SASTENOLE were carried out at four different temperatures (8, 10, 12 and 14°C) and four different frequencies (0.3, 1, 3 and 10Hz). For BM1_C, 27 SASTENOLE tests were conducted, at nine different temperatures (−4, −2, 0, 10, 12, 14, 24, 26 and 28°C) and three different frequencies (0.1, 1 and 10Hz). For each temperature, a thermal conditioning time of four hours is maintained (imposing a nil stress in stress control mode). For each of the combinations of temperature and frequency, the SASTENOLE test consists of a series of loading sequences at different maximum targeted strain amplitudes. For BM1_B, eight loading sequences at four different maximum targeted strain amplitudes (50, 75, 100 and 110μm/m) were applied. For BM1_C, six loading sequences at three different maximum targeted strain amplitudes (50, 85 and 120μm/m) were applied.

Figure 4-3 shows a scheme of the test procedure applied on BM1_B. A detailed scheme for the SASTENOLE test at 14°C and 0.3Hz is also presented as an example in this figure. For each maximum targeted strain amplitude, from the lowest one (50μm/m) to the highest one (110μm/m), two loading sequences are performed. The first is composed of five cycles at the constant maximum targeted strain amplitude, followed by a decreasing sweep of 50 cycles during which strain amplitude decreases linearly to zero. After a rest period of 900s (in strain control mode), the second loading sequence is performed. Strain amplitude is linearly increased from zero to the targeted maximum value during 50 cycles (increasing sweep), after which five cycles are applied at the constant maximum targeted strain amplitude. Before performing the two loading sequences for the next targeted maximum strain amplitude, a 900s rest period is maintained.

Considering the 16 SASTENOLE tests (at four different temperatures and four different frequencies) on BM1_B, the four different targeted maximum strain amplitudes and the two strain amplitude evolution trends during sweeps (decreasing and increasing), a total of 128 testing sequences are applied (test duration is approximately 48 hours). For BM1_C, the 27 SASTENOLE lead to 162 testing sequences. Due to the higher difference in temperature, a particular set of PID control parameters needs to be adjusted for each group of three temperatures (around −2, 12 and 26°C) and the test is run separately. Testing on BM1_C required approximately a week.

Figure 4-3 also shows data obtained for the norm of complex modulus during the SASTENOLE test at 14°C and 0.3Hz), used as an example. At these conditions, a variation of $|E^*|$ of more than 20% of its initial value was observed for some sequences. For the norm of complex modulus, small variations are observed. As it will be seen in the next sections, nonlinearity will affect more importantly the Poisson's ratio at high temperatures and low frequencies. Since the test condition at 14°C, 0.3Hz was the one that presented more nonlinearity, and no effect on Poisson's ratio was observed, it was concluded that for the tested temperature and frequency range applied on BM1_B, no nonlinearity is observed on the Poisson's ratio. A further discussion on this parameter is presented for the results obtained from the second experimental campaign, on BM1_C.

Some outlier data were observed and are explained by the following different reasons:

– Data obtained for cycles performed at very low strain amplitudes can be affected by important relative errors due to the accuracy of the load cell and of the extensometers. Data obtained for strain amplitudes lower than 10μm/m were not considered reliable (due to excessive noise in measurements).

– The strain signal applied in the last cycle of each increasing loading sequence (5th cycle at constant amplitude) was found not to respect exactly the targeted sinusoidal pulse, probably due to the control system of the hydraulic press.

– Transient effects develop in the material just after initial load application, which become negligible after the first two or three cycles (Gayte et al., 2016)(Gayte et al., 2016).

Those outliers were excluded from the analyses presented in this work.

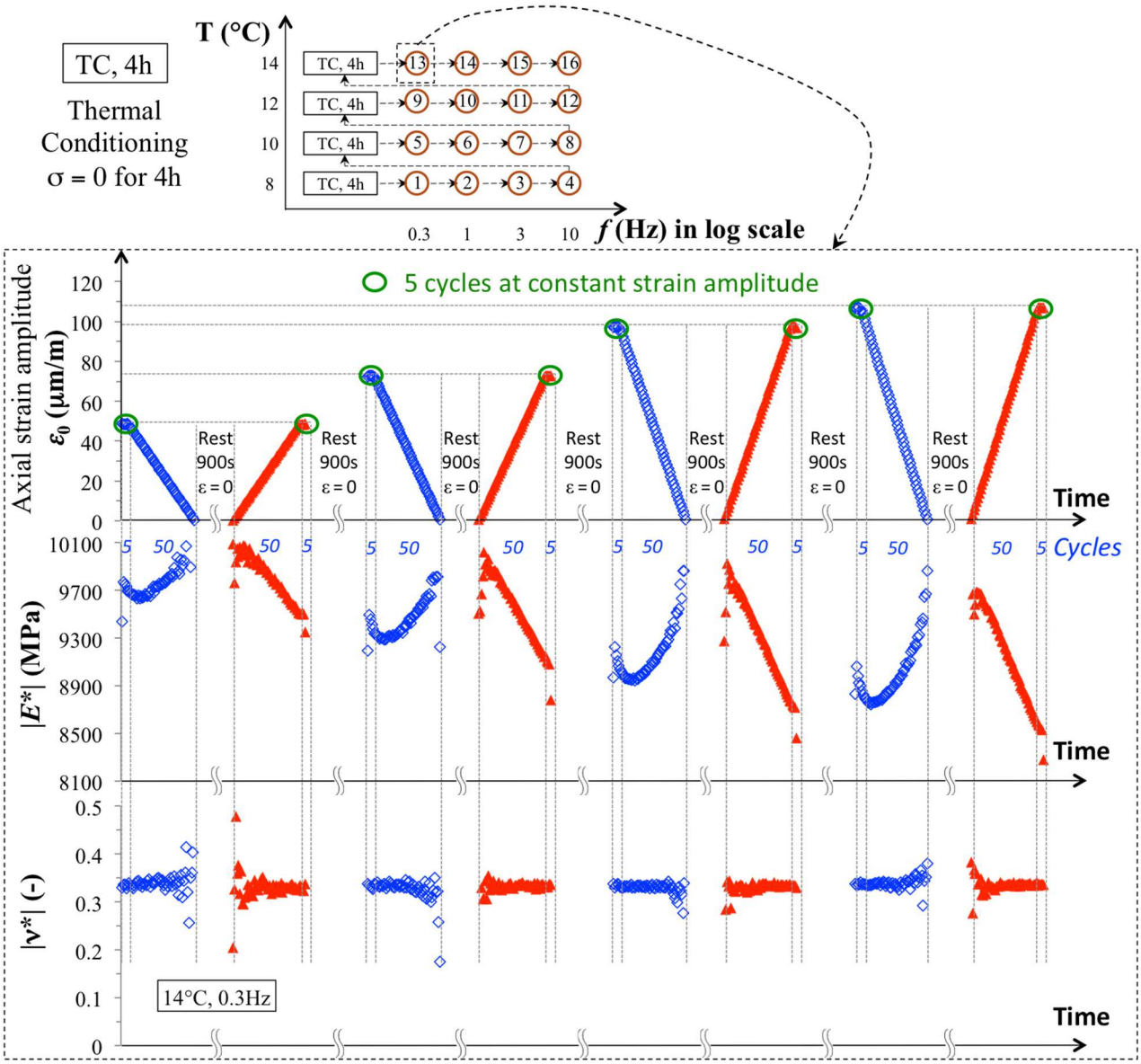

Figure 4-3. Detailed scheme of the 16 Strain Amplitude Sweep Tests for NonLinearity Evaluation (SASTENOLE) applied on BM1_B, with an example of results obtained for the norms of complex modulus and Poisson's ratio during the eight sequences of the SASTENOLE test #13, at 14°C, 0.3Hz. A total of 128 sequences were performed and analysed on BM1_B.

4.2.3. Analysis of SASTENOLE test results on BM1_B

Before proceeding to the analysis of SASTENOLE results, it is important to recall that, rigorously, complex modulus is a material property defined considering Boltzmann's superposition principle (cf. Section 2.3.2), so linearity in material's response is assumed. In the case of small nonlinearities, the concept of equivalent (or apparent) complex modulus is required (cf. definition and discussion on Sections 2.3.2, 2.4.1, 3.2.3, and 4.1). This investigation explores the influence of the applied strain amplitude on the measured equivalent complex modulus.

Figure 4-4 shows examples of the results obtained for increasing and decreasing amplitude sweeps, with a maximum targeted amplitude of 110µm/m, during SASTENOLE tests #4 (8°C,

10Hz) and #13 (14°C, 0.3Hz) on specimen BM1_B. Norm ($|E^*|$) and phase angle φ of complex modulus and dissipated energy per cycle W_N are plotted as functions of the imposed strain amplitude. All obtained results are reported in the figures, including the outlier data previously explained. Results obtained during cycles performed at strain amplitudes lower than 10μm/m are shown in shaded areas and were not considered for further analysis.

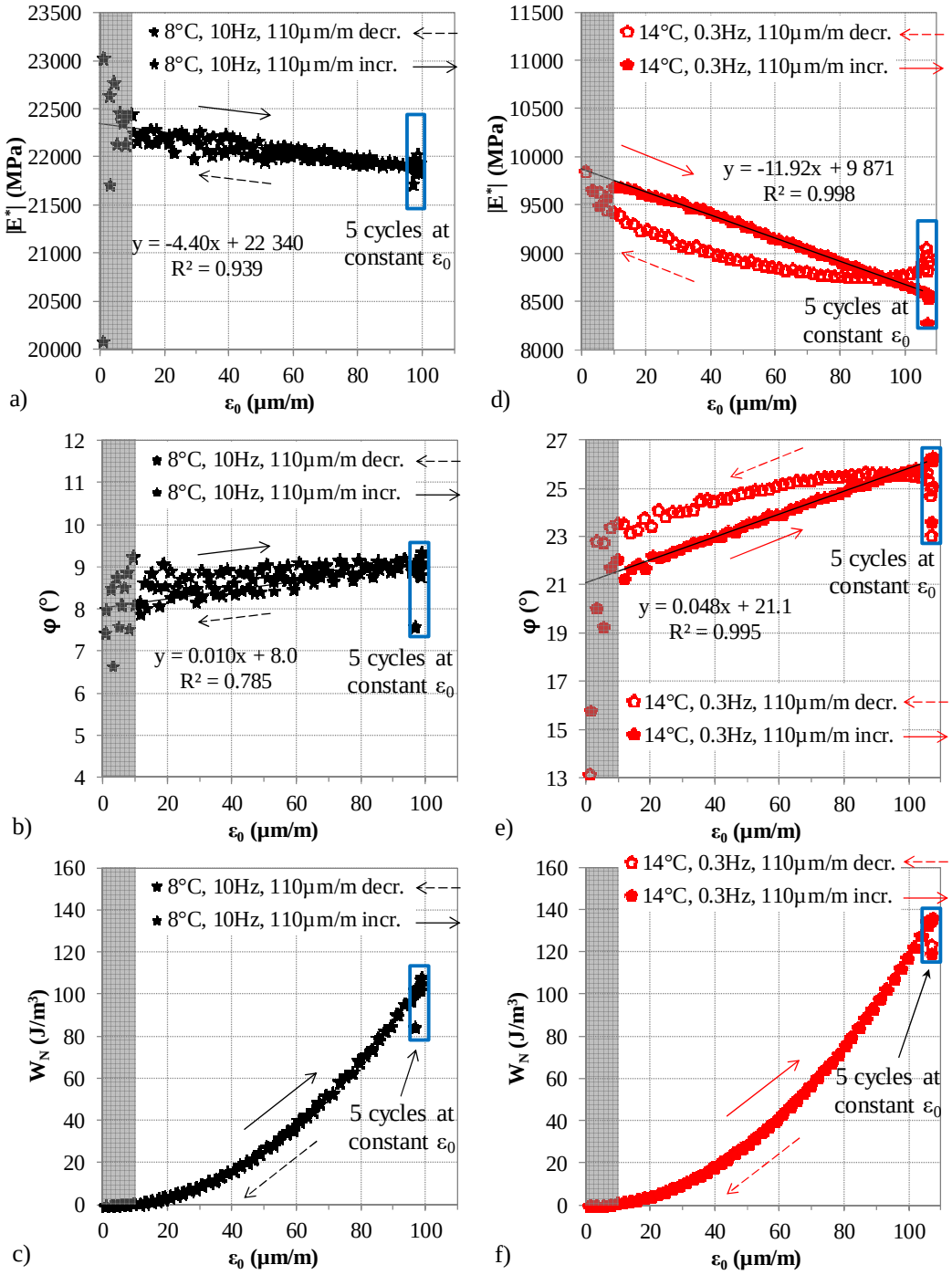

Figure 4-4. Results obtained from SASTENOLE tests at 8°C, 10Hz (a, b, c) and 14°C, 0.3Hz (d, e, f), for maximum targeted strain amplitude of 110µm/m: norm of complex modulus $|E^*|$ (top), phase angle φ (middle) and dissipated energy per cycle W_N (bottom) are plotted as functions of strain amplitude.

A non-negligible strain dependence is observed for both norm and phase angle of equivalent complex modulus for the applied strain amplitudes, which are mostly quite lower than the traditionally considered LVE limit of about 100µm/m. These results confirm the existence of nonlinear behaviour for bituminous mixtures even for strain amplitudes as small as 10µm/m. Therefore, the assumption of LVE behaviour can be accepted only as a first approximation.

However, different results are obtained during decreasing and increasing strain amplitude sweeps for the same combinations of temperature and frequency. During increasing sweeps, the norm of complex modulus decreases with strain amplitude while phase angle increases. As a first approximation, both appear to vary linearly. Linear regressions were performed for both $|E^*|$ and φ values as functions of strain amplitude, using only data obtained during increasing sweeps. Different trends were observed during decreasing sweeps. When strain amplitude decreases, norm of complex modulus appears to decrease for some cycles and then to increase, while phase angle increases initially and then decreases. These differences are evident for the SASTENOLE test performed at 14°C, 0.3Hz, while they appear as negligible at 8°C, 10Hz.

The difference observed between test results obtained during decreasing and increasing sweeps (for the same temperature, frequency and maximum targeted strain amplitude) suggest the existence of a second phenomenon. In fact, nonlinearity, defined as the strain dependence of complex modulus, is expected to be independent of the loading path (increasing or decreasing strain amplitude sweeps). If nonlinearity were the only phenomenon causing complex modulus to vary during loading sequences, the results observed during increasing and decreasing sweeps should coincide. As this does not occur, a hypothesis should be made that a second recoverable phenomenon, related to the applied number of cycles, occurs, causing a decrease of the norm of complex modulus and an increase of its phase angle. During increasing sweeps, both nonlinearity and the second phenomenon contribute to the decrease of $|E^*|$ and the increase of φ, while during decreasing sweeps the two phenomena have opposite effects. The nature of this second phenomenon is still unclear and is not discussed further in this chapter. Available data suggest a possible relationship with energy dissipation. Figure 4-4c and Figure 4-4f show values of dissipated energy per cycle, W_N, calculated as in Eq. 4-1, as functions of strain amplitude ε_0. More investigation on these other reversible phenomena is presented in Chapters 5 and 6, which involve self-heating and thixotropy (fatigue damage is negligible due to the very low number of cycles applied during SASTENOLE tests).

$$W_N = \pi \varepsilon_0^2 |E^*| \sin \varphi \qquad \text{Eq. 4-1}$$

Despite the differences observed for complex modulus, approximately the same values of W_N are found during increasing and decreasing sweeps. In order to quantify the effects of nonlinearity on the complex modulus of the studied material, changes of its norm and phase angle are evaluated as functions of the applied strain amplitude. Results from decreasing and increasing sweeps for the SASTENOLE test at 14°C, 0.3Hz on BM1_B are used as an example to describe the performed analysis, which is replicated to all test conditions. Figure 4-5 shows data obtained during the four increasing sweeps for the four maximum targeted strain amplitudes (50, 75, 100 and 110μm/m). For each loading sequence, the five cycles performed at constant maximum amplitude are not plotted, since any variation observed during these cycles is not related to nonlinearity. In addition, cycles carried out at amplitudes equal or lower than 10μm/m are discarded. Norm and phase angle of complex modulus obtained for each loading cycle are plotted against the corresponding strain amplitude. The results of both norm and phase angle of complex modulus obtained during the four increasing sweeps show a relatively good superposition. These results were used to perform linear regressions of $|E^*|$ and φ with strain amplitude ε_0 (Eq. 4-2 and Eq. 4-4). Slopes of regression lines

of $|E^*|$ and φ are, respectively, coefficients s_E and p_φ, while $|E_0^*|$ and φ_0 represent, respectively, extrapolated values of $|E^*|$ and φ for 0μm/m strain amplitude. These values could also have been experimentally obtained, as a first approximation, using wave propagation tests, inducing very low strain levels within the material (Mounier et al., 2012). The value of s_E is normalized with respect to $|E_0^*|$ (Eq. 4-3).

$$|E^*(\varepsilon_0)| = s_E\varepsilon_0 + |E_0^*| \qquad \text{Eq. 4-2}$$

$$\frac{|E^*(\varepsilon_0)|}{|E_0^*|} = p_E\varepsilon_0 + 1 \quad ; \quad p_E = \frac{s_E}{|E_0^*|} \qquad \text{Eq. 4-3}$$

$$\varphi(\varepsilon_0) = p_\varphi\varepsilon_0 + \varphi_0 \qquad \text{Eq. 4-4}$$

Considering the previous definitions, for a given combination of frequency and temperature, complex modulus can be expressed in complex notation as a function of axial strain amplitude, as in Eq. 4-5, which is a combination of Eq. 4-2, Eq. 4-3 and Eq. 4-4 in complex notation. Its interpretation in the complex plane is given next, in Figure 4-8.

$$E^*(\varepsilon_0) = |E_0^*|e^{i\varphi_0}(1 + p_E\varepsilon_0)e^{ip_\varphi\varepsilon_0} \qquad \text{Eq. 4-5}$$

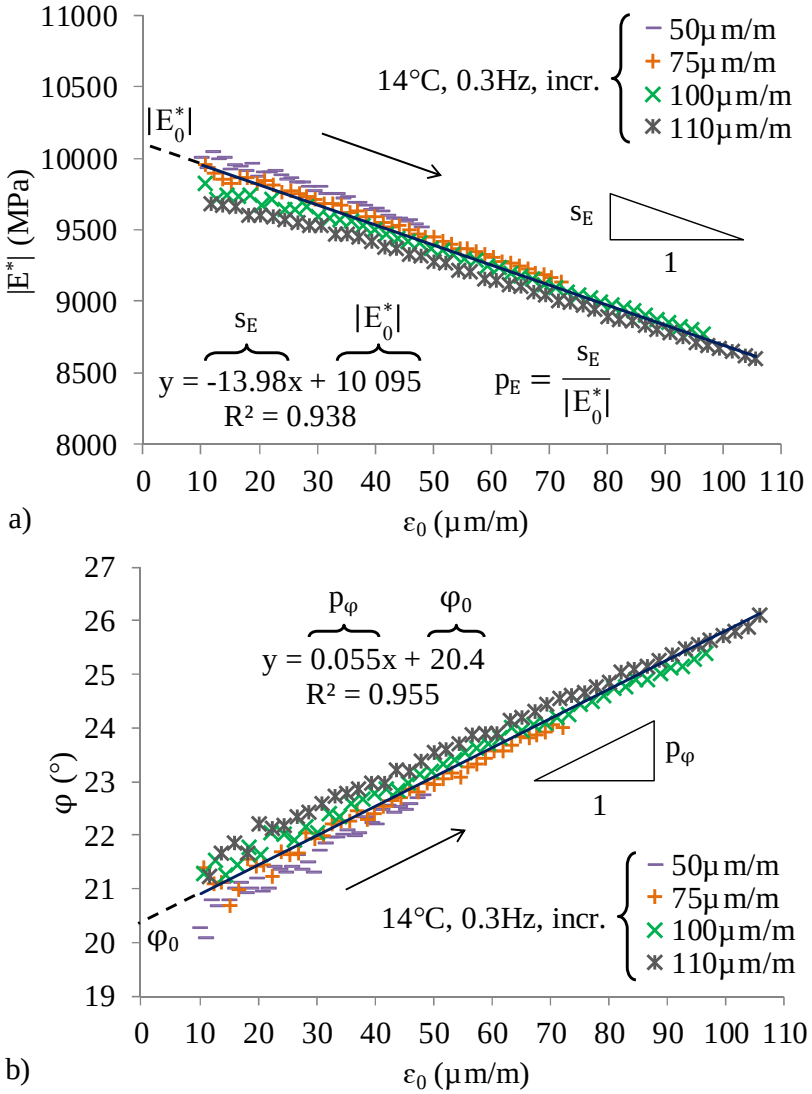

Figure 4-5. Norm of the complex modulus $|E^*|$ (a, top) and phase angle φ (b, bottom) obtained from the SASTENOLE test at 14°C, 0.3Hz, for the four increasing strain amplitude loading paths: s_E and p_φ are the slopes of the nonlinearity envelopes of, respectively, $|E^*|$ and φ.

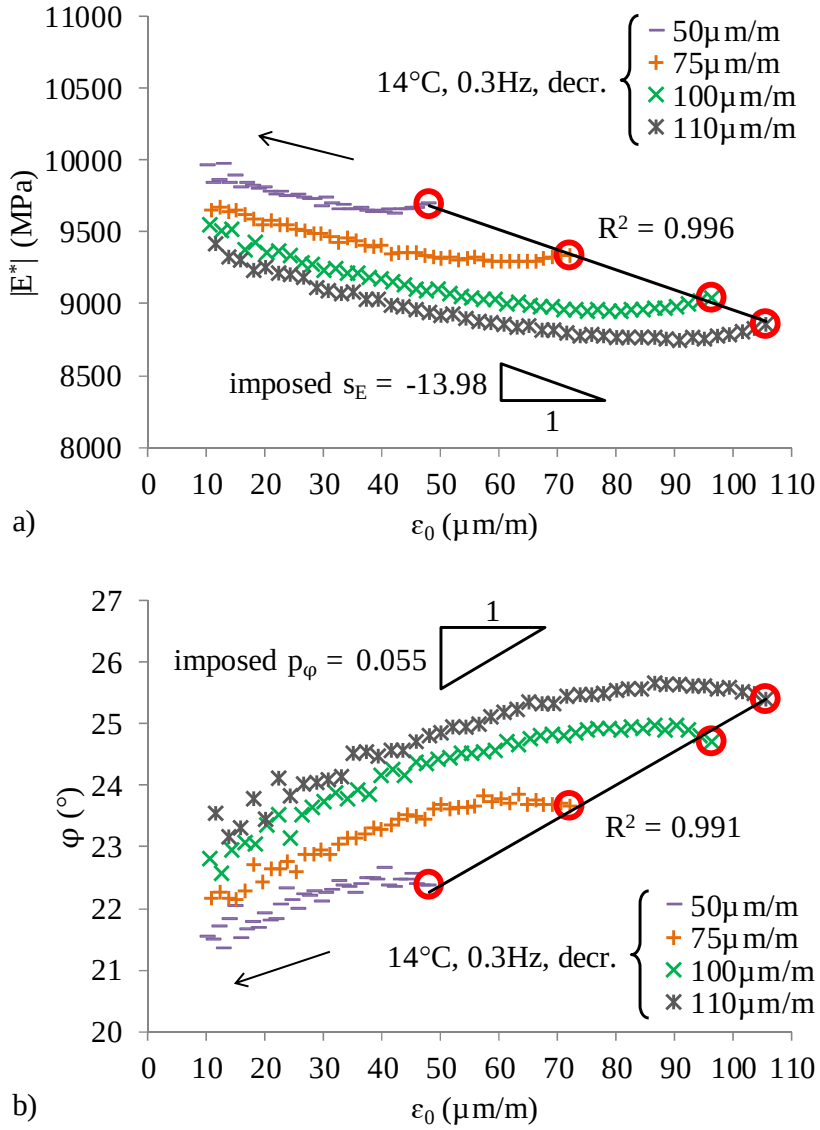

Figure 4-6. Norm of the complex modulus $|E^*|$ (a, top) and phase angle φ (b, bottom) obtained from the SASTENOLE test at 14°C, 0.3Hz, for decreasing strain amplitude loading paths: R^2 values are calculated for the regressions of the initial points with lines of, respectively, s_E and p_φ slopes (as calculated in Figure 4-5 for increasing strain amplitude loading paths).

Results obtained during the four decreasing sweeps at the same temperature and frequency are presented in Figure 4-6. As already explained, differences are found with respect to data obtained during increasing sweeps. In addition to nonlinearity, a second phenomenon occurs at least in the first cycles of the decreasing sweeps, causing a reduction of $|E^*|$ and an increase of φ. This phenomenon becomes less important in the following cycles. For this reason, nonlinearity cannot be estimated by means of linear regressions based on data obtained during decreasing sweeps. The nature of this second phenomenon is still unclear. As shown in Figure 4-6, $|E^*|$ and φ values obtained for the very first cycle of each decreasing sweep (6th cycle of the decreasing loading sequence) were fitted (through least squares optimisation) with linear functions having, respectively, the same s_E and p_φ obtained for increasing sweeps (Figure 4-5). Excellent R^2 values (very close to 1) were obtained (reported in Figure 4-6), for the considered cycle (first of the 50 in

the decreasing sweep). This observation reinforces the hypothesis of two independent phenomena occurring. The first one is nonlinearity, intended as strain dependence of complex modulus (the higher the strain amplitude, the lower the norm of complex modulus and the higher the phase angle). The second one, whose nature needs to be clarified, is also responsible for a variation of complex modulus (decrease of norm and increase of phase angle) with number of cycles.

Table 4-2. Regression parameters p_E and p_φ obtained from nonlinearity envelopes of, respectively, norm and phase angle of complex modulus obtained from all SASTENOLE tests on BM1_B at different temperatures and frequencies, for increasing strain amplitude loading paths.

T (°C)	f (Hz)	Strain ampl. evol.	Norm of complex modulus $\|E^*\|$				Phase angle φ			
			s_E (MPa/µm/m)	$\|E^*_0\|$ (MPa)	$p_E = s_E/\|E^*_0\|$ (1/µm/m)	R^2 (-)	p_φ (°/µm/m)	φ_0 (°)	R^2 (-)	p_E/p_φ (1/°)
8	0.3	Incr.	-12.11	14841	$-8.16\cdot10^{-4}$	0.924	0.036	13.8	0.968	$-2.28\cdot10^{-2}$
	1	Incr.	-8.28	17424	$-4.75\cdot10^{-4}$	0.967	0.023	11.6	0.952	$-2.08\cdot10^{-2}$
	3	Incr.	-5.96	19837	$-3.00\cdot10^{-4}$	0.950	0.015	9.8	0.910	$-2.00\cdot10^{-2}$
	10	Incr.	-4.17	22342	$-1.87\cdot10^{-4}$	0.842	0.009	8.2	0.642	$-2.07\cdot10^{-2}$
10	0.3	Incr.	-13.54	13185	$-1.03\cdot10^{-3}$	0.937	0.043	15.8	0.962	$-2.39\cdot10^{-2}$
	1	Incr.	-9.12	15872	$-5.78\cdot10^{-4}$	0.972	0.028	13.2	0.969	$-2.06\cdot10^{-2}$
	3	Incr.	-6.42	18276	$-3.51\cdot10^{-4}$	0.926	0.019	11.0	0.941	$-1.85\cdot10^{-2}$
	10	Incr.	-3.76	20881	$-1.80\cdot10^{-4}$	0.671	0.012	9.1	0.808	$-1.50\cdot10^{-2}$
12	0.3	Incr.	-14.51	11907	$-1.22\cdot10^{-3}$	0.948	0.051	17.3	0.957	$-2.39\cdot10^{-2}$
	1	Incr.	-10.84	14510	$-7.47\cdot10^{-4}$	0.989	0.033	14.6	0.981	$-2.26\cdot10^{-2}$
	3	Incr.	-8.30	17035	$-4.87\cdot10^{-4}$	0.974	0.023	12.1	0.958	$-2.12\cdot10^{-2}$
	10	Incr.	-5.70	19707	$-2.89\cdot10^{-4}$	0.918	0.015	10.0	0.850	$-1.93\cdot10^{-2}$
14	0.3	Incr.	-13.98	10095	$-1.38\cdot10^{-3}$	0.938	0.055	20.4	0.955	$-2.52\cdot10^{-2}$
	1	Incr.	-11.15	12702	$-8.78\cdot10^{-4}$	0.990	0.037	17.0	0.987	$-2.37\cdot10^{-2}$
	3	Incr.	-8.91	15283	$-5.83\cdot10^{-4}$	0.979	0.028	14.0	0.975	$-2.08\cdot10^{-2}$
	10	Incr.	-6.18	18048	$-3.42\cdot10^{-4}$	0.950	0.018	11.4	0.922	$-1.90\cdot10^{-2}$

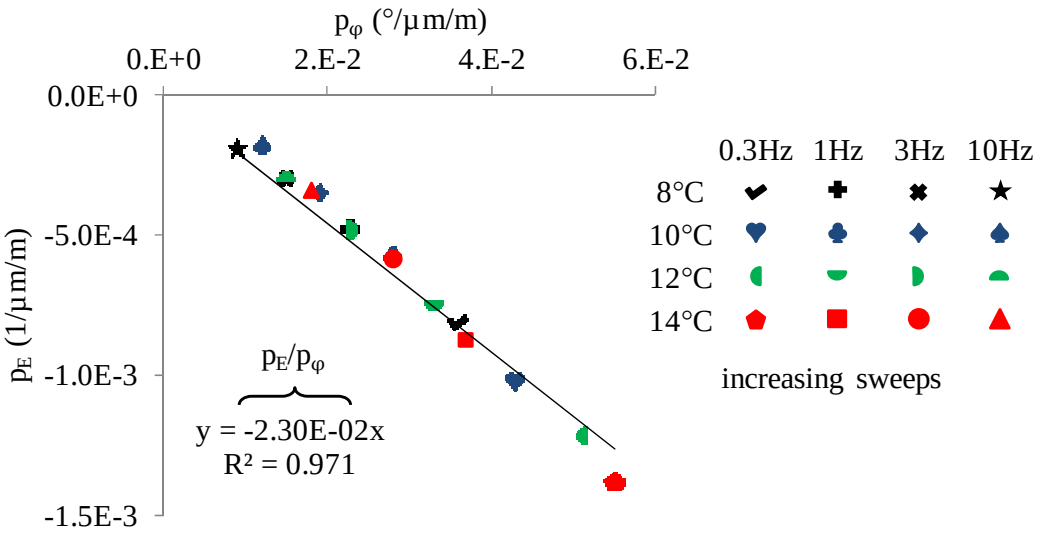

Figure 4-7. Linear regression of p_E values as a function of corresponding p_φ values obtained from all SASTENOLE tests on BM1_B at different temperatures and frequencies, for increasing strain amplitude loading paths (Figure 4-5).

As a first approximation, nonlinearity envelopes obtained from increasing amplitude sweeps were used to estimate the strain dependence of complex modulus. A summary of results obtained for the 16 different combinations of temperatures and frequencies tested on BM1_B is presented in Table 4-2. Values of p_E range between $-1.80 \cdot 10^{-4}$ and $-1.38 \cdot 10^{-3}$ per µm/m, while values of p_φ vary between 0.009 and 0.055 °/µm/m.

Higher absolute values of p_E and p_φ, used as indicators of the effect of nonlinearity on complex modulus, were obtained at high temperatures and low frequencies. It means that for the tested bituminous mixture, strain dependence is more pronounced at higher temperature and lower frequency. Moreover, as shown in Figure 4-7 with results at different temperatures and frequencies, these two coefficients appear to form a unique curve, indicating that a time-temperature superposition (further discussed in the next section with results for BM1_C) is valid. Also, for tests on BM1_B with temperatures between 8 and 14°C and frequencies between 0.3 and 10Hz, the referred parameters seem to correlate linearly. A straight line passing from the origin was imposed and the corresponding R^2 value is reported, both in Figure 4-7. Therefore, as a first approximation, the ratio p_E/p_φ can be considered as a constant. This observation appears to confirm the findings of (Q. T. Nguyen et al., 2015). The referred authors considered that deviations from a constant value of p_E/p_φ were due to experimental problems at higher temperatures. Moreover, the authors showed that, if $|p_E \cdot \varepsilon_0| << 1$, p_E/p_φ can be used to define a direction over which strain dependence imposes a change in complex modulus. According to the referred experimental results, this direction would be a constant for the material, for all frequencies and temperatures. Therefore, when results of amplitude sweeps are plotted in Black space, complex modulus variations due to nonlinearity would follow a unique direction, called “direction of nonlinearity”.

From Eq. 4-2 to Eq. 4-4, the slope of complex modulus variation due to nonlinearity in Black space (defined as a diagram where base 10 logarithm of norm of complex modulus is plotted on the vertical axis and phase angle is plotted on the horizontal axis) is given by Eq. 4-6.

$$\frac{d\log|E^*|}{d\varphi} = \frac{d\log|E^*|}{d\varepsilon_0}\frac{d\varepsilon_0}{d\varphi} = \frac{1}{(\ln 10)(1+p_E\varepsilon_0)}\frac{p_E}{p_\varphi} \quad \text{Eq. 4-6}$$

Natural logarithm appears because $|E^*|$ axis of Black space is defined in base 10 logarithm. Similarly, the nonlinearity direction in Cole-Cole space can be obtained as in Eq. 4-7.

$$\frac{d\big(Im(E^*)\big)}{d\big(Re(E^*)\big)} = \frac{d(|E^*|\sin\varphi)}{d(|E^*|\cos\varphi)} = \frac{\tan\varphi + \frac{p_\varphi}{p_E}(1+p_E\varepsilon_0)}{1-\frac{p_\varphi}{p_E}(1+p_E\varepsilon_0)\tan\varphi} \quad \text{Eq. 4-7}$$

In Eq. 4-7, $Im(E^*)$ represents the imaginary part of the complex modulus (vertical axis of Cole-Cole plot) and $Re(E^*)$ its real part (horizontal axis of Cole-Cole plot). Angle α is defined as in Eq. 4-8.

$$\alpha = -\tan^{-1}\left[\frac{p_\varphi}{p_E}(1+p_E\varepsilon_0)\right] \quad \text{Eq. 4-8}$$

Eq. 4-6 and Eq. 4-7 can be rewritten as Eq. 4-9 and Eq. 4-10, respectively describing α in Black and Cole-Cole spaces:

$$\frac{d\log|E^*|}{d\varphi} = -\frac{1}{(\ln 10)\tan\alpha} \quad \text{Eq. 4-9}$$

$$\frac{d\big(Im(E^*)\big)}{d\big(Re(E^*)\big)} = \frac{d(|E^*|\sin\varphi)}{d(|E^*|\cos\varphi)} = \tan(\varphi-\alpha) \quad \text{Eq. 4-10}$$

Figure 4-8 provides graphical explanations of the identification of nonlinearity directions in Black and Cole-Cole spaces.

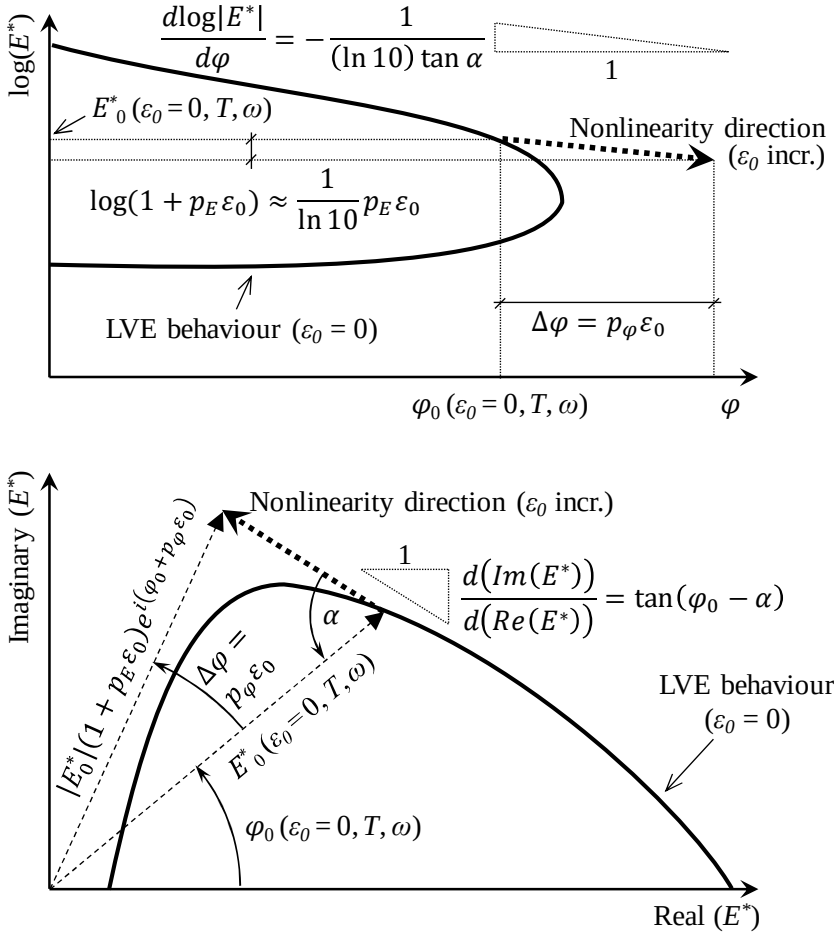

Figure 4-8. Schemes of nonlinearity directions in Black (top) and Cole-Cole (bottom) spaces (cf. Eq. 4-6 and Eq. 4-8).

Eq. 4-6 to Eq. 4-10 show that experimental data plotted in both Cole-Cole and Black spaces are described by linear equations if $|p_E \cdot \varepsilon_0| << 1$. Therefore, nonlinearity directions can be directly determined by performing linear regressions of data obtained from cycles satisfying the $|p_E \cdot \varepsilon_0| << 1$ condition. In order to do so, as a first approximation, p_E values determined from increasing sweeps of SASTENOLE tests (Table 4-2) were used to calculate the maximum strain amplitude so that $|p_E \cdot \varepsilon_0| \leq 0.05$. Calculated values are reported in Table 4. For some combinations of frequency and temperature, the calculated strain amplitude limit is higher than the maximum amplitude used during tests, therefore all cycles could be used for regressions.

Table 4-3. Maximum strain amplitude values satisfying the $|p_E \cdot \varepsilon_0| \leq 0.05$ condition, according to p_E coefficients obtained from increasing sweeps of SASTENOLE tests on BM1_B (Table 4-2).

	0.3Hz	**1Hz**	**3Hz**	**10Hz**
8°C	61µm/m	105µm/m	166µm/m	268µm/m
10°C	49µm/m	87µm/m	142µm/m	278µm/m
12°C	41µm/m	67µm/m	103µm/m	173µm/m
14°C	36µm/m	57µm/m	86µm/m	146µm/m

Results of all SASTENOLE tests on BM1_B, during both increasing and decreasing sweeps, were plotted in Cole-Cole and Black spaces, respectively Figure 4-9 and Figure 4-10. In both figures, a continuous line represents the LVE behaviour of the mixture, as described by the 2S2P1D model previously obtained (Table 4-1). Also, two zooms are shown for data obtained for the two most different test conditions (14°C, 0.3Hz and 8°C, 10Hz). In particular, for the two zooms of the Cole-Cole space (Figure 4-9), axes are orthonormal (same scale on x and y axes) and $|E_0^*|$ and φ_0 are represented as, respectively, norm and inclination of a vector going from the origin to the represented point. For each combination of temperature and frequency, the effect of nonlinearity can be observed from linear or quasi-linear trends in Cole-Cole and Black spaces. Although different trends were found when norm of complex modulus and phase angle of increasing and decreasing sweeps (for each combination of temperature and frequency) were plotted against strain amplitude, the same data appear to superpose in Black and Cole-Cole plots. This could indicate that the direction of the second phenomenon (responsible for the difference observed between increasing and decreasing sweeps) in these diagrams is close to the nonlinearity direction. In this case, using Black and Cole-Cole spaces (and Eq. 4-6 to Eq. 4-10) to characterize nonlinearity appears as a more reliable method than simple regressions of norm and phase angle of complex modulus as functions of strain amplitude.

Another important observation is that the time-temperature superposition principle appears to be respected for nonlinearity, i.e. very similar data are obtained for different combinations of frequency and temperature corresponding to the same equivalent frequency (after applying time-temperature shift factors). Two clear examples are seen in Figure 4-9: coincidence of SASTENOLE results at 12°C, 10Hz and at 8°C, 3Hz; and coincidence between 14°C, 10Hz and 10°C, 3Hz. Other authors reached this conclusion on the time-temperature superposition for non-linear domains (M. L. Nguyen et al., 2013; Q. T. Nguyen et al., 2013).

As a final remark, it can be observed that, both in Cole-Cole and Black diagrams, the 2S2P1D model curve (representing the linear viscoelastic complex modulus of the tested mixture) fitted for 50μm/m strain amplitude crosses the curves obtained from SASTENOLE tests. This shows that the direction of nonlinearity evolution is not along the complex modulus curve obtained when changing frequency and temperature.

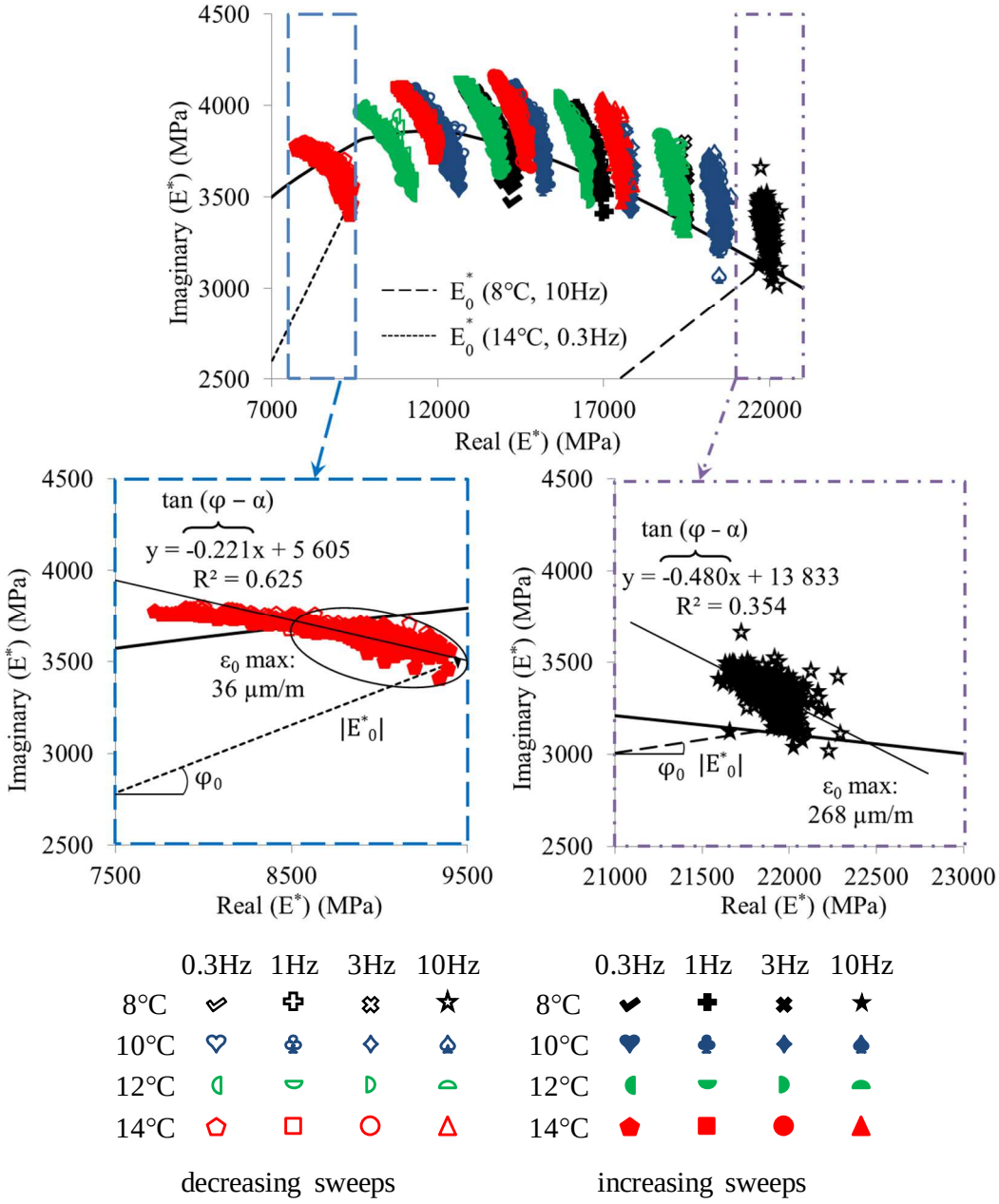

Figure 4-9. Results obtained from all SASTENOLE tests on BM1_B (scheme on Figure 4-3) at different temperatures and frequencies, for both decreasing and increasing strain amplitude loading paths, in Cole-Cole space: zooms are provided for data obtained at 14°C, 0.3Hz (bottom, left) and 8°C, 10Hz (bottom, right). For each combination of temperature and frequency, the regression was performed by combining data from both decreasing and increasing strain amplitude sweeps.

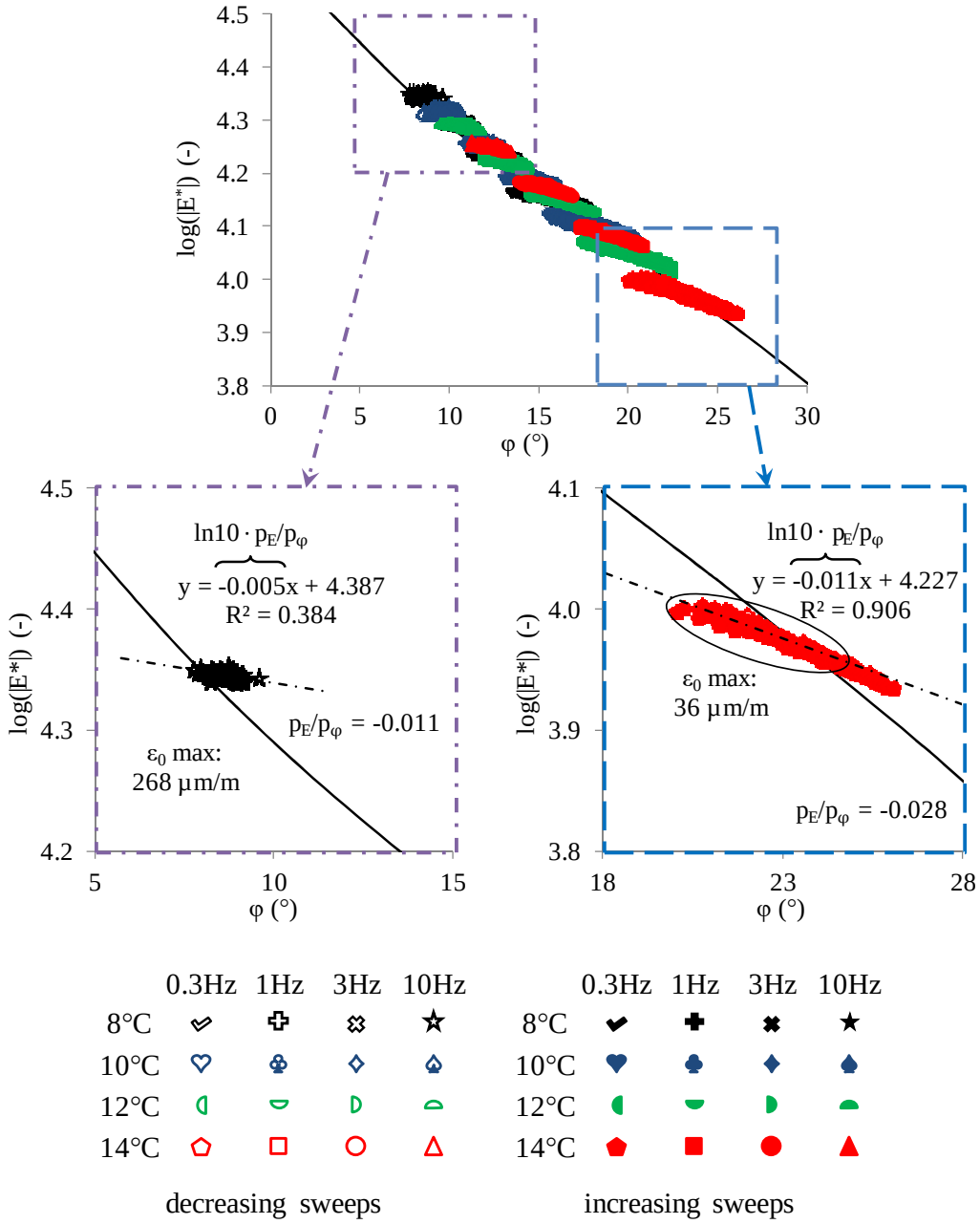

Figure 4-10. Results obtained from all SASTENOLE tests on BM1_B (scheme on Figure 4-3) at different temperatures and frequencies, for both decreasing and increasing strain amplitude loading paths, in Black space: zooms are provided for data obtained at 8°C, 10Hz (bottom, left) and 14°C, 0.3Hz (bottom, right). For each combination of temperature and frequency, the regression was performed by combining data from both decreasing and increasing strain amplitude sweeps.

Values of p_E/p_φ and α were estimated from both Cole-Cole and Black spaces. The obtained results, together with R^2 values of regressions, are reported in Table 4-4. Among the 16 regressions, 10 have R^2 values higher than 0.9. Lower values are found for data obtained at 10Hz. Values of p_E/p_φ and α obtained from Cole-Cole and Black spaces present the same order of magnitude and vary in similar ranges. Mean and standard deviation were calculated for the two sets of values estimated from, respectively, Cole-Cole and Black plots. A lower standard deviation was found for values of p_E/p_φ and α obtained from Cole-Cole plots, with respect to values obtained

from Black space. Overall, the variation range of temperature and frequency used for this study is too narrow to confirm that nonlinearity direction of mixtures do not depend on test conditions. Furthermore, results of SASTENOLE tests were plotted in a normalized Black space (Figure 4-11). For each combination of temperature and frequency, results were normalized with respect to values of $|E_0^*|$ and φ_0 obtained during increasing sweeps (Table 4-2). It can be shown that the slope of the curves plotted in such a graph is p_E/p_φ, as Eq. 4-11.

$$\frac{d\left(\frac{|E^*|}{|E_0^*|}\right)}{d(\varphi-\varphi_0)} = \frac{d\left(\frac{|E^*|}{|E_0^*|}\right)}{d\varepsilon_0}\frac{d\varepsilon_0}{d(\varphi-\varphi_0)} = \frac{1}{|E_0^*|}\frac{d|E^*|}{d\varepsilon_0}\frac{d\varepsilon_0}{d\varphi} = \frac{p_E}{p_\varphi} \qquad \text{Eq. 4-11}$$

From a visual interpretation, all curves appear to be relatively well superposed onto each other, suggesting that a unique p_E/p_φ is valid for all combinations of temperature and frequency. However, the scatter of the data points, especially at low temperature/high frequency, confirms the need for a wider domain of these test conditions in order to confirm this hypothesis.

(Q. T. Nguyen et al., 2015) concluded that p_E/p_φ is a constant. Although they performed tests in a significantly larger domain of frequency and temperature, their finding is based only on the regression of p_E as a function of p_φ, similar to the one shown in Figure 4-7. More research is needed on this point, justifying the second experimental campaign on nonlinearity of bituminous mixture, performed on BM1_C.

Table 4-4. Values of p_E/p_φ and α obtained for all temperatures and frequencies from linear regressions for BM1_B in (a) Cole-Cole and (b) Black spaces. Each value was obtained by combining data from both decreasing and increasing strain amplitude sweeps.

a)

Cole-Cole space				
T (°C)	**f (Hz)**	**p_E/p_φ (1/°)**	**α (°)**	**R^2 (-)**
8	**0.3**	$-2.48\cdot10^{-2}$	35.1	0.829
	1	$-2.26\cdot10^{-2}$	37.6	0.875
	3	$-2.17\cdot10^{-2}$	38.8	0.746
	10	$-2.60\cdot10^{-2}$	33.8	0.591
10	**0.3**	$-2.66\cdot10^{-2}$	33.3	0.784
	1	$-2.29\cdot10^{-2}$	37.4	0.846
	3	$-2.06\cdot10^{-2}$	40.2	0.838
	10	$-1.85\cdot10^{-2}$	43.3	0.580
12	**0.3**	$-2.48\cdot10^{-2}$	35.2	0.810
	1	$-2.42\cdot10^{-2}$	35.8	0.835
	3	$-2.34\cdot10^{-2}$	36.7	0.855
	10	$-2.05\cdot10^{-2}$	40.5	0.787
14	**0.3**	$-2.94\cdot10^{-2}$	30.7	0.941
	1	$-2.44\cdot10^{-2}$	35.6	0.852
	3	$-2.29\cdot10^{-2}$	37.3	0.842
	10	$-2.05\cdot10^{-2}$	40.5	0.807
Mean		$-2.34\cdot10^{-2}$	37.0	
St. dev.		$0.27\cdot10^{-2}$	3.2	

b)

Black space				
T (°C)	**f (Hz)**	**p_E/p_φ (1/°)**	**α (°)**	**R^2 (-)**
8	**0.3**	$-2.16\cdot10^{-2}$	39.0	0.908
	1	$-2.01\cdot10^{-2}$	41.0	0.917
	3	$-1.72\cdot10^{-2}$	45.4	0.792
	10	$-1.11\cdot10^{-2}$	57.5	0.384
10	**0.3**	$-2.29\cdot10^{-2}$	37.3	0.907
	1	$-2.00\cdot10^{-2}$	41.1	0.906
	3	$-1.76\cdot10^{-2}$	44.8	0.857
	10	$-1.13\cdot10^{-2}$	57.0	0.511
12	**0.3**	$-2.16\cdot10^{-2}$	38.9	0.922
	1	$-2.13\cdot10^{-2}$	39.4	0.914
	3	$-2.06\cdot10^{-2}$	40.3	0.908
	10	$-1.56\cdot10^{-2}$	48.2	0.688
14	**0.3**	$-2.52\cdot10^{-2}$	34.8	0.906
	1	$-2.18\cdot10^{-2}$	38.7	0.838
	3	$-2.01\cdot10^{-2}$	41.0	0.907
	10	$-1.63\cdot10^{-2}$	47.0	0.787
Mean		$-1.90\cdot10^{-2}$	43.2	
St. dev.		$0.39\cdot10^{-2}$	6.5	

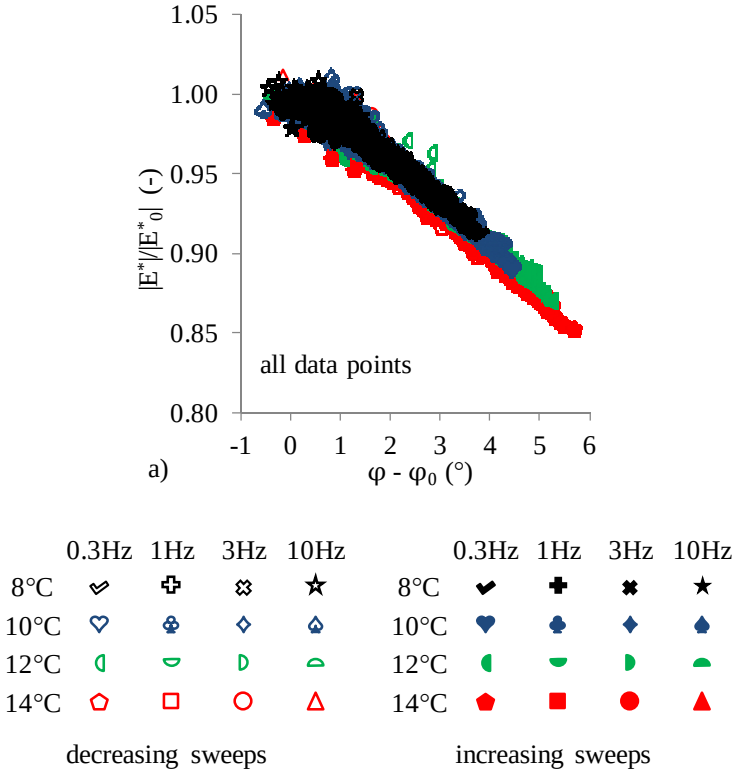

Figure 4-11. Results obtained from all SASTENOLE tests on BM1_B at different temperatures and frequencies, for both decreasing and increasing strain amplitude loading paths, in normalized Black space.

4.2.4. Analysis of SASTENOLE test results on BM1_C

The experimental analysis on BM1_C follows the same logic as on BM1_B. SASTENOLE was applied at different conditions of temperature and frequency, directions of nonlinearity and its intensity were investigated for the tested mixture. This time, as presented in Figure 4-12, a wider range of temperatures and frequencies was used, in order to investigate the hypothesis of a constant direction of nonlinearity, and also the variation of complex Poisson's ratio with the applied axial strain amplitude. The experimental plan included the following temperatures: -4°C, -2°C, 0°C, 10°C, 12°C, 14°C, 24°C, 26°C, 28°C. Frequencies were 0.1Hz, 1Hz and 10Hz. Targeted strain amplitudes were 50μm/m, 85μm/m, and 120μm/m. Test conditions are summarised in Table 4-5.

Table 4-5. Summary of SASTENOLE test conditions on BM1_C (test scheme for BM1_B on Figure 4-3).

Temperature	Frequency	Maximum axial strain amplitude	Strain path	Rest period
-4°C	0.1Hz, 1Hz, 10Hz	50µm/m, 85µm/m, 120µm/m	Increasing, decreasing	4 h before each thermal conditioning (σ=0) 15 min before each loading sequence (ε=0)
-2°C				
0°C				
10°C				
12°C				
14°C				
24°C				
26°C				
28°C				

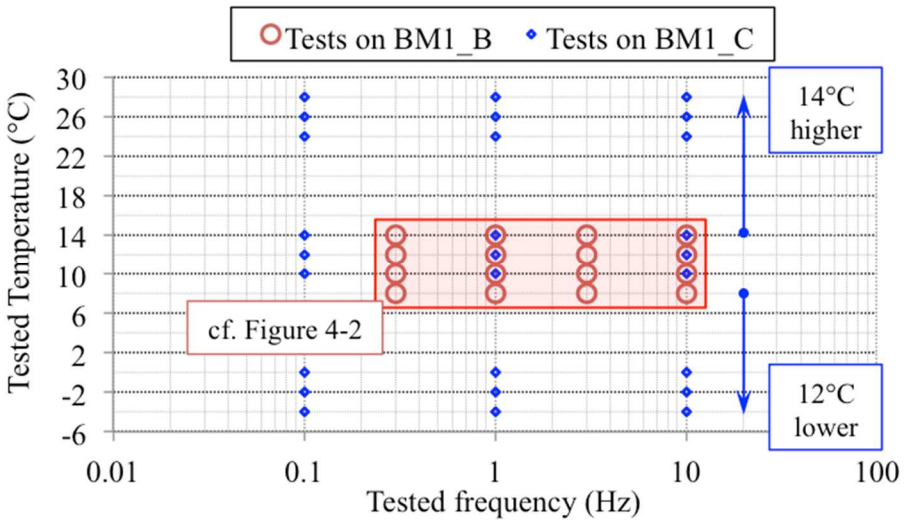

Figure 4-12. Comparison between the test conditions range for the first experimental campaign on bituminous mixture nonlinearity (BM1_B, cf. Figure 4-3) and for the second experimental campaign (on BM1_C). Including all testing sequences (increasing and decreasing sweeps at three different maximum targeted strain amplitudes) a total of 162 sequences were performed and analysed on BM1_C.

4.2.4.1. *Strain dependence of norm of complex modulus and phase angle*

The experimental results for BM1_C complex modulus are presented in Figure 4-13 in Cole-Cole plot (a, comparable to Figure 4-9 for BM1_B), Black diagram (b, comparable to Figure 4-10 for BM1_B), normalized Black space (c, comparable to Figure 4-11 for BM1_B). It can be seen from Figure 4-13a and Figure 4-13b that this second experimental campaign covered the effects of nonlinearity for a wide range of temperatures and frequencies. In the same figures, an indication of the direction on nonlinearity is given. It is aimed in this second experimental study to determine whether the direction of nonlinearity can still be considered a constant for testing conditions wider (-4 to 28°C) than the one used before (8 to 14°C). In Figure 4-13c a normalized Black space presents all results for the SASTENOLE tests on BM1_C (analogous to Figure 4-11 for BM1_B). For tests between 8 and 14°C on BM1_B this representation seemed to present a unique curve for the material, hence a constant direction of nonlinearity. With the wider range of tested

temperatures (-4 to 28°C) on BM1_C, some variation around that unique curve is observed. It seems that for higher temperatures (24 to 28°C), the relative variation of norm of complex modulus becomes higher for the same variation in phase angle due to nonlinearity. For lower temperatures (-4 to 0°C) and strain amplitudes lower than 120µm/m, results were restrained to what has been defined as the "LVE domain" (indicated in Figure 4-13c), a zone where a relative variation in norm of complex modulus is smaller than 5%.

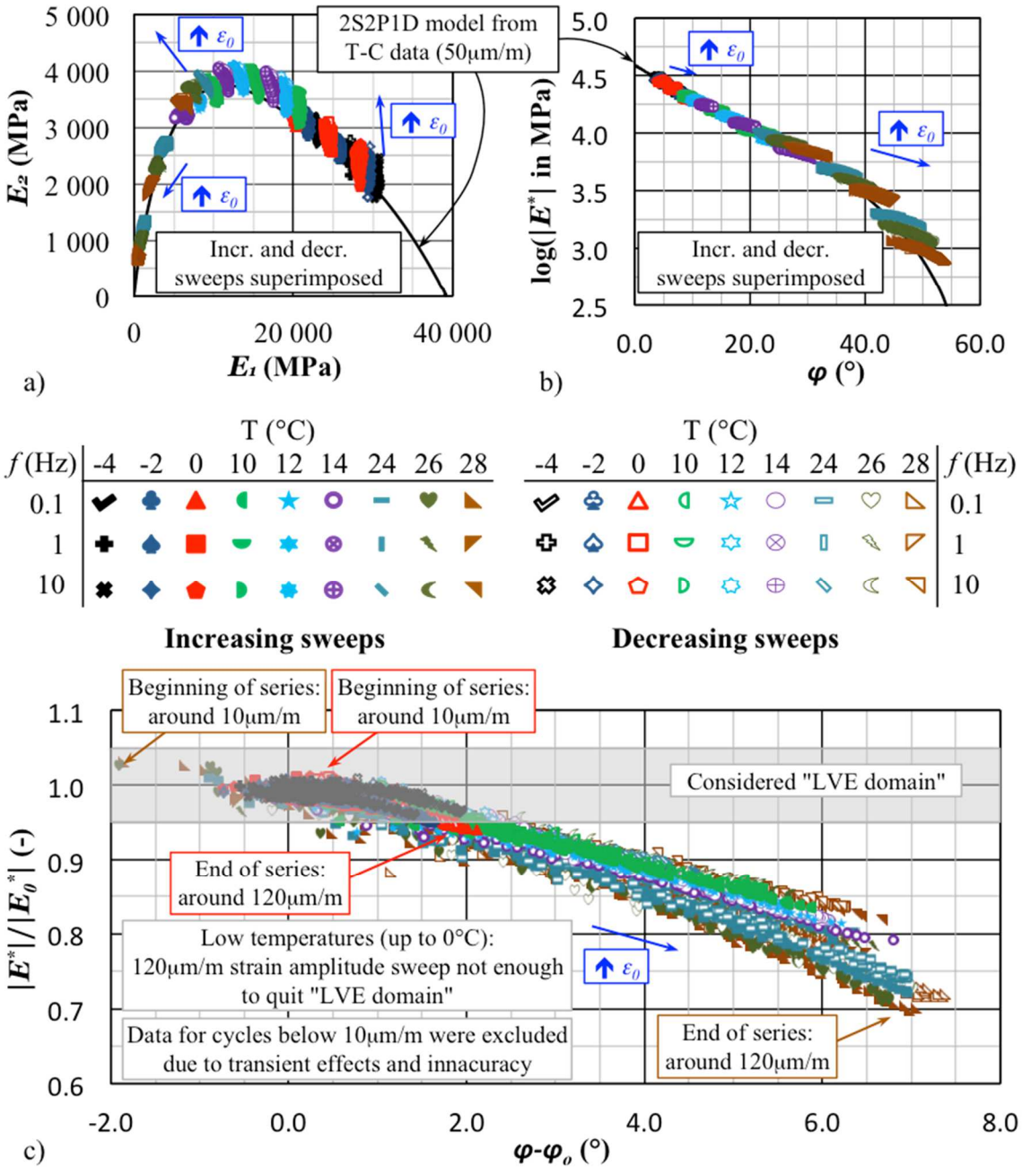

Figure 4-13. Results obtained from all SASTENOLE tests on BM1_C at different temperatures and frequencies, for both decreasing and increasing strain amplitude loading paths, in (a) Cole-Cole plot (comparable to Figure 4-9 for BM1_B), (b) Black space (comparable to Figure 4-10 for BM1_B), and (c) normalized black space (comparable to Figure 4-11 for BM1_B).

In order to further investigate the direction of nonlinearity and its intensity, as done before for results on BM1_B (cf. Figure 4-5), values of p_E and p_φ obtained from nonlinearity envelopes for increasing sweeps were calculated. Results are presented in Table 4-6 (BM1_B results have been presented on Table 4-2). Values of p_E and p_φ were also presented in Figure 4-14. Figure 4-14a (BM1_B results on Figure 4-7), b and c present results with no further analysis, while d, e and f present results in master curves, where reduced frequency was obtained using shift factors calculated using WLF equation fitted to complex modulus experiments (cf. Figure 4-2 and Table 4-1). This set of WLF equation parameters seems to represent correctly the time-shift observed for nonlinearity, i.e. the same parameters govern the time-shifts of both the linear and nonlinear viscoelastic properties.

Table 4-6. Regression parameters p_E and p_φ obtained from nonlinearity envelopes of, respectively, norm and phase angle of complex modulus obtained from all SASTENOLE tests on BM1_C (BM1_B results on Table 4-2) at different temperatures and frequencies, for increasing strain amplitude loading paths.

T (°C)	f (Hz)	Strain ampl. evol.	Norm of complex modulus $\|E^*\|$				Phase angle φ			
			s_E (MPa/µm/m)	$\|E^*_0\|$ (MPa)	$p_E = s_E/\|E^*_0\|$ (1/µm/m)	R^2 (-)	p_φ (°/µm/m)	φ_0 (°)	R^2 (-)	p_E/p_φ (1/°)
	0.1	**Incr.**	-7.20	23511	$-3.06\cdot10^{-4}$	0.879	0.011	6.7	0.931	$-2.83\cdot10^{-2}$
-4	**1**	**Incr.**	-4.40	27256	$-1.61\cdot10^{-4}$	0.848	0.005	5.1	0.617	$-3.27\cdot10^{-2}$
	10	**Incr.**	-5.05	30642	$-1.65\cdot10^{-4}$	0.532	0.002	3.8	0.066	$-7.29\cdot10^{-2}$
	0.1	**Incr.**	-8.50	22234	$-3.82\cdot10^{-4}$	0.940	0.013	7.5	0.932	$-3.01\cdot10^{-2}$
-2	**1**	**Incr.**	-5.27	26115	$-2.02\cdot10^{-4}$	0.897	0.006	5.7	0.679	$-3.46\cdot10^{-2}$
	10	**Incr.**	-4.35	29598	$-1.47\cdot10^{-4}$	0.471	0.003	4.2	0.132	$-4.36\cdot10^{-2}$
	0.1	**Incr.**	-9.99	20678	$-4.83\cdot10^{-4}$	0.952	0.016	8.5	0.951	$-2.96\cdot10^{-2}$
0	**1**	**Incr.**	-6.52	24766	$-2.63\cdot10^{-4}$	0.766	0.008	6.3	0.763	$-3.44\cdot10^{-2}$
	10	**Incr.**	-5.13	28533	$-1.80\cdot10^{-4}$	0.590	0.004	4.7	0.164	$-4.53\cdot10^{-2}$
	0.1	**Incr.**	-15.18	11172	$-1.36\cdot10^{-3}$	0.923	0.049	18.3	0.953	$-2.77\cdot10^{-2}$
10	**1**	**Incr.**	-10.14	16164	$-6.28\cdot10^{-4}$	0.979	0.024	12.8	0.955	$-2.64\cdot10^{-2}$
	10	**Incr.**	-6.81	21187	$-3.21\cdot10^{-4}$	0.906	0.011	8.8	0.654	$-2.97\cdot10^{-2}$
	0.1	**Incr.**	-14.43	9297	$-1.55\cdot10^{-3}$	0.921	0.053	21.6	0.953	$-2.91\cdot10^{-2}$
12	**1**	**Incr.**	-10.57	14335	$-7.37\cdot10^{-4}$	0.977	0.028	14.9	0.957	$-2.66\cdot10^{-2}$
	10	**Incr.**	-7.72	19582	$-3.94\cdot10^{-4}$	0.937	0.014	10.0	0.800	$-2.82\cdot10^{-2}$
	0.1	**Incr.**	-13.43	7599	$-1.77\cdot10^{-3}$	0.928	0.057	25.0	0.954	$-3.08\cdot10^{-2}$
14	**1**	**Incr.**	-11.20	12567	$-8.92\cdot10^{-4}$	0.982	0.034	17.2	0.965	$-2.61\cdot10^{-2}$
	10	**Incr.**	-7.81	17958	$-4.35\cdot10^{-4}$	0.963	0.017	11.4	0.884	$-2.51\cdot10^{-2}$
	0.1	**Incr.**	-5.06	2014	$-2.51\cdot10^{-3}$	0.940	0.067	42.7	0.911	$-3.77\cdot10^{-2}$
24	**1**	**Incr.**	-8.71	5107	$-1.71\cdot10^{-3}$	0.989	0.055	32.5	0.966	$-3.09\cdot10^{-2}$
	10	**Incr.**	-9.90	10099	$-9.80\cdot10^{-4}$	0.985	0.040	21.4	0.967	$-2.48\cdot10^{-2}$
	0.1	**Incr.**	-4.13	1532	$-2.70\cdot10^{-3}$	0.930	0.068	44.9	0.881	$-3.99\cdot10^{-2}$
26	**1**	**Incr.**	-7.74	4145	$-1.87\cdot10^{-3}$	0.985	0.058	35.5	0.953	$-3.21\cdot10^{-2}$
	10	**Incr.**	-10.22	8832	$-1.16\cdot10^{-3}$	0.988	0.044	23.8	0.976	$-2.63\cdot10^{-2}$
	0.1	**Incr.**	-3.23	1139	$-2.84\cdot10^{-3}$	0.921	0.070	46.7	0.854	$-4.04\cdot10^{-2}$
28	**1**	**Incr.**	-6.48	3270	$-1.98\cdot10^{-3}$	0.983	0.069	38.8	0.941	$-2.88\cdot10^{-2}$
	10	**Incr.**	-9.30	7520	$-1.24\cdot10^{-3}$	0.992	0.046	26.7	0.981	$-2.68\cdot10^{-2}$

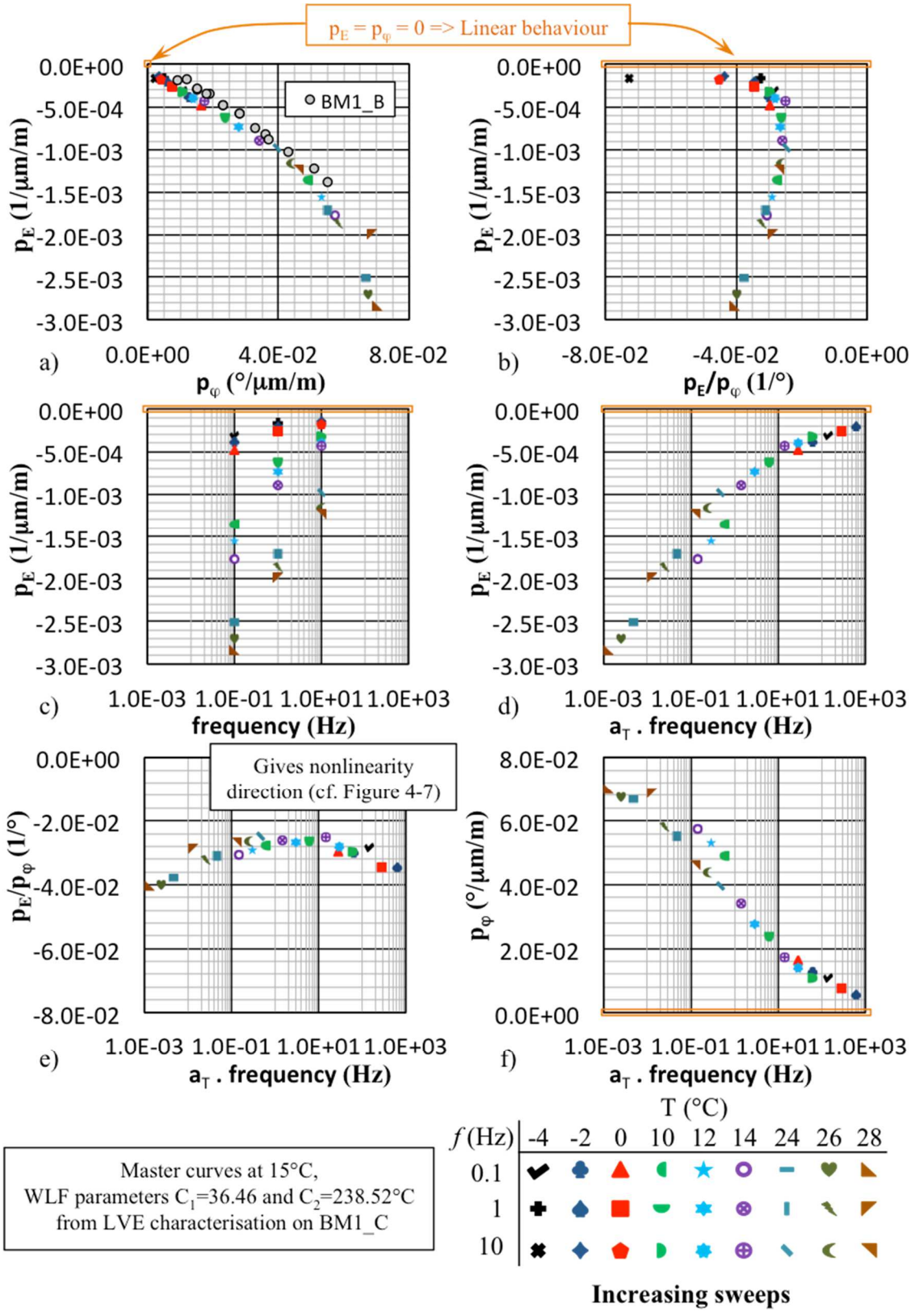

Figure 4-14. p_E and p_φ results obtained from all SASTENOLE tests on BM1_C (BM1_B results on Figure 4-7 also represented here) at different temperatures and frequencies, for increasing strain amplitude loading paths: a) p_E as a function of corresponding p_φ; b) p_E (intensity of nonlinearity effect) as a function of corresponding p_E/p_φ (which gives nonlinearity direction); c) isotherms for p_E; and d) p_E master curve, d) p_E/p_φ master curve, and f) p_φ master curve, all constructed using WLF parameters from LVE characterisation (Table 4-1). The master curves are presented at 15°C.

In Figure 4-14, p_E/p_φ can be interpreted as an indicator of the direction of nonlinearity, while p_E would give its intensity. For low absolute values of p_E/p_φ, low relative variation in norm of complex modulus is observed for a given variation in phase angle. This means that on Black curves a more horizontal path should be observed, while on Cole-Cole plots α (cf. Figure 4-8) would be closer to 90°. Meanwhile, for high absolute values of p_E/p_φ, high relative variation in norm of complex modulus is observed for a given variation in phase angle. This means that on Black curves higher slopes should be observed, while on Cole-Cole plots α (cf. Figure 4-8) would be closer to 0°. In Figure 4-14, indications of the regions corresponding to LVE behaviour (low absolute values of p_E and p_φ) were given.

Using the presented results of p_E, the maximum strain amplitude for which not more than 5% relative variation on norm of complex modulus is expected has been calculated. Results are presented in Table 4-7. From the referred table, it is observed that the strain amplitude necessary to produce non-negligible nonlinearity is temperature and frequency dependent. While the LVE domain could be considered for strain amplitudes lower than around 300μm/m at low temperatures and high frequencies, strain amplitude should be restricted to values as low as 20μm/m at high temperatures and low frequencies. The results from Table 4-7 can also be interpreted as the LVE limit in terms of strain amplitude ($\varepsilon_{0,95\%}$) for the bituminous mixture, and they are plotted in Figure 4-15 as a function of the corresponding norms of complex modulus (extrapolated at 0μm/m, cf. Table 4-6). In the same figure, the calculated LVE limit in terms of stress amplitude ($\sigma_{0,95\%}=|E^*_0|.\varepsilon_{0,95\%}$) is plotted as a function of the corresponding norm of complex modulus. It is observed from that figure that the LVE limit also respects the Time Temperature Superposition Principle (TTSP). Since it appears that a unique relation exists between LVE limit and norm of complex modulus, LVE limit respects the TTSP with the same shift factors as for E^*.

Table 4-7. Maximum strain amplitude values satisfying the $|p_E \cdot \varepsilon_0| \leq 0.05$ condition (5% decrease in norm of complex modulus, similar to the considered LVE limit definition), according to p_E coefficients obtained from increasing sweeps of SASTENOLE tests on BM1_C (Table 4-6) (cf. BM1_B results on Table 4-3).

	0.1Hz	**1Hz**	**10Hz**
-4°C	163μm/m	310μm/m	304μm/m
-2°C	131μm/m	248μm/m	340μm/m
0°C	103μm/m	190μm/m	278μm/m
10°C	37μm/m	80μm/m	156μm/m
12°C	32μm/m	68μm/m	127μm/m
14°C	28μm/m	56μm/m	115μm/m
24°C	20μm/m	29μm/m	51μm/m
26°C	19μm/m	27μm/m	43μm/m
28°C	18μm/m	25μm/m	40μm/m

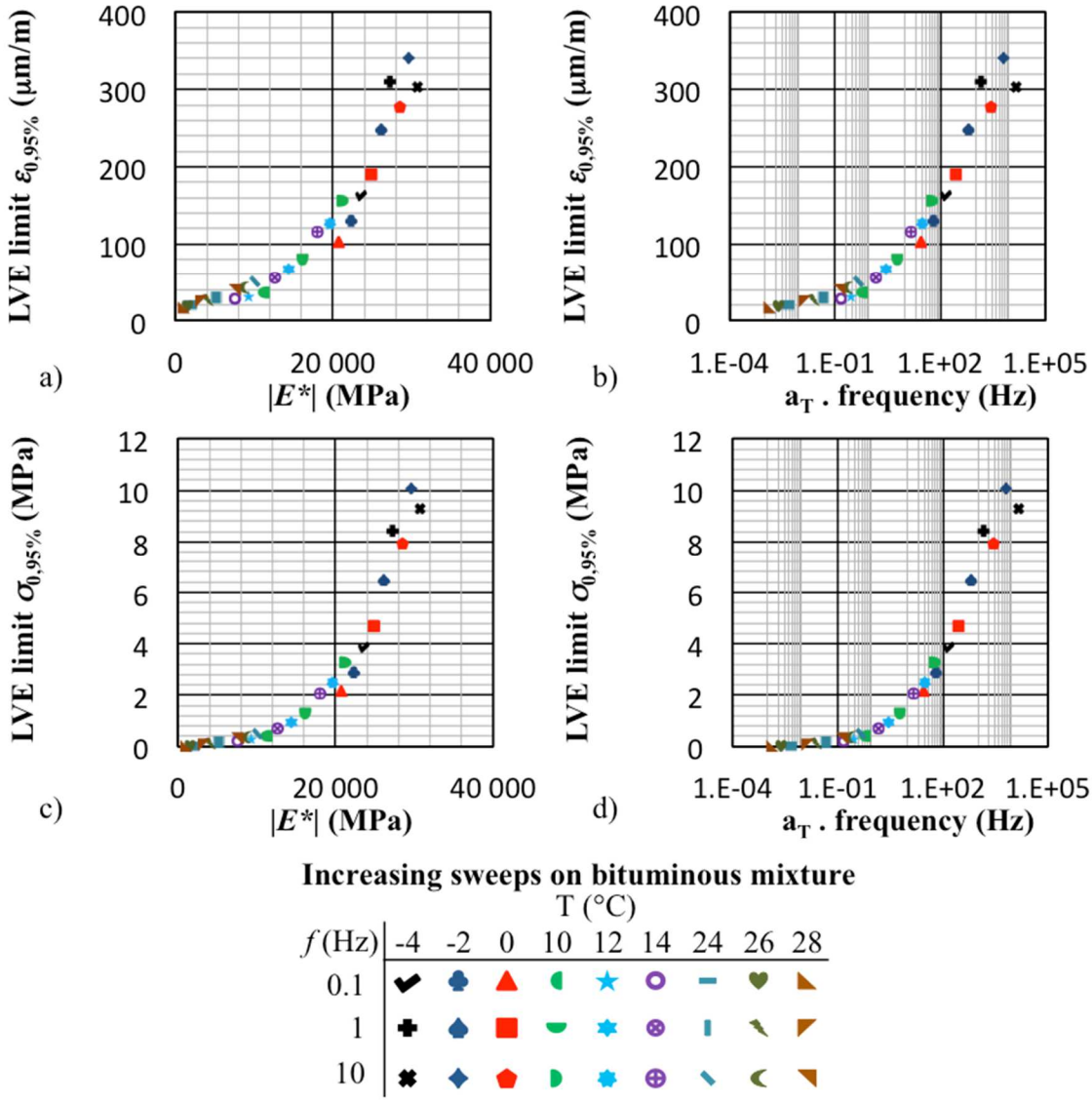

Figure 4-15. LVE limit (in terms of axial strain amplitude, $\varepsilon_{0.95\%}$, figs. a and b, and axial stress amplitude, $\sigma_{0.95\%}$, figs. c and d) obtained from SASTENOLE results (cf. $|p_E \cdot \varepsilon_0| \leq 0.05$ results in Table 4-7) on bitumen BM1_C as a function of norm of complex modulus (figs. a and c) and time-shifted frequency (figs b and d).

Focusing in the direction of nonlinearity as given by Black diagrams and Cole-Cole plots (cf. Figure 4-8 for a scheme, Figure 4-9 and Figure 4-10 for results examples on BM1_B, and Table 4-4 for the summary of results on BM1_B), p_E/p_φ and α have been calculated for SASTENOLE tests on BM1_C. Results are presented in Table 4-8, with indications of the quality of the fit.

Table 4-8. Values of p_E/p_φ and α obtained for all temperatures and frequencies from linear regressions for BM1_C (results for BM1_B on Table 4-4) in (a) Cole-Cole and (b) Black spaces. Each value was obtained by combining data from both decreasing and increasing strain amplitude sweeps.

a)

Cole-Cole space				
T (°C)	**f (Hz)**	**p_E/p_φ (1/°)**	**α (°)**	**R^2 (-)**
-4	**0.1**	$-3.24\cdot10^{-2}$	28.3	0.828
	1	$-3.66\cdot10^{-2}$	25.5	0.517
	10	$-5.48\cdot10^{-3}$	72.6	*1
-2	**0.1**	$-3.27\cdot10^{-2}$	28.1	0.881
	1	$-3.94\cdot10^{-2}$	23.9	0.491
	10	$-3.87\cdot10^{-3}$	77.5	*1
0	**0.1**	$-3.23\cdot10^{-2}$	28.4	0.868
	1	$-4.34\cdot10^{-2}$	21.9	0.489
	10	$-8.50\cdot10^{-3}$	64.0	*1
10	**0.1**	$-3.47\cdot10^{-2}$	26.7	0.346
	1	$-2.77\cdot10^{-2}$	32.3	0.870
	10	$-3.35\cdot10^{-2}$	27.5	0.410
12	**0.1**	$-1.45\cdot10^{-2}$	50.3	*1
	1	$-2.72\cdot10^{-2}$	32.7	0.800
	10	$-2.86\cdot10^{-2}$	31.4	0.623
14	**0.1**	$-3.23\cdot10^{-2}$	28.4	*2
	1	$-2.36\cdot10^{-2}$	36.4	0.751
	10	$-2.72\cdot10^{-2}$	32.7	0.730
24	**0.1**	$-3.93\cdot10^{-2}$	24.0	0.669
	1	$-2.40\cdot10^{-2}$	36.0	*2
	10	$-2.44\cdot10^{-2}$	35.5	0.619
26	**0.1**	$-3.85\cdot10^{-2}$	24.4	0.780
	1	$-2.04\cdot10^{-2}$	40.6	*2
	10	$-2.64\cdot10^{-2}$	33.4	0.531
28	**0.1**	$-3.82\cdot10^{-2}$	24.5	0.772
	1	$-2.27\cdot10^{-2}$	37.5	*2
	10	$-2.49\cdot10^{-2}$	35.0	*2
Mean		$-2.75\cdot10^{-2}$	35.5	
St. dev.		$1.01\cdot10^{-2}$	14.1	

b)

Black space				
T (°C)	**f (Hz)**	**p_E/p_φ (1/°)**	**α (°)**	**R^2 (-)**
-4	**0.1**	$-2.81\cdot10^{-2}$	31.9	0.881
	1	$-2.21\cdot10^{-2}$	38.3	0.597
	10	$-6.91\cdot10^{-4}$	87.7	*2
-2	**0.1**	$-2.95\cdot10^{-2}$	30.6	0.926
	1	$-2.37\cdot10^{-2}$	36.3	*1
	10	$-6.91\cdot10^{-4}$	87.7	*2
0	**0.1**	$-2.88\cdot10^{-2}$	31.2	0.921
	1	$-2.74\cdot10^{-2}$	32.5	0.629
	10	$-2.53\cdot10^{-3}$	81.7	*2
10	**0.1**	$-2.74\cdot10^{-2}$	32.5	0.804
	1	$-2.51\cdot10^{-2}$	34.8	0.935
	10	$-1.87\cdot10^{-2}$	43.1	0.540
12	**0.1**	$-2.88\cdot10^{-2}$	31.2	0.713
	1	$-2.42\cdot10^{-2}$	35.8	0.911
	10	$-2.12\cdot10^{-2}$	39.5	0.736
14	**0.1**	$-3.34\cdot10^{-2}$	27.6	0.759
	1	$-2.05\cdot10^{-2}$	40.4	0.878
	10	$-2.23\cdot10^{-2}$	38.0	0.831
24	**0.1**	$-3.13\cdot10^{-2}$	29.1	0.734
	1	$-2.10\cdot10^{-2}$	39.8	0.850
	10	$-2.10\cdot10^{-2}$	39.8	0.867
26	**0.1**	$-3.36\cdot10^{-2}$	27.4	0.816
	1	$-1.57\cdot10^{-2}$	48.1	0.675
	10	$-2.35\cdot10^{-2}$	36.6	0.900
28	**0.1**	$-2.14\cdot10^{-2}$	39.2	0.854
	1	$-1.68\cdot10^{-2}$	46.1	0.623
	10	$-3.36\cdot10^{-2}$	27.4	0.785
Mean		$-2.23\cdot10^{-2}$	41.3	
St. dev.		$8.86\cdot10^{-3}$	16.6	

*1 For this condition, in Cole-Cole plot, data points present an almost vertical trend (nonlinearity direction is almost vertical). In this case, in order to obtain the slope, an imposed y-intercept needed to be used, and consequent R^2 values were negative, even if nonlinearity produces a clear trend on the measured complex modulus. In Black space, it means that the observed effect of nonlinearity was relatively low, not being perfectly distinguishable from variability around the nonlinearity tren.

*2 For this condition, in Cole-Cole plot, data points present an almost horizontal trend (nonlinearity direction is almost horizontal). In this case, even though there is low variability around the nonlinearity trend, obtained R^2 values are very low, even if nonlinearity produces a clear trend on the measured complex modulus. The same occurred in Black space for results at the lowest temperatures at 10Hz. Other low obtained R^2 values can be explained the same way.

4.2.4.2. *Strain dependence of norm and phase angle of complex Poisson's ratio*

This section presents the effects of nonlinearity on the equivalent complex Poisson's ratio in terms of variations of norm and phase angle as functions of the applied strain amplitude. As for complex modulus, nonlinearity envelopes (measurements as a function of the applied axial strain amplitude) are analysed. Figure 4-16 and Figure 4-17 present results of norm (figure a) and phase angle (figure b) of complex modulus and norm (figure c) and phase angle (figure d) of Poisson's ratio at -4°C, 1Hz and at 28°C, 0.1Hz, respectively. Displayed results are from increasing and decreasing strain sweeps from SASTENOLE on BM1_C, with maximum targeted strain amplitude of 120μm/m. It is observed that even though nonlinearity is clearly observed on complex modulus, this effect is relatively less important on Poisson's ratio. At both testing conditions, variation of norm of complex Poisson's ratio is negligible: less than 3.6% variation in norm of Poisson's ratio is observed for 100μm/m variation on axial strain amplitude, which can be due to the variability of the determined experimental value. When it comes to the phase angle of complex modulus, it can be observed that for the low temperature, negligible variation is also observed, with nonlinearity effects being lower than the noise in experimental results. For the higher temperature (that presented relatively the more significant effect of nonlinearity on complex modulus), some variation was observed: for the applied variation in axial strain amplitude, phase angle of Poisson's ratio varied by around 1°, while its estimated value at very low strain amplitudes is around 3°.

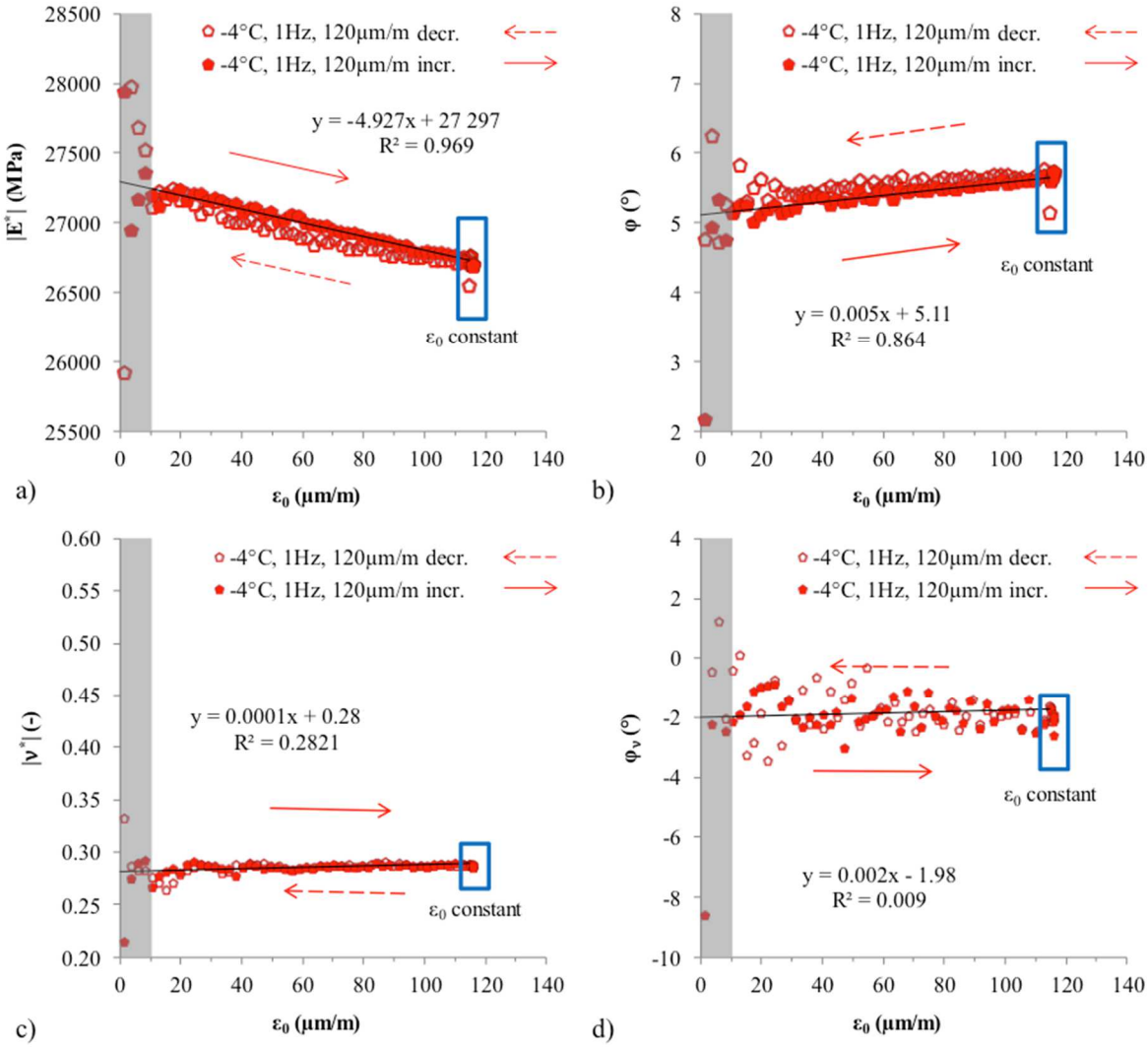

Figure 4-16. Norm and phase angle of complex modulus ($|E^*|$, φ, figures a and b) and of Poisson's ratio ($|\nu^*|$, φ_ν, figures c and d) obtained during increasing and decreasing strain sweeps of SASTENOLE test for maximum targeted strain amplitude of 110µm/m at -4°C, 1Hz.

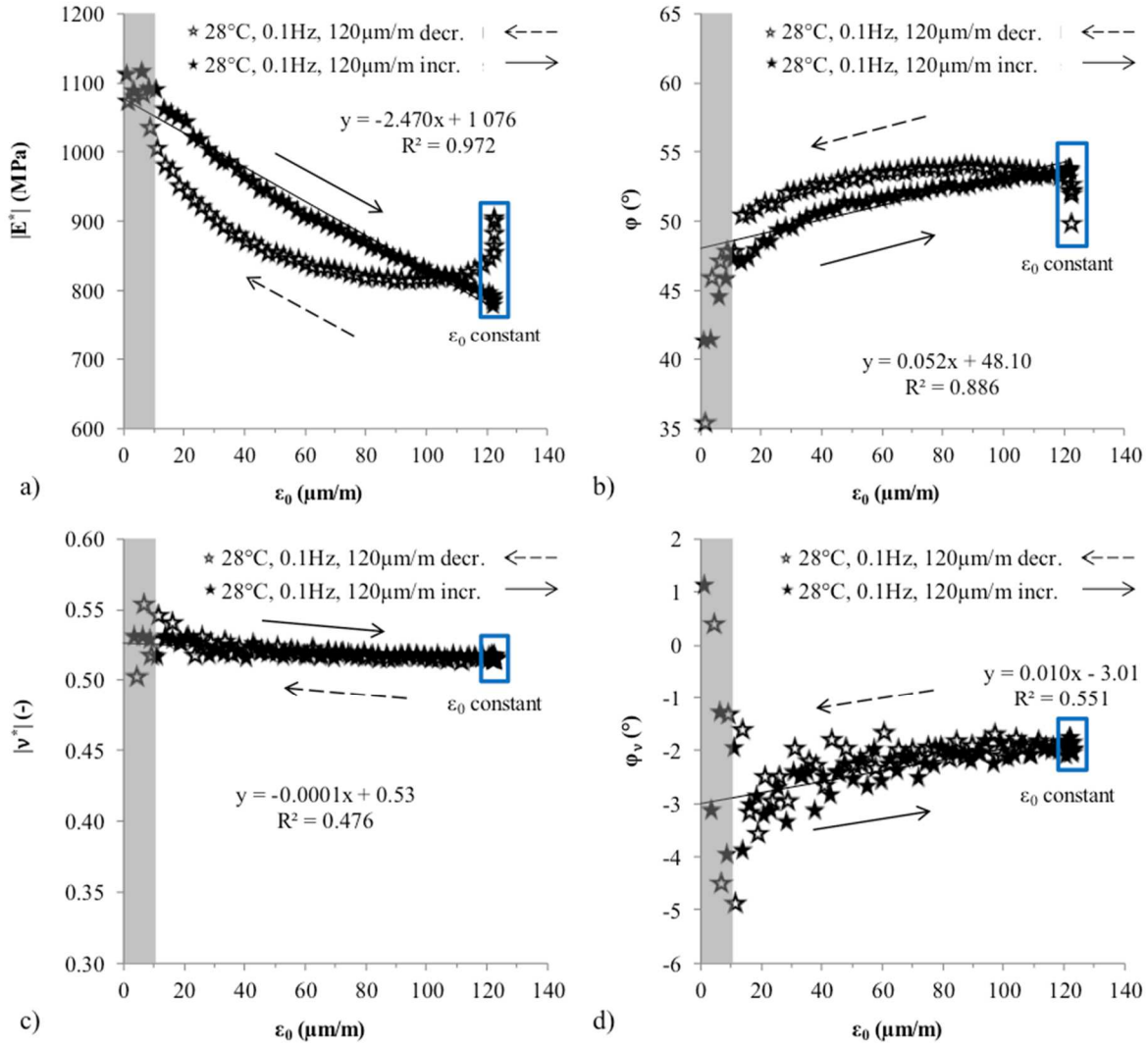

Figure 4-17. Norm and phase angle of complex modulus ($|E^*|$, φ, figures a and b) and of Poisson's ratio ($|\nu^*|$, φ_ν, figures c and d) obtained during increasing and decreasing strain sweeps of SASTENOLE test for maximum targeted strain amplitude of 110µm/m at 28°C, 0.1Hz.

Figure 4-18 and Figure 4-19 present SASTENOLE results including all tested maximum targeted strain amplitudes, with increasing amplitude sweeps separated from the decreasing amplitude sweeps, for -4°C, 1Hz and 28°C, 0.1Hz, respectively. In the figures, as for BM1_B (cf. Figure 4-5 and Figure 4-6), results from increasing and decreasing amplitude sweeps can be compared. Results obtained for the very first cycle of each decreasing sweep (6th cycle of the decreasing loading sequence, first of the 50 cycles in the decreasing sweep) were highlighted in red circles cycle. From Figure 4-18, it is clear that, at low temperature, the effects of nonlinearity are negligible when compared to the noise in experiments. Experimental observation does not provide evidence of a strain dependent Poisson's ratio at low temperature. At higher temperature, variation in the norm of Poisson's ratio is negligible (relative variation of around 3% for 100µm/m variation in axial strain amplitude). So, there is still no evidence supporting a strain dependent norm of Poisson's ratio. However, some variation in its phase angle is observed (Figure 4-19c and d) at higher temperatures: 1°, while its estimated value at very low strain amplitudes is around 3°. This variation can be considered low for modelling purposes.

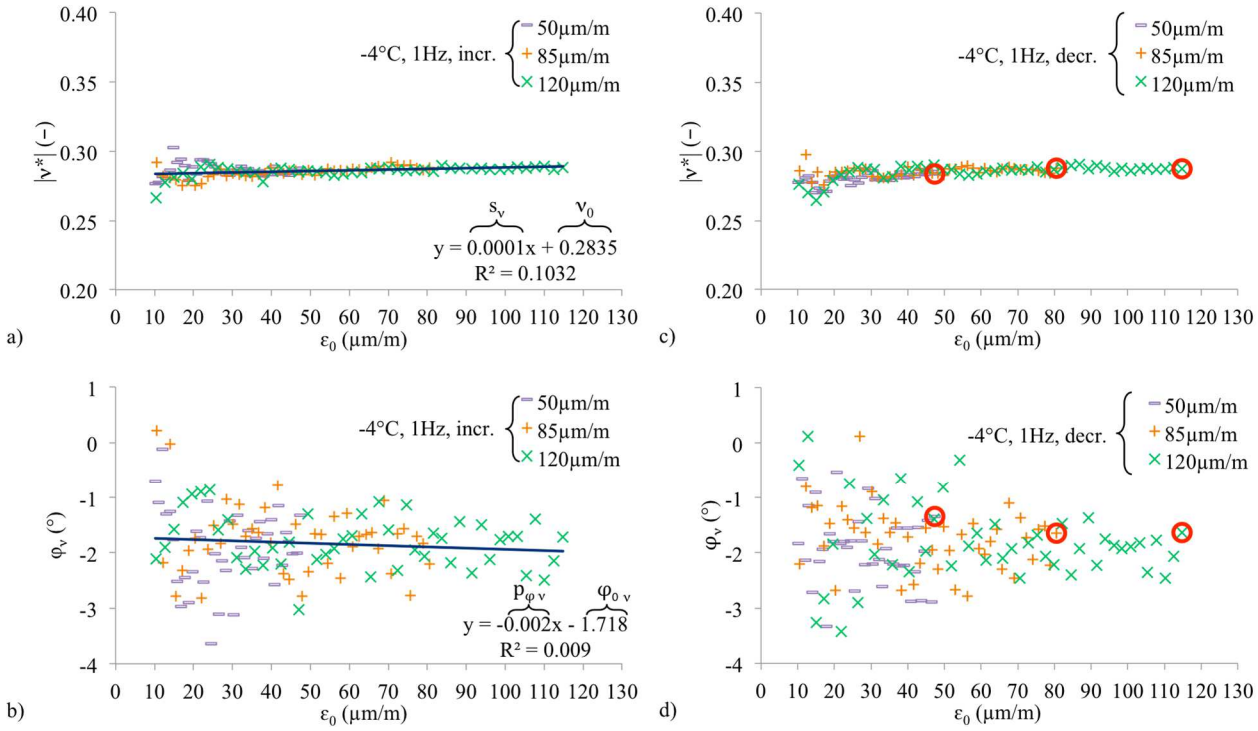

Figure 4-18. Norm $|v^*|$ (top) and phase angle φ_v of Poisson's ratio (bottom) obtained from SASTENOLE test at -4°C, 1Hz, for the three increasing strain amplitude (figures a and b) and for the three decreasing strain amplitude loading paths (figures c and d): s_v and $p_{\varphi v}$ are the slopes of the nonlinearity envelopes of, respectively, $|v^*|$ and φ_v.

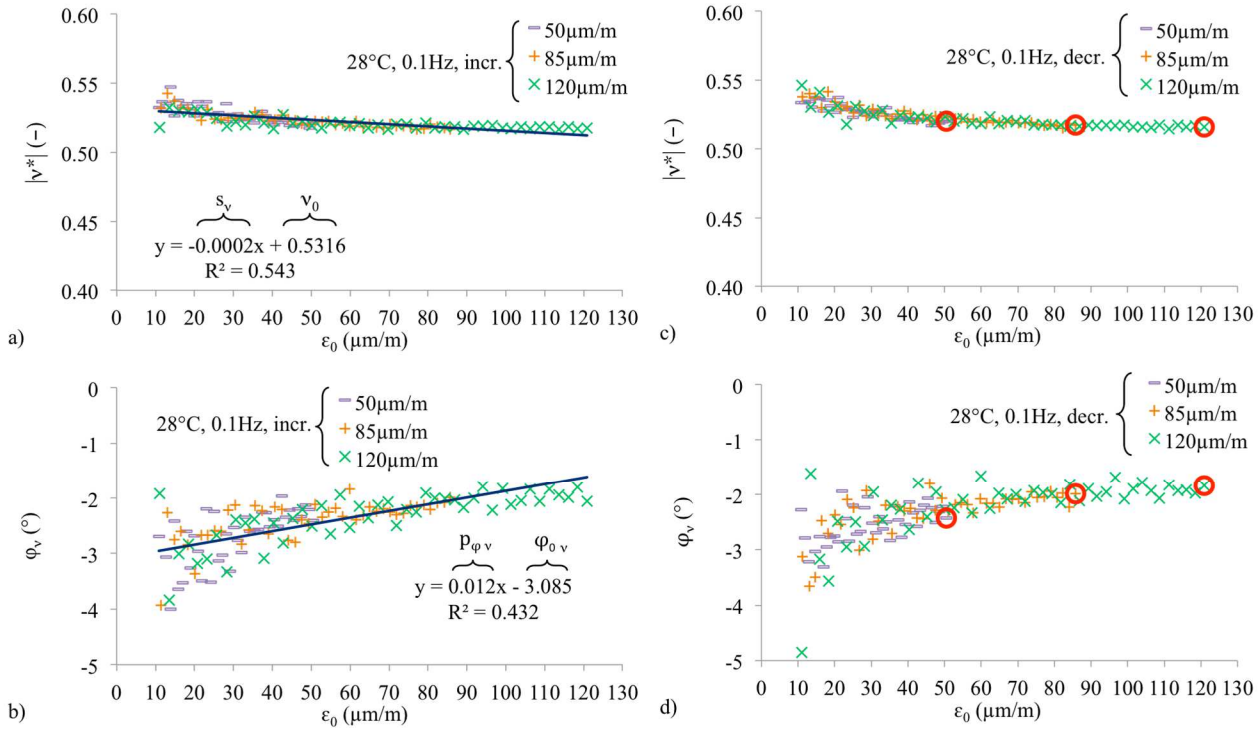

Figure 4-19. Norm $|v^*|$ (top) and phase angle φ_v of Poisson's ratio (bottom) obtained from SASTENOLE test at 28°C, 0.1Hz, for the three increasing strain amplitude (figures a and b) and for the three decreasing strain amplitude loading paths (figures c and d): s_v and $p_{\varphi v}$ are the slopes of the nonlinearity envelopes of, respectively, $|v^*|$ and φ_v.

4.2.5. Transient effects during SASTENOLE tests

Complex modulus and complex Poisson's ratio are defined for steady state conditions, i.e. under sinusoidal loading the transient effects (inherent to viscoelastic materials) are negligible and constant amplitudes are observed both in strain and in stress signals. The test procedure developed in this thesis, called SASTENOLE, proposes a continuous change in strain amplitude, which is in principle in contradiction with the previous definitions. This section intends to demonstrate that transient effects are negligible for most part of the SASTENOLE loading, and that a steady state can be considered in the analysis, thus, used to obtain complex modulus and complex Poisson's ratio.

In order to calculate transient effects expected in SASTENOLE tests, a numerical procedure used to approximate the convolution integral describing LVE behaviour (cf. Eq. 2-12 and Eq. 2-13) was used (Gayte et al., 2016). Input material parameters are the constants associated to a generalised Kelvin-Voigt (GKV) model, presented in Table 4-9. Then, the strain path during SASTENOLE tests is imposed, while the numerical procedure calculates the force necessary to produce that strain. Specimen is considered cylindrical with 75.3mm diameter. The obtained result is the force signal associated to the imposed strain signals. The result may be analysed as done for complex modulus tests: sinusoidal signals are used to approximate the actual results, and, finally, to determine equivalent complex modulus. Equivalent complex modulus results obtained for a purely linear viscoelastic material with GKV model constants compatible with BM1 are presented in Figure 4-20. Also, examples of results for two loading cycles are presented in graphs of force as a function of strain. The chosen cycles are the 2nd and the 10th of increasing amplitude sweeps with maximum targeted strain amplitude of 100μm/m. These cycles were chosen to illustrate when transient effects, which produce defects on strain and/or stress sinusoidal signals, can be considered negligible in order to obtain a reliable equivalent complex modulus measurement.

Table 4-9. Generalised Kelvin-Voigt model (at 14.44°C) with 40 viscoelastic elements and one free elastic constant used to simulate transient effects in the tested bituminous mixture, following numerical calculation from the literature (Gayte et al., 2016). This set of KVG parameters is a discretised form to describe LVE behaviour of BM1, equivalent to 2S2P1D model for BM1_A (cf. Table 4-1, where WLF parameters are also given).

τ_j (s)	D_j (MPa^{-1})	τ_j (s)	D_j (MPa^{-1})
$6.27 \cdot 10^{-14}$	$2.64 \cdot 10^{-7}$	$5.12 \cdot 10^{-2}$	$1.76 \cdot 10^{-5}$
$2.47 \cdot 10^{-13}$	$1.61 \cdot 10^{-7}$	$2.02 \cdot 10^{-1}$	$2.96 \cdot 10^{-5}$
$9.74 \cdot 10^{-13}$	$2.33 \cdot 10^{-7}$	$7.95 \cdot 10^{-1}$	$5.36 \cdot 10^{-5}$
$3.84 \cdot 10^{-12}$	$1.65 \cdot 10^{-7}$	$3.13 \cdot 10^{-0}$	$1.03 \cdot 10^{-4}$
$1.51 \cdot 10^{-11}$	$2.21 \cdot 10^{-7}$	$1.24 \cdot 10^{1}$	$2.08 \cdot 10^{-4}$
$5.96 \cdot 10^{-11}$	$2.77 \cdot 10^{-7}$	$4.87 \cdot 10^{1}$	$4.38 \cdot 10^{-4}$
$2.35 \cdot 10^{-10}$	$3.52 \cdot 10^{-7}$	$1.92 \cdot 10^{2}$	$9.68 \cdot 10^{-4}$
$9.26 \cdot 10^{-10}$	$4.45 \cdot 10^{-7}$	$7.56 \cdot 10^{2}$	$2.39 \cdot 10^{-3}$
$3.65 \cdot 10^{-9}$	$5.65 \cdot 10^{-7}$	$2.98 \cdot 10^{3}$	$7.41 \cdot 10^{-3}$
$1.44 \cdot 10^{-8}$	$7.14 \cdot 10^{-7}$	$1.17 \cdot 10^{4}$	$2.42 \cdot 10^{-2}$
$5.67 \cdot 10^{-8}$	$9.07 \cdot 10^{-7}$	$4.63 \cdot 10^{4}$	$2.15 \cdot 10^{-2}$
$2.23 \cdot 10^{-7}$	$1.15 \cdot 10^{-6}$	$1.82 \cdot 10^{5}$	$1.07 \cdot 10^{-3}$
$8.80 \cdot 10^{-7}$	$1.46 \cdot 10^{-6}$	$7.19 \cdot 10^{5}$	$6.86 \cdot 10^{-4}$
$3.47 \cdot 10^{-6}$	$1.87 \cdot 10^{-6}$	$2.83 \cdot 10^{6}$	$5.90 \cdot 10^{-4}$
$1.37 \cdot 10^{-5}$	$2.39 \cdot 10^{-6}$	$1.12 \cdot 10^{7}$	$5.46 \cdot 10^{-4}$
$5.39 \cdot 10^{-5}$	$3.10 \cdot 10^{-6}$	$4.40 \cdot 10^{7}$	$5.12 \cdot 10^{-4}$
$2.12 \cdot 10^{-4}$	$4.07 \cdot 10^{-6}$	$1.73 \cdot 10^{8}$	$4.81 \cdot 10^{-4}$
$8.37 \cdot 10^{-4}$	$5.48 \cdot 10^{-6}$	$6.83 \cdot 10^{8}$	$4.51 \cdot 10^{-4}$
$3.30 \cdot 10^{-3}$	$7.65 \cdot 10^{-6}$	$2.69 \cdot 10^{9}$	$4.24 \cdot 10^{-4}$
$1.30 \cdot 10^{-2}$	$1.12 \cdot 10^{-5}$	$1.06 \cdot 10^{10}$	$3.98 \cdot 10^{-4}$

*Free elastic constant (glassy compliance): D_g (MPa^{-1}) = $2.48 \cdot 10^{-5}$

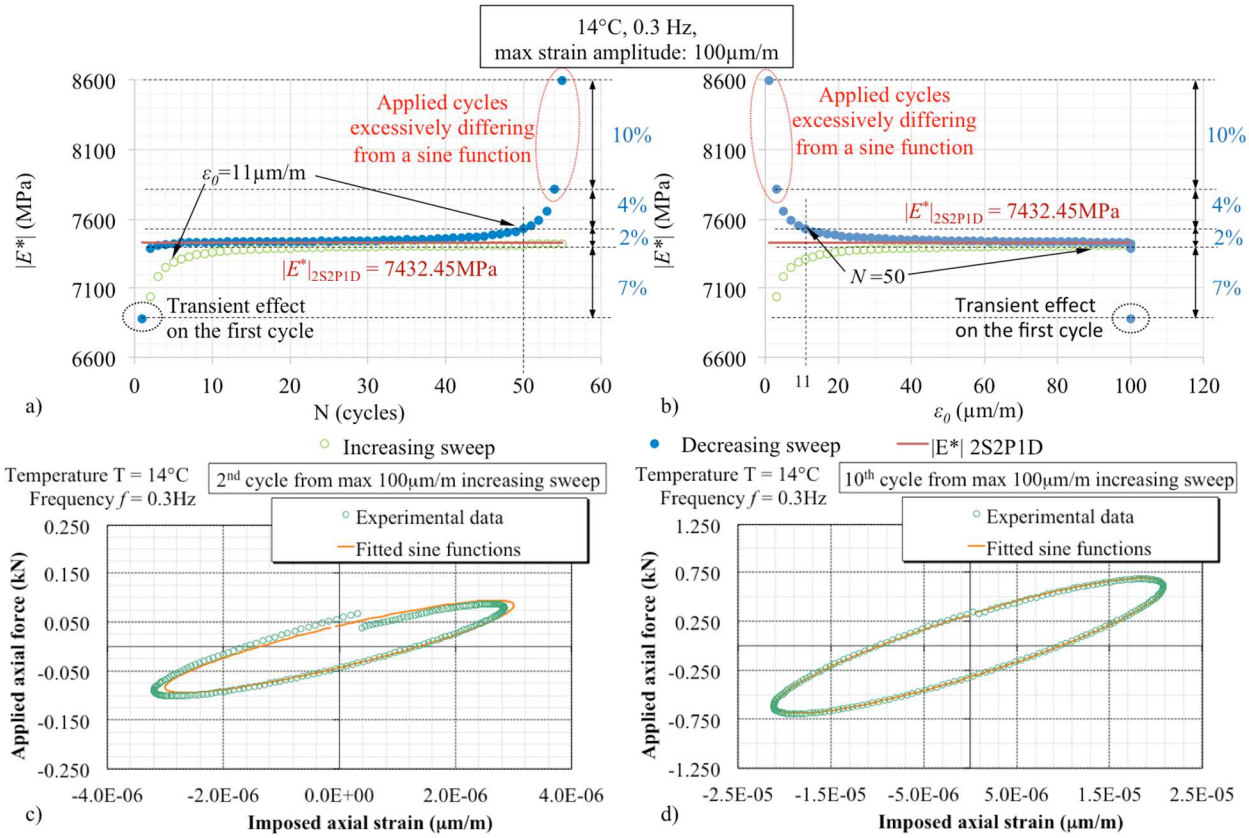

Figure 4-20. Example of results for the simulation of perfectly linear viscoelastic response of BM1_A (using KVG model parameters given in Table 4-9, and specimen diameter 75.3mm), including transient effects, to the SASTENOLE loading path (increasing and decreasing sweeps), obtained at 14°C and 0.3Hz with maximum strain amplitude of 100µm/m: a) Modulus from increasing and decreasing sweeps as a function of loading cycles; a) Modulus from increasing and decreasing sweeps as a function of the applied strain amplitude; and examples of hysteresis loop (including the actual response and the fitted sine functions used to obtain modulus) at c) the 2nd cycle and d) the 10th cycle.

4.3. Annular shear experiments on bitumen and mastic specimens

The Annular Shear Rheometer (ASR) was used to perform tests (cf. Section 3.2.1 for test set-up) for the characterisation of bitumen and mastic. Two materials were studied: bitumen B5070 and mastic M5070_30pc40-70. A characterisation of the "linear" behaviour was performed. It is given by the complex shear modulus (obtained at low shear stress amplitudes, the least possible giving clear force signals, corresponding to an amplitude of around 0.3kN). Then, a characterisation of the nonlinear behaviour (varying strain amplitude) was performed.

4.3.1. Complex shear modulus test at "low" amplitudes

In order to determine the complex shear modulus of bitumen and mastic, ASR complex modulus tests were performed. In the test, on-specimen strain is controlled in order to have

sinusoidal signals. The amplitude of the signal is chosen in order to have sufficiently accurate load signals measured in the 50kN load-cell. Also, a "small" strain is desired, in order to avoid nonlinearities in the mechanical response. The targeted force amplitude during the complex shear modulus tests on bitumen and mastic is 0.3kN. The utilised loading path is represented in Figure 4-21. Figure 4-22 represents the experimental results from the linear viscoelastic characterisation of bitumen B5070 and mastic M5070_30pc40-70, and the 2S2P1D modelling results. It also shows a comparison of the LVE behaviour of the two tested materials with that of the bituminous mixture BM1, evaluated before. The fitted 2S2P1D parameters are given in Table 4-10.

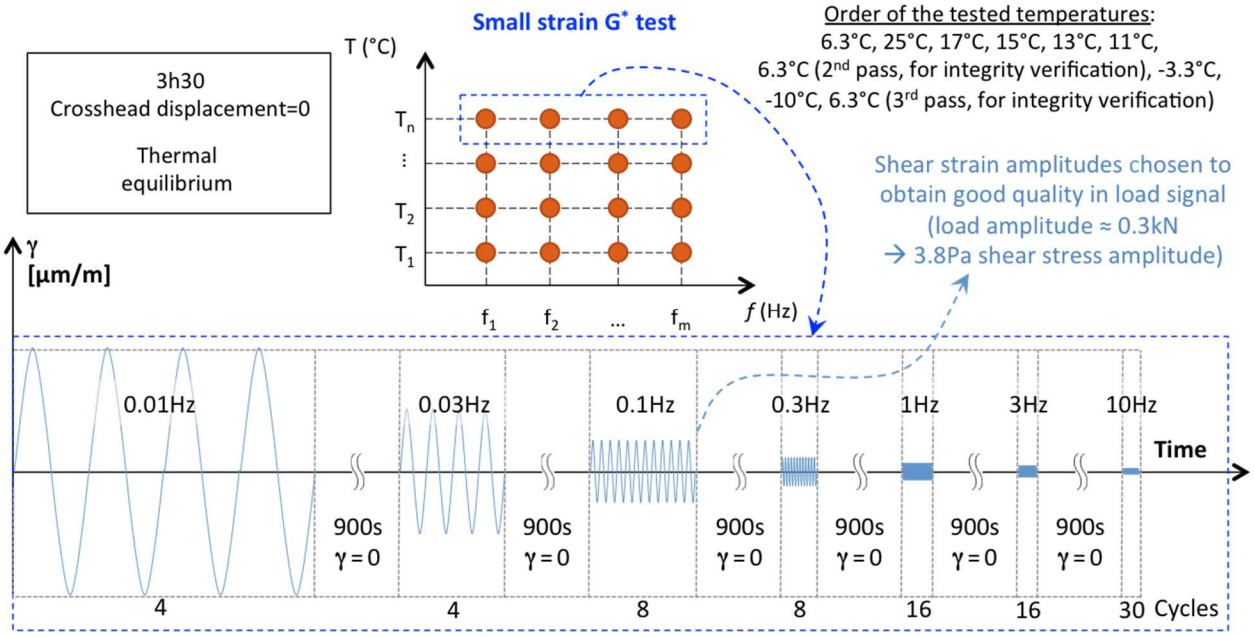

Figure 4-21. Scheme of the bitumen and mastic complex modulus test (ASR setup, cf. Figure 3-2, and Figure 3-4 for a deformation scheme) loading path.

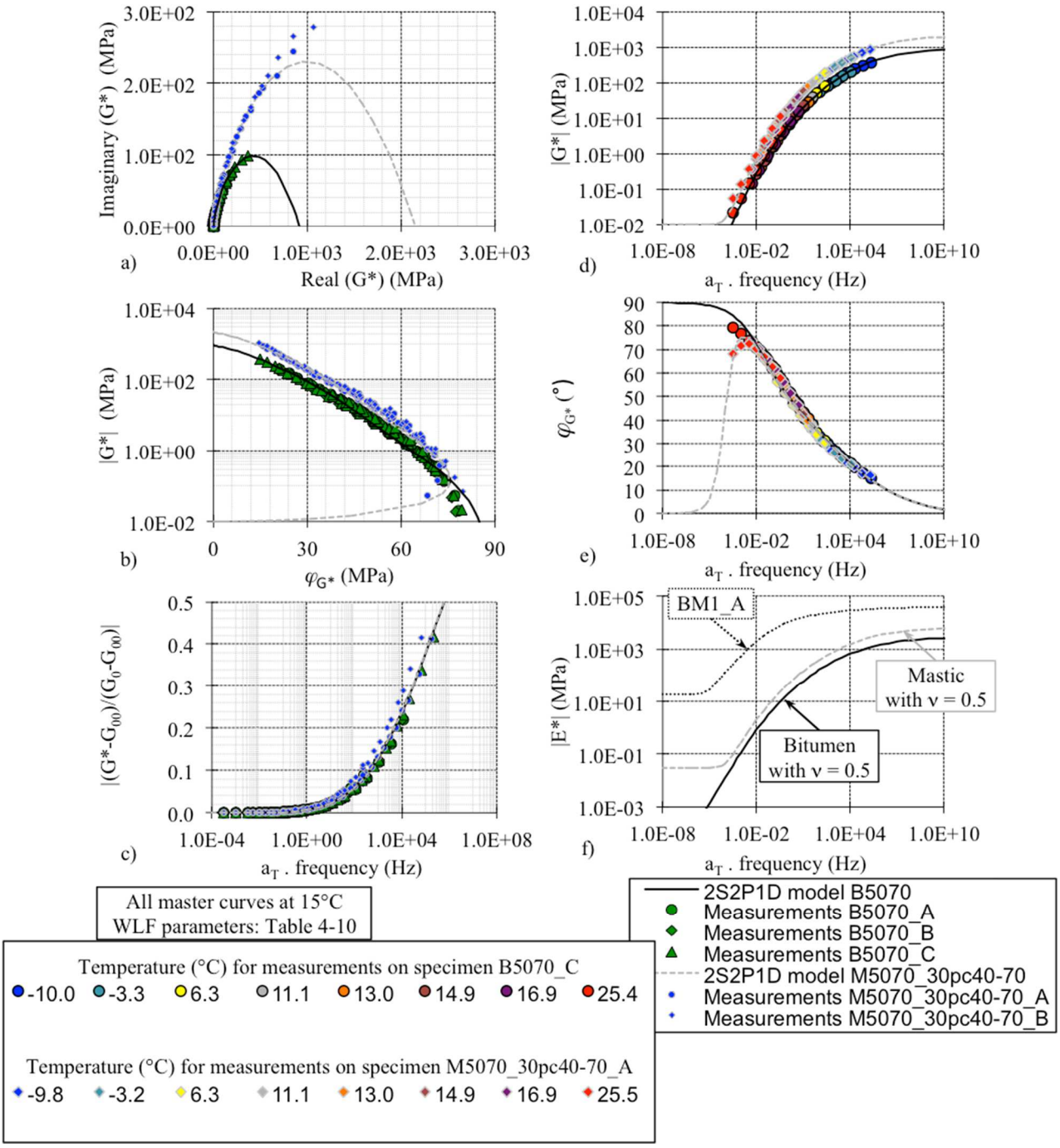

Figure 4-22. 2S2P1D fitting of experimental data (BM1_A and BM1_C specimens) obtained from ASR complex shear modulus tests at low strain amplitude (force signal amplitude around 0.3kN): a) Cole-Cole plot; (b) Black diagram; c) normalized complex modulus master curve (at 15°C); d) norm of complex modulus, and e) phase angle master curves (at 15°C) with details on tested temperatures; and f) comparison of norm of axial complex modulus master curves (at 15°C) for the three studied materials.

Table 4-10. 2S2P1D model and WLF equation parameters used to model the LVE behaviour of the studied bitumen and mastic.

2S2P1D model parameters (T_{ref} = 15°C)								WLF equation		
Specimen	**G_{00} (MPa)**	**G_0 (MPa)**	**k (-)**	**h (-)**	**δ (-)**	**$\tau_{0,G}$ (s)**	**β (-)**	**T_{ref} (°C)**	**C_1 (-)**	**C_2 (°C)**
B5070	0	920	0.250	0.570	3.60	$4.40 \cdot 10^{-5}$	190	15.0	28.5	190.8
M5070_30pc40-70	0.01	2,250	0.250	0.570	3.60	$4.40 \cdot 10^{-5}$	190	15.0	28.5	190.8

From Figure 4-22c and Table 4-10, it is seen that B5070 and M5070_30pc40-70 share most of the LVE modelling parameters. It can also be seen that the mastic, for a wide range of temperatures and frequencies, presents a complex shear modulus increased by an approximately constant factor when compared to the bitumen. Norm of complex modulus is multiplied by approximately 2.45, while the phase angle is the same for almost all tested frequencies and temperatures. At temperatures higher than 17°C, and low frequencies, the phase angle of the mastic is reduced with respect to that of the bitumen. This is expected, since the elastic solid inclusions take over the overall behaviour of the composite. A simple model, which is further discussed in the next chapter (cf. Sections 5.3 and 5.5.3), can explain this observed ratio between mastic modulus and bitumen modulus.

4.3.2. Strain Amplitude Sweep (SAS) tests on bitumen and mastic

Strain Amplitude Sweep (SAS) tests were performed on bitumen and mastic in order to evaluate nonlinearity. Test specimens used were B5070_F (test at 6.3°C) and B5070_G (test at 11.1°C) for bitumen and M5070_30pc40-70_C (tests at all utilised temperatures) for mastic (cf. Table 3-1). Figure 4-23 presents a detailed scheme of the SAS tests, which are performed at different frequencies and strain amplitudes at a given temperature. The figure also presents an example of test results (norm of complex modulus and average temperature of the 4 thermocouples inside the specimen) for bitumen B5070 at 11.1°C and 3Hz. For different frequencies, a different number of loading cycles is applied, similarly as done for typical complex modulus tests. For 0.01, 0.03, 0.1, 0.3, 1, 3, 10Hz, the number of applied cycles was 4, 4, 4, 8, 8, 16, 30, respectively.

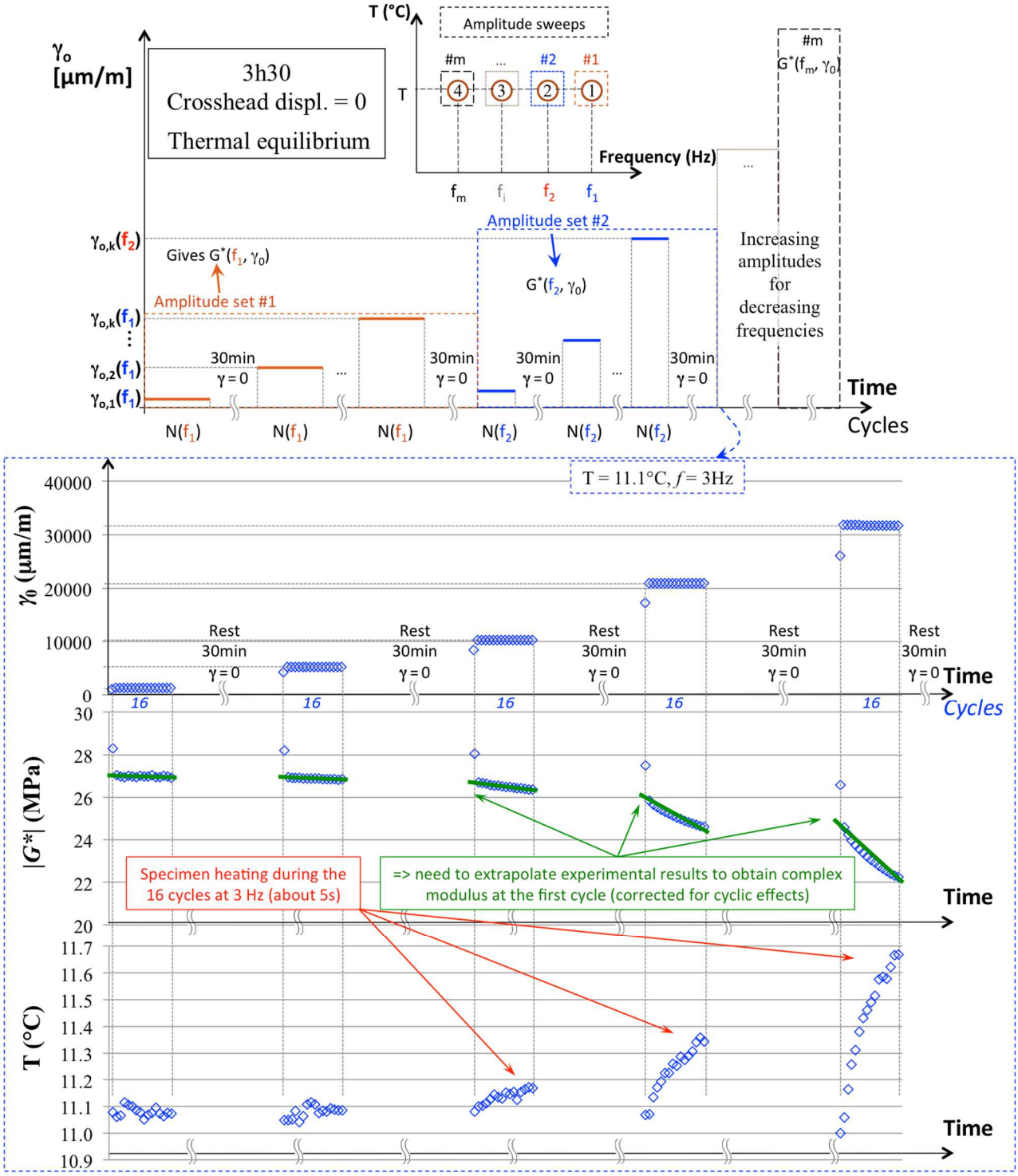

Figure 4-23. Detailed scheme of the Strain Amplitude Sweep (SAS) tests conducted using the ASR, with an example of results for B5070 at 11.1°C, presenting the obtained norm of complex shear modulus and the in-specimen temperature during the loading sequences at 3Hz.

4.3.2.1. *Cyclic effects during Strain Amplitude Sweep (SAS) tests*

The effect of nonlinearity, solely, on the complex modulus should produce a strain dependent mechanical response, but with no variation with respect to the number of cycles. As presented in the example on Figure 4-23, SAS tests introduce a change in complex modulus for fixed strain

amplitude, which is not expected from nonlinearity. This is due to cyclic effects, such as self-heating producing an increase in temperature, which is highlighted in the figure. Figure 4-24 presents results of maximum temperature increase obtained during SAS tests on bitumen and mastic (at various conditions of temperature, frequency and strain amplitude) as a function of the applied shear strain amplitude (average from all cycles except the first one). The figure shows that higher temperature increase is observed for a higher frequency at a given strain amplitude. It is recalled that the number of applied cycles was of 30 for tests and 10Hz, 16 for 3Hz, 8 for 1Hz and 0.3Hz, and 4 for 0.1Hz and 0.03Hz. So, more dissipated energy tends to be injected as heat in the material for tests at higher frequency, and that happens in a shorter period of time.

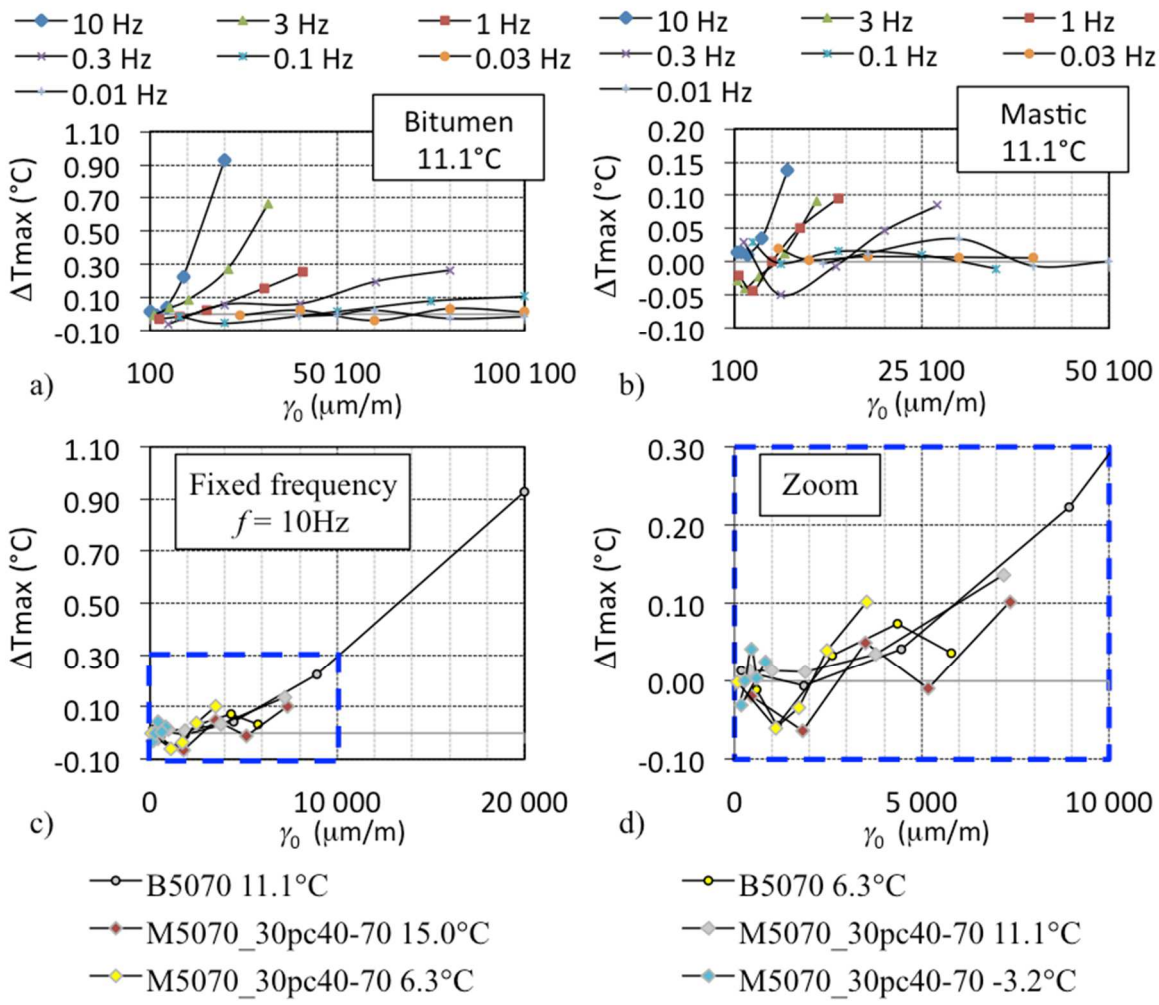

Figure 4-24. Maximum temperature increase during SAS tests on bitumen and mastic (at the last cycle of loading at a given frequency and strain amplitude, cf. Figure 4-23). The figure presents the temperature increase for tests on bitumen at 11.1°C and all frequencies (figure a), on mastic at 11.1°C and all frequencies (figure b), on bitumen and mastic at 10Hz and all temperatures (figure c) and a zoom on these last results (figure d).

The next chapter of this thesis (Chapter 5) treats the self-heating phenomenon. Other cyclic effects include thixotropy, and damage, which is negligible for low number of cycles as applied in the SAS test. All those cyclic effects are addressed in Chapter 6. Other effect that needs to be

taken into account when analysing SAS tests is transient effects (cf. Section 4.2.5 and Figure 4-20 for a thorough discussion). As seen before, initial cycles (around 2 or 3) need to be discarded (Gayte et al., 2016). In order to correct the observed cyclic effects and obtain an observation of nonlinearity, the complex modulus result needs to be obtained at the first cycle of loading at a given amplitude and frequency. This can be done using an extrapolation technique. In this work, linear functions were fitted to the complex modulus versus number of cycles curve, excluding the 2 first cycles. Then, the value of complex modulus was obtained at the first cycle by extrapolation.

4.3.3. Analysis of Strain Amplitude Sweep (SAS) test results

Again, it is recalled that, rigorously, complex modulus is a linear viscoelastic parameter independent of strain amplitude and that, in this investigation of nonlinearity, results of complex modulus are in fact "equivalent" complex modulus. Figure 4-25 presents an example of SAS test result, in terms of complex modulus results as a function of strain amplitude, obtained for M5070_30pc40-70 at 6.3°C and frequencies from 0.01 to 10Hz. Other results are presented in the Appendix B. The figure presents how to determine the asymptotic value of norm and phase angle of complex shear modulus (extrapolated for 0μm/m). These asymptotic values are used to normalise complex modulus. Finally, a LVE limit, defined as the strain amplitude necessary to produce a change of 5% in complex modulus, is obtained. It is seen from the presented results that the LVE limit is frequency-dependent. It is to be observed that, differently from the bituminous mixture results (cf. Figure 4-11 and Figure 4-13), a linear trend of the relative change in modulus and in phase angle can hardly be observed. Then, obtaining values for the parameters studied for bituminous mixtures (p_E and p_φ) from linear fitting is not possible.

From the same results, and using the same asymptotic values for norm and phase angle of complex modulus, normalised Black curves are obtained, as done before for the analysis of nonlinearity in bituminous mixture (cf. Figure 4-11 and Figure 4-13c). As seen before (cf. Section 4.2.3) normalised Black curves give nonlinearity direction. All normalised Black curves results obtained in this work are presented in Figure 4-26. In the figure, each graph represents a SAS result for either bitumen or mastic, at a given temperature, for all tested frequencies and strain amplitudes. It is seen that nonlinearity direction is frequency-dependent: for increasing frequencies, norm of complex modulus relative change decreases for a given change in phase angle. In order to evaluate temperature-dependence of the nonlinearity direction, the same curves are analysed, but with fixed frequencies and varying temperatures. Figure 4-27 presents an example of results for loading at 0.1Hz. It is seen that the direction of nonlinearity is temperature-dependent: as temperature increases the relative modulus change increases for a given change in phase angle. In a less pronounced way, the same kind of temperature- and frequency- dependence was observed in bituminous mixture (cf. Figure 4-13). Since the obtained experimental data (Figure 4-26 and Figure 4-27) present an approximately linear trend, it is possible to estimate the relationship between nonlinearity in modulus and in phase angle from a linear fitting, similarly to what has been done for bituminous mixtures with the parameter p_E/p_φ.

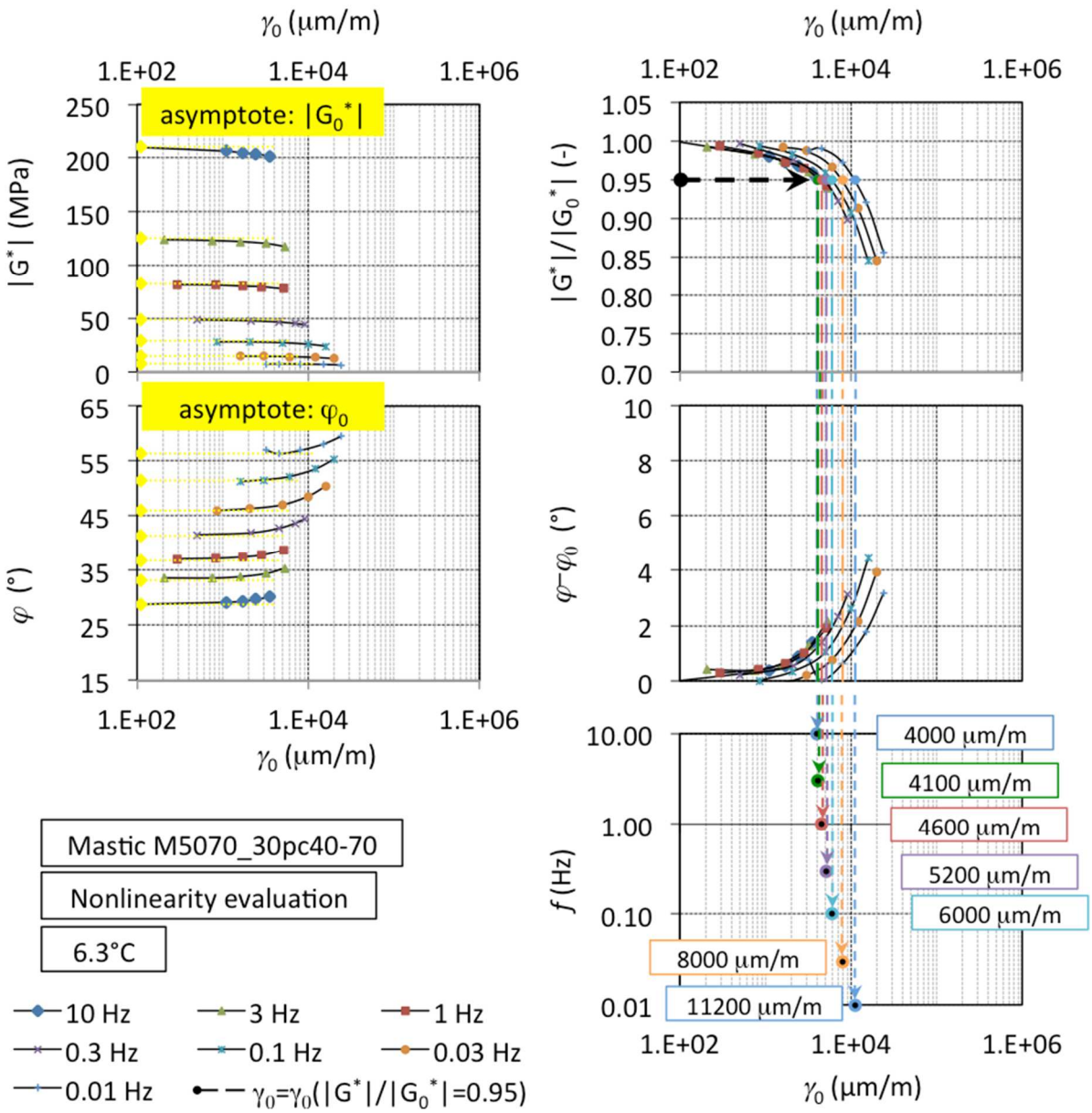

Figure 4-25. Example of a set of experimental results (norm and phase angle of complex shear modulus) for SAS tests using the ASR (tests at 6.3°C on mastic M5070_30pc40-70), with details on the method for determination of the asymptotic "linear" values (at 0µm/m) and of the LVE limit in terms of strain amplitude.

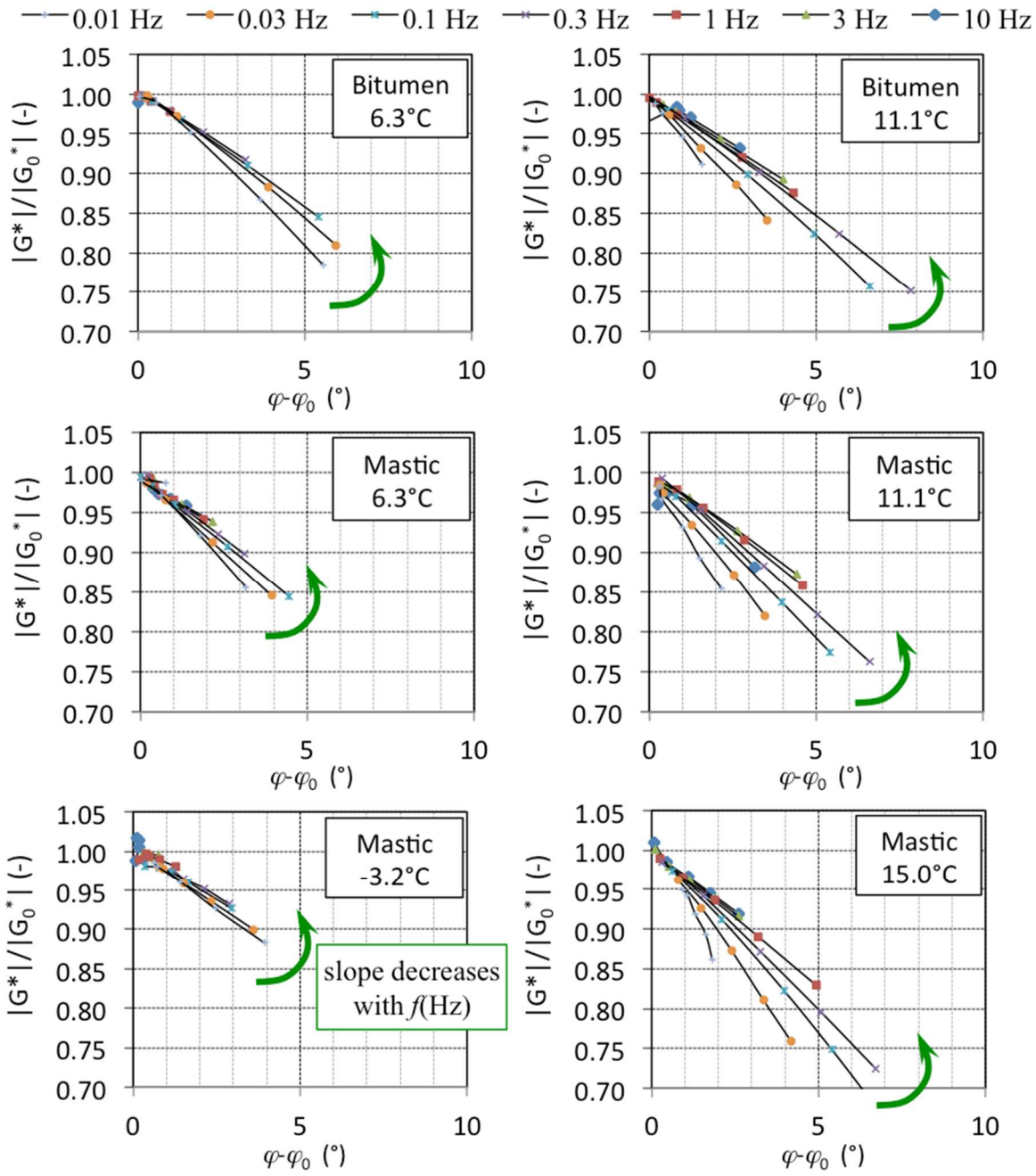

Figure 4-26. SAS experimental results in normalized Black curves (normalized equivalent complex modulus as a function of the normalized phase angle) for all tested temperatures and frequencies on bitumen B5070 and mastic M5070_30pc40-70.

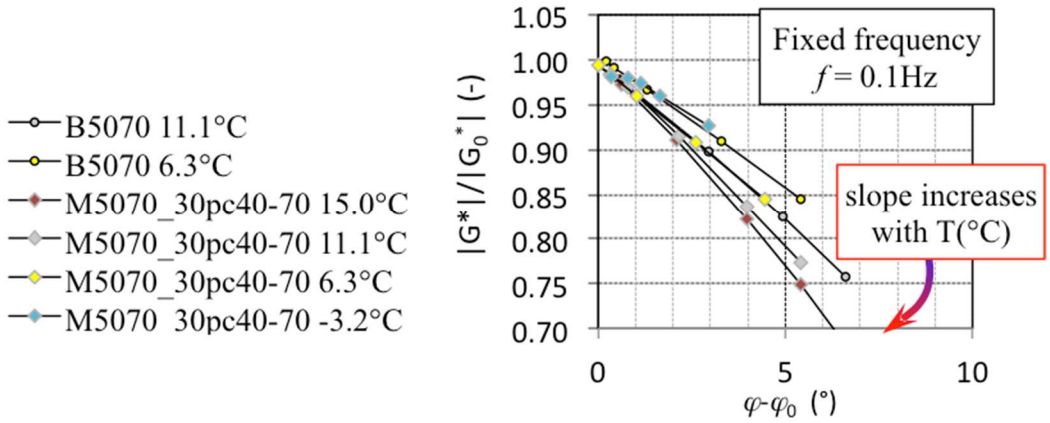

Figure 4-27. SAS experimental results at 0.1Hz for all tested temperatures in normalized Black curves (normalized equivalent complex modulus as a function of the normalized phase angle) for bitumen B5070 and mastic M5070_30pc40-70.

From the linear fitting of the experimental data presented in Figure 4-26, the parameter p_E/p_φ was estimated. This parameter is intrinsically related to the directions of nonlinearity in polar representations of the complex modulus (cf. Figure 4-8, Figure 4-9 and Figure 4-10, and Eq. 4-11). The obtained results are presented in Figure 4-28. The figure suggests that the time-temperature superposition principle apply for the parameter p_E/p_φ in bitumen and in mastic. Also, the same WLF equation parameters used for the LVE characterisation (cf. Table 4-10) have been used to obtain the time-shifted master curves. This indicates that time-temperature superposition follows the same rule for p_E/p_φ as for the complex modulus (linear characterisation). Finally, it is also observed from the figure that bitumen and mastic behave similarly with respect to p_E/p_φ values. This means that, at a given temperature and frequency, the direction of nonlinearity in polar representations is the same for both materials. The same is not observed for the bituminous mixture. For the observed frequency range (10^{-3} to 10^{3} Hz at 15°C), while bitumen and mastic p_E/p_φ varied from about -0.10/° to about -0.02/° in a monotonic way, bituminous mixture p_E/p_φ varied from about -0.04/° to about -0.02/° with a peak around 1Hz at 15°C.

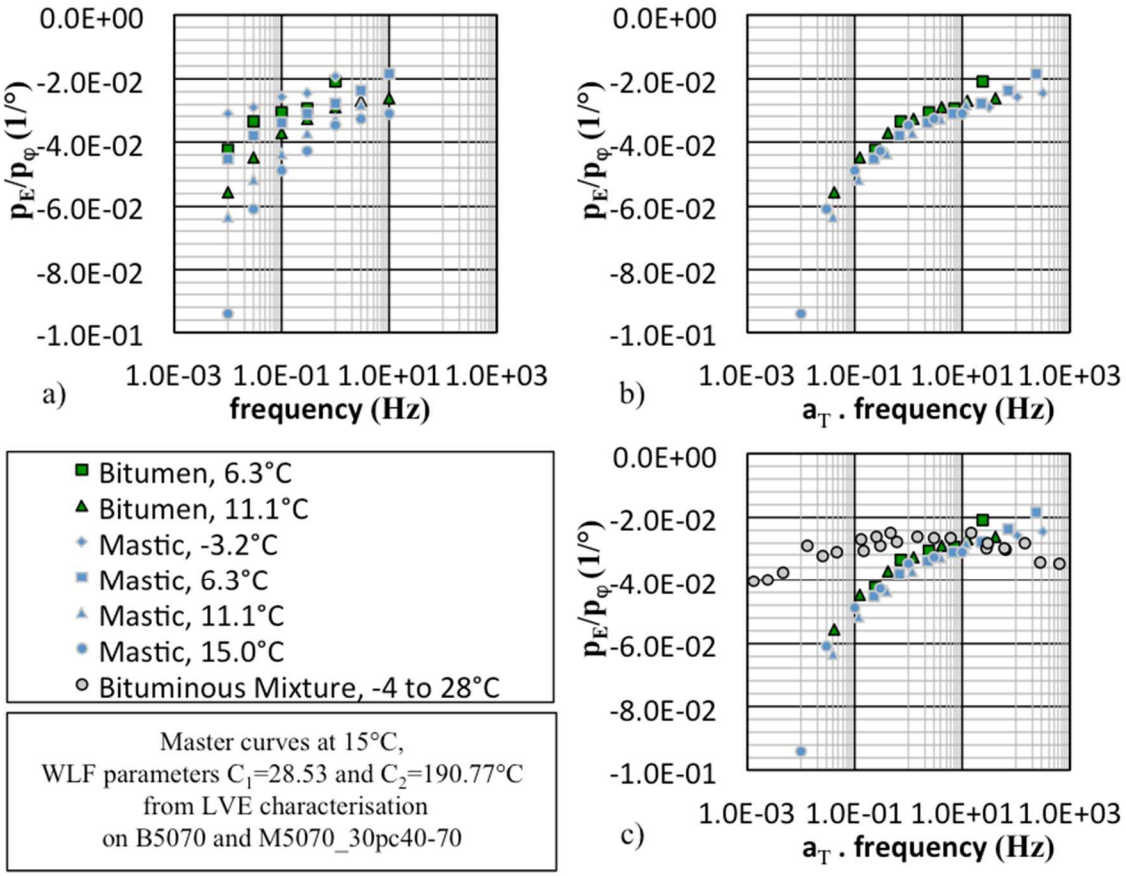

Figure 4-28. p_E/p_φ results obtained from all SAS tests on B5070 and on M5070_30pc40-70 at different temperatures and frequencies: a) p_E/p_φ as a function of frequency; b) p_E/p_φ master curves, constructed using WLF parameters from LVE characterisation (Table 4-10); c) p_E/p_φ master curves including BM1_C results (cf. Figure 4-14). The master curves are presented at 15°C.

Figure 4-29 presents an analysis of the relationship between the LVE limit of bitumen and mastic. All obtained LVE limit results, in terms of shear strain amplitude necessary to produce a 5% relative change in modulus, are represented as functions of the complex shear modulus. Details on test temperatures and frequencies are also given. It is seen from the figures that time-temperature superposition seems to apply to the LVE limit. Unique curves of LVE limit as a function of modulus are obtained. This indicates that time-temperature superposition follows the same rule for LVE limit as for the complex modulus (linear characterisation).

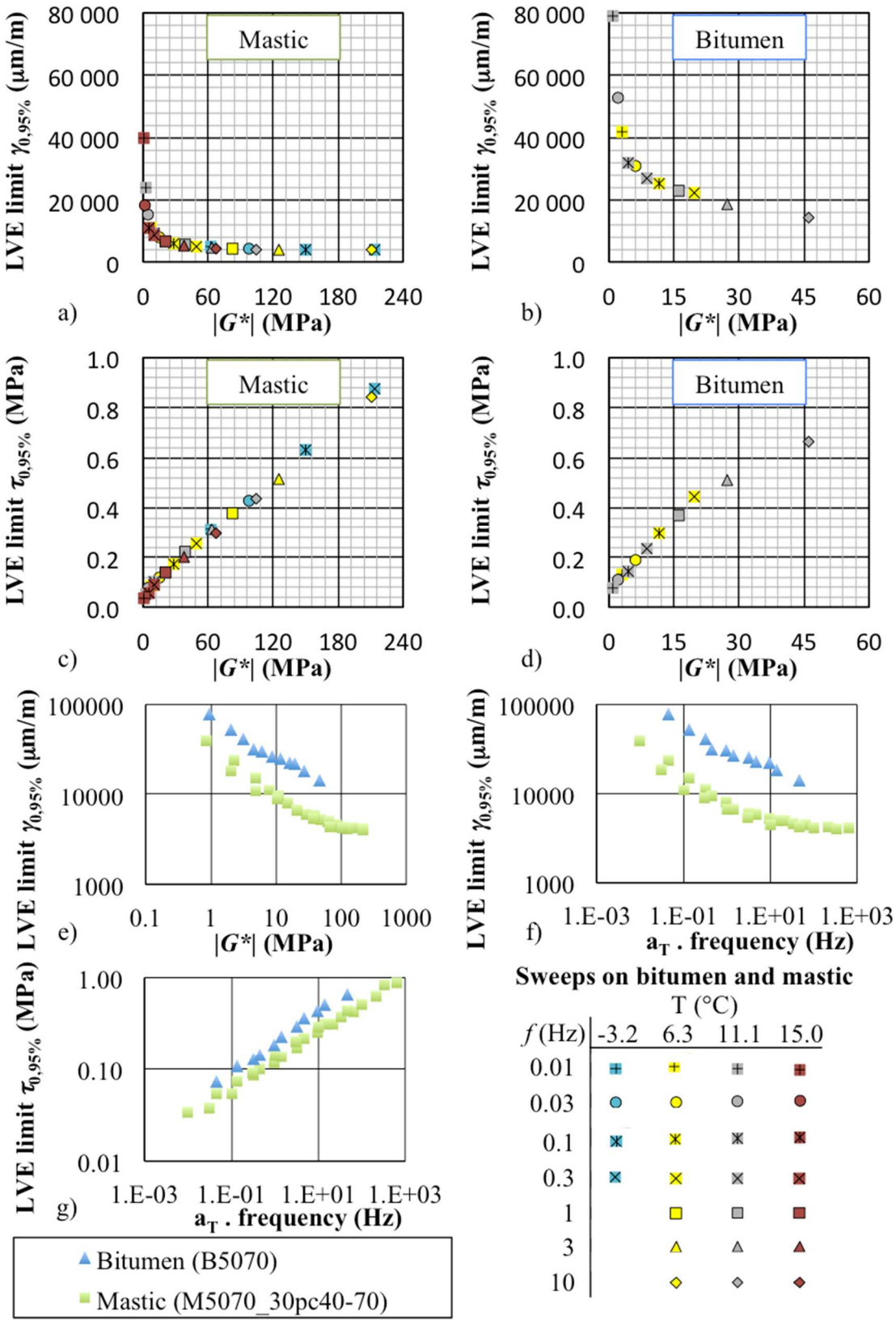

Figure 4-29. LVE limit (in terms of shear strain amplitude, $\gamma_{0.95\%}$, figs. a, b, e, and f, and shear stress amplitude, $\tau_{0.95\%}$, figs. c, d, and g) obtained from SAS test results (cf. example in Figure 4-25) on bitumen B5070 and mastic M5070_30pc40-70 as a function of norm of complex shear modulus (a through e) and time-shifted frequency at 15°C (f and g).

4.4. LVE limits of bituminous materials

This section presents a comparison between results of LVE limits from bitumen, mastic and bituminous mixture testing. A relationship between them is investigated, in order to try to determine if the nonlinearity phenomenon in bituminous mixtures and in mastic can be explained by the nonlinearity observed in bitumen. Figure 4-30 presents LVE limits obtained for bitumen, mastic and bituminous mixture (cf. Figure 4-15 and Figure 4-29 for individually presented results). Results are presented in terms of both strain amplitude (either in shear, $\gamma_{0.95\%}$, or in axial loading, $\varepsilon_{0.95\%}$,) and stress amplitude (either in shear, $\tau_{0.95\%}$, or in axial loading, $\sigma_{0.95\%}$,) necessary to produce a 5% relative change in modulus, as a function of the modulus (either in axial, |E*|, or in shear, |G*|). It is recalled that while the bituminous mixture was tested with axial loading, the bitumen and the mastic were tested in shear.

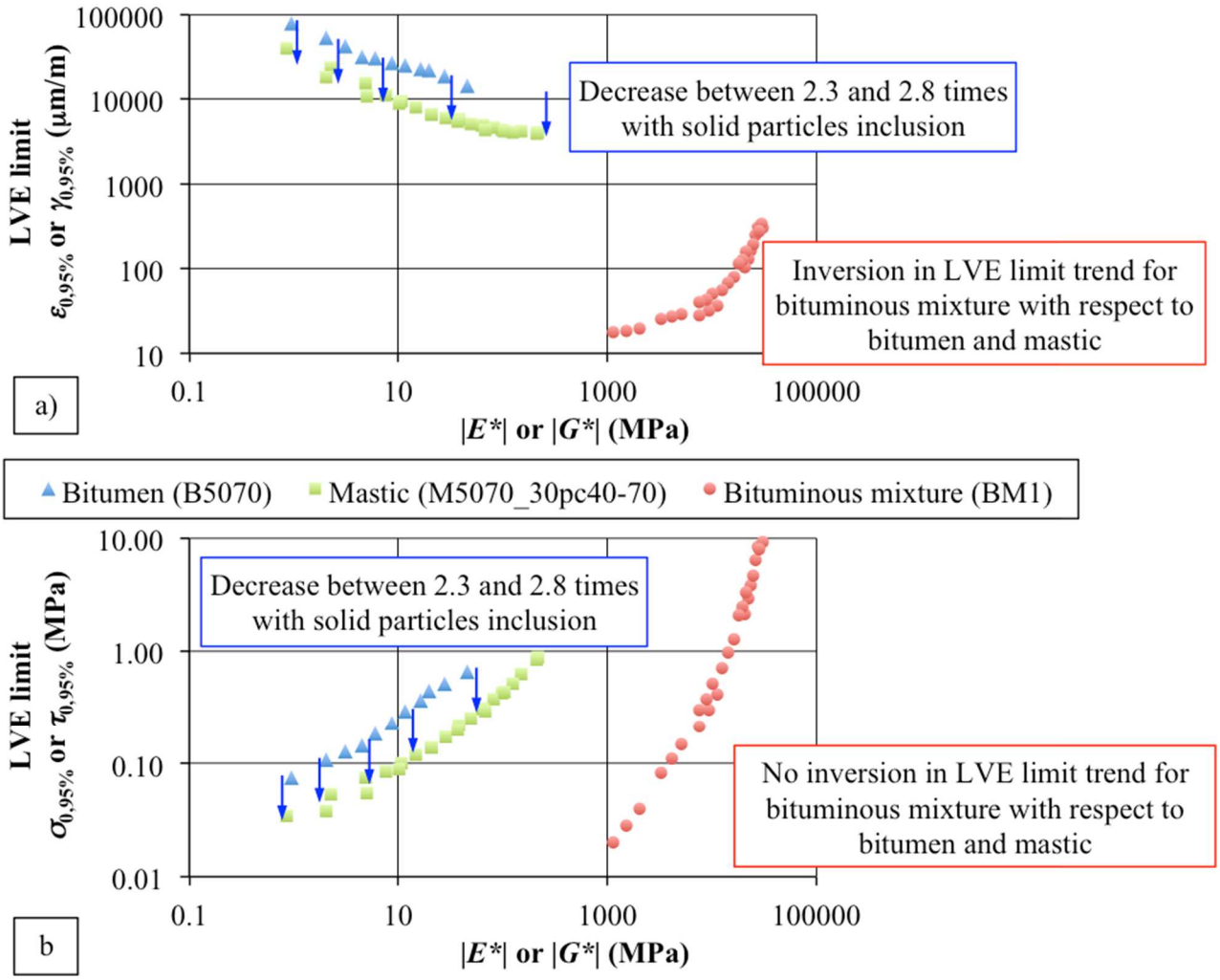

Figure 4-30. Comparison of the determined LVE limits (in terms of axial or shear strain amplitude, $\varepsilon_{0.95\%}$ or $\gamma_{0.95\%}$, figure a, and axial or shear stress amplitude, $\sigma_{0.95\%}$ or $\tau_{0.95\%}$, figure b) obtained from SASTENOLE and SAS test results (cf. Figure 4-15 and Figure 4-29) on bitumen B5070, mastic M5070_30pc40-70 and BM1_C as a function of norm of complex shear modulus.

From Figure 4-30, it is seen that bitumen and mastic behave similarly. LVE limit for mastic can be obtained from LVE limit for bitumen by reducing the stress or the strain amplitude limit by an approximately constant factor between 2.3 and 2.8. In the same figure, in terms of strain amplitude, the trend of bituminous mixture LVE limit as a function of modulus, with respect to the trend of bitumen and mastic LVE limit, is inversed. While bituminous mixture LVE limit is higher for higher modulus (at low temperature and high frequency), bitumen and mastic present narrower LVE domain in terms of strain amplitude for higher modulus (low temperature and high frequency). The same is not observed when analysing LVE limit in terms of stress amplitude (bottom of Figure 4-30). Either way, it is seen from the figure that time-temperature superposition applies for the LVE limit as it did for complex modulus. Then, master curves for the LVE limit can be obtained, both in terms of strain and of stress amplitude, using the same shift factors as for complex modulus (cf. Table 4-1 and Table 4-10). This will allow comparing behaviour for a given frequency, which can be helpful since no coincidence of modulus could be observed for bitumen, mastic and bituminous mixture. Results are presented in Figure 4-31, where LVE limit in terms of strain amplitude or stress amplitude are plotted against the equivalent frequency at 15°C.

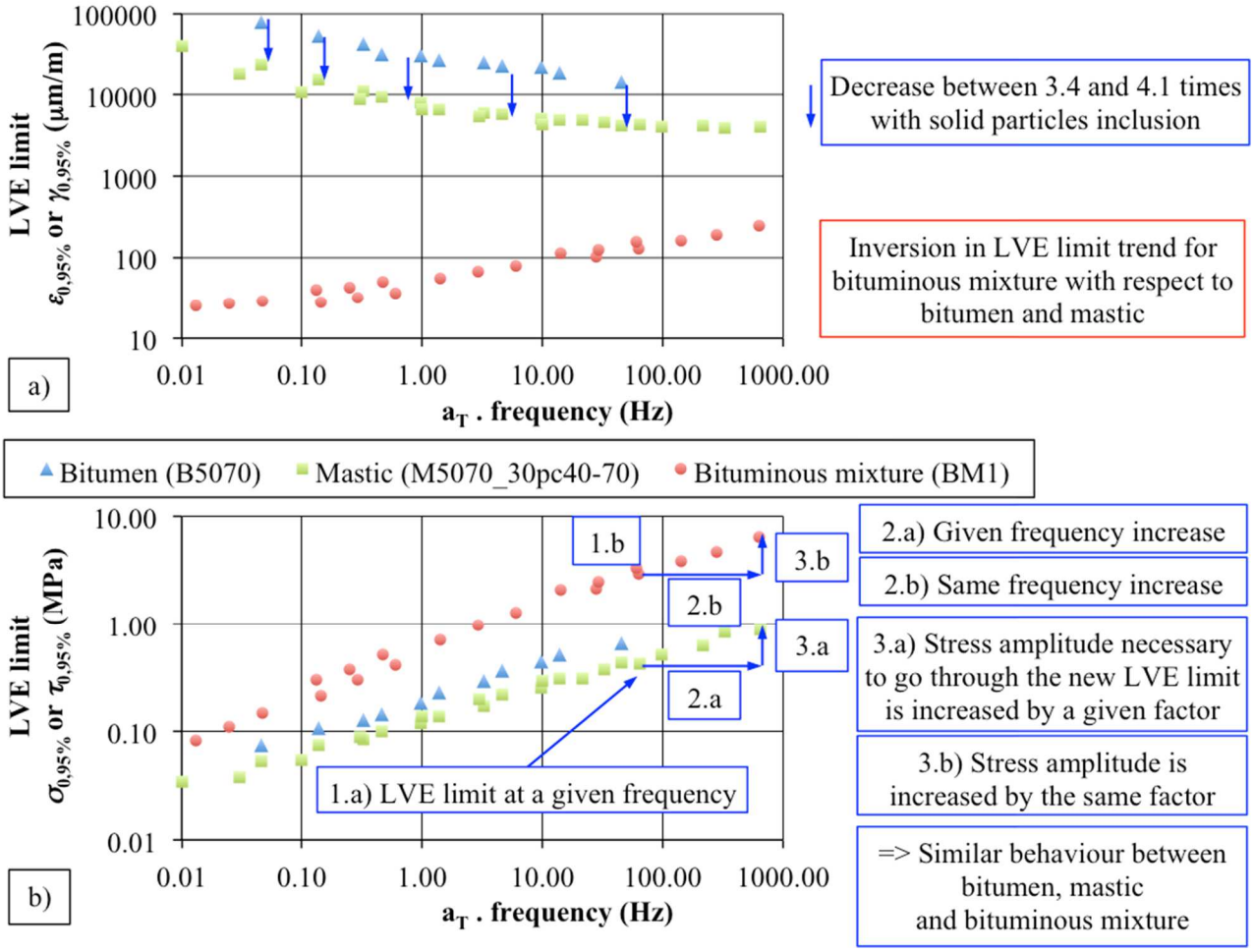

Figure 4-31. Comparison of the determined LVE limits (in terms of axial or shear strain amplitude, $\varepsilon_{0.95\%}$ or $\gamma_{0.95\%}$, figure a, and axial or shear stress amplitude, $\sigma_{0.95\%}$ or $\tau_{0.95\%}$, figure b) obtained from SASTENOLE and SAS test results (cf. Figure 4-15 and Figure 4-29) on bitumen B5070, mastic M5070_30pc40-70 and BM1_C as a function of the time-shifted frequency (with the same WLF parameters as for linear characterisation, cf. Table 4-1 and Table 4-10). The results are presented as master curves at 15°C.

From Figure 4-31, it is seen that approximately parallel curves are obtained for LVE limit in terms of stress amplitude. The inversion in trend is still observed for LVE limit in terms of strain amplitude. The observation can be explained in two steps: i) association in series of nonlinear viscoelastic bitumen and linear elastic aggregate; ii) heterogeneous distribution of strain in a real composite. The first step is to represent the bituminous mixture as an association in series of a volume (continuum) of bitumen with a volume (continuum) of aggregate. The continua present the same shape, but with different lengths, respecting the volume fraction of each material. The association is submitted to axial loading, which translate to stress and strain along the length of the continuum. Since it is an association in series, stress is the same in any cross-section of the association. Then, when stress amplitude equals the bitumen LVE limit, bituminous mixture LVE limit will be reached. In this case, all LVE limit in terms of stress amplitude as a function of frequency should be equal. Then, the second step needs to be considered: actually, strain and stress in the bituminous mixture distributes heterogeneously. A model to represent this is thoroughly

studied later, in Sections 5.3 and 5.5.3. It will be demonstrated that, with heterogeneous distribution of strain and stress, strain amplitude in the bitumen phase is, in most part of the volume, greater than the bulk strain amplitude applied in the bituminous mixture. From the referred model, when considering the studied mastic, strain in the most strained region and in the less strained region in the material would differ by a factor of 4.55, i.e. in thin bitumen films, strain is about 4.55 times higher than the bulk strain applied in the mastic. For the bituminous mixture, a more complex strain distribution results from the wide variety of particles dimension. Also, the modulus of the composite is a result of the modulus of the bituminous matrix and its strain distribution (cf. Sections 5.3 and 5.5.3). Combined, those effects produce a vertical shift in the curve presenting the LVE limit in terms of stress amplitude as a function of frequency. The curves in those axes would be equal in the case of a homogeneous stress/strain distribution. The inversion in trend in LVE limit in terms of strain amplitude that is observed in bituminous mixture when compared to bitumen or mastic may be due to the stiffness difference between the bituminous phase and the aggregate.

It should be underlined that since time-temperature shift factors are not the same for bituminous mixture as for the other materials, the physical frequency corresponding to an equivalent frequency at 15°C could differ between the materials (shifted in the horizontal axis). However, since the obtained master curves are approximately parallel, the explanations given before would still hold. Then, it seems that the bituminous mixture could inherit its nonlinear behaviour from the bitumen predominantly with respect to nonlinearity from the granular skeleton.

4.5. Conclusion on nonlinearity

This work describes the results of an investigation focusing on the characterisation of the nonlinearity of bitumen, mastic and bituminous mixtures. Nonlinearity is defined as the stress/strain dependence of the mechanical behaviour, resulting in a stress/strain dependent measured complex modulus. For bitumen and mastic, typical strain amplitude sweeps were used. It was demonstrated that these tests produce cyclic effects (modulus evolves with the repetition of loading cycles), which need to be corrected in order to evaluate nonlinearity on the measured complex modulus. A linear extrapolation from the test results was successfully used in order to obtain the complex modulus at the first cycle. For bituminous mixtures, a special test protocol (SASTENOLE) was developed, consisting of a series of continuously changing strain amplitude sweeps, performed at different temperatures and frequencies, with different maximum strain amplitudes and two types of loading paths (increasing and decreasing). It was demonstrated that transient effects influence early cycles results from SASTENOLE, but the other cycles can be used in the analysis of nonlinearity.

This investigation provides evidence for the strain dependence of complex modulus of bituminous mixtures, during both increasing and decreasing sweeps, even for strain amplitudes as low as 10μm/m. Obtained results for combinations of temperature and frequency giving the same complex modulus also gave equivalent nonlinearity results. This suggests that nonlinearity effects respect the time-temperature superposition principle with the same time-temperature superposition

law as for classical complex modulus characterisation. The same was observed for bitumen and mastic nonlinearity.

Bituminous mixture complex modulus variations due to nonlinearity are characterized using data obtained from increasing sweeps. Complex modulus is observed to vary in an approximately linear fashion for increasing strain amplitude. The observed relative decrease of the norm of complex modulus (p_E) varies from $-1.5 \cdot 10^{-4}$ to $-2.9 \cdot 10^{-3}$ 1/μm/m, while the rate of increase of phase angle (p_φ) ranges from 0.004 to 0.068°/μm/m, for results obtained from 0.1 to 10Hz at temperatures from -4 to 28°C. Different trends are observed during decreasing sweeps, suggesting the existence of a second phenomenon, possibly related to energy dissipation, causing a decrease of complex modulus and an increase of phase angle. This hypothesis could explain why results obtained during decreasing sweeps do not follow linear variation trends.

Bituminous mixture results of both increasing and decreasing sweeps are also analysed in Cole-Cole and Black spaces. On these diagrams, directions of nonlinearity are directly identified, related to the value of p_E/p_φ ratio. While it seemed from a first experimental campaign (with temperatures from 8 to 14°C and frequencies from 0.3 to 10Hz) that the direction of nonlinearity was independent of test conditions, the second campaign demonstrated that this is not true. The experimental results presented here may be used as basis for the modelling of nonlinearity. This is left as recommendation for future work.

When it comes to the characterisation of nonlinearity in bitumen and mastic, it was also demonstrated that the direction of nonlinearity is temperature- and frequency-dependent. Also, a clear relation between the LVE limits of the two materials was found. Mastic behaves similarly as bitumen with respect to the LVE limit, and its LVE limit can be obtained from the one for bitumen by applying a factor, independently of frequency and temperature.

When comparing the LVE limits of the three studied materials, interesting results were obtained. An explanation was given for the inversion of trends of LVE limit in terms of strain amplitude, based on simple geometrical models for the bituminous mixture and on the assumption that the aggregate is linear elastic and the bitumen is nonlinear viscoelastic. It seems that the bituminous mixture inherits predominantly nonlinearity from the bitumen, with secondary contribution of the granular skeleton.

Results and conclusions of this study can have an impact on characterisation of viscoelastic and fatigue response of bituminous materials. The work highlights strain amplitude dependence of stiffness results obtained from experiments, even for low strain levels in the case of bituminous mixtures. Strain amplitude used in the tests should be reported with complex modulus results. In the same way, the modulus decrease during fatigue tests should be interpreted considering variations in strain amplitude during the tests.

As future work, the study of more materials, containing the same base bitumen should be conducted. Enlarging the range of temperatures studied for nonlinearity of bitumen and mastic may produce interesting results. The investigation of higher temperatures (higher than 28°C) for bituminous mixture would produce nonlinearity results in the region where phase angle starts to decrease with increasing frequency.

Chapter 5: INITIAL MODULUS DECREASE AND SELF-HEATING DURING CYCLIC LOADING

Chapter 5: Initial Modulus Decrease and Self-heating During Cyclic Loading.....132
5.1. Introduction.....133
5.2. Tension-compression experiments description.....135
5.2.1. Complex modulus test (H. M. Nguyen, 2010).....135
5.2.2. Phase I Fatigue test (Q. T. Nguyen, 2011).....136
5.3. Considered heterogeneous cell and relationship with the grading curve.....137
5.4. Thermomechanical coupling and preliminary calculations.....139
5.5. Performed calculations without heat diffusion.....142
5.5.1. Homogeneous heat distribution in the bituminous mixture.....142
5.5.2. Homogeneous heat distribution only in the bitumen.....142
5.5.3. 3D heterogeneous calculation.....143
5.6. Results and analysis without heat diffusion.....147
5.6.1. Example: test on BM3_A at 12.3°C and 3Hz and 116μm/m.....147
5.6.2. Analysis of initial slopes of norm of complex modulus for all tests.....149
5.6.3. Time intervals when calculated slopes are observed in experiments.....154
5.7. 3D heterogeneous calculation with heat diffusion.....156
5.7.1. FEM Calculations.....157
5.7.1.1. FEM characteristics.....159
5.7.1.2. Thermal and Mechanical FEM calculations.....160
5.8. Results and analysis with heat diffusion.....161
5.9. Conclusion on bituminous mixture self-heating.....163

5.1. Introduction

This chapter presents an investigation to determine whether initial modulus decrease observed at the beginning of cyclic loading of bituminous mixtures can be explained by the phenomenon of self-heating. Self-heating is intended as the phenomenon of temperature increase, caused by the fact that mechanical dissipation of energy in the bituminous mixture (due to its viscoelastic properties) produces heat. The investigation described in this chapter is partially presented in one journal paper (Babadopulos et al., 2017a) and two international conference papers (Babadopulos et al., 2017b; Babadopulos, Sauzéat, & Di Benedetto, 2016).

Bituminous mixtures can be seen as granular media composed by particles (larger aggregates) and a bonding phase (a mix of smaller aggregates and bitumen, called bituminous mastic), which presents a viscoelastic behaviour inherited from bitumen. For linear viscoelastic characterisation of bituminous mixtures, usually few sinusoidal cycles are applied with low strain amplitudes in order to obtain complex modulus (both its norm and its phase angle). For fatigue tests, higher strain amplitudes and large number of cycles lead the specimen to failure and the complex modulus evolution can be analysed in order to characterise damage. A decrease in norm of complex modulus, an increase in phase angle and a temperature increase are observed during fatigue experiments (Di Benedetto, Nguyen, et al., 2011; Mangiafico et al., 2015). The stiffness decrease is commonly misinterpreted in the literature as being completely due to damage, which is supposed to be an irreversible process. Among others (such as physical nonlinearity, cf. Chapter 4), one of the possible phenomena behind the observed modulus decrease in bituminous mixtures is self-heating due to thermomechanical coupling (Bodin et al., 2004; De La Roche & Marsac, 1996; Di Benedetto, Nguyen, et al., 2011; Mangiafico et al., 2015; Mengis, 1997; Riahi et al., 2016, 2017). Mechanical loading may produce heat from viscous dissipated energy, inducing thermal changes and, consequently, changes in mechanical behaviour of the bituminous material, which is thermo-sensitive (creating a thermomechanical coupling). The investigation presented in this chapter aims at verifying if self-heating (which is a reversible phenomenon) may explain the modulus decrease observed at the beginning of fatigue tests on a bituminous mixtures. The analysis is proposed for different temperatures, applied strain amplitudes and loading frequencies in tension-compression tests. Since in other works (Di Benedetto, Nguyen, et al., 2011; Mangiafico et al., 2015) temperature measurements in bituminous mixture specimens could not explain stiffness changes at the beginning of cyclic tests, an explanation for the initial modulus decrease based on local thermal effects (local self-heating) is proposed in this chapter. These local effects, which occur at the scale of some tens of microns, could not have been measured using thermocouples (which present diameter of the order of the millimetre, i.e. from about twenty to one hundred times larger than the length scale of the hypothesized phenomenon).

First, using simplified analytical thermomechanical calculations, with no heat diffusion in the bituminous mixture, the possibility of explaining initial modulus changes with only the self-heating phenomenon is investigated. A non-uniform (local) heat production in the mastic is considered using a simplified geometry (monodisperse rigid spheres in a viscoelastic mastic phase). After, a numerical simulation including the effect of heat diffusion in the mastic phase is presented, in order to verify whether the heating necessary to explain the modulus decrease in the bituminous mixture can be achieved in a less particular case. The same non-uniform (local) heat

production in the mastic is considered for the case without diffusion. No heat exchange is considered between mastic and particles. This hypothesis is possible with sufficiently high thermal contact resistance (Somé, Gaudefroy, & Delaunay, 2014) between the large aggregates and the mastic phase, and is a reasonable assumption for short periods of time as studied in this investigation. The local effects of temperature on the observed stiffness change are analysed for the first 100 cycles of loading at 10Hz (10 seconds) for the case including heat diffusion.

Materials used in this chapter were BM2 (specimens A and B) and BM3 (specimens A and B), on which Phase I fatigue tests were performed (cf. Table 3-1, and Sections 3.3.3.3 and 3.3.3.4) in a previous work (Q. T. Nguyen, 2011) and analysed in a different way in this thesis. Tests presenting information on stiffness corresponding to the initial cycles of cyclic tests were selected for the investigation.

For the thermomechanical calculations, the values of the required thermophysical constants were adopted respecting results found in the literature (Highter & Wall, 1984; Hunter et al., 2015; Islam & Tarefder, 2014; Mrawira & Luca, 2006; Q. T. Nguyen, Di Benedetto, & Sauzéat, 2012; Read et al., 2003; Xu & Solaimanian, 2010). Values of the specific heat capacity for the voids, the bitumen and the aggregate particles present in the mastic are $(\rho c)_{air} = 1.2\times10^{3}$J/m^{3}°C, $(\rho c)_{b} = 1.7\times10^{6}$J/m^{3}°C and $(\rho c)_{agg} = 2.2\times10^{6}$J/m^{3}°C, respectively. This leads to a heat capacity of $(\rho c)_{m} = 2.02\times10^{6}$ J/m^{3}°C for the mastic, obtained by homogenisation (with a volume fraction of bitumen in the mastic of 36%). For the whole bituminous mixture, a value of $(\rho c)_{bm} = 2.11\times10^{6}$ J/m^{3}°C was obtained. Considered thermal conductivity within the mastic is 1.0W/m/K, the mastic phase density is 2300kg/m³, with specific heat capacity of 887J/kg/K (giving $\rho c = 2.02\times10^{6}$J/m³K). Those parameters were adopted for both studied mixtures.

It is emphasised that analysing temperature changes in a bituminous mixture specimen involves solving a complex coupled thermomechanical problem. In this investigation, four calculations of modulus decrease due to local self-heating at the beginning of fatigue tests are proposed, each one with different simplification hypotheses, detailed as follows. Figure 5-1 presents schematically these calculations.

i. Homogeneous self-heating of bituminous mixture without heat diffusion (Section 5.5.1);
ii. Homogeneous self-heating of bitumen without heat diffusion (Section 5.5.2);
iii. Heterogeneous self-heating of the mastic in the bituminous mixture without heat diffusion (Sections 5.5.3 and 5.6);
iv. Heterogeneous self-heating of the mastic in the bituminous mixture without heat diffusion (Sections 5.7 and 5.8).

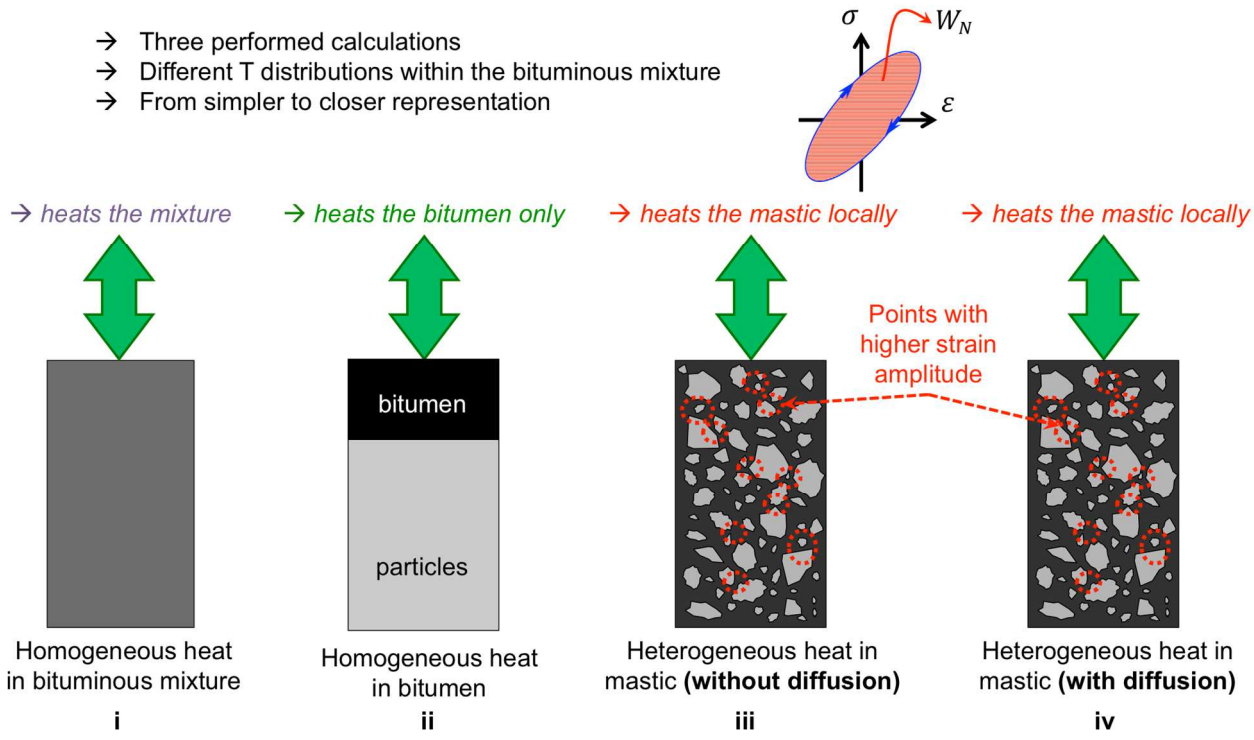

Figure 5-1. Scheme for the proposed thermomechanical calculations.

5.2. Tension-compression experiments description

This section briefly described the tests analysed for the investigation of initial stiffness decrease in this thesis. Tension-compression tests (T-C) were used (cf. Sections 3.1.2 and 3.2.2 for test set-up). Experiments had been previously performed (H. M. Nguyen, 2010; Q. T. Nguyen, 2011), and are analysed in a different way in this thesis. Two kinds of test were analysed: Complex Modulus tests, and Phase I Fatigue tests (called "Pseudo-Fatigue tests", PFT, in (Q. T. Nguyen, 2011). For more details on tests, the reader may refer to the cited works.

5.2.1. Complex modulus test (H. M. Nguyen, 2010)

Complex modulus was obtained for BM3 from strain controlled sinusoidal tests, targeting 50μm/m of strain amplitude (cf. Figure 4-1). Material was tested at the temperatures of -18.6, -8.4, -0.1, 10.1, 20.3, 30.8, and 41.3°C. Tested frequencies were 0.03, 0.1, 0.3, 1, 3, 10Hz. Details can be found in a previous work (H. M. Nguyen, 2010). The experimental results were used to calibrate a 2S2P1D model (Eq. 2-28) (Olard & Di Benedetto, 2003) and Williams-Landel-Ferry (WLF, (Williams et al., 1955) equation (Eq. 2-1) parameters for BM3, using least squares regression (Q. T. Nguyen, 2011). Considering similarities between BM2 and BM3 (same base binder, similar grading curve) and information on complex modulus obtained during the analysed Phase I Fatigue tests, a 2S2P1D model for BM2 was also obtained in this work. 2S2P1D model and WLF equation parameters for both bituminous mixtures are presented in Table 5-1.

Table 5-1. 2S2P1D model and WLF equation parameters used to model the LVE behaviour of the studied bituminous mixtures

	2S2P1D (T_{ref} = 25°C)							WLF		
Bituminous Mixture	**E_{00} (MPa)**	**E_0 (MPa)**	**k (-)**	**h (-)**	**δ (-)**	**τ_0 (s)**	**β (-)**	**T_{ref} (°C)**	**C_1 (-)**	**C_2 (°C)**
BM2	17.5	42,000	0.200	0.600	2.00	$2.00 \cdot 10^{-3}$	100	25.0	23.0	193.0
BM3	15	36,000	0.200	0.600	2.00	$6.50 \cdot 10^{-4}$	100	25.0	23.0	193.0

5.2.2. Phase I Fatigue test (Q. T. Nguyen, 2011)

In order to investigate the initial stiffness decrease occurring in cyclic tests on bituminous mixtures, experimental results from a previous experimental effort (Q. T. Nguyen, 2011) were investigated in this work. The experimental results are obtained from Phase I Fatigue tests (called "Pseudo-Fatigue tests", PFT, in (Q. T. Nguyen, 2011). Phase I Fatigue tests consist in applying cyclic loading, exactly as done for fatigue tests, but stopping loading after some thousands of cycles in order to allow the material to recover its initial modulus before starting loading again. Figure 5-2 presents an example of Phase I Fatigue test loading path, applied to BM2_A, and information of temperature for tests on the other specimens.

Tests presenting experimental information (stiffness measurements) on initial cycles of cyclic tests were selected and analysed in this work. Results for two specimens for each of the studied bituminous mixtures (BM2 and BM3) were investigated (cf. Table 3-1). For BM2, analysed temperatures were 11.3°C, 12.4°C and 21.4°C, with frequency of 10Hz, while for BM3, temperatures were 7.4°C, 11.6°C and 12.3°C, with frequencies of 1Hz, 3Hz and 10Hz. For BM2, 10 tests were analysed, with initial strain amplitudes ranging from around 50 to 131μm/m. For BM3, 13 tests were analysed, with initial strain amplitudes ranging from around 56 to 127μm/m.

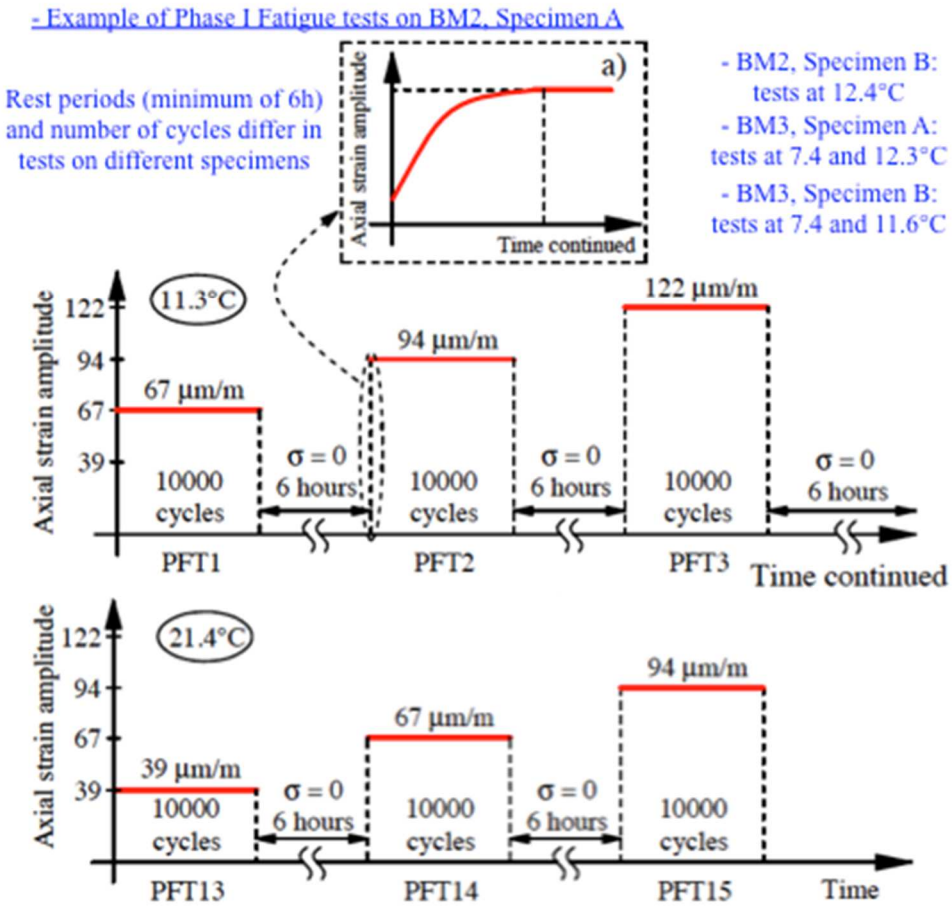

Figure 5-2. Loading scheme (Q. T. Nguyen, 2011) of a Phase I Fatigue test (example of tests on BM2_A).

5.3. Considered heterogeneous cell and relationship with the grading curve

Figure 5-3 presents a scheme of the geometry of the idealized heterogeneous bituminous mixture. This geometry is used for calculation of heterogeneous stress and strain distributions within the material and to obtain temperature increase, both in the case without heat diffusion (Sections 5.5.3 and 5.6) and with heat diffusion (Sections 5.7 and 5.8). The structure in Figure 5-3a gives the representative volume element presented in Figure 5-3b. It is called the Elementary Heterogeneous Volume (EHeV) and it contains $1/8^{th}$ of one spherical rigid particle. There is no contact between particles.

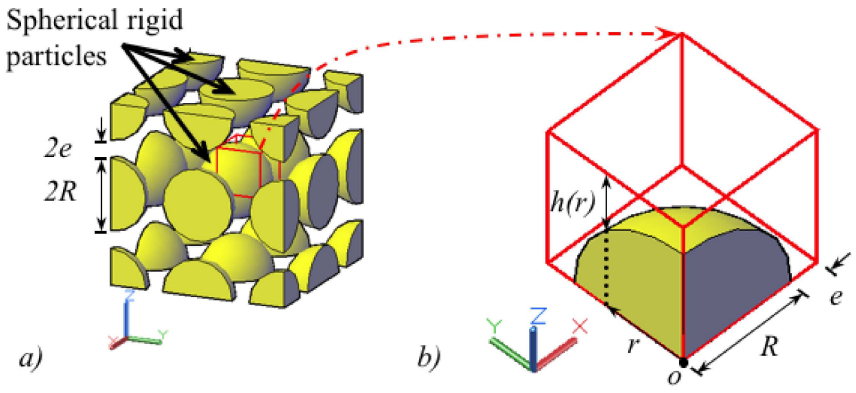

Figure 5-3. a) Considered idealized heterogeneous bituminous mixture (monodisperse spherical particles in a mastic phase) and b) Zoom on the elementary cell called "Elementary Heterogeneous Volume" (EHeV) used for 3D heterogeneous calculation.

The minimal distance between two particles (which is equivalent to the minimum mastic thickness, 2*e*) is considered negligible in comparison to the particle diameter (2*R*). As a consequence, the volume of mastic is equal to 47.6% of the total volume of mixture.

The grading curves for both studied mixtures are very similar and are presented in Figure 5-4, as well as the volume of voids, bitumen and particles passing through a particular sieve (in percentage of the total volume of specimen). In Sections from 5.5.3 to 5.8, the bituminous mixture is represented by monodisperse mineral particles bonded by a mastic phase (Figure 5-3). Considering the volume fraction of mastic imposed by the heterogeneous cell (cf. Figure 5-3), in Figure 5-4, it is possible to determine the maximum diameter of the particles within the mastic (which includes air voids) as 2.4mm.

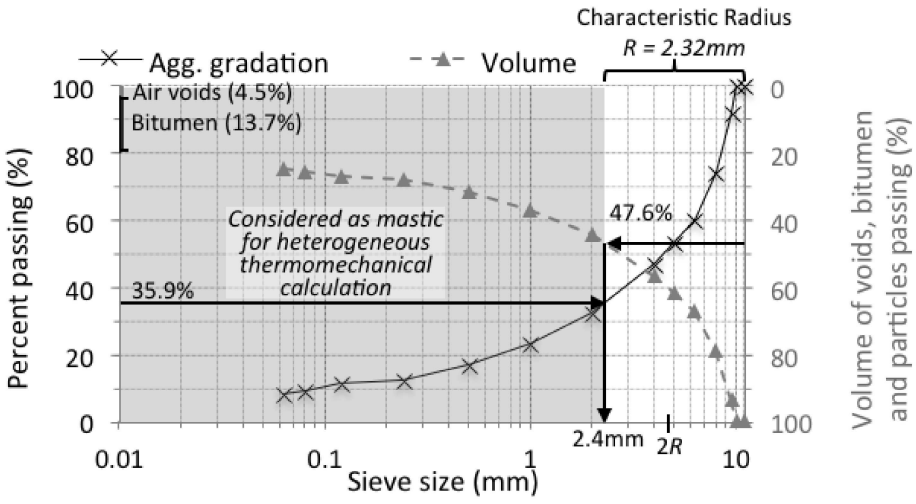

Figure 5-4. Aggregate gradation of the two studied materials: in mass (left axis, classical representation without bitumen) and in volume (right axis, considering air voids and bitumen)

All the particles having less than 2.4mm of diameter represent 35.9% in mass of aggregates (Figure 5-4). The remaining particles are modelled by a set of monodisperse spherical particles organized in a cubic array as discussed later (cf. Figure 5-3a). Their diameter giving the same mass and volume proportions in the mixture, called characteristic diameter, is 4.64mm (characteristic radius of 2.32mm).

5.4. Thermomechanical coupling and preliminary calculations

This section presents the thermomechanical coupling whose effect is investigated in this chapter as a possible explanation for the initial stiffness change observed during cyclic tests. The simplified thermomechanical calculations (without heat diffusion) presented here consists basically of two steps: i) the calculation of the temperature increase per cycle; and ii) the calculation of the consequent complex modulus change per cycle. Figure 5-5 presents a scheme for the calculation.

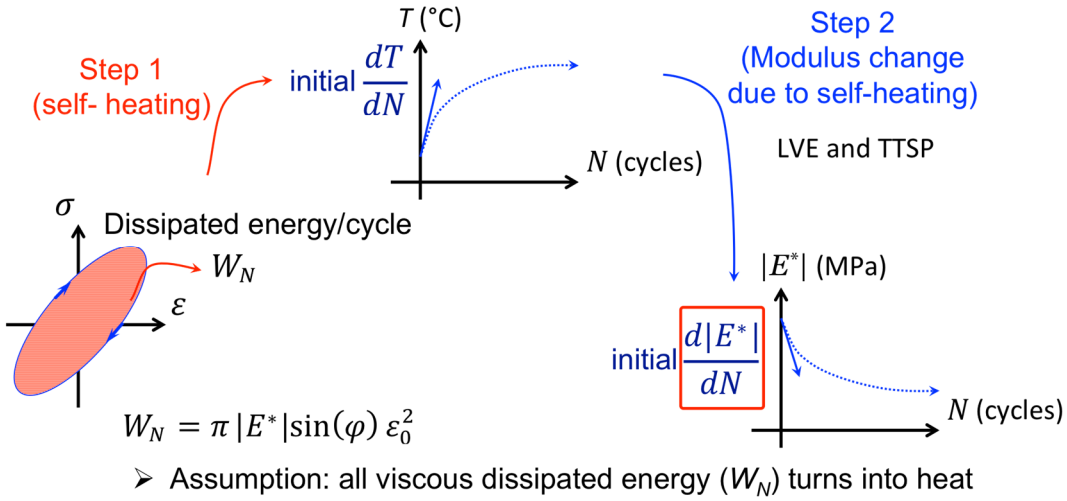

Figure 5-5. Scheme of the steps necessary to the simplified thermomechanical calculations.

For the first step, a thermophysical constant, known as the specific heat capacity ρc is necessary, whose value has been discussed in Section 5.1. For the second step, the complex modulus dependency with respect to temperature is a necessary input. It can be obtained from a Linear ViscoElastic (LVE) model representing material behaviour. For this investigation, this dependency was obtained from the combination of 2S2P1D model (Equation XX-X) (Olard & Di Benedetto, 2003) and Williams-Landel-Ferry (WLF, (Williams et al., 1955) equation (Equation XX-X) fitted to complex modulus test data. Considering that the time-temperature superposition principle (TTSP) holds for the studied material (Q. T. Nguyen et al., 2013), WLF equation can be used to simulate a_T(T) as a function of temperature T and of the material constants C_1 and C_2 (Williams et al., 1955). 2S2P1D and WLF parameters obtained for both studied bituminous mixtures were presented in Table 5-1.

The bituminous mixture, as a viscoelastic material, dissipates energy during its hysteresis in each loading cycle. Most (or all) energy turns into heat and produces an increase in temperature in the material, which changes property due to its thermo-sensitivity (Pouget et al., 2012b). Expansion and contraction thermal effects (Lamothe, Perraton, & Di Benedetto, 2015) are considered negligible for this investigation. Calculations performed in this first part of the investigation of thermal effects consider local adiabatic hypothesis, which implies that the heat flux is nil (no diffusion) all over the bituminous mixture. From this hypothesis, which is strictly valid only at the very beginning of tests (for small time intervals), a linear relationship between the variation of temperature and the injected heat can be considered. That kind of linear relation, which traduces the first principle of thermodynamics, was experimentally observed by (Q. T. Nguyen, 2011) and (Q. T. Nguyen et al., 2012) up to 10,000 cycles at 10Hz (1000s of testing). Eq. 5-1 represents the mentioned relation.

$$\frac{dT}{dN} = \frac{W_N}{\rho c} \qquad \text{Eq. 5-1}$$

In Eq. 5-1, dT/dN represents the temperature variation in the self-heating material during one loading cycle. The self-heating material is at the same time the heat source (originated from the dissipation of mechanical energy) and the heated material. It produces an amount of heat per unit volume during one cycle $W_N = \pi|E^*|\sin(\varphi).\varepsilon_0^2$, where strain amplitude is ε_0 ($\varepsilon(t) = \varepsilon_0\sin(2\pi ft)$, with f the loading frequency). W_N is dissipated in the volume $V_{\text{self-heating}}$ that presents heat capacity ρc. Three cases are considered for calculations in this first part of the investigation: i) the bituminous mixture as a homogeneous continuum medium ($V_{\text{self-heating}}$ is the whole mixture) (Section 5.5.1), ii) the bitumen as a homogeneous continuum medium being homogeneously self-heated ($V_{\text{self-heating}}$ is the bitumen only) (Section 5.5.2), and iii) the bituminous mixture as a heterogeneous medium composed by rigid coarse aggregate particles and homogeneous mastic, which has non-homogeneous strain field and self-heating ($V_{\text{self-heating}}$ is any small volume element in the mastic) (cf. Sections 5.5.3 and 5.6). The first case considers homogeneous heat distributions in the bituminous mixture. It is clear that it underestimates the potential for stiffness change in bituminous mixtures. The second one considers heterogeneous heat distribution in the bituminous mixture (heat is concentrated only in the bitumen) and results in a higher initial change in stiffness. However, it does not account yet for the existent non-homogeneous heat distribution within the mastic. The last proposed thermomechanical calculation accounts for heterogeneous strain and heat distributions within the mastic.

Another general assumption made in this investigation is that all dissipated energy turns into heat. It means that damage or other dissipative effects are considered as negligible. This hypothesis seems to be quite realistic for bituminous materials at the beginning of fatigue test.

It is noticed from Eq. 2-1 and Eq. 2-29 that the parameter "characteristic time", represented by τ, is the only one depending on temperature. The analytical derivative of complex modulus with respect to temperature can be obtained for a given material, as schematically represented in Figure 5-6. Then, the normalized (with respect to linear viscoelastic initial modulus) derivative M can be defined, as seen in Figure 5-6. Table 5-2 and Table 5-3 presents the M values obtained for the tested bituminous mixture at the different test conditions studied in this investigation.

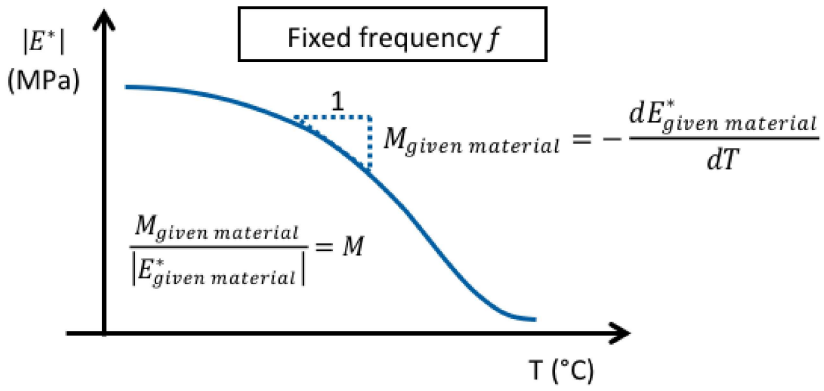

Figure 5-6. Schematic definition of the normalized parameter (M) giving the influence of temperature on $|E^*|$ for a given loading frequency.

Table 5-2. M parameter values obtained from 2S2P1D model and WLF equation (constants given in Table 5-1) for BM2

T (°C)	**11.3**	**12.4**	**21.4**
***f* (Hz)**	10	10	10
M (%/°C)	5.39	5.71	8.95

Table 5-3. M parameter values obtained from 2S2P1D model and WLF equation (constants given in Table 5-1) for BM3

T (°C)	**7.4**			**11.6**	**12.3**		
***f* (Hz)**	1	3	10	10	1	3	10
M (%/°C)	8.76	6.98	5.47	6.88	11.23	9.15	7.15

From the temperature variation dT/dN of the self-heating material, the change in complex modulus (dE^*/dN (which contains information about changes both in modulus and in phase angle) can be evaluated. Material linear viscoelastic model associated to shift factors (considering the time-temperature superposition principle) gives the relationship between them. For a small temperature change, it can be considered as linear, as seen in Eq. 5-2.

$$\frac{1}{|E^*|}\frac{d|E^*|}{dN} = -M\frac{dT}{dN} \qquad \text{Eq. 5-2}$$

5.5. Performed calculations without heat diffusion

5.5.1. Homogeneous heat distribution in the bituminous mixture

For this case, the material producing heat is the whole mix as well as the material that is self-heating. The bituminous mixture is being considered as homogeneous, both for the mechanical and for the thermophysical properties, and the heat distribution is also homogeneous. In this case, Eq. 5-3 represents the obtained slope.

$$\frac{1}{|E^*|_{bm}}\frac{d|E^*|_{bm}}{dN} = -M\frac{(W_N)_{bm}}{(\rho c)_{bm}} = -M\frac{\pi|E^*|_{bm}\sin(\varphi_{bm})\,\varepsilon_{0,bm}^2}{(\rho c)_{bm}} \qquad \text{Eq. 5-3}$$

In Eq. 5-3, the left-hand side represents the relative change in the norm of complex modulus of the bituminous mixture (represented by the subscript "bm"), while the right-hand side presents its calculation for the assumed hypotheses. Finally, $\varepsilon_{0,bm}$ represents the strain amplitude ($\varepsilon_{bm}(t) = \varepsilon_{0,bm}\sin(2\pi ft)$, where f is the loading frequency) applied to the bituminous mixture.

5.5.2. Homogeneous heat distribution only in the bitumen

For this case, the effect of heat acts only in the bitumen (aggregates and fines are not affected). The bituminous mixture is being considered as homogeneous with respect to the mechanical properties, but the thermophysical properties are considered to be heterogeneous this time. Heat is homogeneously distributed in the bitumen. The heat injection can be evaluated from the properties of the whole bituminous mixture, and then concentrated in the self-heating material, which is the bitumen only. Mineral particles are considered as elastic and do not change stiffness with temperature. So, the calculated temperature increase in the bitumen produces the same change in the bituminous mixture complex modulus as if the same temperature increase was applied to the whole material. Those considerations allow using Eq. 5-2 to describe the process, considering E^* and M of the bituminous mixture and the value of dT/dN calculated for the bitumen. For the chosen set of simplification hypotheses, Eq. 5-4 represents the slope obtained. In Eq. 5-4, the subscript "b" represents the bitumen, and the ratio V_b/V_{bm} is the volume fraction of binder in the bituminous mixture.

$$\frac{1}{|E^*|_{bm}}\frac{d|E^*|_{bm}}{dN} = -M\frac{(W_N)_{bm}.V_{bm}}{(\rho c)_b.V_b} = -M\frac{\pi|E^*|_{bm}\sin(\varphi_{bm})\,\varepsilon_{0,bm}^2}{(\rho c)_b}\frac{1}{V_b/V_{bm}} \qquad \text{Eq. 5-4}$$

5.5.3. 3D heterogeneous calculation

A unit cell (cf. Figure 5-3) cross-section is represented schematically in Figure 5-7, which presents the principle of the proposed analysis for the Elementary Heterogeneous Volume (EHeV) element and the corresponding Elementary Homogeneous Volume (EHoV) element.

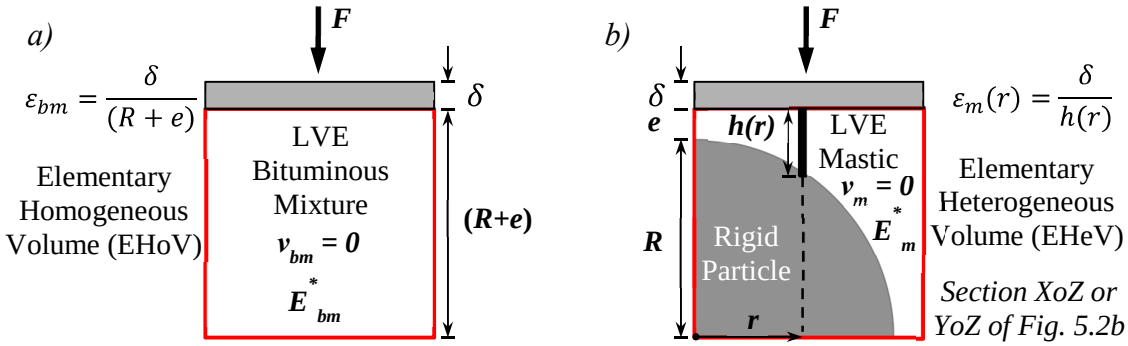

Figure 5-7. Explanation of strain calculation from displacement δ (applied load F in tension-compression): a) Case of the Elementary Homogeneous Volume (EHoV) and b) Case of the Elementary Heterogeneous Volume (EHeV)

For the studied materials (presented in Section 5.3), the EHeV has 2 types of materials: i) rigid spherical particles, having a characteristic radius R = 2.32mm, which represents the coarse aggregates (diameter larger than 2.4mm as obtained in Figure 5-4) and ii) mastic, modelled by a deformable continuum material, including bitumen, void and particles whose diameter is smaller than 2.4mm. With a geometry of the bigger particles fixed, the only geometrical parameter that influences model prediction is e (minimum half-thickness of mastic). The hypothesis of rigid spherical particles is reasonable when comparing the modulus of coarse aggregates (about 70GPa) and the glassy modulus of mastic (of the order of 10GPa, as shown by (Delaporte et al., 2007) and (Delaporte et al., 2009).

To simplify calculations and allow for an analytical calculation of the coupled thermomechanical problem, the Poisson's ratio of the mastic is supposed nil, which gives also a nil Poisson's ratio for the mixture ($\nu_m = 0$, and $\nu_{bm} = 0$). Then, all calculations can be done considering a one-dimensional problem with $\varepsilon = \varepsilon_{zz}$ and $\sigma = \sigma_{zz}$.

As seen in Figure 5-7, the force F and the displacement δ applied on the EHeV and on the EHoV are equal, in order to obtain an equivalent representation of the material. This leads to a homogeneous strain ε_{bm} in the EHoV, and to a non-homogeneous strain $\varepsilon_m(r)$ in the mastic, which depends on the position within the mastic (r). Eq. 5-5 gives the strain in the mastic as a function of the position r in the unit cell.

$$\varepsilon_m(r) = \frac{\varepsilon_{bm}.(R+e)}{h(r)} \quad ; \qquad h(r) = (R+e) - \sqrt{(R^2 - r^2)} \qquad \text{Eq. 5-5}$$

When it comes to the applied force F on the surface S_e of the unit cell (cf. Figure 5-3 and Figure 5-7), equivalence between EHoV and EHeV gives Eq. 5-6. In this equation, the superscript "*" indicates that a sinusoidal loading is applied and that quantities are complex numbers, presenting amplitude and phase angle. dS_e represents an infinitesimal element of S_e.

$$F^* = E^*_{bm}.\varepsilon^*_{bm}.S_e = \int_{S_e} E^*_m.\varepsilon^*_m.dS_e \qquad \text{Eq. 5-6}$$

In Eq. 5-6, S_e represents the upper surface area of the element where loading (F) is applied (cf. Figure 5-3 and Figure 5-7), which is equal to $(R+e)^2$. From the same equation, it is seen that, at the beginning of the loading, when mastic modulus (E_m^*) is approximately spatially constant, bituminous mixtures modulus (E_{bm}^*) and E_m^* are co-linear (ratio between them is a constant that depends on the unit cell geometry), i.e. they present the same phase angle. That is a consequence of the absence of contact between particles. If no heat transfer happens in the unit cell (local adiabatic hypothesis, cf. Eq. 5-1), Eq. 5-7 holds for the calculation of the temperature increase per cycle (dT/dN) as a function of the position r in the unit cell.

$$\frac{dT}{dN}(r) = \frac{W_N(r)}{(\rho c)_m} = \frac{\pi |E^*_m| \sin\varphi_{E^*_m} |\varepsilon^*_m(r)|^2}{(\rho c)_m} \qquad \text{Eq. 5-7}$$

From the equality of force F^* for EHoV and EHeV (Eq. 5-6), E_{bm}^* can be linked to E_m^* and, consequently, their two initial slopes with respect to the number of cycles are also linked. The slope for E_m^* for the mastic at any position is deduced from Eq. 5-2, considering the temperature increase distribution obtained in Eq. 5-7. The coefficient M_m (temperature derivative of mastic modulus, cf. Figure 5-6) is deduced as follows.

As presented in Eq. 5-6, for the chosen model (no contact between particles), co-linearity is imposed between E_{bm}^* and E_m^* (i.e. they present the same phase angle). So, if the time-temperature superposition principle holds, Eq. 5-8 can be obtained, which shows that an equivalent value of M (normalized temperature derivative of norm of complex modulus) works both for the mastic and for the mixture. It should be noticed that M_{bm} and M_m would need to be treated separately for cases where contacts between particles become important for the behaviour of the material (which may happen depending on the tested temperature and frequency).

$$\frac{M_{bm}}{|E^*_{bm}|} = \frac{M_m}{|E^*_m|} = M \qquad \text{Eq. 5-8}$$

As an example, the strain amplitude and the temperature distributions for R = 2.32mm and e = 35.1μm are presented in Figure 5-8. At each position inside the EHeV, a mastic element of height $h(r)$ is subjected to a strain amplitude $\varepsilon_m(r)$. This element is heated and a temperature increase per cycle $dT/dN(r)$, which depends only on r, is obtained. A great heterogeneity is observed in strain amplitude (ratio between maximum and minimum values equals to $R/e+1 \approx 67$ in this example). The consequent heterogeneity in dT/dN (r) is greater, as it depends on the square of the strain

amplitude. In the chosen example, the ratio between maximum and minimum temperature increase per cycle is equal to $(R/e+1)^2 \approx 4{,}500$.

With the resulting temperature increase distribution, a calculation of the consequent change in stiffness can be performed. Eq. 5-9 presents the final result. Parameters for the mastic can be obtained from Eq. 5-6 (modulus and phase angle) and from the introduction of this chapter ($(\rho c)_m$). In Eq. 5-9, dS_e represents an infinitesimal element of the upper surface area of the element where loading (F) is applied (cf. Figure 5-3 and Figure 5-7). It is recalled that S_e is equal to $(R+e)^2$.

$$\frac{1}{|E^*|_{bm}}\frac{d|E^*|_{bm}}{dN} = -M.\pi|E_m^*|\sin\varphi_m \frac{1}{(\rho c)_m}\frac{\int_{S_e}|\varepsilon_m^*|^3 dS_e}{\int_{S_e}|\varepsilon_m^*|dS_e} \qquad \text{Eq. 5-9}$$

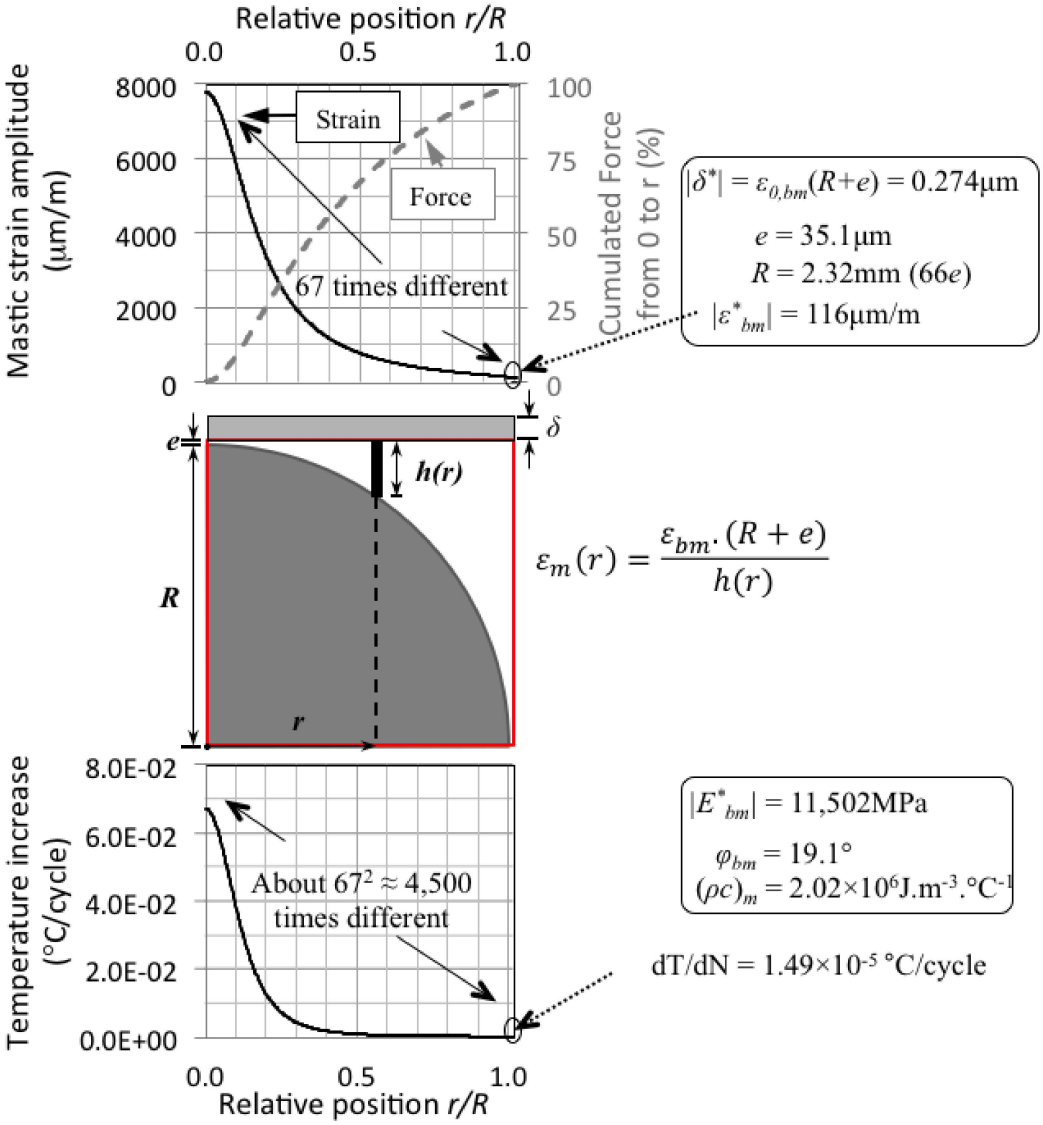

Figure 5-8. 3D heterogeneous calculation results with e/R = 0.015 (fixed parameters corresponding to the studied bituminous mixture, tested at 12.3°C and 3Hz for a strain amplitude of 116µm/m, cf. also test results in Figure 5-10 and Figure 5-11): (above) strain amplitude and cumulated force on a disc of radius r and (below) temperature increase per cycle for local adiabatic conditions (i.e. no heat transfer) as a function of relative position (r/R)

Calculated modulus and relative modulus decreases per cycle as a function of the ratio e/R is presented in Figure 5-9, considering one of the test conditions evaluated in this work (the same as for Figure 5-8, i.e. BM3 tested at 12.3°C and 3Hz). In the same figure, the results for e = 0.015R are highlighted (which corresponds to the value determined for BM3 in Section 5.6, cf. Figure 5-10 and Table 5-4 and Table 5-5). As it can be seen, the modulus decrease is very sensitive to the adopted mastic half-thickness (e). Then, for a given initial modulus decrease per cycle, one is likely to find a value of e that can represent the initial modulus decrease just due to thermomechanical coupling. In the present investigation, however, different test conditions are analysed, and only one value of e is searched for a given bituminous mixture, and it should be used to explain modulus changes for all tested conditions.

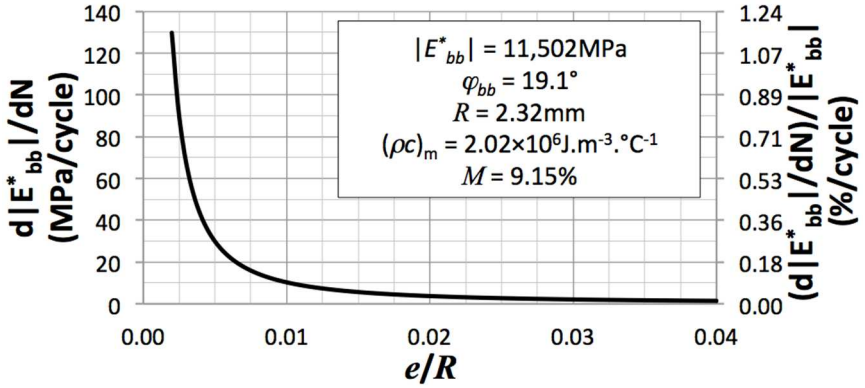

Figure 5-9. Modulus (left axis) and relative modulus (right axis) decrease per cycle as a function of *e*/*R* (fixed parameters correspond to BM3 and tested at 12.3°C and 3Hz for a strain amplitude of around 116µm/m, see also test results Figure 5-10)

From the results presented in Figure 5-9, it is observed that a huge range of modulus decrease per cycle can be obtained when varying *e*/*R*. For *e*/*R* from 0.0025 to 0.04 (corresponding to *e* from 6 to 93µm for *R* = 2.32mm), stiffness decreases from around 0.01% to 0.9% are predicted.

This chapter focuses on the evolution of norm of complex modulus, both from experimental and modelling perspectives. However, it is also possible to obtain the change in phase angle of the bituminous mixture according to the model. The model assumes that each mastic element integrated in the simplified 3D thermomechanical calculation changes its modulus along the LVE Black curve (or Cole-Cole curve), since it consists of a change in temperature. All points in the mastic are initially at the same temperature, and although a different rate of change in temperature is predicted for each point in the mastic, the direction of the change in complex modulus needs to follow the Black (and Cole-Cole) diagram. Then, this implies that the calculated change in complex modulus of the mixture will also follow the LVE Black (and Cole-Cole) curve. Thus, the analysis proposed in this work gives also the evolution of the phase angle when the norm of complex modulus variation is known. A complete analysis of phase angle changes due to self-heating is not presented in this thesis.

5.6. Results and analysis without heat diffusion

5.6.1. Example: test on BM3_A at 12.3°C and 3Hz and 116µm/m

Classical tension-compression strain controlled Phase I Fatigue tests (performed by (Q. T. Nguyen, 2011), also called Pseudo-Fatigue tests, PFT) at temperatures of 11.3, 12.4 and 21.4°C at a frequency of 10Hz for BM2 and of 7.4, 11.6 and 12.3°C at frequencies of 1, 3 and 10Hz for BM3 were used for comparison with modelled results. For BM2, a total of 10 tests was analysed, 5 with sample A, and 6 with sample B (cf. Table 5-4). For BM3, a total of 13 tests was analysed, 9 with sample A and 4 with sample B (cf. Table 5-5). Rest periods (at constant temperature and nil stress on the sample) between each test on the same specimen were of at least 6h for BM2 and 8h

for BM3. For tests on BM2 specimens, applied strain amplitudes varied from 50 to 131μm/m for the analysed loading cycles at the different temperatures and frequencies, while for BM3 they varied from 56 to 127μm/m. When calculating experimental modulus slopes with number of cycles obtained for the thermomechanical analysis, a fixed interval of time from 5 to 7s was chosen for all tested frequencies. The time interval was arbitrarily chosen, taking into consideration the constraints listed below:

- Transient effects, which require to eliminate the first 2 to 3 cycles for the analysis of complex modulus as shown by (Gayte et al., 2016);

- Strain amplitude variation at the beginning of the test, due to the monitoring system of the press, which induces a complex modulus change caused by nonlinearity (Mangiafico et al., 2015). The proposed analysis needs a series of cycles at approximately constant strain amplitude, close to the final one;

- Heat diffusion time scale, which affects temperature distribution in the elementary cell and consequently the stiffness change of the bituminous mixture. It requires: i) fixing the same time interval (and not number of cycles) for the analysis at all frequencies, and ii) fixing a short time interval to respect the adiabaticity hypothesis.

Then, for tests at 1Hz, cycles from 5 to 7 were taken into account, for 3Hz cycles 15 to 21, and 10Hz included cycles from 50 to 70. Force and strain signals were fitted by sinusoidal functions using 2 consecutive cycles in the analysis. For each thermomechanical calculation input (norm of complex modulus, phase angle and strain amplitude), average values from the analysed series of cycles were used. Figure 5-10 presents norm of complex modulus data as a function of the applied number of cycles for one of the Phase I Fatigue tests on BM3_A. For the first 100 cycles, the actual applied strain amplitude is also presented. Results, in terms of slopes for the bituminous mixture modulus decrease with the number of cycles, obtained from the three proposed thermomechanical calculations (without heat diffusion), were plotted in the same figure. These slopes were placed where they better fit experimental results.

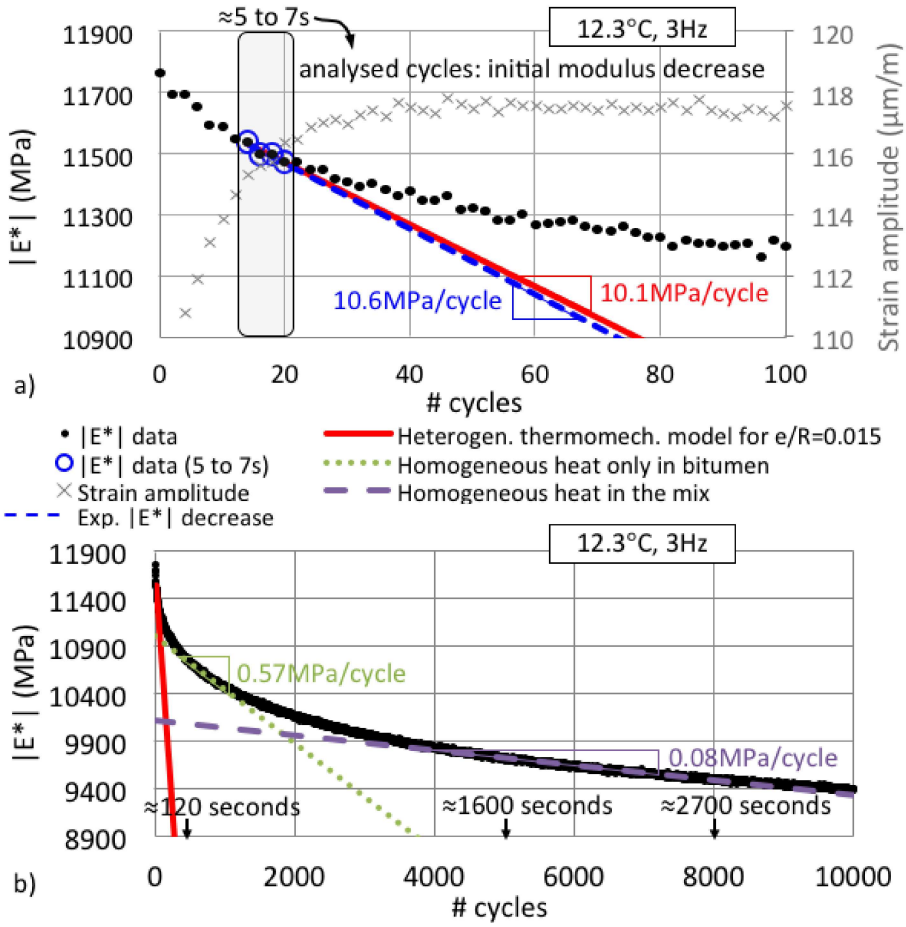

Figure 5-10. Initial decrease of norm of complex modulus for BM3_A, tested at 12.3°C and 3Hz for a strain amplitude of 116µm/m (cf. also test results in Figure 5-11): data and prediction considering the 3 considered calculations: i) homogeneous heat in the mix, ii) Homogeneous heat in bituminous phase and iii) 3D heterogeneous thermomechanical calculation. Up to 10,000 cycles (b) and, zoom up to 100 cycles (a).

Figure 5-10a shows a focus on results from the first 100 cycles. It is to be observed that the applied strain amplitude was not constant at the very beginning of the test (up to about 30 cycles), due to limitations of the monitoring system of the press. Then, nonlinearity may be responsible for a part of the initial stiffness decrease (up to about 30 cycles). A modulus decrease of 10.6MPa/cycle (around 0.09%/cycle) is experimentally obtained for the example given in Figure 5-10a.

5.6.2. Analysis of initial slopes of norm of complex modulus for all tests

Experimental slopes (modulus as a function of number of cycles) were obtained for all tested conditions analysed in this investigation (cf. Figure 5-11, and Figure 5-12 and Table 5-4 and Table 5-5). In the case of the heterogeneous calculation presented in Section 5.5.3, a value of 1.515×10^{-2} for e/R allows obtaining a slope of 10.1MPa/cycle only with the effect of local self-heating. As R = 2.32mm (characteristic particle radius), e (minimum half-thickness of mastic) is approximately

35.1µm. Figure 5-10b presents the experimental modulus values until 10,000 cycles, as well as the slopes calculated from the three proposed approaches (two preliminary and the simplified 3D heterogeneous calculations). Results show that the slope representing the stiffness decrease at the beginning of the test can be obtained using the simplified 3D thermomechanical calculation presented in this work. The slope obtained considering a homogeneous heat distribution concentrated in the bitumen is observed at around 360 cycles (corresponding to 120 seconds). The slope estimated considering a homogeneous heat distribution in the bituminous mixture occurs around 5,000 cycles (around 1600s). From a numerical thermomechanical simulation considering heat diffusion, (Riahi et al., 2016) estimated that the time for completely homogenising temperature distribution between mastic and aggregates was around 100s, or 1,000 cycles for tests at 10Hz.

Table 5-4 and Table 5-5 present the experimental (strain amplitude, bituminous mixture norm of complex modulus, phase angle and initial modulus decrease) and modelling (initial modulus decrease) results (over the evaluated cycles) obtained at the different conditions of temperature and frequency between 5 and 7s (average values for the analysed cycles) on both studied bituminous mixtures. Figure 5-11 presents experimental and modelled results for normalized initial modulus decrease ($(-d|E_{bm}^*|/dN)/|E_{bm}^*|$) obtained for BM2 at different conditions of temperature, frequency and strain amplitude. Figure 5-12 presents the same information for BM3.

Table 5-4. Strain amplitude, norm of complex modulus, phase angle and initial modulus decrease (from the experiment and from simplified 3D thermomechanical calculation using e = 58.6µm/m and R = 2.32mm) for BM2

					From 5 to 7s				
					Experiment				**Model**
BM	**Sp.**	**Test order**	**T (°C)**	***f* (Hz)**	**$\varepsilon_{0,bm}$ (µm/m)**	**$\lvert E^*_{bm}\rvert$ (MPa)**	**φ_{bm} (°)**	**$-d\lvert E^*_{bm}\rvert/dN$ (MPa/cycle)**	**$-d\lvert E^*_{bm}\rvert/dN$ (MPa/cycle)**
2	**A**	1	11.3	10	78	16,185	15.2	2.3	2.1
2	**A**	2	11.3	10	110	16,043	15.7	4.3	4.2
2	**A**	4	21.4	10	50	9,361	24.5	0.8	0.8
2	**A**	5	21.4	10	90	9,140	25.4	2.4	2.4
2	**B**	1	12.4	10	57	14,253	18.5	1.2	1.1
2	**B**	2	12.4	10	81	14,305	18.6	2.3	2.3
2	**B**	3	12.4	10	106	14,002	18.5	3.7	3.7
2	**B**	4	12.4	10	130	13,898	19.1	5.6	5.6
2	**B**	5	12.4	10	131	13,675	19.3	5.6	5.6
2	**B**	6	12.4	10	131	13,288	20.5	5.6	5.6

Table 5-5. Strain amplitude, norm of complex modulus, phase angle and initial modulus decrease (from the experiment and from simplified 3D thermomechanical calculation using e = 35.1µm/m and R = 2.32mm) for BM3

					From 5 to 7s				
					Experiment				**Model**
BM	**Sp.**	**Test order**	**T (°C)**	***f* (Hz)**	**$\varepsilon_{0,bm}$ (µm/m)**	**$\lvert E^*_{bm}\rvert$ (MPa)**	**φ_{bm} (°)**	**$-d\lvert E^*_{bm}\rvert/dN$ (MPa/cycle)**	**$-d\lvert E^*_{bm}\rvert/dN$ (MPa/cycle)**
3	**A**	1	7.4	1	72	13,109	15.6	4.5	4.0
3	**A**	2	7.4	3	63	15,554	13.1	3.5	2.9
3	**A**	3	7.4	10	56	18,316	10.7	2.2	2.0
3	**A**	4	7.4	1	124	12,923	16.5	11.7	12.1
3	**A**	5	7.4	3	111	15,105	14.2	9.5	9.1
3	**A**	6	7.4	10	99	17,940	11.5	6.0	6.5
3	**A**	7	12.3	1	126	9,385	22.1	12.5	11.3
3	**A**	8	12.3	3	116	11,502	19.1	10.6	10.1
3	**A**	9	12.3	10	107	14,334	15.4	8.5	8.5
3	**B**	1	7.4	3	71	14,387	14.5	3.6	3.6
3	**B**	2	7.4	3	127	14,261	15.2	9.5	12.1
3	**B**	3	11.6	10	68	14,289	15.0	3.6	3.6
3	**B**	4	11.6	10	124	13,999	15.8	6.5	10.6

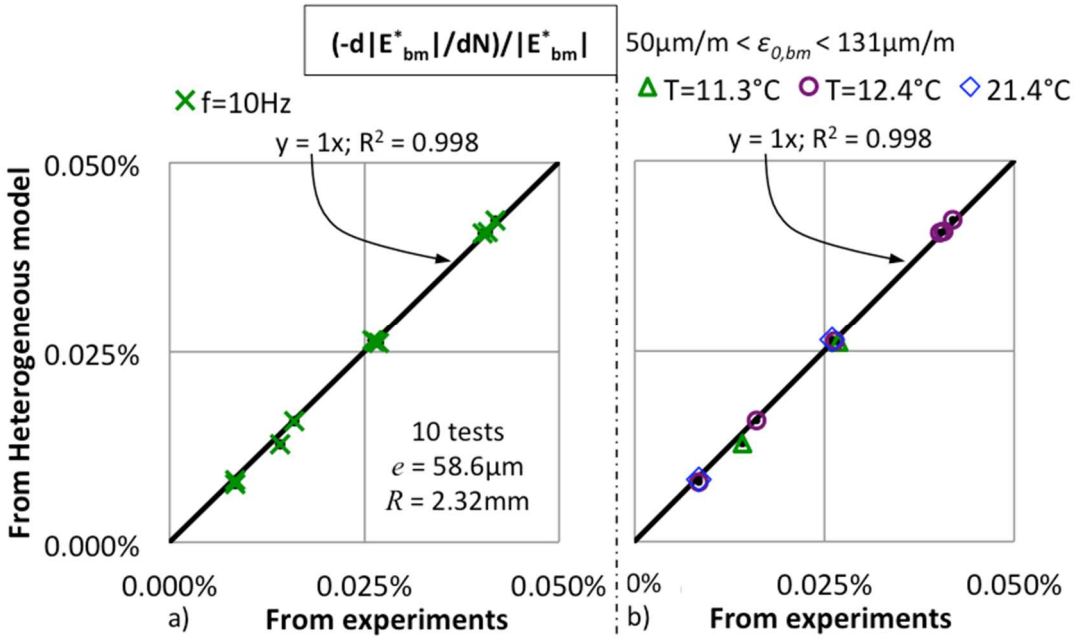

Figure 5-11. For BM2, modelled (3D heterogeneous thermomechanical calculation, cf. Section 5.5.3 and Figure 5-10a) normalized initial modulus decrease ($-d|E_{bm}^*|/dN)/|E_{bm}^*|$) as a function of the results obtained from experiments (for cycles between 5 and 7s of loading) at different temperatures and frequencies with different strain amplitudes (10 tests): a) labelled by frequencies, and b) labelled by temperatures.

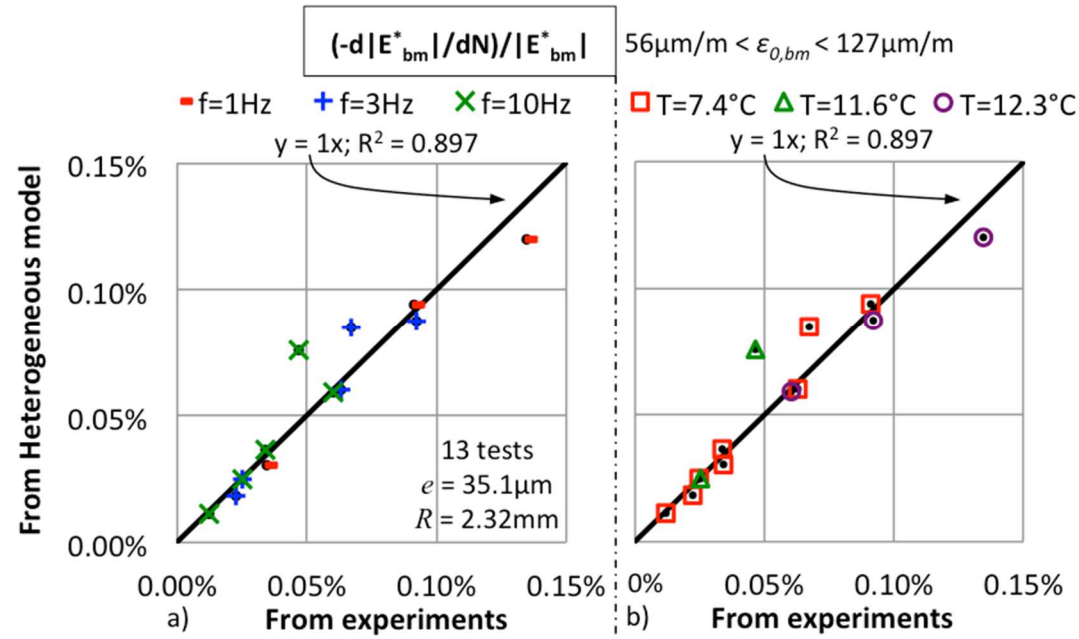

Figure 5-12. For BM3, modelled (3D heterogeneous thermomechanical calculation, cf. Section 5.5.3 and Figure 5-10a) normalized initial modulus decrease ($-d|E_{bm}^*|/dN)/|E_{bm}^*|$) as a function of the results obtained from experiments (for cycles between 5 and 7s of loading) at different temperatures and frequencies with different strain amplitudes (13 tests): a) labelled by frequencies, and b) labelled by temperatures.

Results from Figure 5-11 and Figure 5-12 demonstrate that the simplified 3D heterogeneous model studied in this work can rather correctly simulate the modulus decrease observed at the very beginning of cyclic loading on bituminous mixtures, at least for initial modulus decreases below about 0.15%/cycle. A coefficient of determination between experimental and calculated slopes of modulus decrease of around 0.9 was obtained for BM3, using a parameter e/R of 1.515×10^{-2} for e/R which corresponds to approximately 35.1μm with the determined particle radius of R = 2.32mm. For this material, three different frequencies of loading were applied with different strain amplitudes (from 56 to 127μm/m), for which initial modulus decreases below 0.15%/cycle were obtained. For BM2, the determination was almost perfect (coefficient of determination near 1.0), using a parameter e/R of 2.525×10^{-2} for e/R which corresponds to approximately 58.6μm with the determined particle radius of R = 2.32mm. For this material, only one frequency was applied with different strain amplitudes (from 50 to 131μm/m), for which initial modulus decreases below 0.05%/cycle were obtained.

The obtained results suggest that, if no heat diffusion happens during initial loading cycles, the observed modulus decrease can be explained by a non-uniform temperature increase due to the self-heating phenomenon. This non-uniform temperature increase could not be measured using common thermocouples, since it happens very locally (in zones of about few tens of microns).

5.6.3. Time intervals when calculated slopes are observed in experiments

For all tests, the time for which the thermomechanical calculations corresponded to the experimental observations was investigated. Good correspondence was observed between experimental results from 5 to 7s and calculated results from the simplified 3D thermomechanical calculations. These time intervals correspond to cycles from 5 to 7 at 1Hz, 15 to 21 at 3Hz cycles, and 50 to 70 at 10Hz. It should be underlined that only one value for the model parameter e (mastic half-thickness) was used for a given bituminous mixture. As it was demonstrated (cf. Figure 5-11 and Figure 5-12), calculation and experimental results correlate rather well for those initial cycles during cyclic loading.

For the two other thermomechanical calculations results (considering homogeneous heat in the bitumen and considering homogeneous heat in the mixture), no systematic correspondence was observed, i.e. nor the time for correspondence between experimental and calculated slopes, nor the number of cycles were systematically the same for all tests. Results are summarised in Table 5-6 and Table 5-7. It seems that the time interval for which calculated modulus slopes correspond to the experimental modulus slopes is not independent of the test conditions (strain amplitude, temperature and frequency). Moreover, no relationship between those time intervals has been found, even when considering equivalent frequencies (considering the TTSP as modelled for the investigated bituminous mixture) and normalisation procedures (considering the squared strain amplitude, the modulus, and the sine of the phase angle, all of these intervening in the dissipated energy). This indicates that the calculation considering homogeneous heat in the bitumen has no correspondence with an actual state of temperature increase distribution in the bituminous mixture during cyclic loading. Since after some time it is expected that all the bituminous mixture heats at the same rate, a correspondence was expected for the case of homogeneous heat in the bituminous

mixture, but it has not been found. This seems to indicate that another phenomenon occurs in those time intervals. Figure 5-13 presents the obtained results and some of the tested relationships for BM3.

Table 5-6. Time interval correspondence between calculated and experimental slopes (both for the case of homogeneous heat in the bitumen and homogeneous heat in the bituminous mixture) observed for Phase I Fatigue tests on BM2.

			Homogeneous heat in bitumen				**Homogeneous heat in mixture**			
T (°C)	***f* (Hz)**	**$\varepsilon_{0,bm}$ (μm/m)**	**Beginning cycle**	**Ending cycle**	**Beginning time (s)**	**Ending time (s)**	**Beginning cycle**	**Ending cycle**	**Beginning time (s)**	**Ending time (s)**
11.3	10	95	1,400	5,200	140	520	>10,000	>10,000	>1,000	>1,000
11.3	10	134	2,500	8,000	250	800	>10,000	>10,000	>1,000	>1,000
21.4	10	53	650	2,400	65	240	>10,000	>10,000	>1,000	>1,000
21.4	10	94	1,500	4,000	150	400	6,000	>10,000	600	>1,000
12.4	10	59	220	900	22	90	3,000	9,100	300	910
12.4	10	83	260	830	26	83	6,000	>10,000	600	>1,000
12.4	10	108	330	1,340	33	134	>10,000	>10,000	>1,000	>1,000
12.4	10	133	780	2,530	78	253	>10,000	>10,000	>1,000	>1,000
12.4	10	133	790	2,300	79	230	>10,000	>10,000	>1,000	>1,000
12.4	10	133	1,020	3,300	102	330	>10,000	>10,000	>1,000	>1,000

Table 5-7. Time interval correspondence between calculated and experimental slopes (both for the case of homogeneous heat in the bitumen and homogeneous heat in the bituminous mixture) observed for Phase I Fatigue tests on BM3.

			Homogeneous heat in bitumen				**Homogeneous heat in mixture**			
T (°C)	***f* (Hz)**	**$\varepsilon_{0,bm}$ (μm/m)**	**Beginning cycle**	**Ending cycle**	**Beginning time (s)**	**Ending time (s)**	**Beginning cycle**	**Ending cycle**	**Beginning time (s)**	**Ending time (s)**
12.3	1	117	280	940	280	940	2,400	6,900	2,400	6,900
12.3	3	117	350	940	117	313	4,000	8,100	1,333	2,700
12.3	10	119	340	1,100	34	110	9,500	>10,000	950	>1,000
7.4	1	67	350	1,350	350	1,350	3,000	>10,000	3,000	>10,000
7.4	3	67	380	1,600	127	533	5,300	>10,000	1,767	>3,333
7.4	10	68	120	2,500	12	250	>10,000	>10,000	>1,000	>1,000
7.4	1	117	150	800	150	800	3,500	>10,000	3,500	>10,000
7.4	3	118	290	1,030	97	343	4,700	>10,000	1,567	>3,333
7.4	10	119	250	1,650	25	165	8,500	>10,000	850	>1,000
7.4	3	73	380	1,150	127	383	6,400	>10,000	2,133	>3,333
7.4	3	130	140	760	47	253	>5000	>5,000	>1,667	>1,667
11.6	10	72	380	1,250	38	125	7,200	>10,000	720	>1,000
11.6	10	130	120	1,050	12	105	8,100	>10,000	810	>1,000

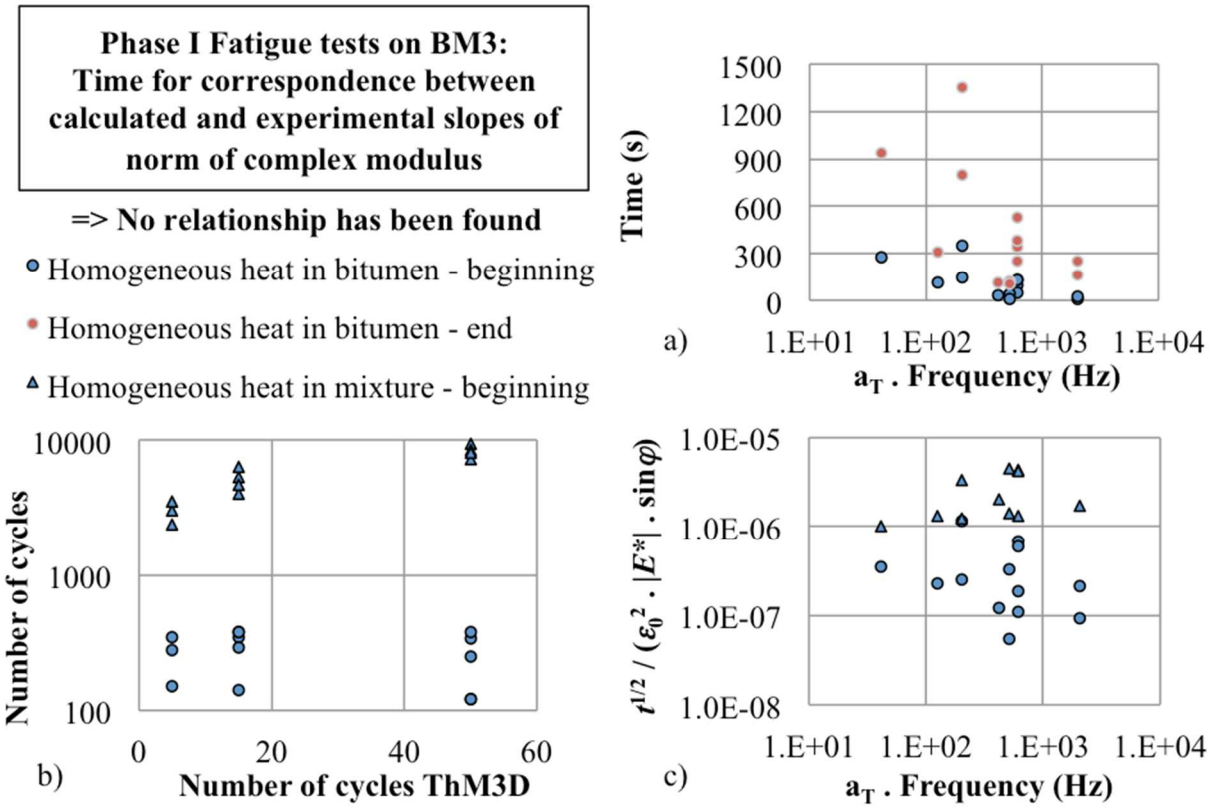

Figure 5-13. Investigation of relationships of the time for correspondence between calculated and experimental slopes of norm of complex modulus observed for Phase I Fatigue tests. Example on BM3. a) Time correspondence (beginning and end of correspondence) for the calculation considering homogeneous heat in bitumen as a function of the time-shifted frequency. b) Number of cycles for the beginning of correspondence for the calculation considering homogeneous heat in bitumen and homogeneous heat in mixture as a function of the number of cycles for the beginning of correspondence for the calculation considering heterogeneous heat in mastic. c) A normalised parameter (involving correspondence time, strain amplitude, and complex modulus) as a function of the time-shifted frequency.

5.7. 3D heterogeneous calculation with heat diffusion

In this section, a particular test condition (11.6°C and 10Hz on BM3) is studied in detail, considering the effect of heat diffusion. Since calculation hypotheses are different, a new value of *e* should be determined. For the study of modulus evolution considering heat diffusion within the mastic phase, a set of linear viscoelastic parameters is needed for the mastic. For this problem considering heat diffusion, an evolution of modulus decrease as a function of loading time is obtained, instead of only one value of modulus decrease per cycle (slope calculation). The model geometry is the same as for the case without heat diffusion (set of monodisperse rigid spheres, cf. Figure 5-3).

Norm of complex modulus and phase angle of approximately 14,500MPa and 14.5° are obtained from complex modulus tests on BM3 at 11.6°C and 10Hz. Also, sensitivity to small (infinitesimal) temperature changes of −6.88%/°C (relative change in norm of complex modulus per degree) is obtained (cf. Table 5-3 and a scheme on Figure 5-6).

Calculation of heat distribution over time in the EHeV is performed for three values for *e*: 3, 10 and 100μm. This is done in order to evaluate if local effects can still explain initial modulus decrease now considering heat diffusion, and also for which value of *e* this would be possible. Focus is given to results obtained with e = 3μm. For each fixed value of *e*, the modulus of the mastic phase is calculated in order to obtain an EHeV presenting apparent modulus equivalent to the one of the Elementary Homogeneous Volume (EHoV). This is due to the strain distribution in the EHeV, as previously discussed (cf. Figure 5-7 and Eq. 5-6).

The mastic phase is considered viscoelastic and modelled using 2S2P1D model (Olard & Di Benedetto, 2003). For FEM calculations, a Generalised Maxwell (GM) model fitted on the 2S2P1D model (Tiouajni et al., 2011), containing only viscoelastic terms, is used. The GM model represents a discretisation of the continuous spectrum given by the 2S2P1D model. In this investigation, 8 viscoelastic elements were used for the discretisation. Complex modulus is obtained from Eq. 5-10 using parameters given in Table 5-8. As a simplification, Poisson's ratio (ν) is considered nil, as previously done for the calculation without heat diffusion.

$$E^* = E' + iE''; \; E' = \sum_{j=1}^{n} E_j \frac{\omega^2 \rho_j^2}{1 + \omega^2 \rho_j^2} \; and \; E'' = \sum_{j=1}^{n} E_j \frac{\omega \rho_j}{1 + \omega^2 \rho_j^2} \qquad \text{Eq. 5-10}$$

Where ω is the angular frequency of the sinusoidal loading and i is the complex number defined by $i^2 = -1$. The parameter n is the number of viscoelastic elements in the GM model, E_j and ρ_j represent the modulus of the spring and the relaxation time (ratio between viscosity of the damper and modulus of the spring in a given viscoelastic element) of the element j, respectively.

Table 5-8. Bituminous mastic Generalised Maxwell model constants (cf. Eq. 5-10), chosen to give, for R = 2.32mm, a bituminous mixture with initial norm of complex modulus of 14,500MPa and phase angle of 14.5° at 11.6°C and 10Hz, compatible with BM3 characterisation.

ρ_j (s)	$1 \cdot 10^{-4}$	$1 \cdot 10^{-3}$	$1 \cdot 10^{-2}$	$1 \cdot 10^{-1}$	$1 \cdot 10^{0}$	$1 \cdot 10^{1}$	$1 \cdot 10^{2}$	$1 \cdot 10^{3}$
E_j (MPa) for e = 3μm	816.8	634.4	589.2	515.5	515.5	331.5	15.1	9.5
E_j (MPa) for e = 10μm	1030.0	800.0	743.0	650.0	650.0	418.0	19.0	12.0
E_j (MPa) for e = 100μm	1967.0	1527.8	1419.0	1241.3	1241.3	798.3	36.3	22.9

5.7.1. FEM Calculations

For simplicity sake, the fully coupled thermomechanical phenomenon observed in bituminous mixtures was modelled as a one-way coupled phenomenon (viscous dissipated energy is not re-evaluated at each calculation step), as presented in Figure 5-14. For the cases analysed in this study (with resulting local temperature increases of the order of 1°C), not re-evaluating the viscous dissipated energy has little effect on the obtained results (even if locally that may induce a 10% modulus change in the mastic, the effect on the bituminous mixture is negligible). Moreover, with test conditions in the vicinity of 10°C and 10Hz, a small temperature increase induces a decrease in the imaginary part of the complex modulus, which is related to the energy injection. Then, this

simplification maximises the calculated temperature increase, not altering the obtained conclusions, as it will be seen. This modelling procedure consists of two steps: a thermal problem FEM calculation and a mechanical problem FEM calculation.

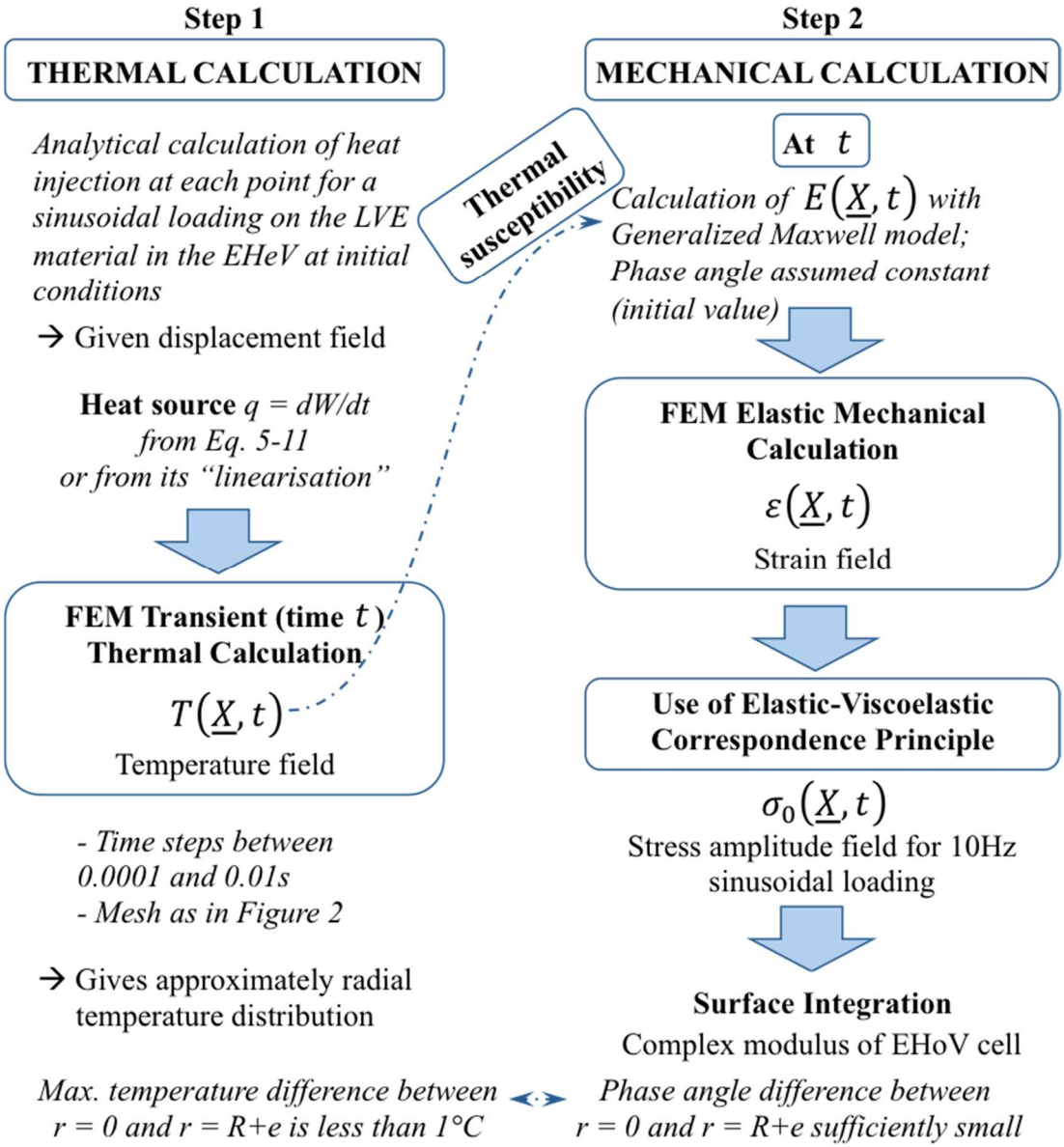

Figure 5-14. Flowchart describing performed FEM calculations: thermal analysis and mechanical analysis.

For the first step, the thermal problem associated with the calculated heat production from a sinusoidal loading, including the heat diffusion within the mastic, is solved numerically using FEM. This calculation gives the temperature field within the EHeV at any time. The heat production at each point in the mastic phase has been obtained from the analytical solution of the mechanical problem at the initial conditions, where temperature and linear viscoelastic properties are the same at any point in the mastic within the EHeV. The heat production corresponds to the

dissipated energy in the material. This dissipated energy can be calculated using the Generalised Maxwell model and it will be called here "real" heat production. The "real" heat production (dW/dt) is given by Eq. 5-11. It corresponds to the energy dissipation in all the dashpots in the GM model. The dissipated power in each of the dashpots (dW_i/dt) corresponds to the stress in the dashpot times its strain rate. In the equation, n represents the number of viscoelastic GM elements.

$$\frac{dW}{dt} = \sum_{i=1}^{n} \frac{dW_i}{dt} = \sum_{i=1}^{n} \frac{1}{\eta_i} \left[\varepsilon_0 \frac{\omega E_i}{\left(\frac{E_i}{\eta_i}\right)^2 + \omega^2} \left(\frac{E_i}{\eta_i} \cos \omega t + \omega \sin \omega t - \frac{E_i}{\eta_i} e^{-\frac{E_i}{\eta_i} t} \right) \right]^2 \qquad \text{Eq. 5-11}$$

Another calculation of heat injection was made considering that the dissipation of energy occurs in a linear way with respect to time over a cycle. This calculation produced what was called here the "linearised" results. "Linearisation" consists in distributing all the dissipated energy that happens in a cycle in a linear way with respect to time over this cycle. This means that heat injection would occur at a constant power, instead of the actual variable power obtained from Eq. 5-11. The total heat injected in the mastic within a cycle is equal in both cases. The "linearisation" procedure allows utilising greater time steps in the FEM calculation, hence reducing calculation time. However, possible oscillations in temperature obtained locally in the mastic cannot be calculated.

For the second step, the FEM thermal calculation solution is used in the FEM mechanical calculation. At any given time, the obtained temperature field is used as input to adjust the mastic modulus for each point in the mastic region in the EHeV, respecting temperature-dependence of the material. The FEM mechanical calculation results are interpreted by applying the Elastic-Viscoelastic Correspondence Principle (EVCP) (Biot, 1955). In order to apply this principle, it is supposed that negligible phase difference of the complex moduli of the mastic points in the EHeV is produced after self-heating. This assumption will be proven to be reasonable when analysing the temperature distributions in the EHeV (cf. Figure 5-16). It provides a means of evaluating the complex modulus of the equivalent EHoV. Thermal expansion is neglected.

5.7.1.1. *FEM characteristics*

Figure 5-15 presents the FEM calculations (mesh, boundary conditions, materials properties) performed using COMSOL 5.2 software. The FEM mesh (with tetrahedral elements used in the mastic) is the same for the thermal and for the mechanical calculations. It is constructed using the physics-controlled mesh generator and is considered as "fine" by the software, resulting in a different number of elements for each of the thicknesses of mastic analysed. When analysing the problem with mastic half-thickness (e) of 3µm, 10µm, and 100µm, 18,561, 17,369, and 16,534 elements were used, respectively.

5.7.1.2. *Thermal and Mechanical FEM calculations*

Figure 5-16 presents temperature fields obtained for sinusoidal loading at 10Hz and 150µm/m strain amplitude (ε_0) on the studied bituminous mixture, using a EHeV with e = 3µm, at different times (0.1, 1 and 10s). The main results from the FEM mechanical analysis is also given: the relative modulus change. Figure 5-16 shows that, as expected, temperature increase initially concentrates in the thinnest region of mastic phase where the distance between particles is minimal and the vertical strain is maximal. Point A in Figure 5-16c represents the hottest point in the EHeV. At the beginning of the loading (from zero seconds to approximately 1s) the size of the "hot" region increases rapidly until a rather identical steady state temperature evolution is obtained for all mastic points. Point B in Figure 5-16c indicates the coldest point in the EHeV. As expected, it is located opposite to point A, in a region where mastic presents lower strain.

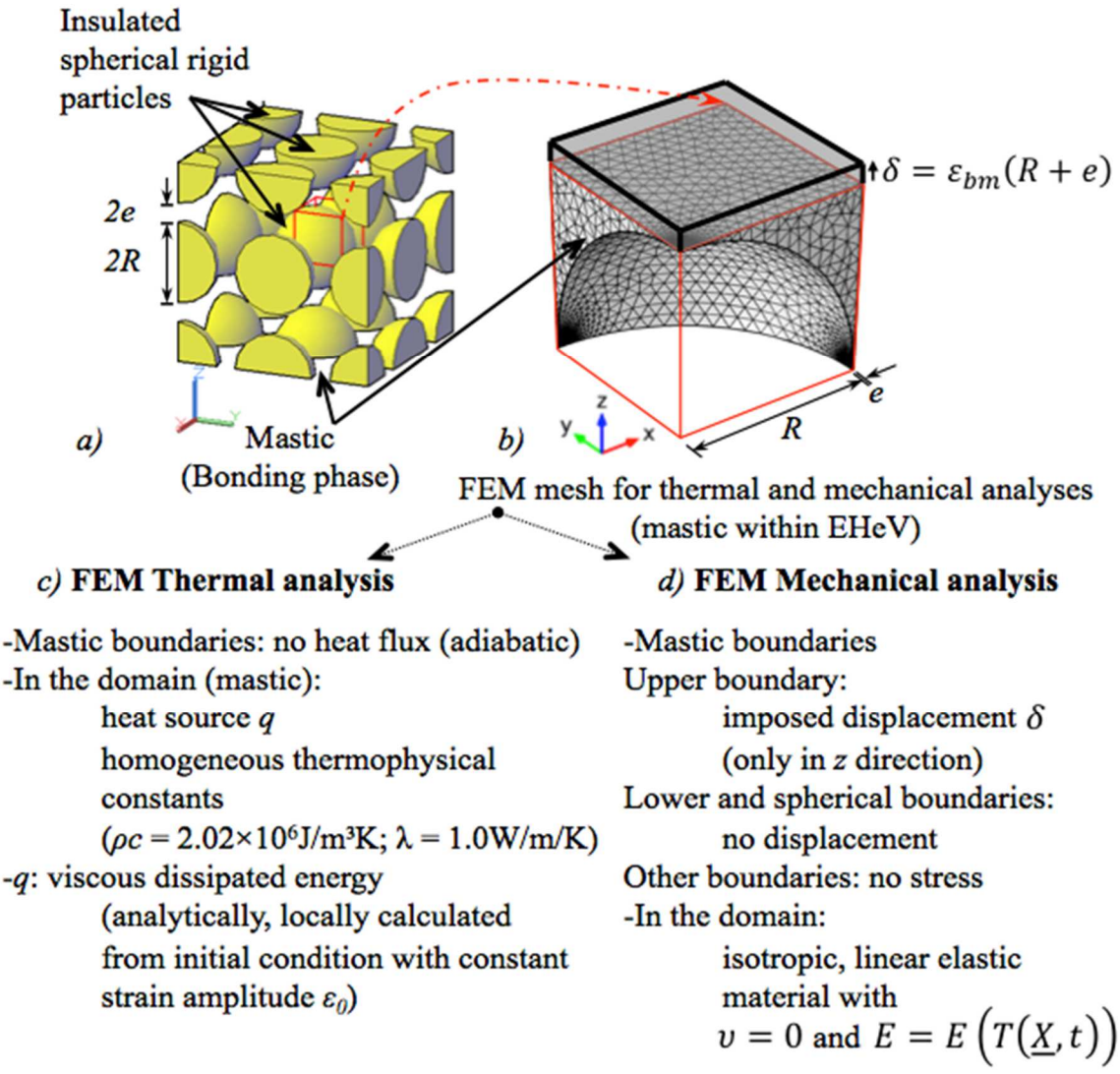

Figure 5-15. a) Idealized heterogeneous bituminous mixture; b) Zoom on the meshed elementary cell called "Elementary Heterogeneous Volume" (EHeV) used for 3D FEM analysis; c) considerations for FEM thermal analysis; d) considerations for FEM mechanical analysis.

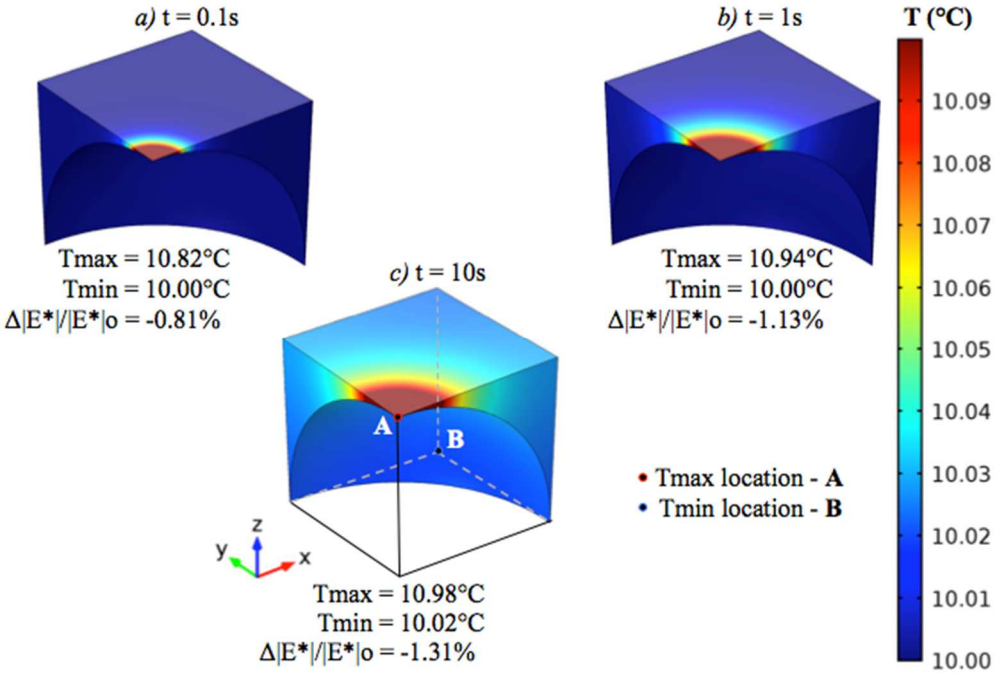

Figure 5-16. Temperature distribution and bituminous mixture relative modulus change at a) 0.1s; b) 1s; and c) 10s for e = 3µm and sinusoidal loading at 10Hz and 150µm/m strain amplitude applied on the bituminous mixture (the model represents BM3).

5.8. Results and analysis with heat diffusion

Figure 5-17a presents the "linearised" temperature change (considering that the heat produced in a whole sinusoidal cycle is injected at a constant rate within the cycle), calculated at point A (hottest one) and point B (coldest one) for an EHeV cell with e = 3µm, representing BM3. The calculated relative modulus change is also presented (dotted grey line in secondary axis), as well as experimental results (data points in secondary axis, Nguyen, 2011). Figure 5-17b and Figure 5-17c present details on the temperature change at points A and B, respectively, from 9.8 to 10s (cycles 99 and 100). The dotted lines represent the results obtained considering directly the heat production from cyclic loading while the continuous line is the output after "linearisation" of heat production. Figure 5-17b shows that the temperature increase at point A (hottest) oscillates around the value calculated with "linearisation". The oscillation amplitude is about 0.2°C and its frequency is 20 Hz. At point B (coldest), oscillation is negligible (Figure 5-17c). The frequency of 20Hz was expected since heat production is a function of the square of the strain rate, which oscillates at 10Hz. Results validate the use of the "linearised" procedure, which makes calculations faster. Temperature increase at points A and B and bituminous mixture modulus changes depend on the mastic half-thickness (e) used. Results are summarised in Table 5-9.For R = 2.32mm, after 10 cycles, the calculated temperature increase in point A (resp. B) is about 0.74°C (resp. 0.01°C) for e = 3µm, 0.29°C (resp. 0.01°C) for e = 10µm and 0.06°C (resp. 0.01°C) for e = 100µm. Corresponding modulus decreases are 1%, 0.5% and 0.1%, respectively.

Table 5-9. Calculated temperatures at points A (hottest one) and B (coldest one) in the EHeV and calculated bituminous mixture relative modulus decrease after 10s of loading at 10Hz and 150µm/m (with different values of mastic half-thickness, 3, 10, and 100µm, particle radius R = 2.32mm, and mastic's Generalised Maxwell model constants given in Table 5-8.

	Temperature increase at point A after 10s (°C)	**Temperature increase at point B after 10s (°C)**	**Bituminous mixture relative modulus decrease (%)**
***e* = 3µm**	0.74	0.01	1
***e* = 10µm**	0.29	0.01	0.5
***e* = 100µm**	0.06	0.01	0.1

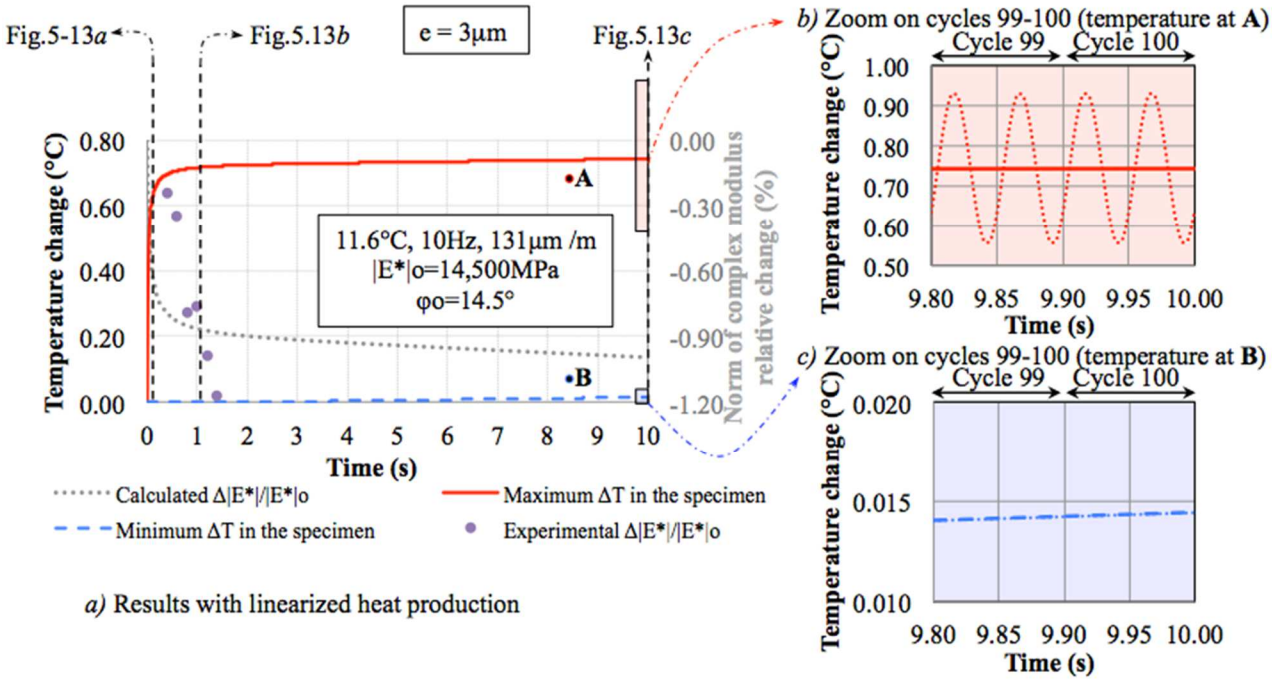

Figure 5-17. Results for the first 100 cycles of sinusoidal loading for e = 3µm. a) Modulus and temperature changes calculated with a "linearized" heat production during each cycle; and b) and c) zoom for cycles #99 and #100 including the temperature change considering "real" heat production at points A (maximum temperature change) and B (minimum temperature change).

From Figure 5-17, it is observed that, until about 1s of loading (10 cycles), the temperature change occurs very rapidly. After this transient state, a steady state is established (between 1 to 2 seconds after the beginning of the loading), where average temperature increase is the same in each point of the mastic. In the previous sections, in order to calculate modulus change at the very beginning of the test, an analytical method considering that no heat transfer exists within the mastic (local adiabatic hypothesis) was proposed. When considering heat diffusion, as in this section, that hypothesis of adiabaticity seems not applicable at a time scale of some seconds, and that the modulus decrease cannot be fully explained by the thermomechanical coupling phenomenon.

As a final remark, it may be concluded that a fully coupled thermomechanical model is not required for the purpose of this work. Since viscous dissipation would be lower with increasing

temperature at 10°C (material parameters available in Table 5-8), calculated modulus changes due to thermomechanical coupling would be lower in fully coupled calculation. Hence, the conclusions obtained in this investigation still hold.

5.9. Conclusion on bituminous mixture self-heating

In this chapter, an investigation of the stiffness decrease with the number of loading cycles of bituminous mixtures at the beginning of cyclic tests is presented. Results showed that local thermal effects, as modelled through a simplified thermomechanical calculation considering material heterogeneity, could explain the initial stiffness decrease. For the considered strain levels (up to 131μm/m) and number of applied cycles (less than 10,000 cycles, considered as Phase I of a fatigue test), this decrease is completely reversible, as shown in the literature (Coutinho et al., 2014; Di Benedetto et al., 1996; Di Benedetto, de La Roche, et al., 2004; Di Benedetto, Olard, et al., 2004; Gauthier et al., 2010; Gayte et al., 2016; Mangiafico, 2014; Mangiafico et al., 2015, 2017; Q. T. Nguyen, 2011; Q. T. Nguyen et al., 2015; C. V. Phan, Di Benedetto, Sauzéat, Dayde, et al., 2017; Riahi et al., 2017; Soltani & Anderson, 2005). Then, damage is assumed as negligible. Three adiabatic thermomechanical calculations were proposed, differing with respect to their simplification hypotheses. The first one is performed considering homogeneous strain and heat distributions in the bituminous mixture. The second one considered that viscous dissipated energy heats only the bitumen and resulted in a higher initial change in stiffness, but still far from the experimental observed decrease. The last one consists in a simplified 3D thermomechanical calculation, which accounted for heterogeneous strain and heat distributions within the mastic.

A particle radius (R) of 2.32mm was adopted, determined from geometrical considerations on the studied mixture. A minimum half-thickness of mastic (e) of 58.6μm for BM2 and of 35.1μm for BM3, which seems physically reasonable, enabled the calculation of the experimentally observed initial stiffness decreases, with good agreement (R^2 of at least 0.9) to test results. Relative modulus decreases ranging from 0.01%/cycle to 0.14%/cycle, obtained at different testing conditions (varying temperature, frequency and strain amplitude), could be simulated. This rather simple thermomechanical calculation shows that local self-heating could explain stiffness decrease at the beginning of fatigue or any other cyclic tests on bituminous mixtures, provided that the necessary temperature increase indeed happens within the mastic. That means that if significant temperature increase occurs in some regions of the bituminous phase, it would be possible to produce the observed stiffness decrease in the whole bituminous mixture during cyclic tests. The calculation shows that this significant temperature increase is reached under certain conditions (absence of heat diffusion, which is true for small time intervals, and sufficiently thin mastic coating). These conditions can only be true only at the very beginning of tests. As a complementary remark, the simplified 3D thermomechanical calculation allows also prediction of the phase angle evolution with number of cycles. It results that complex modulus evolution follows the LVE Black curve.

After demonstrating that local thermal effects could explain modulus decrease in the beginning of cyclic tests in adiabatic conditions, a calculation considering heat diffusion was presented. Results show that heat diffusion happens excessively fast. A steady state phase, with homogeneous

rate of temperature increase, is reached in about 1 to 2s (10 to 20 cycles at 10Hz), independently of the mastic half-thickness (*e*). Even within a loading cycle (0.1s), noticeable oscillation of temperature can be observed in the hottest regions of the mastic (cf. Figure 5-17). The presented calculation cannot simulate the rapid initial stiffness change observed experimentally on bituminous mixtures. Hence, despite simplification made for calculations, it is likely that another phenomenon, which is not temperature increase due to self-heating, contributes for the modulus decrease. However, the simulations made before in local adiabatic conditions proved to well represent the initial modulus decrease (for different conditions of frequency, temperature and strain amplitude). This could be explained by the existence of another reversible phenomenon consistent with the definition of thixotropy (Barnes, 1997), which magnifies thermal effects while producing equivalent consequences on material behaviour (Van Rompu et al., 2012). Regarding the obtained results from the calculation with no heat diffusion, thixotropy seems to produce an effect equivalent to the one of a change in temperature.

Chapter 6: COMBINED EFFECTS OF DIFFERENT PHENOMENA DURING CYCLIC TESTS

Chapter 6: Combined Effects of Different Phenomena During Cyclic Tests 165
6.1. Introduction.....166
6.2. Annular Shear Rheometer experiments description 168
6.2.1. Complex shear modulus tests.....168
6.2.2. Alternating Strain Amplitudes (ASA) test 168
6.2.3. Load and Rest Periods (LRP) tests.....169
6.3. Complex shear modulus test results: the effect of temperature 171
6.4. ASA test results 173
6.5. LRP test results: quantification of biasing effects on bitumen and mastic specimens 177
6.5.1. An example of LRP test results: 5 LRP loops with 10,000 cycles and 4h rest on bitumen submitted to 20,000µm/m sinusoidal loading.....177
6.5.2. Damage.....184
6.5.3. Nonlinearity and self-heating.....187
6.5.4. Thixotropy.....194
6.6. Number of cycles and rest time effect 196
6.7. Failure analysis 199
6.8. Conclusion on biasing effects on bitumen and mastic.....202

6.1. Introduction

Fatigue of bituminous materials (bitumen, mastic and bituminous mixtures) is commonly studied by applying cyclic loading until failure. Two kinds of information are searched: the damage behaviour of the material, and its fatigue life. When looking to the damage behaviour, which is capable of producing a change in stiffness, literature commonly considers that the complex modulus variation observed during fatigue tests is due to damage (Bahia et al. 1999; Carpenter et al. 2003; Darabi et al. 2013; Ghuzlan and Carpenter 2000; Ghuzlan and Carpenter 2006; Ghuzlan and Carpenter 2003; Kim et al. 1997; Shen et al. 2006; Underwood et al. 2012; You et al. 2014, among others). Then, if rest is applied and a recovery of the complex modulus is observed, this would call for the existence of another phenomenon, capable of reversing the effects of damage. This phenomenon is called in the literature "self-healing" of microcracks (Bhasin et al., 2008; Canestrari et al., 2015; Daniel & Kim, 2001; Karki et al., 2015; Palvadi et al., 2012).

The tests interpretation approach considering damage and self-healing most frequently completely neglects phenomena such as nonlinearity (cf. Chapter 4), self-heating (cf. Chapter 5) and thixotropy. These are reversible phenomena capable of producing complex modulus variation during loading that is completely reversible during rest, and this variation is most frequently much higher than the complex modulus variation due to damage (Coutinho et al., 2014; Di Benedetto et al., 1996; Di Benedetto, de La Roche, et al., 2004; Di Benedetto, Olard, et al., 2004; Gauthier et al., 2010; Gayte et al., 2016; Mangiafico, 2014; Mangiafico et al., 2015, 2017; Q. T. Nguyen, 2011; Q. T. Nguyen et al., 2015; C. V. Phan, Di Benedetto, Sauzéat, Dayde, et al., 2017; Riahi et al., 2017; Soltani & Anderson, 2005). The effects of these phenomena on the measured complex modulus can be seen as biasing effects to the interpretation of fatigue tests, since they lead analysts to overestimate damage during loading, and postulate the existence of another phenomenon in order to explain recovery during rest. Separating these phenomena (the reversible phenomena from damage and self-healing) is a difficult task, because they are likely to occur simultaneously during loading. Some authors used models for that (Bhasin et al., 2008; Canestrari et al., 2015; Daniel & Kim, 2001; Karki et al., 2015; Palvadi et al., 2012), but there is no guarantee that the model is fitted to the complex modulus variation corresponding only to the phenomenon it is trying to describe. Thus, in different loading conditions (frequency, strain amplitude, temperature), the models are likely to produce unsatisfactory results. Due to this reason, making a clear difference between thixotropy and the combination of damage and self-healing seems to be more than just a semantics issue.

When looking to the fatigue life of the bituminous materials, authors apply rest and observe that the material endures some additional cycles before fatigue failure, which is considered to be due to self-healing. However, in a test with rest, due to self-heating during loading and cooling during rest in a thermal chamber, the material is not subjected to the loading history at the same temperature as in a test without rest. Since bitumen fatigue life is likely to be temperature dependent as other bituminous materials properties, a different fatigue life is expected for a different thermal history. Moreover, sometimes the fatigue failure criterion of a fixed relative change in modulus is used, which is perturbed by the other phenomena that induce a modulus change without any damage or fatigue life consumption (number of already applied cycles over the number of expected cycles at failure).

In the literature, authors investigated self-healing as the effect behind the possible recovery of consumed fatigue life of bituminous mixtures specimens (Moreno-Navarro et al., 2017; Moreno-Navarro, Sol-Sánchez, et al., 2015). When no failure had yet been observed, some "prolongation" of the fatigue life is usually obtained (Canestrari et al., 2015; Moreno-Navarro, Sol-Sánchez, et al., 2015). However, this may be due to the confusion in the test interpretation and to the utilised failure criterion (which is influenced by the biasing effects, not considered in the analysis). For example if 50% modulus decrease is set as a failure criterion, stopping a test before 50% modulus decrease, allowing recovery (due to a change in the temperature back to the original one, for example), the specimen is likely to reach again the 50% modulus change before breaking if most part of this change comes from reversible phenomena. An investigation of the recovery properties of bituminous mixtures specimens presenting a discrete crack, produced by a fatigue test, were presented by (Moreno-Navarro et al., 2017). After failure had been clearly produced, no prolongation (one of the tests presented a maximum of 5% recovery) of the fatigue life has been achieved, either by applying external compressive forces between the crack tips during short (1h) or long (60h) periods of time at temperatures around 60°C. The external force was applied by using a clamp, forcing the beam specimens to their original lengths. The mentioned results appear to be strong evidence that self-healing is not the phenomenon behind the "prolongation" of the fatigue life after rest. On the other hand, some more aggressive methods include the use of conductive fillers (such as steel fibres or steel wools) in the bituminous mixture and submitting the damaged mixture to an inductive process that heats up the inductive fillers, then the bitumen around them, provoking microcracks closure and an "forced" healing. In these cases, where the specimen surface temperature elevation is of the order of 100°C (Q. Liu, Schlangen, García, & van de Ven, 2010; Q. Liu, Schlangen, van de Ven, et al., 2010) significant material properties recovery may be achieved.

This chapter focuses on the aforementioned phenomena during cyclic loading and during rest of bituminous materials. It aims at identifying and quantifying the phenomena intervening on the material, and influencing the measured complex modulus of bituminous materials. From the results presented in Chapter 5 on self-heating, it was concluded that temperature effects could not explain all the reversible complex modulus change observed at constant strain amplitude at the beginning of cyclic loading of bituminous mixtures. Then, another reversible phenomenon, such as thixotropy is investigated. This phenomenon is likely to take place in bitumen, since this material is an example of colloidal dispersions (Behzadfar & Hatzikiriakos, 2014; Lesueur, 2009), which are commonly thixotropic (Barnes, 1997; Mewis & Wagner, 2009). Bitumen (B5070) and mastic (M5070_30pc40-70) specimens were tested using the Annular Shear Rheometer (cf. Chapter 3, and Table 3-1 and Table 3-2 for details on the materials and on the test configuration). Different tests were performed: complex modulus test, Alternating Strain Amplitudes (ASA) tests, Load and Rest Periods (LRP) test (including small Strain Amplitude Sweep test before LRP), and classical Fatigue tests. The complex modulus tests present negligible effects of the mentioned phenomena, due to the small strain amplitudes applied, and is used only to capture the temperature dependence of the material behaviour. This is needed in the interpretation of the other analysed tests. Meanwhile, the other tests are used to provide evidence of the existence of the mentioned reversible phenomena in bitumen and mastic, and quantify them. Load and Rest periods with different strain amplitudes during loading were performed. LRP tests differing on the rest time (4h and 14h) and on the number of applied cycles (10,000 and 20,000) during loading loops are used

to discuss the possible existence of self-healing in bitumen during rest. Results of all tests are presented either in the body of this chapter, or in Appendix C. All tests used for the investigation of biasing effects were carried out at 11°C. The effect of the strain amplitude is investigated, by testing different levels on bitumen and mastic.

6.2. Annular Shear Rheometer experiments description

Test results presented in this chapter were all obtained using experiments conducted with the Annular Shear Rheometer (ASR) (cf. Figure 3-2 for test setup, and Figure 3-4 for deformation scheme) on bitumen (B5070) and mastic (M5070_30pc40-70). Three extensometers were used to measure specimen shear strain, and four thermocouples were used to measure in-specimen temperature (cf. Section 3.2.1). The different tests presented here are complex shear modulus tests, Alternating Strain Amplitudes (ASA) tests, Load and Rest Periods (LRP) tests and classical Fatigue tests. The former ones were performed immediately after the last rest loop of the LRP test, using the same specimen.

6.2.1. Complex shear modulus tests

A complete description of complex shear modulus tests has already been presented in Chapter 4 for both bitumen and mastic. A scheme of the loading path used for the complex shear modulus tests has been presented in Figure 4-21. The test allowed characterising the material's frequency- and temperature- dependence in the linear viscoelastic domain. This is a necessary input for the interpretation of the cyclic tests investigated in this chapter.

6.2.2. Alternating Strain Amplitudes (ASA) test

In order to evaluate the complex modulus evolution during continuous cyclic loading when increasing and when decreasing the applied strain amplitude, an Alternating Strain Amplitudes (ASA) test was performed at 11°C, 10Hz. This test consists in continuous cyclic loading (no rest periods are applied), applied in a series of loading blocks that differ by the applied strain amplitude. Test loading path performed in this investigation is presented in Figure 6-1. As seen in the figure, different numbers of cycles were used for each of the applied strain amplitudes. The last loading block is similar to a classical fatigue test, i.e. only one strain amplitude is used and the test is carried out until failure of the specimen.

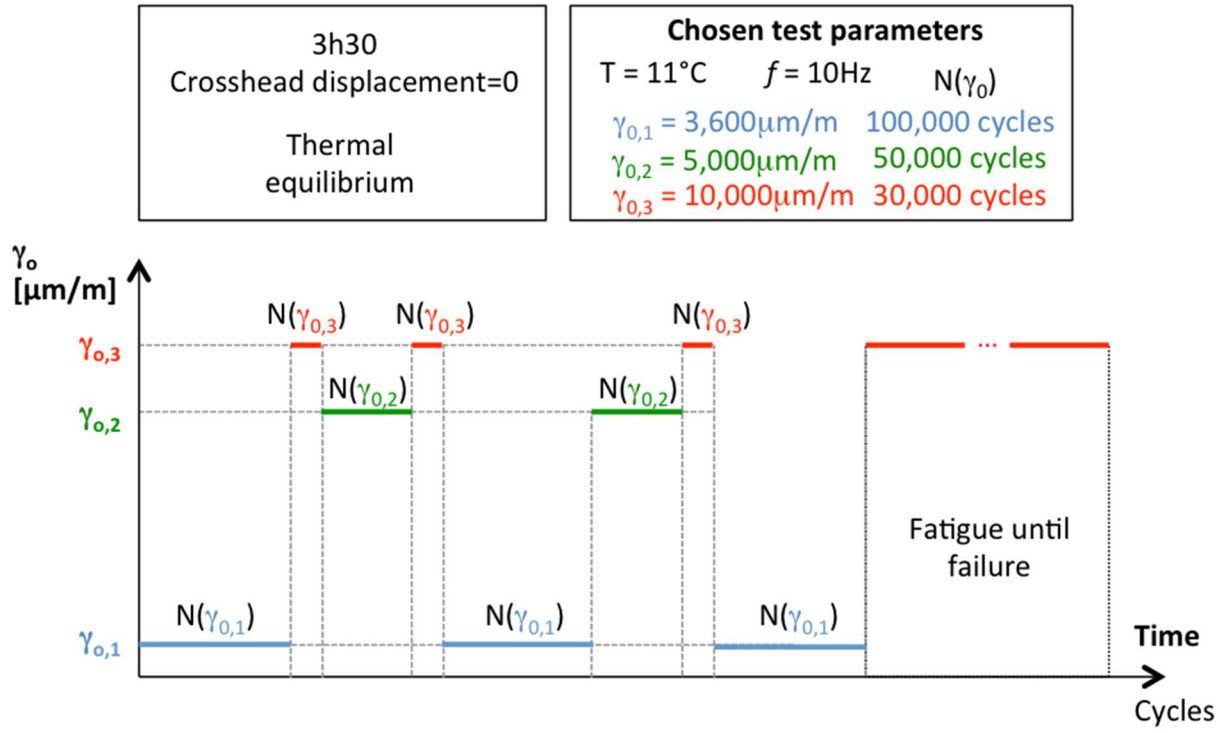

Figure 6-1. Scheme of the Alternating Strain Amplitude test loading path, including details on the applied strain amplitudes during loading (no rest periods are applied).

6.2.3. Load and Rest Periods (LRP) tests

In order to investigate the combined effects of different phenomena during cyclic tests, Load and Rest Periods (LRP) tests were performed on bitumen and mastic. These tests involve the application of a series of loading and rest loops on the material. The loading loop consists in a continuous cyclic loading, at fixed frequency and strain amplitude. The frequency used in this research is 10Hz (commonly used for fatigue tests), and different amplitudes were investigated (3,600μm/m, 10,000μm/m, 20,000μm/m on bitumen and 1,000μm/m, 3,300μm/m, 8,500μm/m on mastic). The rest loop consists of a fixed time interval where the specimen is allowed to recover its mechanical properties and to cool back to its initial temperature. During the rest loop, "small" strain complex modulus tests are performed in order to track the stiffness change during "rest". Figure 6-2 presents a scheme of the LRP tests loading path, including details on the "small" strain complex modulus tests applied during rest, for a LRP with application of 10,000 cycles per loading loop and 4h rest per rest loop, with a total duration of 5 LRP loops. The figure also shows the times chosen for the beginning of the "small" strain complex modulus tests during rest: 0, 5, 10, 20, 40, 80, 120, and 240min. The total time required for each small test is 3.35min. As seen in the detail of the "small" strain complex modulus test, two measurements at 10Hz are performed, one at the beginning and one at the end (3.25min apart) of the time span where the "small" strain complex modulus test is performed. This allows having more information on the stiffness change at the very beginning of the rest loop, where faster temperature decrease and stiffness change are expected. That means that, for this configuration of LRP test, complex modulus is tracked during the rest time with 16 measurements at 10Hz. At 10Hz, the strain amplitude applied, during a very

brief time span, is much lower than the one applied during the loading loop. The loading is verified to produce insignificant temperature increase and modulus change in the specimen.

Another configuration of the LRP test used in this research included rest loops of 14h of duration and loading loops with 20,000 cycles. During the 14h of rest, additional small complex modulus tests were performed at 360, 480, 600, 720, and 840min (10 supplementary complex modulus measurements at 10Hz during the 10h supplementary rest). Before all LRP tests performed in this research, a SAS test only at 10Hz (cf. Figure 4-23), using 30 loading cycles (3s of loading), is performed. Four different strain amplitudes are used, starting from the strain amplitude used in the complex modulus test and ending with the strain amplitude used in the LRP test. This is done in order to have a measurement of the nonlinearity of the specimen tested using the LRP loading path. This information is used in order to interpret the test after. Between each of the loading sequences, 15min rest between each of the loading sequences and before the LRP test is allowed to the specimen.

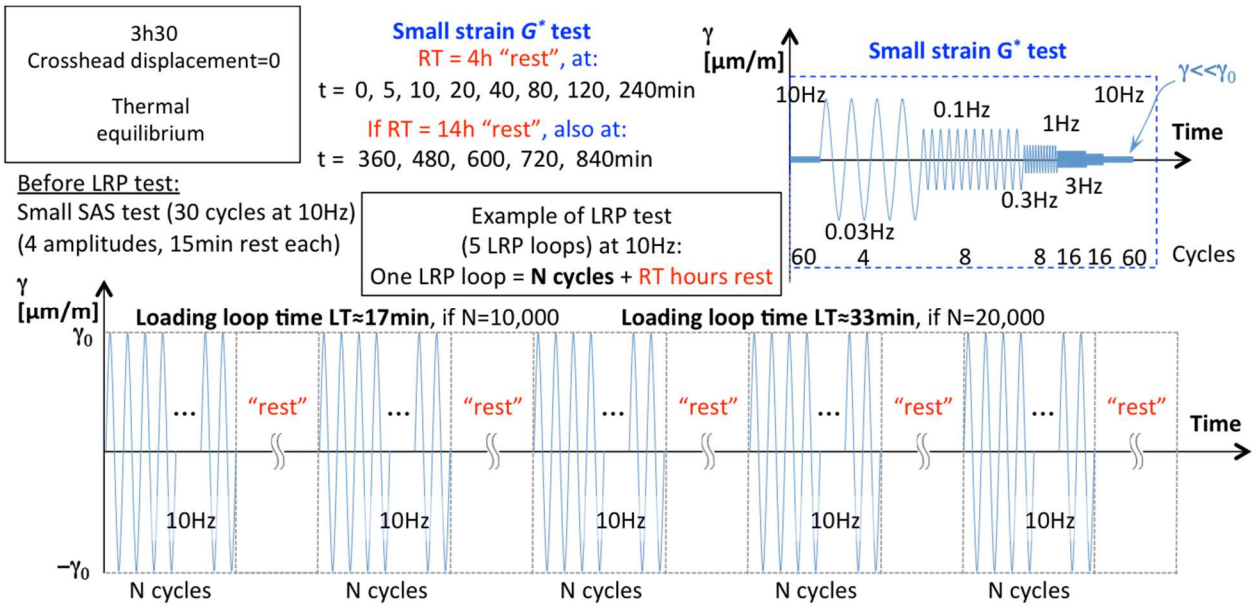

Figure 6-2. Scheme of Load and Rest Periods tests loading path, including representation of the applied strain amplitudes during loading and of the applied small strain amplitudes during rest.

Specimens used in LRP tests were bitumen B5070_A, B, C, D and E, and mastic M5070_30pc40-70_A, B and C. (cf. Table 3-1). Loading conditions (strain amplitude, number of cycles during loading loops and rest time applied during rest loops) are presented in Table 6-1. As seen in the table, bitumen specimen B5070_E was used to investigate the effect of longer loading and rest times.

Table 6-1. Specimens used in Loading and Rest Periods (LRP) tests and tested loading conditions (strain amplitude, number of cycles during loading loops and rest time applied during rest loops). All tests were performed using 5 LRP loops, started with mean in-specimen temperature of 11°C.

Material/Specimen	Strain Amplitude during LRP loading loops	Number of applied cycles during each LRP loading loop	Rest time during each LRP rest loop
B5070_A	10,000μm/m	10,000	4h
B5070_B	20,000μm/m	10,000	4h
B5070_C	3,600μm/m	10,000	4h
B5070_D	20,000μm/m	10,000	4h
B5070_E	20,000μm/m	20,000	14h
M5070_30pc40-70_A	3,300μm/m	10,000	4h
M5070_30pc40-70_B	8,500μm/m	10,000	4h
M5070_30pc40-70_C	1,000μm/m	10,000	4h

6.3. Complex shear modulus test results: the effect of temperature

The experimental results obtained from the complex shear modulus tests on bitumen and mastic have already been presented in detail in Chapter 4. Data is presented in Figure 4-22 and 2S2P1D model parameters in Table 4-10. In this chapter, the effect of temperature is investigated during LRP tests (loading at 10Hz) on bitumen and mastic. In-specimen temperature is measured, and the consequent effect of the temperature change must be evaluated. This temperature effect on the complex modulus is calculated by a combination of the 2S2P1D model and the WLF equation, fitted to the experimental results of complex shear modulus tests. Here, a focus on the effect of temperature is made, for complex modulus at a fixed frequency of 10Hz, in the temperature range from 10°C to 21°C. Figure 6-3 presents the complex shear modulus given by the combination of 2S2P1D model and WLF equation, with indication of temperatures used for the calculation of modulus at 10Hz. The figure shows the complex modulus in two representations: Cole-Cole plot and Black space (with natural non-log scale for the norm of complex modulus, as used throughout all this chapter).

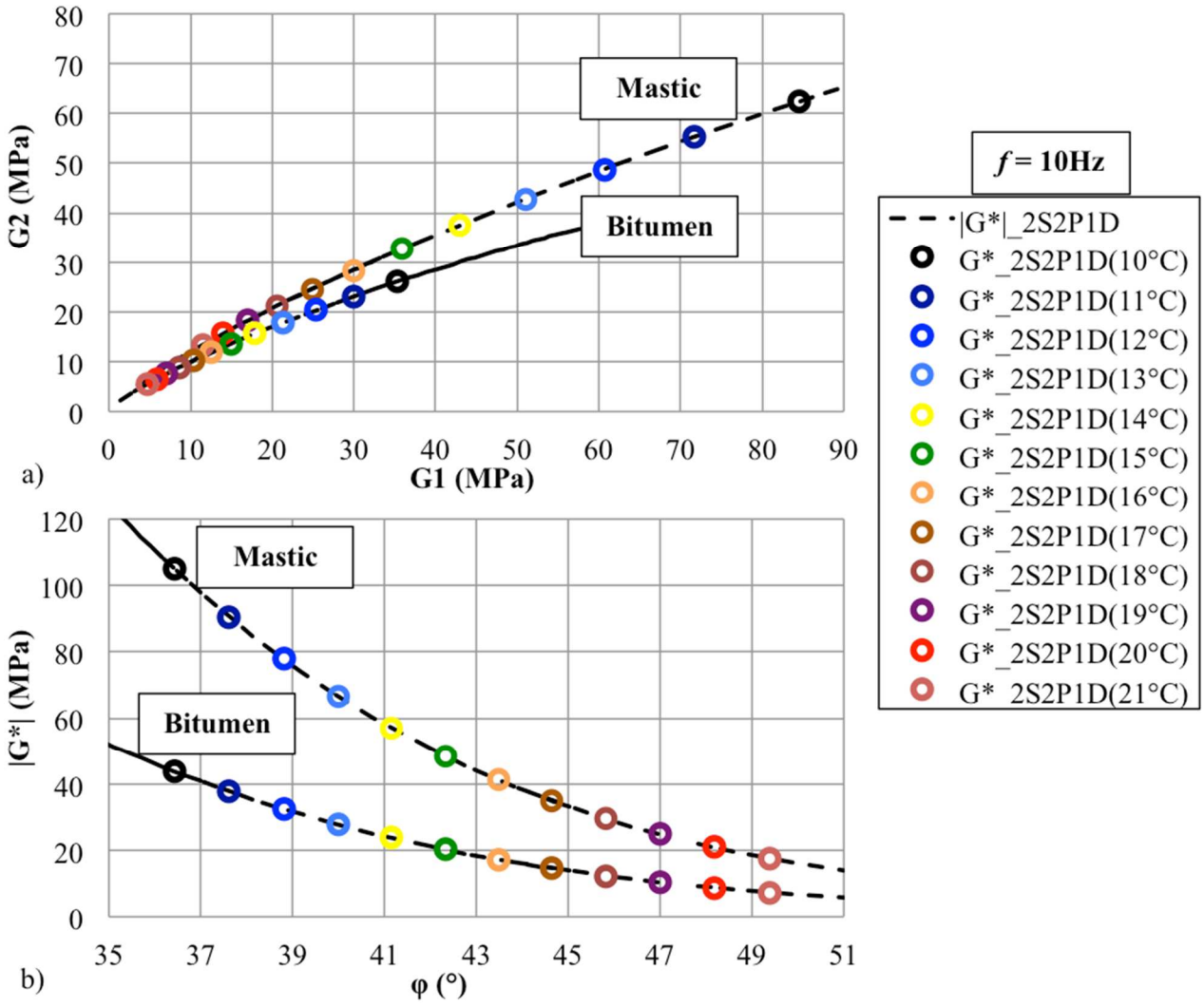

Figure 6-3. 2S2P1D model (cf. Chapter 4, Figure 4-22 and Table 4-10) for bitumen (B5070) and mastic (M5070_30pc40-70), with indications of complex modulus obtained at 10Hz at various temperatures from 10 to 21°C: Representation on a) Cole-Cole plot and b) Black diagram (with arithmetic scale for the norm of complex modulus).

From Figure 6-3b, it is possible to track the complex modulus change due to a temperature effect, i.e., if during a sinusoidal test a temperature increase is measured, the effect of the temperature on the modulus can be calculated (assuming LVE behaviour). For bitumen, a change in temperature from 11°C to 13°C produces a change in norm of complex modulus from 37.8MPa to 27.9MPa (26% decrease) and a change in phase angle from 37.6° to 40° (1.4° increase). For mastic, those changes are from 90.6MPa to 66.7MPa and 37.6° to 40° (same relative changes). With a higher temperature increase of 11°C to 16°C, the relative changes obtained are 55% and 3.6°C. Then, it is clear that depending on the temperature increase observed in the material, a major part of the complex modulus change during sinusoidal tests is due to a temperature effect. For the interpretation of the cyclic loading test results, this temperature effect on the complex modulus needs to be corrected. Since cyclic loading tests may use a different strain amplitude from the one used to fit the 2S2P1D model and the WLF equation, considerations on the temperature

effect at different strain amplitudes must be done. A detailed discussion on this is provided in Section 6.5.3.

6.4. ASA test results

The experimental results obtained from the ASA test performed on bitumen (B5070_G) are presented in Figure 6-4 in terms of the evolution of norm of complex modulus (figure a), phase angle (figure b), mean in-specimen temperature (figure c), and applied strain amplitude (figure d). Sinusoidal loading is applied at a constant frequency of 10Hz. Different strain amplitudes are applied in different loading blocks, without any rest between them. Extracting quantitatively the effects of all different physical phenomena on the measured complex modulus during this test is a difficult task. However, it is useful to observe qualitatively what happens i) when changing the applied strain amplitude and ii) when maintaining the application of this amplitude for many cycles.

In Figure 6-4a, it is seen that the first loading block, 100,000 cycles at 3,600μm/m, the modulus decreases from 44.6MPa to 41.0MPa (8% relative decrease), while the phase angle increases from 36.9° to 37.7° (0.8° relative increase) (cf. Figure 6-4b). This is accompanied by a temperature increase from 11.0°C to 11.6°C. This measured temperature increase is expected, at small strain (cf. Figure 6-3), to induce complex modulus relative changes of approximately the same values obtained experimentally (8% relative modulus decrease and 0.8° phase angle increase). During the following loading block (30,000 cycles at 10,000μm/m), modulus changes from 41.0MPa to 25.0MPa (39% decrease) and phase angle changes from 37.7° to 42.9° (5.2°). This time, the predicted complex modulus relative changes due to temperature increase, using the small strain 2S2P1D model are 36.4% for the modulus (approximately the experimental value), and 3.4° for the phase angle (1.8° less than the experimental value). It appears that, for this higher strain amplitude, other phenomena change the direction of the complex modulus change in Black space (there is more change in phase angle than what is expected as a consequence of self-heating in the LVE material). The following loading sequence presents a continuous increase in norm of complex modulus and a continuous decrease in phase angle during loading (there is no rest). Modulus changes from 25.0MPa to 34.8MPa (39% relative increase) and phase angle changes from 42.9° to 39.2° (3.7° decrease), while temperature is reduced from 14.5°C to 12.2°C. From the LVE behaviour of the bitumen, the expected changes in modulus would be from 22.0MPa to 31.5MPa (43% increase) and in phase angle from 41.7 to 39.0 (2.7° decrease). Again, this suggests that, although a change in norm of complex modulus in the same order is expected from LVE behaviour, the change in phase angle is lower than expected (not following the same direction in Black space, which indicates the presence of other phenomena). This analysis can be done for the following loading sequences with similar conclusions. Other important observation from the results presented in Figure 6-4 is that, at the end of each of the loading block, complex modulus change is small compared to the changes in the beginning of the same loading block. An asymptotic behaviour could be extrapolated. The asymptotic phase angles (Figure 6-4b) estimated this way seem to be the same for all loading blocks at the same strain amplitude: 38° at 3,600μm/m; 39° at 5,000μm/m; and more than 43° at 10,000μm/m. These coincidence in asyptotic values is not observed for the norm of complex modulus (Figure 6-4a), with the asymptotic value

decreasing from 41MPa to 33MPa to 30MPa, for the 1st, the 2nd, and the 3rd loading blocks at 3,600μm/m, respectively. These complex modulus measurements are obtained at the same temperature of 11.5°C. This indicates the accumulation of the effects of damage in the material behaviour. At the last loading block, which is similar to a fatigue test (continuous cyclic loading until failure), the specimen fails.

From the above analysis, it can be seen that, although at low strain amplitudes the observed complex modulus change seem to be due to the temperature increase due to self-heating, at higher strain amplitudes this is not the case. Also, the specimen seems to cumulate damage during the test. Qualitatively, the phenomena that may produce effects on the measured complex modulus during the ASA test may be commented as follows.

- Transient effects, which perturb the measurement of complex modulus for few (2 to 3) cycles after a sudden change in the applied strain amplitude (cf. Chapters 4 and 5). These first applied cycles after the transition present a deviation with respect to the sinusoidal functions (cf. Figure 4-20);
- Nonlinearity, that introduces an immediate (and reversible) change in complex modulus for a given strain amplitude change (cf. Chapter 4 for details on this phenomenon), producing either an decrease of norm of complex modulus and increase in phase angle as a consequence of an amplitude increase, or the inverse in the case of a decrease in amplitude;
- Temperature effect (cf. Figure 6-3), which produces either a “recovery” or a “loss” of the complex modulus, depending if the temperature is decreasing or increasing. As observed in Figure 6-4, a qualitative relationship can be established between complex modulus and temperature changes. At the tested loading conditions (11°C, 10Hz, systematically, when temperature increases norm of complex modulus decreases and phase angle increases. The opposite is observed when temperature decreases. That suggests an intimate relation between temperature changes and complex modulus evolution during cyclic tests (as investigated in Chapter 5). However, as it will be seen for the next tests, for which a more thorough quantitative investigation is presented, the temperature change alone is not sufficient to explain at the same time the norm of complex modulus changes and the phase angle changes;
- Thixotropy (cf. Chapters 1, 2 and 5), that can either produce a decrease or an increase in norm of complex modulus, depending on either the build-up phenomenon is being predominant over the breakdown in the bitumen (Barnes, 1997; Mewis & Wagner, 2009). It is expected that, after an increase in strain amplitude, the breakdown phenomenon (modulus “loss”) is predominant, while if strain amplitude decreases the build-up should prevail (modulus “recovery”). Then, with the continuous application of cycles at constant strain amplitude, the complex modulus continues to evolve in the same direction as observed due to nonlinearity. For example, after a sudden strain amplitude decrease, even keeping the strain amplitude constant, the modulus continuously increases (recovery of modulus during loading) and the phase angle continuously decreases (recovery of phase angle during loading);
- Damage, which always produces a decrease in norm of complex modulus. In classical damage mechanics, the phenomenon is seen as a loss in resistant cross-section of the

material. In the presented test results, it is possible to observe, from a loading block at a given strain amplitude to the next one at the same amplitude, that a decrease in norm of complex modulus is obtained. This shows that some unrecovered modulus decrease is produced due to damage. The same unrecovered change is not clearly observed for the measured phase angle. This is expected since, in principle, the loss in resistant cross-section should not have en effect on the phase angle. At the last loading block (classical fatigue test with 10,000μm/m strain amplitude), the specimen fails. This happens when the modulus is 70% lower to the initial measured modulus. This 70% decrease in modulus is a result of the effects of all referred phenomena combined.

The same results are presented in Figure 6-5 on a Black space, where the direction of the complex modulus change can be better observed. The failure zone is also depicted in the figure.

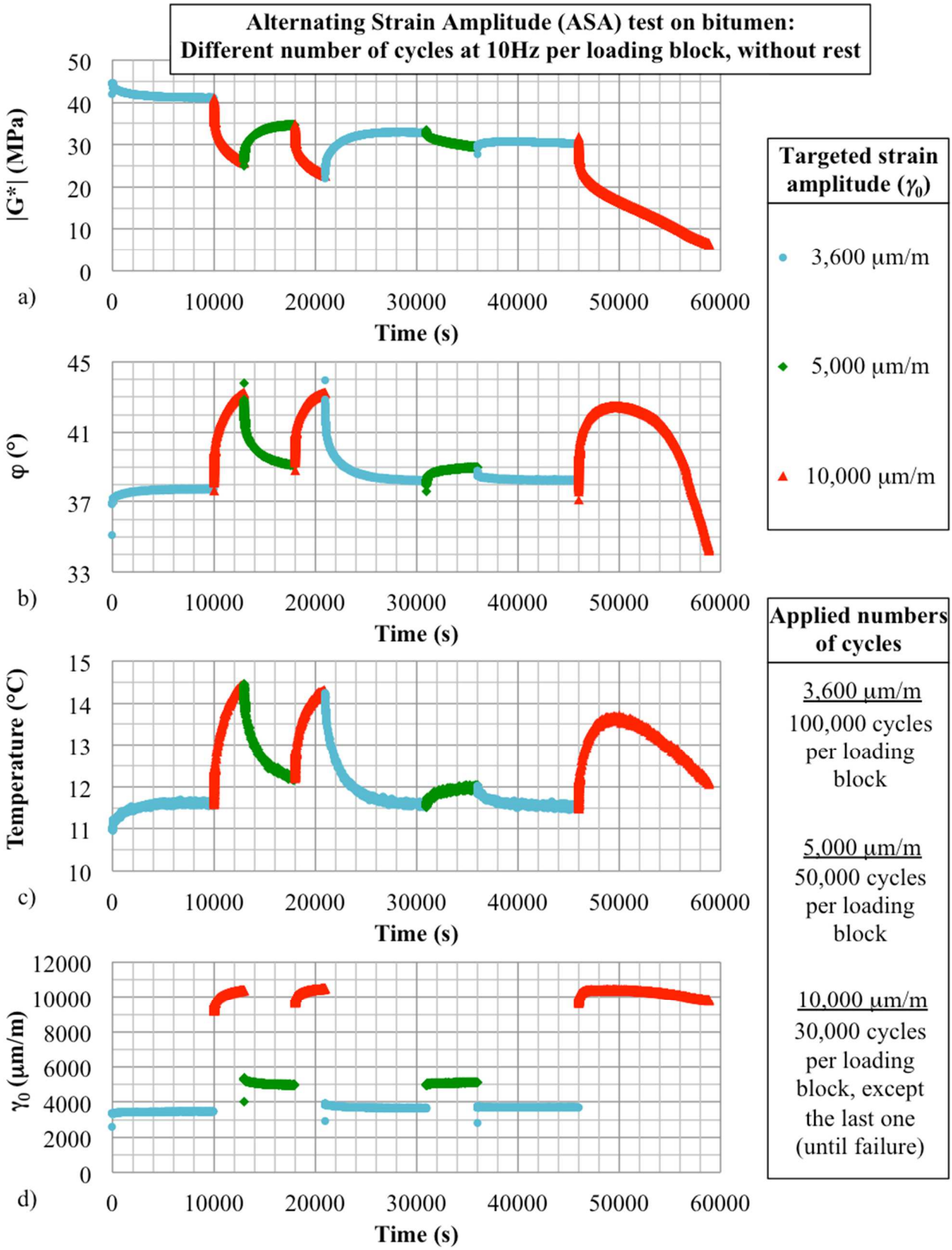

Figure 6-4. Alternating Strain Amplitudes (ASA) test results for bitumen (B5070_G): a) Norm of complex modulus, b) phase angle, c) mean in-specimen temperature, and d) shear strain amplitude as a function of time, for a test performed at constant frequency of 10Hz (1s = 10cycles).

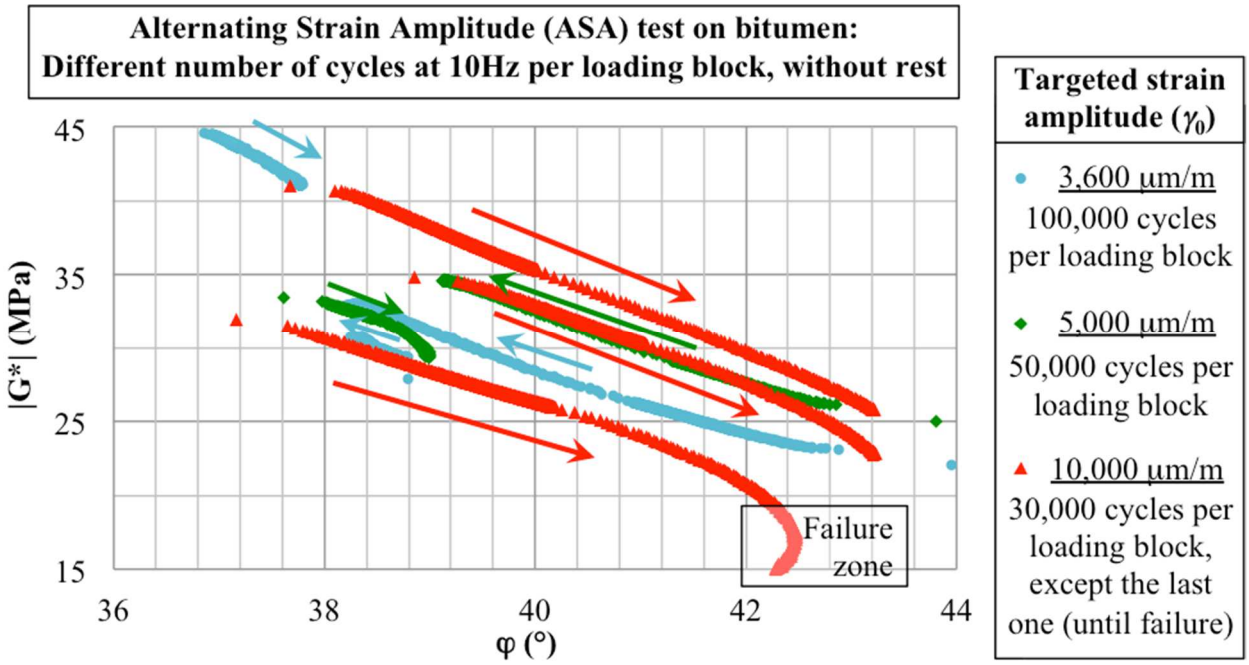

Figure 6-5. Alternating Strain Amplitudes (ASA) test results for bitumen (B5070_G) represented in Black space (natural non-log axis for norm of complex modulus as a function of the phase angle.

6.5. LRP test results: quantification of biasing effects on bitumen and mastic specimens

In this section, the results of Load and Rest Periods (LRP) tests (cf. Table 6-1) are analysed in order to quantify the effect of each of the investigated phenomena in bitumen and mastic during sinusoidal loading. A total of 8 LRP is analysed, 5 on bitumen and 3 on mastic. Different strain amplitudes are investigated. The effect of a longer rest period on the complex modulus is also investigated. Results for an example of test are discussed in details: 5 LRP loops on bitumen submitted to 10,000 cycles of 20,000µm/m sinusoidal loading followed by 4h rest (test on specimen B5070_D). The other test results are available on Appendix C, presented in the same figures as the example of test.

6.5.1. An example of LRP test results: 5 LRP loops with 10,000 cycles and 4h rest on bitumen submitted to 20,000µm/m sinusoidal loading

The test condition chosen as an example is the most extreme tested, in terms of the applied strain amplitude (cf. results and discussion on Chapter 4). Rigorously, due to non-negligible nonlinearity, the notion of equivalent complex modulus must be applied (cf. Sections 4.1 and 4.3.3). For simplicity sake, the equivalent complex modulus is called complex modulus or measured complex modulus in this chapter. It is the test performed on the bitumen specimen

B5070_D. The raw experimental data are presented in different figures, from Figure 6-6 to Figure 6-9, as follows:

- Figure 6-6 presents results of both the loading and the rest loops (where strain is controlled to produce no deformation in the specimen, except during very brief small strain complex modulus tests, cf. details on Section 6.2.3). It is to be underlined that the strain amplitudes used during loading and during rest are not the same. Then, even at constant temperature and with no effect of other phenomena (such as damage and thixotropy) the expected measured modulus is not the same due to nonlinearity (cf. Chapter 4). In Figure 6-6a, norm and phase angle of complex modulus are represented as a function of time. In Figure 6-6b, the applied strain amplitude and the temperature are represented as a function of time. Only the results of complex modulus measured at 10Hz are presented, even if other frequencies were also tested (cf. Figure 6-2). This is done in order to facilitate visualising and understanding the figure. Also, results at frequencies different from 10Hz during rest could not be directly compared to the results obtained during the loading loops. In Figure 6-6a, it is seen that while the norm of complex modulus is not fully recovered after 4h rest, the phase angle practically completely recovered. Since some fluctuation is observed in the measured temperature (of about 0.2°C) some fluctuation is also expected on the measured modulus and phase angle. It seems that the norm of complex modulus could have continued to recover after a longer period of rest, which is further discussed in Section 6.6. In Figure 6-6b, it is seen that the on-specimen strain amplitude is rather well controlled. After few seconds (few tens of cycles), the targeted strain amplitude is reached with good precision. PID control system was fin-tuned for each of the tests in order to obtain this result (cf. Table A-1). It is also seen that during rest loops the strain amplitude used in the small strain complex modulus tests is negligible when compared to the strain amplitude applied continuously during the loading loops. In the same figure, it is seen that the specimen temperature at the initial of a loading loop is recovered near the end of the 4h rest period. With the utilised test geometry and test conditions (10,000 cycles at 10Hz with 20,000μm/m strain amplitude, with the utilised thermal chamber), if less than 4h rest is used, the initial specimen temperature would probably not recover completely. As a complementary remark, it is seen in Figure 6-6b that the very first cycle of each loading loop has very different strain amplitude with respect to the others. This is due to a defect in the signal with respect to a sinusoidal function. This is expected at the first loading cycle due to the hydraulic press control system that is starting a sinusoidal loading from rest. This cycle must then be ignored from the analysis. Then, during the following cycles, the press control system will adjust the applied strain amplitude depending on the targeted strain amplitude, on the PID control parameters (cf. Table A-1), and on the material state.
- Figure 6-7 presents experimental results from the loading loops. The measured norm of complex modulus ($|G^*|$, figure a), the measured phase angle (φ, figure b), the measured mean in-specimen temperature (figure c), and the dissipated energy per cycle (figure d, $W_N = \pi|G^*|\sin(\varphi).\gamma_0^2$, where γ_0 is the applied shear strain amplitude) are represented as functions of the number of applied cycles during the test. It is possible to observe that the initial norm of complex modulus (Figure 6-7a) at each loading loop (which follows

from rest) seems to form a straight line, while the phase angle (Figure 6-7b) seems to practically completely recover after rest. The temperature measured during all the loading loops increases (of about 5°C at the first loading loop and of about 2.5°C at the last loading loop). It is also observed that, after the 4h rest between each loading loop, the specimen cools back to its initial temperature from before loading (Figure 6-7c). The dissipated energy during a loading loop decreases, because the norm of complex modulus decreases and the phase angle increases, changing the result of calculation ($W_N = \pi|G^*|\sin(\varphi).\gamma_0^2$). This energy turns at least partially into heat, inducing the 5°C temperature increase during the first loading loop, when the specimen is stiffer, and 2.5°C during the 5th loading loop, when the specimen is softer. The dissipated energy per cycle obtained during the test depends on the specimen temperature. Since temperature is changing during the test, during to self-heating, the dissipated energy also changes. Then, this parameter could only be an indicator of a change in the other phenomena (damage, for instance) if the temperature was considered constant.

- Figure 6-8 presents experimental results from the loading loops. The measured complex modulus is represented in a Black space (figure a) and in a Cole-Cole plot (figure b). In the Black space it is seen that approximately parallel curves are obtained. However, the evolution of complex modulus does not reach the same final value at the end of the loading loop. Since the temperature reached at the end of the first loops is higher, it was expected that the modulus would decrease more and the phase angle would increase more in the first loops. At the beginning of each of the loading loops (left-hand side of the figure), the initial complex moduli present approximately the same phase angle, between 38 and 39°. It is recalled that some effect of nonlinearity is expected since not exactly the same strain amplitudes were applied in these initial cycles. In the last loops, it is seen that the phase angle tends to vary less for the same variation of norm of complex modulus. This may be an indicator that the specimen is approaching the fatigue failure. In Cole-Cole plot, the same observations can be made, but it is less simple to read the results. At the beginning of each of the loading loops (right-hand side of the figure), the initial complex moduli present approximately the same phase angle (same slope of the line going from the origin to the complex modulus point). The norm of complex modulus (distance from the point to the origin) is higher for the initial loops. During each loading loop, the modulus evolves in the direction of the left-hand side of the Cole-Cole plot, with an increasing phase angle. Since the figure does not represent an orthogonal spatial system (x and y axis variations are not in the same length-scale in the figure), phase angle representation is dirtorted.
- Figure 6-9 presents experimental results from the loading loops. In these figures, complex modulus is normalised with respect to the initial complex modulus (at the first loading loop) at the tested strain amplitude. The values of the initial norm and phase angle of complex modulus, used for the normalisation procedure, are evaluated at the 3rd loading cycle. For this tests, these values were 38.8MPa and 38.7°, respectively. Figure 6-9a and Figure 6-9b present normalised norm of complex modulus, and normalised phase angle as a function of the number of applied cycles, respectively. Figure 6-9c presents the normalised norm of complex modulus as a function of the normalised phase angle (normalised Black space with respect to the complex modulus

at the 3rd loading cycle of the first loading loop). It is seen that during the 5 loading loops, more than 70% modulus decrease is observed. Depending on the loading loop, the phase angle increase varied from 5° to 11°. As seen before on Figure 6-7, temperature at the end of those loading loops varied from 2.5°C to 5°C. In Figure 6-9c the two first cycles with non-negligible transient effects are clearly seen for each of the loading loops. These effects are also present in the other figures presenting experimental results (cf. Figure 6-7b, Figure 6-7d, and Figure 6-8a). The measured complex modulus in these cycles cannot be used in the analysis of the material behaviour since they present significant deviation from sinusoidal signals (cf. Figure 4-20).

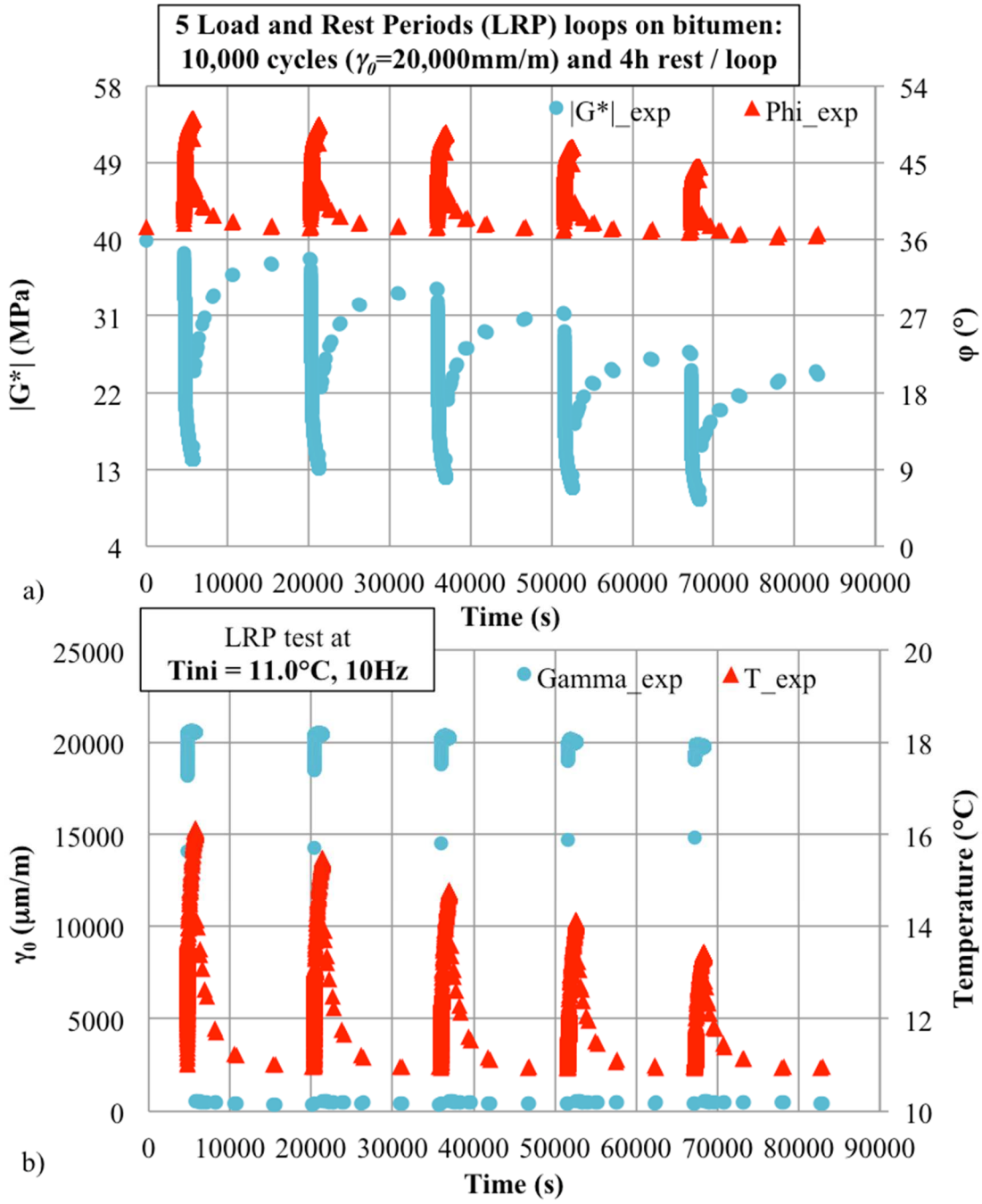

Figure 6-6. Experimental results (B5070_D) for LRP tests: 5 LRP loops with 10,000 cycles and 4h rest on bitumen submitted to 20,000µm/m sinusoidal loading: a) Norm of complex modulus and phase angle as a function of time, and b) shear strain amplitude and temperature as a function of time.

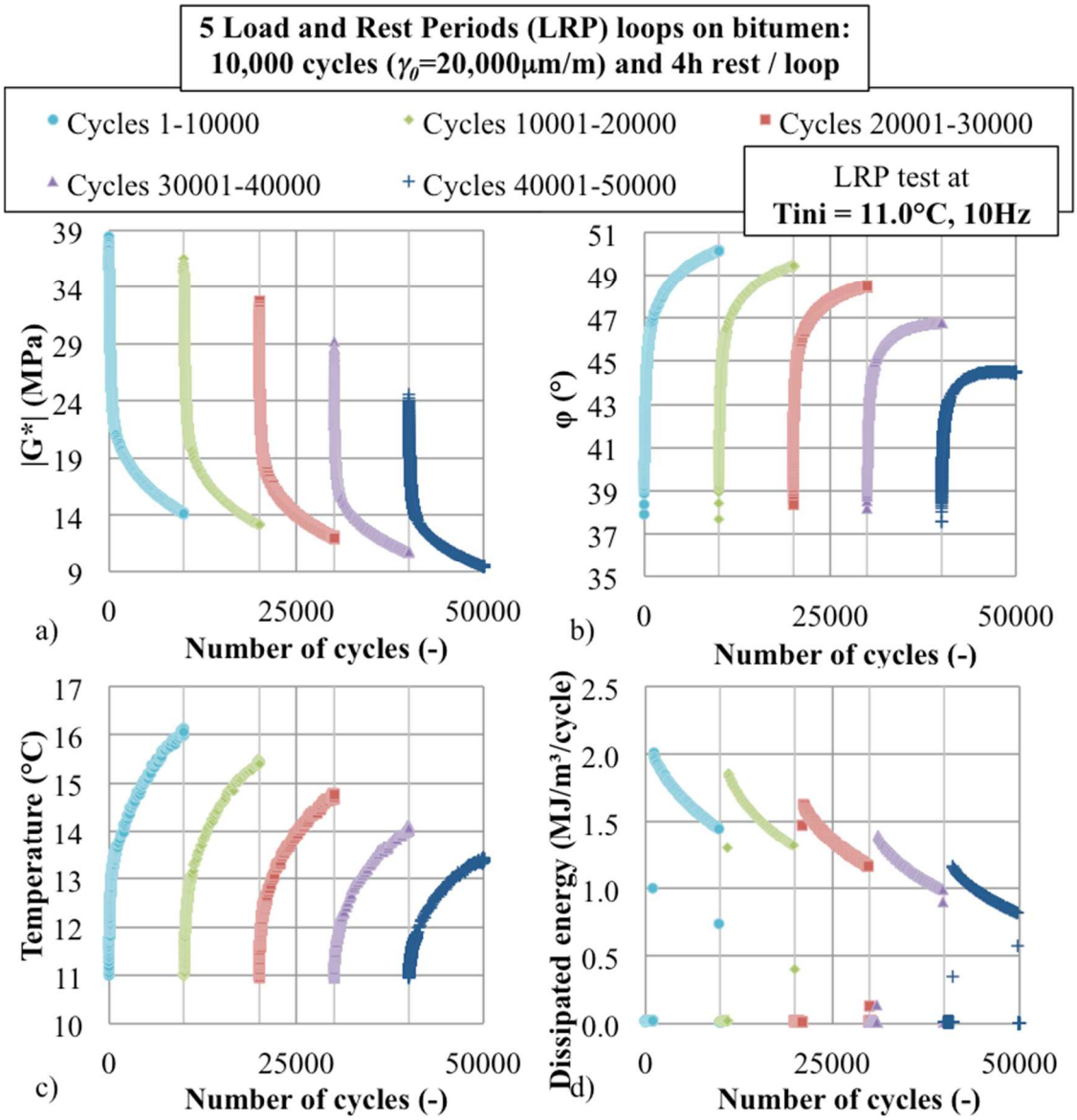

Figure 6-7. Experimental results (B5070_D) for LRP tests: 5 LRP 20,000µm/m sinusoidal loading loops with 10,000 cycles each on bitumen: a) Norm of complex shear modulus, b) phase angle, c) mean in-specimen temperature, and d) dissipated energy per cycle as a function of the number of applied cycles.

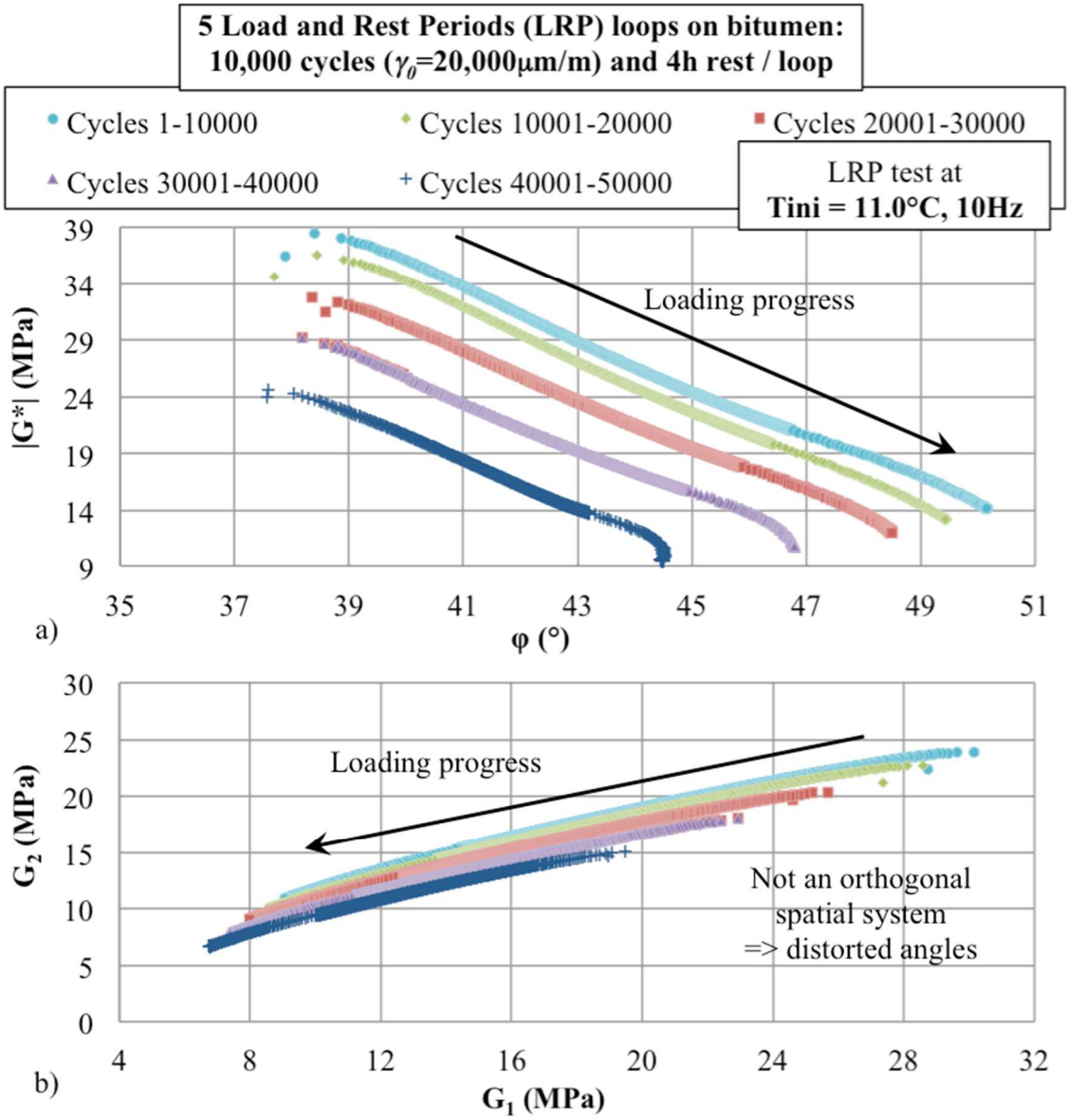

Figure 6-8. Experimental results (B5070_D) for LRP tests: 5 LRP 20,000µm/m sinusoidal loading loops with 10,000 cycles each on bitumen: representation on a) Black space, and b) Cole-Cole diagram.

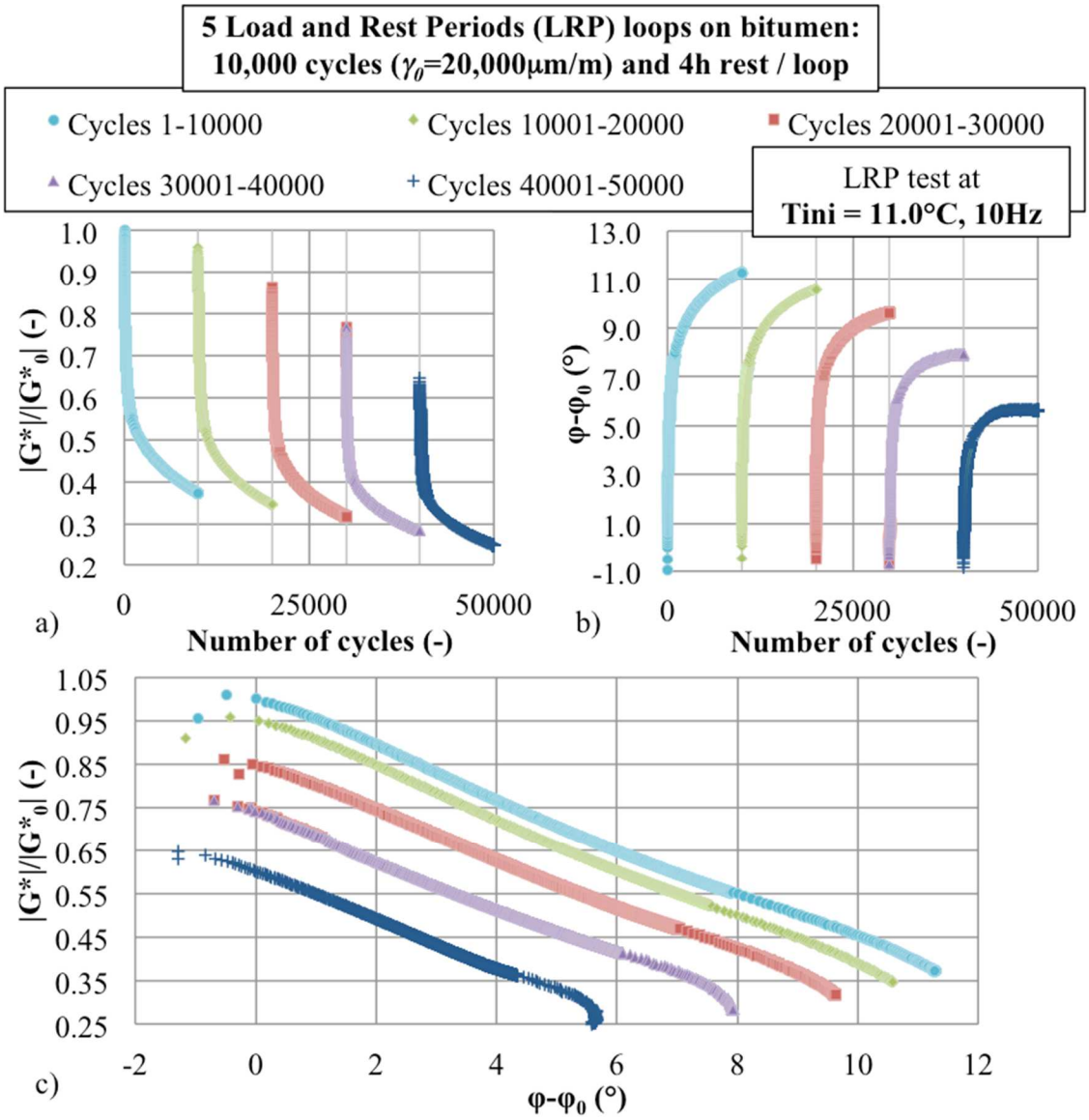

Figure 6-9. Experimental results (B5070_D) for LRP tests: 5 LRP 20,000µm/m sinusoidal loading loops with 10,000 cycles each on bitumen: a) Normalised (the initial modulus being considered as the result at the 3rd cycle) norm of complex shear modulus, and b) normalised phase angle as a function of number of applied cycles; and c) representation of the results on a normalised Black space.

6.5.2. Damage

In order to evaluate damage, the unrecovered complex modulus change after the 4h rest was evaluated. This was done by comparing trends in the complex modulus evolution (in Black space) at two regions of interest: i) at the end of rest periods two successive and ii) at the beginning of loading loops. Successive LRP loading loops are compared. A value of unrecovered norm of complex modulus is affected to each of the LRP loops in order to obtain equal complex modulus from a loop to the other, after accounting for this unrecovered complex modulus change. The unrecovered norm of complex modulus change is normalised with respect to the initial value of norm of complex modulus at the first loading loop, evaluated at the 3rd cycle (38.8MPa), in order

to obtain a relative modulus change. The resulting relative modulus change (left-axis in blue) and phase angle change (right-axis in green) are plotted in Figure 6-10 against the cumulated number of cycles applied during the LRP test. The figure presents results for four tests on bitumen (specimens B5070_A through D), at three different strain amplitudes (3,600μm/m; 10,000μm/m; and 20,000μm/m in figures a, b and c, respectively), and three tests on mastic (specimens M5070_30pc50-70_A through C), at three different strain amplitudes (1,000μm/m; 3,300μm/m; and 8,500μm/m in figures d, e and f, respectively).

Results show that, for all tests, a linear relationship between the unrecovered modulus and the applied number of cycles represents rather well the test results ($R^2 > 0.9$ for all tests presenting damage). As seen before (cf. Figure 6-6), some variation in the on-specimen strain amplitude is observed during the test. This is inherent to the press control system, working on a material whose mechanical properties are changing during the test. This variation induces, at least partially, the small deviation from a straight line observed in Figure 6-10.

As observed in Figure 6-10, no damage was observed after 50,000 cycles at 3,600μm/m on bitumen (figure a), and after 50,000 cycles at 1,000μm/m on mastic (figure d). Bitumen cumulated a 8.5% unrecovered change in norm of complex modulus after 50,000 cycles at 10,000μm/m (figure b), and 60% at 20,000μm/m (figure c). Mastic cumulated a 7% unrecovered change in norm of complex modulus after 50,000 cycles at 3,300μm/m (figure e), and 34% at 8,500μm/m (figure f). Observed unrecovered phase angle is less than 1° for all tests, except for one of the tests on bitumen at the highest strain amplitude (20,000μm/m), which had probably failed at the last LRP loop. This unrecovered change in phase angle is negligible in comparison to the unrecovered change in norm of complex modulus. Then, it is possible to state that damage provokes a change in norm of complex modulus that is not accompanied by a change in the phase angle, differently from the other phenomena studied in this research. This had also been previously observed in the literature (Gauthier et al., 2010). In Section 6.5.4, a damage correction is applied onto the test results, using the linear relationship with the number of applied cycles demonstrated in Figure 6-10. Figure 6-11, the relationship between the slopes of the unrecovered change in norm of complex modulus (considered as a result of fatigue damage) obtained from LRP tests on bitumen and mastic are plotted as a function of the applied shear strain amplitude. It is observed that the slope of damage grows rapidly when increasing strain amplitude and it is negligible for shear strain amplitudes of less than 3,600μm/m on bitumen and for less than 3,300μm/m on mastic. More data points would be needed o establish a more accurate relationship.

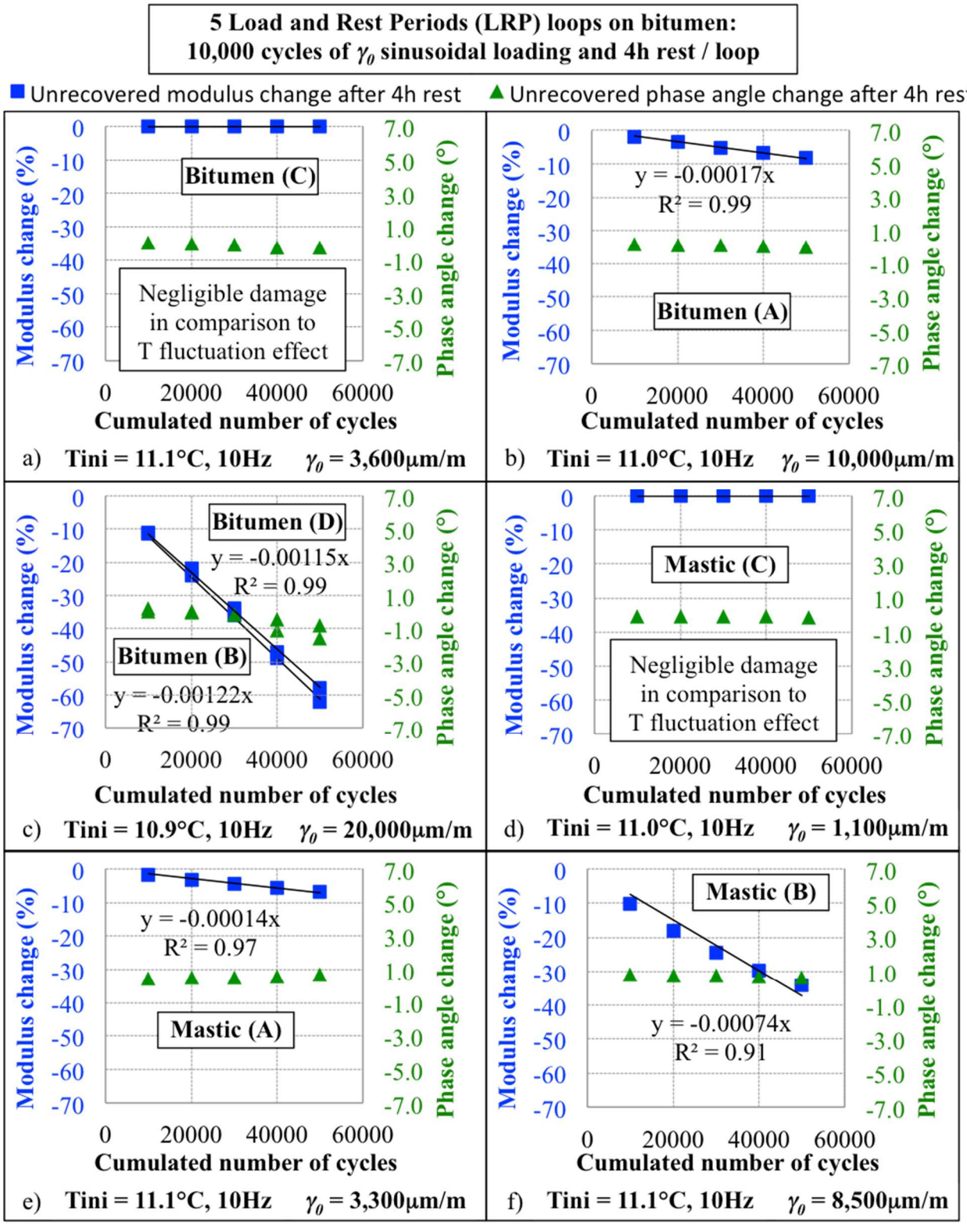

Figure 6-10. Experimental results for LRP tests: analysis of the unrecovered relative change in complex modulus after 4h rest: a) bitumen (B5070_C) with 3,600µm/m sinusoidal loading, b) bitumen (B5070_A) with 10,000µm/m, c) bitumen (B5070_B and B5070_D) with 20,000µm/m, d) mastic (M5070_30pc40-70_C) with 1,000µm/m, e) mastic (M5070_30pc40-70_A) with 3,300µm/m, and f) mastic (M5070_30pc40-70_B) with 8,800µm/m.

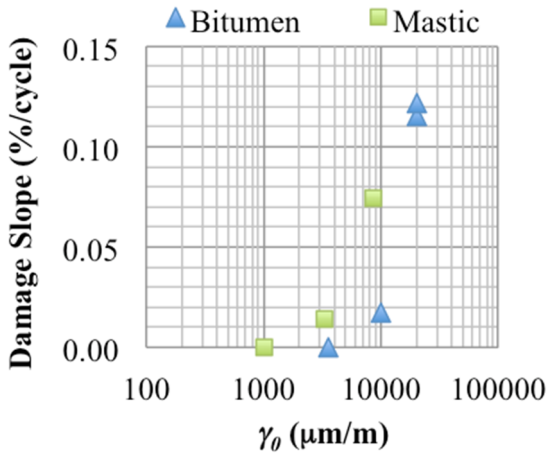

Figure 6-11. Slopes of the unrecovered change in norm of complex modulus obtained from LRP tests on bitumen and mastic as a function of the applied shear strain amplitude.

6.5.3. Nonlinearity and self-heating

In this section, the effect of two phenomena are evaluated in the LRP test: nonlinearity and self-heating (cf. Chapters 4 and 5, respectively, for a detailed analysis of those phenomena). The quantification of the effect of temperature on the measured complex modulus, based on the measured in-specimen temperature, is a necessary input for its correction. This information may be obtained using the 2S2P1D model combined to the WLF equation. Together, these models give complex modulus values for different measured temperatures, and hence, its information may be used in order to correct the effect of the self-heating phenomenon on the measured complex modulus. However, it is to be noticed that the 2S2P1D model represents the small strain complex modulus of the linear viscoelastic material. The information on thermo-sensitivity given by the WLF equation comes from complex modulus tests at small strain amplitudes, whereas the LRP tests results are obtained at higher strain amplitudes during the loading loops. Also, as demonstrated in Chapter 4, nonlinearity is dependent on the specimen temperature (cf. Figure 4-27). Then, a coupled effect of nonlinearity and self-heating is expected during LRP loading loops, since temperature at the end of the loading is higher than at the beginning. Then, the change in complex modulus calculated with 2S2P1D (small strain amplitude) cannot be directly applied in the investigation of the temperature effect on the measured complex modulus at high strain amplitude. In order to correct the effect of temperature for the results obtained from LRP tests, a supplementary hypothesis is needed. Also, a specimen-adjusted 2S2P1D model avoids sample-to-sample variation issues when calculating the effect of temperature for the LRP test specimen. In the following paragraphs, the 2S2P1D specimen-adjustment procedure, and the adopted hypothesis for the correction of the effect of self-heating (taking into account the coupled effect of the change in strain amplitude), are explained.

Nonlinearity of each specimen tested using the LRP loading path was evaluated using the small SAS test performed before the LRP test (cf. Figure 6-2). This provided a means of adjusting the previously obtained 2S2P1D model (cf. Figure 4-22 and Table 4-10 for a complete characterisation of small strain complex modulus) for each of the tested specimens, accounting for

sample-to-sample variation. Details on the test performed on bitumen specimen B5070_D are given next (cf. comments on Figure 6-14 presented later).

In Figure 6-12, the adopted hypothesis for the analysis of the temperature effect on the measured complex at high strain amplitude is explained. Figure 6-12a recalls the effect of temperature on the small strain complex modulus taking bitumen as an example (cf. Figure 6-3 for bitumen and mastic) in a Black diagram (norm of complex modulus in natural non-log axis). Figure 6-12b presents a scheme of the different complex moduli ($G^*(\gamma_{0,1})$ and $G^*(\gamma_{0,2})$) obtained at two strain amplitudes ($\gamma_{0,2} > \gamma_{0,1}$). The temperature effect on the measured complex modulus (T-effect) at small strain amplitude is represented, as well as the nonlinearity that is expected at the initial temperature (Tini) when changing from $\gamma_{0,1}$ to $\gamma_{0,2}$. After some time of sinusoidal loading, the temperature is different. Then, the expected nonlinearity is also different. This is represented in Figure 6-12c, as well as the T-effect at the new strain amplitude ($\gamma_{0,2}$). This T-effect at $\gamma_{0,2}$ is not known a priori and a hypothesis is needed for its calculation. The hypothesis used in this thesis is shown in Figure 6-12d: the ratio of the complex moduli at two different temperatures is independent of the applied strain amplitude. The consequences of this hypothesis on the phase angle and on the norm of complex modulus are:

- Phase angle change ($\Delta\varphi$ (T) = φ (T) - φ (Tini)) due to T-effect is independent of the strain amplitude. Then, the corrected phase angle at a given strain amplitude ($\varphi_{T\text{-}corrected}$) can be obtained from the measured phase angle ($\varphi_{measured}$ (T)) and the calculated phase angle change with 2S2P1D ($\Delta\varphi_{2S2P1D}$ (T)) (cf. Eq. 6-1);
- Norm of complex modulus change (($\Delta|G^*|$ (T) = $|G^*|$ (T) - $|G^*|$ (Tini)) due to the T-effect is dependent on the strain amplitudes (cf. Figure 6-12d). Then, the corrected norm of complex modulus at a given strain amplitude ($|G^*|_{T\text{-}corrected}$) can be obtained from the measured norm of complex modulus ($|G^*|_{measured}$ (T)) and the calculated norm of complex modulus relative change with 2S2P1D ($\Delta|G^*|_{2S2P1D}$ (T)/$|G^*|_{2S2P1D}$ (Tini)) (cf. Eq. 6-2).

$$\varphi_{T-corrected} = \varphi_{measured} - \Delta\varphi_{2S2P1D}(T, Tini) \quad \text{Eq. 6-1}$$

$$|G^*|_{T-corrected} = |G^*|_{measured} \Big/ \left[1 + \frac{\Delta|G^*|_{2S2P1D}(T, Tini)}{|G^*|_{2S2P1D}(Tini)}\right] \quad \text{Eq. 6-2}$$

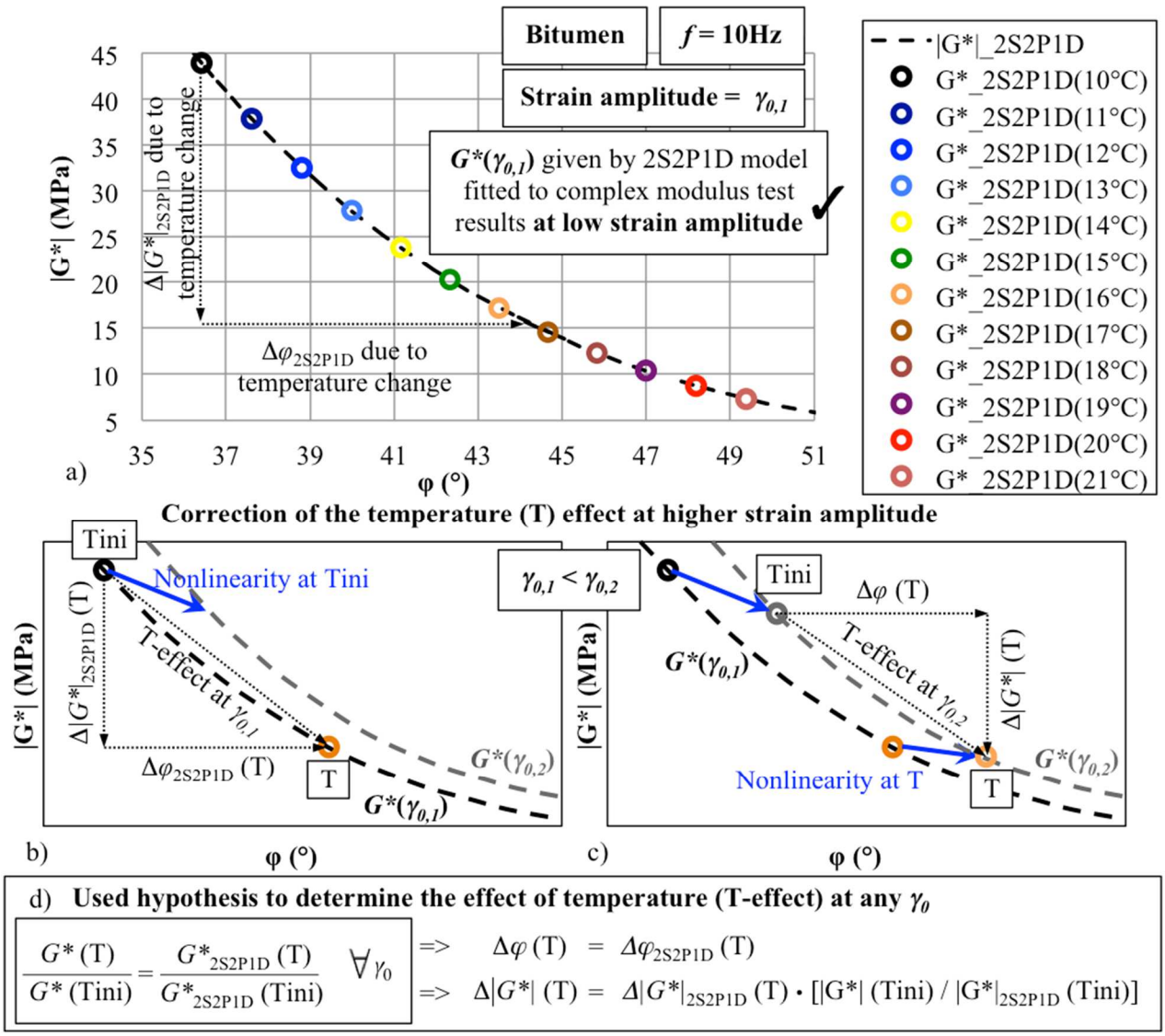

Figure 6-12. Scheme of the utilised correction for the temperature effect (T-effect) on the complex modulus, with an example for bitumen (the hypothesis for correction is the same for mastic). The correction uses as input parameters the 2S2P1D complex moduli (G^*_{2S2P1D}, fitted for low strain amplitudes) at the initial (Tini) and the current (T) measured temperatures, and the measured complex modulus (G^*) during the LRP test (performed at higher strain amplitudes). a) Complex modulus at different temperatures on a Black diagram (cf. Figure 4-22 and Table 4-10 and Figure 6-3). b) Temperature effect on the calculated 2S2P1D complex modulus (low strain amplitude, $\gamma_{0,1}$) and indication of nonlinearity effect on . c) Scheme of the temperature effect on the measured complex modulus (at higher strain amplitude, $\gamma_{0,2}$), after the effect of nonlinearity is obtained (cf. Chapter 4).

Firstly, using the presented calculation hypothesis for the temperature correction at any strain amplitude, the possibility to explain the observed variations in complex modulus during a LRP test is investigated. The first 10,000 cycles from LRP test on bitumen specimen B5070_D are chosen for this analysis. Two temperature evolutions are calculated: i) the temperature evolution necessary to explain the phase angle variations during loading, and ii) the temperature evolution necessary to explain the norm of complex modulus variations during loading. The results are then compared to the measured mean in-specimen temperature. From the figure, it is seen that both the necessary

temperatures to explain complex modulus variation during loading are higher than the measured in-specimen temperature. At the end of the 10,000 cycles, to explain the modulus variation a temperature of 17.3°C (6.3°C increase) would be required, to explain phase angle variation a temperature of 20.7°C (9.7°C increase) would be required, while the measured temperature is 16.1°C (5.1°C increase). Not only the necessary temperatures to explain norm of complex modulus variations and phase angle variations observations are not reached, but also they diverge (variation to explain norm of complex modulus is 90% higher than the measured one, while the one to eplain phase angle variation is 24%). This means that, in complex representations (such as Black space), the complex modulus variation during loading does not follow the same direction as the one of a temperature change. This demonstrates that self-heating is not the only phenomenon behind the observed complex modulus changes during loading, and justifies the following analyses. The results of calculated temperatures are obviously influenced by the adopted calculation hypothesis (cf. Figure 6-12). However, it is unlikely that another physically acceptable hypothesis would produce results of calculated temperature increases explaining at the same time the norm of complex modulus and the phase angle changes observed during cyclic loading.

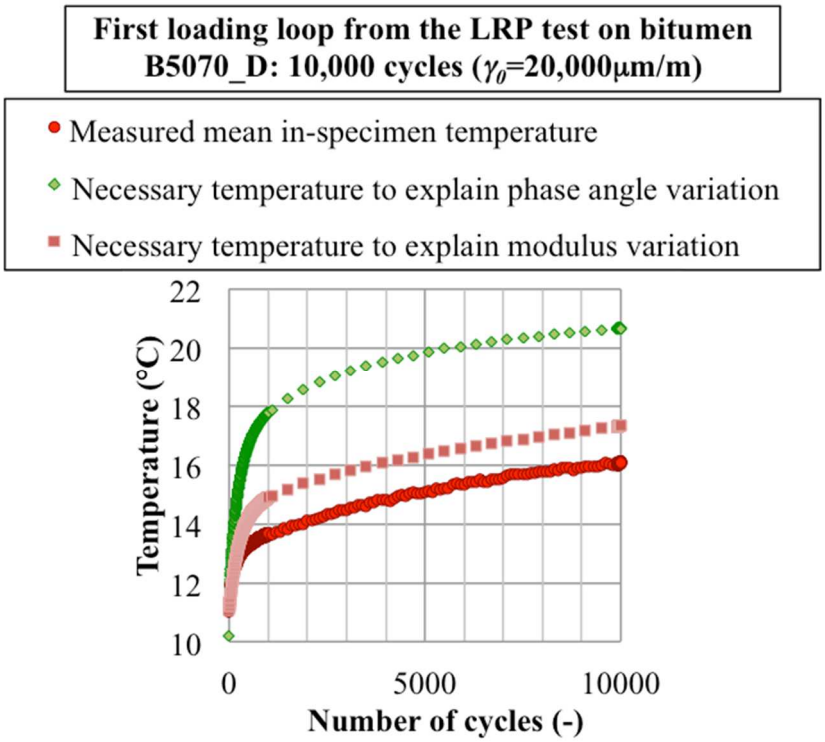

Figure 6-13. Temperature evolution as a function of the number of applied cycles during the first loading loop of LRP test on bitumen specimen B5070_D. Three temperature evolution curves are presented: measured mean in-specimen temperature, necessary temperature to explain phase angle variation during loading, and necessary temperature to explain modulus variation during loading.

Figure 6-14a presents the measured complex modulus during the 5 LRP loops on bitumen specimen B5070_D. It also presents results from a 2S2P1D model (combined with WLF equation), which represents what should be expected as a change in small strain complex modulus due to the temperature effect. In the figure, for each of the loading loops, cycles #3, 10, 30, 100,

1,000, and 10,000 are represented with special markers, which allow identifying the progress of the loading. The same is made for the rest loops, where the rest time can be tracked by special markers, which differ between the different rest loops.

Using the measurement of nonlinearity (from the small SAS test performed before the LRP test) it is possible to calculate the small strain complex modulus of the specimen, accounting for sample-to-sample variation. The measured complex modulus at the 3rd loading cycle (avoiding transient effects) was used in order to back-calculate the small strain complex modulus. Its value is 38.8MPa modulus and 38.7° phase angle, as previously stated. From the small SAS tests on B5070_D, it was determined that, on this bitumen specimen, nonlinearity produces an effect of 6.3% modulus decrease and 1.7° phase angle increase when changing strain amplitude from the one used in small strain complex modulus tests to the one used during LRP loading loops. The small strain complex modulus back-calculated this way is 41.4MPa modulus and 37.0° phase angle. The resulting small strain complex modulus is represented by a blue triangle in Figure 6-14a and b. Another calculation of this small strain complex modulus is made using the 2S2P1D model and the WLF equation (cf. Figure 4-22 and Table 4-10). The resulting small strain complex modulus is represented by a blue circle on the 2S2P1D line in Figure 6-14a and b. Since these two results should be coincident (which is not the case due to sample-to-sample variation), this process provides a means of fine-tuning the 2S2P1D model for the LRP test specimen. This was done by changing only the asymptotic elastic moduli parameters (G_0 and G_{00}) and the characteristic time parameter ($\tau_{0,G}$). The specimen-adjusted parameters are given in Figure 6-14 (G_0 = 940MPa and $\tau_{0,G}$ = 5.2×10^{-5}s, slightly changed with respect to the original values of G_0 = 920MPa and $\tau_{0,G}$ = 4.4×10^{-5}s). Then, the effect of nonlinearity obtained at the very beginning of the test is represented by a blue arrow linking the small strain complex modulus (coincident blue triangle and circle) and the measured complex modulus at the 3rd cycle. This arrow gives the direction of nonlinearity, and its intensity, at the initial temperature. In order to calculate the effect of nonlinearity between the end of the load loop (high strain amplitude) and the beginning of the rest loop (small strain amplitude), the hypothesis explained in Figure 6-12 is used. The second blue arrow, pointing in the reverse direction ("recovery" of complex modulus, due to the decrease in strain amplitude), is represented going from the point representing the measured complex modulus 10,000th loading cycle. It is seen that the other end of the arrow is very close to the complex modulus measured at the first small complex modulus test at small strain amplitude. Less than 0.1MPa error in modulus and less than 0.2° error in phase angle is obtained, which justifies the adopted hypothesis for the correction of the temperature effect on the complex modulus.

Then, the phenomenon of self-heating was evaluated by combining the measured mean in-specimen temperature and the specimen-adjusted 2S2P1D model. Combined with the hypothesis for correction of the temperature effect on the measured complex modulus (cf. Eq. 6-1 and Eq. 6-2), this gives the complex modulus after correction of the temperature effect, presented in Figure 6-14b. In this figure, the effects of nonlinearity (explicitly indicated in the end and in the beginning of loading), damage, and possibly another phenomenon, still appear. This other phenomenon is shown to recover after rest, and is, thus, reversible. It is hypothesised in this research as thixotropy.

Figure 6-14b adopts the same labelling system as Figure 6-14a, which allows tracking the progress of the LRP test. It is seen in the figure that, in the tested conditions (20,000μm/m), the

change in complex modulus from the 3rd cycle to the 100th cycle (around 5MPa in modulus and 2° in phase angle) is approximately the same as from the 100th cycle to the 1,000th cycle. Also, these changes are much higher than the one observed from the 1,000th cycle to the 10,000th (less than 2MPa in modulus and less than 1° in phase angle). Since nonlinearity, self-heating and thixotropy are phenomena that stabilise with time, it is possible to conclude that the effect of damage during the 10,000 first cycles of loading is small compared to the other effects combined. This demonstrates the need for taking into account the reversible phenomena when analysing the complex modulus change during fatigue tests.

Another result from the interpretation of Figure 6-14b is that, in the tested conditions, all the complex modulus change cannot be explained by a temperature effect. The complex modulus evolution does not follow the same direction as the one of a temperature change. For this test, approximately half of the change in complex modulus can be explained by the measured temperature, which increased by 5°C during the first loading loop (cf. Figure 6-6).

Finally, after temperature correction, approximately parallel lines for each of the loading loops are obtained. This suggests again that the damage cumulated in each of the loading loops is equal, producing an even modulus loss after a given amount of cycles. This is an indication that the hypothesis of damage being produced uniformly on the norm of complex modulus for cycles at fixed strain amplitude can be applied (cf. Figure 6-10). Phase angle variation due to damage is negligible. This linear relationship of the norm of complex modulus with the number of applied cycles at fixed strain amplitude is used in the next section (Section 6.5.4) in order to correct the effect of damage on the complex modulus.

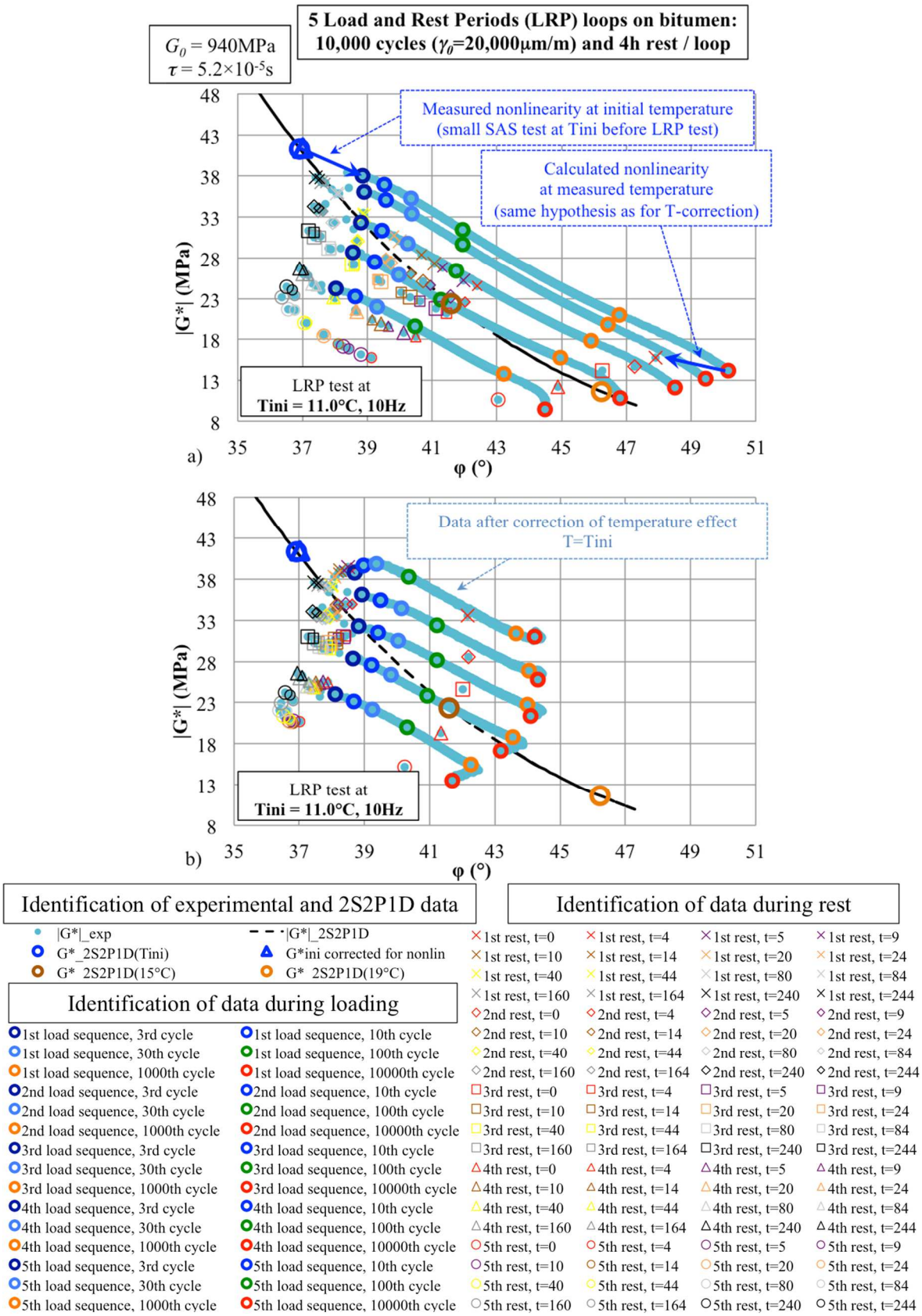

Figure 6-14. Experimental results (B5070_D) for LRP tests (5 LRP tests with 10,000 cycles of 20,000µm/m sinusoidal loading and 4h rest loops on bitumen): a) Black diagram representation of the results including details of the number of cycles during loading and the time of rest during rest periods, and a representation of the nonlinearity effect; b) results after temperature correction. The figure present also a 2S2P1D model prediction, with indication of LVE complex modulus at 10Hz and three temperatures, 11.1°C (Tini), 15°C and 19°C.

6.5.4. Thixotropy

Based on the conclusions previously presented (cf. Figure 6-10 and Figure 6-14) concerning the complex modulus evolution due to damage (linear relationship with the number of applied cycles at a given strain amplitude, cf. Figure 6-10 for the values of damage used in the correction), experimental data were corrected for this phenomenon. Figure 6-15a presents on a same graph the data from Figure 6-14a (measured complex modulus results) and from Figure 6-14b (complex modulus results after correction of the temperature effect), without all the details on the LRP test progress, facilitating visualisation. By applying the damage correction hypothesis (linear relationship with the number of applied cycles at fixed strain amplitude) with the results obtained after the correction of temperature effect, a new data set is obtained. These data, presented in Figure 6-15b, is corrected for the effect of temperature and damage on the measured complex modulus. All data points from loading and rest loops are presented. They form a unique curve, where only the effects of nonlinearity and thixotropy have not been corrected. Nonlinearity is still seen in the noticeable difference between the cycles at small strain amplitude during rest (at the upper left corner of the graph, relatively high modulus and low phase angle) and the cycles at higher strain amplitude during loading. The direction of nonlinearity, obtained for the tested specimen and presented before in Figure 6-14a, is again represented on this figure. It is seen that in Black space (natural non-log axis for the norm of complex modulus) this direction is parallel to the one of the curve obtained after the correction of the effects of temperature and damage. It seems then that the direction of nonlinearity and thixotropy is the same. This was observed for both bitumen and mastic (cf. Appendix C for results at different strain amplitudes on bitumen and mastic). This provides evidence for an intrinsic relation between nonlinearity and thixotropy. It seems that thixotropy provokes a delayed complex modulus change in the same direction as nonlinearity. This is possibly due to a common microstructural origin of these phenomena, as observed in shear-thinning and thixotropic fluids (Barnes, 1997; Mewis & Wagner, 2009), which include some colloidal systems. In these materials, shear-dependent thermodynamically stable microstructures (from by inter-particle attractions) are obtained after a period of shearing. If these stable microstructures are obtained instantly, no thixotropy (which is a change over time) is observed. This definition is similar to the one used for the effect of nonlinearity in this thesis: a reversible strain-dependent complex modulus change. If the metastable microstructures take time to be reached, then thixotropy is observed. From the obtained experimental results, it seems that in bitumen and mastic, a part of the complex modulus change occurs instantly (compared to the time for one cycles, 0.1s seconds), while the other develops with time. For the test conducted on bitumen B5070_D with 20,000μm/m strain amplitude, approximately 4MPa and 2° complex modulus change seems to come instantly (nonlinearity) and 10MPa and 5° complex modulus change seems to come with time (thixotropy), with this maximum complex modulus change occurring after a number of cycles between 4,500 or 5,500 (between 7.5min and 9.2min of loading at 10Hz), depending on the analysed loading loop on B5070_D.

In Figure 6-15b, it is also seen that in the end of the 3 first loading loops, the effect of thixotropy seems to reverse, and slightly change direction. Still, this reversion and change in direction is small compared to the changes observed during a whole loading loop. It is possibly due to a temperature dependence of the thixotropy effect. In this test, temperature increases from 4 to 6°C were observed at the end of the 3 first loading loops. In the other tests (lower amplitudes

and temperature increases during the loading loops), this effect is less pronounced (cf. Appendix C).

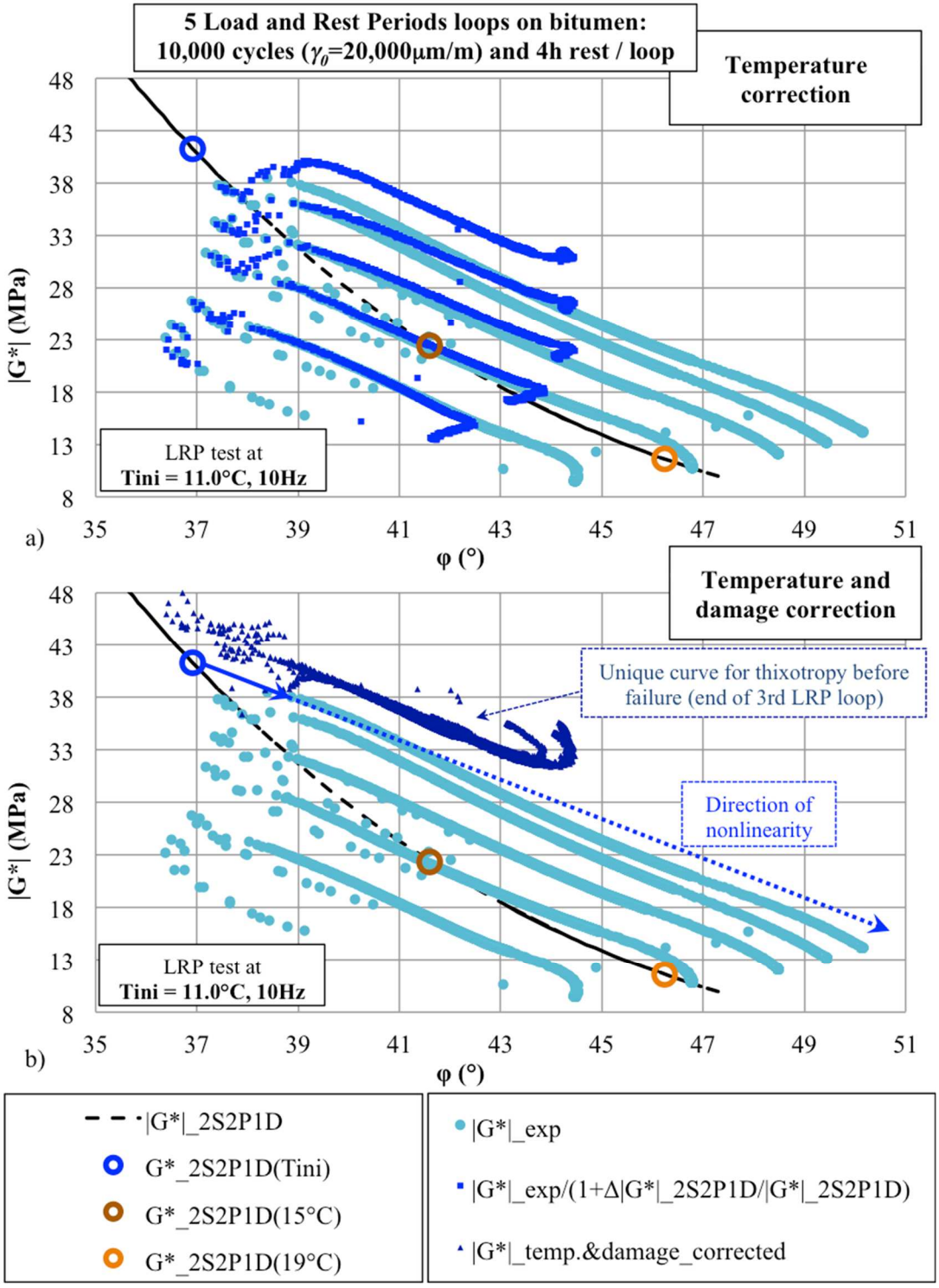

Figure 6-15. Experimental results (B5070_D) for LRP tests (5 LRP tests with 10,000 cycles of 20,000µm/m sinusoidal loading and 4h rest loops on bitumen): Black diagram representation of a) the raw experimental results and the results after the temperature correction and b) the experimental results after temperature and damage correction. The figure present also a 2S2P1D model prediction, with indication of LVE complex modulus at 10Hz and three temperatures, 11.1°C (Tini), 15°C and 19°C.

6.6. Number of cycles and rest time effect

In this section, the effect of the duration of the rest time is evaluated using a LRP test on bitumen (specimen B5070_E) with rest loops of 14h. The loading loops present 20,000 cycles instead of the 10,000 cycles used in the previously presented LRP test. The same strain amplitude was used, i.e. 20,000μm/m. Figure 6-16 presents the obtained results for the longer LRP test in terms of the measured norm and phase angle of complex modulus (Figure 6-16a) and the applied strain amplitude and mean in-specimen temperature (Figure 6-16b) as a function of the testing time. This figure presents the same axes (same scale) as the one displaying the results for the shorter LRP (Figure 6-6).

During the first loading loop (20,000 cycles), the specimen presented a total norm of complex modulus decrease of approximately 70%, with no sign of fatigue failure (no inversion in the trends of norm of complex modulus and phase angle, no disturbance in the strain control system). Signs of fatigue failure appear in the third loading loop. In the shorter test, the modulus decrease at the end of the first loading loop (10,000 cycles) was approximately 65%, i.e. 10,000 more cycles only led to a 5% more modulus decrease. When it comes to the phase angle, the observed increase in the longer test is around 12.5°, while it was of 12° in the shorter LRP test. The temperature increase during the longer loop is around 7°C, while it was 5°C in the shorter loop. Even with this difference in the temperature increase, after 4h of rest, initial temperature of 11°C was obtained (within the thermocouples measurement precision).

During the rest loops, it is seen that the phase angle recovery happens as fast as the temperature decrease during the first 4h (specimen cooling back to the initial temperature). During the next 10h of rest, negligible variation is observed in the phase angle. However, some modulus recovery is still observed after the first 4h, even if it happens much slower than what has been seen for the first 4h. The effect observed is a slow modulus recovery with negligible phase angle variation (vertical direction in Black space). The only phenomenon described before presenting this particular direction in Black space was damage, with a decreasing norm of complex modulus (the opposite of the observed effect for long periods of rest). This secondary effect of modulus recovery (with negligible phase angle variation), which may be seen as caused by the phenomenon called “self-healing” in the literature (Bhasin et al., 2008; Canestrari et al., 2015; Daniel & Kim, 2001; Karki et al., 2015; Palvadi et al., 2012), produces a modulus recovery during LRP tests much less important than what is being treated as thixotropy in this thesis (it is possible to observe that modulus recovers approximately 2.5MPa with less than 0.5°C recovery of phase angle after 10h of rest, while during 4h 23MPa and 13° variation had been observed). The phenomena differ on their fundamental explanation (self-healing is a consequence of the closure of micro-cracks produced by damage, while thixotropy is a consequence of a reversible weakening of the bitumen microstructure). They also differ on the rate they seem to produce an effect on complex modulus, thixotropy happening faster. During the first 4h of rest, the effect of self-healing seems negligible compared to the effect of thixotropy and temperature, which validates the 4h rest LRP test interpretation presented before. Finally, the directions of these phenomena on Black space are not the same, since thixotropy shares direction with nonlinearity and self-healing seems to slightly recover modulus with negligible change in phase angle.

Figure 6-17 presents in Black space the measured complex modulus on both the shorter and the longer LRP tests presented. During the longer LRP test, after a cumulated number of cycles of 92,420 (5th loading loop), the specimen completely broke and on-specimen strain controlled became impossible, no further cycles data being presented. From the third loading loop, signs of fatigue failure were appearing, with an inversion in the trend of phase angle. The total modulus decrease observed during the 20,000 cycles loading loop is comparable to a modulus decrease produced by a change in temperature from 11°C to 19°C, as shown in the 2S2P1D model curve (same one as in Figure 6-14). It is recalled that the temperature increase measured at the end of this loading loop was from 11°C to 18°C. When looking to the measured complex modulus during the longer periods of rest, it is possible to observe that modulus recovers (approximately 2.5MPa) with very small recovery of phase angle (less than 0.5°C). This may be linked to the commented "self-healing" phenomenon. Since, during the first 4h, the recovery of modulus was of approximately 23MPa, and of phase angle of about 13°, this phenomenon is considered to produce only a secondary effect during the first 4h of rest. This validates the analysis for the LRP tests with 4h of rest. As observed in the literature, while after a rest period of 4h where significant recovery is observed in bituminous mixture material properties (following 25% modulus decrease during loading), negligible effect is measured at 20°C during rest from 4h to 8h (Isailović et al., 2017).

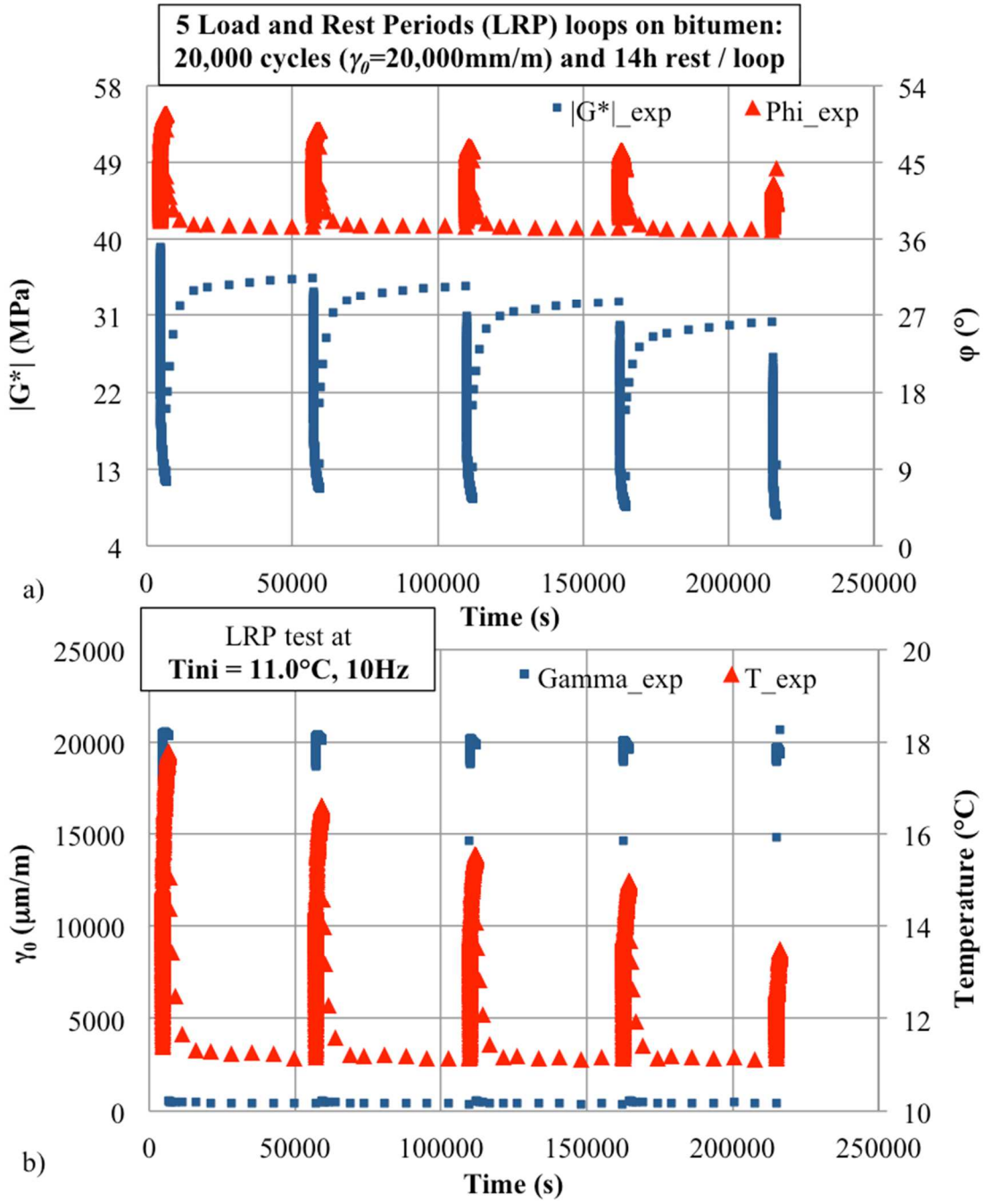

Figure 6-16. Experimental results (B5070_E) for LRP tests: 5 LRP loops with 20,000 cycles and 14h rest on bitumen submitted to 20,000µm/m sinusoidal loading. a) Norm of complex modulus and phase angle as a function of time, and b) shear strain amplitude and temperature as a function of time.

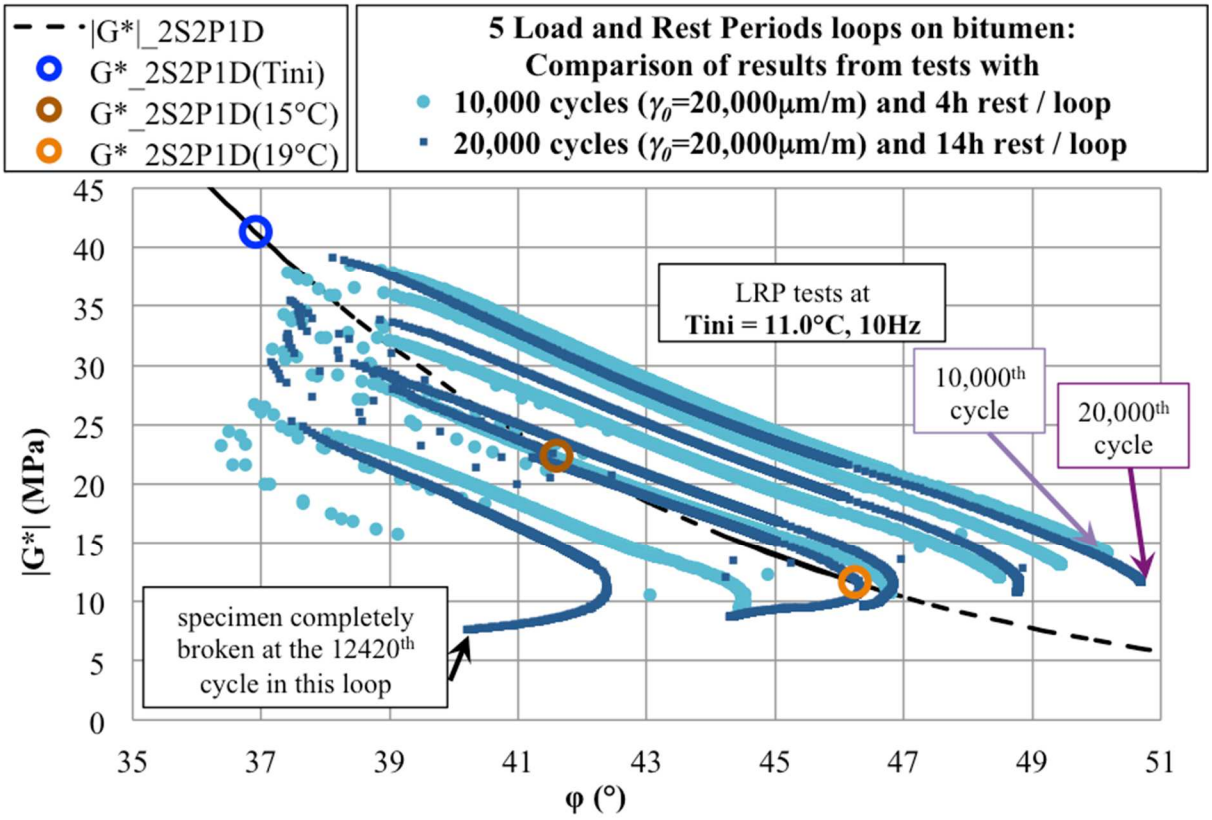

Figure 6-17. Comparison (in Black space) of LRP test results with different test parameters: LRP test with 10,000 cycles of sinusoidal loading at 20,000µm/m and 4h rest loops and 20,000 cycles of sinusoidal loading at 20,000µm/m and 14h rest loops on bitumen (B5070_E) at 11.0°C and 10Hz.

6.7. Failure analysis

After all the LRP tests that did not present clearly a fatigue failure, classical fatigue tests (continuous sinusoidal strain loading) were performed. The tests were carried immediately after the last rest loop from the LRP test, using the same strain amplitude as during LRP loading loops. A total of 8 tests is analysed, 5 on bitumen specimens and 3 on mastic specimens. Figure 6-18 presents the obtained norm of complex modulus and phase angle (figure a) and the measured on-specimen strain amplitude and temperature (figure b) as a function of the applied loading cycles for the bitumen specimen B5070_D (same as in the previous figures). The initial measured complex modulus is of about 23MPa, while at the beginning of the first LRP loop, it was of 38.8MPa (the specimen has already cumulated damage). The classical trends in norm of complex modulus and phase angle are observed: phase angle increases at the beginning of the test, until it stabilises and starts to decrease; norm of complex modulus decreases fast at the beginning of the test, then it presents an approximately linear decrease with the number of cycles, until a perturbation in its trend occurs. These changes in the trends of evolution of norm of complex modulus (perturbation in the linear trend) and phase angle (perturbation in the decrease trend after a maximum has occurred) may be used as indicators of fatigue failure. Literature commonly associates these changes in trend of complex modulus evolution with the coalescence of microcracks into a macrocrack, even if the peak phase angle is more commonly used (Goodrich,

1991). Due to the phenomena experimentally demonstrated in this thesis, it does not seem reasonable to consider the phase angle peak ass associated to a failure. Then, other perturbations in the complex modulus evolution trend are used to determine fatigue failure.

From the curves presented in Figure 6-18, it is seen that determining the failure from this process is not so simple, and imprecision in the results is expected. The considered fatigue failure zone and the considered number of cycles at failure (*Nf*) are indicated in Figure 6-18a. Slope perturbations are observed in this zone both for the norm of complex modulus and for the phase angle. For the considered number of cycles at failure, mean in-specimen temperature is around 13°C, i.e., a 2°C temperature increase with respect to the initial test temperature.

Considering this method for determining the number of cycles at failure (*Nf*), *Nf* was obtained for all fatigue tests conducted after the LRP tests, on both bitumen (five specimens, at three different strain amplitudes, 3,600μm/m, 10,000μm/m, 20,000μm/m) and mastic (three specimens, at three different strain amplitudes, 1,000μm/m, 3,300μm/m, 8,500μm/m). The obtained results are presented in Table 6-2. For the specimens broken during the LRP test, the same method was applied in order to determine *Nf* (considering the cumulated cycles during all LRP loading loops). Then, for all tested specimens, the total number of cycles at failure is presented, considering a cumulative rule for fatigue life consumption (number of already applied cycles over the number of expected cycles at failure) with the number of applied cycles during LRP loading loops and classical fatigue tests. The table also presents the applied shear strain amplitudes during the tests.

Using the data presented in Table 6-2, Whöler curves (*Nf* as a function of the applied strain amplitude, in log-log axis) were constructed, either not considering the cumulated cycles from LRP tests (Figure 6-19a) or considering the cumulated cycles from the LRP tests (Figure 6-19b). When not considering the cumulated cycles from LRP loops, the fatigue behaviour of bitumen and mastic seemed to diverge in terms of the strain amplitude dependence of the fatigue life. This was changed when considering the cumulated cycles, i.e. strain amplitude dependences of the fatigue life of bitumen and mastic are similar. The same similarity between bitumen and mastic (with 30% volume fraction of particles) fatigue strain dependence has been observed before in the literature (Van Rompu et al., 2012). Considering the cumulated cycles in this analysis is consistent with the hypothesis made in Section 6.5.4 (cf. Figure 6-15) to correct the effect of damage on the measured complex modulus: the effects of damage seems to cumulate. The presented results suggest that this accumulation happens both on the relative modulus change (cf. Figure 6-10 and Figure 6-15) and on the fatigue life consumption (cf. Figure 6-18 and Figure 6-19).

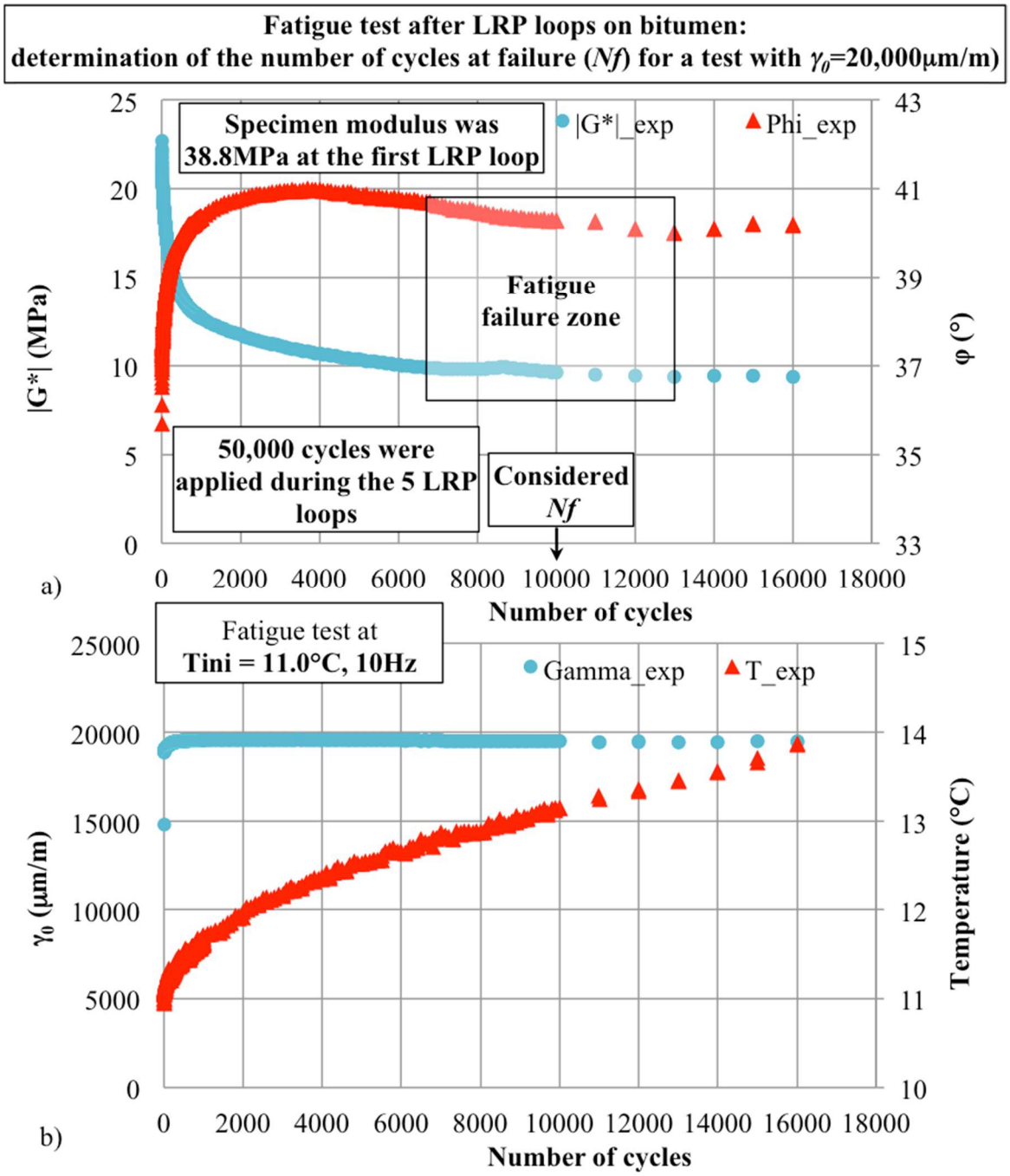

Figure 6-18. Experimental results (B5070_D) for the fatigue test performed immediately after the last rest loop of the LRP test (cf. Figure 6-6) with to 20,000µm/m sinusoidal loading and determination of the number of cycles at failure (*Nf*). a) Norm of complex modulus and phase angle as a function of the number of applied cycles, and b) shear strain amplitude and temperature as a function of the number of applied cycles.

Table 6-2. Results from the fatigue tests performed immediately after the last rest loop of the LRP tests, in terms of the number of cycles at failure defined considering changes in trend on the rate of change in modulus and on the phase angle.

Material/Specimen	Strain Amplitude (μm/m)	Number of cycles at failure *Nf* during LRP tests	Number of cycles at failure *Nf* during the fatigue test	Number of cycles at failure *Nf* considering the cycles from LRP tests
B5070_A	10,000	Not failed	68,000	118,000
B5070_B	20,000	39,000	Failed during LRP	39,000
B5070_C	3,600	Not failed	940,000	990,000
B5070_D	20,000	Not failed	10,000	60,000
B5070_E	20,000	53,000	Failed during LRP	53,000
M5070_30pc40-70_A	3,300	Not failed	170,000	220,000
M5070_30pc40-70_B	8,500	Not failed	35,000	85,000
M5070_30pc40-70_C	1,000	Not failed	2,500,000	2,550,000

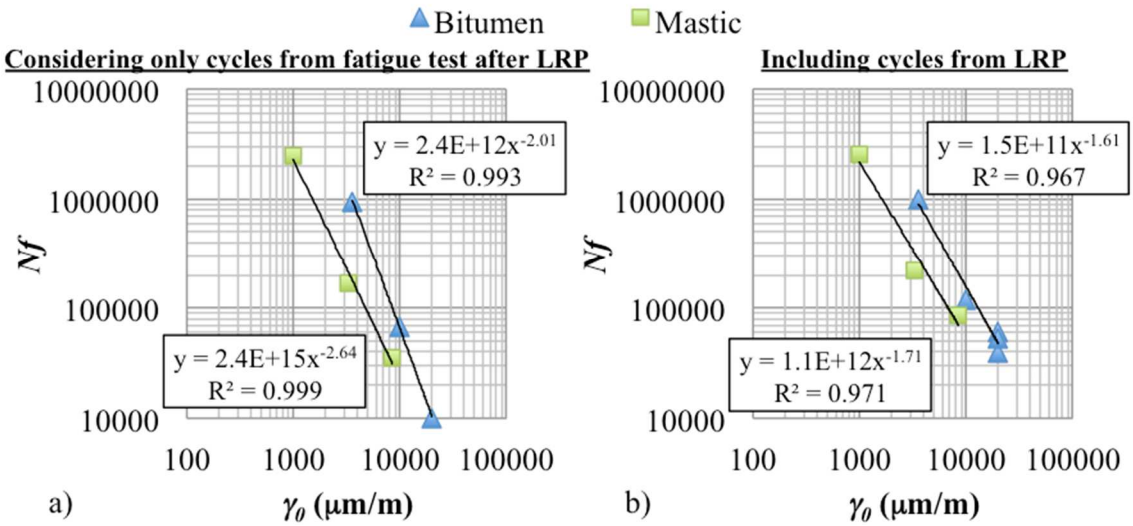

Figure 6-19. Experimental results from the fatigue tests performed immediately after the last rest loop of the LRP tests: number of cycles at failure (*Nf*), defined considering changes in trend on the rate of change in modulus and on the phase angle, as a function of the shear strain amplitude (Whöler curves). a) Results considering only cycles from the fatigue test, and b) results considering both the cycles from the LRP and the cycles from the fatigue test (the effect of all cycles on the fatigue damage is considered to cumulate).

6.8. Conclusion on biasing effects on bitumen and mastic

This chapter presented the effects of different physical phenomena occurring during cyclic tests on bituminous materials. Bitumen (B5070) and mastic (M5070_30pc40-70) were tested. Four types of tests were discussed: complex modulus test, Alternating Strain Amplitudes (ASA) tests, Load and Rest Periods (LRP) test (including small Strain Amplitude Sweep test before LRP), and classical Fatigue tests. Complex modulus test results were used to evaluate the effect of temperature on the complex modulus. This is done using a combination of the 2S2P1D model and the WLF equation. For all performed tests, mean in-specimen temperature is measured continuously using four thermocouples. The ASA test results were used to qualitatively present the

effects of nonlinearity, temperature and thixotropy, and damage. During the tests, a recovery of complex modulus during loading was observed over time when the applied strain amplitude was decreased, which is typical for thixotropic materials. Then, the LRP tests, whose results were used to quantify all the phenomena, were presented.

With the LRP tests results presented in this chapter, evidence was provided that damage cumulates with a linear relationship with the number of applied cycles at fixed strain amplitude. All cycles at a given strain amplitude produce the same irreversible modulus change (damage), independently if they happened at the beginning or at the end of loading. The experimental results of unrecovered complex modulus after 4h rest demonstrated this. Also, when it comes to fatigue failure, a comparison of Whöler curves for bitumen and mastic, presenting number of cycles at fatigue failure relationship with the number of applied cycles, demonstrated that even with 4h rest after less than 17min of 10Hz loading, the fatigue life consumed during loading is not recovered, as seems to believe an important part of the literature. When considering the cumulated number of cycles (including the ones from LRP tests) to the analysis of fatigue life consumption (number of already applied cycles over the number of expected cycles at failure), the strain amplitude dependence of the fatigue lives of bitumen and mastic, in terms of their Whöler curves slopes in log-log scale, were similar.

A method for calculating the effects of nonlinearity and self-heating effects was proposed. It is based on the hypothesis that the ratio of the complex moduli at two different temperatures is independent of the applied strain amplitude. Combining this hypothesis with the 2S2P1D model and the WLF equation (fitted to small strain amplitude behaviour), the effect of temperature at higher strain amplitudes was corrected. The consequences of this hypothesis were discussed and the nonlinearity effects observed at the very beginning of a loading loop and of a rest loop (which occur at different temperatures) were used to validate it.

After correcting the effects of temperature and damage on the measured complex modulus, the results suggest that nonlinearity and thixotropy share the same direction. It seems that these reversible phenomena share an intrinsic relation, possibly on the microstructural level, which is the case for other shear-thinning and thixotropic materials. While nonlinearity happens instantly (in a shorter time scale than one loading cycle), thixotropy happens over time.

The effect of longer rest periods and longer loading was also investigated in this chapter for the tests on bitumen with 20,000μm/m shear strain amplitude. Regarding the longer loading loop, it only provoked 5% more modulus decrease, while the shorter one had produced already 65% modulus decrease. Regarding the rest loop, even if phase angle seems to completely recover after 4h rest, the norm of complex modulus presents a slow recovery even after 4h. This effect is negligible in comparison to the other investigated phenomena during the first 4h of rest. This secondary effect is probably what is called in the literature as “self-healing”, which differ on the fundamental explanation from thixotropy. The directions of the phenomena are also not the same in Black space, since thixotropy shares direction with nonlinearity and self-healing seems to slightly recover modulus with negligible change in phase angle.

Chapter 7: CONCLUSIONS AND PERSPECTIVES

This thesis identified and quantified the effects of different physical phenomena happening during cyclic tests on bituminous materials, aiming at improving the interpretation of such tests. The fundamental behaviour of bituminous materials was investigated using experiments especially designed for the study of different phenomena: transient effects, non-linearity, self-heating, thixotropy, damage, and self-healing. From the experimental observations, conclusions on these phenomena could be drawn. These conclusions can be summarised as follows.

- Due to transient effects typical of viscoelastic behaviour, when starting sinusoidal loading on a bituminous material, some cycles are needed before reaching approximate steady-state loading-response behaviour, where measurement of stiffness can be done using classical signals analysis for complex modulus determination. When starting loading from rest, 2 or 3 cycles are necessary. When changing the applied loading amplitude from a cycle to the other, the error in the measured norm of complex modulus is negligible if the change is less than 10%. Results can be found in Chapter 4.
- Bituminous mixtures present strain dependence of complex modulus (nonlinearity) even for strain amplitudes as low as 10μm/m. In bitumen, mastic and bituminous mixtures, nonlinearity can be characterised by two parameters, defining its intensity (complex modulus change by unit change in stress/strain amplitude) and direction in complex representations (relationship between change in norm and in phase angle of complex modulus). The definition of nonlinearity limits applied for bitumen, mastic and bituminous mixture used in this thesis is the maximum stress or strain amplitude that can be applied producing 5% relative decrease in norm of complex modulus with respect to asymptotic small amplitude behaviour. From the comparison of nonlinearity limits of bitumen, mastic and bituminous mixture in terms of stress amplitude, it was concluded that mastic and bituminous mixture inherit nonlinearity primarily from the bitumen, granular skeleton nonlinearity being a secondary contribution. Mastic nonlinearity limits could be obtained from bitumen nonlinearity limits by applying a simple factor, independent of frequency and temperature. Nonlinearity limits and the nonlinearity parameters defined in this work are time- and frequency- dependent and respect the time-temperature superposition principle with the same time-shift law (same WLF equation parameters) as parameters from linear viscoelasticity (determined from complex modulus tests). This was observed for all tested materials (bitumen, mastic and bituminous mixture). Results can be found in Chapter 4.
- A simplified thermomechanical model (with no heat diffusion) enabled the calculation of the experimentally observed initial stiffness decreases from cyclic loading, with good agreement to test results, using only one fitting parameter per bituminous mixture (mastic film thickness coating coarser aggregate particles). This modulus decrease explanation relies on significant temperature increases occurring in some regions of the bituminous phase (local self-heating), which can be achieved in locally adiabatic conditions (only true at the very beginning of tests). These regions are small (mastic

films of some tens of micrometres in between coarser aggregate particles), and thermocouples cannot be used to measure them because of their size. However, heat diffusion seems to happen excessively fast, as demonstrated by a more sophisticated calculation. Due to heat diffusion, the existence of progressive local temperature differences seems not physically possible (calculated maximum difference is not higher than 1°C, and is obtained in less than 2s, being approximately constant after that). Then, another reversible phenomenon, which is not temperature increase due to self-heating, contributes for the modulus decrease. The phenomenon seems consistent with the definition of thixotropy. From the performed cyclic tests on bitumen, temperature increases up to 7°C, after 20,000 cycles at 11°C and 10Hz using 20,000μm/m, were obtained. In only 30 cycles at those conditions, temperature increase is around 1°C. Experimental results indicate that after 10,000 cycles following rest, the effect of temperature corresponds to about 1/3 to 2/3 of the measured changes in norm of complex modulus and phase angle. The effect of temperature on the measured complex modulus cannot be neglected during fatigue tests. Temperature needs to be measured in the tested specimen to allow for correction of its effects. Results can be found in Chapters 5 and 6.

- The obtained experimental results from tests including rest periods seem to indicate that damage cumulates following a linear relationship with the cumulated number of applied cycles. Rest periods of 4h produce negligible recovery of the effects of the damage phenomenon. The recovery of complex modulus observed during 4h of rest can be almost completely explained by the reversible character of phenomena such as nonlinearity, thixotropy and self-heating. By considering this cumulative rule for the number of applied cycles on the damage evolution, which was also applied to fatigue life consumption (number of already applied cycles over the number expected of cycles at failure), it was demonstrated that the strain amplitude dependence of the fatigue lives of bitumen and mastic, in terms of their Whöler curves slopes in log-log scale, are similar. Results can be found in Chapter 6.
- After a fast and nonlinear recovery of complex modulus (norm and phase angle) during the first 4h of rest, some recovery of norm of complex modulus was observed between 4h and 14h of rest. This recovery is approximately linear (approximately 2.5MPa in 10h, while in 4h 23MPa had been recovered) with time and accompanied by a negligible change in phase angle (this parameter is practically completely recovered after 4h rest). This effect may be due to the phenomenon called in the literature self-healing. As seen in the tests performed, it is of secondary importance compared to the effect of the reversible phenomena during the first 4h of rest. It seems, from the analysed experimental results, that most of the effects considered in the literature as consequences of self-healing are simply due to the reversible effects studied in this thesis. Results from this work demonstrated that less than 4h rest is not suitable if a self-healing behaviour is searched, since the effects of this phenomenon are negligible in comparison to the one of the occurring reversible phenomena. Results can be found in Chapter 6.
- After correction of the effects of temperature and damage, thixotropy could be analysed. In this investigation, a classical interpretation of damage was used: a loss in resistant cross-section of the material. This loss is expected to produce a change in the

measured modulus, but in principle no phase angle change is to be expected. Self-healing, interpreted as the inverse phenomenon, i.e. somewhat of a sealing of microcracks, should produce a recovery of the measured modulus, also with no variation in phase angle. Thixotropy is seen as the reversible phenomenon appearing during continuous and cyclic loading, as in other materials. It was concluded that thixotropy shares the same direction in complex planes (relationship between norm of complex modulus change and phase angle change) as the one of nonlinearity. This appears to be an indication that these phenomena present the same micro-structural origin. While nonlinearity happens instantly (with respect to the time-scale of a loading cycle), thixotropy happens over time. This is consistent with thixotropy as observed in other materials, which are also nonlinear (shear-thinning fluids, which are frequently thixotropic). Results can be found in Chapter 6.

- The effects of thixotropy and self-healing do not appear to present a similar direction of change in complex modulus in polar representations. While thixotropy shares direction with nonlinearity, thixotropy seems to produce the opposite effect of damage: a slow recovery of norm of complex with negligible change in phase angle. This could be seen as just a semantics issue, but since these phenomena may differ in their fundamental explanation, they can also produce different predictions of material behaviour depending on how they are characterised from tests. Moreover, thixotropy is not a behaviour expected in the field, since continuous loading is not applied and much rest is allowed to the material. Then, if self-healing is confounded with thixotropy during characterisation (thixotropy producing much faster modulus recovery at the beginning of tests), over-estimation of the self-healing capability of bituminous materials is expected. The explanations given in this thesis on all the reversible phenomena, on damage and on self-healing appear physically acceptable, but much wok is still needed in order to confirm the observations.

The aforementioned physical phenomena need to be taken into account for sufficiently high stress/strain amplitudes used in cyclic tests. This is the case of fatigue tests, commonly used for bituminous materials characterisation. When fatigue tests are analysed, modulus decrease is commonly explained as damage, without any consideration of the aforementioned reversible phenomena. Even for more advanced analysis, all modulus recovery is considered as caused only by the self-healing phenomenon. The results from this thesis demonstrated that such considerations are at least an excessive simplification, if not a complete mistake. This obviously leads to overestimation of damage and also of self-healing properties of bituminous materials. Moreover, when comparing the behaviour of two materials without considering the other reversible phenomena, complete misinterpretation is very likely, since the reversible phenomena produce more effect on the measured complex modulus than damage and healing.

In this thesis, only homogeneous tests were used, i.e., tests producing theoretically homogeneous stress and displacement fields in the material. Due to the investigated phenomena, which are highly dependent on the strain levels in the material, the interpretation of non-homogeneous fatigue tests results becomes very difficult. These tests should not be recommended for the study of the fatigue damage (or self-healing) behaviour of bituminous materials.

It is hoped that the results and conclusions of this thesis have an impact on the characterisation of viscoelastic and fatigue response of bituminous materials. The work highlights the importance of systematically reporting the stress/strain amplitude used in complex modulus tests on bituminous mixtures, since these materials are nonlinear even for very low strain amplitude. For bitumen and mastic, the lowest strain amplitude possible, giving accurate load measurements, should be used, and also reported. Performing a test (with at least two strain amplitudes) to verify linearity is recommended for studies on new materials or with new test configurations. For fatigue tests on bituminous materials, it is highly recommended to measure in-specimen temperature, and to correct the effects of temperature on the complex modulus before drawing any conclusions on its evolution. The obtained number of cycles at failure should be reported with the corresponding measured in-specimen temperature throughout the test.

Some recommendations for future work can also be made, as follows.

- Testing more materials could provide insight on the studied phenomena and confirm the conclusions made on the studied materials. This could confirm for bituminous materials with other compositions that: i) thixotropy shares direction in complex planes with nonlinearity; ii) nonlinearity in bituminous mixtures is primarily inherited from bitumen with secondary contribution from the aggregate skeleton; iii) nonlinearity respects time-temperature superposition with the same shift factors as for stiffness; iv) damage and fatigue life consumption (number of already applied cycles over the number of expected cycles at failure) cumulate linearly with the number of cycles; and v) self-healing is a secondary effect for rest times below 4h.
- A more thorough modelling of nonlinearity would be useful for the analysis of the performed cyclic tests. For the Load and Rest (LRP) periods tests interpretation in this thesis, a hypothesis involving nonlinearity and self-heating was needed, which may be seen as a simplified model. This hypothesis may be a first step to nonlinearity modelling, and a preliminary experimental verification was provided for the used hypothesis. The nonlinearity experimental results provided in this thesis consist of a valuable input for nonlinearity modelling procedures.
- Even if the direction of thixotropy has been established (relationship between modulus and phase angle changes, the same as for nonlinearity, at least at 11°C, 10Hz), the intensity of this phenomenon over time still needs to be modelled. For this, results at other temperatures and loading frequencies are needed. This could confirm that thixotropy effects on complex representations share direction with nonlinearity effects also at other loading conditions. This would also reinforce the hypothesis that these phenomena are linked by the same micro-structural origin. Results on other materials are also desirable in order to model thixotropy for bituminous materials. Modelling this phenomenon would be another step to allow better interpretation of cyclic tests results on bituminous materials.
- More tests with long periods of rest (more than 4h) could be used to investigate the self-healing phenomenon, which was found negligible for less than 4h rest when compared to the effect of the observed reversible phenomena. This could provide information for the modelling of this phenomenon, which is still not understood in the asphalt community.

- Investigations on the molecular level (using either experimental techniques such as electronic microscopy or modelling techniques such as molecular dynamics) should help understand the thixotropy phenomenon in bitumen. Studying this phenomenon would require the closer work of chemists and physicists with engineering scientists and mechanical behaviour experts working on bitumen. Improving the understanding of thixotropy will help interpreting the fatigue behaviour of bituminous materials, which is of importance to the asphalt community.
- After advancing with the proposed developments, a better understanding of the phenomena producing complex modulus changes during cyclic tests will be achieved. This includes understanding the effects of temperature and frequency on each of them. It will, then, be possible to model those phenomena, particularly the “real” damage. The proposed analysis procedure can be used to interpret cyclic fatigue tests (at different frequencies), taking into account different physical phenomena occurring simultaneously, and obtaining the effects of the “real” damage. It is believed that modelling correctly the “real” fatigue damage observed in tests (after correction of the biasing phenomena) will facilitate filling the gap between laboratory fatigue observations and field fatigue observations, which is a major interest for road engineering. While in laboratory fatigue tests many phenomena produce more complex modulus change than the “real” fatigue damage, in the field, due to very frequent rest periods between each loading cycle, the effects of the other phenomena, except for nonlinearity, are negligible.

RESUME EN FRANÇAIS

Résumé en Français.....209
Introduction.....210
Généralités sur les matériaux bitumineux.....214
Matériaux et Matériels.....216
Non-linéarité.....216
Auto-échauffement.....217
Effets combinés des différents phénomènes lors des essais cycliques.....219
Conclusions et Perspectives.....220

Introduction

Les routes sont des infrastructures nécessaires pour le développement économique d'un pays. Les chaussées bitumineuses (qui possèdent une ou plusieurs couches constituées d'enrobé bitumineux) sont la solution technique la plus utilisée pour des voies à fort trafic. Dans certaines méthodes de dimensionnement, les chaussées sont conçues pour une durée de vie donnée, qui peut être déterminée suivant des considérations mécanistiques et empiriques. Les informations sur la structure proposée et ses conditions d'utilisation (climat, géométrie, trafic, etc.) et sur les matériaux utilisés (obtenues à partir d'essais en laboratoire) sont utilisées pour la prédiction de l'intégrité structurelle au cours du temps (simulation de performance). Un des principaux mécanismes de dégradation observés dans les chaussées bitumineuses, et qui doit être simulé pendant la conception de la chaussée, est la fissuration par fatigue.

La fissuration par fatigue de la couche d'enrobé bitumineux est produite à partir du cumul de dommage dû au trafic. Même si un seul cycle de chargement est incapable de produire la rupture dans l'enrobé, la répétition des charges peut induire, après beaucoup de cycles, la rupture du matériau, accélérant la dégradation de la chaussée. Le dommage est vu comme étant le développement de microfissures dans le matériau, qui produit macroscopiquement une perte apparente de rigidité. En laboratoire, tester la fatigue des matériaux bitumineux consiste le plus souvent à appliquer des cycles répétés de manière continue jusqu'à la rupture. Les cycles appliqués de manière répétée accélèrent le processus d'endommagement qui est observé dans les enrobés bitumineux appliqués sur des chaussées in situ. La rigidité des matériaux peut être suivie au cours des essais, et son changement peut être utilisé comme indicateur du dommage dans le matériau (Di Benedetto et al., 2004, Tapsoba et al., 2015). Dans certaines approches, ces changements sont utilisés pour caler des modèles d'endommagement, utilisés ensuite pour simuler la performance de chaussées. Il est donc particulièrement important d'interpréter correctement les changements de rigidité perçus lors des essais de fatigue, identifiant les phénomènes physiques qui y ont lieu.

Il est possible de distinguer trois phases dans les essais de fatigue sur enrobé bitumineux (Di Benedetto et al. 2004a). La première (Phase I) est caractérisée par une chute rapide et non linéaire de la rigidité (telle que donnée par un paramètre matériau appelé module complexe) avec le nombre de cycles au début de l'essai. Dans cette phase, d'autres phénomènes qui ne sont pas l'endommagement paraissent être prédominants. Ces phénomènes sont : les effets transitoires (Gayte et al. 2016), la dépendance avec l'amplitude de déformation, ou non-linéarité, (Airey et al. 2003; Di Benedetto et al. 2011a; Gauthier et al. 2010; Mangiafico et al. 2017; Mangiafico et al. 2015), l'auto-échauffement distribué dans le volume (Di Benedetto et al. 2011a; Lundström et al. 2004; Riahi et al. 2016) et la thixotropie (Barnes 1997; Di Benedetto et al. 2011a; Mangiafico et al. 2015; Riahi et al. 2017). La Phase II présente une évolution quasi-linéaire du module complexe. La Phase III présente généralement un changement dans la tendance d'évolution du module complexe par rapport à la Phase II. Ce changement indique que des défauts distribués dans le volume ont coalescé dans une macrofissure (Goodrich 1991) et que les résultats ne sont plus exploitables pour obtenir des propriétés de volume comme la rigidité du matériau. Par exemple, dans le cas d'essais de fatigue en traction-compression, les champs de contrainte et déformation ne sont plus homogènes, alors que c'était le cas avant la coalescence de la macrofissure. La limite entre les Phases II et III peut être interprétée comme étant le moment de la rupture de l'éprouvette, et constitue un important résultat d'un essai de fatigue (appelé durée de vie, *Nf*). En revanche, cette

limite peut ne pas se manifester très clairement de manière systématique. Des résultats expérimentaux (Di Benedetto et al. 2011a; Isailović et al. 2017; Mangiafico et al. 2017; Mangiafico 2014; Nguyen 2011; Phan et al. 2017a; Riahi et al. 2017; Soltani and Anderson 2005) montrent que la plupart des effets observés pendant la Phase I sont complètement réversibles. Ces effets sont produits par des processus qui peuvent être décrits comme distribués dans le volume et réversibles.

Pour estimer la performance, des modèles de comportement de matériaux sont nécessaires. Ils doivent décrire les propriétés du matériau de la manière la plus simple et précise possible, respectant le comportement du matériau. Ce travail porte sur le comportement fondamental des matériaux bitumineux observé en laboratoire. Une attention particulière est portée sur les différents phénomènes capables de produire des effets sur la rigidité du matériau. Ces effets impactent directement l'interprétation des essais de fatigue, pour lesquels la littérature (Bahia et al. 1999; Carpenter et al. 2003; Darabi et al. 2013; Ghuzlan and Carpenter 2000; Ghuzlan and Carpenter 2006; Ghuzlan and Carpenter 2003; Kim et al. 1997; Shen et al. 2006; Underwood et al. 2012; You et al. 2014, parmi d'autres) considère souvent que seulement l'endommagement par fatigue peut produire des changements de rigidité.

Les phénomènes étudiés dans cette thèse sont :

- La non-linéarité, qui est un phénomène réversible qui fait que la rigidité est dépendante du niveau de chargement (comme, par exemple, de l'amplitude de déformation d'un chargement sinusoïdal). Comme les essais de fatigue sont souvent utilisés pour déterminer la quantité de cycles nécessaire pour produire la rupture en fonction du niveau de chargement utilisé, différents niveaux de chargement sont testés et un effet de la non-linéarité sur la rigidité est attendu. De plus, lors des essais cycliques, quelques cycles peuvent être nécessaires avant que l'amplitude de chargement désirée soit atteinte, donc des effets de la non-linéarité sur la rigidité se produisent au moins au début des essais ;
- L'auto-échauffement, qui est une conséquence du comportement dissipatif du matériau viscoélastique. Le matériau dissipe de l'énergie mécanique dans son volume au cours du chargement. Cette énergie dissipée se transforme en chaleur et produit une augmentation de température dans le matériau. En conséquence, une diminution de rigidité est observée dans le matériau bitumineux, qui est thermosusceptible. De plus, dû à la différence de rigidité entre les granulats et le mastic les recouvrant, un auto-échauffement hétérogène est attendu. Dans des films de mastic minces, ces effets locaux d'auto-échauffement peuvent produire localement une diminution de rigidité relativement importante, impactant de manière plus prononcée la rigidité de l'enrobé. L'augmentation de température due à l'auto-échauffement local est difficile à mesurer, car l'échelle à laquelle il peut se produire est de l'ordre de la dizaine de microns. Cela fait de l'auto-échauffement local un phénomène qui peut se confondre à la thixotropie (expliquée ci-après). Les effets de l'auto-échauffement dans un matériau hétérogène, comme l'enrobé bitumineux, sont aussi étudiés dans ce travail. Si le matériau est laissé au repos jusqu'à ce qu'il se refroidisse à la température initiale, la rigidité initiale est retrouvée, i.e. l'auto-échauffement est un phénomène réversible ;

- La thixotropie, qui est un phénomène apparaissant dans certains fluides, comme les colloïdes (desquels le bitume fait partie), présentant sous chargement continu une diminution de viscosité (ou rigidité) au cours du temps. Ce changement se passe jusqu'à ce qu'une viscosité (ou rigidité) d'équilibre soit atteinte. Quand le chargement est arrêté (application de temps de repos), la viscosité (ou rigidité) originale est récupérée après un certain temps, i.e. le phénomène est réversible. La diminution de rigidité au cours du chargement et l'augmentation de rigidité pendant le repos sont toutes les deux des manifestations du phénomène de thixotropie. Le phénomène peut être vu comme la combinaison de deux sous-phénomènes, le *breakdown* et le *build-up* de la microstructure du matériau, et les deux ont lieu de manière simultanée. L'équilibre de ces deux sous-phénomènes mène à la viscosité (ou rigidité) d'équilibre obtenue, qui est dépendante du niveau de chargement ;
- L'endommagement, qui en mécanique des milieux continus est vu comme un phénomène de perte d'aire de section résistante à une échelle inférieure à celle du matériau (phénomène distribué dans le volume), produisant une perte de rigidité apparente. La rigidité apparente peut être utilisée comme un indicateur de l'évolution du dommage. Comme la perte d'aire de section résistante produit une discontinuité au niveau microscopique, à l'exception de la possibilité que le matériau puisse fluer pour défaire cette discontinuité, l'endommagement est un phénomène irréversible. Quelques auteurs croient que le phénomène où le matériau flue pour refermer des microfissures a lieu dans les enrobés bitumineux, à une température suffisamment haute. Ce phénomène est appelé souvent "*self-healing*" ou auto-cicatrisation de microfissures. La combinaison de l'endommagement avec l'auto-cicatrisation peut facilement être confondue avec la thixotropie. Comme remarque supplémentaire, il est observé que pendant des essais de fatigue, les autres phénomènes, qui sont réversibles, produisent des biais pour l'interprétation de l'essai de fatigue, qui est supposé donner des informations sur l'endommagement et la rupture par fatigue. Ces phénomènes sont appelés quelques fois effets biaisants dans cette thèse.

Comme on peut l'apercevoir à partir des commentaires précédents, accéder aux propriétés mécaniques des matériaux bitumineux à partir des essais peut être une tâche difficile à cause de tous les phénomènes physiques qui doivent être pris en compte. Certaines hypothèses simplificatrices nécessaires à l'analyse de certains essais peuvent ne pas être valides et par conséquent influencer les paramètres matériaux déterminés à partir de l'essai. En plus de la méthode d'analyse expérimentale, la géométrie de l'essai en soi doit être choisie avec soin pour obtenir des résultats de propriétés fondamentales fiables. Si les effets des phénomènes cités auparavant sont relativement importants, des géométries d'essai produisant des champs de contrainte et déformation non-homogènes (e.g. essais de flexion, traction indirecte, torsion de cylindre, etc.) ne sont pas adaptés pour obtenir les propriétés mécaniques du matériau. Analyser ces essais (i.e. obtenir les champs de contrainte et déformation à partir de la force appliquée et du déplacement mesuré) requiert une hypothèse supplémentaire sur le comportement du matériau (e.g. viscoélasticité linéaire isotrope), dont la détermination est le but même de l'essai. En outre, comme mentionné auparavant, les phénomènes apparaissant lors des essais sont dépendants du niveau de contrainte/déformation. Comme les essais non-homogènes produisent des champs de contrainte et déformation non-homogènes, l'hypothèse supplémentaire nécessaire doit prendre en

compte la dépendance avec la contrainte/déformation, i.e. basée sur la connaissance à priori du type de comportement du matériau. Le type de comportement n'est pas accessible sans utilisation d'essais homogènes.

En vue du contexte présenté, le problème de recherche traité dans cette thèse sont les erreurs d'interprétation des résultats d'essais cycliques en général et des essais de fatigue sur les matériaux en particulier, qui rendent difficile la tâche d'obtenir des propriétés du matériau de manière fiable, dû aux effets combinés de différents phénomènes physiques. L'objectif général du travail est d'identifier et de quantifier les effets de chacun des phénomènes physiques, de manière à améliorer l'interprétation des résultats d'essais cycliques. Spécifiquement, les buts de la thèse sont :

- D'évaluer l'effet de la non-linéarité sur du bitume, du mastic et de l'enrobé bitumineux à différentes conditions de température et de fréquence et d'étudier comment est reliée la non-linéarité dans ces différentes échelles du matériau ;
- D'analyser l'effet de l'auto-échauffement local lors d'essais cycliques en enrobés bitumineux à différentes conditions de température, fréquence et amplitude de chargement. Aussi, il doit être vérifié si l'auto-échauffement local pourrait expliquer la chute initiale de module observé dans les essais. Cela indiquerait qu'il n'y aurait pas besoin de postuler l'existence d'un autre phénomène réversible (comme la thixotropie) pour expliquer les résultats expérimentaux observés ;
- De démontrer expérimentalement les effets combinés des phénomènes étudiés (non-linéarité, auto-échauffement, thixotropie et endommagement) et comment décomposer ses effets.

Cette thèse de doctorat se concentre sur le domaine de la Mécanique des Matériaux, appliquée aux matériaux bitumineux. Elle a été préparée au sein du Laboratoire de Tribologie et Dynamique des Systèmes (LTDS) à l'Ecole Nationale des Travaux Publics de l'Etat (ENTPE), en France, avec le support du programme brésilien Science sans Frontières (CsF – *Ciência sem Fronteiras*) (bourse de thèse), et avec la participation de l'ENTPE à travers sa coopération de recherche (Chaire) avec l'entreprise Eiffage Routes. En plus de l'Introduction (Chapitre 1) présentant le contexte de l'étude et ses objectifs, la thèse contient des approches expérimentales et de modélisation, dont les résultats sont organisés comme suit.

- Le Chapitre 2 présente des généralités sur le comportement mécanique des matériaux bitumineux. Il communique des points importants de la littérature pour le travail présenté dans la thèse, comme la composition des matériaux bitumineux et la description de leur comportement thermomécanique en général. Le chapitre se conclut avec la description de l'approche générale pour interpréter les essais de fatigue prenant en compte les phénomènes physiques réversibles (non-linéarité, auto-échauffement et thixotropie) au cours du chargement cyclique des matériaux bitumineux ;
- Le Chapitre 3 décrit le matériel expérimental utilisé dans la thèse. Il donne aussi des détails sur les matériaux étudiés et sur l'interprétation des résultats des essais mécaniques (traitement des signaux) ;
- Le Chapitre 4 porte sur le phénomène de non-linéarité dans les matériaux bitumineux, compris dans cette thèse comme étant la dépendance du comportement mécanique du matériau avec le niveau de déformation. Les effets de l'amplitude de déformation sur la

rigidité du matériau ont été étudiés pour du bitume, du mastic et de l'enrobé bitumineux. Des comparaisons sont faites entre les comportements des ces différentes échelles du matériau et une proposition pour l'origine physique du phénomène dans les enrobés est présentée ;

- Le Chapitre 5 couvre le phénomène d'auto-échauffement dû au couplage thermomécanique dans les enrobés bitumineux. Il décrit l'étude réalisée pour vérifier si l'auto-échauffement local pourrait expliquer la chute initiale de module observée dans les essais de chargement cyclique. Cela indiquerait qu'il n'y aurait pas besoin de postuler l'existence d'un autre phénomène réversible (comme la thixotropie) pour produire les résultats expérimentaux observés ;
- Le Chapitre 6 décrit le travail expérimental prévu pour déterminer les contributions de chacun des comportements mentionnés auparavant au cours d'essais cycliques sur du bitume et du mastic. Une description de la séparation de l'impact des phénomènes étudiés est présentée et une approche pour l'interprétation du comportement du matériau au cours des essais, et conséquemment la modélisation du comportement du matériau, est présentée ;
- Le Chapitre 7 présente la conclusion générale de cette thèse avec les impacts sur l'analyse des essais de chargement cyclique, et aussi des recommandations de travaux futurs.

Généralités sur les matériaux bitumineux

Ce chapitre présente différents aspects importants pour l'étude du comportement thermomécanique des enrobés bitumineux. Une approche générale a été développée à l'ENTPE/Université de Lyon pour l'interprétation de résultats expérimentaux obtenus à partir de chargements cycliques et d'essais de fatigue (Mangiafico 2014; Nguyen 2011). Cela inclut des considérations sur les différents phénomènes physiques (non-linéarité, auto-échauffement, thixotropie et endommagement) qui induisent des variations de module complexe pendant le chargement. Parmi ces phénomènes, on considère que ceux qui sont réversibles produisent des effets biaisants par rapport à l'analyse de l'endommagement. Cette considération est faite car pendant des essais de fatigue en laboratoire, les effets (changements de module) liés aux phénomènes réversibles apparaissent, mais cela n'est pas le cas pour le chargement in-situ, où il n'y a que peu de cycles, toujours suivis par du repos. Pour permettre l'interprétation de l'essai en prenant en compte les effets biaisants, des périodes de repos doivent être introduites. Pendant l'essai (pendant le chargement, avec une relativement grande amplitude de déformation, et pendant le repos, avec très petite déformation et pendant très peu de temps), le module complexe est mesuré. Les changements dans la valeur mesurée de norme de module complexe (notée $E(\varepsilon_0,T,N)$, comme une fonction de l'amplitude de déformation, de la température et du nombre de cycles) et d'angle de phase, peuvent être dus aux phénomènes physiques suivants :

- Non-linéarité : Ce phénomène est étudié en détail dans le Chapitre 4. À température et fréquence fixées, la non-linéarité fait que le module mesuré dépend de l'amplitude de déformation axiale (ε_{01}). À très petite amplitude de déformation (domaine linéaire) la norme du module complexe est notée $E(0,T_0,1)$. Donc ce phénomène est observé quand

l'amplitude de déformation change (ce qui est le cas au début de l'essai de fatigue), mais une variation de module n'est pas attendue pour ce phénomène ensuite, quand l'amplitude de déformation est constante. Au début du chargement à l'amplitude de déformation désirée, la norme du module complexe est notée $E(\varepsilon_{01},T,1)$. Le changement de module dû à la non-linéarité est instantané et réversible, et noté ici $\Delta E_{\text{Non-linéarité}}$. Il peut être calculé comme:

- $\Delta E_{\text{Non-linéarité}} = E(\varepsilon_{01},T_0,1) - E(_0,T_0,1)$.

- Auto-échauffement (et refroidissement pendant le repos) : l'effet de ce phénomène pour le module complexe est observé quand la température de l'éprouvette change. Même si l'enceinte thermique est à température constante, la température de l'éprouvette peut changer. Pendant le chargement, la température de l'éprouvette augmente. Pendant le repos, elle diminue jusqu'à l'équilibre thermique initial. Les mesures de température dans l'éprouvette, associées avec des modèles rhéologiques, donnent des informations sur l'effet de l'auto-échauffement sur le module complexe. Le changement de module complexe dû à cet effet est réversible. La variation dans la norme du module complexe (à un cycle N donné) dû à l'auto-échauffement est noté ici $\Delta E_{\text{Échauffement}}$.
  - $\Delta E_{\text{Échauffement}} = E(\varepsilon_{01},T,N) - E(\varepsilon_{01},T0,N)$.
- Thixotropie : l'effet de ce phénomène est perçu au cours du chargement et du repos, quand la microstructure du matériau est en train de se modifier (cf. Section 2.7), jusqu'à ce qu'un état d'équilibre soit atteint. La variation dans la norme du module complexe dû à la thixotropie est notée ici $\Delta E_{\text{Thixotropie}}$.
  - $\Delta E_{\text{Thixotropie}}$ = changement réversible restant.
- Endommagement : l'effet de ce phénomène dans le module complexe est observé au cours du chargement. Pendant le chargement, la section résistante du matériau se réduit (microfissures) et la rigidité apparente est réduite. Avec le cumul de dommage, les microfissures peuvent coalescer en une macrofissure et le matériau entre en rupture. Le phénomène est irréversible. La variation de norme du module complexe dû à l'endommagement est notée ici $\Delta E_{\text{Fatigue}}$.
  - $\Delta E_{\text{Fatigue}}$ = changement irréversible.
- Pris ensemble, thixotropie et endommagement sont appelés « effets cycliques », car ils produisent un changement de rigidité avec la répétition des cycles. La variation de norme du module complexe dû aux effets cycliques est notée ici $\Delta E_{\text{Effets Cycliques}}$.
  - $\Delta E_{\text{Effets Cycliques}} = \Delta E_{\text{Fatigue}} + \Delta E_{\text{Thixotropie}} = E(\varepsilon_{01},T,N) - E(\varepsilon_{01},T,1)$.

Des essais réalisés sur différents enrobés bitumineux, avec l'application de 100 000 cycles à 100 μm/m suivis de 24h de repos montrent que le changement non récupéré dans la norme du module complexe est autour de 10 % (par rapport au changement total de module observé pendant le chargement) (Mangiafico 2014). Le changement non récupéré d'angle de phase est autour de 1°. Le changement dans le module complexe est possiblement lié au dommage, qui est considéré comme le responsable de la rupture par fatigue du matériau. Dû à la petite importance relative de ce phénomène dans le changement total de module complexe pendant le chargement, il est clair que les effets biaisants doivent être pris en compte pendant l'analyse de la fatigue des enrobés bitumineux. Pour les mêmes raisons, des analyses du phénomène d'auto-cicatrisation doivent inclure des considérations sur la thixotropie (Shan et al. 2011; Shan et al. 2010), même si une

méthode plus précise pour la distinction entre les deux phénomènes pendant le repos est encore nécessaire.

Matériaux et Matériels

Ce chapitre présente les géométries d'essais utilisées, les méthodes de traitement des signaux obtenus pour déterminer les paramètres matériaux, ainsi que les matériaux testés. Une vision générale des essais réalisés est aussi donnée. Il est important d'observer que les géométries d'essais choisies sont pour obtenir des essais homogènes (Di Benedetto et al. 2004a; Di Benedetto et al. 2001), i.e., des essais produisant des champs de contrainte et de déformation homogènes dans le matériau (considérant l'hypothèse d'homogénéité du matériau de la mécanique des milieux continus, i.e. les particules les plus grandes sont relativement petites comparées à la plus petite dimension de l'éprouvette). Les essais homogènes permettent d'obtenir les champs de contrainte et de déformation directement à partir de mesures faites aux limites du volume matériau, sans avoir besoin d'hypothèses supplémentaires pour l'analyse. Donc, ces essais donnent accès directement au comportement du matériau étudié, ce qui est un intérêt majeur.

Le bitume testé est classé à l'essai de pénétration comme un bitume 50/70 et est le même que celui du Projet National (PN) IMPROVMURE. Le mastic est constitué de ce même bitume et de billes de verre (composés principalement d'oxyde de silice) sphériques dont le diamètre est compris à 90% entre 40 et 70 μm. Le taux volumique de billes de verre dans le mastic est de 30 %. Des résultats expérimentaux sur trois différents enrobés bitumineux ont été étudiés. Pour l'étude de non-linéarité (Chapitre 4), un grave-bitume a été testé. Des résultats de la littérature (Nguyen, 2011) sur des bétons bitumineux semi-grenus ont été utilisés pour la comparaison avec les résultats de modélisation dans le Chapitre 5 sur l'auto-échauffement.

Non-linéarité

Ce chapitre décrit les résultats de l'étude sur la non-linéarité du bitume, du mastic et des enrobés bitumineux. Pour le bitume et le mastic, des essais classiques de balayage d'amplitude ont été utilisés. Il a été démontré que pour ces essais des effets cycliques peuvent être observés à amplitude constante, i.e. pour certaines amplitudes de déformations suffisamment grandes le module chute à amplitude constante. Ces effets doivent être corrigés pour l'étude de l'effet de la non-linéarité sur le module complexe mesuré. Pour cela, une extrapolation linéaire a été utilisée pour obtenir le module complexe au premier cycle de chargement. Pour les essais sur enrobé bitumineux, un protocole d'essai particulier a été proposé (SASTENOLE), consistant en une série de chargements en balayage continu d'amplitude. 50 cycles sont appliqués avec une amplitude qui varie linéairement entre zéro et l'amplitude maximale visée, et 5 cycles sont appliqués à amplitude constante. Des séries de chargement à amplitude croissante et à amplitude décroissante ont été utilisées. Différentes températures (–4 à 28 °C) et fréquences (0,1 à 10 Hz) ont été testées, avec des amplitudes de déformation maximales jusqu'à 120 μm/m. Il a été démontré que les effets transitoires influencent les résultats seulement des cycles initiaux de chaque série de chargement,

ce qui est aussi le cas d'un essai classique. Les autres cycles peuvent être utilisés dans l'analyse de non-linéarité.

Cette étude fournit des données expérimentales qui confirment la dépendance avec la déformation du module complexe des enrobés bitumineux, même pour des amplitudes aussi petites que 10 μm/m. Cela est observé pour des séries à amplitude croissante, où le module baisse, et pour des séries à amplitude décroissante, où le module augmente. Des résultats obtenus à des combinaisons de température et fréquence qui donnent le même module complexe ont aussi donnée un comportement équivalent en termes de non-linéarité. Cela suggère que les effets de non-linéarité respectent le principe de superposition temps-température avec la même loi de superposition temps-température que pour la caractérisation classique du module complexe. Des observations similaires ont été faites pour les essais sur bitume et mastic.

Les variations de module dues à la non-linéarité ont été caractérisées à partir des séries de chargement à amplitude croissante. Une relation linéaire du module avec l'amplitude de déformation est obtenue. Différentes tendances sont obtenues pour les séries à amplitude décroissante, ce qui a été expliqué qualitativement par les effets des autres phénomènes (possiblement liés à la dissipation d'énergie) qui ont lieu simultanément dans le matériau. Les résultats de SASTENOLE pour des séries à amplitude croissante ou décroissante décrivent une même courbe quand présentés dans des espaces de Black et Cole-Cole. À partir de ces courbes, il est possible d'identifier des directions caractéristiques de non-linéarité. Les résultats obtenus peuvent être utilisés pour la modélisation de la non-linéarité dans les matériaux bitumineux, ce qui constituera un élément de futurs travaux.

Avec les résultats expérimentaux obtenus pour bitume et mastic, il a aussi été démontré que le principe de superposition temps-température peut être appliqué pour les effets de non-linéarité avec les mêmes coefficients de translation temps-température que pour la caractérisation linéaire du module complexe. De plus, une relation claire entre les résultats de limites de non-linéarité entre bitumes et mastics a été observée. Le mastic se comporte de manière similaire au bitume quant à ces limites, avec la simple application d'un facteur multipliant la limite de non-linéarité du bitume pour obtenir celle du mastic, indépendamment de la fréquence ou de la température.

Quand on compare les limites de non-linéarité des trois matériaux étudiés, des résultats intéressants sont obtenus. Les limites de non-linéarité de bitumes et mastic sont plus grandes en termes d'amplitudes de déformation quand on augmente la température, alors que l'inverse est observé pour les enrobés. Un explication cette inversion a été donnée, basée sur des considérations géométriques simples sur l'enrobé bitumineux, présentant des granulats purement élastiques relativement très rigides par rapport à la matrice bitumineuse non linéaire viscoélastique. Il apparaît que la non-linéarité dans l'enrobé est héritée principalement du bitume, avec une contribution secondaire de l'agencement granulaire.

Auto-échauffement

Dans ce chapitre, une étude de la chute de module avec le nombre de cycles de chargement sur enrobés bitumineux au début des essais est présentée. Des procédures de modélisation du

problème thermomécanique ont été proposées et les résultats ont été comparés avec des résultats expérimentaux de la littérature (Nguyen 2011). Dans un premier temps, les résultats ont démontré que des effets thermiques locaux, tels que modélisés par un calcul thermomécanique simplifié considérant l'hétérogénéité du matériau, pourraient expliquer les chutes initiales de module. Pour les amplitudes de déformation considérées (jusqu'à 131 μm/m) et les nombres de cycles observés (moins de 10 000 cycles, considérés comme la Phase I des essais d'un essai de fatigue), cette chute est complètement réversible, comme il a été montré dans la littérature (Coutinho et al. 2014; Di Benedetto et al. 2004a; Di Benedetto et al. 2004b; Di Benedetto et al. 1996; Gauthier et al. 2010; Gayte et al. 2016; Mangiafico et al. 2017; Mangiafico et al. 2015; Mangiafico 2014; Nguyen et al. 2015; Nguyen 2011; Phan et al. 2017a; Riahi et al. 2017; Soltani and Anderson 2005). Donc l'endommagement est considéré comme négligeable. Trois calculs adiabatiques ont été proposés, ayant chacun différentes hypothèses simplificatrices. Le premier considère une distribution de déformation et de chaleur homogènes dans l'enrobé. Le deuxième considère que toute l'énergie dissipée est utilisée pour chauffer uniquement le bitume. Il résulte en une chute de module calculée plus importante, mais encore loin de ce qui est observé expérimentalement au début des essais. Le dernier calcul consiste en un calcul thermomécanique 3D simplifié, qui prend en compte l'hétérogénéité des distributions de déformation et de chaleur dans le mastic.

Un rayon de particule de 2,32 mm a été utilisé pour les deux enrobés étudiés. Ce rayon est choisi pour respecter les fractions volumiques de granulats et bitume dans l'enrobé réel. Une demi-épaisseur de mastic de 58,6 μm pour BM2, et de 35,1 μm pour BM3, ce qui semble physiquement raisonnable, a permis le calcul des diminutions initiales de module observées expérimentalement à différentes températures, fréquences et amplitudes de déformation. Ce modèle simple montre que l'auto-échauffement local pourrait potentiellement expliquer les diminutions initiales de modules observées dans les essais de fatigue et d'autres essais cycliques sur des enrobés bitumineux, à partir du moment où les distributions de température calculées dans le mastic sous des conditions adiabatiques sont effectivement atteintes. Ces conditions sont possibles uniquement au tout début du chargement. Un calcul prenant en compte la diffusion de chaleur a été utilisé pour vérifier à quel point (jusqu'à quel cycle) ces conditions pourraient se justifier.

Les résultats du calcul avec la diffusion démontrent que la diffusion de chaleur se produit de façon très rapide par rapport à la chute de module observée expérimentalement. Un régime permanent, présentant une chute de module et des taux d'augmentation de température constants, est obtenu après environ 1 ou 2 s (10 à 20 cycles à 10Hz), indépendamment de l'épaisseur de mastic étudiée (qui a varié de 3 à 100 μm). Même au sein d'un cycle de chargement, des oscillations de température peuvent être observées dans le mastic. (cf. Figure 5–17). Le calcul ne peut donc pas simuler la chute initiale rapide et non linéaire observée expérimentalement pour les enrobés bitumineux. Finalement, malgré les simplifications faites, il est probable qu'un autre phénomène réversible, qui n'est pas lié à l'augmentation de température due à l'auto-échauffement, contribue à la chute de module. On remarque que le calcul adiabatique considérant l'hétérogénéité de l'enrobé a bien représenté les résultats expérimentaux pour différentes conditions de température, fréquence et amplitude de déformation. Cela pourrait être expliqué par l'existence d'un autre phénomène réversible compatible avec la définition de la thixotropie (Barnes 1997), qui amplifie les effets thermiques locaux pendant qu'il produit des conséquences semblables dans le comportement du matériau (Van Rompu et al. 2012).

Effets combinés des différents phénomènes lors des essais cycliques

Ce chapitre présente une étude sur les effets des différents phénomènes physiques ayant lieu au cours d'essais cycliques sur les matériaux bitumineux. Bitumes et mastics ont été testés. Quatre types d'essais sont présentés : essais de module complexe, essais avec application d'amplitudes de déformation alternées (*Alternating Strain Amplitudes* - ASA), essais avec application de chargement et de repos (*Load and Rest Periods* - LRP), et essais classiques de fatigue. Les résultats des essais de module complexe ont été utilisés pour évaluer l'effet du changement de température (associé à l'auto-échauffement) dans le module complexe mesuré. Pour tous les essais réalisés dans ce chapitre, la température moyenne de l'éprouvette a été mesurée de manière continue utilisant quatre thermocouples. Les résultats d'essai ASA ont été utilisés pour présenter qualitativement les effets de la non-linéarité, de la température (auto-échauffement) et de la thixotropie, ainsi que celui de l'endommagement. Pendant ces essais, une récupération de module complexe pendant le chargement a été observée après une diminution d'amplitude de déformation, ce qui est typique des matériaux thixotropes. Ensuite, les résultats d'essais LRP ont été utilisés pour quantifier tous les phénomènes.

Avec les résultats des essais LRP présenté dans ce chapitre, des indices ont été trouvés montrant que le dommage se cumule suivant une relation linéaire avec le nombre de cycles appliqués à une amplitude de déformation donnée. Tous les cycles à une amplitude de déformation donnée produisent le même changement irréversible de module (dommage), indépendamment qu'ils aient été appliqués au début ou à la fin du chargement, avec un changement négligeable d'angle de phase. Les résultats expérimentaux de module complexe non récupéré à la fin de 4 h de repos ont démontré cela. Quant à la rupture par fatigue, il semble que la partie consommée de la durée de vie du matériau n'est pas récupérée après le repos. De plus, si on considère le nombre de cycles cumulés au cours de toutes les séquences de chargement, la dépendance de la durée de vie sur l'amplitude de déformation tel qu'évaluée sur des courbes de Whöler (Nf vs ε_0 en espace log-log) est similaire pour bitume et mastic.

Une méthode pour calculer les effets de la non-linéarité et de l'auto-échauffement a été proposée. Après correction de l'effet de température sur le module complexe utilisant cette méthode et correction de l'effet de l'endommagement utilisant l'hypothèse de cumul linéaire avec le nombre de cycles sans changement d'angle de phase, il a été démontré que les résultats expérimentaux suggèrent que la non-linéarité et la thixotropie possèdent la même direction caractéristique. Il semble que ces phénomènes partagent une relation intrinsèque, possiblement au niveau microstructurel, ce qui est le cas pour d'autres matériaux rhéo-fluidifiants et thixotropes. Alors que la non-linéarité se manifeste de manière instantanée (dans une échelle de temps plus petite que celle d'un cycle), la thixotropie se manifeste au cours du temps.

L'effet de périodes de repos plus longues et de plus de cycles de chargement a aussi été étudié dans ce chapitre avec un essai sur bitume à 20 000 μm/m d'amplitude de déformation présentant 20 000 cycles (à comparer aux résultats avec 10 000 cycles) de chargement et 14 h de repos (à comparer aux résultats avec 4 h de repos). Le chargement plus long n'a produit que 5 % de plus de changement de module, alors que le plus court avait déjà produit 65 % de diminution de module au cours des 10 000 premiers cycles de chargement. Quant au repos, même si l'angle de phase paraît être complètement récupéré après les 4 h de repos, la norme du module complexe continue à

présenter une lente récupération même après 4 h. Cet effet est négligeable en comparaison aux autres pendant les quatre premières heures de repos. Cet effet secondaire est probablement celui dû au phénomène appelé auto-cicatrisation dans la littérature, et diffère fondamentalement dans son explication de la thixotropie. Les directions de ces phénomènes ne sont pas les mêmes dans les espaces de Black, étant donné que la thixotropie partage sa direction avec la non-linéarité et que l'auto-cicatrisation paraît produire une lente récupération de module sans changement d'angle de phase (dans un effet opposé à celui du dommage).

Conclusions et Perspectives

Au cours de cette thèse, les effets des différents phénomènes physiques ayant lieu lors de chargements cycliques de matériaux bitumineux ont été identifiés et quantifiés, visant à l'amélioration de l'interprétation des résultats d'essais cycliques. Le comportement fondamental des matériaux bitumineux a été étudié en utilisant des expériences planifiées spécifiquement pour l'étude des différents phénomènes : effets transitoires, non-linéarité, thixotropie, endommagement et auto-cicatrisation. À partir des observations expérimentales, des conclusions spécifiques à chacun de ces phénomènes ont pu être obtenues, décrites auparavant. De manière plus générale, il peut être conclu que ces phénomènes doivent être pris en compte si des amplitudes de déformations suffisamment grandes sont utilisées, comme celles employées dans les essais de fatigue ou dans certains protocoles d'essai de module. Pour les essais de fatigue, dont les résultats de chute de module sont souvent interprétés comme dû à l'endommagement, il a été clairement démontré que cela est une simplification excessive, très éloignée de la réalité. Cela induit une surestimation du dommage et des effets d'auto-cicatrisation dans les matériaux bitumineux, parce que les changements observés dans le module viennent principalement d'autres phénomènes, qui sont réversibles. En comparant le comportement de deux matériaux différents sans prendre en compte les effets de phénomènes réversibles, une faute d'interprétation est très probable, faussant les conclusions obtenues.

Dans cette thèse, seuls des essais homogènes ont été utilisés, i.e. des essais produisant théoriquement des champs de contrainte et déplacement homogènes dans le matériau. A cause des phénomènes étudiés, qui sont fortement dépendants de l'amplitude de déformation, l'interprétation de résultats d'essais non-homogènes dévient très difficile. Ce type d'essai ne devrait pas être recommandé pour l'étude de l'endommagement par fatigue (ou de l'auto-cicatrisation) dans les enrobés bitumineux.

Il est espéré que les résultats et conclusions de ce travail auront un impact sur la caractérisation de la réponse viscoélastique en fatigue des matériaux bitumineux. Le travail souligne l'importance de reporter systématiquement les amplitudes de déformations/contraintes utilisées dans les essais de module complexe sur enrobés bitumineux, étant donné que le comportement de ces matériaux est non linéaire même pour des amplitudes de déformation très petites. Pour le bitume et le mastic, la plus petite amplitude possible donnant des résultats suffisamment précis doit être employée, et également reportée. Réaliser un essai (avec au moins deux amplitudes de déformation) pour vérifier la linéarité est recommandé pour des études sur de nouveaux matériaux ou de nouvelles configurations d'essai. Pour des essais de fatigue sur les matériaux bitumineux, il est recommandé

de prendre des mesures de température dans l'éprouvette, et de corriger les effets de la température (auto-échauffement) sur le module complexe avant de tirer des conclusions sur l'évolution du module au cours de l'essai. Le nombre de cycles à la rupture par fatigue doit être reporté avec la température mesurée dans l'éprouvette, qui est différente de celle de l'enceinte thermique.

Des recommandations pour des travaux futurs peuvent aussi être faites, comme suit.

- Tester plus de matériaux pourrait donner plus d'informations sur les phénomènes étudiés et confirmer les hypothèses faites au cours de cette étude. Cela pourrait confirmer que des matériaux bitumineux avec d'autres compositions : i) présentent de la thixotropie, qui partage la même direction dans des plans complexes que la non-linéarité; ii) présentent de la non-linéarité héritée principalement du bitume avec une contribution secondaire de l'empilement granulaire; iii) présentent un comportement de non-linéarité respectant le principe de superposition temps-température avec les mêmes translations temps-température que pour la caractérisation de la rigidité; iv) manifestent un endommagement et une consommation de la durée de vie (nombre de cycles déjà appliqué sur le nombre de cycles espéré pour la rupture) qui se cumule linéairement avec le nombre de cycles; et v) présentent une auto-cicatrisation qui est un effet secondaire pour des temps de repos en dessous de 4h.

- Une modélisation plus complète des effets du phénomène de non-linéarité serait utile pour l'analyse des essais cycliques. Pour les essais LRP analysés dans cette thèse, une hypothèse autour de la non-linéarité et de l'auto-échauffement a été faite, basée sur les données expérimentales à la température des essais LRP. Cette hypothèse peut être un premier pas vers la modélisation des effets de non-linéarité. Les résultats expérimentaux de la caractérisation de la non-linéarité présentés dans cette thèse constituent une précieuse source d'information pour des procédures de modélisation du phénomène.

- Même si les directions de thixotropie (relation entre le changement dans le module et dans l'angle de phase) ont été identifiées, au moins à 11 °C et 10 Hz, l'intensité de l'effet de ce phénomène au cours du temps reste à modéliser. Pour cela, des résultats expérimentaux à d'autres températures et fréquences devront être obtenus. Cela pourrait aussi confirmer la relation intrinsèque entre la non-linéarité et la thixotropie, qui partagent la direction en plans complexes pour d'autres conditions d'essai. La modélisation du phénomène de thixotropie serait un autre pas pour l'amélioration de l'interprétation des résultats d'essais cycliques sur matériaux bitumineux.

- Plus d'essais avec des temps de repos longs (plus de 4 h) pourraient être utilisés pour étudier le phénomène d'auto-cicatrisation, qui a été négligeable pour les premières 4 h de repos comparé aux autres phénomènes réversibles. Cela pourrait donner des informations pour la modélisation de ce phénomène, qui est encore peu compris par la communauté.

- Des études au niveau moléculaire (soit avec des méthodes expérimentales comme la microscopie électronique, soit avec des méthodes de modélisation comme la dynamique moléculaire) pourraient aider à comprendre la thixotropie dans le bitume. Pour étudier ce phénomène, un rapprochement du travail de chimistes, physiciens, ingénieurs scientifiques, et experts sur le comportement des matériaux bitumineux serait nécessaire. Améliorer la compréhension du phénomène de thixotropie aidera à interpréter le comportement de fatigue des matériaux bitumineux, ce qui est de grande importance pour la communauté scientifique.

- Après avoir avancé sur ces développements scientifiques, une meilleure compréhension des phénomènes produisant des changements du module complexe au cours d'essais cycliques sera obtenue. Cela inclut la compréhension des effets de température et de fréquence sur chacun d'entre eux. Il sera donc possible de modéliser ces phénomènes, particulièrement le dommage « réel ». La modélisation du dommage « réel » (après correction des phénomènes biaisants) facilitera la compréhension des importantes différences observées entre les comportements de matériaux bitumineux en laboratoire et in-situ, ce qui est un intérêt majeur pour le génie routier. Alors qu'en laboratoire plusieurs phénomènes interviennent sur le comportement du matériau, produisant plus de changement de module complexe que le dommage « réel », in-situ, à cause des longues périodes de repos entre chaque chargement, les effets des autres phénomènes, à l'exception de la non-linéarité, sont négligeables.

REFERENCES

AASHTO M320. (2009). Standard Specification for Performance-Graded Asphalt Binder. American Association of State Highway and Transportation officials.

AASHTO PP6. (1994). Standard practice for grading or verifying the performance grade of an asphalt binder. American Association of State Highway and Transportation officials.

AASHTO T313. (2012). Standard Method of Test for Determining the Flexural Creep Stiffness of Asphalt Binder Using the Bending Beam Rheometer (BBR). American Association of State Highway and Transportation officials.

AASHTO T314. (2012). Standard Method of Test for Determining the Fracture Properties of Asphalt Binder in Direct Tension (DT). American Association of State Highway and Transportation officials.

AASHTO T315. (2012). Standard Method of Test for Determining the Rheological Properties of Asphalt Binder Using a Dynamic Shear Rheometer (DSR). American Association of State Highway and Transportation officials.

Abu Al-Rub, R. K., Darabi, M. K., Kim, S.-M., Little, D. N., & Glover, C. J. (2013). Mechanistic-based constitutive modeling of oxidative aging in aging-susceptible materials and its effect on the damage potential of asphalt concrete. *Construction and Building Materials, 41*, 439–454. https://doi.org/10.1016/j.conbuildmat.2012.12.044

Abu Al-Rub, R. K., Darabi, M. K., Masad, E. A., & Little, D. N. (2011). A Unified Continuum Damage Mechanics Model for Predicting the Mechanical Response of Asphalt Mixtures and Pavements. *International Journal of Roads and Airports, 1*(1).

https://doi.org/10.5568/ijra.2011-01-05.6884

Airey, G. D., & Rahimzadeh, B. (2004). Combined bituminous binder and mixture linear rheological properties. *Construction and Building Materials*, *18*(7), 535–548. https://doi.org/10.1016/j.conbuildmat.2004.04.008

Airey, G. D., Rahimzadeh, B., & Collop, A. C. (2002). Linear viscoelastic limits of bituminous binders. *Journal of the Association of Asphalt Paving Technologists*, *71*, 89–115.

Airey, G. D., Rahimzadeh, B., & Collop, A. C. (2003). Viscoelastic linearity limits for bituminous materials. *Materials and Structures*, *36*(10), 643–647. https://doi.org/10.1007/BF02479495

Alavi, M. Z., Hajj, E. Y., & Morian, N. E. (2013). Approach for quantifying the effect of binder oxidative aging on the viscoelastic properties of asphalt mixtures. *Transportation Research Record: Journal of the Transportation Research Board*, *2373*, 109–120.

Anderson, D. A., & Goetz, W. H. (1973). Mechanical behavior and reinforcement of mineral filler-asphalt mixtures. *Journal of the Association of Asphalt Paving Technologists*, *42*, 37–66.

Baaj, H. (2002). *Comportement à la fatigue des matériaux granulaires traités aux liens hydrocarbonés* (Doctoral Thesis). Institut National des Sciences Appliquées (INSA) de Lyon, Lyon.

Baaj, H., Di Benedetto, H., & Chaverot, P. (2003). Fatigue of mixes: an intrinsic damage approach. In *Proceedings of the 6th RILEM Symposium PTEBM* (pp. 394–400). Zurich.

Baaj, H., Di Benedetto, H., & Chaverot, P. (2005). Effect of Binder Characteristics on Fatigue of Asphalt Pavement Using an Intrinsic Damage Approach. *Road Materials and Pavement Design*, *6*(2), 147–174. https://doi.org/10.1080/14680629.2005.9690003

Babadopulos, L. F. A. L. (2014). *A Contribution to couple aging to hot mix asphalt (HMA)*

mechanical characterization under load-induced damage (M.Sc. Thesis). Federal University of Ceará, Fortaleza, Brazil.

Babadopulos, L. F. A. L., Ferreira, J. L. S., & Soares, J. B. (2016). An approach to couple aging to stiffness and permanent deformation modeling of asphalt mixtures. *Materials and Structures*. https://doi.org/10.1617/s11527-016-0834-4

Babadopulos, L. F. A. L., Ferreira, J. L. S., Soares, J. B., Nascimento, L. A. H., & Castelo Branco, V. T. F. (2016). Aging-Effect Incorporation into the Fatigue-Damage Modeling of Asphalt Mixtures Using the S-VECD Model. *Journal of Materials in Civil Engineering*, *28*(12), 4016161. https://doi.org/10.1061/(ASCE)MT.1943-5533.0001676

Babadopulos, L. F. A. L., Sauzéat, C., & Di Benedetto, H. (2016). Calculation of stiffness change induced by self-heating during cyclic loading of bituminous mixtures considered as heterogeneous medium. Presented at the International Society for Asphalt Pavements (ISAP) 2016 Symposium, Jackson Hole, USA.

Babadopulos, L. F. A. L., Sauzéat, C., & Di Benedetto, H. (2017a). Softening and local self-heating of bituminous mixtures during cyclic loading. *Road Materials and Pavement Design*, 1–14. https://doi.org/10.1080/14680629.2017.1304260

Babadopulos, L. F. A. L., Sauzéat, C., & Di Benedetto, H. (2017b). Thermomechanical coupling in bituminous mixtures considered as bonded granular media. Presented at the 6th Biot Conference on Poromechanics, Paris, France.

Babadopulos, L. F. A. L., Soares, J. B., & Castelo Branco, V. T. F. (2015). Interpreting fatigue tests in hot mix asphalt (HMA) using concepts from viscoelasticity and damage mechanics. *TRANSPORTES*, *23*(2), 85. https://doi.org/10.14295/transportes.v23i2.898

Baek, C., Underwood, B., & Kim, Y. (2012). Effects of Oxidative Aging on Asphalt Mixture

Properties. *Transportation Research Record: Journal of the Transportation Research Board*, *2296*, 77–85. https://doi.org/10.3141/2296-08

Bahia, H. U., & Anderson, D. A. (1995). The Development of the Bending Beam Rheometer; Basics and Critical Evaluation of the Rheometer. In J. C. Hardin (Ed.), *Physical Properties of Asphalt Cement Binders* (pp. 28-28–23). 100 Barr Harbor Drive, PO Box C700, West Conshohocken, PA 19428-2959: ASTM International. https://doi.org/10.1520/STP18187S

Bahia, H. U., Zhai, H., Onnetti, K., & Kose, S. (1999). Non-Linear Viscoelastic and Fatigue Properties of Asphalt Binders. *Journal of the Association of Asphalt Paving Technologists*, *68*, 1–34.

Bari, J., & Witczak, M. W. (n.d.). Development of a new revised version of the Witczak E* predictive model of hot mix asphalt mixtures. *Journal of the Association of Asphalt Paving Technologists*, *75*, 381–424.

Barnes, H. A. (1997). Thixotropy—a review. *Journal of Non-Newtonian Fluid Mechanics*, *70*(1–2), 1–33. https://doi.org/10.1016/S0377-0257(97)00004-9

Bastos, J. B. S., Babadopulos, L. F. A. L., & Soares, J. B. (2017). Relationship between multiple stress creep recovery (MSCR) binder test results and asphalt concrete rutting resistance in Brazilian roadways. *Construction and Building Materials*, *145*, 20–27. https://doi.org/10.1016/j.conbuildmat.2017.03.216

Bastos, J. B. S., Torquato e Silva, S. A., Soares, J. B., Nascimento, L. A. H., & Kim, Y. R. (2016). Triaxial stress sweep test protocol considerations for permanent deformation characterisation of asphalt mixtures. *Road Materials and Pavement Design*, 1–14. https://doi.org/10.1080/14680629.2016.1261729

Behzadfar, E., & Hatzikiriakos, S. G. (2014). Rheology of bitumen: Effects of temperature,

pressure, CO2 concentration and shear rate. *Fuel*, *116*, 578–587. https://doi.org/10.1016/j.fuel.2013.08.024

Bhasin, A., Little, D. N., Bommavaram, R., & Vasconcelos, K. (2008). A Framework to Quantify the Effect of Healing in Bituminous Materials using Material Properties. *Road Materials and Pavement Design*, *9*(sup1), 219–242. https://doi.org/10.1080/14680629.2008.9690167

Biot, M. A. (1954). Theory of stress-strain relations in anisotropic viscoelasticity and relaxation phenomena. *Journal of Applied Physics*, *25*(11), 1385–1391.

Biot, M. A. (1955). Dynamics of Viscoelastic Anisotropic Media. In *Proceedings of the 4th Midwestern Conference on Solid Mechanics* (p. Publication #129). Lafayette, USA: Engineering Experiment Station.

Bodin, D., Soenen, H., & De La Roche Saint-André, C. (2004). Temperature effects in binder fatigue and healing tests. Presented at the Eurasphalt & Eurobitume Conference, Vienna.

Brinson, H. F., & Brinson, L. C. (2015). *Polymer Engineering Science and Viscoelasticity*. Boston, MA: Springer US. https://doi.org/10.1007/978-1-4899-7485-3

Canestrari, F., Virgili, A., Graziani, A., & Stimilli, A. (2015). Modeling and assessment of self-healing and thixotropy properties for modified binders. *International Journal of Fatigue*, *70*, 351–360. https://doi.org/10.1016/j.ijfatigue.2014.08.004

Cardona, D. A. R. (2016). *Characterisation of thermomechanical properties of bituminous mixtures used for railway infrastructures* (Doctoral Thesis). École Nationale des Travaux Publics de l'État (ENTPE) de l'Université de Lyon (UdL), Vaulx-en-Velin.

Carpenter, S., Ghuzlan, K., & Shen, S. (2003). Fatigue Endurance Limit for Highway and Airport Pavements. *Transportation Research Record: Journal of the Transportation Research Board*, *1832*, 131–138. https://doi.org/10.3141/1832-16

Carpenter, S. H., & Vandam, T. (1987). Laboratory performance comparisons of polymer-modified and unmodified asphalt concrete mixtures. *Transportation Research Record: Journal of the Transportation Research Board, 1115,* 62–74.

Chen, J.-S., & Peng, C.-H. (1998). Analyses of Tensile Failure Properties of Asphalt-Mineral Filler Mastics. *Journal of Materials in Civil Engineering*, *10*(4), 256–262. https://doi.org/10.1061/(ASCE)0899-1561(1998)10:4(256)

Choi, Y.-T., & Kim, Y. R. (2013). Development of characterisation models for incremental permanent deformation model for asphalt concrete in confined compression. *Road Materials and Pavement Design*, *14*(sup2), 266–288. https://doi.org/10.1080/14680629.2013.812847

Choi, Y.-T., & Kim, Y. R. (2014). Implementation and verification of a mechanistic permanent deformation model (shift model) to predict rut depths of asphalt pavement. *Road Materials and Pavement Design*, *15*(sup1), 195–218. https://doi.org/10.1080/14680629.2014.927085

Choi, Y.-T., Subramanian, V., Guddati, M., & Kim, Y. (2012). Incremental Model for Prediction of Permanent Deformation of Asphalt Concrete in Compression. *Transportation Research Record: Journal of the Transportation Research Board*, *2296*, 24–35. https://doi.org/10.3141/2296-03

Coutinho, R. P., Babadopulos, L. F. A. L., Freire, R. A., Castelo Branco, V. T. F., & Soares, J. B. (2014). The use of stress sweep tests for asphalt mixtures nonlinear viscoelastic and fatigue damage responses identification. *Materials and Structures*, *47*(5), 895–909. https://doi.org/10.1617/s11527-013-0101-x

Daniel, J. S., & Kim, Y. R. (2001). Laboratory Evaluation of Fatigue Damage and Healing of Asphalt Mixtures. *Journal of Materials in Civil Engineering*, *13*(6), 434–440. https://doi.org/10.1061/(ASCE)0899-1561(2001)13:6(434)

Daniel, J. S., Kim, Y. R., & Lee, J. (1998). Effects of aging on viscoelastic properties of asphalt-aggregate mixtures. *Transportation Research Record: Journal of the Transportation Research Board*, *1630*, 21–27.

Darabi, M., Abu Al-Rub, R., Masad, E., & Little, D. (2013). Constitutive Modeling of Fatigue Damage Response of Asphalt Concrete Materials. *Transportation Research Record: Journal of the Transportation Research Board*, *2373*, 11–21. https://doi.org/10.3141/2373-02

Darabi, M. K., Abu Al-Rub, R. K., Masad, E. A., & Little, D. N. (2013). Constitutive modeling of fatigue damage response of asphalt concrete materials with consideration of micro-damage healing. *International Journal of Solids and Structures*, *50*(19), 2901–2913. https://doi.org/10.1016/j.ijsolstr.2013.05.007

De La Roche, C., & Marsac, P. (1996). Caractérisation expérimentale de la dissipation thermique dans un enrobé bitumineux sollicité en fatigue. In *Proceedings of the Eurasphalt & Eurobitume Congress*. Strasbourg.

Delaporte, B. (2007). *Étude de la rhéologie des mastics bitumineux à l'aide d'un rhéomètre à cisaillement annulaire* (Doctoral Thesis). Institut National des Sciences Appliquées (INSA) de Lyon, Lyon.

Delaporte, B., Di Benedetto, H., Chaverot, P., & Gauthier, G. (2007). Linear Viscoelastic Properties of Bituminous Materials: from Binders to Mastics. *Journal of the Association of Asphalt Paving Technologists*, *76*, 455–494.

Delaporte, B., Di Benedetto, H., Chaverot, P., & Gauthier, G. (2009). Linear Viscoelastic Properties of Bituminous Materials Including New Products Made with Ultrafine Particles. *Road Materials and Pavement Design*, *10*(1), 7–38. https://doi.org/10.1080/14680629.2009.9690180

Delgadillo, R., Bahia, H. U., & Lakes, R. (2012). A nonlinear constitutive relationship for asphalt binders. *Materials and Structures*, *45*(3), 457–473. https://doi.org/10.1617/s11527-011-9777-y

Di Benedetto, H., Ashayer Soltani, A., & Chaverot, P. (1996). Fatigue damage for bituminous mixtures: a pertinent approach. *Journal of the Association of Asphalt Paving Technologists*, *65*, 142–158.

Di Benedetto, H., & Corté, J.-F. (2005). *Matériaux routiers bitumeux 2: constitution et propriétés thermomécaniques des mélanges*. Paris: Hermès Science Publications.

Di Benedetto, H., de La Roche, C., Baaj, H., Pronk, A., & Lundström, R. (2004). Fatigue of bituminous mixtures. *Materials and Structures*, *37*(3), 202–216. https://doi.org/10.1007/BF02481620

Di Benedetto, H., Delaporte, B., & Sauzéat, C. (2007). Three-Dimensional Linear Behavior of Bituminous Materials: Experiments and Modeling. *International Journal of Geomechanics*, *7*, 149–157. https://doi.org/10.1061/(ASCE)1532-3641(2007)7:2(149)

Di Benedetto, H., Gabet, T., Grenfell, J., Perraton, D., Sauzéat, C., & Bodin, D. (2013). Mechanical Testing of Bituminous Mixtures. In M. N. Partl, H. U. Bahia, F. Canestrari, C. de la Roche, H. Di Benedetto, H. Piber, & D. Sybilski (Eds.), *Advances in Interlaboratory Testing and Evaluation of Bituminous Materials* (Vol. 9, pp. 143–256). Dordrecht: Springer Netherlands. https://doi.org/10.1007/978-94-007-5104-0_4

Di Benedetto, H., Mondher, N., Sauzéat, C., & Olard, F. (2007). Three-dimensional Thermo-viscoplastic Behaviour of Bituminous Materials: The DBN Model. *Road Materials and Pavement Design*, *8*(2), 285–315. https://doi.org/10.1080/14680629.2007.9690076

Di Benedetto, H., Nguyen, H. M., Pouget, S., & Sauzéat, C. (2008). Time-temperature

superposition principle for bituminous mixtures: three dimensional approach and extension in the nonlinear domain (pp. 178–188). Presented at the First International Conference on Transportation Infrastructure (ICTI), Beijing.

Di Benedetto, H., Nguyen, Q. T., & Sauzéat, C. (2011). Nonlinearity, Heating, Fatigue and Thixotropy during Cyclic Loading of Asphalt Mixtures. *Road Materials and Pavement Design*, *12*(1), 129–158. https://doi.org/10.1080/14680629.2011.9690356

Di Benedetto, H., Olard, F., Sauzéat, C., & Delaporte, B. (2004). Linear viscoelastic behaviour of bituminous materials: From binders to mixes. *Road Materials and Pavement Design*, *5*(sup1), 163–202. https://doi.org/10.1080/14680629.2004.9689992

Di Benedetto, H., Partl, M. N., Francken, L., & De La Roche Saint André, C. (2001). Stiffness testing for bituminous mixtures. *Materials and Structures*, *34*(2), 66–70. https://doi.org/10.1007/BF02481553

Di Benedetto, H., Sauzeat, C., Bilodeau, K., Buannic, M., Mangiafico, S., Nguyen, Q. T., … Van Rompu, J. (2011). General overview of the time-temperature superposition principle validity for materials containing bituminous binder. *International Journal of Roads and Airports*, *1*(1). https://doi.org/10.5568/ijra.2011-01-03.3552

Di Benedetto, H., Sauzéat, C., & Clec'h, P. (2016). Anisotropy of bituminous mixture in the linear viscoelastic domain. *Mechanics of Time-Dependent Materials*, *20*(3), 281–297. https://doi.org/10.1007/s11043-016-9305-0

Di Benedetto, H., Sauzéat, C., & Sohm, J. (2009). Stiffness of Bituminous Mixtures Using Ultrasonic Wave Propagation. *Road Materials and Pavement Design*, *10*(4), 789–814. https://doi.org/10.3166/rmpd.10.789-814

Di Benedetto, H., Tatsuoka, F., Lo Presti, D., Sauzéat, C., & Geoffroy, H. (2003). *Time effects on*

the behaviour of geomaterials. Keynote lecture in: Deformation characteristics of geomaterials, proceedings of the Third International Symposium on Deformation Characteristics of Geomaterials. (H. Di Benedetto, T. Doanh, H. Geoffroy, & C. Sauzéat, Eds.) (Vol. 2, pp. 59–124). Lyon: A.A. Balkema.

Doan, T. H. (1977). Les études de fatigue des enrobés bitumineux au LCPC. *Bulletin de Liaison Des Laboratoires Des Ponts et Chaussées, Numéro Spécial V*, 215–228.

Doolittle, A. K., & Doolittle, D. B. (1957). Studies in Newtonian Flow. V. Further Verification of the Free-Space Viscosity Equation. *Journal of Applied Physics*, *28*(8), 901–905. https://doi.org/10.1063/1.1722884

Doubbaneh, E. (1995). *Comportement mécanique des enrobés bitumineux des "petites" aux "grandes" déformations* (Doctoral Thesis). ENTPE-INSA Lyon, Lyon.

Dougan, C. E., Stephens, J. E., Mahoney, J., & Hansen, G. (2003). *E* - Dynamic modulus test protocol - Problems and solutions* (No. CT-SPR-0003084-F-03-3) (p. 70p). University of Connecticut, Connecticut Transportation Institute.

Einstein, A. (1906). Eine neue Bestimmung der Moleküldimensionen. *Annalen Der Physik*, *19*, 289–306.

Emri, I. (2005). Rheology of solid polymers. In D. M. Binding, K. Walters, & British Society of Rheology (Eds.), *Rheology reviews 2005* (pp. 49–100). Place of publication not identified: British Society of Rheology.

Fan, W. (2016). *Etude du phénomène de non-linéarité au cours des sollicitations cycliques sur un enrobé bitumineux* (Master's thesis). Vaulx-en-Velin.

Ferry, J. D. (1980). *Viscoelastic properties of polymers* (3d ed). New York: Wiley.

Findley, W. N., Lai, J. S., & Onaran, K. (1976). *Creep and relaxation of nonlinear viscoelastic*

materials, with an introduction to linear viscoelasticity. North-Holland Pub. Co Sole distributors for the U.S.A. and Canada Elsevier/North Holland.

Gauthier, G., Bodin, D., Chailleux, E., & Gallet, T. (2010). Non Linearity in Bituminous Materials during Cyclic Tests. *Road Materials and Pavement Design*, *11*(sup1), 379–410. https://doi.org/10.1080/14680629.2010.9690339

Gayte, P., Di Benedetto, H., Sauzéat, C., & Nguyen, Q. T. (2016). Influence of transient effects for analysis of complex modulus tests on bituminous mixtures. *Road Materials and Pavement Design*, *17*(2), 271–289. https://doi.org/10.1080/14680629.2015.1067246

Ghuzlan, K. A., & Carpenter, S. H. (2003). Traditional fatigue analysis of asphalt concrete mixtures. In *Proceedings of the 2003 TRB Annual Meeting*.

Ghuzlan, K. A., & Carpenter, S. H. (2006). Fatigue damage analysis in asphalt concrete mixtures using the dissipated energy approach. *Canadian Journal of Civil Engineering*, *33*(7), 890–901. https://doi.org/10.1139/l06-032

Ghuzlan, K., & Carpenter, S. (2000). Energy-Derived, Damage-Based Failure Criterion for Fatigue Testing. *Transportation Research Record: Journal of the Transportation Research Board*, *1723*, 141–149. https://doi.org/10.3141/1723-18

Glover, C. J., Martin, A. E., Chowdhury, A., Han, R., Prapaitrakul, N., Jin, X., & Lawrence, J. (2008). *Evaluation of binder aging and its influence in aging of hot mix asphalt concrete: literature review and experimental design* (No. FHWA/TX-08/0-6009-1).

Goddard, J. D., & Miller, C. (1967). Nonlinear effects in the rheology of dilute suspensions. *Journal of Fluid Mechanics*, *28*(4), 657. https://doi.org/10.1017/S0022112067002381

Goodrich, J. L. (1991). Asphalt binder rheology, asphalt concrete rheology and asphalt concrete mix properties. *Journal of the Association of Asphalt Paving Technologists*, *60*, 80–120.

Green, A. E., & Rivlin, R. S. (1957). The mechanics of non-linear materials with memory: Part I. *Archive for Rational Mechanics and Analysis*, *1*(1), 1–21. https://doi.org/10.1007/BF00297992

Green, A. E., Rivlin, R. S., & Spencer, A. J. M. (1997). The Mechanics of Non-Linear Materials with Memory. In G. I. Barenblatt & D. D. Joseph (Eds.), *Collected Papers of R.S. Rivlin* (pp. 1127–1136). New York, NY: Springer New York. https://doi.org/10.1007/978-1-4612-2416-7_70

Gross, B. (1968). *Mathematical Structure of the Theories of Viscoelasticity*. Paris: Hermann et Cie.

Gudmarsson, A., Ryden, N., Di Benedetto, H., & Sauzéat, C. (2015). Complex modulus and complex Poisson's ratio from cyclic and dynamic modal testing of asphalt concrete. *Construction and Building Materials*, *88*, 20–31. https://doi.org/10.1016/j.conbuildmat.2015.04.007

Herrington, P. R., & Ball, G. F. A. (1996). Temperature dependence of asphalt oxidation mechanism. *Fuel*, *75*(9), 1129–1131. https://doi.org/10.1016/0016-2361(96)00042-7

Highter, W. H., & Wall, D. J. (1984). Thermal properties of some asphaltic concrete mixes. *Transportation Research Record: Journal of the Transportation Research Board*, *968*, 38–45.

Hopman, P. C., Kunst, P. A. J., & Pronk, A. C. (1989). A renewed intepretation method for fatigue measurements: verification of Miner's rule. In *Proceedings of the 4th Eurobitume Symposium* (Vol. 1, pp. 557–561).

Huang, S.-C., & Di Benedetto, H. (Eds.). (2015). *Advances in asphalt materials: road and pavement construction*. Oxford: Woodhead Publishing.

Huang, Y. H. (2004). *Pavement analysis and design* (2nd ed). Upper Saddle River, NJ:

Pearson/Prentice Hall.

Huet, C. (1963). *Étude par une méthode d'impédance du comportement viscoélastique des matériaux hydrocarbonés* (Doctoral Thesis). Université de Paris.

Hunter, R. N., Self, A., & Read, J. (2015). *The Shell Bitumen handbook* (Sixth edition). Westminster, London: Published for Shell Bitumen by ICE Publishing.

IEC 60584-1. (2013). Thermocouples - Part 1: EMF specifications and tolerances. International Electrotechnical Comission.

IEC 60751. (2008). Industrial platinum resistance thermometers and platinum temperature sensors. International Electrotechnical Comission.

Isacsson, U., & Zeng, H. (1998). Low-temperature cracking of polymer-modified asphalt. *Materials and Structures, 31*(1), 58–63. https://doi.org/10.1007/BF02486415

Isailović, I., Wistuba, M. P., & Cannone Falchetto, A. (2017). Investigation on mixture recovery properties in fatigue tests. *Road Materials and Pavement Design*, 1–11. https://doi.org/10.1080/14680629.2017.1300598

Islam, M. R., & Tarefder, R. A. (2014). Determining thermal properties of asphalt concrete using field data and laboratory testing. *Construction and Building Materials, 67*, 297–306. https://doi.org/10.1016/j.conbuildmat.2014.03.040

Kachanov, L. M. (1958). Rupture time under creep conditions. *Izvestia Akademii Nauk SSSR, Otdelenie Tekhnicheskich Nauk*, (8), 26–31.

Kachanov, L. M. (1986). *Introduction to continuum damage mechanics* (Vol. 10). Dordrecht: Springer Netherlands. https://doi.org/10.1007/978-94-017-1957-5

Karki, P., Li, R., & Bhasin, A. (2015). Quantifying overall damage and healing behaviour of

asphalt materials using continuum damage approach. *International Journal of Pavement Engineering*, *16*(4), 350–362. https://doi.org/10.1080/10298436.2014.942993

Kim, Y. R. (Ed.). (2009). *Modeling of asphalt concrete*. Reston, VA : New York: ASCE Press ; McGraw-Hill.

Kim, Y. R., Lee, H.-J., & Little, D. N. (1997). Fatigue characterization of asphalt concrete using viscoelasticity and continuum damage theory. *Journal of the Association of Asphalt Paving Technologists*, *66*, 520–569.

Kim, Y.-R., Little, D. N., & Lytton, R. L. (2003). Fatigue and Healing Characterization of Asphalt Mixtures. *Journal of Materials in Civil Engineering*, *15*(1), 75–83. https://doi.org/10.1061/(ASCE)0899-1561(2003)15:1(75)

King, G. N., Muncy, H. W., & Prudhomme, J. B. (1986). Polymer modification: Binder's effect on mix properties. *Journal of the Association of Asphalt Paving Technologists*, *55*, 519–540.

Kongkitkul, W., Tatsuoka, F., Duttine, A., Kawabe, S., Enomoto, T., & Di Benedetto, H. (2008). Modelling and simulation of rate-dependent stress-strain behaviour of granular materials in shear. *SOILS AND FOUNDATIONS*, *48*(2), 175–194. https://doi.org/10.3208/sandf.48.175

Lamothe, S. (2014). *Endommagement d'un enrobé bitumineux partiellement saturé en eau ou en saumure soumis à des sollicitations cycliques de gel-dégel et mécaniques* (Doctoral Thesis). Cotutelle École de Technologie Supérieure (ÉTS), Canada, et École Nationale des Travaux Publics de l'État (ENTPE), France, Montréal, Canada.

Lamothe, S., Perraton, D., & Di Benedetto, H. (2015). Contraction and expansion of partially saturated hot mix asphalt samples exposed to freeze–thaw cycles. *Road Materials and Pavement Design*, *16*(2), 277–299. https://doi.org/10.1080/14680629.2014.990917

Lau, C. K., Lunsford, K. M., Glover, C. J., Davison, R. R., & Bullin, J. A. (1992). Reaction Rates

and Hardening Susceptibilities as Determined from Pressure Oxygen Vessel Aging of Asphalts. *Transportation Research Record: Journal of the Transportation Research Board*, *1342*, 50–57.

Lee, D. Y., & Huang, R. J. (1973). Weathering of Asphalts as Characterized by Infrared Multiple Internal Reflection Spectra. *Applied Spectroscopy*, *27*(6), 435–440. https://doi.org/10.1366/000370273774333236

Lee, H.-J., & Kim, Y. R. (1998). Viscoelastic Constitutive Model for Asphalt Concrete under Cyclic Loading. *Journal of Engineering Mechanics*, *124*(1), 32–40. https://doi.org/10.1061/(ASCE)0733-9399(1998)124:1(32)

Lemaître, J., & Chaboche, J.-L. (1990). *Mechanics of solid materials*. Cambridge: Cambridge University Press.

Lesueur, D. (2009). The colloidal structure of bitumen: Consequences on the rheology and on the mechanisms of bitumen modification. *Advances in Colloid and Interface Science*, *145*(1–2), 42–82. https://doi.org/10.1016/j.cis.2008.08.011

Lira, B., Jelagin, D., & Birgisson, B. (2013). Gradation-based framework for asphalt mixture. *Materials and Structures*, *46*(8), 1401–1414. https://doi.org/10.1617/s11527-012-9982-3

Little, D. N., & Petersen, J. C. (2005). Unique Effects of Hydrated Lime Filler on the Performance-Related Properties of Asphalt Cements: Physical and Chemical Interactions Revisited. *Journal of Materials in Civil Engineering*, *17*(2), 207–218. https://doi.org/10.1061/(ASCE)0899-1561(2005)17:2(207)

Liu, M., Ferry, M. A., Davison, R. R., Glover, C. J., & Bullin, J. A. (1998). Oxygen Uptake As Correlated to Carbonyl Growth in Aged Asphalts and Asphalt Corbett Fractions. *Industrial & Engineering Chemistry Research*, *37*(12), 4669–4674. https://doi.org/10.1021/ie980450o

Liu, M., Lunsford, K. M., Davison, R. R., Glover, C. J., & Bullin, J. A. (1996). The kinetics of carbonyl formation in asphalt. *AIChE Journal*, *42*(4), 1069–1076. https://doi.org/10.1002/aic.690420417

Liu, Q., Schlangen, E., García, Á., & van de Ven, M. (2010). Induction heating of electrically conductive porous asphalt concrete. *Construction and Building Materials*, *24*(7), 1207–1213. https://doi.org/10.1016/j.conbuildmat.2009.12.019

Liu, Q., Schlangen, E., van de Ven, M., & García, Á. (2010). Healing of Porous Asphalt Concrete *via* Induction Heating. *Road Materials and Pavement Design*, *11*(sup1), 527–542. https://doi.org/10.1080/14680629.2010.9690345

Lockett, F. J. (1965). Creep and stress-relaxation experiments for non-linear materials. *International Journal of Engineering Science*, *3*(1), 59–75. https://doi.org/10.1016/0020-7225(65)90020-0

Lockett, F. J. (1972). *Nonlinear viscoelastic solids*. London, New York: Academic Press.

Loeber, L., Sutton, O., Morel, J., Valleton, J.-M., & Muller, G. (1996). New direct observations of asphalts and asphalt binders by scanning electron microscopy and atomic force microscopy. *Journal of Microscopy*, *182*(1), 32–39. https://doi.org/10.1046/j.1365-2818.1996.134416.x

Lundström, R., Ekblad, J., & Isacsson, U. (2004). Influence of Hysteretic Heating on Asphalt Fatigue Characterization. *Journal of Testing and Evaluation*, *32*(6), 12284. https://doi.org/10.1520/JTE12284

Lundstrom, R., & Isacsson, U. (2003). Asphalt Fatigue Modelling Using Viscoelastic Continuum Damage Theory. *Road Materials and Pavement Design*, *4*(1), 51–75. https://doi.org/10.1080/14680629.2003.9689940

Mangiafico, S. (2014). *Linear viscoelastic properties and fatigue of bituminous mixtures produced with Reclaimed Asphalt Pavement and corresponding binder blends* (Doctoral Thesis). École Nationale des Travaux Publics de l'État (ENTPE) de l'Université de Lyon (UdL), Vaulx-en-Velin.

Mangiafico, S., Babadopulos, L. F. A. L., Sauzéat, C., & Di Benedetto, H. (2017). Nonlinearity of bituminous mixtures. *Mechanics of Time-Dependent Materials*. https://doi.org/10.1007/s11043-017-9350-3

Mangiafico, S., Sauzéat, C., Di Benedetto, H., Pouget, S., Olard, F., & Planque, L. (2015). Quantification of biasing effects during fatigue tests on asphalt mixes: non-linearity, self-heating and thixotropy. *Road Materials and Pavement Design*, *16*(sup2), 73–99. https://doi.org/10.1080/14680629.2015.1077000

Masad, E., Al-Rub, R. A., & Little, D. N. (2012). Recent Developments and Applications of Pavement Analysis Using Nonlinear Damage (PANDA) Model. In A. Scarpas, N. Kringos, I. Al-Qadi, & L. A. (Eds.), *7th RILEM International Conference on Cracking in Pavements* (pp. 399–408). Dordrecht: Springer Netherlands. https://doi.org/10.1007/978-94-007-4566-7_39

Masad, E., Tashman, L., Little, D., & Zbib, H. (2005). Viscoplastic modeling of asphalt mixes with the effects of anisotropy, damage and aggregate characteristics. *Mechanics of Materials*, *37*(12), 1242–1256. https://doi.org/10.1016/j.mechmat.2005.06.003

Mengis, M. (1997). *Contribution à l'interprétation des essais de fatigue par une approche thermo-mécanique* (Master's thesis). ENTPE, Vaulx-en-Velin.

Mewis, J., & Wagner, N. J. (2009). Thixotropy. *Advances in Colloid and Interface Science*, *147–148*, 214–227. https://doi.org/10.1016/j.cis.2008.09.005

Miner, M. A. (1945). Cumulative damage in fatigue. *Journal of Applied Mechanics*, *67*, 159–164.

Moreno-Navarro, F., Ayar, P., Sol-Sánchez, M., & Rubio-Gámez, M. C. (2017). Exploring the recovery of fatigue damage in bituminous mixtures at macro-crack level: the influence of temperature, time, and external loads. *Road Materials and Pavement Design*, *18*(sup2), 293–303. https://doi.org/10.1080/14680629.2017.1305149

Moreno-Navarro, F., Rubio-Gámez, M. C., Miró, R., & Pérez-Jiménez, F. (2015). The influence of temperature on the fatigue behaviour of bituminous materials for pavement rehabilitation. *Road Materials and Pavement Design*, *16*(sup1), 300–313. https://doi.org/10.1080/14680629.2015.1029676

Moreno-Navarro, F., Sol-Sánchez, M., & Rubio-Gámez, M. C. (2015). Exploring the recovery of fatigue damage in bituminous mixtures: the role of healing. *Road Materials and Pavement Design*, *16*(sup1), 75–89. https://doi.org/10.1080/14680629.2015.1029706

Mounier, D., Di Benedetto, H., & Sauzéat, C. (2012). Determination of bituminous mixtures linear properties using ultrasonic wave propagation. *Construction and Building Materials*, *36*, 638–647. https://doi.org/10.1016/j.conbuildmat.2012.04.136

Moutier, F. (1991). Étude statistique de l'effet de la composition des enrobés bitumineux sur leur comportement en fatigue et leur module complexe. *Bulletin de Liaison Des Laboratoires Des Ponts et Chaussées*, *172*, 33–41.

Mrawira, D. M., & Luca, J. (2006). Effect of aggregate type, gradation, and compaction level on thermal properties of hot-mix asphalts. *Canadian Journal of Civil Engineering*, *33*(11), 1410–1417. https://doi.org/10.1139/l06-076

Neifar, M. (1997). *Comportement thermomécanique des enrobés bitumineux: expérimentation et modélisation* (Doctoral Thesis). Institut National des Sciences Appliquées (INSA) de Lyon,

Lyon.

Neifar, M., & Di Benedetto, H. (2001). Thermo-viscoplastic law for bituminous mixes. *Road Materials and Pavement Design, 2*(1), 71–95. https://doi.org/10.1080/14680629.2001.9689894

NF EN 1426. (2007). Bitumen and bituminous binders. Determination of needle penetration. European standard.

NF EN 1427. (2007). Bitumen and bituminous binders. Determination of the softening point. Ring and Ball method. European standard.

NF EN 12593. (2007). Bitumen and bituminous binders. Determination of the Fraass breaking point. European standard.

NF EN 12597. (2014). Bitumen and bituminous binders. Terminology. European standard.

NF EN 12697-24. (2012). Bituminous mixtures. Test methods for hot mix asphalt. Part 24: Resistance to fatigue. European standard.

NF EN 12697-33. (2007). Bituminous mixtures. Test methods for hot mix asphalt. Part 33: specimen prepared by roller compactor. European standard.

NF EN 12697-35. (2007). Bituminous mixtures. Test methods for hot mix asphalt. Part 35: laboratory mixing. European standard.

NF EN 13108-1. (2007). Bituminous mixtures. Materials specifications. Part 1: Asphalt concrete. European standard.

Nguyen, H. M. (2010). *Comportement cyclique aux déformations permanentes des enrobés bitumineux* (Doctoral Thesis). École Nationale des Travaux Publics de l'État (ENTPE) de l'Université de Lyon (UdL), Vaulx-en-Velin.

Nguyen, H. M., Pouget, S., Di Benedetto, H., & Sauzéat, C. (2009). Time-temperature superposition principle for bituminous mixtures. *European Journal of Environmental and Civil Engineering*, *13*(9), 1095–1107. https://doi.org/10.1080/19648189.2009.9693176

Nguyen, M. L., Sauzéat, C., Di Benedetto, H., & Tapsoba, N. (2013). Validation of the time–temperature superposition principle for crack propagation in bituminous mixtures. *Materials and Structures*, *46*(7), 1075–1087. https://doi.org/10.1617/s11527-012-9954-7

Nguyen, Q. T. (2011). *Comportement thermomécanique des enrobés bitumineux sous sollicitations cycliques dans les domaines linéaire et non-linéaire* (Doctoral Thesis). École Nationale des Travaux Publics de l'État (ENTPE) de l'Université de Lyon (UdL), Vaulx-en-Velin.

Nguyen, Q. T., Di Benedetto, H., & Sauzéat, C. (2012). Determination of thermal properties of asphalt mixtures as another output from cyclic tension-compression test. *Road Materials and Pavement Design*, *13*(1), 85–103. https://doi.org/10.1080/14680629.2011.644082

Nguyen, Q. T., Di Benedetto, H., & Sauzéat, C. (2015). Linear and nonlinear viscoelastic behaviour of bituminous mixtures. *Materials and Structures*, *48*(7), 2339–2351. https://doi.org/10.1617/s11527-014-0316-5

Nguyen, Q. T., Di Benedetto, H., Sauzéat, C., & Tapsoba, N. (2013). Time Temperature Superposition Principle Validation for Bituminous Mixes in the Linear and Nonlinear Domains. *Journal of Materials in Civil Engineering*, *25*(9), 1181–1188. https://doi.org/10.1061/(ASCE)MT.1943-5533.0000658

Oakley, J. G., Giacomin, A. J., & Yosick, J. A. (1998). Molecular origins of nonlinear viscoelasticity. *Mikrochimica Acta*, *130*(1–2), 1–28. https://doi.org/10.1007/BF01254586

Olard, F. (2003). *Comportement thermomécanique des enrobés bitumineux à basses températures: Relations entre les propriétés du liant et de l'enrobé* (Doctoral Thesis). Institut National

des Sciences Appliquées (INSA) de Lyon, Lyon.

Olard, F., & Di Benedetto, H. (2003). General “2S2P1D” Model and Relation Between the Linear Viscoelastic Behaviours of Bituminous Binders and Mixes. *Road Materials and Pavement Design*, *4*(2), 185–224. https://doi.org/10.1080/14680629.2003.9689946

Olard, F., Di Benedetto, H., Dony, A., & Vaniscote, J.-C. (2005). Properties of bituminous mixtures at low temperatures and relations with binder characteristics. *Materials and Structures*, *38*(1), 121–126. https://doi.org/10.1007/BF02480584

Orozco, G. (2016). *Etude du comportement thermomécanique d’un bitume à l’aide d’un rhéomètre à cisaillement annulaire* (Master’s thesis). ENTPE, Vaulx-en-Velin.

Palmgreen, A. (1924). Die Lebensdauer von Kugellagem. *Zeitschrift des Vereins deutscher Ingenieure*, *68*(339–341).

Palvadi, S., Bhasin, A., & Little, D. (2012). Method to Quantify Healing in Asphalt Composites by Continuum Damage Approach. *Transportation Research Record: Journal of the Transportation Research Board*, *2296*, 86–96. https://doi.org/10.3141/2296-09

Park, S. W., Kim, Y. R., & Schapery, R. A. (1996). A viscoelastic continuum damage model and its application to uniaxial behavior of asphalt concrete. *Mechanics of Materials*, *24*(4), 241–255. https://doi.org/10.1016/S0167-6636(96)00042-7

Park, S. W., & Schapery, R. A. (1997). A viscoelastic constitutive model for particulate composites with growing damage. *International Journal of Solids and Structures*, *34*(8), 931–947. https://doi.org/10.1016/S0020-7683(96)00066-2

Park, S. W., & Schapery, R. A. (1999). Methods of interconversion between linear viscoelastic material functions. Part I—a numerical method based on Prony series. *International Journal of Solids and Structures*, *36*(11), 1653–1675. https://doi.org/10.1016/S0020-

7683(98)00055-9

Partl, M. N., Bahia, H. U., Canestrari, F., de la Roche, C., Di Benedetto, H., Piber, H., & Sybilski, D. (Eds.). (2013). *Advances in Interlaboratory Testing and Evaluation of Bituminous Materials* (Vol. 9). Dordrecht: Springer Netherlands. Retrieved from http://link.springer.com/10.1007/978-94-007-5104-0

Petersen, J. C., Branthaver, J. F., Robertson, R. E., Harnsberger, P. M., Duvall, J. J., & Ensley, E. K. (1993). Effects of physicochemical factors on asphalt oxidation kinetics. *Transportation Research Record: Journal of the Transportation Research Board*, *1391*, 1–10.

Pham, N. H., Sauzéat, C., Di Benedetto, H., González-León, J.-A., Barreto, G., Nicolaï, A., & Jakubowski, M. (2015). Reclaimed asphalt pavement and additives' influence on 3D linear behaviour of warm mix asphalts. *Road Materials and Pavement Design*, *16*(3), 569–591. https://doi.org/10.1080/14680629.2015.1021108

Pham, N. H., Sauzéat, C., Di Benedetto, H., González-León, J. A., Barreto, G., Nicolaï, A., & Jakubowski, M. (2015). Analysis and modeling of 3D complex modulus tests on hot and warm bituminous mixtures. *Mechanics of Time-Dependent Materials*, *19*(2), 167–186. https://doi.org/10.1007/s11043-015-9258-8

Phan, C. V., Di Benedetto, H., Sauzéat, C., Dayde, J., & Pouget, S. (2017). Quantification of different effects occurring during fatigue tests on bituminous mixtures. *Fatigue & Fracture of Engineering Materials & Structures*. https://doi.org/10.1111/ffe.12646

Phan, C. V., Di Benedetto, H., Sauzéat, C., Lesueur, D., Pouget, S., Olard, F., & Dupriet, S. (2017). Complex modulus and fatigue resistance of bituminous mixtures containing hydrated lime. *Construction and Building Materials*, *139*, 24–33. https://doi.org/10.1016/j.conbuildmat.2017.02.042

Phan, T. K. (2015). *Etude des non-linéarités au cours des sollicitations cycliques sur un enrobe bitumineux* (Master's thesis). ENTPE, Vaulx-en-Velin.

Pipkin, A. C., & Rogers, T. G. (1968). A non-linear integral representation for viscoelastic behaviour. *Journal of the Mechanics and Physics of Solids*, *16*(1), 59–72. https://doi.org/10.1016/0022-5096(68)90016-1

Poncelet, J. V. (1839). *Introduction à la mécanique industrielle, physique ou expérimentale: Deuxième édition, entièrement corrigée et contenant un grand nombre de considération nouvelles*. Metz: Mme Thiel.

Pouget, S. (2011). *Influence des propriétés élastiques ou viscoélastiques des revêtements sur le comportement des ponts à dalle orthotrope* (Doctoral Thesis). École Nationale des Travaux Publics de l'État (ENTPE) de l'Université de Lyon (UdL), Vaulx-en-Velin.

Pouget, S., Sauzéat, C., Di Benedetto, H., & Olard, F. (2012a). Modeling of viscous bituminous wearing course materials on orthotropic steel deck. *Materials and Structures*, *45*(7), 1115–1125. https://doi.org/10.1617/s11527-011-9820-z

Pouget, S., Sauzéat, C., Di Benedetto, H., & Olard, F. (2012b). Viscous Energy Dissipation in Asphalt Pavement Structures and Implication for Vehicle Fuel Consumption. *Journal of Materials in Civil Engineering*, *24*(5), 568–576. https://doi.org/10.1061/(ASCE)MT.1943-5533.0000414

Qin, Q., Schabron, J. F., Boysen, R. B., & Farrar, M. J. (2014). Field aging effect on chemistry and rheology of asphalt binders and rheological predictions for field aging. *Fuel*, *121*, 86–94. https://doi.org/10.1016/j.fuel.2013.12.040

Read, J., Whiteoak, D., & Hunter, R. N. (2003). *The Shell Bitumen handbook* (5th ed). London: Thomas Telford.

Riahi, E., Allou, F., Botella, R., Fakhari Tehrani, F., Dubois, F., Absi, J., … Pérez-Jiménez, F. E. (2017). Modelling self-heating and thixotropy phenomena under the cyclic loading of asphalt. *Road Materials and Pavement Design*, 1–9. https://doi.org/10.1080/14680629.2017.1305145

Riahi, E., Allou, F., Ulmet, L., Absi, J., Dubois, F., & Petit, C. (2016). Numerical simulation of local temperature evolution in bituminous materials under cyclic loading. *European Journal of Environmental and Civil Engineering*, *20*(10), 1214–1232. https://doi.org/10.1080/19648189.2016.1139511

Rigden, P. J. (1947). The use of fillers in bituminous road surfacings. A study of filler-binder systems in relation to filler characteristics. *Journal of the Society of Chemical Industry*, *66*(9), 299–309. https://doi.org/10.1002/jctb.5000660902

Rivlin, R. S. (1965). Nonlinear Viscoelastic Solids. *SIAM Review*, *7*(3), 323–340. https://doi.org/10.1137/1007067

Roberts, F. L., Khandal, P. S., Brown, E. R., Lee, D. Y., & Kennedy, T. W. (1996). *Hot mix asphalt materials, mixture design and construction* (2nd Edition). Lanham, MD: NAPA Education Foundation.

Romeo, E., Birgisson, B., Montepara, A., & Tebaldi, G. (2010). The effect of polymer modification on hot mix asphalt fracture at tensile loading conditions. *International Journal of Pavement Engineering*, *11*(5), 403–413. https://doi.org/10.1080/10298436.2010.488735

Sabouri, M., & Kim, Y. (2014). Development of a Failure Criterion for Asphalt Mixtures Under Different Modes of Fatigue Loading. *Transportation Research Record: Journal of the Transportation Research Board*, *2447*, 117–125. https://doi.org/10.3141/2447-13

Safaei, F., Castorena, C., & Kim, Y. R. (2016). Linking asphalt binder fatigue to asphalt mixture fatigue performance using viscoelastic continuum damage modeling. *Mechanics of Time-Dependent Materials*, *20*(3), 299–323. https://doi.org/10.1007/s11043-016-9304-1

Sauzéat, C. (2003). *Comportement du sable dans le domaine des petites et moyennes déformations : rotations « d'axes » et effets visqueux* (Doctoral Thesis). Institut Nacional des Sciences Appliquées (INSA) de l'Université de Lyon (UdL), Lyon.

Sayegh, G. (1965). *Variations des modules de quelques bitumes purs et enrobés bitumineux* (Doctoral Thesis). Université de Paris.

Schapery, R. A. (1969). On the characterization of nonlinear viscoelastic materials. *Polymer Engineering and Science*, *9*(4), 295–310. https://doi.org/10.1002/pen.760090410

Schapery, R. A. (1991). Simplifications in the Behavior of Viscoelastic Composites with Growing Damage. In G. J. Dvorak (Ed.), *Inelastic Deformation of Composite Materials* (pp. 193–214). New York, NY: Springer New York. https://doi.org/10.1007/978-1-4613-9109-8_10

Shan, L., Tan, Y., Underwood, B., & Kim, Y. (2011). Separation of Thixotropy from Fatigue Process of Asphalt Binder. *Transportation Research Record: Journal of the Transportation Research Board*, *2207*, 89–98. https://doi.org/10.3141/2207-12

Shan, L., Tan, Y., Underwood, S., & Kim, Y. (2010). Application of Thixotropy to Analyze Fatigue and Healing Characteristics of Asphalt Binder. *Transportation Research Record: Journal of the Transportation Research Board*, *2179*, 85–92. https://doi.org/10.3141/2179-10

Shen, S., Airey, G. D., Carpenter, S. H., & Huang, H. (2006). A Dissipated Energy Approach to Fatigue Evaluation. *Road Materials and Pavement Design*, *7*(1), 47–69. https://doi.org/10.1080/14680629.2006.9690026

Soltani, M. A. A. (1998). *Comportement en fatigue des enrobes bitumineux* (Doctoral Thesis). Institut National des Sciences Appliquées (INSA) de Lyon, Lyon.

Soltani, M. A. A., & Anderson, D. A. (2005). New Test Protocol to Measure Fatigue Damage in Asphalt Mixtures. *Road Materials and Pavement Design*, *6*(4), 485–514. https://doi.org/10.1080/14680629.2005.9690017

Somé, S. C., Gaudefroy, V., & Delaunay, D. (2014). A new laboratory method to evaluate the influence of aggregate temperature on the binder-aggregate bonding: first results. *Materials and Structures*, *47*(6), 963–976. https://doi.org/10.1617/s11527-013-0106-5

Specht, L. P., Babadopulos, L. F. A. L., Di Benedetto, H., Sauzéat, C., & Soares, J. B. (2017). Application of the theory of viscoelasticity to evaluate the resilient modulus test in asphalt mixes. *Construction and Building Materials*, *149*, 648–658. https://doi.org/10.1016/j.conbuildmat.2017.05.037

Tapsoba, N. (2011). *Comportement des enrobés bitumineux à base de matériaux recyclés et/ou fabriqués à température réduite* (Doctoral Thesis). École Nationale des Travaux Publics de l'État (ENTPE) de l'Université de Lyon (UdL), Vaulx-en-Velin.

Tapsoba, N., Sauzéat, C., & Di Benedetto, H. (2013). Analysis of Fatigue Test for Bituminous Mixtures. *Journal of Materials in Civil Engineering*, *25*(6), 701–710. https://doi.org/10.1061/(ASCE)MT.1943-5533.0000636

Tapsoba, N., Sauzéat, C., Di Benedetto, H., Baaj, H., & Ech, M. (2015). Three-dimensional analysis of fatigue tests on bituminous mixtures. *Fatigue & Fracture of Engineering Materials & Structures*, *38*(6), 730–741. https://doi.org/10.1111/ffe.12278

Tatsuoka, F., Kohata, Y., & Lo Presti, D. (1995). Deformation characteristics of soils and soft rocks under monotonic and cyclic loads and their relationships. In *Proceedings: Third*

International Conference on Recent Advances in Geotechnical Earthquake Engineering and Soil Dynamics (Vol. 2, pp. 851–879). St. Louis, Missouri.

Tatsuoka, F., & Shibuya, S. (1992). Deformation characteristics of soils and rocks from laboratory and field tests. In *Proceedings of the 9th Asian Regional Conference on Soils Mechanics and Foundations Engineering.* (Vol. 2, pp. 101–170). Bangkok.

Tayebali, A. A., Goodrich, J. L., Sousa, J. B., & Monismith, C. L. (1991). Relationships between modified asphalt binders rheology and binder-aggregate mixture permanent deformation response. *Journal of the Association of Asphalt Paving Technologists*, *60*, 121–159.

TCSA. (2016). *Traité de thermométrie par thermocouple et résistance*. France.

Tiouajni, S., Di Benedetto, H., Sauzéat, C., & Pouget, S. (2011). Approximation of Linear Viscoelastic Model in the 3 Dimensional Case with Mechanical Analogues of Finite Size: Application to Bituminous Materials. *Road Materials and Pavement Design*, *12*(4), 897–930. https://doi.org/10.1080/14680629.2011.9713899

Underwood, B., Baek, C., & Kim, Y. (2012). Simplified Viscoelastic Continuum Damage Model as Platform for Asphalt Concrete Fatigue Analysis. *Transportation Research Record: Journal of the Transportation Research Board*, *2296*, 36–45. https://doi.org/10.3141/2296-04

Underwood, B., & Kim, Y. (2013). Nonlinear Viscoelastic Behavior of Asphalt Concrete and Its Implication for Fatigue Modeling. *Transportation Research Record: Journal of the Transportation Research Board*, *2373*, 100–108. https://doi.org/10.3141/2373-11

Underwood, B. S. (2016). A continuum damage model for asphalt cement and asphalt mastic fatigue. *International Journal of Fatigue*, *82*, 387–401. https://doi.org/10.1016/j.ijfatigue.2015.08.020

Underwood, B. S., & Kim, Y. R. (2012). Comprehensive Evaluation of Small Strain Viscoelastic Behavior of Asphalt Concrete. *Journal of Testing and Evaluation*, *40*(4), 104521. https://doi.org/10.1520/JTE104521

Uzan, J., & Levenberg, E. (2007). Advanced Testing and Characterization of Asphalt Concrete Materials in Tension. *International Journal of Geomechanics*, *7*(2), 158–165. https://doi.org/10.1061/(ASCE)1532-3641(2007)7:2(158)

Van Rompu, J., Di Benedetto, H., Buannic, M., Gallet, T., & Ruot, C. (2012). New fatigue test on bituminous binders: Experimental results and modeling. *Construction and Building Materials*, *37*, 197–208. https://doi.org/10.1016/j.conbuildmat.2012.02.099

Vavrik, W. R., Pine, W. J., Huber, G., Carpenter, S. H., & Bailey, R. (2001). The Bailey method of gradation evaluation: the influence of aggregate gradation and packing characteristics on voids in the mineral aggregate. *Journal of the Association of Asphalt Paving Technologists*, *70*, 132–175.

Von Quintus, H., Mallela, J., & Buncher, M. (2007). Quantification of Effect of Polymer-Modified Asphalt on Flexible Pavement Performance. *Transportation Research Record: Journal of the Transportation Research Board*, *2001*, 141–154. https://doi.org/10.3141/2001-16

Whiteoak, D., & Shell Bitumen. (1991). *The shell bitumen handbook*. Chertsey, Angleterre: Shell Bitumen.

Williams, M. L., Landel, R. F., & Ferry, J. D. (1955). The Temperature Dependence of Relaxation Mechanisms in Amorphous Polymers and Other Glass-forming Liquids. *Journal of the American Chemical Society*, *77*(14), 3701–3707. https://doi.org/10.1021/ja01619a008

Wöhler, A. (1870). Über die Festigkeitsversuche mit Eisen und Stahl. *Zeitschrift für Bauwesen*, *20*, 73–106.

Wright, J. R. (1965). *Weathering: Theoretical and Practical Aspects of Asphalt Durability. Ch. 8 In Bituminous Materials: Asphalts, Tars and Pitches, pp. 249-306*. (A. J. Hoiberg, Ed.) (Vol. II). New York: Interscience Publishers.

Xu, Q., & Solaimanian, M. (2010). Modeling temperature distribution and thermal property of asphalt concrete for laboratory testing applications. *Construction and Building Materials*, *24*(4), 487–497. https://doi.org/10.1016/j.conbuildmat.2009.10.013

You, T., Al-Rub, R. K. A., Masad, E. A., Kassem, E., & Little, D. N. (2014). Three-Dimensional Microstructural Modeling Framework for Dense-Graded Asphalt Concrete Using a Coupled Viscoelastic, Viscoplastic, and Viscodamage Model. *Journal of Materials in Civil Engineering*, *26*(4), 607–621. https://doi.org/10.1061/(ASCE)MT.1943-5533.0000860

You, T., Masad, E., Al-Rub, R., Kassem, E., & Little, D. (2014). Calibration and Validation of a Comprehensive Constitutive Model for Asphalt Mixtures. *Transportation Research Record: Journal of the Transportation Research Board*, *2447*, 13–22. https://doi.org/10.3141/2447-02

APPENDIX A – UTILISED PID CONTROL PARAMETERS

Table A-1. MTS® press's (FlexTest SE) Proportional-Derivative-Integral (PID) controller parameters (controlled channel is the mean shear strain for three extensometers) used for tests on mastic M5070_30pc40-70 at the given approximate values of targeted shear strain amplitude (γ_0).

Material	Type of test	T (°C)	f (Hz)	γ_0 (μm/m)	P (**)	I (**)	D (**)
Bitumen	Complex Modulus	25.4	0.01-10	5,000-100,000	400	150	5
Bitumen	Complex Modulus	16.9	0.01-10	1,800-100,000	1,000	150	5
Bitumen	Complex Modulus	14.9	0.01-10	1,500-80,000	1,000	150	5
Bitumen	Complex Modulus	13.0	0.01-10	1,300-70,000	1,000	150	5
Bitumen	Complex Modulus	11.1	0.01-10	1,100-40,000	1,000	150	5
Bitumen	Complex Modulus	6.3	0.01-10	450-12,000	2,800	150	5
Bitumen	Complex Modulus	-3.2	0.01-10	200-1,600	6,000	150	5
Bitumen	Complex Modulus	-10	0.01-10	90-300	8,000	150	5
Bitumen	Load and Rest	11.1	10	3,600	1,000	150	5
Bitumen	Load and Rest	11.1	10	20,000	800	150	5
Bitumen	Load and Rest	11.1	10	32,000	700	150	5
Mastic	Complex Modulus	25.4	0.01-10	2,000-100,000	450	10	1
Mastic	Complex Modulus	16.9	0.01-10	600-70,000	1,100	10	1
Mastic	Complex Modulus	14.9	0.01-10	400-35,000	1,700	50	1
Mastic	Complex Modulus	13.0	0.01-10	400-20,000	2,000	50	1
Mastic	Complex Modulus	11.1	0.01-10	350-12,000	2,000	50	1
Mastic	Complex Modulus	6.3	0.01-10	180-3,200	3,000	100	5
Mastic	Complex Modulus	-3.2	0.01-10	150-1,100	5,000	100	5
Mastic	Complex Modulus	-10	0.01-10	150-380	6,000	100	5
Mastic	Load and Rest	11.1	10	3,125	3,000	100	5
Mastic	Load and Rest	11.1	10	6,125	2,000	50	1
Mastic	Load and Rest	11.1	10	10,000	1,800	50	1

[*] *During thermal conditioning, loading was controlled using the actuator displacement channel. Values are given in the dimensions required by the press software. PID controller parameters for SAS tests were the same as those for complex modulus tests, the only difference in the control being the targeted strain amplitudes. Strain amplitudes in ASR complex modulus tests are chosen to give approximately constant and low force amplitudes with sufficient precision (force amplitude was between 0.2kN and 0.7kN).*

[**] *Units not clearly state by the software.*

Table A-2. Instron® 8800 press's Proportional-Derivative-Integral (PID) controller parameters (controlled channel is the mean axial strain for three extensometers[*]) used for tests on BM1 at the given approximate values of targeted axial strain amplitude (ε_0).

Material	Type of test	T (°C)	f (Hz)	ε_0 (μm/m)	P (dB)	I (1/s)	D (ms)
BM1	Complex Modulus	-25–50	0.003-10	50	16.0	2.0	0.1
BM1	SASTENOLE	-4–0	0.1-10	0-120	35.0	2.0	0.1
BM1	SASTENOLE	8–14	0.1-10	0-120	25.6	2.0	0.1
BM1	SASTENOLE	24–28	0.1-10	0-120	16.0	2.0	0.1

[*] *During thermal conditioning, loading was controlled using the load cell. Values are given in the dimensions required by the press software.*

APPENDIX B – BITUMEN AND MASTIC NONLINEARITY CHARACTERISATION RESULTS

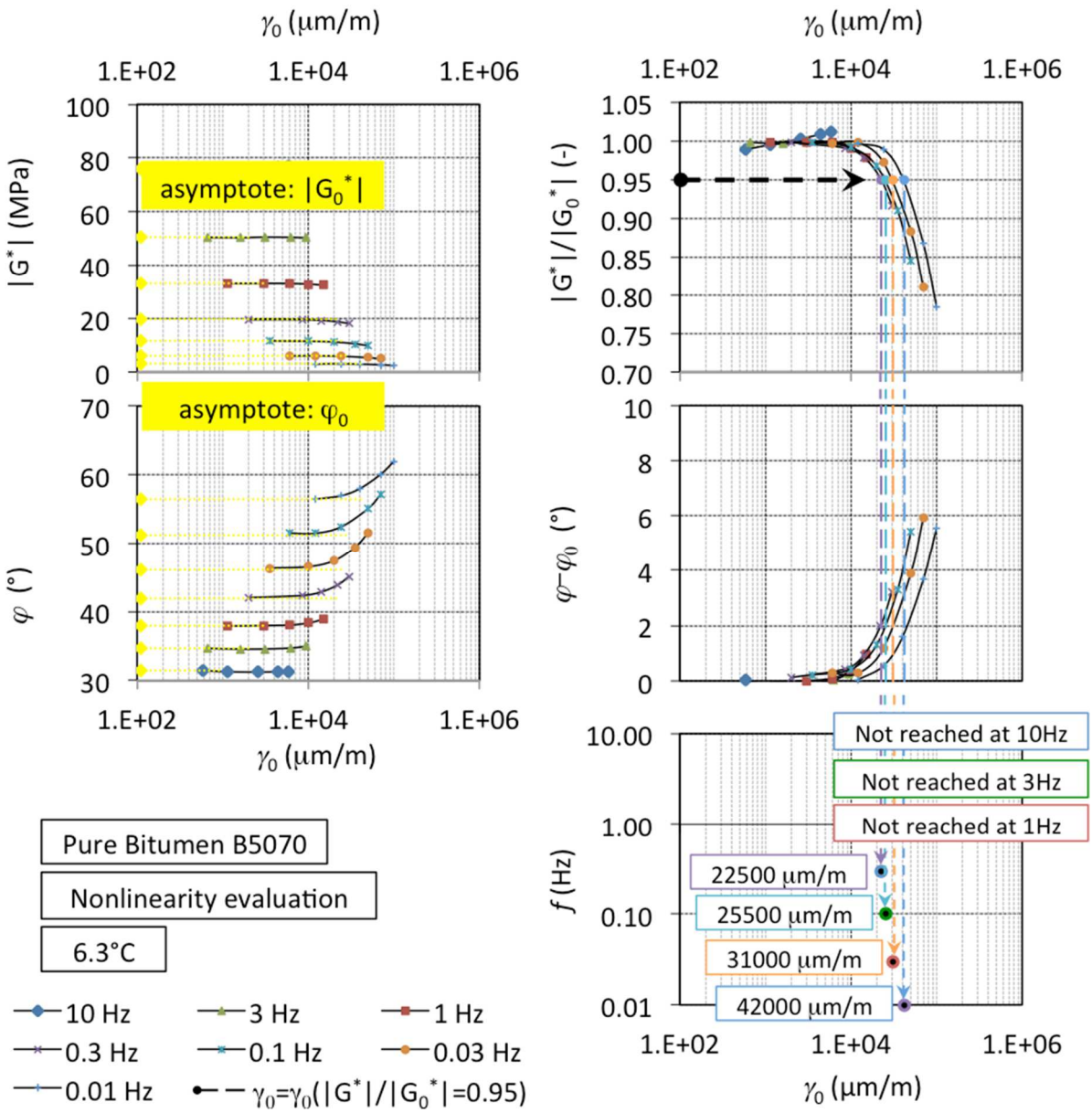

Figure B-1. Set of experimental results (norm and phase angle of complex shear modulus) for SAS tests using the ASR (tests at 6.3°C on bitumen B5070), with details on the method for determination of the asymptotic “linear” values (at 0µm/m) and of the LVE limit in terms of strain amplitude.

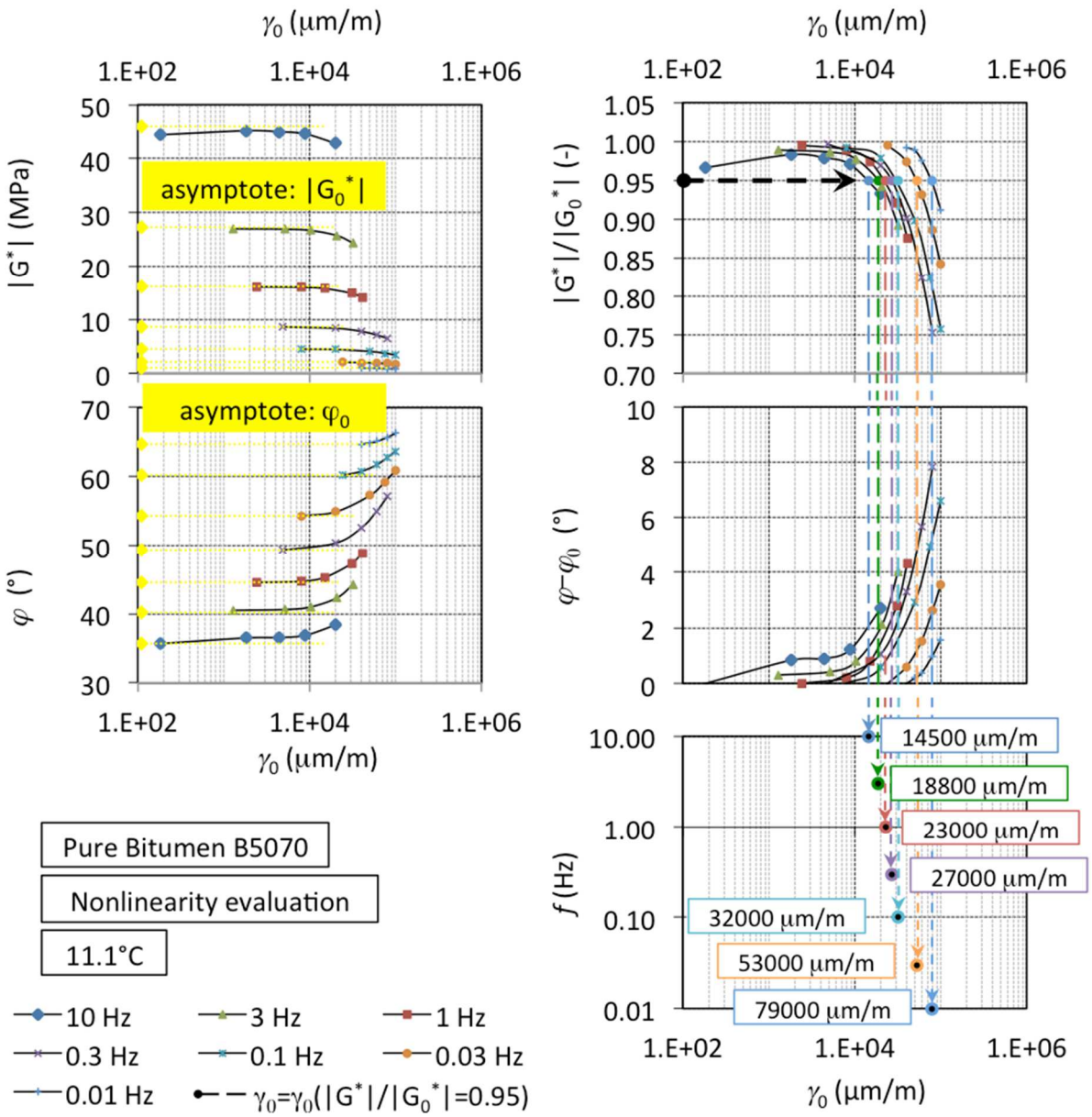

Figure B-2. Set of experimental results (norm and phase angle of complex shear modulus) for SAS tests using the ASR (tests at 11.1°C on bitumen B5070), with details on the method for determination of the asymptotic “linear” values (at 0μm/m) and of the LVE limit in terms of strain amplitude.

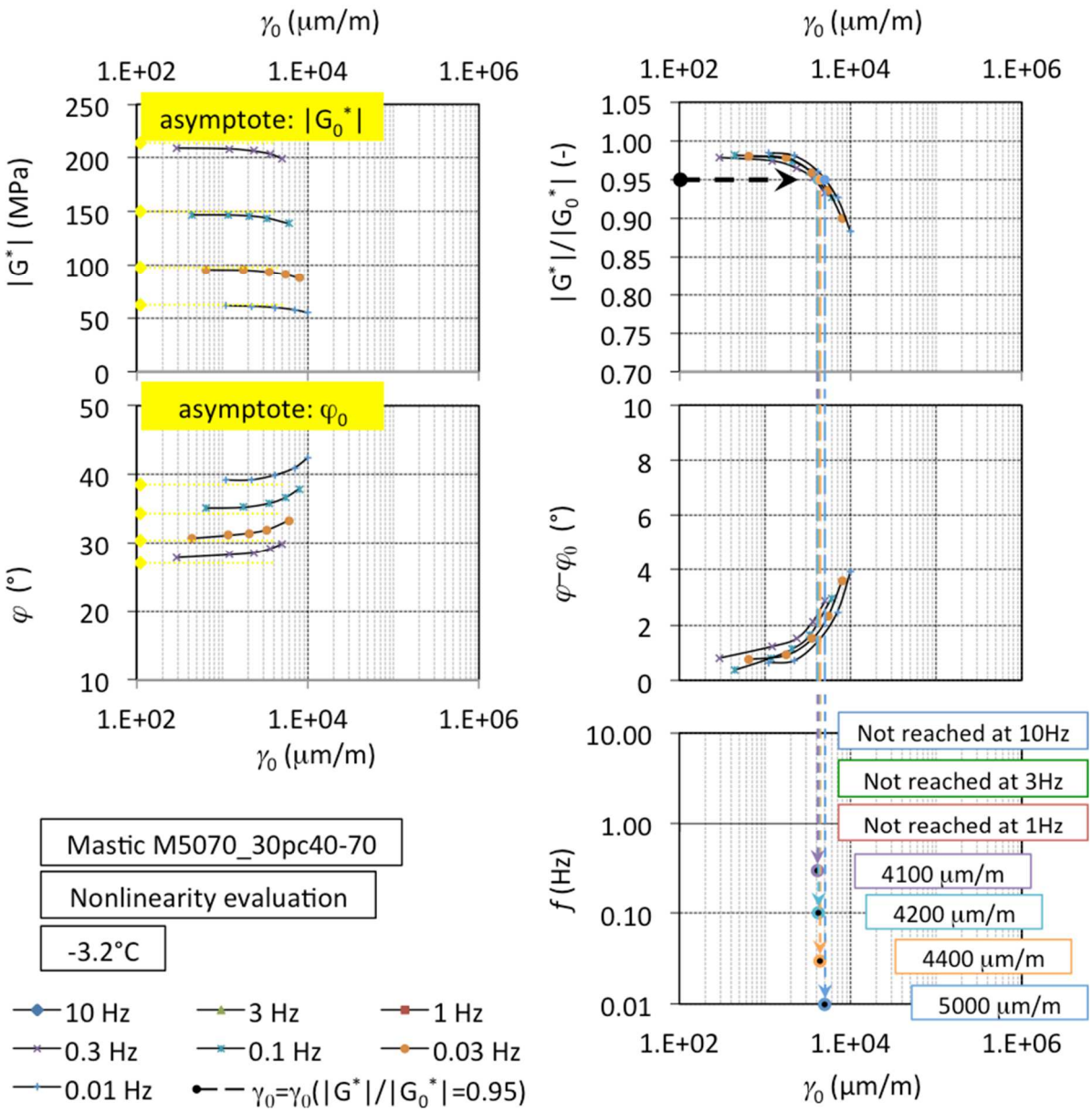

Figure B-3. Set of experimental results (norm and phase angle of complex shear modulus) for SAS tests using the ASR (tests at -3.2°C on mastic M5070_30pc40-70), with details on the method for determination of the asymptotic "linear" values (at 0µm/m) and of the LVE limit in terms of strain amplitude.

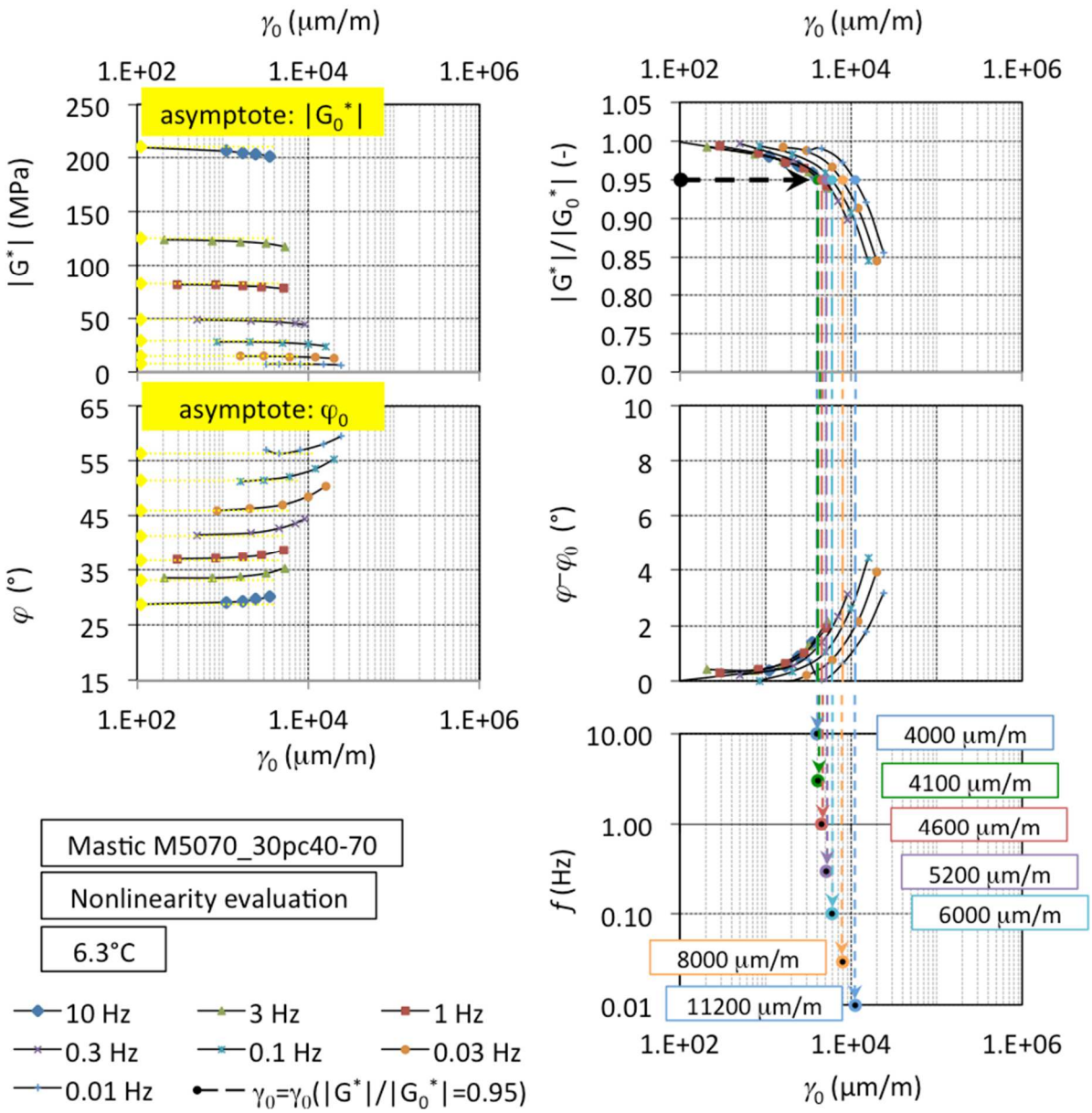

Figure B-4. Set of experimental results (norm and phase angle of complex shear modulus) for SAS tests using the ASR (tests at 6.3°C on mastic M5070_30pc40-70), with details on the method for determination of the asymptotic “linear” values (at 0µm/m) and of the LVE limit in terms of strain amplitude.

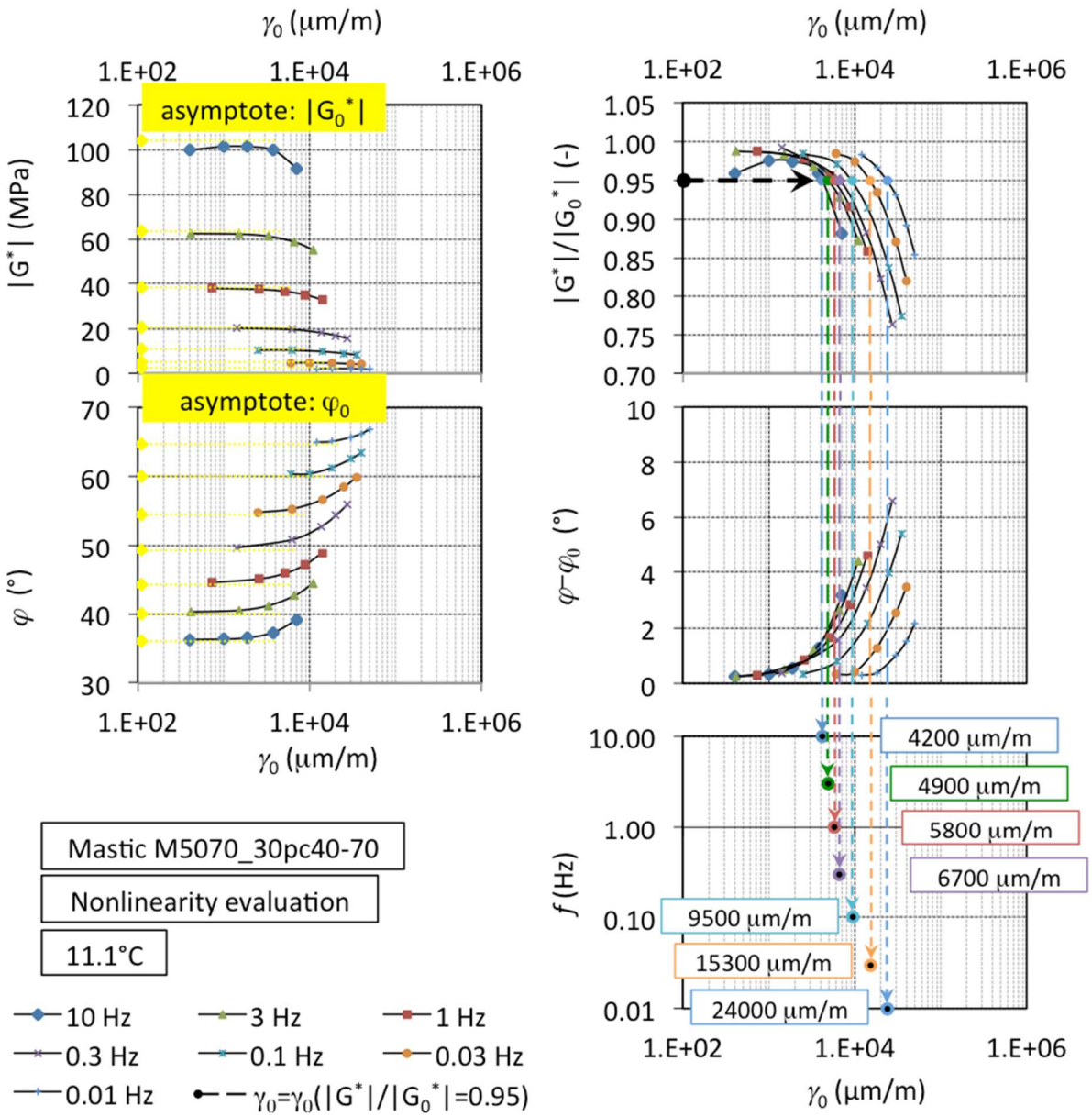

Figure B-5. Set of experimental results (norm and phase angle of complex shear modulus) for SAS tests using the ASR (tests at 11.1°C on mastic M5070_30pc40-70), with details on the method for determination of the asymptotic “linear” values (at 0μm/m) and of the LVE limit in terms of strain amplitude.

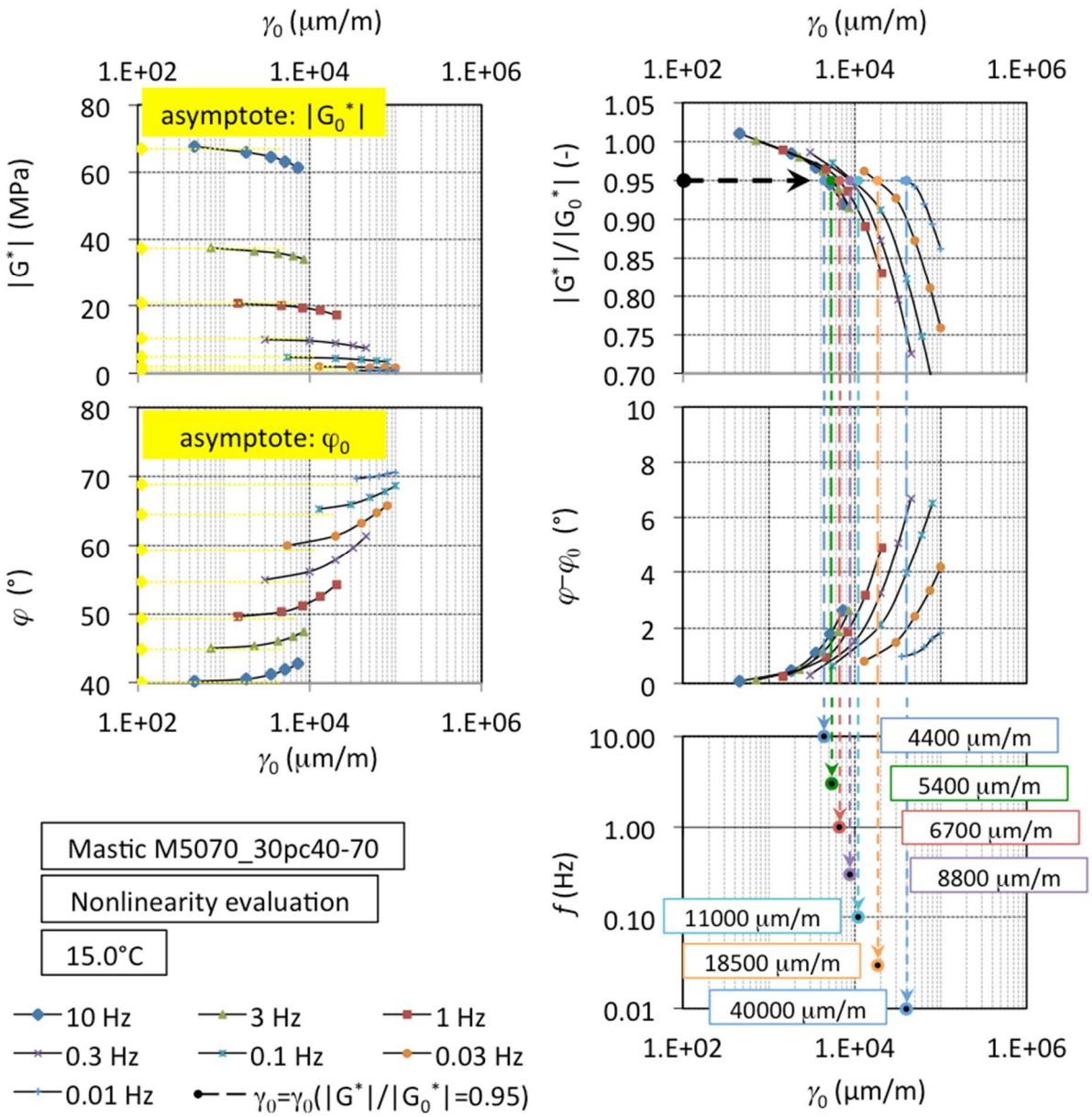

Figure B-6. Set of experimental results (norm and phase angle of complex shear modulus) for SAS tests using the ASR (tests at 15.0°C on mastic M5070_30pc40-70), with details on the method for determination of the asymptotic “linear” values (at 0µm/m) and of the LVE limit in terms of strain amplitude.

APPENDIX C – BITUMEN AND MASTIC LOAD AND REST PERIOD TEST RESULTS

LRP test results on Bitumen

B5070_C with 3,600µm/m strain amplitude

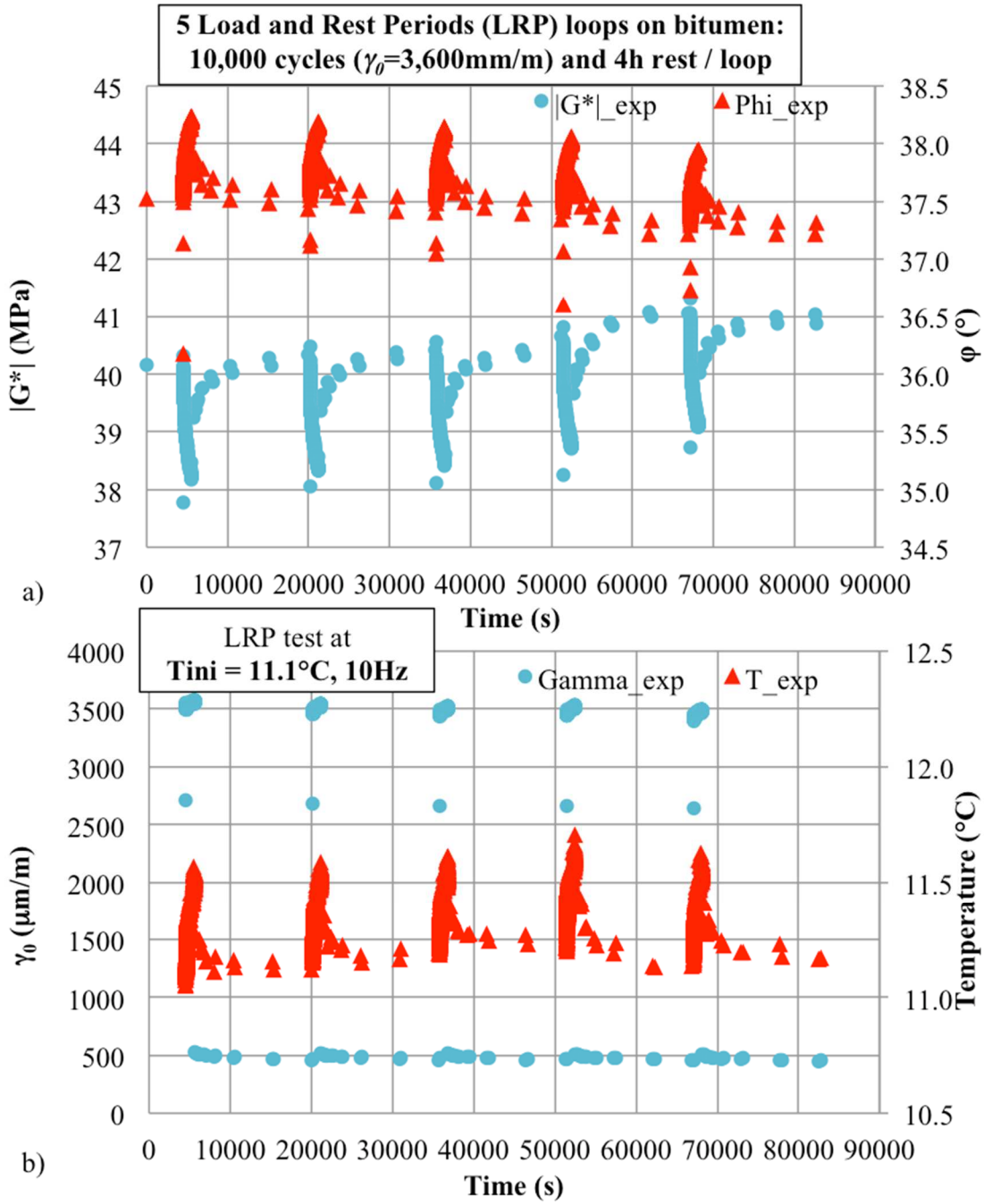

Figure C-1. Experimental results (B5070_C) for LRP tests: 5 LRP loops with 10,000 cycles and 4h rest on bitumen submitted to 3,600µm/m sinusoidal loading: a) Norm of complex modulus and phase angle as a function of time, and b) shear strain amplitude and temperature as a function of time.

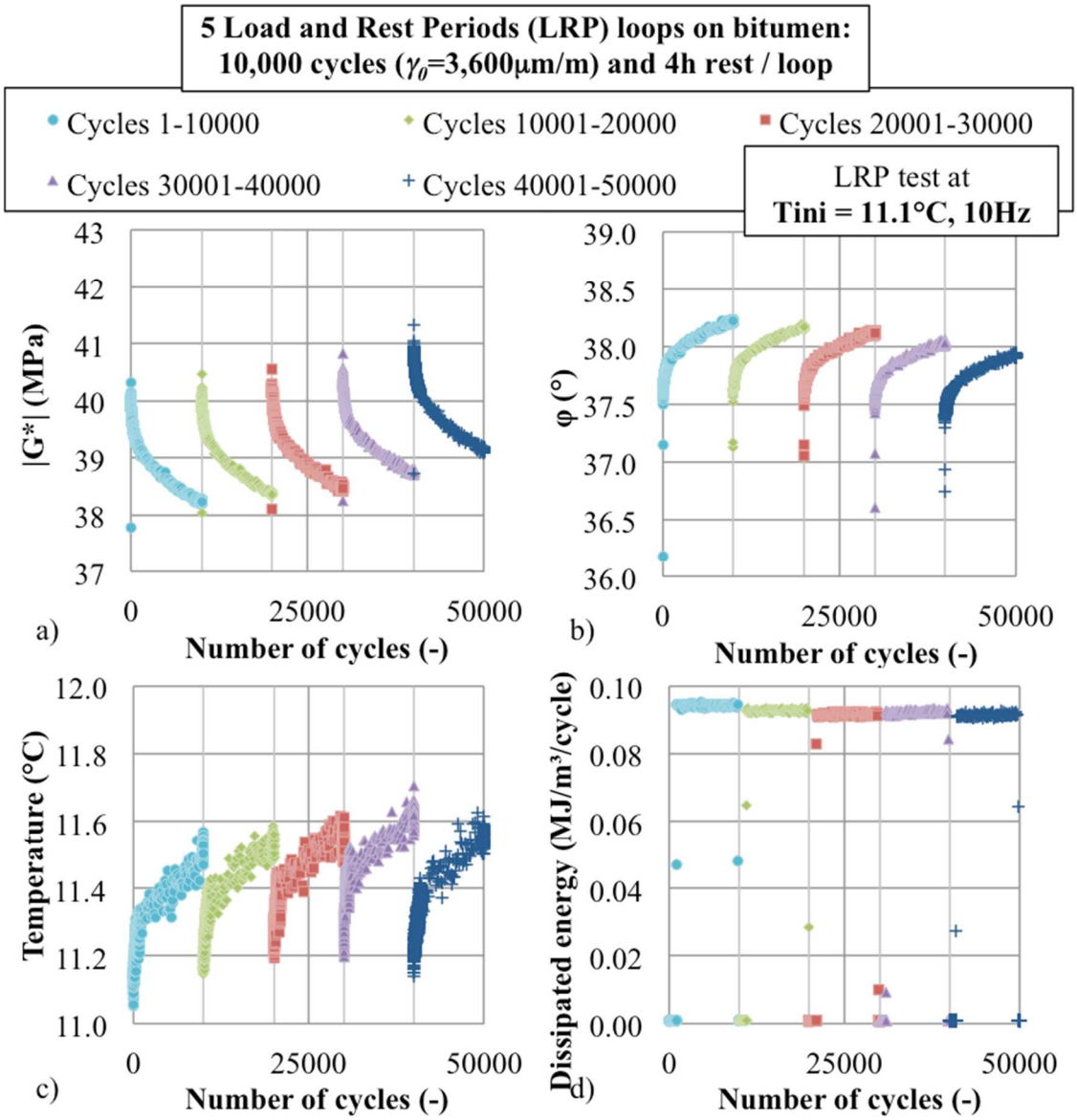

Figure C-2. Experimental results (B5070_C) for LRP tests: 5 LRP 3,600µm/m sinusoidal loading loops with 10,000 cycles each on bitumen: a) Norm of complex shear modulus, b) phase angle, c) mean in-specimen temperature, and d) dissipated energy per cycle as a function of the number of applied cycles.

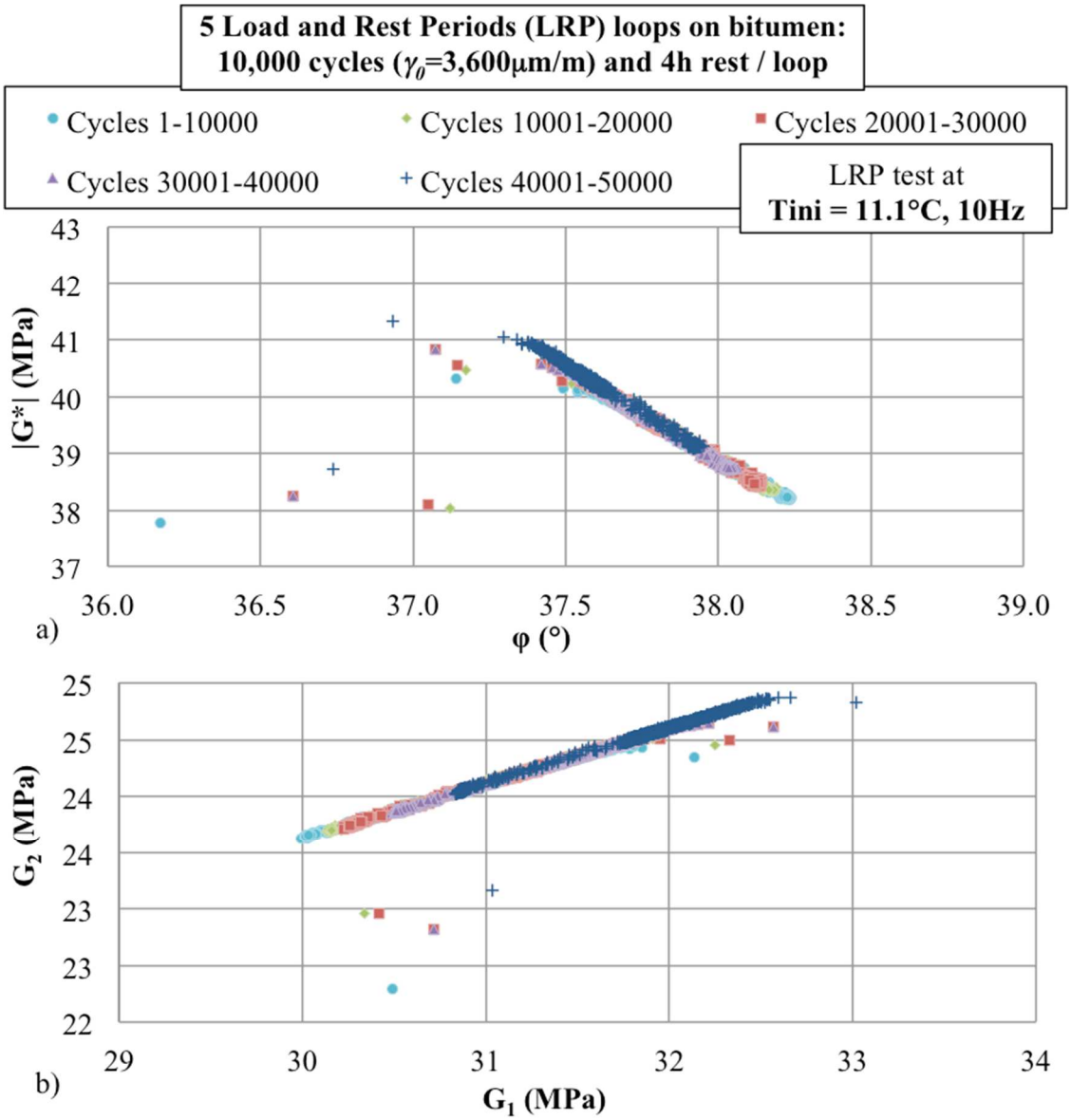

Figure C-3. Experimental results (B5070_C) for LRP tests: 5 LRP 3,600µm/m sinusoidal loading loops with 10,000 cycles each on bitumen: representation on a) Black space, and b) Cole-Cole diagram.

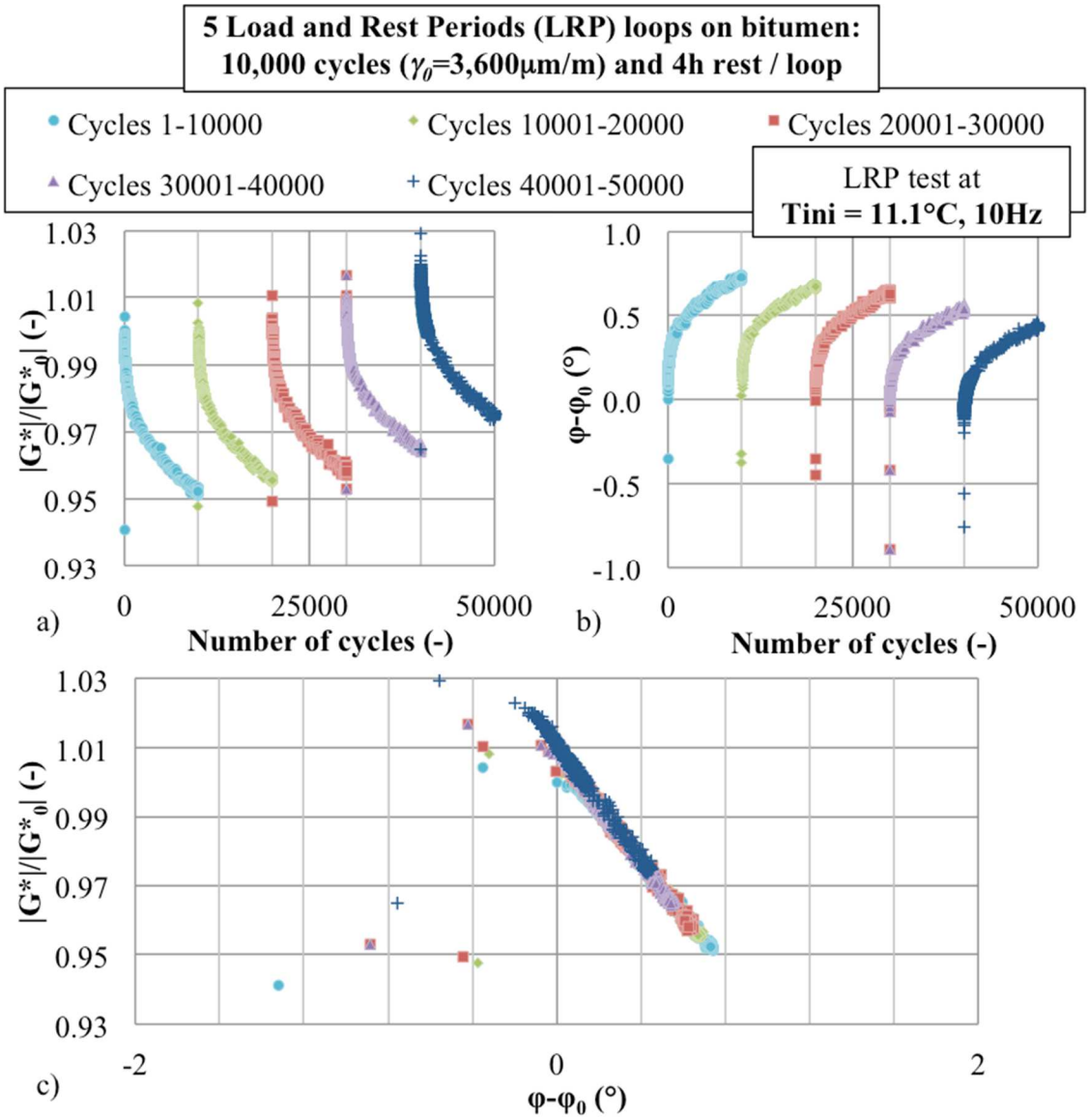

Figure C-4. Experimental results (B5070_C) for LRP tests: 5 LRP 3,600µm/m sinusoidal loading loops with 10,000 cycles each on bitumen: a) Normalised (the initial modulus being considered as the result at the 3rd cycle) norm of complex shear modulus, and b) normalised phase angle as a function of number of applied cycles; and c) representation of the results on a normalised Black space.

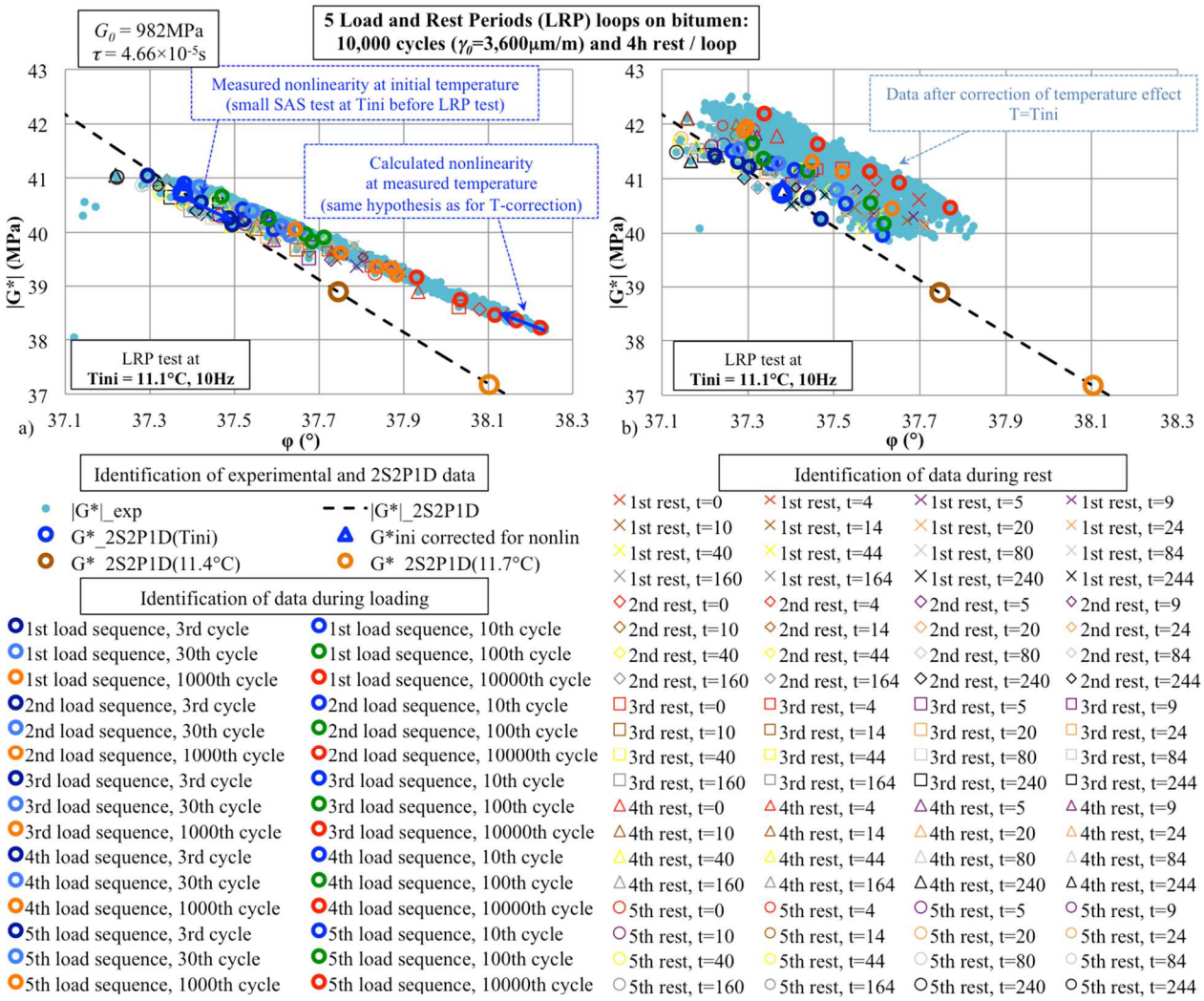

Figure C-5. Experimental results (B5070_C) for LRP tests (5 LRP tests with 10,000 cycles of 3,600µm/m sinusoidal loading and 4h rest loops on bitumen): a) Black diagram representation of the results including details of the number of cycles during loading and the time of rest during rest periods, and a representation of the nonlinearity effect; b) results after temperature correction. The figure present also a 2S2P1D model prediction, with indication of LVE complex modulus at 10Hz and three temperatures, 11.1°C (Tini), 11.4°C and 11.7°C.

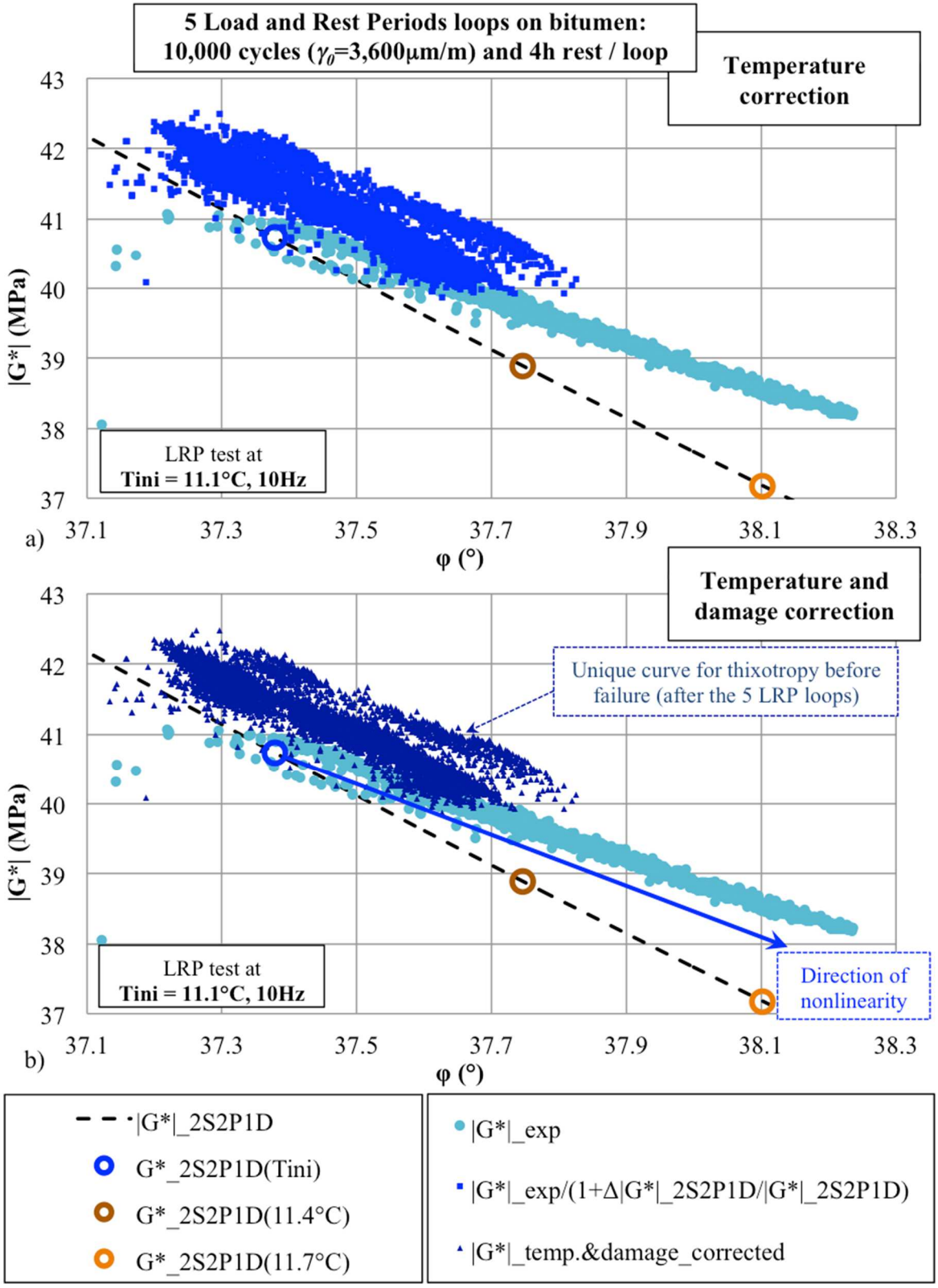

Figure C-6. Experimental results (B5070_C) for LRP tests (5 LRP tests with 10,000 cycles of 3,600µm/m sinusoidal loading and 4h rest loops on bitumen): Black diagram representation of a) the raw experimental results and the results after the temperature correction and b) the experimental results after temperature and damage correction. The figure present also a 2S2P1D model prediction, with indication of LVE complex modulus at 10Hz and three temperatures, 11.1°C (Tini), 11.4°C and 11.7°C.

B5070_A with 10,000μm/m strain amplitude

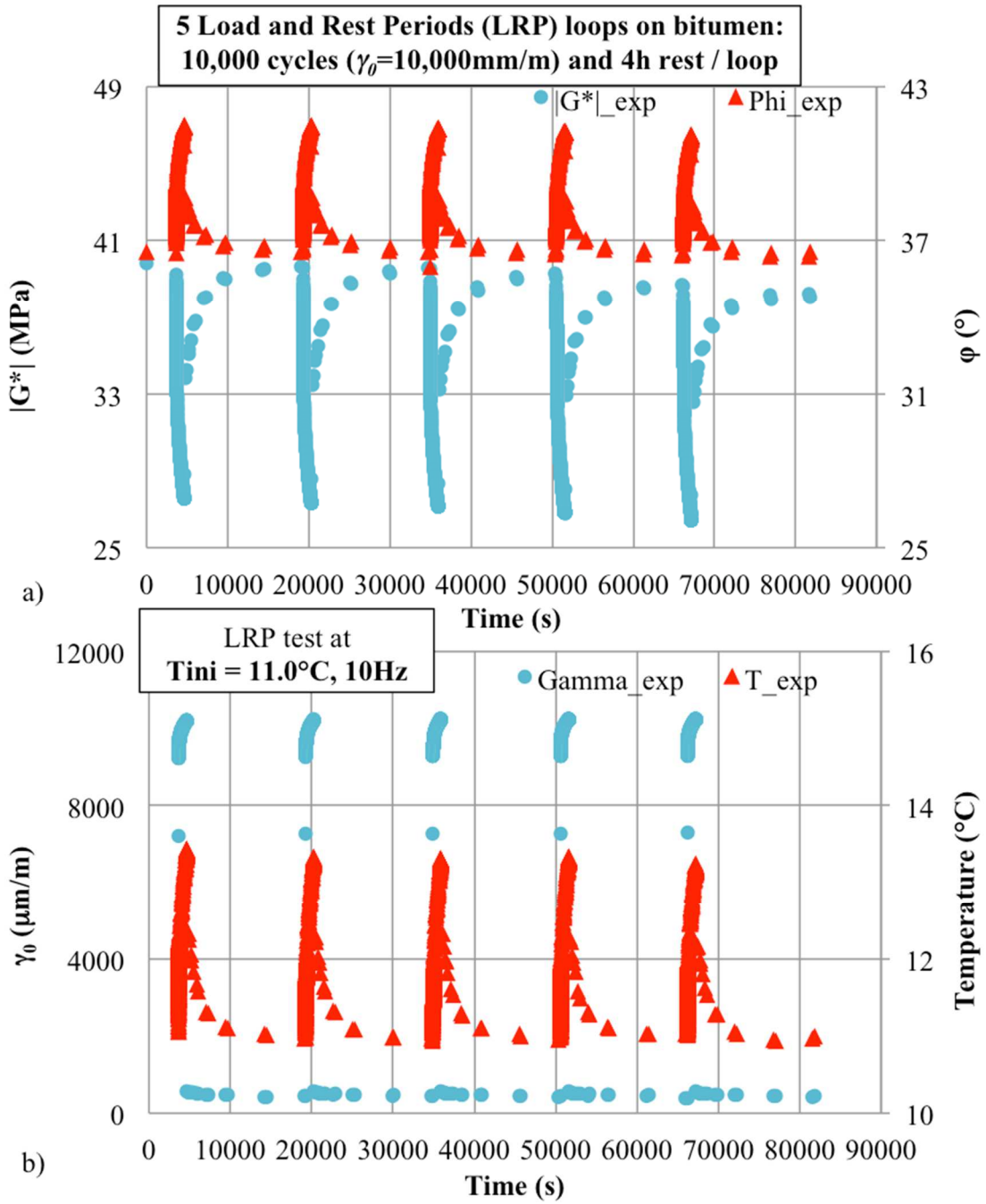

Figure C-7. Experimental results (B5070_A) for LRP tests: 5 LRP loops with 10,000 cycles and 4h rest on bitumen submitted to 10,000μm/m sinusoidal loading: a) Norm of complex modulus and phase angle as a function of time, and b) shear strain amplitude and temperature as a function of time.

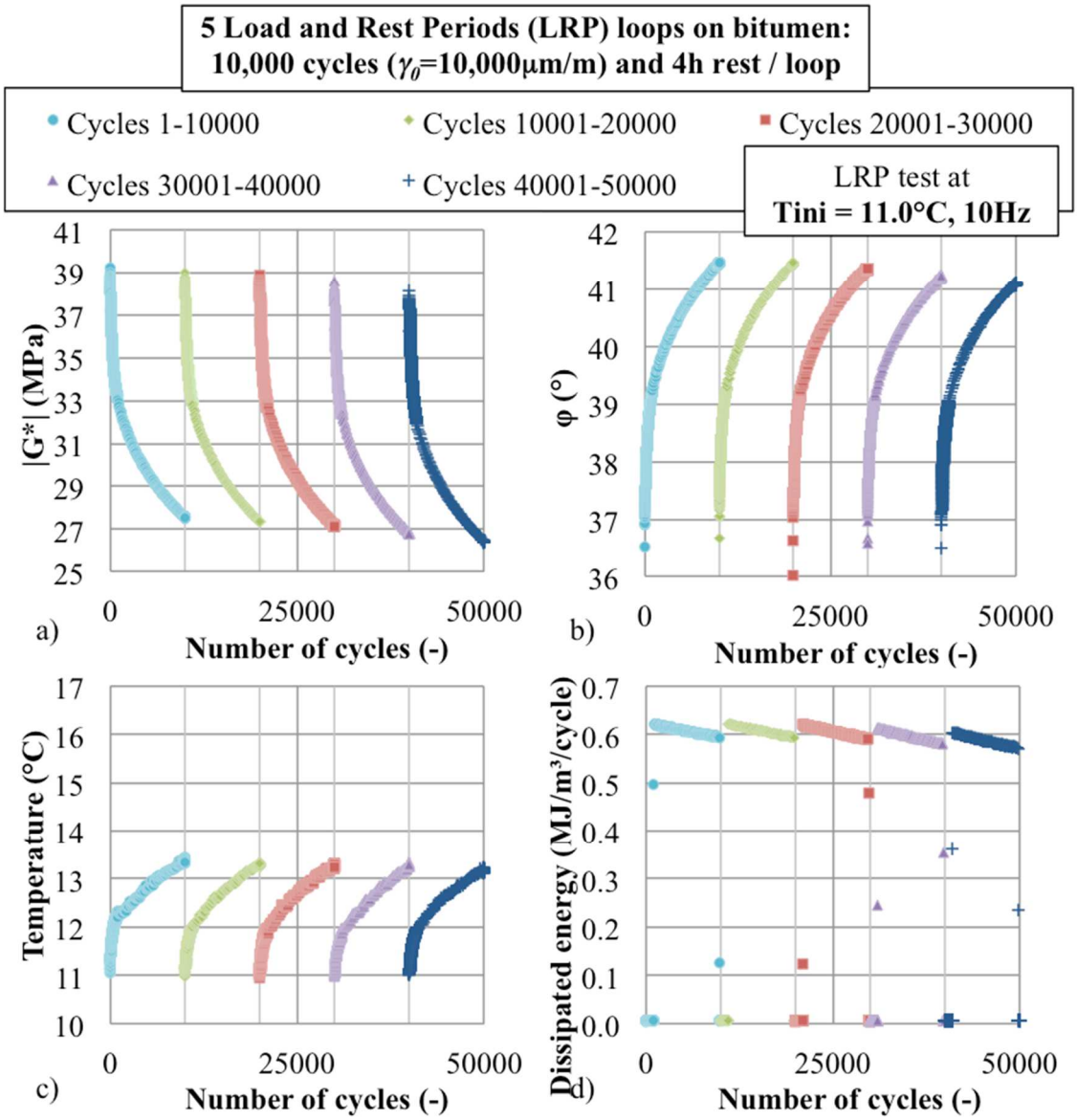

Figure C-8. Experimental results (B5070_A) for LRP tests: 5 LRP 10,000µm/m sinusoidal loading loops with 10,000 cycles each on bitumen: a) Norm of complex shear modulus, b) phase angle, c) mean in-specimen temperature, and d) dissipated energy per cycle as a function of the number of applied cycles.

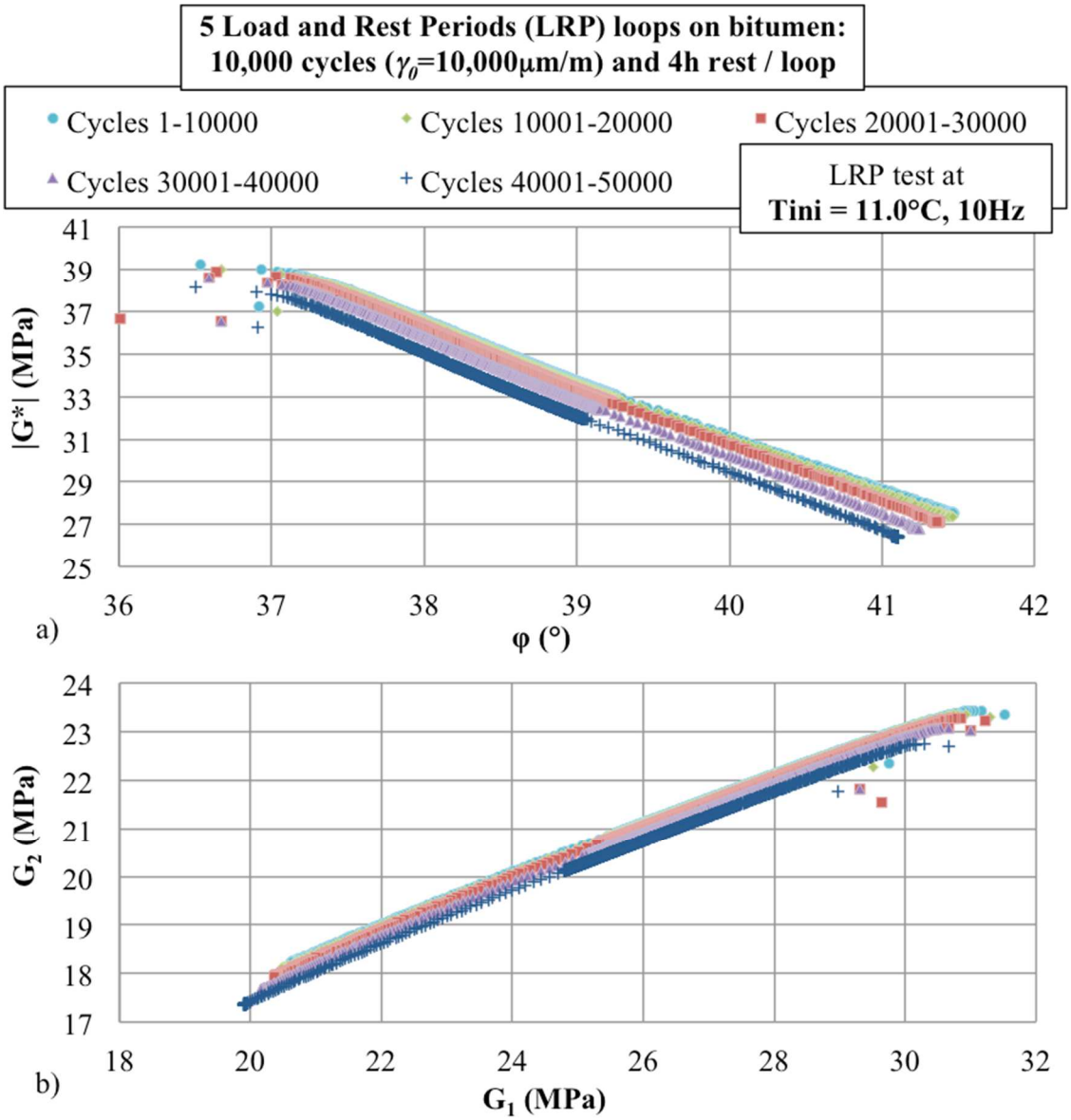

Figure C-9. Experimental results (B5070_A) for LRP tests: 5 LRP 10,000µm/m sinusoidal loading loops with 10,000 cycles each on bitumen: representation on a) Black space, and b) Cole-Cole diagram.

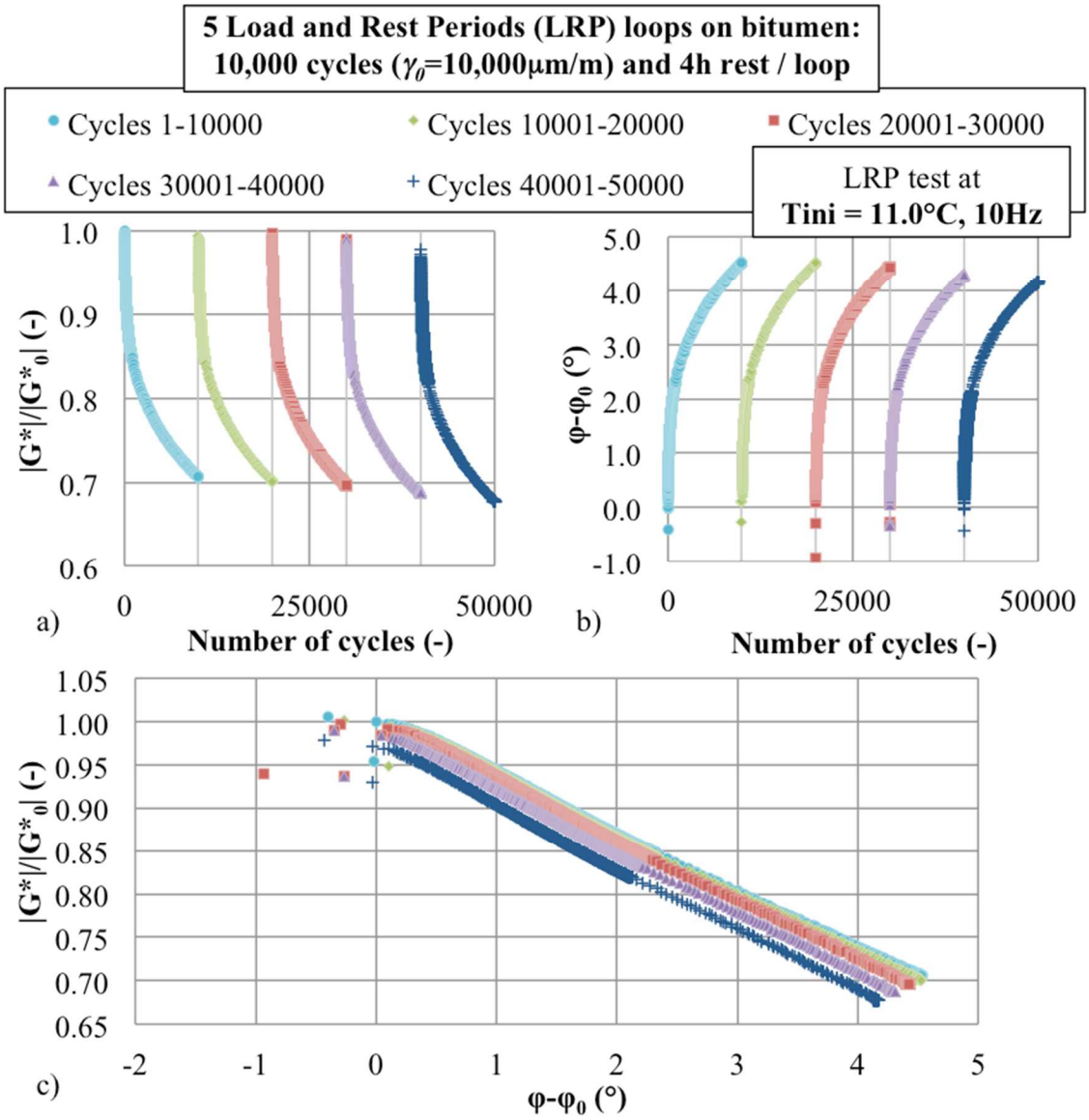

Figure C-10. Experimental results (B5070_A) for LRP tests: 5 LRP 10,000µm/m sinusoidal loading loops with 10,000 cycles each on bitumen: a) Normalised (the initial modulus being considered as the result at the 3rd cycle) norm of complex shear modulus, and b) normalised phase angle as a function of number of applied cycles; and c) representation of the results on a normalised Black space.

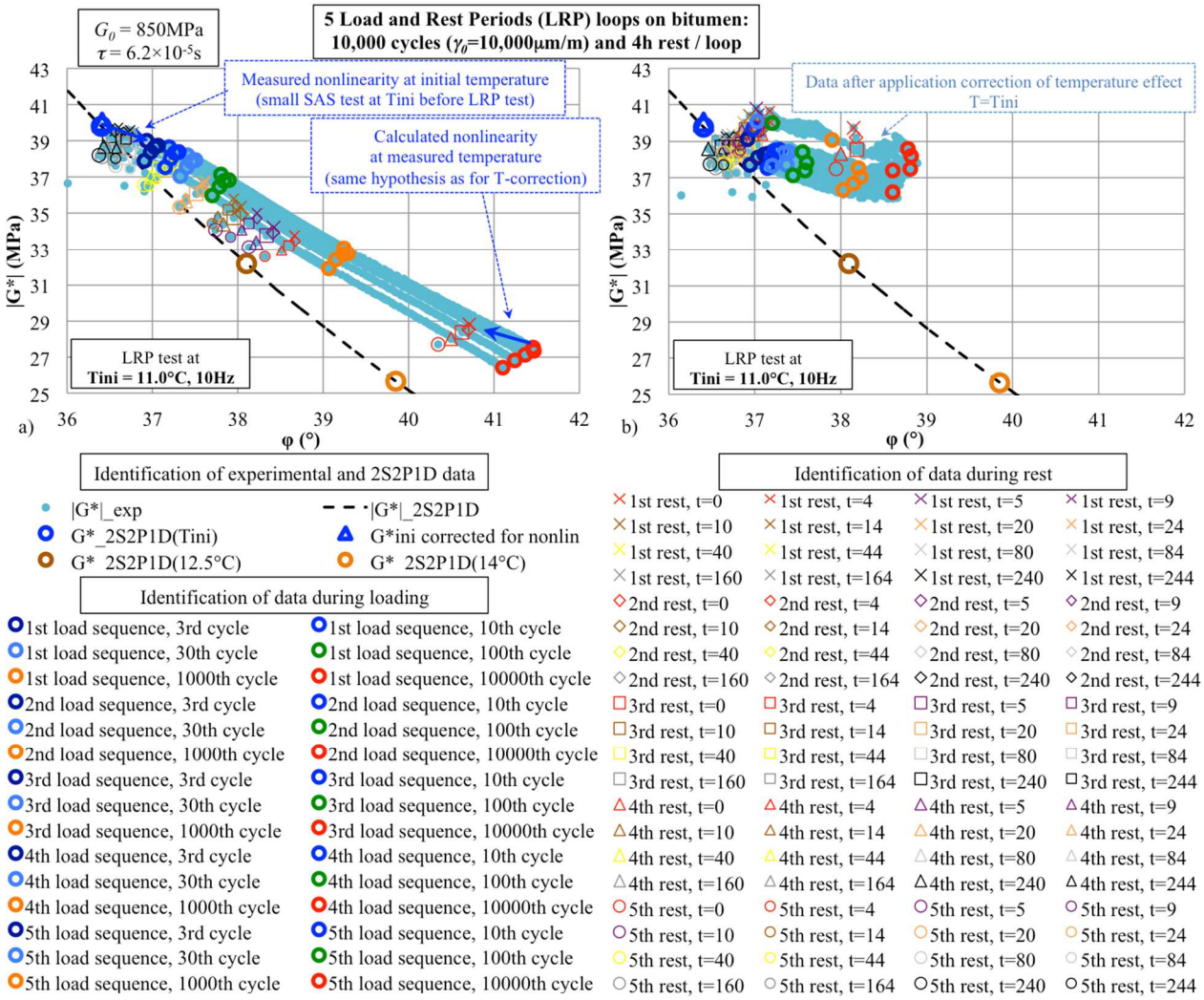

Figure C-11. Experimental results (B5070_A) for LRP tests (5 LRP tests with 10,000 cycles of 10,000µm/m sinusoidal loading and 4h rest loops on bitumen): a) Black diagram representation of the results including details of the number of cycles during loading and the time of rest during rest periods, and a representation of the nonlinearity effect; b) results after temperature correction. The figure present also a 2S2P1D model prediction, with indication of LVE complex modulus at 10Hz and three temperatures, 11.0°C (Tini), 12.5°C and 14°C.

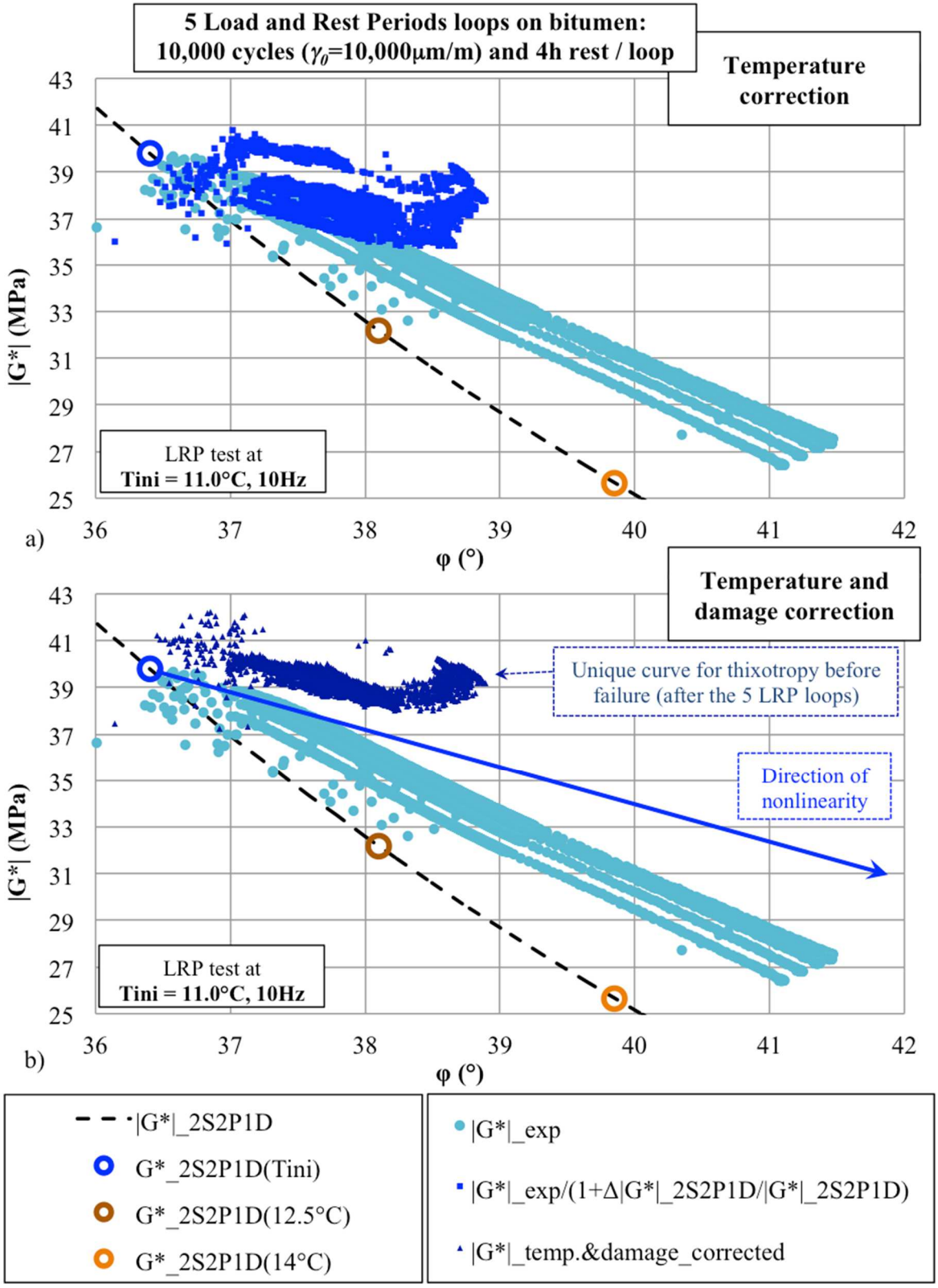

Figure C-12. Experimental results (B5070_A) for LRP tests (5 LRP tests with 10,000 cycles of 10,000µm/m sinusoidal loading and 4h rest loops on bitumen): Black diagram representation of a) the raw experimental results and the results after the temperature correction and b) the experimental results after temperature and damage correction. The figure present also a 2S2P1D model prediction, with indication of LVE complex modulus at 10Hz and three temperatures, 11.0°C (Tini), 12.5°C and 14°C.

B5070_B with 20,000μm/m strain amplitude

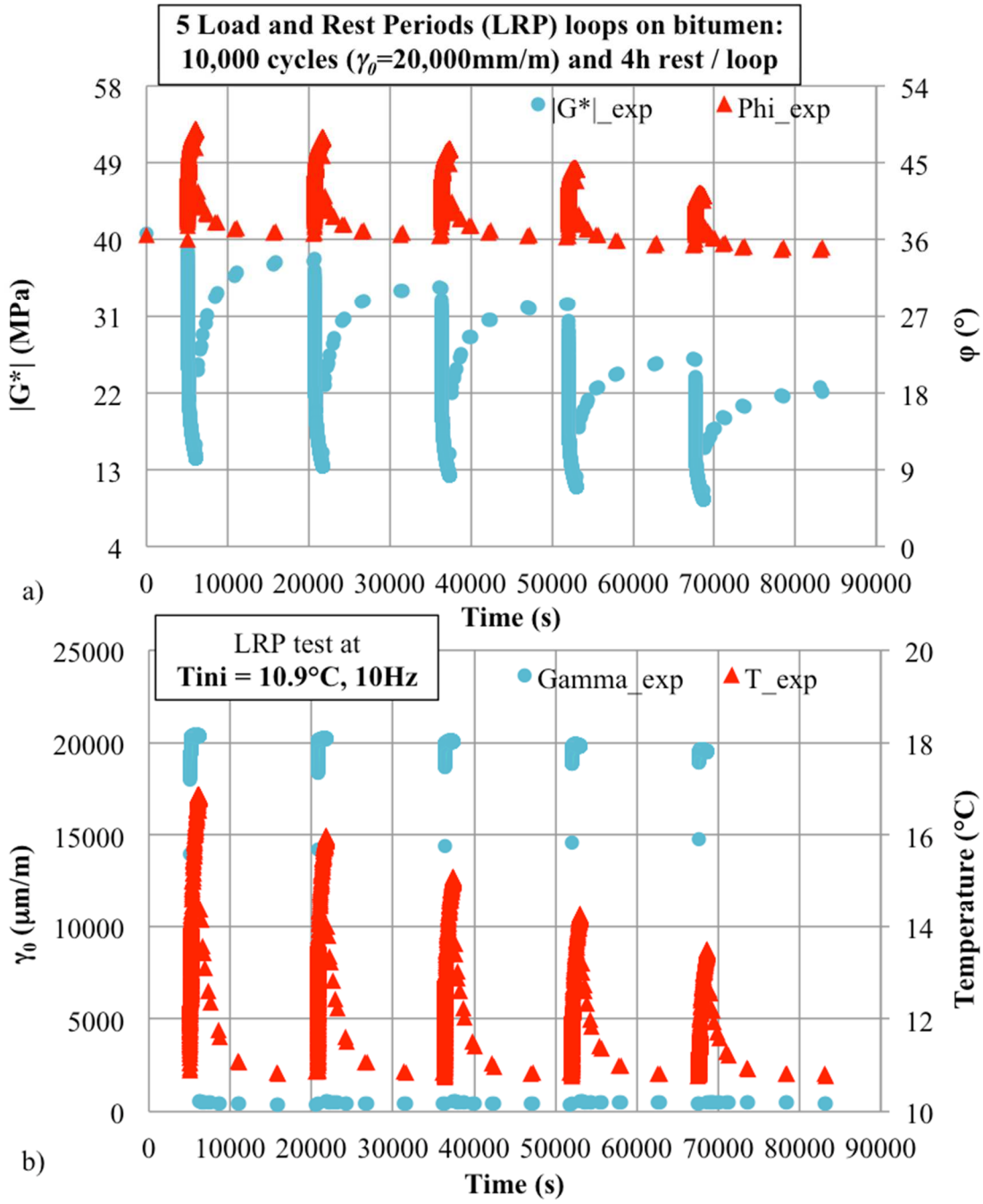

Figure C-13. Experimental results (B5070_B) for LRP tests: 5 LRP loops with 10,000 cycles and 4h rest on bitumen submitted to 20,000μm/m sinusoidal loading: a) Norm of complex modulus and phase angle as a function of time, and b) shear strain amplitude and temperature as a function of time.

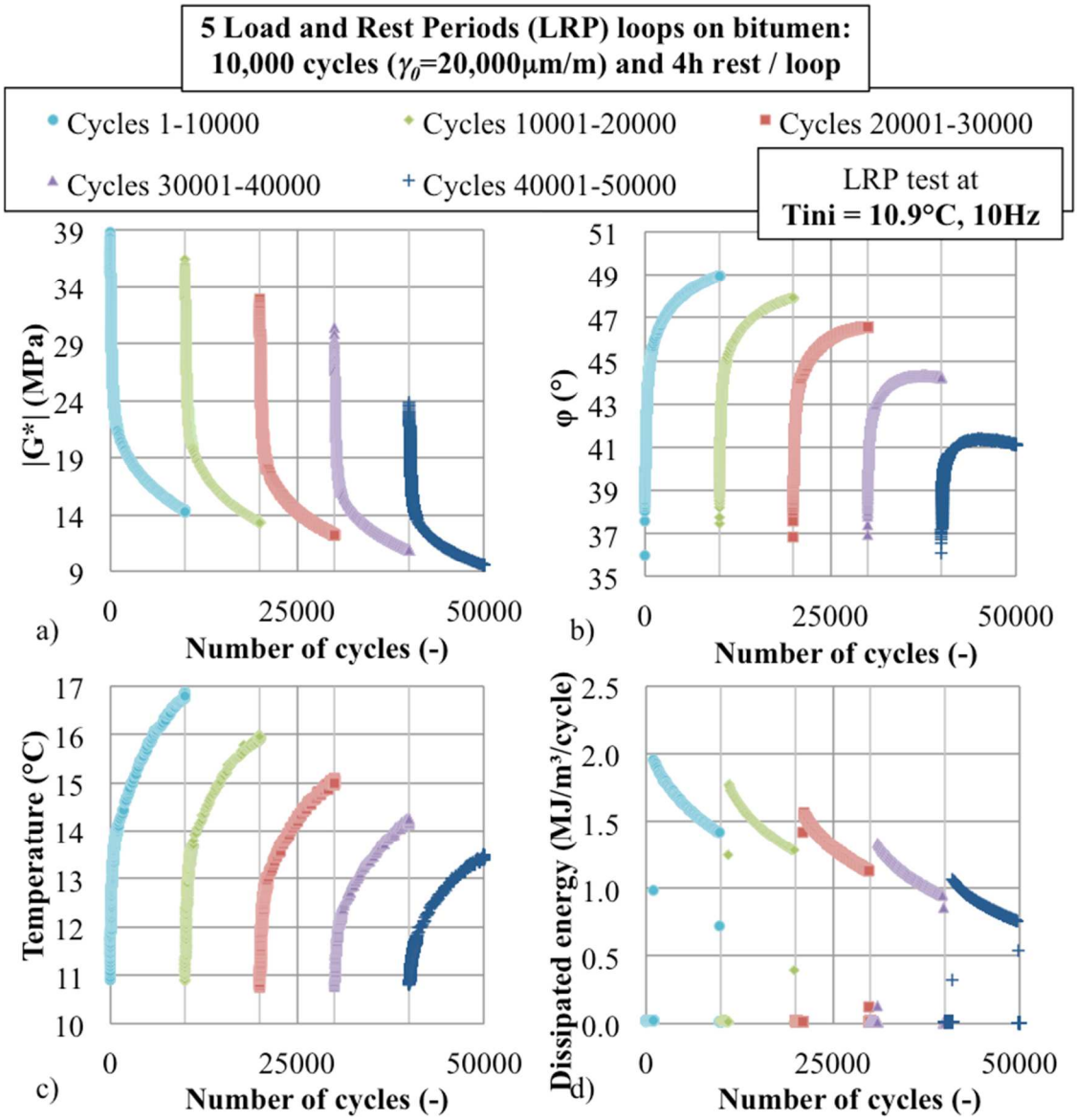

Figure C-14. Experimental results (B5070_B) for LRP tests: 5 LRP 20,000µm/m sinusoidal loading loops with 10,000 cycles each on bitumen: a) Norm of complex shear modulus, b) phase angle, c) mean in-specimen temperature, and d) dissipated energy per cycle as a function of the number of applied cycles.

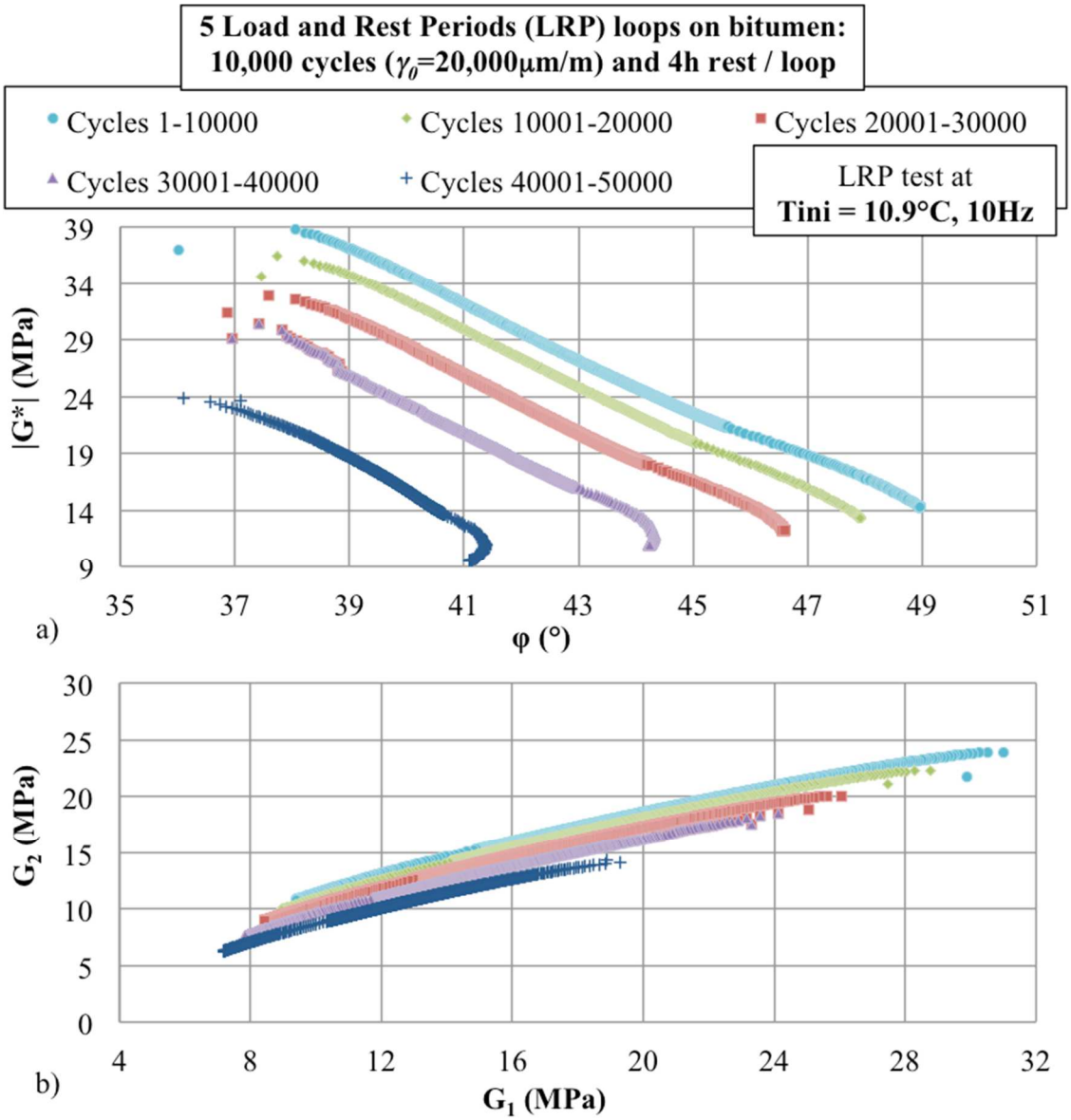

Figure C-15. Experimental results (B5070_B) for LRP tests: 5 LRP 20,000µm/m sinusoidal loading loops with 10,000 cycles each on bitumen: representation on a) Black space, and b) Cole-Cole diagram.

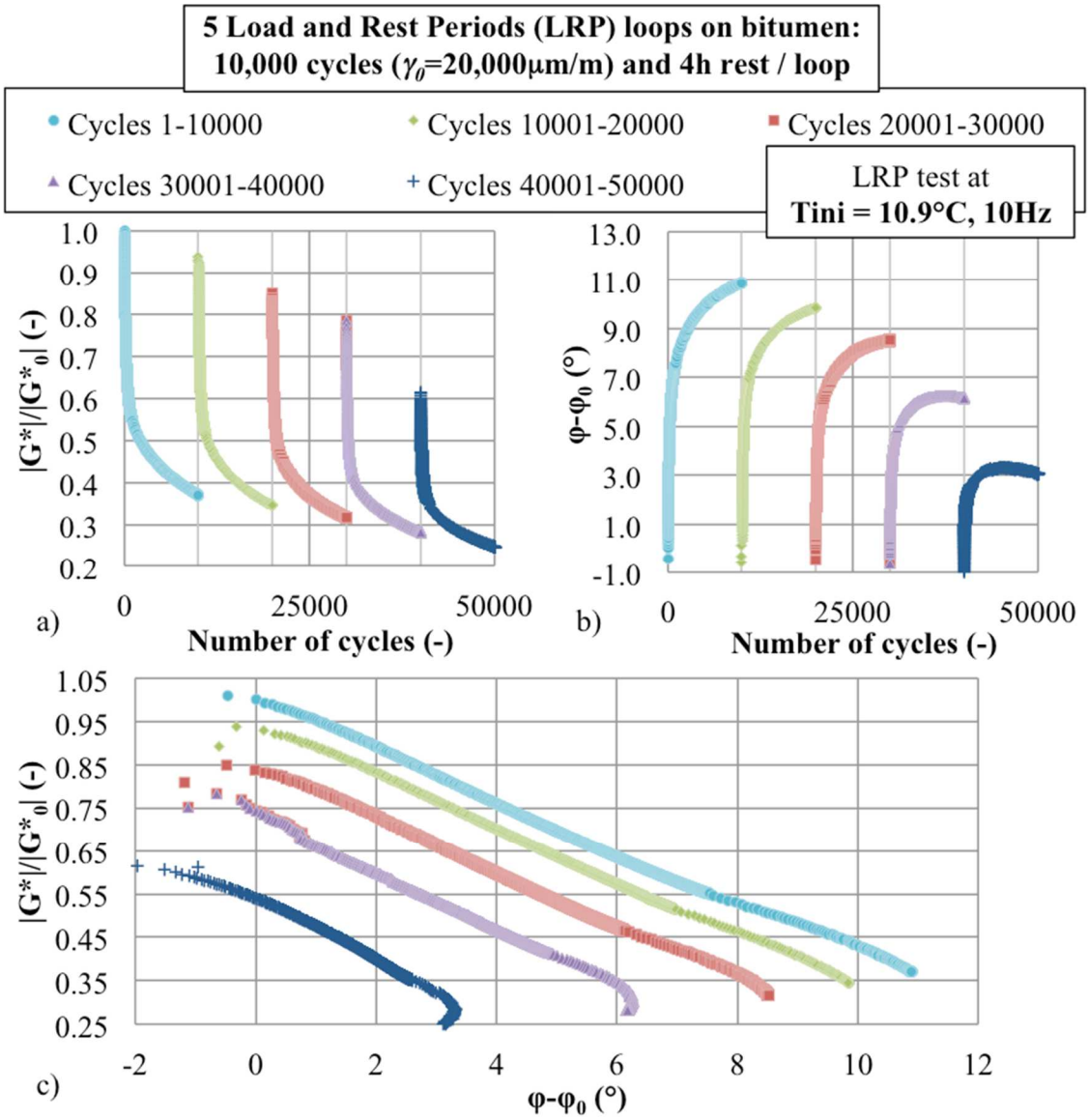

Figure C-16. Experimental results (B5070_B) for LRP tests: 5 LRP 20,000µm/m sinusoidal loading loops with 10,000 cycles each on bitumen: a) Normalised (the initial modulus being considered as the result at the 3rd cycle) norm of complex shear modulus, and b) normalised phase angle as a function of number of applied cycles; and c) representation of the results on a normalised Black space.

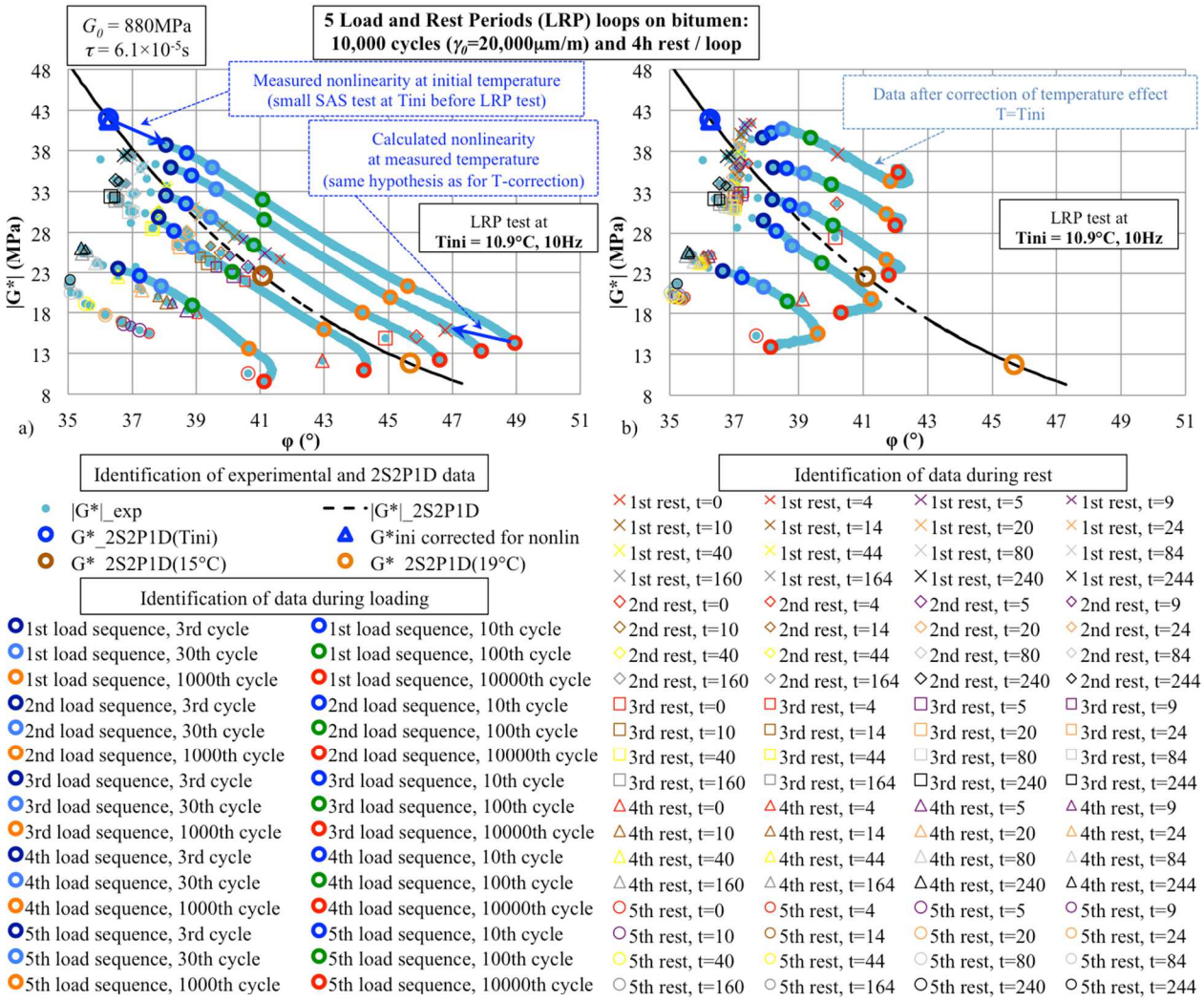

Figure C-17. Experimental results (B5070_B) for LRP tests (5 LRP tests with 10,000 cycles of 20,000µm/m sinusoidal loading and 4h rest loops on bitumen): a) Black diagram representation of the results including details of the number of cycles during loading and the time of rest during rest periods, and a representation of the nonlinearity effect; b) results after temperature correction. The figure present also a 2S2P1D model prediction, with indication of LVE complex modulus at 10Hz and three temperatures, 10.9°C (Tini), 15°C and 19°C.

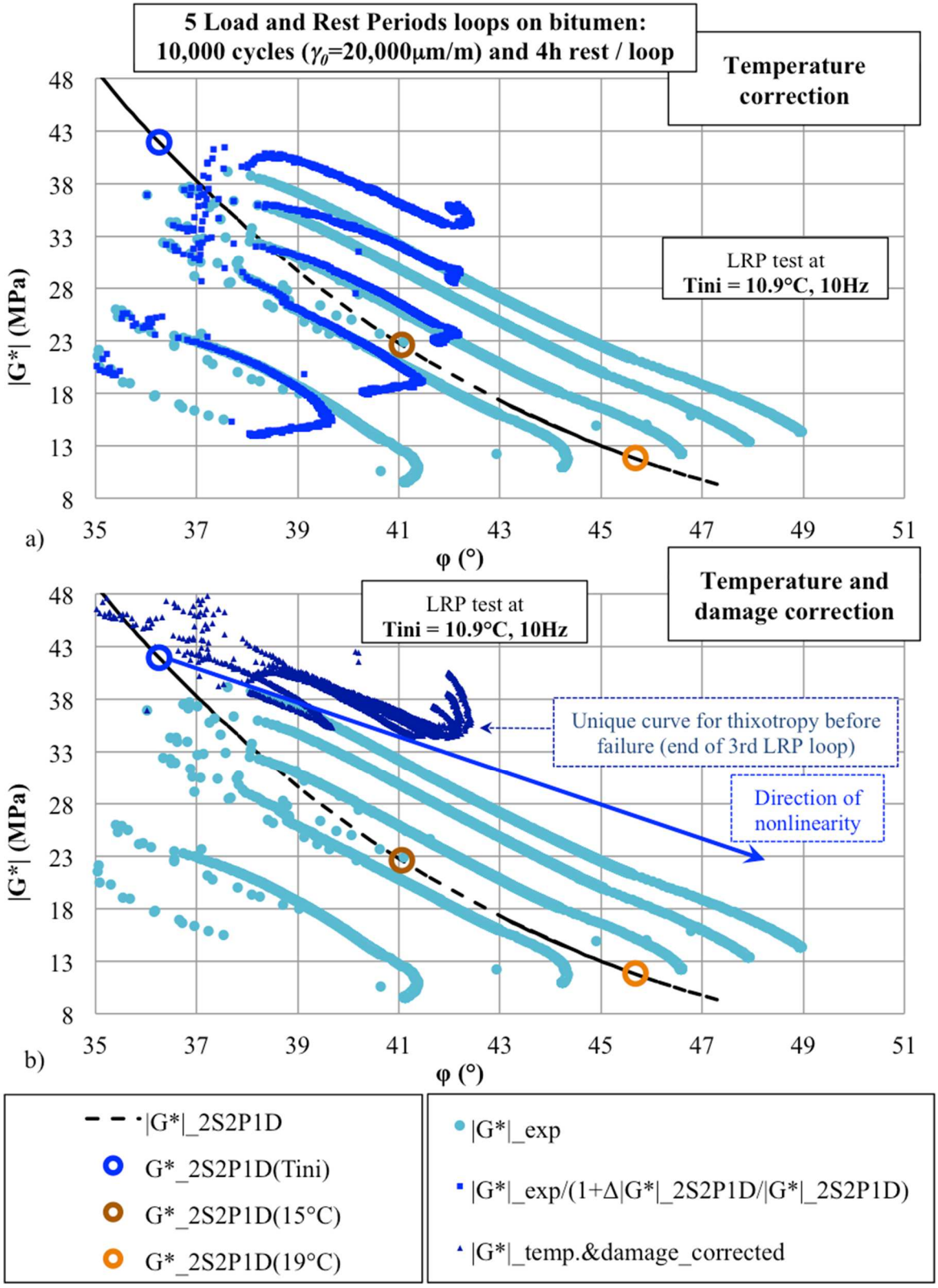

Figure C-18. Experimental results (B5070_B) for LRP tests (5 LRP tests with 10,000 cycles of 20,000µm/m sinusoidal loading and 4h rest loops on bitumen): Black diagram representation of a) the raw experimental results and the results after the temperature correction and b) the experimental results after temperature and damage correction. The figure present also a 2S2P1D model prediction, with indication of LVE complex modulus at 10Hz and three temperatures, 10.9°C (Tini), 15°C and 19°C.

B5070_D with 20,000μm/m strain amplitude

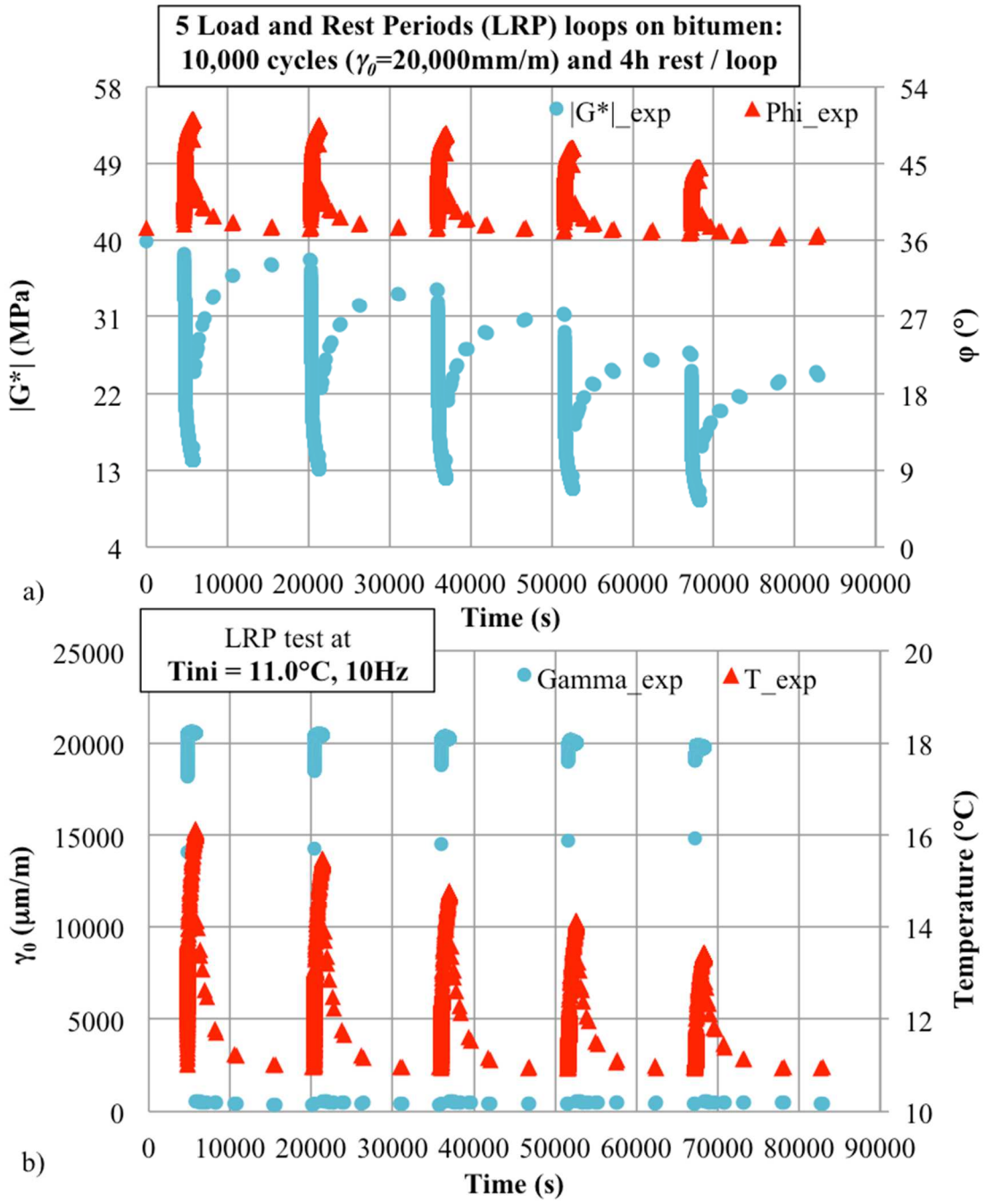

Figure C-19. Experimental results (B5070_D) for LRP tests: 5 LRP loops with 10,000 cycles and 4h rest on bitumen submitted to 20,000μm/m sinusoidal loading: a) Norm of complex modulus and phase angle as a function of time, and b) shear strain amplitude and temperature as a function of time.

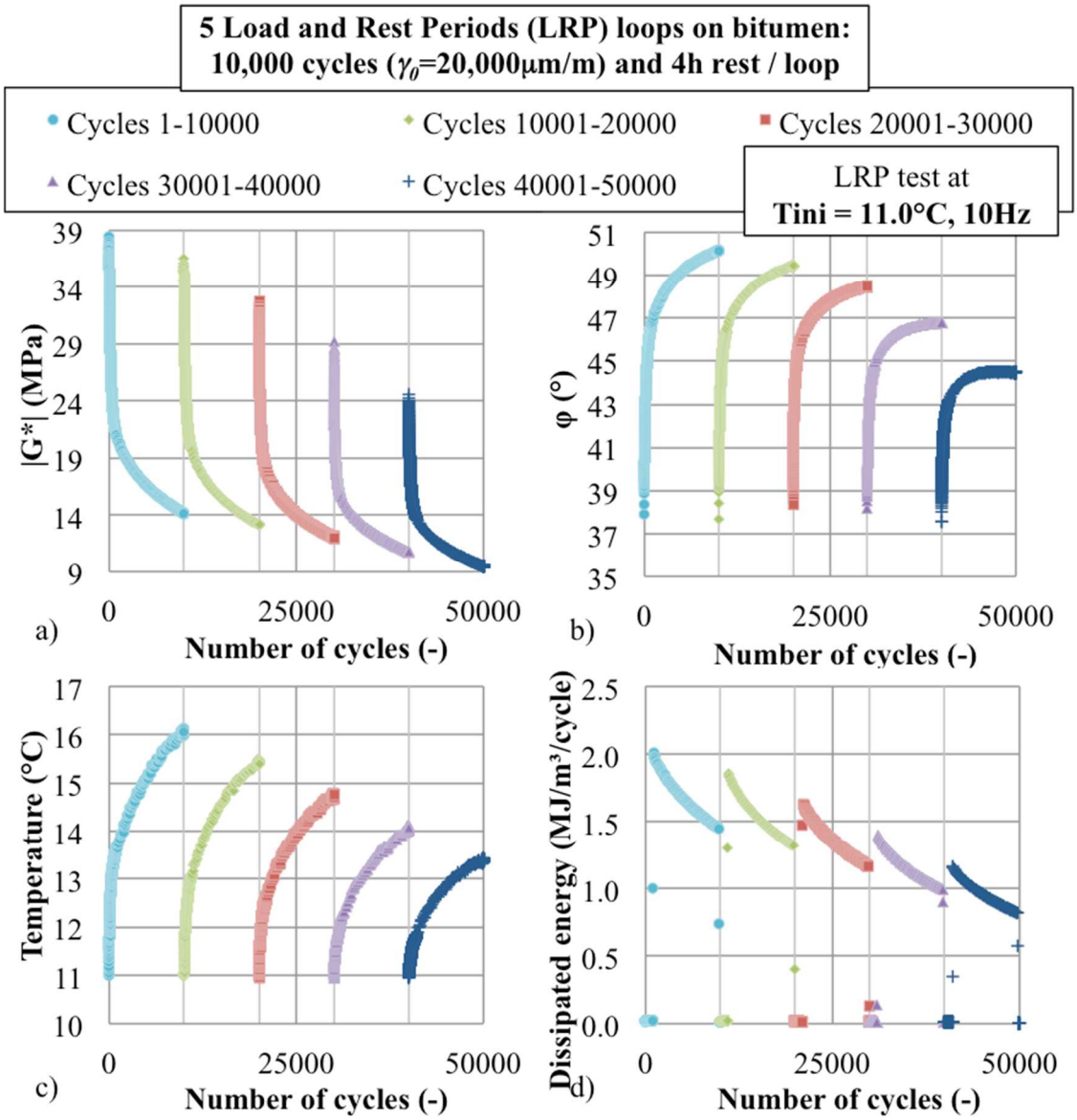

Figure C-20. Experimental results (B5070_D) for LRP tests: 5 LRP 20,000µm/m sinusoidal loading loops with 10,000 cycles each on bitumen: a) Norm of complex shear modulus, b) phase angle, c) mean in-specimen temperature, and d) dissipated energy per cycle as a function of the number of applied cycles.

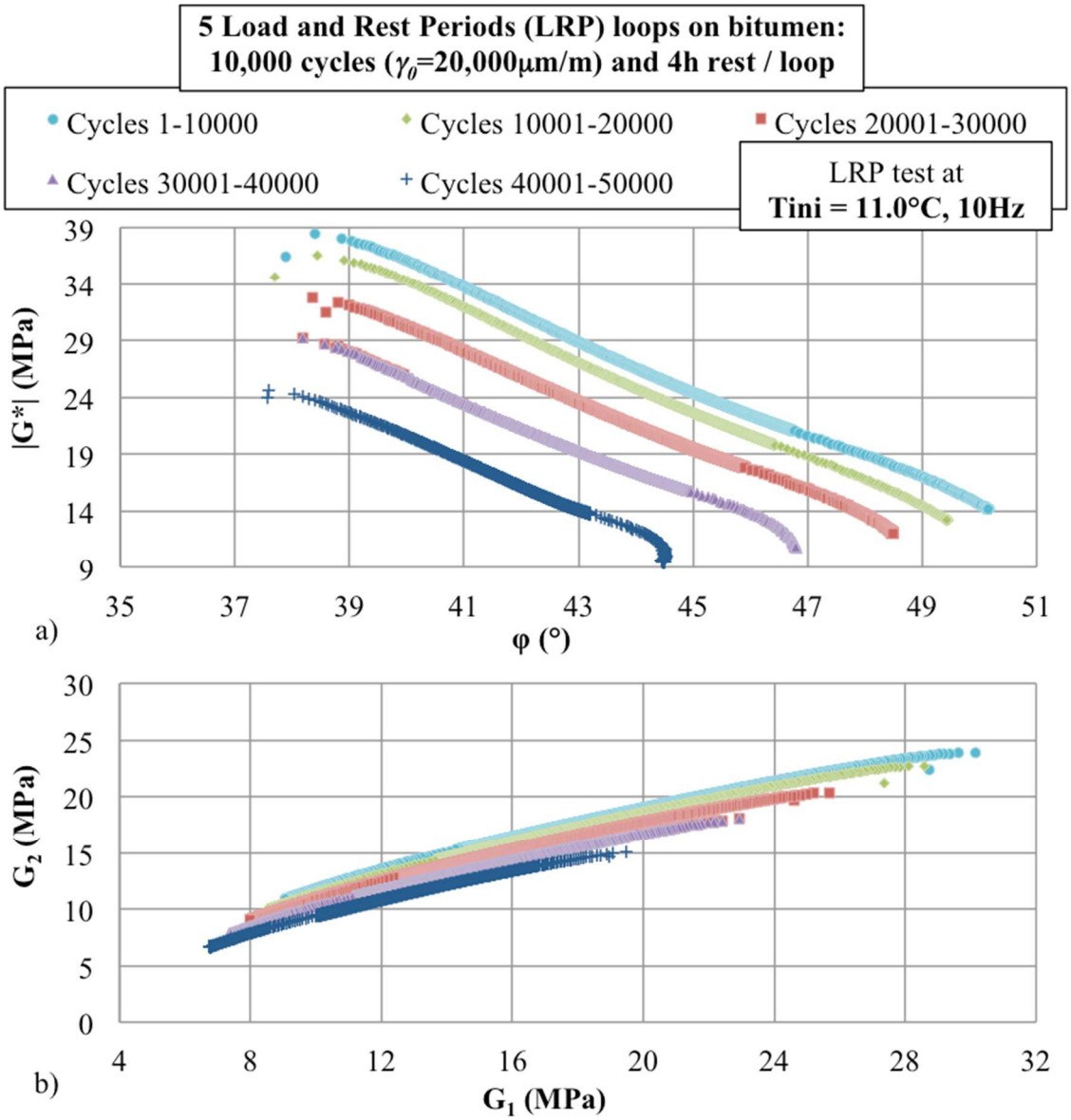

Figure C-21. Experimental results (B5070_D) for LRP tests: 5 LRP 20,000µm/m sinusoidal loading loops with 10,000 cycles each on bitumen: representation on a) Black space, and b) Cole-Cole diagram.

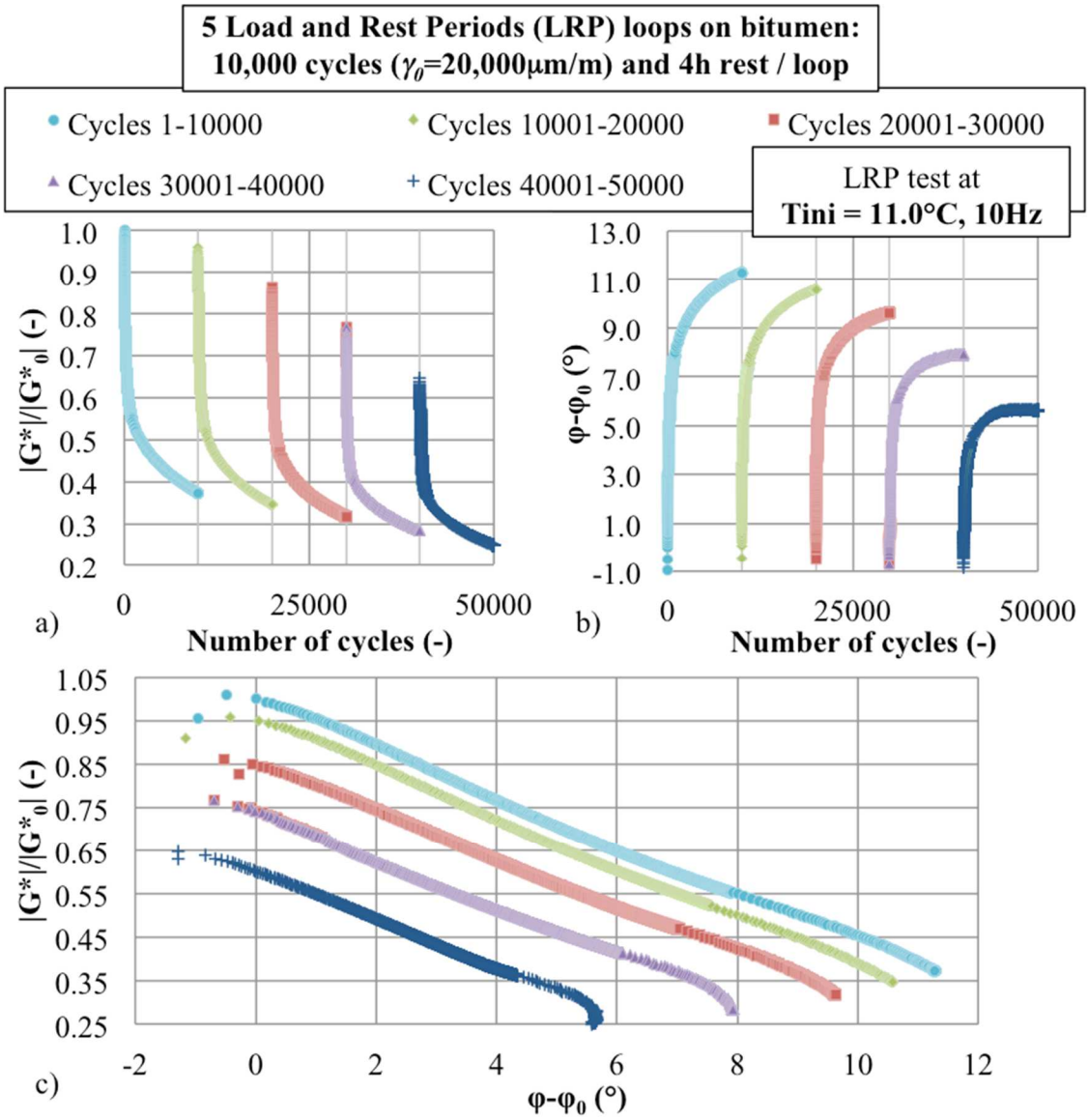

Figure C-22. Experimental results (B5070_D) for LRP tests: 5 LRP 20,000µm/m sinusoidal loading loops with 10,000 cycles each on bitumen: a) Normalised (the initial modulus being considered as the result at the 3rd cycle) norm of complex shear modulus, and b) normalised phase angle as a function of number of applied cycles; and c) representation of the results on a normalised Black space.

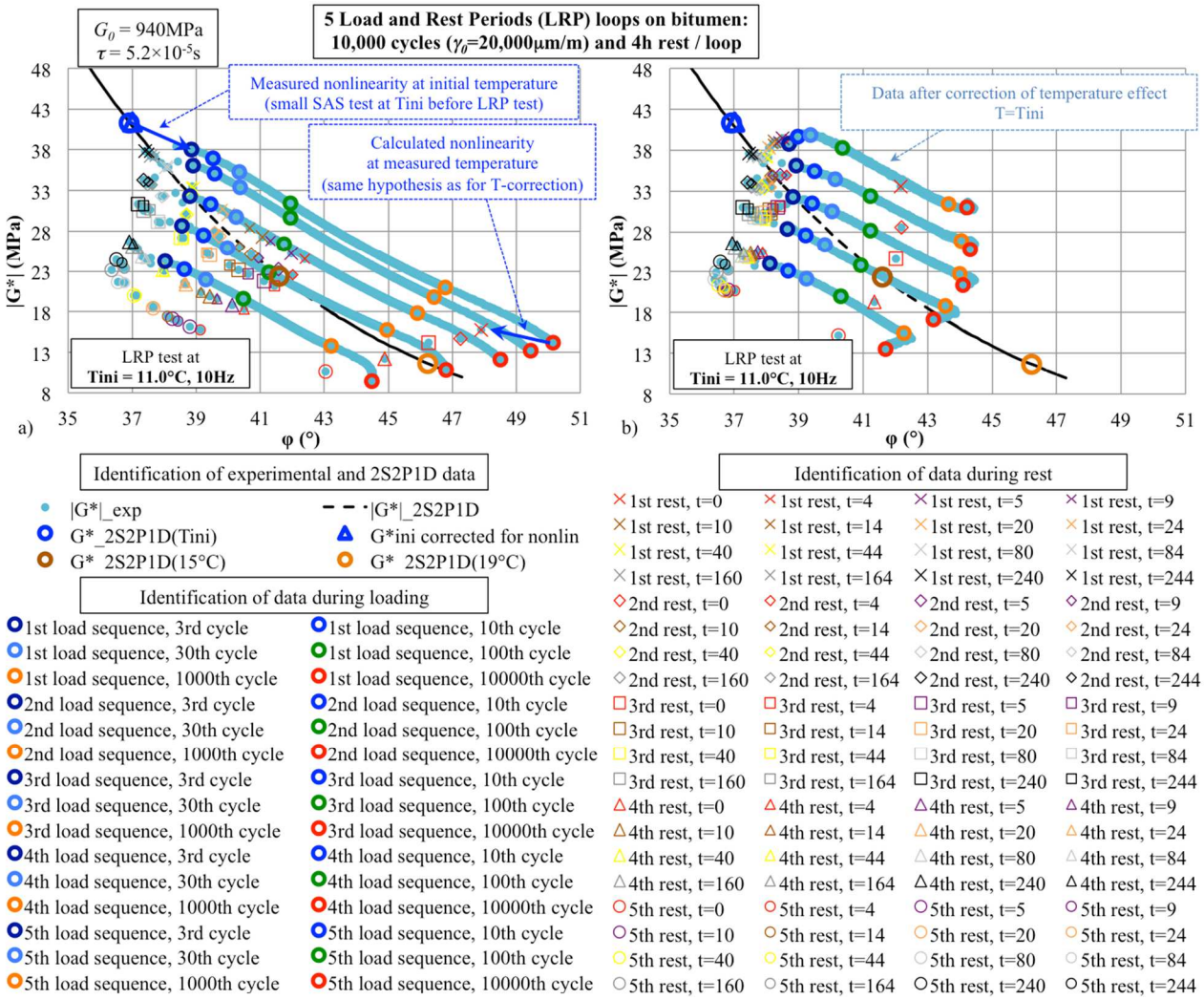

Figure C-23. Experimental results (B5070_D) for LRP tests (5 LRP tests with 10,000 cycles of 20,000µm/m sinusoidal loading and 4h rest loops on bitumen): a) Black diagram representation of the results including details of the number of cycles during loading and the time of rest during rest periods, and a representation of the nonlinearity effect; b) results after temperature correction. The figure present also a 2S2P1D model prediction, with indication of LVE complex modulus at 10Hz and three temperatures, 11.0°C (Tini), 15°C and 19°C.

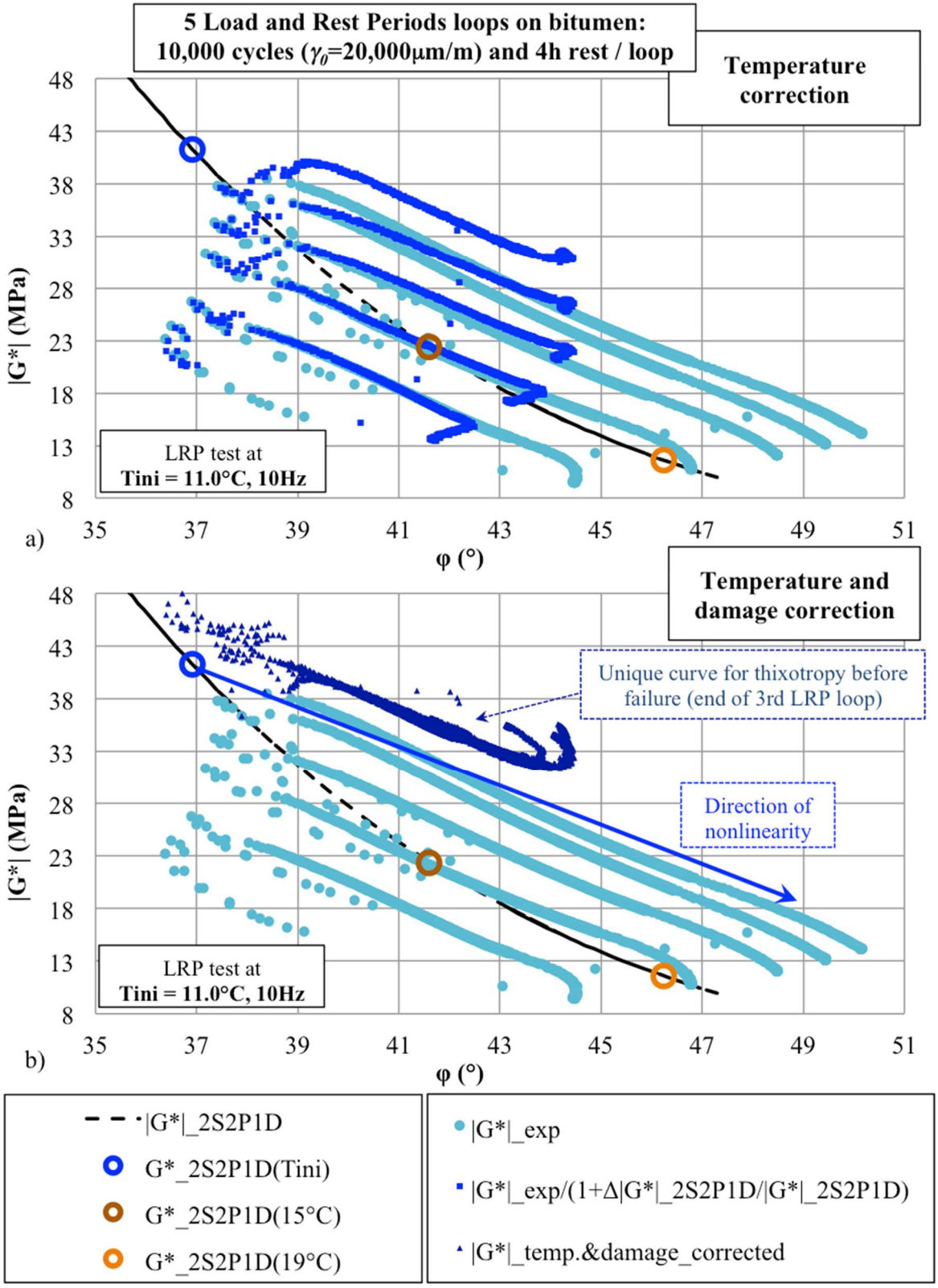

Figure C-24. Experimental results (B5070_D) for LRP tests (5 LRP tests with 10,000 cycles of 20,000µm/m sinusoidal loading and 4h rest loops on bitumen): Black diagram representation of a) the raw experimental results and the results after the temperature correction and b) the experimental results after temperature and damage correction. The figure present also a 2S2P1D model prediction, with indication of LVE complex modulus at 10Hz and three temperatures, 11.0°C (Tini), 15°C and 19°C.

LRP test results on Mastic

M5070_30pc40-70_C with 1,000μm/m strain amplitude

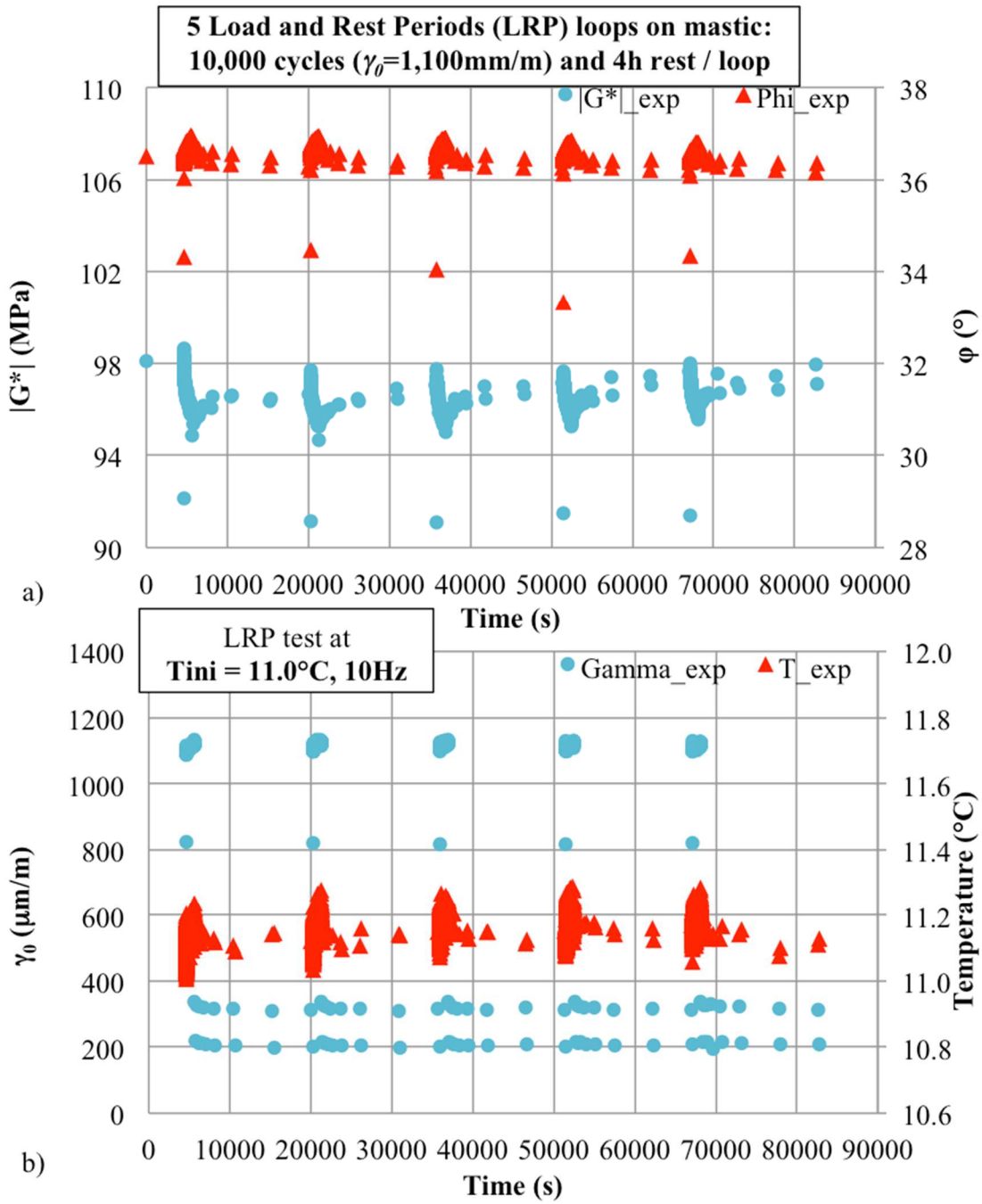

Figure C-25. Experimental results (M5070_30pc40-70_C) for LRP tests: 5 LRP loops with 10,000 cycles and 4h rest on bitumen submitted to 1,100μm/m sinusoidal loading: a) Norm of complex modulus and phase angle as a function of time, and b) shear strain amplitude and temperature as a function of time.

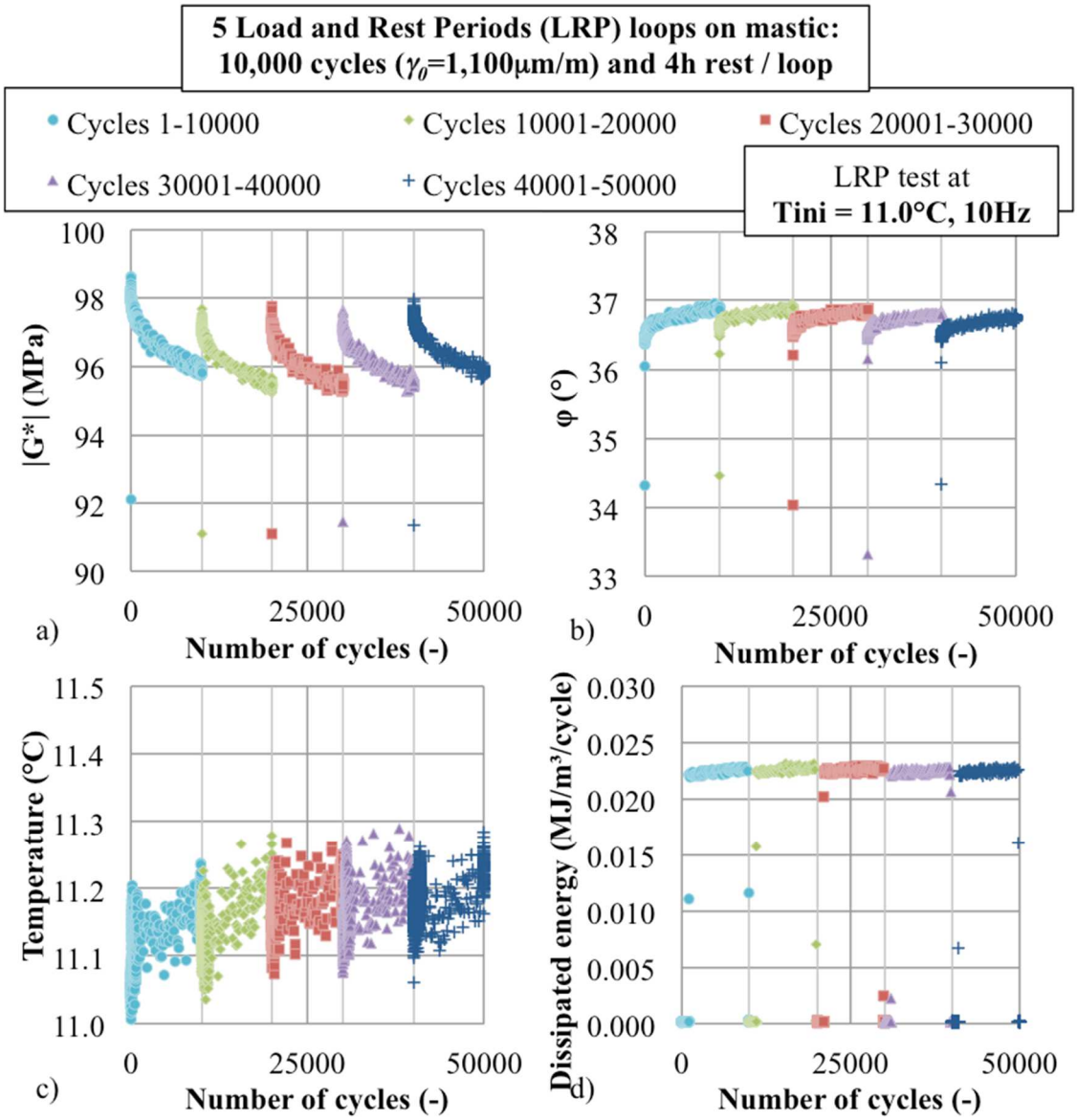

Figure C-26. Experimental results (M5070_30pc40-70_C) for LRP tests: 5 LRP 1,100µm/m sinusoidal loading loops with 10,000 cycles each on bitumen: a) Norm of complex shear modulus, b) phase angle, c) mean in-specimen temperature, and d) dissipated energy per cycle as a function of the number of applied cycles.

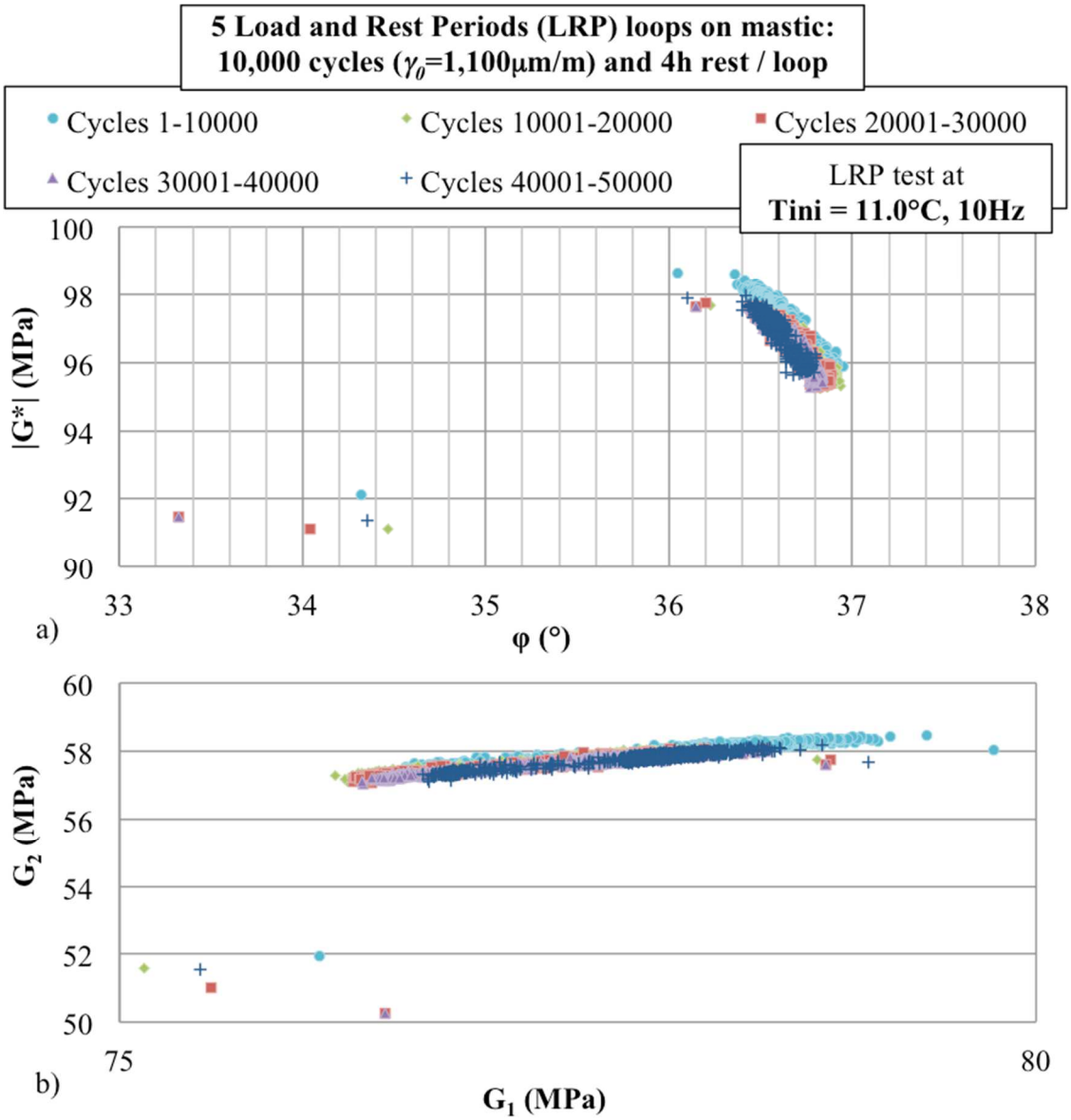

Figure C-27. Experimental results (M5070_30pc40-70_C) for LRP tests: 5 LRP 1,100µm/m sinusoidal loading loops with 10,000 cycles each on bitumen: representation on a) Black space, and b) Cole-Cole diagram.

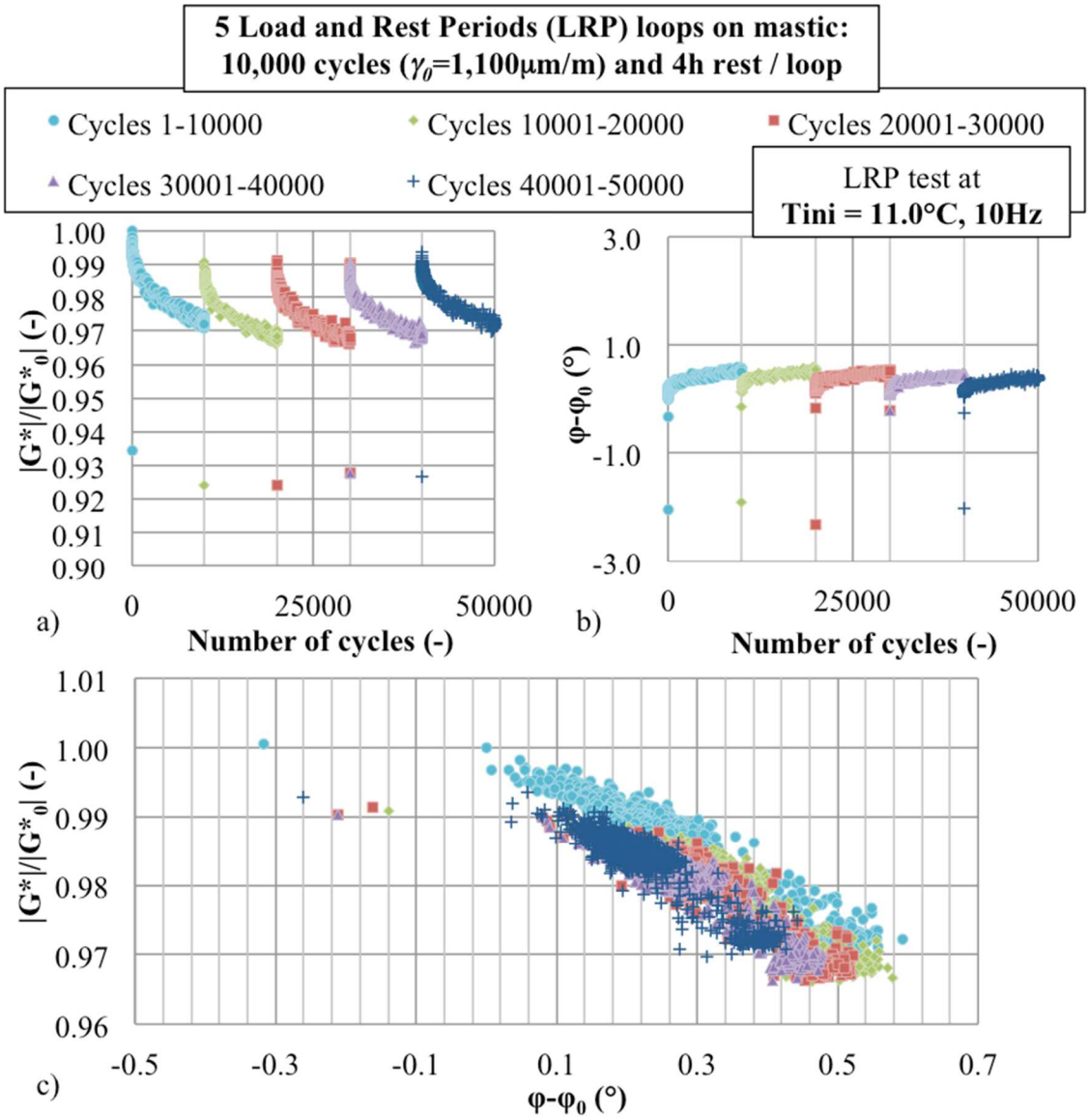

Figure C-28. Experimental results (M5070_30pc40-70_C) for LRP tests: 5 LRP 1,100µm/m sinusoidal loading loops with 10,000 cycles each on bitumen: a) Normalised (the initial modulus being considered as the result at the 3rd cycle) norm of complex shear modulus, and b) normalised phase angle as a function of number of applied cycles; and c) representation of the results on a normalised Black space.

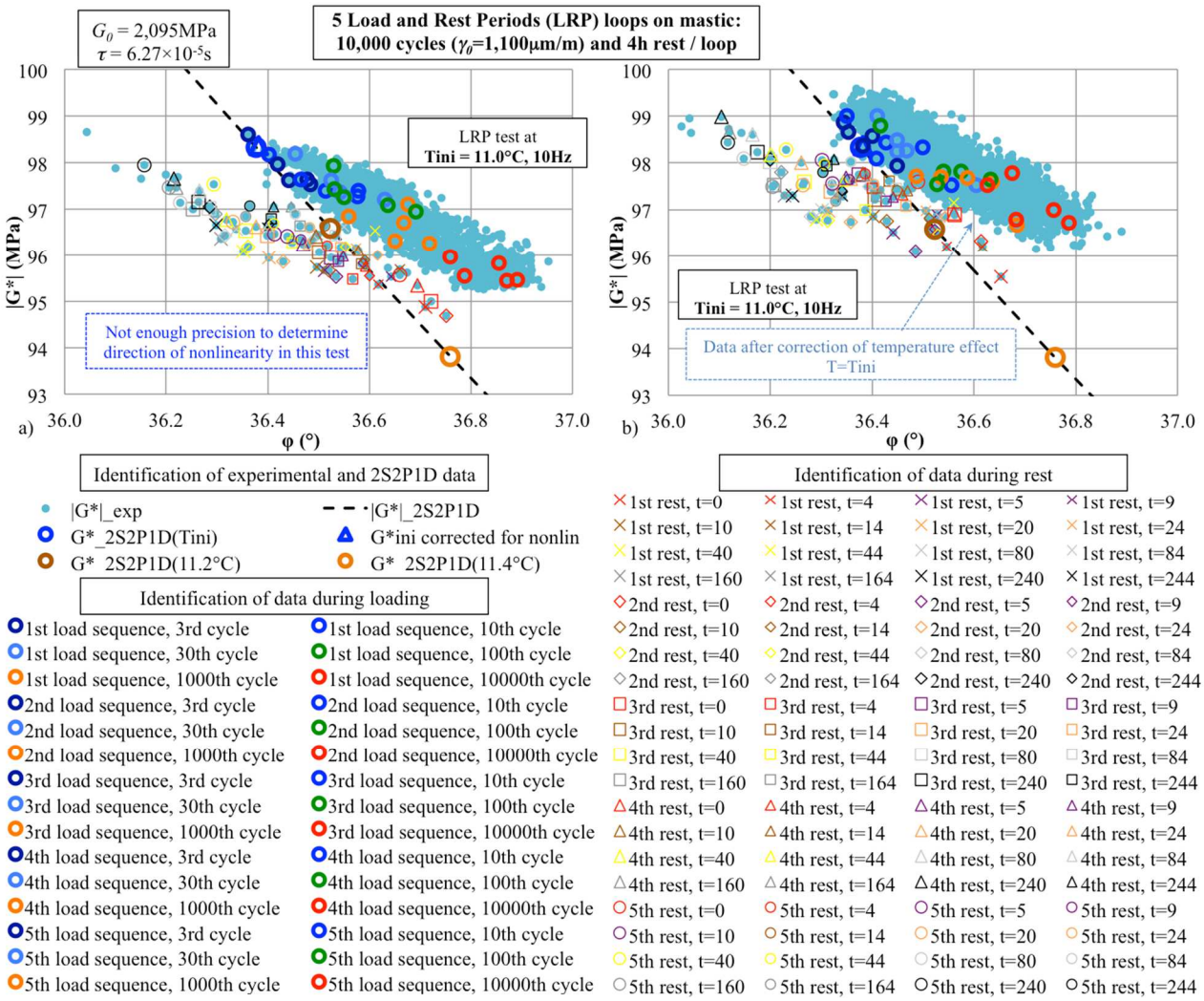

Figure C-29. Experimental results (M5070_30pc40-70_C) for LRP tests (5 LRP tests with 10,000 cycles of 1,100µm/m sinusoidal loading and 4h rest loops on bitumen): a) Black diagram representation of the results including details of the number of cycles during loading and the time of rest during rest periods, and a representation of the nonlinearity effect; b) results after temperature correction. The figure present also a 2S2P1D model prediction, with indication of LVE complex modulus at 10Hz and three temperatures, 11.1°C (Tini), 11.2°C and 11.4°C.

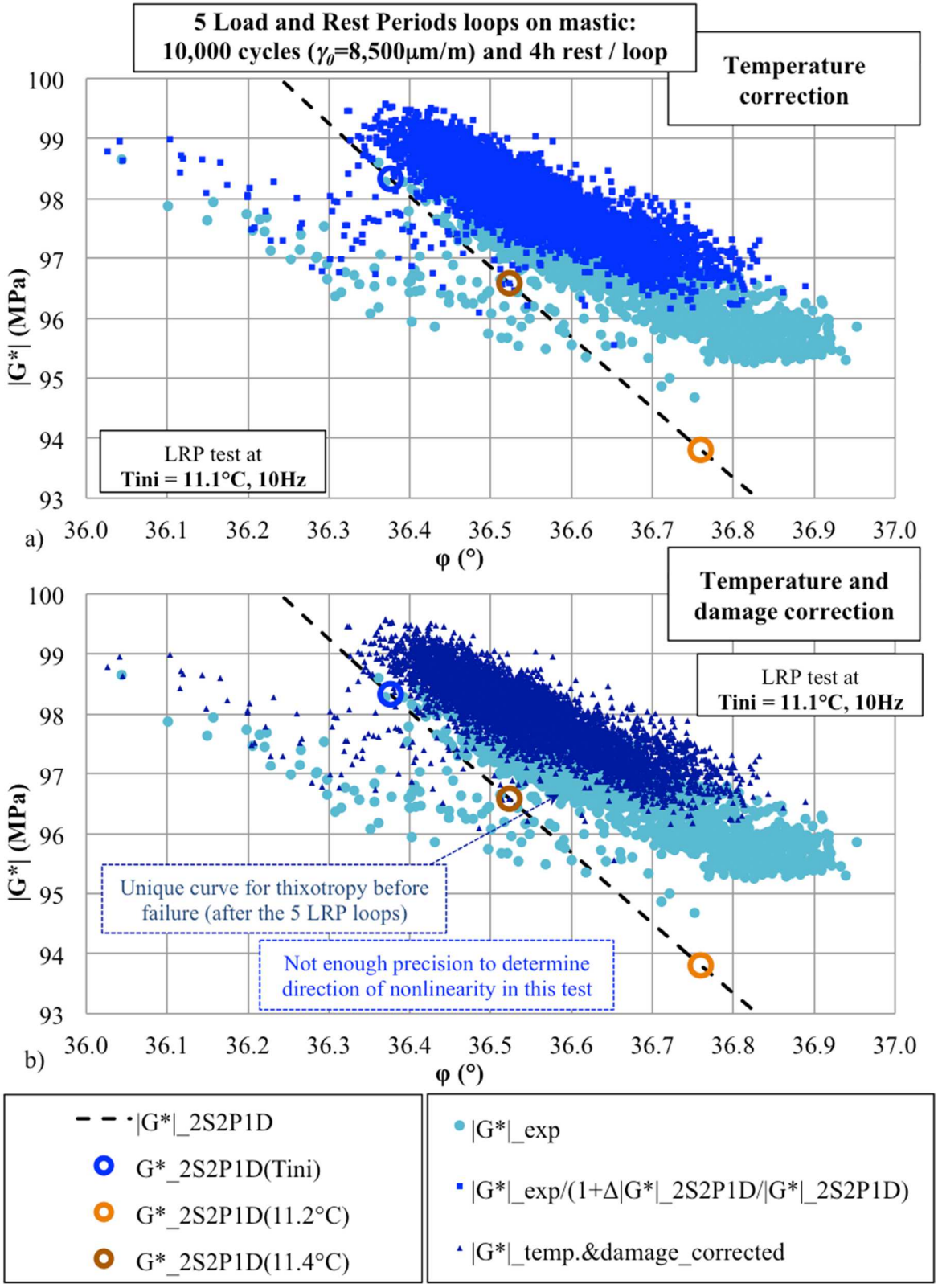

Figure C-30. Experimental results (M5070_30pc40-70_C) for LRP tests (5 LRP tests with 10,000 cycles of 1,100µm/m sinusoidal loading and 4h rest loops on bitumen): Black diagram representation of a) the raw experimental results and the results after the temperature correction and b) the experimental results after temperature and damage correction. The figure present also a 2S2P1D model prediction, with indication of LVE complex modulus at 10Hz and three temperatures, 11.1°C (Tini), 11.2°C and 11.4°C.

M5070_30pc40-70_A with 3,300μm/m strain amplitude

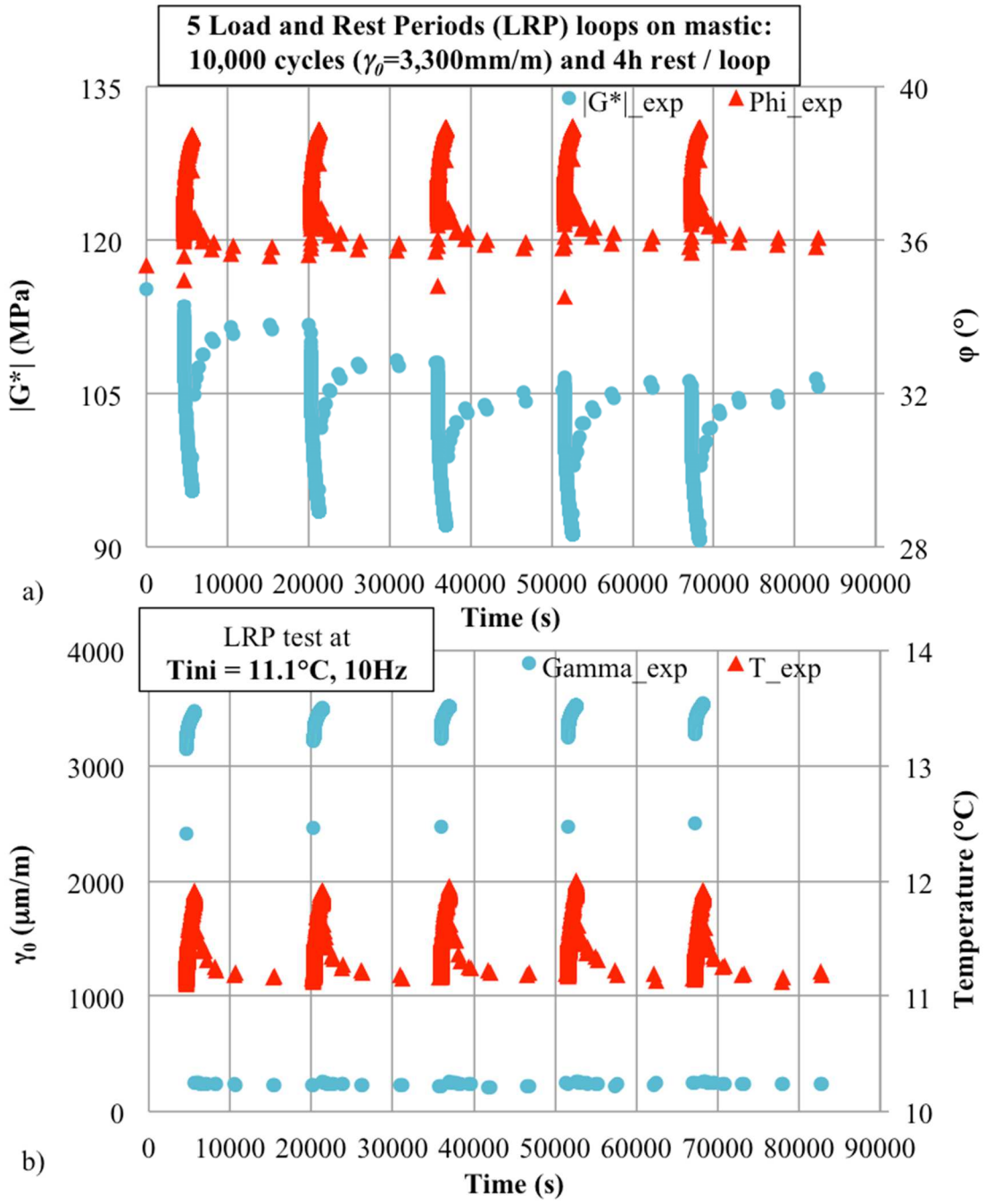

Figure C-31. Experimental results (M5070_30pc40-70_A) for LRP tests: 5 LRP loops with 10,000 cycles and 4h rest on bitumen submitted to 3,300μm/m sinusoidal loading: a) Norm of complex modulus and phase angle as a function of time, and b) shear strain amplitude and temperature as a function of time.

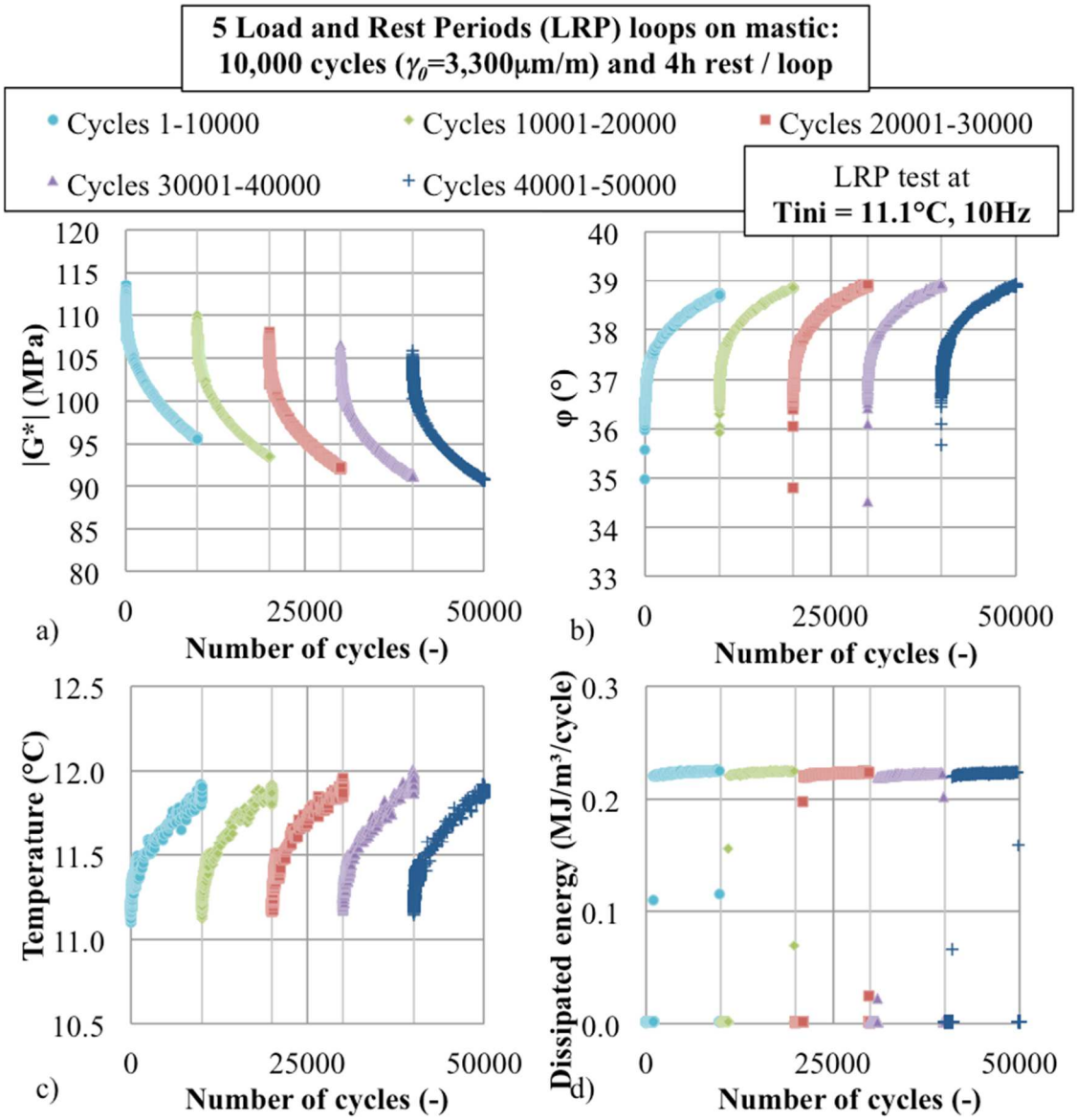

Figure C-32. Experimental results (M5070_30pc40-70_A) for LRP tests: 5 LRP 3,300µm/m sinusoidal loading loops with 10,000 cycles each on bitumen: a) Norm of complex shear modulus, b) phase angle, c) mean in-specimen temperature, and d) dissipated energy per cycle as a function of the number of applied cycles.

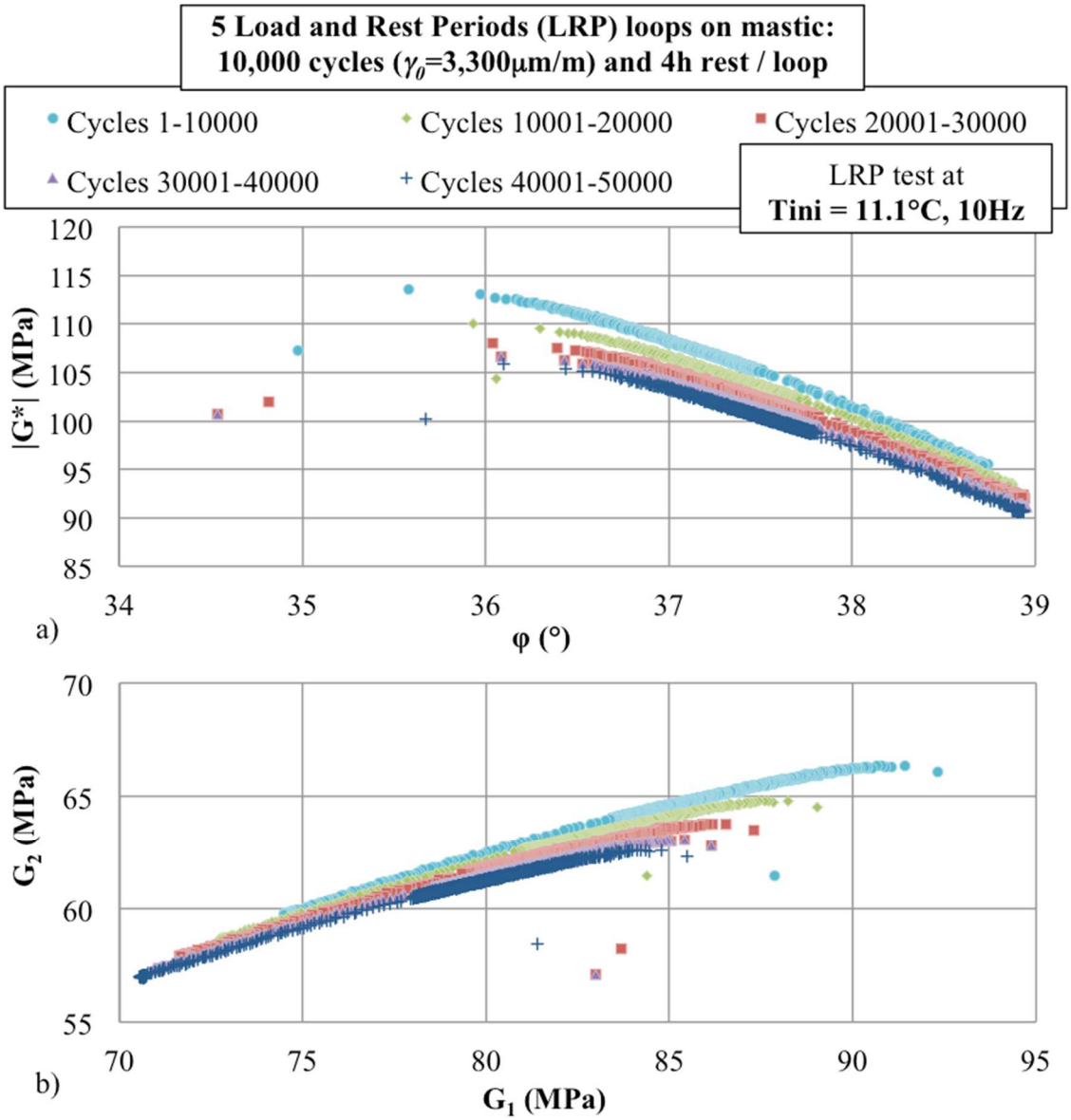

Figure C-33. Experimental results (M5070_30pc40-70_A) for LRP tests: 5 LRP 3,300µm/m sinusoidal loading loops with 10,000 cycles each on bitumen: representation on a) Black space, and b) Cole-Cole diagram.

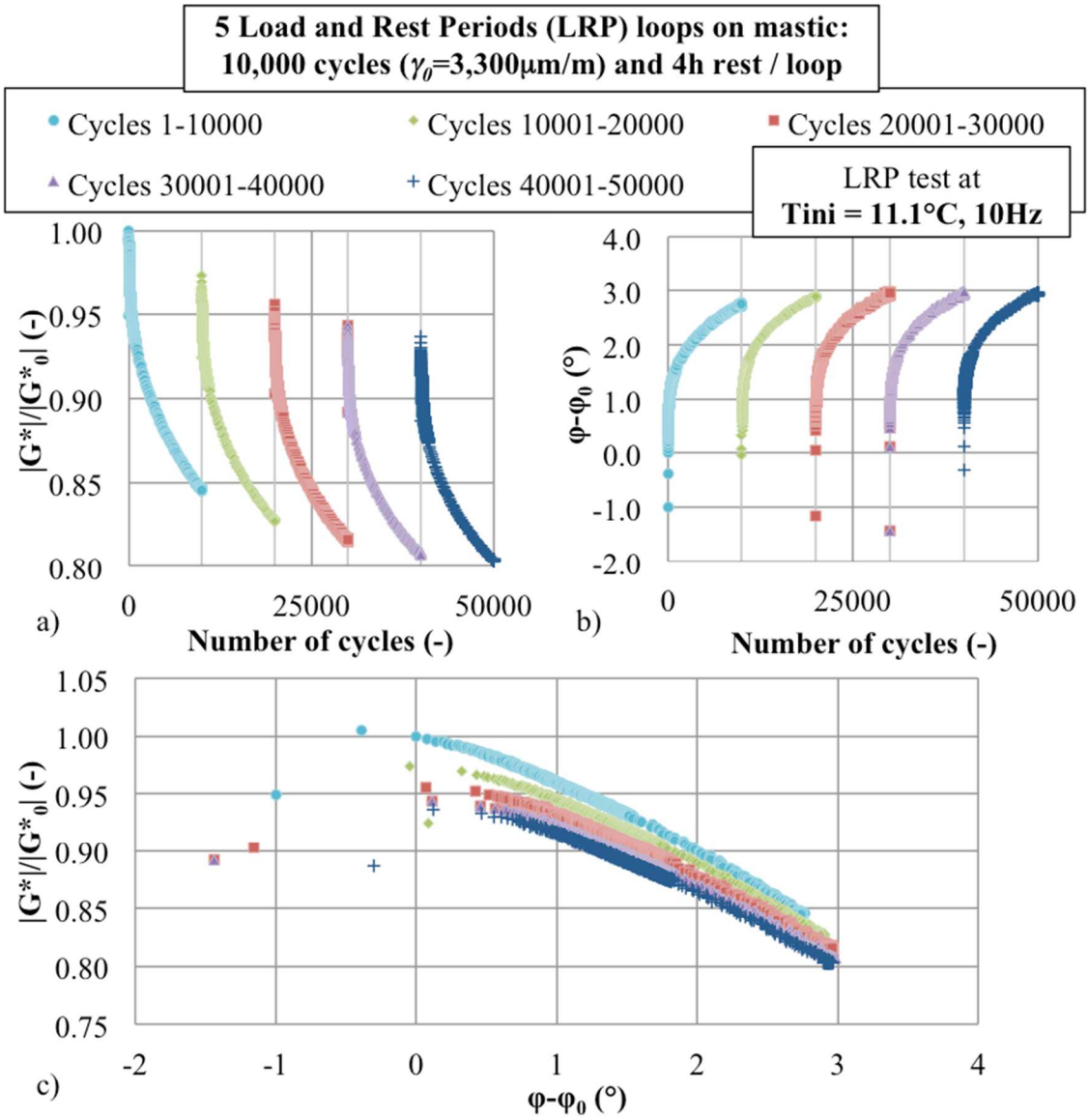

Figure C-34. Experimental results (M5070_30pc40-70_A) for LRP tests: 5 LRP 3,300µm/m sinusoidal loading loops with 10,000 cycles each on bitumen: a) Normalised (the initial modulus being considered as the result at the 3rd cycle) norm of complex shear modulus, and b) normalised phase angle as a function of number of applied cycles; and c) representation of the results on a normalised Black space.

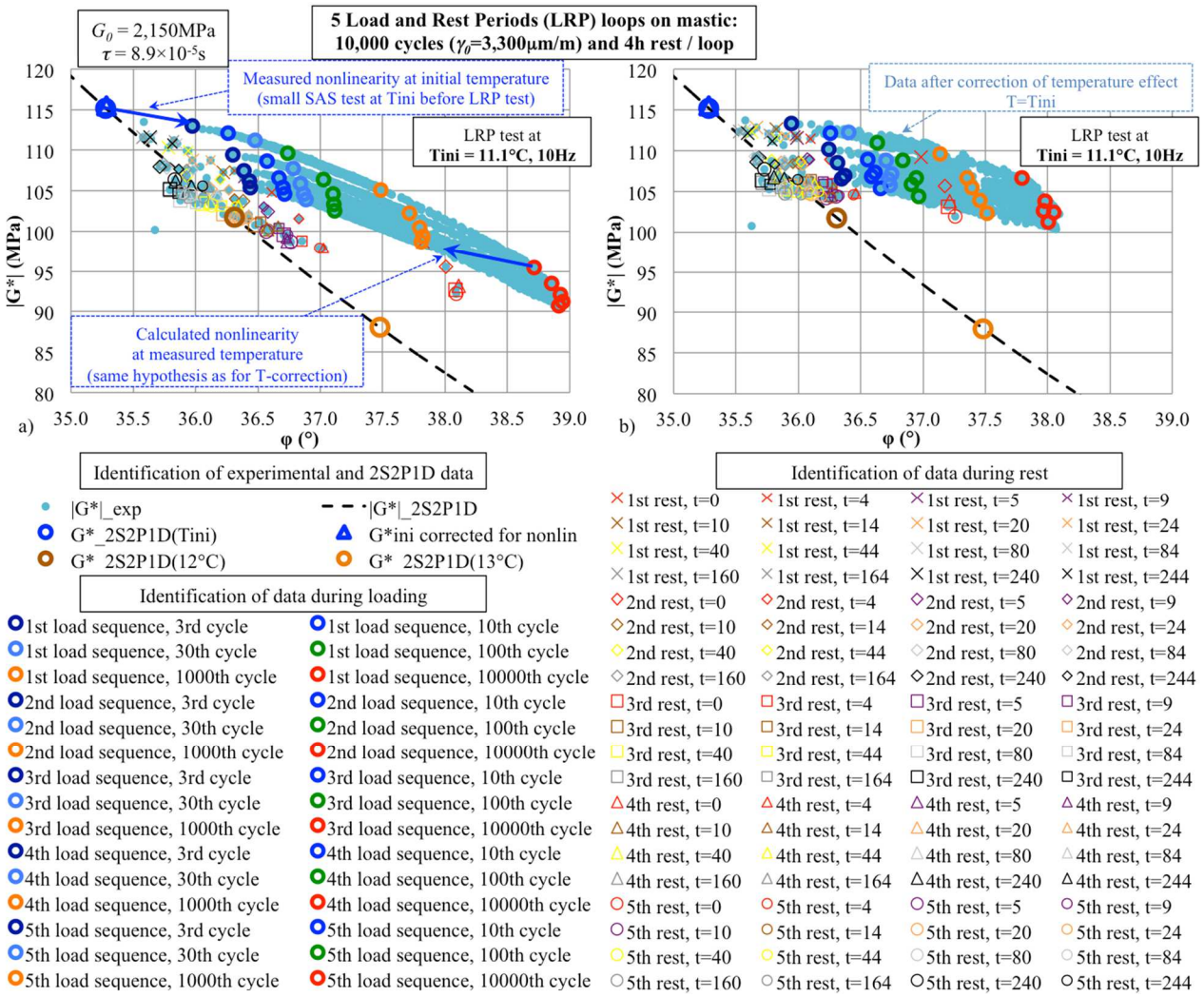

Figure C-35. Experimental results (M5070_30pc40-70_A) for LRP tests (5 LRP tests with 10,000 cycles of 3,300µm/m sinusoidal loading and 4h rest loops on bitumen): a) Black diagram representation of the results including details of the number of cycles during loading and the time of rest during rest periods, and a representation of the nonlinearity effect; b) results after temperature correction. The figure present also a 2S2P1D model prediction, with indication of LVE complex modulus at 10Hz and three temperatures, 11.1°C (Tini), 12°C and 13°C.

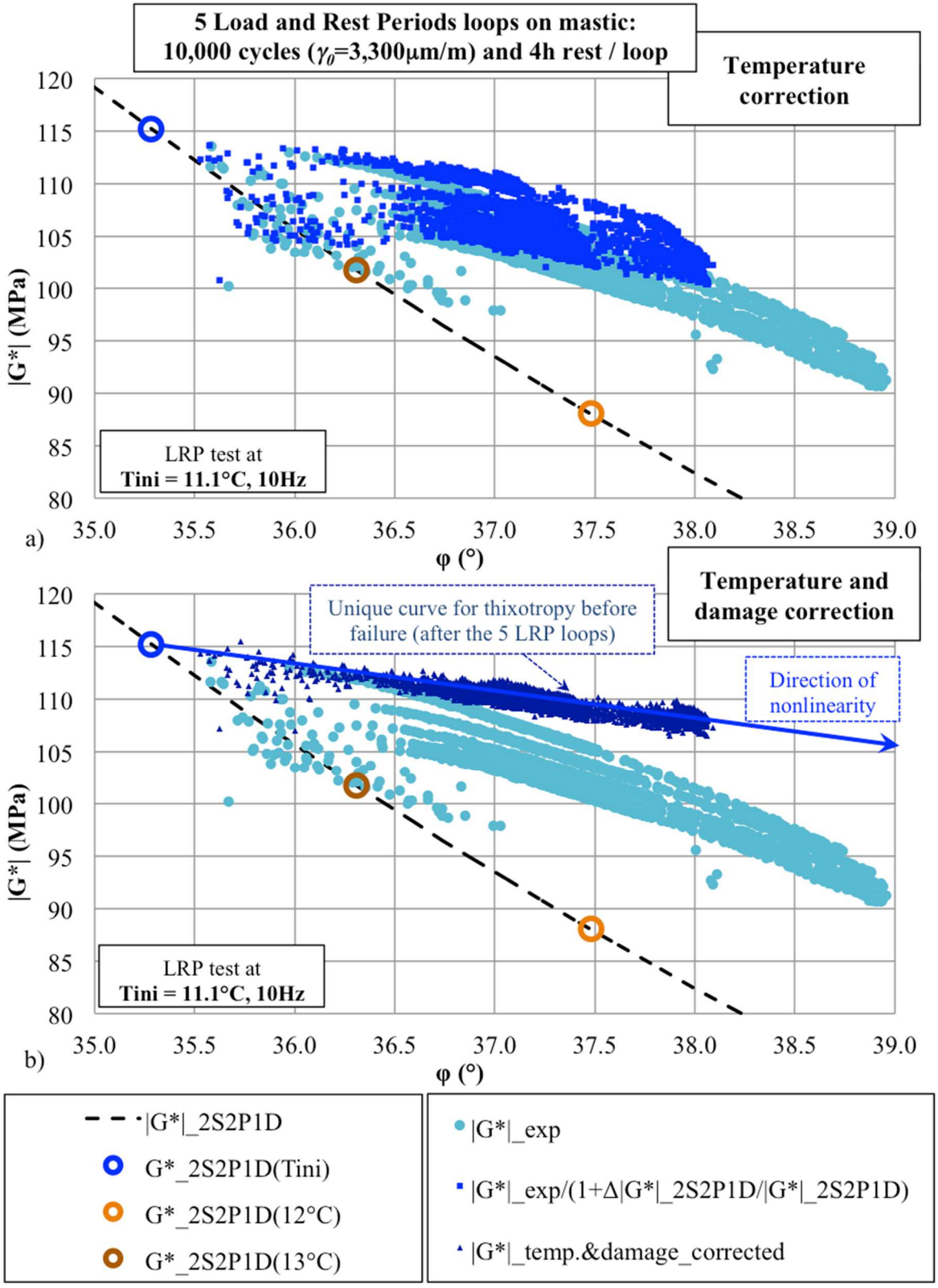

Figure C-36. Experimental results (M5070_30pc40-70_A) for LRP tests (5 LRP tests with 10,000 cycles of 3,300µm/m sinusoidal loading and 4h rest loops on bitumen): Black diagram representation of a) the raw experimental results and the results after the temperature correction and b) the experimental results after temperature and damage correction. The figure present also a 2S2P1D model prediction, with indication of LVE complex modulus at 10Hz and three temperatures, 11.1°C (Tini), 12°C and 13°C.

M5070_30pc40-70_B with 8,500μm/m strain amplitude

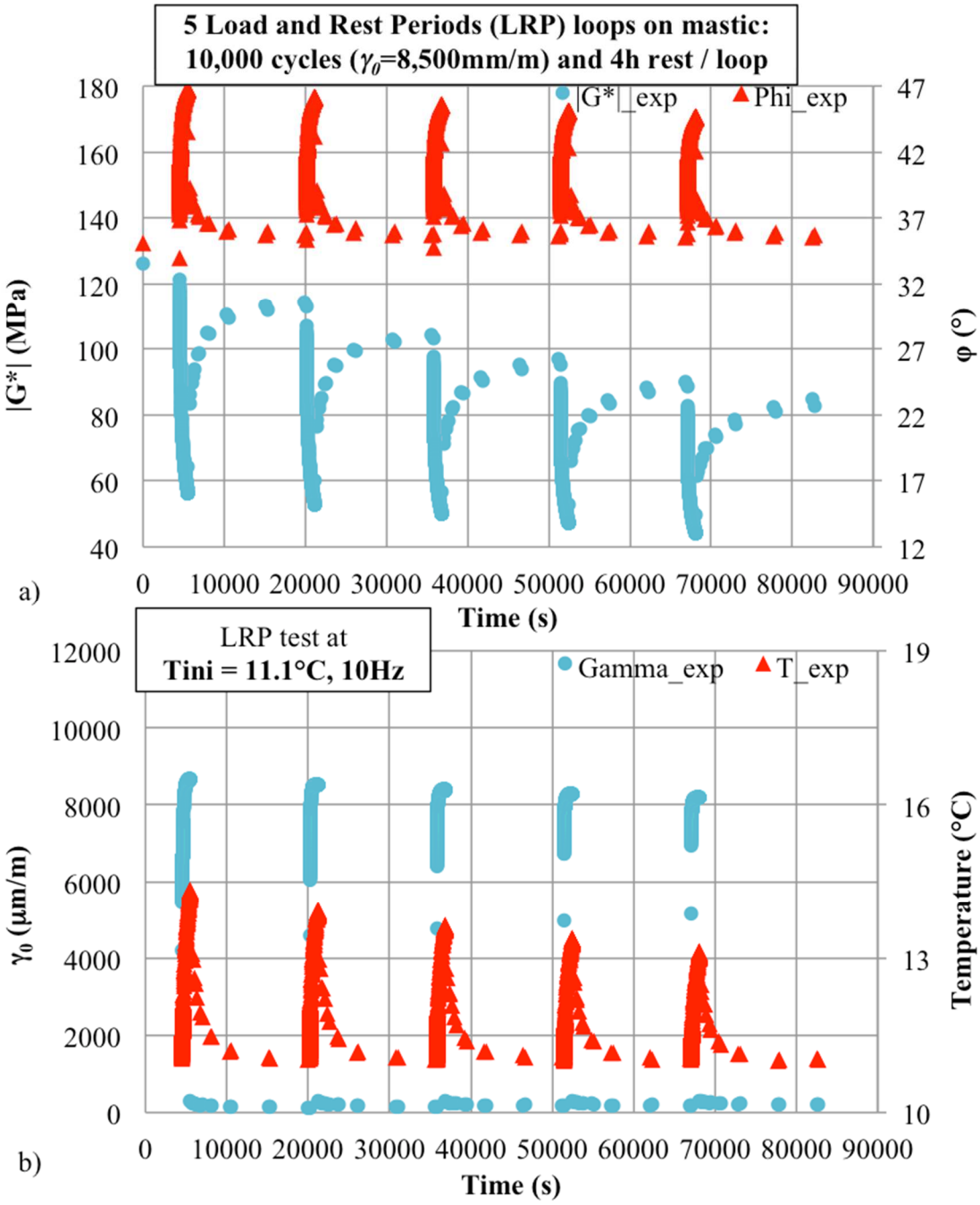

Figure C-37. Experimental results (M5070_30pc40-70_B) for LRP tests: 5 LRP loops with 10,000 cycles and 4h rest on bitumen submitted to 8,500μm/m sinusoidal loading: a) Norm of complex modulus and phase angle as a function of time, and b) shear strain amplitude and temperature as a function of time.

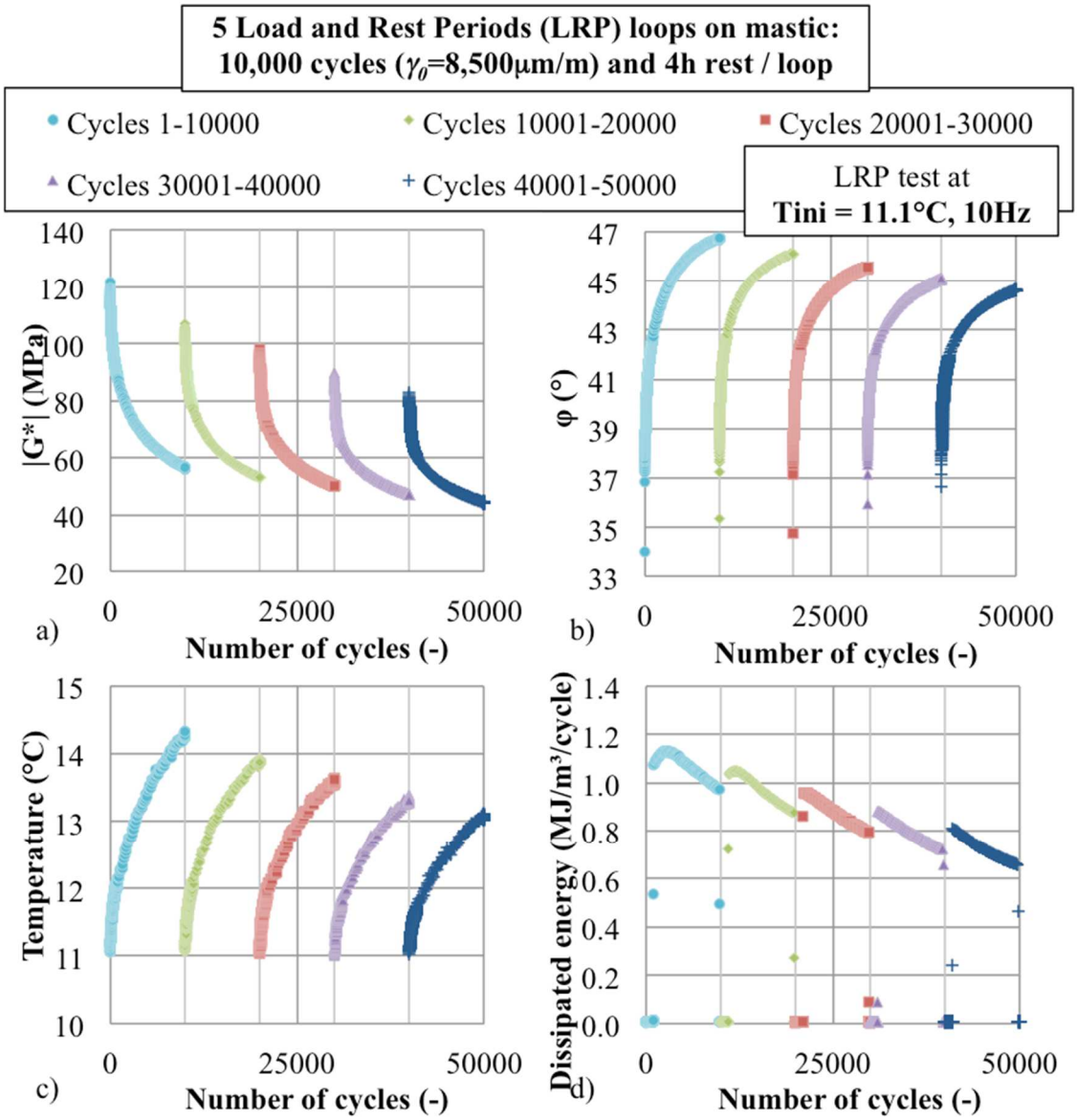

Figure C-38. Experimental results (M5070_30pc40-70_B) for LRP tests: 5 LRP 8,500µm/m sinusoidal loading loops with 10,000 cycles each on bitumen: a) Norm of complex shear modulus, b) phase angle, c) mean in-specimen temperature, and d) dissipated energy per cycle as a function of the number of applied cycles.

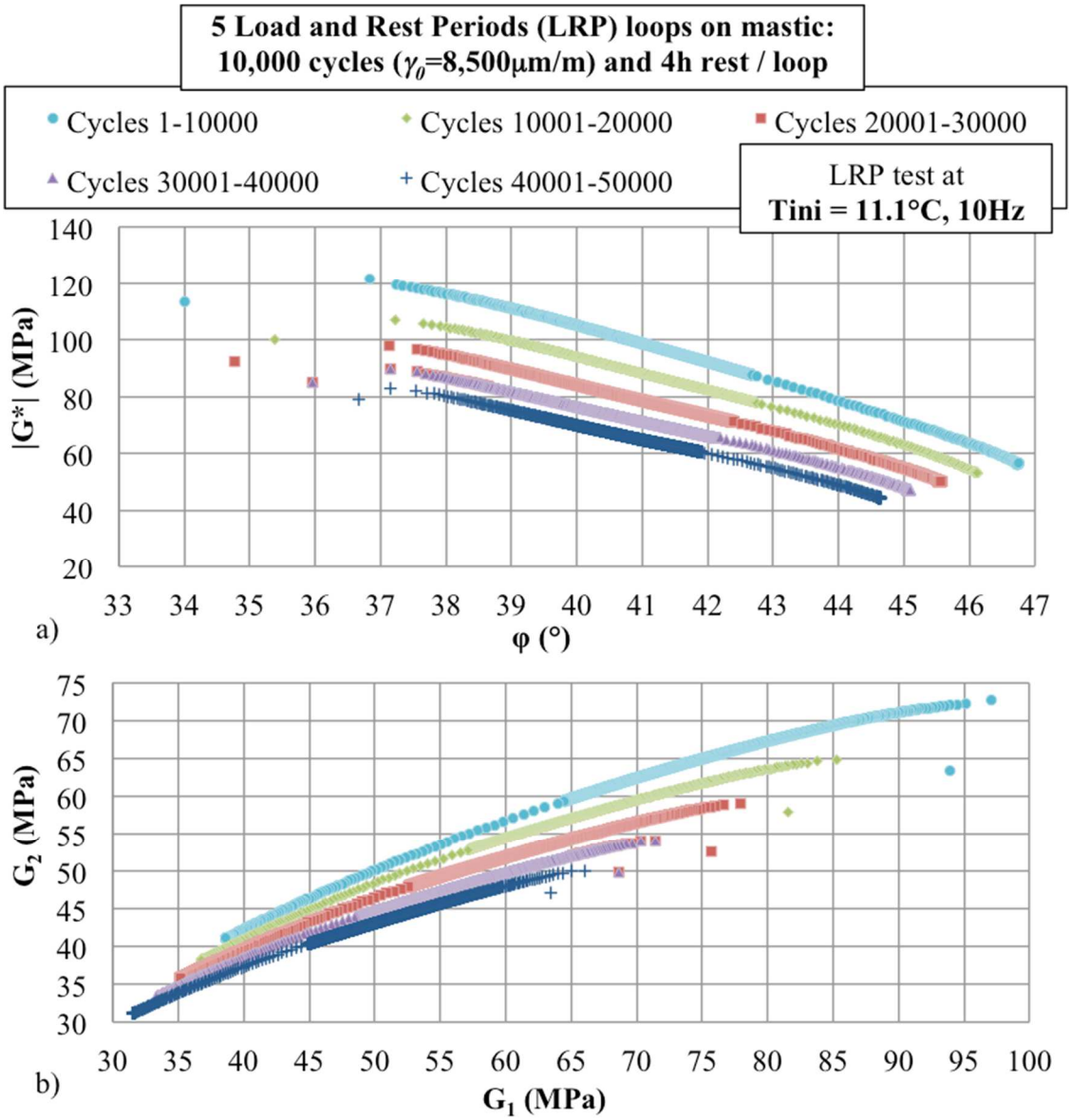

Figure C-39. Experimental results (M5070_30pc40-70_B) for LRP tests: 5 LRP 8,500µm/m sinusoidal loading loops with 10,000 cycles each on bitumen: representation on a) Black space, and b) Cole-Cole diagram.

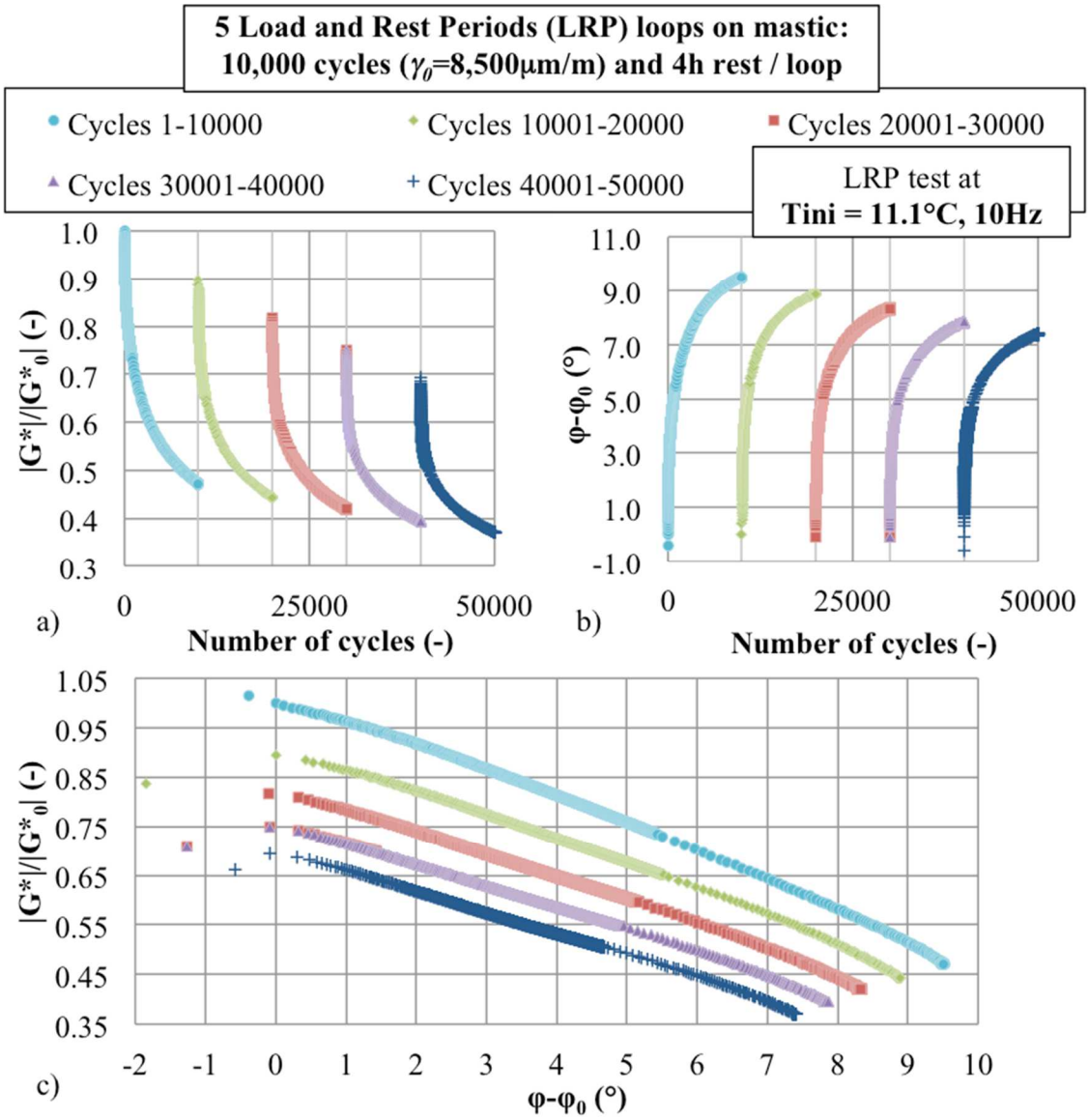

Figure C-40. Experimental results (M5070_30pc40-70_B) for LRP tests: 5 LRP 8,500µm/m sinusoidal loading loops with 10,000 cycles each on bitumen: a) Normalised (the initial modulus being considered as the result at the 3rd cycle) norm of complex shear modulus, and b) normalised phase angle as a function of number of applied cycles; and c) representation of the results on a normalised Black space.

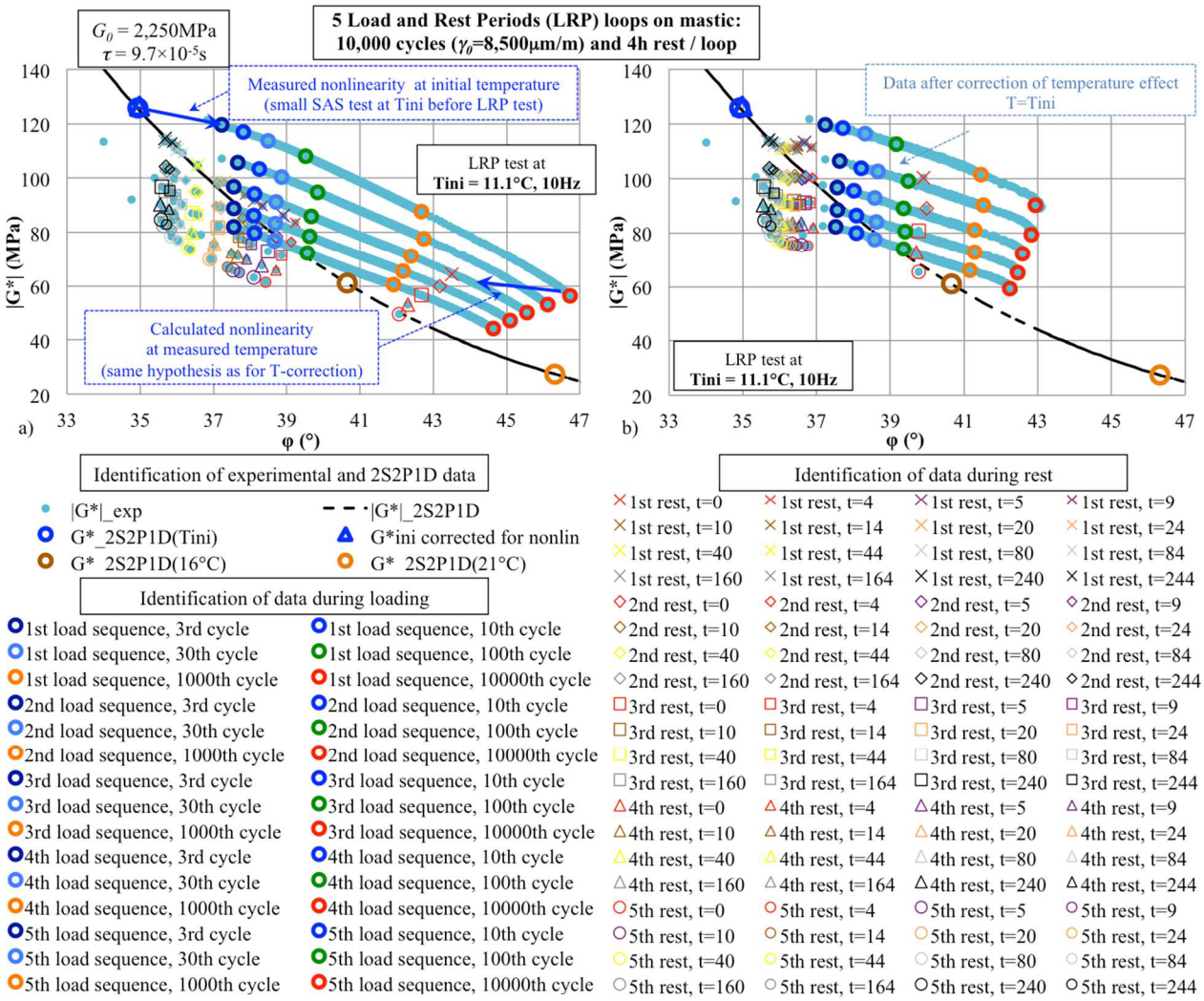

Figure C-41. Experimental results (M5070_30pc40-70_B) for LRP tests (5 LRP tests with 10,000 cycles of 8,500µm/m sinusoidal loading and 4h rest loops on bitumen): a) Black diagram representation of the results including details of the number of cycles during loading and the time of rest during rest periods, and a representation of the nonlinearity effect; b) results after temperature correction. The figure present also a 2S2P1D model prediction, with indication of LVE complex modulus at 10Hz and three temperatures, 11.1°C (Tini), 16°C and 21°C.

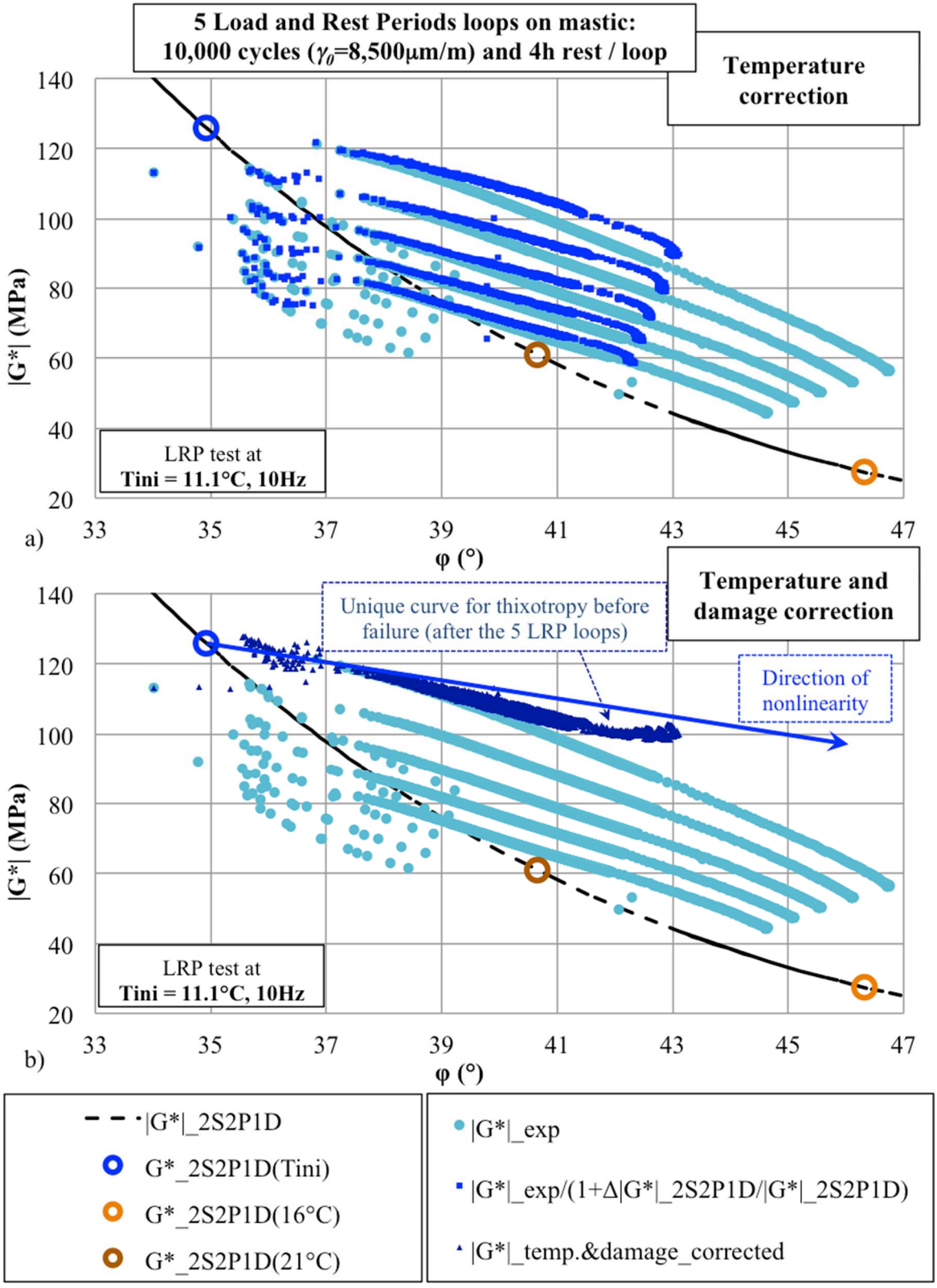

Figure C-42. Experimental results (M5070_30pc40-70_B) for LRP tests (5 LRP tests with 10,000 cycles of 8,500µm/m sinusoidal loading and 4h rest loops on bitumen): Black diagram representation of a) the raw experimental results and the results after the temperature correction and b) the experimental results after temperature and damage correction. The figure present also a 2S2P1D model prediction, with indication of LVE complex modulus at 10Hz and three temperatures, 11.1°C (Tini), 16°C and 21°C.